Ultimate Load Behaviour of Steel Box Girder Stiffened Compression Flanges

A Thesis submitted for the degree of Doctor of Philosophy in the Faculty of Engineering of the University of London

by Firoz Mohamedali Moolani
BSc(Eng),MSc,DIC

Imperial College of Science and Technology, London

April 1976

To my Wife

and my Parents

ABSTRACT

The study reported in this thesis deals with experimental and analytical investigations into the collapse behaviour of stiffened compression flanges of box girders.

The experimental work described covers tests on six box girder models, fabricated on a realistic scale, in which the compression flanges were the critical components. The tests were of two types: central point load tests on simply supported sections of box girders which simulated the conditions that occur near the support region of a continuous girder, and pure bending tests which represented, in an idealised way, the conditions in the span region of a continuous structure. Of the six models tested, two were centrally point loaded beam tests while the rest were pure moment tests. In one of the point loaded models pronounced shear lag was included in the flange. Details of the behaviour of the models are described for loads in the elastic range and beyond, up to collapse.

A theoretical method for analysing the ultimate load behaviour of stiffened compression panels is developed. The method is based on the column approach in which the longitudinally stiffened plate between cross-frames is treated as a series of columns consisting of the stiffeners and associated widths of flange plating. An iterative numerical procedure is used to analyse the response of such columns of various proportions and having varying degrees of initial imperfections. The theoretical treatment also includes multi-span stiffened panel analysis; for this analysis the plate/stiffener assembly is considered as a beam-column supported at the cross-girder

positions by springs which simulate the stiffnesses of the girders. The effects of continuity on the compressive strength of the panel are studied using this multi-span approach. Two modes of stiffened panel failure, namely, plate-initiated and stiffener-initiated failure are investigated. The buckling behaviour of plate panels is allowed for by using average stress-strain curves - instead of the material stress-strain curve - derived from elasto-plastic large-deflection analysis of constrained plate panels subjected to uniform end displacements. It is shown that the analytical method developed predicts satisfactorily the behaviour of the stiffened compression panels of the models.

The analytical work includes a parametric study of stiffened compression panels using the beam-column approach. A range of geometric and initial imperfection parameters which control the behaviour of the panels is considered. For the multi-span panels various patterns of geometric initial deflections in adjacent spans are assumed. Effective stiffener initial deflections which are used to relate multi-span to single-span failure are derived and it is shown that empirical formulations for the effective values can be satisfactorily used to predict multi-span panel behaviour.

ACKNOWLEDGEMENTS

The experimental and theoretical investigations reported in this thesis were initiated by and carried out under the supervision of Dr. P.J. Dowling, Reader in Steel Structures. The author is deeply grateful for his guidance, constant encouragement and expert advice throughout the duration of the work. The author is also most grateful to Professor B.G. Neal, Professor of Engineering Structures, under whose general direction the research was conducted, for his continued support and interest in the project. The experimental investigation was begun under the general direction of the late Professor S.R. Sparkes, formerly Professor of Engineering Structures, who was a source of constant encouragement to the author.

The author would like to thank the Bridges Engineering Design Standards Division of the Department of the Environment, for their sponsorship of both the experimental and theoretical investigations.

The author expresses gratitude and thanks to: Mr. J. Neale and the staff of the Engineering Structures Laboratories for their intensive efforts and the willingness with which they participated in the experimental work; Mr. P.J.D. Guile and the staff of R.M.E. Ltd. for their help in the fabrication of the models; Mrs. Jean Slatford for the care and patience with which she handled the extensive task of data preparation for the parametric study; Dr. P.A. Frieze for his co-operation with the experimental work and for his willingness and help in providing the results of his computer program on large-deflection analysis of plates; Mrs. Hazel Guile

for her high standard of draughtsmanship; Miss Joyce Gurr for carefully preparing the photographs; Mrs. Maxine Frieze for typing this thesis expertly and with great patience.

Thanks are also due to: Mr. J. Cima and Miss Susan Ford for their help in tracing some of the diagrams; colleagues who assisted in various ways during the tests. The author is also grateful for the benefit of many discussions with colleagues, including those who were engaged in parallel investigations, who freely gave their time over the period of this study.

Finally, but in no way least, the author is deeply grateful to his wife, Nashir, for her support and the extreme patience and understanding she has shown during the course of the study.

CONTENTS

CHAPTER 1

INTRODUCTION AND LITERATURE REVIEW

1.0 INTRODUCTION

In recent years, stiffened steel box girders have been increasingly used in bridge construction due to their economic and aesthetic appeal. The adoption of plated box girders as structural forms for bridges has also been facilitated by post-war developments in welding and fabrication techniques. These new methods allowed prefabrication of structural components on a very large scale with the result that bridge designers ventured into more flexible and economic choices of structural forms in which plates were the principal elements. Numerous box girder bridges have thus been built in the last two decades. The designs of such bridges were, however, based mainly on the experience of plate girder bridges since there were no comprehensive codes of practice covering box girder design. Although there are some aspects of plate girder behaviour which are common to box girders, the design of a box girder involves consideration of many effects which are of secondary importance or non-existent in conventional plate girder design. The inadequacies of bridge codes to deal with box girder problems were highlighted by the recent collapse of major box girder bridges in Austria, Gt. Britain, Germany and Australia. Several lives were lost in these disasters. The British Code of Practice, BS153[(1)] which has been used for steel girder bridges does not specifically refer to the requirements for box girders; it was written for simply supported bridges up

to 300 ft in span and hence does not give guidance for the design of continuous structures. Inevitably, therefore, the designer confronted with the problems of a box girder structure has had to seek guidance elsewhere. Some of the clauses in the German DIN[2] standards are relevant to box girder problems and thus designers have used these rules in the past.

One component of a box girder that presents particular difficulties for the designer is the compression flange. Generally, the flange will consist of a relatively thin plate which may be either stiffened or unstiffened depending on the overall geometry of the girder, that is, whether it is wide or narrow. The design of unstiffened compression plates is covered by BS153 but the rules, which are based on an effective width approach, do not provide for any variations in the severity of initial imperfections to be considered.

A stiffened compression flange will normally have a number of fairly closely spaced stiffeners in the longitudinal direction, and fewer, more widely spaced cross-girders or cross-frames in the transverse direction. Such thin stiffened compression plates are not within the scope of BS153 design rules. Frequently, however, the stiffened compression flange has been designed by using the strut approach (that is, treating the stiffened panel between cross-frames as a strut) based on the Perry Robertson formula in BS153. But, since this formula was derived for struts of symmetrical shapes its application to the design of eccentrically stiffened plates could only be a crude approximation. Moreover, the kind of initial imperfections that are encountered

in welded thin plate structures have not been covered by BS153 and thus the formula cannot be applied to such structures with confidence.

Following the collapse of Milford Haven (Gt. Britain) and West Gate (Australia) Bridges, the British government appointed a committee of enquiry, the Merrison Committee[3] to examine the methods of analysis and design used for steel girder bridges with a view to producing new design rules. A major programme of research was thus initiated. The various problems that needed investigation have recently been reviewed by Dowling[4].

The initial part of the experimental work described in this thesis (Models 1 and 2 - Chapter 2) was already in progress at Imperial College, under the sponsorship of the Department of the Environment, at the time the Merrison Committee was set up. The scope of this research programme was extended by the Committee to include more tests on stiffened steel box girder models covering a wider range of parameters. Following the work of the Merrison Committee, a joint Department of the Environment and Transport and Road Research Laboratory Working Group on steel box girders was established, whose purpose was to co-ordinate the research programmes started by the Committee and to initiate further theoretical studies. The theoretical work described in this thesis, in connection with stiffened compression flanges, was part of the research programme initiated by the Working Group. Reference (5) gives a summary of the basis of the various theoretical approaches that have been developed at Imperial College.

1.1 UNSTIFFENED FLANGES

1.1.1 Analytical Work

Considerable research efforts have now gone into studying the buckling behaviour of unstiffened rectangular plate panels, which are subjected to compressive loads in the plane of the plates. A review of the historical development of the work on this subject can be found in references 6 and 7. The problems of predicting elastic critical buckling loads of panels with various boundary conditions have received extensive treatment[6-9]. However, it is now well recognised that the critical buckling stress of a plate panel does not necessarily indicate its load-carrying capacity. Unlike slender columns, in which the buckling load is often a good indication of its ultimate strength, a plate panel may be able to sustain an ultimate load which is considerably higher than the buckling load. The difference between buckling and ultimate loads becomes particularly important in thin plates. Moreover, a real plate will inevitably have initial geometrical imperfections and thus there will be no bifurcation of the equilibrium position; the plate will have lateral deflections even at low loads. At loads above the critical buckling values, the lateral deflections become large and this results in membrane stress redistribution. Under these circumstances, the deflections can no longer be assumed to be small and it is necessary to use large-deflection theory to define the plate behaviour. An exact solution of the elastic large-deflection equations of the plate presents great difficulty. A number of approximate analyses have thus been performed. Foremost among the analysts dealing with this problem are Timoshenko[7] and Marguerre[6]. By making different assumptions regarding conditions

of the boundary restraints at the unloaded edges, several solutions[10,11,12,13] have since been obtained. The results of such analyses have often been used to obtain ultimate strength predictions in conjunction with some limiting criteria such as the attainment of membrane yield along the unloaded edges.

With the increasing power of electronic computers, it has now been possible to carry out elasto-plastic large-deflection analysis of thin plates. Moxham[14], using a Raleigh-Ritz procedure obtained elasto-plastic load-shortening curves; plasticity was included in the analysis by means of a volume integration in which the plate was considered to be multi-layered. Recently, Crisfield[15,16] has presented a finite element method. He uses two approaches, the 'volume approach' and the 'area approach'. The first approach involves a volume integral and is based on von Mises' yield criterion, while the second approach is based on an area integration using Ilyushin's[17] yield criterion which assumes a sudden plastification through the plate depth. In both methods, the relationship between stress and strain in the plastic stage is determined by the Prandtl-Reuss[18] flow rule.

A computer program for the elasto-plastic analysis of plates using the 'area approach' has also been developed by Frieze[19]. It differs from Crisfield's program in that it uses the finite difference formulations of the governing equations which are then solved by the dynamic relaxation method. A similar formulation of the 'volume approach' has been developed by Harding[20].

Frieze, Dowling and Hobbs have carried out a comprehensive study[21] of the effects of geometric imperfections and residual

stresses in plate panels with various longitudinal edge restraints and subjected to uniaxial compression. Load-end shortening curves are presented for a range of practical plate panel slendernesses. These curves have been used in the parametric study (based on the beam-column or strut approach) on stiffened compression plates, described in Chapter 5.

1.1.2 Tests

The major problem facing an experimentalist when testing isolated plate panels in compression is setting up a test rig which will simulate realistic boundary conditions for the panels. The inadequacies of much of the early work in providing the correct boundary conditions are pointed out by Davidson[22] in his review of the post-buckling behaviour of unstiffened rectangular plates subjected to uniaxial compression. Recently, Ractliffe[23] and Moxham[24] have conducted tests on a number of isolated plate panels with simply supported or clamped edges using a rig which allowed the boundary conditions to be more clearly defined. Both as-rolled and welded plates were considered. The load-end shortening curves obtained from these tests have been found to give satisfactory agreement with Moxham's theoretical solutions[14].

1.2 STIFFENED FLANGES

The load-carrying capacity of a stiffened compression panel can, in general, be limited by elastic buckling, elasto-plastic buckling or yielding. Although there are methods for calculating elastic critical stresses, the effects of initial imperfections and material non-linearity on the buckling stresses cannot

be assessed easily. In recent years, however, with the availability of test data and computer solutions on some of the complex aspects of plate and stiffener behaviour, several simplified methods for predicting the collapse loads of stiffened compression panels have been developed.

The buckling modes that may occur in a compression flange depend on the relative sizes of plate and stiffeners. These modes may be of the following form:

(1) Local buckling of the flange plate panels between longitudinal stiffeners.

(2) Local buckling of the stiffener outstand.

(3) Buckling of the longitudinally stiffened panel between transversals.

(4) Overall buckling of the stiffened panel involving both longitudinal and transverse stiffeners.

The above four modes are not necessarily independent and they may interact with each other depending on the relative proportions of the component elements. In general, modes (1) - (3) present the main problems to the designer; the overall buckling mode is usually avoided by providing sufficiently stiff cross-girders. There are essentially four different approaches on which stiffened compression panel design may be based:-

(1) *The column approach,* in which the longitudinally stiffened plate between cross-frames is treated as a series of columns consisting of the stiffeners and some associated widths of flange plating.

(2) *The orthotropic plate approach,* which assumes that the stiffened plate can be treated as an equivalent ortho-

tropic plate, that is, the stiffener properties can be considered to be 'smeared' over the width of the plate.

(3) *The hybrid approach,* which may be of two forms:

(i) the approach in which the column is employed as a behavioural model but where the analysis involves further considerations, such as the use of orthotropic plate properties in determining the response of the column;

(ii) the approach involving elastic large-deflection analysis of the stiffened plate with the stiffener treated as a discrete member acting with an effective width of flange plating.

(4) *The discretely stiffened plate approach,* in which the plated grillage is analysed as an eccentrically stiffened plate using the finite element or finite difference methods.

1.2.1 The Column Approach

The primary consideration in any column-type analysis of the stiffened plate is the establishment of a procedure to allow for the effects of plate buckling. One approach is to assume that the idealised plate/stiffener column consists of the longitudinal stiffener and a width of the flange plate equal to the spacing of stiffeners, and allow for plate buckling effects by considering the stresses in the plate to be limited to the levels predicted by a buckling analysis of the plate panel. The theoretical work described in this thesis is based on this approach. The alternative method is to assume an effective width of flange plating, derived from a buckling analysis, and then study the response of the plate/stiffener column using the yield stress as the limiting stress.

The design method suggested by Dwight[25] has evolved from an analytical treatment similar in principle to that described in this thesis. Dwight's design method employs a modified version of the Perry formula as a basis for establishing column curves suitable for application to stiffened plating. The modifications made to the Perry formula are: (a) the yield stress is replaced by a fictitious yield stress when considering plate-initiated column failure, (b) the imperfection parameter in the formula is allowed to vary so that a range of column curves similar to the European Column Curves[26] is obtained. Both modes of column failure, that is, failure towards stiffener outstand and away from it, are investigated. In the former case, the fictitious yield stress is taken to be the local plate buckling stress as derived from a set of curves based on experimental[24] and theoretical[14] data on elasto-plastic plate buckling. The reduction in plate strength due to the presence of shear is allowed for by using an effective yield stress instead of the true yield stress. In the case where residual stress is likely to cause sudden deterioration of plate stiffness (a procedure for identifying this situation being given), a separate criterion is used to establish the fictitious yield stress. For outstand-initiated failure, the limiting stress is taken as the yield stress on the assumption that the outstand is of stocky cross-section so that torsional buckling is prevented. To allow for the orthotropic action of the stiffened flange between cross-frames a column of reduced effective length is used in the analysis. The use of the modified Perry formula to predict collapse loads gives this method considerable versatility in that the empirical parameters in the formula can be varied conveniently to obtain a good fit between theoretical and experimental

results. It should be noted, however, that the plate strength curves given in Dwight's design method are based on experimental and theoretical data relating to plates with the unloaded edges free to pull in. While column strength predictions from the use of such data might be pessimistic, the assumption that the edges are unrestrained does not adequately represent the conditions in a multi-stiffened panel, where the column-type analysis is particularly well suited. In such a panel, although the longitudinal edges of internal panels will be free to pull in, conditions of continuity will constrain these edges to remain straight.

Murray[27] also adopts the column approach but uses the alternative method of assuming an effective width of flange plating. However, in the case where the elastic critical buckling stress of the plate is greater than the Euler stress for the column (calculated using the full flange width between stiffeners) the flange plate is considered to be fully effective. It is assumed, therefore, in view of the use of Perry formula, that at collapse the full squash capacity of the plate can be realised; this follows from the fact that the Perry formula gives the intensity of loading that will produce yielding in the most stressed fibre of the column. Such an assumption could, therefore, lead to optimistic strength predictions. In the case of more slender plate panels the effective widths used in the analysis are derived from consideration of the plate behaviour in the post-critical range. Expressions for the effective widths at collapse have been developed in terms of an initial imperfection coefficient considering both, plates with unloaded edges free to pull in and plates with edges held straight. Results of tests on welded steel plates with stress-free edges have been used to establish the

value of the imperfection parameter suitable for stiffened plate design. The shift in the centroid of the effective section relative to that of the gross section of the column is expressed as an equivalent eccentricity which is then added algebraically to the initial deflection of the stiffener. The collapse load is predicted by the Perry formula applied to the effective column. Both modes of column failure are considered.

Horne and Narayanan[28] use the effective width approach based on elastic large-deflection analyses of plates. However, unlike Murray they allow for the reduction in plate stiffness irrespective of the column slenderness. The stiffener outstands are assumed to be of sufficiently stocky cross-section so as to be able to develop yield at their extreme fibres before collapsing by torsional buckling. To allow for such factors as residual stresses, transverse stresses along the unloaded edges and earlier yielding due to the combined action of membrane and plate bending stresses, an empirical approach is used. It is assumed that the geometric initial imperfections of the plate panels can be modified to incorporate the effects of the above factors. Expressions for evaluating the effective width factor for any imperfection level are given. The collapse load of the stiffened panel is obtained by applying the Perry formula to the effective column section. The shift of the centroidal axis of the effective section relative to the gross section is converted into an equivalent initial stiffener deflection which is added to the overall initial bow of the stiffener. Also, the imperfection parameter in the Perry formula is modified to avoid the failure loads of very stocky columns

falling below the squash loads. Stiffener-initiated failure is not considered.

1.2.2 The Orthotropic Plate Approach

The method developed by Massonnet and Maquoi[29] treats the stiffened plate as an equivalent orthotropic plate which is then analysed according to elastic large-deflection theory for orthotropic plates. The effects of weld-induced residual stresses are not considered. To allow for the effects of eccentric stiffening of the flange plate, the extensional, flexural and torsional rigidities used for the substitute plate are modified according to Pflüger[30]. The failure criterion adopted is that of limiting the mean longitudinal stress along the unloaded edges of the orthotropic panel to the yield value. An expression for evaluating the average stress at collapse is given. To allow for the effects of buckling of plate panels between longitudinal stiffeners, an approximate effective width approach, based on Faulkner's[31] formula, is used to modify the collapse stress. The main limitation of this orthotropic plate approach is that it does not allow for the possibility of failure occurring by yielding of the outstand.

1.2.3 The Hybrid Approach

In the hybrid approach while some form of column idealisation based on effective flange width is used, the calculations also involve allowance for the orthotropic behaviour of the stiffened plate. This is the philosophy behind the Design Rules[32] (the Merrison Rules). The longitudinal stiffener is assumed to act with an effective width of flange plating to take account of

the effects of plating buckling. This effective width is derived from an elastic large-deflection analysis[12] of an initially imperfect plate subjected to in-plane loading. The stresses in the plate/stiffener column are determined from a Perry-type formula, assuming that the initial stiffener deflection is in the critical buckling mode. The failure criteria adopted for establishing the maximum load-carrying capacity of the column under the combined effects of applied stress, residual stresses and magnified flexural stresses are:

(a) The total stress in the mid-plane of the flange plate must not exceed the average stress that would produce yielding on the outer surface of an initially imperfect plate; this limiting average stress is derived from elastic large-deflection analysis.

(b) The maximum stress in the outer fibre of stiffener outstand must not exceed the yield stress or two-thirds of the elastic critical torsional buckling stress.

In determining the effects of magnification of initial deflections, the elastic critical buckling stress of the orthotropic plate, instead of that of the isolated plate/stiffener column, is used. The effects of in-plane shear or transverse stresses are considered by including these stresses in the critical stress calculations; also a reduced value of yield stress is used, based on the von Mises yield criterion. By using a mixture of criteria involving concepts of elastic buckling, maximum stress and stress redistribution, the Design Rules have covered a number of basic considerations that affect the behaviour of a box girder. However, the Rules have

one main limitation. By adopting the criterion that failure of the plate occurs when surface yielding is predicted by elastic large-deflection theory, the Rules ignore the reserve of strength that may be present beyond the attainment of surface yield.

Chatterjee and Dowling[33] also use the hybrid behavioural model in their proposed design method. Loss of effectiveness of the flange plate is accounted for by using an effective width derived from simplified forms of plate panel load-end shortening curves. From the results of elastic, and elasto-plastic large-deflection analyses of initially imperfect plates[21], it has been deduced that the plate panel behaviour can be described with sufficient accuracy by bilinear load-end shortening curves. Thus such curves have been established and the effective width factors for plate panels have been derived from these curves. The total stresses at the mid-plane of the flange plate and at the tip of the outstand of the effective column are then checked for the applied factored axial loading and the bending moment due to flexure of the column; the effects of magnification of stiffener initial bow being included in these calculations. For plate-initiated failure, the ultimate stress of the column is assumed to have been reached when the stress in the mid-plane of the plate equals the limiting plate capacity as derived from theoretical plate analysis. The effects of any shear stresses are allowed for by taking a reduced value for the yield stress, based on the von Mises yield criterion. For outstand initiated failure, the ultimate stress is reached when the stress in the extreme fibre of the outstand attains the yield value. Limiting stiffener proportions are specified on the basis of the results obtained from elastic large-deflection analysis of stiffeners of

flat section. A column with varying axial load as in a region of bending moment gradient is also considered. In such an analysis, the first two terms of the Fourier series are used to obtain the buckling mode, the critical buckling load, and the maximum bending moment for an assumed initial stiffener bow. Suitable coefficients have been derived for use in the Perry-type analysis. The orthotropic behaviour of the stiffened panel is considered by an analysis of similar nature but in which the coefficients are based on elastic large-deflection theory for orthotropic plates. In the column analysis, the shift of the centroidal axis due to the loss of stiffness of the flange plate, and the eccentricity due to overall curvature of the flange are also included.

The method developed by Rubin[34] is based on elastic large-deflection analysis of stiffened plates, but instead of considering equivalent orthotropic plate properties, Rubin treats the stiffener as a discrete member acting with an adjoining effective width of flange plating, this width being that given by Faulkner[31]. It is assumed that both initial and final out-of-plane deflections of the stiffened panel are in the sinusoidal mode along the span, but in the transverse direction the deflection mode is established by minimising the total potential energy. The calculation of energy involves consideration of bending in both directions, twisting of the flange plate and extensional deformations in the longitudinal direction. Torsional deformations of the stiffener, membrane shear and transverse deformations of the flange plate are ignored in these calculations. The stiffened panel is assumed to have reached its load-carrying capacity when either the longitudinal edges of the panel or the extreme fibres of the central

longitudinal stiffener, attain the yield stress. Graphs for establishing these limiting conditions are given for a limited range of practical parameters.

1.2.4 The Discretely Stiffened Plate Approach

This approach involves the elasto-plastic large-deflection analysis of the stiffened panel; the plate being considered to be eccentrically stiffened by discrete stiffeners. An elastic analysis of such a plate has been developed at Imperial College by Djahani[35], and the approach is currently being extended to include elasto-plastic behaviour[36]. Solutions using the finite element formulation have more recently been obtained by Moan and Söreide[37].

1.2.5 Review of Theoretical Work on Column Approach

The pioneering work on treating the stiffened compression flange between transverse frames as a beam-column comprised of the stiffener and an associated width of plating was carried out at Lehigh University under the direction of Professor Ostapenko. The research related to compressive strength predictions of stiffened panels of the type used in a ship's hull. Since such panels must be designed for sufficient compressive strength to withstand vertical bending of the ship's hull as well as lateral loading due to water pressure, the work at Lehigh involved beam-columns subjected to combined in-plane and lateral loading; the relative proportions of the component elements of the beam-columns are therefore not comparable to those used in a box girder bridge. Nevertheless, the analytical techniques developed had considerable scope and these have been extended and applied to stiffened plating used in bridge construction.

Following the experimental work of Ostapenko and Lee[38], who observed that the stiffened panel behaviour could be analysed by a beam-column model, Kondo[39] developed an analytical procedure for describing the ultimate strength behaviour of such a model. Kondo's analysis was restricted to plates with small b/t so that local instability was avoided. He assumed that the material stress-strain characteristic was ideal elastic-perfectly plastic, and allowed for residual stresses in the plate and in the stiffener flange. He obtained the ultimate strength of the beam-column by a procedure which involved evaluation of moment-thrust-curvature relationship and determination of the relationship between the ultimate axial load, lateral load, and panel length. For the latter analysis, he established panel length-deflection curves for varying axial loads and then determined the ultimate strength for any given length from the condition of zero gradient of the load-deflection curve. He examined columns with both pinned and fixed ends and developed design charts for such columns. The results of his study established the effects of varying the geometric parameters of the cross-section. The results also showed that residual stresses in the flange plate can cause considerable reductions in the load-carrying capacities of the columns.

Davidson[22] carried out a survey of the methods that were available for describing the post-buckling behaviour of long rectangular plates subjected to longitudinal compression. On the basis of some test results he concluded that for plates with large b/t, the elastic post-buckling behaviour was best described by average stress-edge strain curves as given by Koiter's equation[40]. Accordingly, Tsuiji[41] extended the treatment of the stiffened

plate problem to include the effects of plate buckling in panels of large b/t (such a panel being defined as one whose buckling stress is less than its yield stress). Since Koiter's solution related to an initially flat elastic plate, the maximum average stress was limited to the membrane edge stress causing first yield. Results of some tests on stiffened panels gave support to this approach and consequently Vojta and Ostapenko[42] developed design charts for panels with large b/t. To examine the validity of the assumption of a constant stress in the inelastic post-buckling range, Rutledge and Ostapenko[43] extended the analysis further and arbitrarily modified the assumed portion of the average stress-edge strain relationship. They concluded that the plate behaviour in the inelastic post-buckling range had little effect on the ultimate strength of panels commonly used in ship structures.

By adopting similar procedures for describing the average stress-edge strain relationships, Parsanejad[44] developed a method for analysing the behaviour of plated grillages subjected to combined axial and lateral loading. Using a step-wise numerical integration procedure to establish the deflected configuration of the grillage, he developed a computer program for determining the ultimate strength. He examined the scope of the method by analysing some sample grillages and concluded that the method could be used to predict the ultimate strength but that more test data was needed to establish its accuracy.

To investigate the suitability of the beam-column approach for analysing stiffened compression flanges of box girders, Mittleman[45] adopted Virdi's[46] computer program (which was developed for predicting the ultimate loads of composite columns)

and used it to study the inelastic behaviour of some typical plate-stiffener configurations. For stocky sections, Mittleman assumed the stress-strain relationship to be elastic-perfectly plastic. To allow for local buckling in slender plate panels, he used the average stress-strain curves derived by Moxham[24]. By treating the plate-stiffener combinations as eccentrically loaded columns and assuming the deflections to be defined by 'part-cosine' curves, he obtained a limited number of solutions. Both, initial deflections and residual stresses were considered in the analyses. This exploratory work was then extended by Virdi[47], who while still retaining the cosine wave assumption for deflections, considered in some detail the effects of initial imperfections and the mode of failure on the ultimate strength. Virdi also based his analysis on bilinear stress-strain characteristics for stocky sections but used Ractliffe's[23] experimental load-end shortening curves to study the influence of local plate buckling on the ultimate column strength. Although Virdi considered only one representative case of plate panel with local buckling, his results did demonstrate the extent to which local plate buckling can reduce the stiffened plate strength.

In both, Mittleman's and Virdi's analyses, equilibrium was considered only at the centres of the columns in view of the cosine wave assumption for deflections. Recently, Little[48] has presented a method for analysing the plate-stiffener column by satisfying equilibrium at several positions along the span. To allow for local plate buckling, Little used Moxham's theoretical average stress-strain curves; the limitations of using these curves in column analyses were indicated in Section 1.2.1. Using

some typical plate-stiffener configurations, Little examined the effects of varying the geometric parameters and initial imperfections. The results of his analyses provided the basis for assigning suitable values to the empirical parameters used in the design method proposed by Dwight[25].

1.2.6 Tests on Stiffened Compression Panels

At the time that the experimental work described in this thesis was already underway, there was practically no information on the ultimate load behaviour of stiffened compression flanges of box girders. In the past few years, however, several tests[27,49-51] on the behaviour of stiffened compression panels have been reported. The majority of these tests have considered the stiffened panels in isolation. Dorman and Dwight[49] tested twelve such panels. The panels were simply supported along the edges and five bays were used in order to isolate the centre panel from the influence of the end supports. The plate slenderness, b/t, varied from 33 to 50. Both bulb flat and flat bar stiffeners were used. Varying degrees of welding residual stresses and initial stiffener imperfections were considered. The investigation involved both, plate- and stiffener-initiated failures.

Horne and Narayanan[50] have tested a series of isolated stiffened panels subjected to uniaxial compression. The tests covered a range of variables in b/t (46 to 70), ℓ/r (19 to 95), initial imperfections of various types and differing types of plate/stiffener welds. Both loading and unloading characteristics of the panels were recorded.

Tests on large-scale panels have been reported by Murray[27] (b/t = 54 to 62, ℓ/r = 35 to 75) and Smith[51] (b/t = 34 to 96, ℓ/r = 21 to 66). The tests by Smith were in connection with the type of grillages used in ship-bottom structures.

Massonnet and Maquoi[29] conducted tests on six stiffened panels, all of which had plate panels with b/t of 48 but the proportions and the spacings of longitudinal stiffeners were varied (ℓ/r = 46 to 120). To simulate realistic boundary conditions, the stiffened panels were built into U-section girders so that the panels formed their compression flanges. The girders were then subjected to pure bending moment. Of the six panels tested, results of the first three panels have been published[29]; in these panels, initial stiffener deflections were in the direction of the plate and collapse also occurred in this direction with local buckling of the stiffener outstands.

Tests on complete box girder sections such as those described in this thesis were undertaken by Dibley and Manoharan[52]. They considered an 8 ft × 3 ft × 140 ft continuous two-span box girder. The main objectives of their tests were to investigate the effects of shear lag and to study the moment distributions in the girder up to collapse. The tests indicated some shear lag at the support region but at other locations the behaviour was influenced by the presence of bolted splice joints. On the whole, shear lag effects were not properly demonstrated due to inadequate strain gauging.

1.3 SCOPE OF THESIS

The research work described in this thesis covers:

(a) Tests on six steel box girder models to study the collapse behaviour of the stiffened compression flanges, and to assess the influence of shear lag on flange behaviour.

(b) Ultimate load analyses of stiffened compression panels, based on the column approach (or beam-column approach as it is referred to in this thesis).

In the analytical work, an iterative numerical procedure is developed to generate information about the behaviour of panels of various proportions subjected to axial thrusts. Varying degrees of initial imperfections are considered. Both modes of failure, that is, plate-initiated and stiffener-initiated failures are investigated. The buckling behaviour of plate panels is allowed for by using average stress-strain curves as derived from elasto-plastic analysis[21] of constrained plate panels subjected to uniform end displacement.

In addition, the analysis is extended to multi-span stiffened panels in order to establish the effects of continuity on the compressive strength of the panels; geometric imperfections of various patterns and magnitudes are considered for this study. A method of analysing a grillage of beam-columns, that is, a series of beam-columns supported on discrete transverse stiffeners, is also presented.

1.4 LAYOUT OF THESIS

Chapter 2 describes details of the box girder models, the testing procedures and the behaviour of the models up to collapse.

In Chapter 3, a method of analysing the stiffened compression panel as a beam-column is developed. The effect of continuity of spans is considered by assuming the beam-column to be supported by springs which simulate the stiffnesses of cross-girders. The extension of the beam-column treatment to grillage analysis is described in the appendix to Chapter 3 (Appendix A).

In Chapter 4, model test results are compared with the theoretical predictions obtained by the method developed in Chapter 3.

Chapter 5 describes the results of a parametric study on the ultimate load behaviour of single-span and multi-span beam-columns.

Chapter 6 contains the conclusions of the research programme and suggestions for future work.

CHAPTER 2

TESTS

2.0 INTRODUCTION

The tests described in this chapter formed part of a programme of research into the behaviour of steel box girders and their components. The purpose of the experimental programme was to carry out ultimate load tests on model box girders with components of varying proportions and to obtain data on the various aspects of box girder behaviour. In all, ten models were tested. Since this thesis is concerned with compression flange behaviour only the results of those tests in which the flange elements were critical are described. Of the ten models tested, six were designed specifically to produce compression flange failure. Details of these models and their behaviour up to collapse are discussed in the following sections.

2.1 DESCRIPTION OF TESTS

2.1.1 Outline of Test Types

The tests carried out were of two types: (a) centre point load tests on simply supported models simulating the conditions near the support region of a continuous box girder bridge; and (b) pure bending moment tests representing approximately the conditions in the span region of a continuous girder. Of the six models described herein two were tested as centrally loaded beams, while the remaining four were subjected to uniform bending moments.

One of the two centrally loaded models was tested primarily to investigate the influence of pronounced shear lag on the collapse behaviour; the model was loaded such that the centre point loads acted directly on the webs while the central support diaphragm was omitted.

2.1.2 Description of Models

The box sections tested were roughly quarter-scale models of girders used in practice. The minimum plate size used in the construction of the models was 1/8 in thick. This enabled the use of normal welding processes with realistic weld sizes, although the minimum weld size used (1/8 in fillet measured across throat) would be somewhat larger than that used in full size girders. Apart from the corner welds which were laid by the mixed inert gas (MIG) process, all welding was normal manual arc welding. In general, the models were designed such that normal fabrication procedures and design details could be employed. Reports on the construction sequence of each of the girders and other fabrication details are given in references 53 and 54.

Since the six models that will be described in this chapter formed part of a larger experimental programme consisting of a series of ten models, the identification numbers originally assigned to the models are being retained for ease of reference.

Details of the structural features of each model are presented in Table 2.1. Information on the test types, principal structural parameters and critical elements of the compression flange of each girder, is summarised in Table 2.2. An examination of the data will show that, in general, the main parameter varied

between models was the slenderness of either the plate panels (b/t) or the stiffeners (ℓ/r). For the centrally loaded models (Models 1 and 9) the additional test features were the presence of shear and associated shear lag. To investigate the effects of shear on the collapse of these models, their cross-sectional geometries were made comparable to models loaded under pure bending conditions. Thus Models 1 and 9 were similar to Models 2 and 10 respectively. For such comparisons, ideally the material properties must also be similar but unfortunately this was not achieved in Models 1 and 2. For Models 9 and 10 special efforts were made to ensure that similar material was used in fabricating the models.

2.1.3 Material Properties

The models were fabricated using material specified to meet the requirements of BS4360 Grade 43A steel. Values of yield stress and Young's Modulus for the different components of the model were determined from ultimate tensile tests conducted on coupons cut from surplus material. For each component at least four coupons were tested. Straight, parallel-sided specimens 3/4 in wide by 22 in long, cut and prepared according to the procedures recommended in BS18, were used. Elongations of the coupons were measured with an 8 in extensometer connected to an automatic x-y plotter. A 10 ton Amsler testing machine calibrated in accordance with BS1610 and conforming to Grade A classification was used to determine the yield strengths. Each test was carefully controlled with a strain rate of approximately 300 μstrain/minute. This strain rate was maintained even when measuring the yield stress. Thus the observed values of tensile yield stresses given in Table 2.1 are the dynamic yield stress values.

It may be remarked here that some recent research[55] carried out with the objective of establishing a standard testing procedure for the measurement of material yield stresses has shown that the static yield stress (i.e. the reduced value of stress measured at zero strain rate two minutes after stopping the cross-heads) is a more consistent measure of the yield properties of a steel than the dynamic yield stress. This is so because the strain rate has a significant effect on the dynamic yield stress level as has been shown by Rao, et al.[56] However, it has also been established that the measurement of dynamic yield stress at closely controlled strain rates is not likely to be too variable.

The observed yield stress values presented in Table 2.1 are average values for the component parts of the model. The variation in yield stress within components was very small but the scatter between the average values of components is significant. It may be noted that in some cases the measured yield stresses were lower than the guaranteed minimum value of 16.0 tonf/in^2 specified for the material.

Also listed in Table 2.1 are measured thicknesses of the plated components of the model. These thicknesses varied by up to 6 per cent from the nominal rolling thicknesses.

2.1.4 Details of Test Rigs

2.1.4.1 *Centre Point Load Tests:* The rigs used for testing the centrally loaded girders, Models 1 and 9, were similar in principle but differed in detail with regard to the way in which the centre reactions were provided (Fig. 2.1). Both models were tested by applying hydraulic jack loading at one end, while the

other end of each girder rested on cylindrical rockers and roller bearings supported by concrete blocks on the laboratory floor. For Model 1 the centre reaction was achieved by means of bearings mounted on an overhead cross-beam. The bearings were symmetrically placed about the centre-line but were set inboard of the webs. The model was thus tested in the upside-down position in relation to conditions at the support region of a continuous girder. Testing the model in this position simplified the design of the loading and deflection rigs and facilitated observation of the compression flange. Figure 2.2 shows a photograph of the model and the test rig.

Since the main object of the test on Model 9 was to study the effect of shear lag on compression flange behaviour, the central reaction system was modified so as to leave the critical mid-span region of the compression flange free from any interference by support bearings. Loading the model in this manner obviated the need for a full-width diaphragm and thus also eliminated the complications in compression flange stresses associated with the presence of a diaphragm. Transfer of load from the webs to the centre reaction units was achieved by means of 2 in thick tapered plates welded to the webs, Fig. 2.3, and providing pinned links between the attached tapered plate systems and bolted-down reaction units. Details of the jacking arrangement and support condition at the ends of the model were similar to those of Model 1.

2.1.4.2 *Pure Bending Tests:* Except for the tests on Model 10, all pure bending tests (Models 2, 4 and 8) were carried out using the rig shown diagrammatically in Fig. 2.4. Pure bending moment

condition was achieved by applying jack loads to the extreme ends of purpose-built loading arms welded to each of the box sections. Each model was supported at its junctions with the loading cantilevers by holding-down bolts which prevented vertical displacements at the junctions. These bolts had spherical bearing attachments which allowed rotation of the models in all directions. Although the loading system was self-stabilising, longitudinal and transverse movements of the girders were restricted by flexible stays anchored at one end to the loading arms and at the other to the laboratory floor. The loading units were so designed that they were re-usable. Thus the same pair of loading arms was used on Models 2, 4 and 8. Figure 2.5 shows a view of the loading unit.

Since the flanges of Model 10 were wider than those of the other models, the loading arms for Model 10 had to be redesigned. Details of the loading sections are given in Figs 2.6a to 2.6d. The holding-down arrangement used for this test was also modified. The reactions were provided by a system of link plates and pin joints connecting the model/loading arms assembly to reaction beams bolted to the floor.

2.1.5 Instrumentation

2.1.5.1 *Residual Strain Measurement:* Weld-induced residual strains in the models were measured by using a demountable Demec Mechanical Strain Gauge. The measurements were made over 2 in and 4 in gauge lengths between punched reference marks on the plate surface. A pair of specially ground centre punches was employed to prepare the gauge points. Both faces of the plate were marked so that the mean residual strain could be determined. Readings

were taken at three stages of fabrication: after cutting and butt welding of the component full length plates, after welding of the stiffeners to the plates to form sub-assemblies of stiffened sections, and after welding of all sub-assemblies together to form the completed model.

Since the measurements were spread over the period of fabrication, it was necessary to correct the readings for temperature changes. This was done by using the readings taken on gauge points marked on a small piece of unstressed steel plate.

2.1.5.2 *Deflection Measurements:* Initial out-of-plane deformations and deflections under load of each model were measured by a bank of electrical deflection transducers mounted on an inverted U-frame. The frame could be moved along the girder spans on a pair of rails which were supported at three points on the compression flange. At each of the sections chosen for deflection measurement, the U-frame could be accurately located by resting it on a set of balls fixed to the rails. The heights of the balls were accurately adjusted so as to define a datum plane under the weight of the U-frame. A photograph of the deflection rig used for the tests on Models 2, 4 and 8 can be seen in Fig. 2.7. The arrangement of deflection rig for Model 1 was similar in principle, but due to the presence of central support bearings, two U-frames were employed, one on each side of the central diaphragm. For Models 9 and 10, a wider frame had to be used to cope with the increased flange width (Fig. 2.8).

2.1.5.3 *Strain Measurement:* Strains in stiffeners and the plating were measured by means of electrical resistance strain gauges. Between 400 and 500 strain gauge elements of linear, cross and rosette type were used in each model. Several parts of the models were strain gauged but the majority of gauges were bonded to the critical components. In order to determine axial and bending components of strain in the plating, gauges were placed on both faces of the plate. Where it was adequate to measure the strain in one direction only such as over stiffeners and on stiffener outstands, linear gauge elements were used, but where transverse and shear components were needed cross and rosette type gauges were used. Layout of the gauges, gauge factors and other relevant information on instrumentation are given in references 53 and 54. Details of strains measured in various parts of the compression flanges of the models are given later in this chapter. In all models, some parts of the webs and tension flange were also strain gauged; details of these strain measurements are discussed in references 57 to 59.

2.2 TEST PROCEDURE

2.2.1 Initial Measurements

After installing each model on the test rig and prior to any load application, residual strain readings were taken at some selected locations to check if any relaxation of residual stresses had occurred due to transportation and handling of the models. Upon completion of these measurements, initial deflection profiles of the models were determined using the deflection rig described in the last section. For models with stocky plate panels, only profiles

along stiffener locations were recorded whereas in those models where plate panels were critical, deflections of plate panels along lines mid-way between stiffeners were also measured. In all cases, readings were taken at selected cross-sections located at regular intervals along the span.

2.2.2 Initial Tests

Before commencing the collapse tests, each model was subjected to loads well within the elastic range to obtain information on the elastic behaviour of the model. On satisfactory completion of these tests, further tests were carried out on some of the models so as to study their response at higher loads. The behaviour of the models during these tests is discussed later in this chapter.

2.2.3 Tests to Collapse

After completing all the elastic tests the models were loaded incrementally to collapse. The loading was applied by hydraulic jacks connected to a central control system which enabled the models to be loaded progressively by the application of either load or deflection increments. In the initial stages of testing, load increments were used but in later stages deflections were incremented using the strain control facility. This procedure enabled the load carried by the model to be controlled very satisfactorily on approaching the peak load and beyond.

2.3 INITIAL IMPERFECTIONS

2.3.1 Out-of-Plane Deformations

Longitudinal and transverse initial deflection profiles of the compression flange of each girder were deduced from trans-

ducer readings taken at the cross-sections chosen for deflection measurements. For each model, the profiles are presented separately in the appropriate section.

It was noted that, in general, plate panels deflected towards the surface to which the stiffeners were welded. Longitudinal profiles of the plate panels often showed small ripples superimposed on an otherwise gentle curve, although in the vicinity of transverse stiffener welds large local curvatures were observed.

Table 2.3 gives the maximum values of measured transverse bows in the plates. In all cases the values are well within the tolerances specified in the Design Rules [32]. It should be noted, however, that deflections of magnitudes indicated in Table 2.3 occurred at only a few locations; the average deformation levels were very much smaller.

Profiles of longitudinal stiffeners showed that the deformation modes assumed by the stiffeners were of variable nature. Only in one model, Model 10, were the initial deflections clearly in the preferred buckling mode that is, alternate inward and outward deflections in adjacent spans. In general, the longitudinal stiffeners in internal bays tended to bow towards their outstands between transverse stiffeners, while in the end bays the stiffeners often deflected in the opposite direction.

The maximum values of measured stiffener initial deformations in the direction of the outstand and away from it, are shown in Table 2.3. Also included are the average panel deformations for each model. It is evident that in some instances the maximum values for individual stiffeners are in excess of the tolerances

specified in the Design Rules[32]. However, if the average panel values are considered (which is allowed in the Design Rules) the panels which were deformed towards the outstands of stiffeners, complied with the clauses contained within the Rules; the deformations in the opposite direction generally tended to exceed the requirements.

2.3.2 Weld-Induced Residual Strains

The average levels of compressive residual strain in the compression flange plate panels of each model are given in Table 2.3. Typical distributions of residual strain across the flange widths of each model are shown in Fig. 2.9. It may be seen that except in the plate panels close to the corner and diaphragm welds, the residual strains in the plate away from stiffener welds were fairly uniform. This observation justifies the assumption usually made in stiffened plate analysis, that the compressive residual strains in the centre portion of a plate panel are distributed in a constant way.

Comparing the average levels of residual strain in the different models, it is readily seen that the magnitude of strain is controlled by the amount of welding used. In Models 4 and 8 as there were twice as many longitudinal stiffeners for a given flange width compared with the other models, the amount of welding used was more and hence the residual strains were higher.

In some models, in addition to the longitudinal residual strains, transverse residual strains were also measured but their magnitudes varied considerably and no definite pattern could be established. The variation in the transverse readings was partic-

ularly high in regions adjacent to transverse welds, such as near the centre diaphragm of Model 1.

In Models 9 and 10, residual strains in the longitudinal stiffeners were also recorded (Fig. 2.9b) but the values were very erratic to the extent that, on the tips of outstands, both tensile and compressive residual strains were recorded. It would seem from these observations that the outstand strains are much more dependent on such factors as, the sequence of welding and the clamping methods used. The variables involved in such a process thus make the task of predicting reliably the residual strains in stiffener outstands very complex.

2.4 TESTS ON MODEL 1

2.4.1 General

The 16 ft span of Model 1 was sub-divided into six equal bays by two cross-frames and an end ring-stiffener placed symmetrically on either side of a central diaphragm. Detailed drawings of the model are shown in Figs 2.10a to 2.10d. It will be noted that the longitudinal stiffeners used were simulated bulb flats prepared from 2 in × 1½ in × 3/16 in rolled angle sections. Except for an additional longitudinal stiffener in the compression zone of each web, the cross-section of the model was symmetrically stiffened.

2.4.2 Initial Out-of-Plane Deflections

Prior to testing, initial deflection profiles of the compression flange were determined at some selected cross-sections. Details of these locations are given, Fig. 2.11, while the deflection profiles are shown in Fig. 2.12.

2.4.3 Behaviour under Load

Since the compression flange and webs of Model 1 were designed to be critically stressed simultaneously under the applied loading, information on the collapse behaviour of both components was obtained. Three tests were carried out on the model. In the first test the largest plate panels of the end web bays buckled in shear at a central point load of 120.0 tonf. Compression flange plate panels adjacent to the central diaphragm (around section I) also showed signs of buckling, but the growth of buckles was prevented by the failure of end web panels. After stiffening the end web bays by diagonal bracing on the outsides, a second test was carried out. This test too ended in shear failure with buckling of web plate panels in the intermediate web bays. The maximum load reached was 132.0 tonf corresponding to mid-plate flange stress, σ_n of 13.0 tonf/in^2 and at that stage it was noted the compression flange plate panel buckles had also been amplified.

After bracing the intermediate web bays in the same way as the outer web bays, the model was loaded again incrementally to failure. The maximum load attained in this test was 128.0 tonf (σ_n = 12.6 tonf/in^2), with failure occurring simultaneously in the flange on one side of the central diaphragm and in the web on the opposite side (Fig. 2.13). On the flange side, the critical section was situated at about one-third panel distance between the diaphragm and the first transverse stiffener.

The loading history of the model during the final test may be traced by reference to the overall load-deflection relationship shown in Fig. 2.15. Up to a central point load of 80.0 tonf

the observed deflections agreed closely with those predicted by simple elastic beam theory in which allowance was made for deflections due to shear and shear lag (which accounted for 40% and 6% of total deflection respectively), but at higher loads the response of the model became non-linear. There was no significant loss in overall stiffness until after the maximum load was reached. The load-deflection curve thus shows a sharp peak with a drooping unloading path, a characteristic which may be attributed to the average stress-strain curve of the compression flange after collapse.

Stresses determined from measured strains for central point loads of 80.0 tonf and 128.0 tonf are shown in Fig. 2.17, while out-of-plane deflections of plate panels and stiffeners at some selected locations are shown in Figs 2.15 and 2.16. It may be seen that at the section where failure occurred, the longitudinal stiffeners deflected inwards towards their outstands. In the adjacent spans the stiffeners deflections were small initially but as more deformations were applied to the model, increased deflections in the opposite direction were recorded. The large out-of-plane deformations that occurred at high loads also caused local lateral failure of stiffener outstands near the transversals.

Figure 2.14 shows also that the longitudinal flange stiffeners failed at the same section where the collapse of plate panels occurred. In fact, stiffener failure was triggered off by collapse of plate panels as shown by curves 2, 3 and 4 of Fig. 2.15.

Details of failure on the web side are not included here. However, it should be noted that the test ended in simultaneous failure of the compression flange and web, and consequently the

response of the model may have been influenced to some extent by the interaction of the two failure modes.

2.4.4 Shear Lag in Model 1

Figure 2.18 shows the longitudinal stresses calculated from strain measurements at a cross-section close to mid-span, with the model under a central point load of 80.0 tonf. The distribution of measured stresses is clearly non-uniform due to the influence of shear lag. Stresses obtained from a finite element analysis[60] are also plotted and it will be seen that in the compression flange and web the agreement is satisfactory. In the tension flange, however, the edge strains are higher than those predicted by the analysis, probably due to the relaxation of residual stress in the boundary weld. The effective width ratio, ψ, for the flanges as determined from the finite element solution was 0.59 while the value obtained from the Design Rules[32] (which were based on similar finite element analyses) was 0.61.

2.5 TESTS ON MODEL 2

2.5.1 General

The cross-section of Model 2 was nominally similar to that of Model 1 with the diaphragm omitted to simulate the mid-span region of a continuous box girder. Detailed drawings of the model are shown in Figs 2.19a and 2.19b. The model was tested by applying pure bending using the rig described in Section 2.1.4.2.

Two tests were conducted on Model 2. In the first test (Test 2A), failure occurred in an end bay of the compression flange, at a section close to where the model was welded to the end

loading unit. The end bays were subsequently strengthened by adding longitudinal stiffeners on the outside of the model in line with the internal ones, and the model was retested (Test 2B) to produce failure in one of the centre bays.

2.5.2 Initial Out-of-Plane Deflections

The reference grid adopted for deflection and strain measurements is shown in Fig. 2.20. Longitudinal and transverse initial deflection profiles of the compression flange are given in Figs 2.21a and 2.21b. From the longitudinal profiles, it is evident that the deflections of stiffeners between cross-girders were generally outwards, that is, away from stiffener outstands. It may be seen also that the outward deflections in the end bays were of greater magnitudes than those in inner bays. The average stiffener deflections for each bay are shown in Table 2.3.

2.5.3 Test 2A: Behaviour under Load

The load-deflection relationship of the model during Test 2A is shown in Fig. 2.22. Up until 59.0 tonf jack load the observed deflections increased almost linearly with load but with further loading buckling of a flange plate panel adjacent to the end cross-frame (section W) occurred and the load-deflection path became non-linear. With the next increment of applied loading, to a jack load of 64.5 tonf, that is, σ_n = 13.3 tonf/in^2, buckling occurred in the other flange plate panels close to section W (Figs 2.23 and 2.24). All flange panels, except for an internal one, deflected inwards while the longitudinal stiffeners in the critical end bay deflected outwards, away from the outstands. This caused stiffeners in the adjacent span to deform inwards in sympathy (Fig. 2.25). On apply-

ing further deflection increments to the model, the load sustained by the model dropped to 62.0 tonf, indicating the commencement of unloading. The final increment amplified further the flange plate buckles and also produced complementary outward movements in the adjacent web panels.

Since the section at which collapse occurred was not extensively strain gauged, as it was hoped to collapse one of the internal stiffened bays, information on the nature of strain distribution at the critical section is lacking. However, strains measured in the adjacent span, at section R (Fig. 2.26) indicate the general trend in the level of plate straining. The distribution of strain corresponding to the peak load of 64.5 tonf shows that yield strain had been exceeded at several locations, indicating that the maximum capacity of the model was reached almost immediately after the plate panels became ineffective due to yielding. Another interesting feature of the observed strains at section R is that very little change in strain occurred as the model was loaded past the peak load. This suggests that other parts of the model, mainly in the critical end bay, must have suffered a significant amount of straining.

Figure 2.27 shows strains in the longitudinal stiffeners S1, S3 and S4. Here again strains in the outstands of stiffeners in panel U-W were not recorded but the readings taken at other sections show that as a result of out-of-plane bending, considerable secondary strains were imposed on the stiffeners. Although the first visible sign of distress in the end bay was the buckling of a flange plate panel, it is quite likely that the stiffener out-

stands in this bay were also highly stressed due to the deflections being in a direction away from the outstand. An examination of the initial shape of the compression flange (Fig. 2.21a) will show that the deformations of stiffeners in the end bays were away from the outstands and were of relatively greater magnitudes than those in the inner bays. Under load, the stiffeners continued to deflect in the direction of initial deflections thus increasing the compressive stresses in the tips of the outstands.

Considering the conditions in the flange panels in the vicinity of the failed section, it would seem that there were possibly two factors which contributed to failure in the end bay. The first of these is the proximity of the end plate panels to the continuous transverse fillet weld connecting the end ring-stiffener to the compression flange, and the full strength butt weld joining the model plating to the end loading section. As a result of these welds the plating close to the end ring-stiffeners may have been heavily stressed under the combined action of residual and applied stresses. A second factor is that poor fit-up between the flange plate and that of the loading arm may have introduced a local eccentricity of applied loading in the flange plate. However, the effects of these factors were probably not very significant. Tests by Dwight[49] have shown that the weakening influences of such factors become appreciable only in extreme situations.

2.5.4 Strengthening of End Bays

After completion of Test 2A, both end bays of the model were strengthened by welding additional longitudinal stiffeners to

the outside of the model in line with the internal stiffeners. To avoid any abrupt change in section, the stiffeners were tapered uniformly from full depth at the centres of the end panels (sections B and V) to zero at the transverse stiffener positions (sections C and U). The fillet welding used to connect these stiffeners was also varied. Over the loading section, the welding was continuous but along the model proper intermittent welding was used. Strengthening the end bays in this manner ensured that the internal bays were not subjected to any eccentric loading. Figure 2.28 shows a view of a section of the model and the additional stiffening.

2.5.5 Test 2B: Behaviour under Load

Figure 2.22 shows the overall load-deflection behaviour of the model during the second test. Up to a jack load of 63.0 tonf the observed deflections increased linearly with load and agreed well with deflections computed from simple bending theory. The apparent increase in bending stiffness from Test 2A to Test 2B is due to the reduced length (3 bays instead of 5) used in deducing the deflections under load. The departure from linearity at 63.0 tonf, i.e. σ_n = 13.0 tonf/in^2 coincided with the first visible signs of flange plate buckling. The critical section in this test was the centre of the stiffened bay O-U, the bay adjacent to that which failed previously. As shown in Fig. 2.29, all flange plate panels, except one, buckled inwards while the adjoining compression web panels again deflected in a compatible mode. Longitudinal stiffeners between sections O and U also deflected inwards (Fig. 2.30). In the initial stages of loading the stiffener deflections were small (curve 3B, Fig. 2.31) but with the buckling of plate panels (indicated by curves 2A to 2D) the deflections increased rapidly.

As in Test 2A, the maximum load sustained by the model was 64.5 tonf, i.e. σ_n = 13.3 tonf/in^2. When further deformations, beyond the maximum load stage, were applied to the model, a fall-off in sustained load occurred with mid-plate strains at several locations exceeding the yield value (Fig. 2.32). This was accompanied by further amplification of plate panel buckles and the formation of hinges in longitudinal stiffeners at locations mid-way between transversals. The mechanism of failure can be seen in Fig. 2.33a. An inside view of the model, Fig. 2.33b, shows the lateral buckling of stiffener outstands close to the transversals. These local deformations occurred as a result of additional compression imposed on the stiffener outstands by restraining moments developed at the cross-frame regions of the failing bay. The growth of strains in these regions is shown in Fig. 2.34.

Despite the increased initial deflections in Test 2B arising out of plastic deformations from Test 2A, the maximum moments sustained by the model in the two tests were identical. This indicates, therefore, that the outward deflections of longitudinal stiffeners in the end bay in the first test had a weakening effect on the load-carrying capacity of the flange.

2.6 TESTS ON MODEL 4

2.6.1 General

The cross-section of Model 4 (Fig. 2.35) differed from that of Models 1 and 2 in that the slenderness ratios (panel width/thickness) of plate panels were considerably reduced. This was done to ensure that instability of plate panels in the elastic

range was prevented and that failure of the compression flange occurred by buckling of stiffened panels between transversals. The flange plates of Model 4 were nominally of the same thickness (3/16 in) as those of Models 1 and 2 but with approximately twice as many longitudinal stiffeners. Simulated 'bulb flats' were used as longitudinal stiffeners in the compression flange and webs while flats were used in the tension flange. Cross-frames provided at regular intervals of 31 in divided the span of the model into five bays.

The girder was tested under a condition of pure bending moment, in a rig similar to that of Model 2.

2.6.2 Initial Out-of-Plane Deflections

Details of the reference grid used for deflection and strain data recording are shown in Fig. 2.20. Profiles showing the initial shape of the compression flange are presented in Figs 2.36a and 2.36b. Since the longitudinal stiffeners were very closely spaced in this model, the measurement of out-of-plane deflections of compression flange plate panels was omitted.

The profiles of longitudinal stiffeners (Fig. 2.36a) show that the stiffeners had distinct outward bows in the end bays while in the intermediate bays the stiffeners tended to deform sympathetically. The maximum and the average values of measured stiffener deflections are given in Table 2.3.

2.6.3 Behaviour under Load

The overall load-deflection relationship for Model 4 is shown in Fig. 2.37. Up to a jack load of 63.0 tonf, the observed

deflections increased linearly with load and agreed very well with deflections calculated from engineering beam theory when the entire cross-section of the model was assumed to be fully effective. Over this load range the growth of strains at almost all locations (Figs 2.38 and 2.39) was also linear. There was generally good agreement between measured strains and those computed from bending theory for the constant curvature condition. Beyond 63.0 tonf, however, the stiffness of the girder began to decrease while the growth of mid-plane strain in some flange plate panels showed deviation from linearity (curves 4B and 5B, Fig. 2.40). Buckling of the stiffened panels between transversals was first observed at a jack load of 87.0 tonf, i.e. σ_n = 13.9 tonf/in^2. When further deformations beyond this load stage were applied to the model, the entire compression flange could be seen to have deflected into a sinusoidal waveform (Figs 2.41 and 2.42). The deformation mode, which closely followed the initial shape of the flange, was similar to the classical elastic buckling mode, i.e. outward and inward deflections alternating in adjacent bays.

An inspection of the inside of the model indicated that in the end bays where the longitudinal stiffeners had deflected outwards, i.e. away from the outstands, some lateral deflections of the stiffeners had occurred. The deformations became fairly pronounced at higher loads. It may be noted in Fig. 2.36a that initial deformations in the end bays were also directed outwards and were somewhat larger in magnitude than those in internal bays. It is therefore likely that the tips of outstands in the end bays yielded first and triggered off the buckling of flange panels. Unfortunately,

the end bays were not strain gauged and hence it is not possible to establish the degree of stressing in these bays.

The maximum load sustained by the model was 92.5 tonf corresponding to mid-plate flange stress, σ_n, of 14.8 tonf/in^2. Beyond the peak load, as more deformations were applied to the model, overall girder deflections continued to increase without any fall-off in the sustained load. The load-deflection curve of the girder thus shows a stable plateau at peak load and indicates the capacity of the model to sustain the collapse moment while undergoing further rotation. The moment at collapse was nearly 85 per cent of the full plastic moment of resistance of the box cross-section calculated using the measured yield stresses of all the components. However, when the limiting moment was calculated on the basis of flange capacity alone, then the maximum moment achieved was approximately 113 per cent of the calculated value.

Figure 2.43 shows views of the compression flange after collapse. The regular buckled pattern of the stiffened flange panels can be clearly seen in Fig. 2.43a. Failure of the panels occurred without any noticeable buckling of plate panels between stiffeners. The few local plate buckles that can be seen in the picture, in regions where the stiffened panels deflected inwards, occurred only after large rotations had been applied to the model, beyond the maximum load stage. However, it is interesting to note that the growth of strain in the plate panels (curves 4B and 5B, Fig. 2.40) became non-linear at a relatively early stage of loading. This may be attributed to the presence of high compressive residual stresses in the flange plating. These stresses were of

the order of 8 tonf/in^2, and this may have caused earlier plastic redistribution of strain due to the combined applied and residual compressive stress reaching the yield value. The fact that the limitsof linear behaviour in the overall load-deflection relationship and the plate strain werereached at almost the same load, before any stiffener movements were observed, suggests that residual stresses were responsible for causing the loss in overall girder stiffness. However, residual stresses do not seem to have had any significant effect on the collapse strength of the compression flange, as under the maximum applied moment almost the full squash capacity of the flange plate was achieved.

There is no evidence in this test of any large-deflection or post-buckling behaviour of the compression flange. Referring to Fig. 2.40 it will be seen that the loss of in-plane stiffness of the flange plate under longitudinal compression (curves 4B and 5B) continued without any significant increase in transverse strains. Curves 4A and 5A show that almost up to the maximum load stage, the measured transverse strains were merely the Poisson strains associated with longitudinal compression.

One other interesting feature relating to the strains measured on the compression flange at its junctions with the webs, is that strains measured at the locations of cross-frames were somewhat greater than those measured at the surrounding locations. This was the case even for loads in the elastic range (Fig. 2.38) when strains elsewhere in the flange agreed well with those predicted by simple bending theory. The phenomenon causing this behaviour appears to be one of stress concentration due to the restraining

effects of cross-frames on lateral in-plane movements of the flange, that is, Poisson effect. The restricting influence on the flange caused local curvatures at the corners and this produced local stresses which were of the same sign as the overall bending stresses. It is worth noting here that stress concentrations of similar nature but of much higher intensities have been observed to occur at the flange/web/diaphragm junction of a centrally loaded box girder (Model 3, reference 61).

2.7 TESTS ON MODEL 8

2.7.1 General

The main object of the test on Model 8 was to study the behaviour of stiffened compression flanges having stocky flange plate construction and slender longitudinal stiffeners. The width-to-thickness (b/t) ratio of flange plate panels was 25.6, approximately the same as that for Model 4, but the slenderness ratio (ℓ/r) of flange stiffeners in Model 8 was 114.5 compared with 44.7 in Model 4. Details of the geometry of the model are given in Figs 2.44a and 2.44b.

One other object of the test was to investigate the effects of longitudinal compression in the flange on the behaviour of intermediate cross-girders. For this reason the cross-girders were made slender and were pre-dished in the direction of the outstand. Although it was intended to have equal initial deflections of 1/8 in (= span/385) in each of the two internal transverse stiffeners, the deflections on completion of fabrication were span/310 at E (location indicated in Fig. 2.45) and span/

430 at I. Referring to Fig. 2.44b it will be noted that the transverse members were deliberately made discontinuous at the flange/web corners. The purpose of this was to achieve approximately pinned end conditions at the corners and thereby reduce the effects of any restraining end moments.

2.7.2 Initial Out-of-Plane Deflections

Longitudinal and transverse initial deflection profiles of the compression flange are shown in Figs 2.46a and 2.46b respectively. It may be seen that the pattern of longitudinal stiffener deflections was a very consistent one. In panels A-E and E-I the stiffeners bowed inwards towards the outstands but in the end bay I-M, the deflections were outwards and nearly twice as much as those in the other bays.

2.7.3 Behaviour under Load

The load-deflection behaviour of the model is shown in Fig. 2.47. Up to a jack load of 21.0 tonf the observed deflections agreed well with those calculated from engineering beam theory. Beyond 21.0 tonf load, although the observed deflections were marginally more, there was no significant loss in girder stiffness until a jack load 46.0 tonf, i.e. σ_n = 8.5 tonf/in^2, was reached. The small loss of stiffness at 21.0 tonf load could be attributed to the presence of high residual stress in the flange plating (of the order of 6 tonf/in^2). Referring to Fig. 2.48, it will be seen that up to a jack load of 31.0 tonf, there was satisfactory agreement between stresses determined from measured strains and those predicted by simple beam theory, but at higher loads the observed stresses were markedly non-linear. On loading the model beyond

50.0 tonf, i.e. σ_n = 9.3 tonf/in^2, there was a significant increase in out-of-plane deformations of both the longitudinal stiffeners and the transverse stiffener E. It is interesting to note that although the flange buckled as an orthotropic plate between transverse stiffeners, the deflections of the panels were not in the lowest buckling mode, i.e. alternating inward and outward deflections in adjacent bays. The buckling mode (Figs 2.49 and 2.50) followed closely the initially deflected shape of the compression flange. Considerable spalling of mill scale from the outstands of longitudinal stiffeners was observed in bay I-M, where the stiffeners deflected away from the outstands. Strains recorded in the outstands (Fig. 2.51) at the 51.0 tonf load stage confirmed that yielding had occurred in this bay. When further deformations were applied to the model, a peak sustained load of 55.0 tonf, i.e. σ_n = 10.2 tonf/in^2, was reached. This occurred when the girder deflection at mid-span was approximately twice that at 46.0 tonf load, the load which marked the start of deterioration of girder stiffness. Out-of-plane deformations of flange panels had also been considerably amplified. As more deformations were applied after the peak load had been reached, the model continued to deform while sustaining a load of just under 55.0 tonf. On completion of the test, local lateral buckling of the longitudinal stiffener outstands was observed to have occurred in the end bay I-M.

Photographs of the model, Figs 2.52a and 2.52b, taken after the collapse test, show the fully developed deformations of the flange panels. It would seem from these photographs that the failure mode of the compression flange was one of overall buckling with a half wave-length extending over two bays (A to I). However,

this was not the case, for strain measurements indicated collapse was in fact triggered off by the attainment of compressive yield strain in the outer fibres of stiffener outstands in bay I-M. Substantial deformations of the transverse stiffener at E occurred only after the longitudinal stiffeners had buckled. Since the stiffeners on both sides of the transversal E were deflecting inwards, and also because the transverse stiffener itself had a large initial bow, it was loaded by the vertical component of in-plane compressive loading in the flange. Consequently, as large deformations were applied to the model, the deflections of the transverse stiffener increased considerably. The growth of strains in the cross-girders is shown in Fig. 2.53.

Referring to the overall load-deflection characteristic of the model, Fig. 2.47, it will be noted that although the compression flange had slender longitudinal stiffeners ($\ell/r = 114.5$), the model sustained its peak load, without any significant fall-off, while undergoing increased rotations. In fact, the maximum load (55.5 tonf) compared very well with the load (55.4 tonf) required to produce a nominal stress, as calculated by simple bending theory, at the centroid of the compression flange equal to the elastic critical buckling stress of the flange. The ability of the flange to sustain its critical buckling load, in spite of the high level of residual stress in the plating and pronounced initial stiffener deflections, indicates that there was significant post-buckling reserve in the flange. The presence of membrane action is confirmed by the growth of transverse strains, curves 4 and 5 in Fig. 2.54. In the initial stages of loading, these strains were merely the tensile Poisson's

strains associated with longitudinal compression (curves 2 and 3) but at loads approaching the peak value, the transverse strains increased substantially. In particular, curves 3 and 5 show that in bay I-M although buckling of the stiffeners produced a decrease in longitudinal strain, the transverse strain continued to increase. This reflected the development of tensile membrane stresses as the deflections of the panel became large. The effect of these stresses was to restrict the growth of buckling and thereby help sustain the applied loading. Figures 2.55a to 2.55c show that the more or less uniform distribution of longitudinal strains in the compression flange changed as the maximum load was approached, to a typical plate post-buckling distribution, that is, strains at the edges were higher than those measured at locations inside the flange.

2.8 TESTS ON MODEL 9

2.8.1 General

Model 9 was tested primarily to investigate the effects of shear lag on the collapse behaviour of a compression flange in which both the plate elements and the stiffeners are of intermediate slenderness, that is, are within the imperfection sensitive range. The model was tested as a simply supported girder with a point load at the centre of the span so as to induce shear and shear lag. The flanges of the model were made wide in relation to the span (width-to-span ratio of approximately 0.5) in order to exaggerate the shear lag effect.

The model had an 8 ft wide by 3 ft deep cross-section and a total span of 16 ft. The box section was stiffened by two

cross-frames, one at each end of the model, and internal transverse stiffeners which divided the 186 in clear span of the model into three equal-length bays as shown in Fig. 2.56a. The compression flange plate was nominally 3/16 in thick and was longitudinally stiffened by nine equally-spaced $2\frac{3}{4}$ in deep by 5/16 in thick rolled flats. The width-to-thickness ratio (b/t) of the flange plate panels was thus 49.3 (based on measured plate thickness of 0.192 in).

Transverse stiffening was provided by 5 × 3 × 3/8 in angle sections which were chosen to preclude overall buckling of the stiffened compression flange. The column slenderness ratio (ℓ/r) for the plate/stiffener combination of length equal to transverse stiffener spacing, was 75.4, on the assumption that the entire flange plate was fully effective.

The 36 in deep webs of the model were unstiffened longitudinally but were made 1/2 in thick to prevent any shear failure.

The tension flange was 1/4 in thick and was unstiffened longitudinally. Both the webs and tension flange had transverse stiffening similar to that on the compression flange. Other details of the model are shown in Figs 2.56b to 2.56e.

After all initial measurements were completed, two separate tests on the model were carried out. The first test, Test 9A, was essentially a 'first yield' test in which the model was loaded incrementally until yielding was recorded at the edges of the compression flange at mid-span. In Test 9B, the model was loaded again incrementally from zero load to failure.

2.8.2 Initial Out-of-Plane Deflections

The reference grid adopted for deflection and strain measurements is shown in Fig. 2.57. Transverse initial deflection profiles of the compression flange, Fig. 2.58a, show that at all sections the flange had an overall upward bow with the plate panels between stiffeners almost invariably deflecting inwards towards the stiffener outstands.

Figure 2.58b shows the longitudinal profiles of the flange. It may be seen that the deflections in this case do not exhibit any regular pattern. In general, the deflections of longitudinal stiffeners in this model were small compared with those observed in Models 1 and 2.

2.8.3 Test 9A: Behaviour under Load

The overall load-deflection relationship of the model is shown in Fig. 2.59. Up to a centre point load of 120.0 tonf, that is, σ_n = 4.9 tonf/in^2, the behaviour of the model was linear, with the observed deflections agreeing very well with theoretically predicted values. The theoretical deflections were calculated from engineering beam theory using the shear lag effective widths given in reference 32. Shear deflections of the webs, which in this model accounted for nearly 27 per cent of the total girder deflection, were also included. The values of effective width ratio ψ for the flanges, used in calculating the deflections due to bending and shear lag effects were, ψ = 0.60 for the compression flange and ψ = 0.68 for the tension flange.

Between 120.0 tonf and the maximum applied load of 258.0 tonf there was a small drop in the stiffness of the girder, which

could be attributed to the increased out-of-plane deflections of the compression flange (Figs 2.60 and 2.61). The loss of stiffness may also have been caused by earlier yielding in the highly stressed edge panels of the compression flange as a result of the combined applied and residual compressive stresses reaching the yield stress of the material.

Strains measured at several locations of the flange are shown in Figs 2.62 to 2.64. At 258.0 tonf strain recordings indicated the start of yielding in the compression flange at the flange/web junctions and consequently the model was unloaded. The residual centre deflection of the girder upon unloading was 0.012 in.

Referring to Figs 2.60 and 2.61 which show the deformations of the compression flange under load, the following features will be noted:

(a) The stiffened panel between transversals E and Q deflected inwards while panels A-E and Q-U deflected inwards in areas adjacent to the centre-line of the flange, but outwards in regions nearer to the webs.

(b) In bay E-Q, the longitudinal stiffeners that were closer to the webs and were thus subjected to higher direct stress due to shear lag deflected more than the innermost stiffeners.

(c) The relatively greater inward movements of the panels closer to the webs in bay E-Q appear to have influenced the corresponding panels in the outer bays A-E and Q-U and caused them to deflect outwards in sympathy.

(d) The out-of-plane deflections in panel A-E and Q-U were also affected by the deformations of the flange at the cross-frame positions. The outward deflections at sections A and U occurred as a result of the end reactions being located inboard of the webs, while the centre supports were situated exactly along the centre-lines of the webs. In addition, the way in which the angle bracings were positioned on the end cross-frames (Fig. 2.56e), may have had some effect on the deflections. However, as the model was subjected to a moment gradient, it is unlikely that the deformations at the ends of the model would have had any significant influence on the behaviour of the highly stressed mid-span region.

2.8.4 Shear Lag in Model 9

To show the stress distribution in the compression flange due to shear lag, the stresses corresponding to a centre point load of 40.0 tonf (σ_n = 1.6 tonf/in^2) are plotted in Fig. 2.65. Only a few sections where a reasonable number of experimental values were recorded are shown in the figure. The experimental stresses shown were derived from strains measured in both longitudinal and transverse directions. The theoretical stresses were calculated by using the shear lag effective widths for flanges as given in the Design Rules [32] but following a slightly modified procedure in obtaining the distribution of longitudinal stress. The modifications made were as follows:

(a) In determining the distribution of longitudinal stress across any transverse section of the compression flange,

the formula used was,

$$\sigma_{1\bar{x}} = \sigma_{1max}\left[\left(\frac{\bar{x}}{\bar{B}}\right)^4 + \frac{5\psi - 1}{4}\left\{1 - \left(\frac{\bar{x}}{\bar{B}}\right)^4\right\}\right]$$

where ψ = Effective width ratio as given in the Design Rules

σ_{1max} = Longitudinal stress at the flange/web junctions calculated from engineering beam theory using the effective widths of flanges

$\bar{B}$ = Half width of flange between web centre-lines

$\bar{x}$ = Distance from the centre-line of flange.

The above formula, which has recently been suggested by Moffatt and Dowling[62], gives a much better fit with the finite element values than the formula given in the Design Rules which is based on a simple parabolic distribution.

(b) The values of effective width ratios for cross-sections other than at mid-span were obtained from the report[63] covering the parametric study which formed the basis of shear lag clauses in the Design Rules. The reason for taking this alternative course was that the effective width ratios presented in the Design Rules correspond exactly with the finite element values only at the mid-span and quarter-span positions, whereas for all other intermediate positions the Rules give approximate values based on simple interpolations. While this is quite a reasonable approach for design, it may not provide a fair comparison between test and theory. Reference was thus made to the original report and more accurate values of effective width ratios were obtained by interpolating

between the exact distribution curves as given by the finite element values.

Referring to Fig. 2.65, it may be seen that the experimental and theoretical stresses compare very well. The comparison is particularly good at the mid-span section K, where the effective width ratios were known exactly. The ratios for the mid-span section were as follows:

Compression flange : $\psi = 0.41$
Tension flange : $\psi = 0.45$

For higher load levels, a comparison of the measured and theoretical longitudinal strains at the compression flange/web junctions is made, and this is shown in Fig. 2.63a. It may be seen that at 158.0 tonf centre point load, the measured strains are fairly close to the theoretically predicted values while at 258.0 tonf, the experimental values can be seen to depart from the theoretical distribution. In the inner parts of the flange, however, the differences in strains became greater at somewhat lower loads due to increased out-of-plane deflections of the flange panels.

2.8.5 Test 9B: Behaviour under load

The overall load-deflection relationship of the model for Test 9B is shown in Fig. 2.59. Up to a centre point load of 260.0 tonf, that is, $\sigma_n = 10.7$ tonf/in^2, the response of the model was linear with the overall stiffness being somewhat less than that observed during the initial stages of loading in Test 9A. The limit of linear behaviour in Test 9B occurred at nearly the same load as

the maximum load reached in the previous test (maximum load in Test 9A was 258.0 tonf). The various features observed in loading the model to collapse are summarised below.

(a) At 260.0 tonf edges of the compression flange at mid-span reached yield strain, while at a centre point load of 296.8 tonf (σ_n = 12.2 tonf/in^2) average mid-plane plate strain in the edge panels equalled the yield strain.

(b) On loading the model to 316.0 tonf, out-of-plane deformations of the plate panels became just noticeable. In the more highly loaded edge panels, spalling of mill scale was also observed.

(c) With further loading, both the overall girder deflection and out-of-plane plate panel deflections increased at faster rates. At 420.0 tonf, that is, σ_n = 17.3 tonf/in^2, there were several well-defined plate buckles in the middle-third-span region of panel E-Q. The buckles generally alternated in direction with half-wave lengths approximately equal to plate panel width. A sketch indicating the development of plate buckles is shown in Fig. 2.66.

(d) The maximum centre point load sustained by the model was 440.0 tonf, i.e. σ_n = 18.1 tonf/in^2. The load was maintained in a steady state for about ten minutes, during which time the longitudinal stiffeners still appeared to be holding up as at 420.0 tonf. However, soon after, all the stiffeners in bay E-Q suddenly deflected inwards and the load sustained by the model dropped to 376.0 tonf.

At that stage the deformations in the mid-span region were fairly extensive. When further deflection increments were applied to the model, the load continued to fall while the deformations became even more pronounced. Photographs of the model, taken on completion of the tests, are shown in Figs 2.67a to 2.67c. The deflections of the model under load for various load stages are shown in Figs 2.68 and 2.69.

(e) After the highly stressed edge panels had yielded, inner panels of the compression flange continued to take more strain. When collapse occurred there was extensive yielding across the flange in the mid-span region. The plastic zones extended to approximately one plate panel width on either side of the mid-span section. Strains measured at several locations on the flange are shown in Figs 2.70 and 2.71.

(f) Figure 2.72 shows that in panel E-Q all longitudinal stiffeners, except for the lowly stressed centre one, deflected inwards with respect to the cross-girders; stiffeners closer to the webs deflected more than inner ones. As for the centre stiffener, although the graph shows inward deflections (positive values on graph, Fig. 2.72) the net out-of-plane deflections after allowing for curvatures due to overall bending, were outwards. At low loads, however, these out-of-plane deflections were very small. Stiffener 8 also exhibited similar behaviour but the outward movements remained small throughout. In fact,

above 420.0 tonf, the deflections showed a definite inward trend. In bays A-E and Q-U, the stiffeners deflected outwards although initially small inward deflections were recorded. Figures 2.72 and 2.73 show also that when the ultimate capacity of the model was reached, there was a sudden loss in the flange stiffness as all longitudinal stiffeners in bay E-Q, including the centre stiffener, collapsed inwards.

(g) The distribution of shear strain in the compression flange at section I-J ($7\frac{3}{4}$ in from mid-span), shown in Fig. 2.74, is one that would be associated with varying longitudinal strain due to high shear lag. At higher loads, however, due to the increased participation of the inner flange panels in carrying the longitudinal compression, the shear carried by the inner panels also increased.

(h) The presence of high shear lag in the flange resulted in a gradual spread of plasticity from the edges into the inner panels. The effect of this on the overall response was to produce a gradual deterioration of stiffness as the maximum load was approached.

(i) The maximum mid-span moment sustained by the model was 82 per cent of the calculated plastic moment for the entire box cross-section.

2.9 TESTS ON MODEL 10

2.9.1 General

Model 10 was essentially similar to Model 9 with regard to geometry and material properties, but was tested under a uniform moment condition so as to provide a basis for comparing the results of the centre point load test on Model 9. The only significant difference in the construction of the models was the additional longitudinal stiffening in the end bays of Model 10. The purpose of introducing further stiffeners was to ensure that the middle panel was a critical one, and that the failed section was not influenced by the loading units (Fig. 2.6) welded to the ends of the model. To further ensure that the reinforcing of end panels did not unduly alter the boundary conditions for the critical middle panel, the intermediate stiffeners were tapered uniformly from full depth ($2\frac{3}{4}$ in) at mid-panel positions to zero by the internal cross-girders. Details of these stiffeners and other dimensions of the model are given in Figs 2.75a to 2.75d.

Based on measured thicknesses and gross sections, the slenderness ratios for the compression flange plate panels and stiffeners were as follows:

b/t for flange plate panels = 48.8 (cf. 49.3 for Model 9)
ℓ/r for plate/stiffener combination = 75.6 (cf. 75.4 for Model 9)

The model was subjected to three loading cycles. In the first cycle, Test 10A, the model was loaded in several increments to 158.0 tonf (total load on each loading arm) and then unloaded. In Test 10B the loading was applied again incrementally to a maximum value of 180.5 tonf. The final test, Test 10C, was the collapse

test in which the model was loaded from zero load to the maximum load it could sustain, that is, 196.0 tonf.

2.9.2 Initial Out-of-Plane Deflections

Transverse and longitudinal initial deflection profiles of the compression flange are shown in Figs 2.76a and 2.76b. Details of the reference grid used for Model 10 are similar to those forModel 9 (Fig. 2.58a).

Profiles along transverse sections of the middle bay of the compression flange, exhibit overall outward deflections with plate panels between longitudinal stiffeners bowing inwards in the same way as in Model 9. In the end bays A-E and Q-U, however, the pattern of transverse deformations was different due to the presence of additional longitudinal stiffeners.

Referring to the longitudinal profiles, Fig. 2.76b, it may be seen that the initial stiffener deflections were in the preferred buckling mode with deflections in the middle bay directed outwards, that is, away from stiffener outstands. The maximum and average measured deformations of the stiffeners are given in Table 2.3.

2.9.3 Test 10A: Behaviour under Load

The overall load-deflection behaviour of the model is shown in Fig. 2.77. Two sets of curves are plotted: the first shows centre deflections of the entire girder length A-U (span = 186 in, i.e. 3 bays at 62 in), while the curves on the second graph show centre deflections for span E-Q. For the purpose of comparing the observed deflection values with those predicted theoretically, the

latter graph was used, as it was convenient to compute deflections for the length of girder lying between sections E and Q (which contained the critical compression flange panel) where the cross-sectional geometry was uniform. In the end bays of the model, the cross-section varied due to the presence of tapered longitudinal stiffeners.

Figure 2.77 shows that the response of the model was linear up to a load of 139.0 tonf (σ_n = 11.5 tonf/in^2), with the observed deflections agreeing well with those computed from simple beam theory. Between 139.0 tonf and 158.0 tonf (σ_n = 13.1 tonf/in^2) the overall stiffness of the model was marginally lower. Out-of-plane deflections of the compression flange, Figs 2.78 and 2.79, indicate that the directions in which the stiffened panels deflected followed the initial shape of the compression flange, i.e. the middle panel (E-Q) deflected outwards away from stiffener outstands, while the adjacent end panels deflected inwards. Graphs indicating the growth of out-of-plane stiffener deflections, Fig. 2.80, show that up to about 99.0 tonf the deflections increased almost linearly with load. It should be noted that the curves in Fig. 2.80 show out-of-plane deflections relative to cross-girders and include deflections due to overall bending of the girder. Although the curves do not show true stiffnesses as the loads indicated are total loads on the model and not loads on individual stiffeners, they nevertheless give a good indication of the trend in out-of-plane deflection behaviour.

Figures 2.81a to 2.81d show that up to a load of 99.0 tonf, the distribution of longitudinal strain across transverse sections of the compression flange was nearly uniform with the observed values

being close to those predicted by simple beam theory. Strain distributions in the longitudinal direction are shown in Figs 2.82a to 2.82d. It will be seen that in the vicinity of cross-girders the longitudinal strains tended to vary locally. These variations appear to have been caused by local curvatures resulting from out-of-plane deformations at the cross-girder positions being restricted. On the outer fibres of the compression flange at locations where the webs intersected with the transversals, the local strain concentrations were due to the restraining effects of cross-frames on lateral in-plane movements of the flange, i.e. Poisson effect (as in Models 4 and 8).

The maximum load to which the model was subjected in Test 10A, was 158.0 tonf. At that stage the average longitudinal strain in the outstands of inner longitudinal stiffeners at mid-span was approximately 90 per cent of the yield strain.

Upon unloading the residual centre deflection of the girder of span A-U was 0.012 in while the centre deflection for girder span E-Q was 0.002 in. The maximum value of residual out-of-plane stiffener deflection in the middle bay was of the order of the transverse stiffener spacing/2500, directed outwards. In the end bays, residual deflections were opposite in mode and the maximum value was approximately half that observed in the middle panel.

2.9.4 Test 10B: Behaviour under Load

In the second test, the deflections of the girder increased linearly with load until 160.0 tonf (σ_n = 13.2 tonf/in^2). The overall bending stiffness of the model over this load range was fractionally higher than that observed in Test 10A. The out-of-plane

deflections of the compression flange (Figs 2.83 to 2.85) continued to develop in the preferred buckling mode as observed in the first test. On loading beyond 160.0 tonf, there was a gradual loss in the overall stiffness of the girder. Strain readings taken at 168.0 tonf indicated the start of compressive yielding in the outer fibres of stiffener outstands at the mid-span section of the girder. With further loading the outstand strains increased very rapidly. This was accompanied by increased magnification of out-of-deflections of stiffeners (Fig. 2.85) and a reduction in the overall bending stiffness to approximately half the initial value.

Up to a load of approximately 171.0 tonf (σ_n = 14.1 tonf/in^2) the transverse membrane strains at the mid-span section of the compression flange (Fig. 2.87) were merely the Poisson strains associated with the strains applied longitudinally (that is, the transverse strains were 0.3 times the longitudinal strains) but at higher loads the transverse strains increased significantly; this indicates, therefore, that there was some post-buckling or membrane action in the centre bay of the compression flange.

In Test 10B, the maximum load applied on the model was 180.5 tonf, that is, σ_n = 14.9 tonf/in^2, and at that load stage there was significant spalling of mill scale in the highly stressed regions of the stiffener outstands at mid-span. Over the cross-girder regions, some outer surface yielding of the compression flange plate was also observed. Upon unloading the residual centre deflection of the girder was 0.019 in for span A-U and 0.003 in for the middle span E-Q; the load-deflection curves for both spans are given in Fig. 2.77.

Referring to Figs 2.89a to 2.89e it may be seen that the distribution of longitudinal strain across the flange exhibits an unexpected feature in that mid-plane plate strains between stiffeners exceeded the strains measured over the stiffeners. This is very unusual for a plate subjected to compressive loading. It will be noted that the pattern of strain distribution was extremely consistent and that the difference in the strains became greater as the applied load was increased. It is interesting to note that the distribution of secondary longitudinal strain (i.e. component of longitudinal strain tending to modify the overall bending strain, to produce the observed distribution pattern) is somewhat analogous to the strain distribution due to shear lag in a wide flange beam under lateral loading. The secondary strains in the plate, which were tensile due to the bending of the stiffened panel (E-Q) away from stiffener outstands, were always higher at the longitudinal stiffeners and lower between them. It would appear, therefore, that there was some kind of lag in the distribution of bending components of longitudinal strains. Of course, this reasoning could equally be applied to the case when out-of-plane deflections occur in the direction of stiffener outstands and the result under such a situation would be a post-buckling type strain distribution between stiffeners. From the observations made in this test, it would seem that the phenomenon is associated with large-deflection behaviour and one that could possibly be explained by a large-deflection analysis of discretely stiffened plates. A computer program for just such an analysis is currently being developed[36]

2.9.5 Test 10C: Behaviour under Load

The load-deflection relationship of the girder section E-Q, Fig. 2.77, shows that up to 160.0 tonf (σ_n = 13.2 tonf/in^2) the stiffness of the girder was comparable to that observed in the previous test. However, as further loading was applied, there was a gradual deterioration in the overall bending stiffness. At 192.0 tonf spalling of mill scale was observed in areas of the compression flange plate adjacent to web/flange/transversal intersections. As the loading was increased, out-of-plane deflections of plate panels in the above locations became noticeable, while near mid-span the outstands of longitudinal stiffeners exhibited slight lateral deflections.

The maximum load sustained by the model was 196.0 tonf, corresponding to mid-plane compression flange plate stress, σ_n, of 16.2 tonf/in^2. Application of further deflection increments resulted in increased out-of-plane deflections of the compression flange, and this in turn produced further lateral deflections of stiffener outstands. Photographs of the compression flange, taken after completion of the test, are shown in Figs 2.90a to 2.90c.

Deflections of the compression flange, measured at several stages of loading (Figs 2.91 to 2.93) indicate that the stiffened panels continued to deform in the modes observed in earlier tests but the rates of growth of deflections were much greater in Test 10C. This was because the initial deflections of the panels were more pronounced in the final test due to plastic deformations that occurred in previous tests.

The growth and distribution of strains in the compression flange, for Test 10C, are shown in Figs 2.94 to 2.97. Generally, the strains exhibited similar features to those observed in Test 10B but the level of straining was much higher in the final test. In particular, longitudinal strains in the outer fibres of stiffener outstands at mid-span assumed very high values and at collapse these strains were several times the yield value. Transverse membrane strains in the compression flange plate (Fig. 2.95) also continued to develop at an accelerated pace. One further feature that may be noted is that at collapse longitudinal compressive strains in areas of the compression flange plate adjacent to the webs were very close to the yield strain.

The maximum moment carried by the model was 1.17 times that which initiated yielding in the outer fibres of stiffener outstands at mid-span. In terms of the full plastic moment capacity of the box sections, the maximum moment developed by the model was 74 per cent.

From the results of the tests on Model 10, it is evident that there was some post-buckling reserve in the compression flange. The presence of longitudinal stiffeners of compact cross-section ($d/t_s = 8.8$) enabled the flange to retain much of its load-carrying capacity.

CHAPTER 3

THEORY: BEAM-COLUMN APPROACH

3.0 GENERAL

In the introductory chapter some approaches to the problem of analysing the behaviour of stiffened compression panels were indicated. The methods of analysis described in this thesis are (a) the beam-column or strut approach, and (b) the beam-column grillage approach. In both these methods the stiffened panel is idealised by a series of repeating struts consisting of the individual stiffeners and associated widths of plating. For the beam-column approach, the idealised struts are assumed to be supported on springs which simulate the stiffnesses of cross-girders. By representing the cross-girders in this manner, the problem in effect reduces to that of analysing just one beam-column with intermediate spring supports. In the grillage approach, on the other hand, the series of idealised struts are assumed to be supported at the cross-girder positions by discrete transverse members consisting of the individual cross-girders acting together with effective widths of plating. Thus, in this latter method, the analysis involves a grillage of beam-columns. Details of the extension of the beam-column treatment to grillage analysis are given in Appendix A.

In the present chapter, the method of analysis used for the beam-column problem is described. Since it is not necessary to restrict the number of spring supports for the column, the problem is formulated for the general case of a beam-column with any number of spring supports. The analysis of a single-span pin-ended column is considered by simply assigning zero values to the spring con-

stants. However, as will be shown later, if the springs are specifically excluded from the analysis, the solution process can be simplified.

3.1 MOMENT-THRUST-CURVATURE RELATIONS

Having idealised the stiffened plate as a beam-column, the solution process involves determining the equilibrium shape of the column for the required load and boundary conditions. For this purpose it is necessary that the moment-thrust-curvature relations for the cross-section of the column be known. Any analytical procedure for determining these relationships would have severe limitations due to such factors as non-linearity of the material and the presence of welding residual stresses. The problem becomes even more acute when the component plated elements are slender and buckling of these elements has to be considered. For the present study, therefore, an iterative numerical procedure is adopted in which the behaviour of plate panels is described by their load-end shortening characteristics instead of the material stress-strain curves.

The assumptions made in deriving the moment-thrust-curvature relations and details of the computation procedure are described in the following sections.

3.1.1 Assumptions

(1) Plane cross-sections of the beam-column before bending remain plane and normal to the centroidal axis after any load application. Thus it follows that the strain distribution over the cross-section depth is linear, i.e.

the strain varies in proportion to the distance from the neutral axis.

(2) The stress-strain relationship for the plate in compression can be described by average stress-strain curves as derived from large-deflection elasto-plastic analyses of isolated plate panels suitably idealised with respect to the boundary conditions and loading. This assumption enables the effects of elastic-plastic buckling of plate panels of medium to large slenderness to be included in the column analysis.

(3) The stiffener is sufficiently stocky in cross-section so that no local flexural or torsional buckling of the stiffener itself occurs.

(4) The stress-strain curves are reversible. In other words it is assumed that the relationship of stress to strain during unloading is the same as that for loading. Any value of strain thus uniquely defines a stress value.

It is recognised that this assumption does not strictly represent the true behaviour as unloading in most yielded materials occurs in a nearly elastic manner. However, the errors resulting from this assumption are not likely to be of any significance in columns subjected to progressive loading.

(5) Shear stresses are small so that their effects on yielding in any combined stress situation can be considered to be small too.

3.1.2 Residual Stresses

Residual stresses in steel occur mainly as a result of differential cooling. In the case of rolled shapes these stresses are produced during the process of cooling from rolling temperature to air temperature, when some parts of the section cool more rapidly than others. In fabrication by welding the cooling of the region affected by a welding bead also produces residual stresses. The region in the vicinity of the weld is left with tensile stresses at the yield value of the material which are balanced by compressive stresses in the surrounding material. The magnitudes of the compressive residual stresses depend on a variety of factors such as the type of welding process used, the welding sequence, the rapidity of cooling of the weld, the thickness of the welded component and clamping procedures. The task of predicting these stresses accurately for use in any analysis is, therefore, not an easy one. Considerable research work has gone into this subject, the study carried out by Dwight and Moxham[64] is one example. More recently, a lot of work went into collecting information on weld-induced residual stresses in plated components used in actual bridges[65] Much data was also obtained from the box girder models described in this thesis. But the problem of accurately predicting the levels of residual stresses and their distribution patterns still remains. Thus, in making allowances for residual stresses in any computations one has to make some approximations with regard to the magnitudes of the shrinkage forces involved, and also it is necessary to assume some idealised form of stress distribution.

Except in very stocky plates, residual stresses generally have some effect on the carrying capacities of the plates. In the

case of stocky components, residual stresses influence the behaviour of the components in compression only in that they cause non-linearity to occur earlier. This is because the residual stresses are self-equilibrating and the in-plane performance of the elements is affected only through earlier yielding in regions where the combined residual and applied compressive stresses attain the yield value of the material.

From the data that has been collected by researchers it has become apparent that the compressive residual stresses in the plate between stiffeners, are distributed more or less uniformly. Consequently, an idealised form of stress distribution that is often used in calculations is the self-equilibrating rectangular stress pattern, shown in Fig. 3.1a. This form of stress distribution was first suggested by Dwight and Moxham[64].

Measurements made so far indicate that the pattern of residual stress in the stiffener outstand cannot be predicted reliably. Hence, if stiffener residual stresses are to be included in any theoretical analysis, assumptions have to be made with regard to the pattern of stress distribution.

In the beam-column analysis, residual stresses in the plate/stiffener cross-section are incorporated in the following ways:-

(1) For the plate panels the residual stresses are considered in the derivation of the average stress-strain relations. Thus in the column analysis the plate panels are assumed to be stress-free initially. However, if the residual stresses need to be considered separately, such as in

stocky sections when material stress-strain curves are used, an idealised self-equilibrating distribution such as that shown in Fig. 3.1a could be easily included.

(2) For the stiffener outstand any idealised form of residual stress distribution could be considered. One method that may be used to obtain such a stress pattern is to assume that the residual stress distributions in the stiffener and in the plate are separately self-equilibrating. This approach was first suggested by Nagaraja Rao et al.[66] in connection with residual stresses in welded Tee-shapes and was later used by Little[48]. The stress distribution for the stiffener is shown in Fig. 3.1b. Assuming that the variation of residual stress with depth outside the yield tension block, is linear, a self-equilibrating stress distribution for the stiffener may be obtained using either of the following two conditions:

(a) The yield tension block at the base of the stiffener is of fixed width, the size being determined by some empirical means such as that recommended by Dwight and Moxham[64].

(b) The width of the tension block is varied such that when the linear stress distribution in the rest of the stiffener is extrapolated to the mid-plane of the flange plate, the resulting stress is equal to the residual compressive stress (σ_R) in the plate (Fig. 3.1b). This form of stress distribution produces tension blocks in the stiffeners of much

smaller widths compared to those in the plates. The main drawback of this method, using either condition, is that it always produces tensile residual stresses at the tips of the outstands, whereas in practice, compressive stresses at these locations have often been recorded [67,68].

An alternative approach for determining the stiffener residual stresses is to assume a known width of tension block in the stiffener in the same way as in the last method, and then determine the stresses in the remainder of the cross-section (including the plate) such that equilibrium of the resulting normal forces and moments on the section, is satisfied. The method has been used before by Virdi [47] and the stress distribution that results is shown in Fig. 3.1c. Calculations of this kind can produce both compressive and tensile residual stresses on the tip of stiffener outstand, depending on the size of the tension block and the depth of outstand. However, the fact that the plate has to take more residual stresses, in addition to those already included in obtaining the average stress-strain curves, means that the capacity of the plate is often underestimated.

Whichever residual stress distribution is employed, the stresses are first converted to strain values and these are then used in the column analysis.

3.1.3 Expressions for Deriving Moment-Thrust-Curvature Relationship

The procedure described in this section for deriving the relationship between bending moment, axial force and curvature for

any given cross-section can be applied to any column problem in which bending occurs in the plane containing the axis of symmetry. Any cross-sectional shape which can be adequately defined by a set of rectangular dimensions may be considered in the analysis.

The cross-section of the beam-column is considered to be sub-divided into rectangular elements as shown in Fig. 3.2. Since bending is assumed to occur about an axis perpendicular to the axis of symmetry, the number of sub-divisions of the cross-section in the direction of this axis need not be more than those required to define the geometry of the cross-section. However, if residual stresses of the plate have to be included in the column analysis, then further sub-divisions of the plate may be necessary to ensure that the assumed residual stress distribution is incorporated properly.

Figure 3.2 shows the strain distribution in a typical cross-section. Consistent with the assumption that plane sections before bending remain plane after bending, the strain at any location on the cross-section can be considered to be proportional to the distance from the neutral axis. If the neutral axis is located at a distance h_n from the reference axis a-a (top surface of the plate in Fig. 3.2), the strain ε_a at a-a for any curvature, ϕ, is given by

$$\varepsilon_a = \phi \times h_n \qquad \ldots. \quad 3.1$$

The strain ε at the centroid of any element of area δA is,

$$\varepsilon = \phi \cdot (h_n - h) \qquad \ldots. \quad 3.2$$

where h is the distance of the centroid of the element from the reference axis.

Equation 3.2 gives the value of strain due to curvature and axial thrust on the cross-section. If there are any residual strains to be considered, then these are included to obtain the total strain ε_T, that is,

$$\varepsilon_T = \varepsilon + \varepsilon_R \quad \ldots\ 3.3$$

where ε_R is the residual strain in any element.

The stress σ in an element is a function of the total strain ε_T. Thus using any suitable stress-strain relationship expressed either in a mathematical form as

$$\sigma = f\ (\varepsilon_T) \quad \ldots\ 3.4$$

or as represented numerically, the stress for each element can be determined.

With the stress in each element known, the element force is given by

$$\delta P = \sigma \cdot \delta A \quad \ldots\ 3.5$$

Summation of the element forces for the entire cross-section results in the total axial force P acting on the section. Hence,

$$P = \Sigma\ \delta P \quad \ldots\ 3.6$$

The moment M_a is obtained by summing up the moments of all the element forces about a-a, that is,

$$M_a = \Sigma(\delta P \cdot h) \quad \ldots\ 3.7$$

If the centroid of the cross-section is located at a distance h_c from the reference axis, the moment M about the

centroidal axis is,

$$M = P \cdot h_c - M_a \qquad \ldots\ 3.8$$

The axial force on the section is often expressed as a ratio of the squash capacity P_o. This capacity is evaluated from the relation,

$$P_o = \Sigma(\sigma_o \cdot \delta A) \qquad \ldots\ 3.9$$

where σ_o is the yield stress for the element. The cross-section may be composed of more than one material and hence σ_o may vary.

In the above expressions, all strains, stresses and hence forces of compressive nature are treated as positive. Curvature and moment causing greater compression in the cross-section at a-a are also considered as positive.

3.1.4 Method of Computation

Using the expressions derived in the last section values of moment and thrust can be generated for any specified curvature ϕ, by simply varying the depth of neutral axis h_n. To obtain the neutral axis position for any given P and ϕ, either an interpolation scheme or an iteration procedure may be used. The method adopted for the beam-column analysis involves both interpolation and iteration. The steps involved in the computations are as follows:

(a) As a first guess, any arbitrary value for h_n is chosen. Then, for the given curvature a set of values of axial thrust and moment is evaluated in the vicinity of h_n, using any small increment for h_n.

(b) By linear extrapolation from the values obtained, an approximate position for the neutral axis corresponding to the given load P, is found. If necessary, step (a) is repeated with an improved estimate for h_n until the evaluated axial thrust is close to P.

(c) The final solution for h_n, which establishes the required moment-thrust-curvature relation to within any specified degree of accuracy, is then determined by iteration.

Once a neutral axis position h_{n1} for any given curvature ϕ_1 and axial load P is located, the data is used to provide a very good starting value for any subsequent calculations. Hence if h_{n2} corresponding to another curvature ϕ_2 but same axial load P, is to be found, the value may be guessed from elastic considerations using the relation,

$$h_{n2} = h_{n1} + (h_{n1} - h_c)\left(\frac{\phi_1}{\phi_2} - 1\right) \qquad \ldots\ 3.10$$

With the use of equation 3.10 the number of extrapolations is reduced and often iteration is not needed.

3.2 DETERMINATION OF EQUILIBRIUM SHAPE

Knowing the relationship of moment to curvature for any axial thrust on the section, the next step in the analysis is to determine the deflected shape of the beam-column under the action of the external loads. Figure 3.3a shows a pin-ended beam-column subjected to compressive end load P and lateral load Q. The deflected shape of the column is obtained from equilibrium

considerations. At every point along the length of the beam-column, equilibrium between external and internal moments and thrusts must be satisfied, that is, the following conditions must be met:

$$P = \int_A \sigma \cdot dA \quad \ldots\ldots 3.11$$

and $$M_E = M_I \quad \ldots\ldots 3.12$$

where M_E is the bending moment due to external loads in the deflected state, and M_I = internal moment = f (P, ϕ).

Due to the inelastic nature of the problem, any analytical attempts to achieve a simultaneous solution of the equilibrium equations for every point on the column, must face limitations. Consequently, the problem is best solved by an iterative numerical technique, with equilibrium satisfied at several discrete points along the length of the beam-column. The procedure for setting up the equilibrium equations and the method chosen to solve them are described in the following sections. Since a beam-column which is laterally supported by springs at some intermediate positions is analysed in a similar way, the procedure is presented for the general case of such a beam-column. The particular case of a beam-column with no lateral supports is obtained by assuming zero values for the spring constants. Any constant lateral loading, that is, loading not varying with P can also be considered but the details of including such loading in the analysis are given later in this chapter.

3.2.1 Assumptions

The following assumptions are made in addition to those used in deriving the moment-thrust-curvature relationship for the cross-section.

(1) The deflections of the beam-column are such that the slopes at all points along the length are small, so that the curvatures can be represented by the second derivatives of the deflections y. Thus,

$$\phi = -\frac{d^2y}{dx^2} \qquad \ldots\ 3.13$$

(2) Deflections due to shear strain are small and can be neglected.

(3) The assumed residual stress distribution for the cross-section is constant over the whole length of the column.

(4) The average compressive stress-strain curves for the plate apply to all stations along the span.

3.2.2 Equilibrium Equations for the Beam-Column Problem

Figure 3.3b shows a pin-ended beam-column of length L and consisting of N number of spans. The column is subjected to compressive end load P and is supported at the (N-1) intermediate positions by springs of stiffnesses K_1, K_2 ... K_s etc. It is assumed that under the action of the compressive loading, the lateral forces exerted by the springs on the beam-column are proportional to the deflections of the column at the spring locations. Hence at any support s,

$$F_s = K_s \cdot \Delta_s \qquad \ldots\ 3.14$$

where F_s is the spring reaction and Δ_s the beam-column deflection at the location of the spring.

Let the length L of the beam-column be divided into n equal segments such that the spring locations coincide with the nodal points as shown in Fig. 3.3b. At any section r of the column let the initial deflection of the centroidal axis be y_{or} and the total deflection (under load) be y_r. In all subsequent notations the suffix r will be used to denote quantities relating to station r.

To establish the deflected shape of the beam-column under load P, the equilibrium equations need to be written for each station and a simultaneous solution obtained. The steps involved in writing these equations are now described while the solution process which involves numerical iteration using a generalised form of the Newton-Raphson convergence criterion is given in the following section.

As a first step, a deflected shape for the beam-column is assumed. From the trial values of deflections for the spring supports $\Delta_i (i=1,N-1)$ the spring reactions $F_i (i=1,N-1)$ are determined from equation 3.14. The end reactions R_A and R_B (Fig. 3.3b) are then obtained from a consideration of the statics of all lateral forces. If the bending moment due to the lateral forces only is denoted by $(M_L)_r$ then the total external moment $(M_E)_r$ is given by,

$$(M_E)_r = P \cdot y_r + (M_L)_r \qquad \ldots\ 3.15$$

Using equation 3.13, the curvature at any station r can be expressed in the finite difference form as,

$$\phi_r = -\frac{1}{\delta x^2}(y_{r-1} - 2y_r + y_{r+1}) - \phi_{or} \qquad \ldots\ 3.16$$

where δx is the beam-column segment length and ϕ_{or} is the initial curvature.

With the curvature known the procedure given in Section 3.1.4 is used to determine the internal moment $(M_I)_r$ corresponding to the load P. Now, if equilibrium is to be satisfied the following condition must hold at each station.

$$P \cdot y_r + (M_L)_r = (M_I)_r \qquad \ldots\ 3.17$$

For a pin-ended beam-column, we have,

$$y_{r=o} = y_{r=n} = 0 \qquad \ldots\ 3.18$$

Thus the analysis now involves solving (n-1) non-linear simultaneous equations.

3.2.3 Solution of the Equilibrium Equations

Equation 3.17 can be rearranged and written as,

$$y_r = \frac{1}{P}\left[(M_I)_r - (M_L)_r\right] \qquad \ldots\ 3.19$$

Now for any given load P, the moment $(M_I)_r$ is a function of the curvature only while $(M_L)_r$ depends only on the spring forces, that is,

$$(M_I)_r = f(\phi_r) \qquad \ldots\ 3.20$$

and

$$(M_L)_r = f(F_1, F_2, \ldots F_{N-1}) \qquad \ldots\ 3.21$$

Since the curvature and spring force both depend on the assumed deflected shape, for any trial deflection vector $\{y_j\}_{j=1,n-1}$ a function Y_r can be computed for each station r, so that,

$$Y_r = W_r - \chi_r \qquad \ldots\ 3.22$$

where W_r and χ_r represent respectively the functions $\frac{1}{P}(M_I)_r$ and $\frac{1}{P}(M_L)_r$ corresponding to the assumed deflections. The function

vector $\{Y_j\}_{j=1,n-1}$, therefore, represents the computed deflections corresponding to the trial values $\{y_j\}$. In the equilibrium state, the assumed and computed deflections of the beam-column must converge. Hence the equilibrium conditions may be expressed in another, more general, form as,

$$E_j(y_k) = y_j - Y_j(y_k) = 0 \quad j=1,n-1 \ (k=1,n-1) \qquad \ldots\ 3.23$$

The solution of the above equations is achieved by iteration using the generalised Newton-Raphson method in which successive approximations of the solution vector converge at a quadratic rate. The convergence criterion used in the iteration process may be derived as follows:

Let $\{\bar{y}_k\}$ be an approximation to the solution vector, and let $\{\delta y_k\}$ denote the vector for the correction terms that must be applied to obtain the solution vector $\{y_k\}$. Then,

$$\{y_k\} = \{\bar{y}_k\} + \{\delta y_k\} \qquad \ldots\ 3.24$$

Equation 3.23 then becomes,

$$E_j(\bar{y}_k + \delta y_k) = 0 \qquad \ldots\ 3.25$$

Expanding the above equations by Taylor's formula and ignoring second and higher order terms for small δy_k, we have:

$$\{E_j(\bar{y}_k)\} + \left[\frac{\partial E_j(y_k)}{\partial y_k}\right]_{y_k=\bar{y}_k} \cdot \{\delta y_k\} = 0 \qquad \ldots\ 3.26$$

where $\left[\frac{\partial E_j(y_k)}{\partial y_k}\right]_{y_k=\bar{y}_k}$ is the Jacobian matrix of the function $E_j(y_k)$ about the vector $\{y_k\} = \{\bar{y}_k\}$.

Equation 3.26 represents a set of linear equations of order (n-1). A simultaneous solution of these equations yields the correction terms $\{\delta y_k\}$, and hence a better approximation for the deflection vector, that is,

$$\{\bar{y}_k\}^{(2)} = \{\bar{y}_k\}^{(1)} + \{\delta y_k\} \qquad \ldots\ 3.27$$

where the superscripts (1) and (2) indicate two successive approximations.

The above iteration scheme is continued until the solution vector is found to within any specified degree of accuracy.

In setting up the Jacobian matrix of equation 3.26, a numerical procedure is followed. The expressions needed to evaluate the elements of the matrix will now be given.

Differentiation of equation 3.23 with respect to y_k, gives:

$$\frac{\partial E_j}{\partial y_k} = \delta_{jk} - \frac{\partial Y_j}{\partial y_k} \qquad \ldots\ 3.28$$

where δ_{jk} is the Kronecker Delta, i.e. $\delta_{jk} = 0$ if $j \neq k$, and $\delta_{jk} = 1$ if $j = k$. From equations 3.20 to 3.22, we have,

$$\frac{\partial Y_j}{\partial y_k} = \frac{\partial W_j}{\partial \phi_\ell} \cdot \frac{\partial \phi_\ell}{\partial y_k} - \frac{\partial X_j}{\partial y_k} \cdot \qquad \ldots\ 3.29$$

Let the computed values of W_r corresponding to assumed curvatures ϕ_r and $(\phi_r + \Delta y/\delta x^2)$ be w_r and w'_r respectively, where Δy is any small quantity. Then, using the finite difference expression (3.16) for curvature and noting that $\frac{\partial W_j}{\partial \phi_\ell} = 0$ for $j \neq \ell$, we get:

for j = k = r,

$$\frac{\partial W_r}{\partial \phi_r} \cdot \frac{\partial \phi_r}{\partial y_r} = \frac{(w'_r - w_r)}{(\Delta y/\delta x^2)} \cdot (2/\delta x^2) \qquad \ldots\ 3.30$$

for j = r and, k = r-1 or k = r+1,

$$\frac{\partial W_r}{\partial \phi_r} \cdot \frac{\partial \phi_r}{\partial y_{r-1}} = \frac{\partial w_r}{\partial \phi_r} \cdot \frac{\partial \phi_r}{\partial y_{r+1}} = \frac{(w'_r - w_r)}{(\Delta y/\delta x^2)} \cdot (-1/\delta x^2)$$

$$\ldots\ 3.31$$

for j = r and all other values of k,

$$\frac{\partial W_r}{\partial \phi_r} \cdot \frac{\partial \phi_r}{\partial y_k} = 0 \qquad \ldots\ 3.32$$

Now, for j = r

$$\frac{\partial \chi_r}{\partial y_k} = -\frac{(L - x_k)}{L} \cdot x_r \cdot C \qquad \ldots\ 3.33$$

where $C = K_s$ for k coinciding with the spring location s, and $C = 0$ for all other k.

Thus, with all the elements of the Jacobian matrix now known, equations 3.26 may be solved for the correction vector $\{\delta y_k\}$, by the Gaussian elimination method.

It is worth noting at this stage that in the particular case of all spring constants being zero, the only non-zero elements of the Jacobian matrix are those given by equations 3.30 and 3.31. These elements, in fact, form a diagonally centred banded matrix of width 3. Thus, advantage may be taken of this feature in solving the equations.

3.3 ULTIMATE LOAD OF THE BEAM-COLUMN

In the previous sections, a procedure was given for determining the equilibrium shape of a beam-column under any specified axial loading P. To establish the maximum load that the beam-column is capable of carrying for any given initial imperfections, an incremental approach is used. The axial loads for which equilibrium shapes are to be found, are varied systematically in small increments. The ultimate capacity of the beam-column is then taken to be that load beyond which an equilibrium shape cannot be established. By specifying the size of the smallest load increment, the ultimate capacity can be found to any desired degree of accuracy.

Using the incremental approach outlined above, the speed with which the maximum load can be determined depends on the size of the load increment. Maintaining, at all stages of loading, an increment equal to the specified load accuracy would slow down the computation procedure. Consequently, by adopting a scheme whereby the increments are progressively reduced as the ultimate load is approached, the numbers of trials can be reduced significantly. Also, by evaluating the stiffness $\frac{(P_2 - P_1)}{\{(y_r)_2 - (y_r)_1\}}$ for each station r, where the subscripts 1 and 2 denote the load stages prior to any trial load P (Fig. 3.4), the data can be used to obtain a trial deflected shape for load P. In this way, the number of iteration cycles required for convergence is reduced and often convergence is achieved in only two iterations. For loads approaching the ultimate value, convergence can generally be achieved within five iterations.

3.4 SUMMARY OF THE COMPUTATION PROCEDURE

The following is a summary of the steps involved in obtaining a computerised solution of the beam-column problem.

(1) Read in all initial data relating to:

(a) cross-section and span, including spring constants,

(b) stress-strain curves,

(c) initial deflections and residual stresses.

(2) Assume a trial value for the axial load P, and also read in a trial deflected shape for the beam-column. As an initial guess, the deflected profile under load is assumed to follow the initial shape.

(3) Evaluate curvatures for each station from equation 3.16 in which

$$\phi_{or} = -\frac{1}{\delta x^2}\left(y_{or-1} - 2y_{or} + y_{or+1}\right) \qquad \ldots\ 3.34$$

where y_{or-1}, y_{or} and y_{or+1} are the initial deflections at nodes r-1, r and r+1 respectively.

(4) For the assumed deflections, compute the spring forces from equation 3.14 and then from statics, evaluate reactions R_A and R_B. For each station r, evaluate the bending moments, $(M_L)_r$, due to lateral forces only.

(5) Using the procedure described in Section 3.1.4 for establishing moment-thrust-curvature relationships, determine the internal moments $(M_I)_r$ corresponding to curvature ϕ_r and axial load P.

(6) With $(M_L)_r$ and $(M_I)_r$ known, compute w_r and hence Y_r from equation 3.22.

(7) Change curvatures by $\Delta y/\delta x^2$ and obtain w'_r.

(8) Set up the Jacobian matrix of equations 3.26, using relations 3.30 to 3.33.

(9) Solve equations 3.26 to obtain the corrections $\{\delta y_k\}$, and hence a better approximation for the deflections $\{y_k\}$.

(10) Repeat steps (3) to (9) until the following condition is satisfied:

$$\left|\frac{y_r - Y_r}{y_r}\right| \leq \xi y \qquad \ldots\ 3.35$$

where ξy is a small specified value depending on the accuracy desired. If the number of iterations exceeds the maximum specified, then the load increment ΔP is reduced by a factor (which may vary from zero to 1.0) and steps (2) to (9) are repeated.

If convergence is achieved, the load P is incremented. Trial deflections for the new trial load $(P + \Delta P)$ are obtained by extrapolation from previous data. Steps (2) to (9) are then implemented for the new load value.

(11) In the above stages of computations, if an equilibrium shape cannot be established, and the load increment ΔP is such that,

$$\frac{\Delta P}{P_o} < \xi P \qquad \ldots\ 3.36$$

where ξP is the accuracy to which the ultimate load is

required then the maximum load for which an equilibrium state has been found is taken as the ultimate load for the beam-column.

3.5 UNLOADING PATH

Using the procedure described in Section 3.4 the loading branch of the load-deflection characteristic can be traced. A similar procedure may be used to trace the unloading path. However, in doing so it is important that the trial deflected shape of the column for any given axial load is closer to the equilibrium shape on the unloading path, rather than on the loading path. Thus, after the peak load has been established, the trial deflection values for a slightly reduced value of axial load are guessed by assuming the slope of the load-deflection curves to be negative. On obtaining an equilibrium shape along the unloading path, the trial deflection values for another reduced value of axial load are obtained by extrapolation using a procedure similar to that adopted for the loading path.

3.6 LATERAL LOADING

In the foregoing sections the analysis described involved a beam-column with no applied lateral loading. However, the method is very well suited for incorporating the effects of any lateral loads on the column. The only additional step in the computation procedure is the evaluation of 'free bending moment', that is, bending moment due to applied lateral loads considered as acting over a simple span L. These moments are evaluated for each station r along

the beam-column and are then included, at every iteration stage, with the moments $(M_L)_r$ due to the spring reactions. Any forms of lateral load distributions, such as those shown in Fig. 3.5 may be considered.

It is, of course, also possible to include in such an analysis lateral loading which varies proportionally with the applied thrust.

3.7 LINE OF ACTION OF APPLIED THRUST

The method presented in this chapter for establishing the equilibrium shape of a beam-column for any specified end thrust P, need not be restricted to the case when the line of action of applied load is through the geometric centroid of the cross-section. In general, the position of line of thrust may vary so that the analysis can be applied to the cases when either equal or unequal end eccentricities have to be considered. In addition, the situation when the line of thrust is required to vary at different thrust levels can also be tackled. The need for this latter case of 'shifting' thrust line arises when the cross-section being analysed is asymmetric and the stress-strain behaviour of the component elements is different. Under such conditions the geometric centroid of the cross-section does not coincide with the location of resultant thrust line when the curvature is zero (that is, uniform strain condition as shown in Fig. 3.6). Consequently, if the line of resultant thrust is assumed to act through the geometric centroid, the thrust on the column is in effect applied eccentrically. This can be of considerable significance in stiffened plate analysis

since the average stress-strain curves used to represent plate behaviour can often be very different from the stress-strain curves assumed for the stiffener outstands. In fact, if the line of thrust is considered to be fixed and acting through the centroid, the resulting eccentricity of loading can in some cases exceed the initial deflection of the stiffener. Where initial deflections are in the direction of the plate, the eccentricities can be large enough as to offset the effects of initial deformations.

In the parametric study described in Chapter 5, the line of action is allowed to shift with applied thrust. For any specified thrust the location of 'effective' centroid, that is, the axis about which the moment on the cross-section is zero, for uniform strain on the cross-section, is found by iteration. The line of resultant thrust is then assumed to act through this new centroid.

3.8 ACCURACY OF RESULTS

The main factors which can influence the accuracy of solution of the beam-column problem are:

(a) idealisation of the cross-section, that is, the number of sub-divisions used,

(b) number of segments assumed for the beam-column, and

(c) the accuracy with which stress-strain data is represented numerically, where multi-linear stress-strain curves are used to approximate continuous curves.

In general, where the stress-strain behaviour is assumed to be that of the material, the flange plate may be sub-divided into layers; for the parametric study, five layers were considered. However, where buckling of the plate is accounted for by an average stress-strain curve, the flange plate is not sub-divided into layers (Fig. 3.2). Also, since the stiffened panel analysis as described in this chapter deals with uniaxial bending only, the number of sub-divisions along the width of the plate need not be more than those required to define the geometry of the cross-section. Of course, where residual stresses within the flange plate have to be included, more sub-divisions may be necessary. When stiffeners of flat section were considered, it was found that fifteen sub-divisions along the depth were adequate and further sub-divisions had little effect on the ultimate load of the beam-column. The effect, on accuracy, of the number of segments assumed along the length of the beam-column was also investigated. This is one major factor which greatly affects the total computer time needed for the solution. With ten sub-divisions of the beam-column length between cross-girders, it was found that the ultimate load was conservatively estimated, generally to within 0.5 per cent of the load obtained when more sub-divisions were used. Thus, ten sub-divisions of the length between cross-girders were assumed in all subsequent studies.

Table 3.1 shows a comparison of the results as obtained from the present analysis and those given by Virdi[47]. The cross-sectional geometry was similar to that shown in Fig. 3.2. Virdi's solutions are based on the assumption that the deflected shape of the column can be represented by a sine wave. It has been shown[47] that for axially loaded columns this assumption leads to reasonable

predictions of the ultimate loads. Table 3.1 shows that the ultimate loads for the plate/stiffener columns also compare well, the values obtained from the present analysis in which equilibrium was satisfied at several stations along the span, being higher and within 3 per cent of the loads obtained using the sine wave assumption.

CHAPTER 4

COMPARISON OF EXPERIMENTAL AND THEORETICAL RESULTS

4.0 INTRODUCTION

In Chapter 2 of this thesis, the observed collapse behaviour of the stiffened compression flanges of six box girder models was described. This chapter deals with the comparisons between experimental and theoretical collapse strengths of the flanges. The theoretical values were derived using the column-type treatment in which the stiffened flange was assumed to be represented by a series of repeating struts consisting of the stiffener and associated flange plating. For this idealisation the width of the flange plate considered to act with the stiffener was equal to the spacing of the stiffeners, b. Details of the geometries of the various flanges and the material properties of the component elements have been summarised in Table 2.1. The slenderness parameters for the plate/stiffener columns are given in Table 2.2.

4.1 AVERAGE STRESS-STRAIN CURVES OF THE PLATE PANELS

Before the behaviour of the stiffened compression panels could be analysed it was necessary to establish the average stress-strain characteristics of the plate panels in compression. For this purpose Frieze's computer program[19] for the large-deflection elasto-plastic analysis of plate panels was used. The boundary conditions for the plate panels and the assumptions in the analysis are described in detail in Section 5.1.1 in connection with the

parametric study. The initial imperfections used in the analyses and the resulting average stress-strain curves of the flange plate panels are given, Figs 4.1 and 4.2. For Models 1, 2, 9 and 10, the plate initial deflection (δ_o), that is, the initial bow prior to any load application was assumed to be b/400; this value of δ_o is less than the maximum value of measured initial bow (Table 2.3) and was adopted as a representative average initial deflection for the plate panels in the models listed above. In Models 4 and 8, in which the plate panels were stocky, the initial deformations of plate panels were not measured; for these models δ_o was taken as b/800. For each model, the level of weld-induced compressive residual stress assumed in the plate panel analysis was the average value of the measured residual stress in the compression flange plate. (Figs 4.1 and 4.2, and Table 2.3.)

4.2 ANALYSES OF THE STIFFENED PANELS

The stiffened compression panels of the models that were subjected to uniform bending moment were analysed in two ways as follows:

(a) Using the single-span approach, the collapse strengths of the sections of the flanges between cross-girders were determined. The initial stiffener deflections considered for these analyses were the maximum values of the average deflections in the various bays (Table 2.3). Both modes of the initial bow, that is, in the direction of the stiffener outstand and away from it, were considered. In Model 2, the average deflection in each bay

was directed away from the stiffener outstand; thus, in this case the strength of the stiffened panel for failure in the alternative mode was obtained by considering the maximum value of the measured initial bow in an individual stiffener.

(b) Using the multi-span beam-column approach, the stiffened compression panels were analysed as continuous members and were considered to be supported by springs at the cross-girder positions. In calculating the stiffnesses of the springs, the cross-girders were assumed to act with effective widths of the flange plate equal to B/8 on each side of the girders, where B is the width of the compression flange. The total number of spans in each multi-span beam-column corresponded to the number of bays in the compression flange of the model. The stiffener initial deflections used for the analyses were the average values given in Table 2.3; within each span of a beam-column, the initial stiffener bow was assumed to be of sinusoidal form. The procedure used for determining the applied curvatures at the positions where cusps in initial deflections occurred is given in Appendix B.

In the case of the point load tests (Models 1 and 9), the stiffened panels were analysed as single-span pin-ended columns subjected to equal end thrusts. Thus, the variation in axial thrust due to the longitudinal moment gradient and shear lag was ignored. Also, the effect of continuity of spans was not considered for these cases.

4.3 PRESENTATION AND DISCUSSION OF THE RESULTS

The collapse strengths obtained from the single-span and multi-span analyses of the various stiffened compression panels are given, Tables 4.1a to 4.1d. The panels were analysed as axially loaded members and also as eccentrically loaded members so as to include the effects of curvatures due to overall bending of the girders. Considering the linear variation of strain over the depth of the girder and using elastic theory it can be shown that the eccentricity, e, is given by the expression,

$$e = \frac{r^2}{H} \qquad \ldots\ (4.1)$$

where r is the radius of gyration of the plate/stiffener combination about its centroidal axis parallel to the plate, and H is the distance between the centroidal axis of the plate/stiffener combination and the neutral axis of the box girder.

The effects of the eccentricity of loading due to overall bending were considered in both, single-span and multi-span analyses, and the results obtained are tabulated in the appropriate sections in Tables 4.1a to 4.1d.

Except for Models 4 and 9 the experimental values for the collapse strengths of the stiffened compression flanges were derived by the application of simple bending theory; considering gross section properties of the girder, the longitudinal stress at the centroid of the plate/stiffener assembly, and hence the average flange force, was computed. This procedure was adopted in view of the difficulties involved in establishing the exact stress distribution in the flange as collapse conditions were approached. The forces obtained by simple

bending theory will be good approximations of the actual forces provided that the webs do not buckle or yield prematurely.

In Model 4, the webs were significantly stronger than the flanges and hence allowance had to be made for the contribution of the webs to the moment capacity of the girder (see Section 4.3.3). In Model 9, on the other hand, extensive yielding in the webs near mid-span occurred before the maximum capacity was reached; the flange force at mid-span was thus computed allowing for plasticity in the webs (see Section 4.3.5). The collapse values of the flange forces*, that is, the forces corresponding to the maximum applied moments on the girders are given in Tables 4.1 and are identified as $(P_m)_{test}$. In the case of central point load tests, that is, Models 1 and 9, where the girders were subjected to longitudinal moment gradients, the value of $(P_m)_{test}$ indicated for each girder was evaluated as follows:

$$(P_m)_{test} = 0.6\ P_{m1} + 0.4\ P_{m2} \qquad \ldots\ (4.2)$$

where P_{m1} and P_{m2} are respectively the maximum and minimum flange forces* in the middle bay of the compression flange. The above expression, in fact, gives the flange force at a distance of 0.4ℓ for Model 1 and $0.4\ (\ell/2)$ for Model 9.

In addition to the collapse strengths, Tables 4.1 also give the ratios $(P_m)_{theory}/(P_m)_{test}$ for all the cases analysed. Note that the values shown underlined in these Tables, are also the collapse strengths listed under the heading 'present theory' in Table 4.2; this latter Table gives a comparison of the strengths predicted by BS153, the Interim Design Appraisal Rules (IDAR)[69],

*forces on plate/stiffener columns

and the present theory. Details relating to the IDAR calculations can be found in reference 70.

4.3.1 Model 1

As indicated in Chapter 2, Model 1 was subjected to three loading cycles. In the first two loading cycles, the load-carrying capacities of the model were reached due to buckling of web panels in the outer bays of the model while in the final test, collapse occurred in the centre bays with buckling of compression flange panels on one side of the central diaphragm and web panels on the opposite side. The theoretical analysis of the compression flange was thus carried out for three different conditions as follows:

(i) First Test: The plate/stiffener combination was analysed with the stiffener initial deflection considered as the average measured value for bay D-I'. The average stress-strain curve for the plate panel was derived using the levels of initial imperfections shown in Fig. 4.1.

(ii) Second Test: After completion of the first test, the residual initial stiffener deflections in bay D-I' were determined and these were treated as additional initial deflections for the second test. Although the plate panels also had residual deflections after the first test, the average stress-strain curve for this exercise was assumed to be similar to that of the first test.

(iii) Final Test: Using the residual stiffener deflections from the first two tests, the plate/stiffener column was analysed for the total initial deflection, that is,

including the initial bow measured prior to the first test. The average stress-strain curve used to describe the plate panel behaviour for this case is shown in Fig. 4.1; the curve was derived using a much larger plate panel initial bow, δ_o = b/50, but with initial stresses as for the previous tests.

The collapse strengths of the stiffened panel for the various cases investigated are given in Table 4.1a. It will be seen that the theoretical strengths for all three tests are higher than the experimental values, the difference being least (4 per cent) for the final test in which compression flange panel failure occurred. In the first two tests, the load-carrying capacities of the model were limited by collapse of the web panels in shear, in the outer bays. Therefore, the observed flange strengths given for these cases are not necessarily the maximum values; this explains why the theoretical values are higher than the observed values. In the final test, both flange and web buckling contributed to the collapse of the girder, and hence the moment capacity may have been reduced due to the effects of interaction between the two failure modes.

4.3.2 Model 2

Model 2, which was tested under pure bending moment conditions, was subjected to two loading cycles, Test 2A and Test 2B. Average stress-strain curves for the plate panels for the two tests are shown in Fig. 4.1. The theoretical strengths of the stiffened panels, as derived from the single-span and multi-span analyses, are given in Table 4.1b. The results corresponding to Test 2A were

obtained using the initial stiffener deflections, measured before any load was applied, while for Test 2B the residual stiffener deflections from Test 2A were considered as further initial deflections.

(i) Test 2A:- When the multi-span beam-column was analysed for axial loading only, that is, with e = 0 (case e in Table 4.1b) it was noted that the deflections in adjacent bays were sympathetic. There were two zones of weakness in the beam-column, namely, the tips of the stiffener outstand in the end bay U-W and the plate in the adjacent bay O-U. At the maximum load (P_m/P_o = 0.744) the tip of the stiffener in the end bay had yielded while the plate panel in bay O-U had attained the maximum value of the stress as given by the stress-strain curve (Fig. 4.1). However, when the beam-column was analysed as an eccentrically loaded member (case f, Table 4.1b), collapse of the beam-column occurred due to failure of the plate panel in the regions adjacent to Sections A and W. It is interesting to note here that in the test, the maximum load-carrying capacity of the model was also reached due to collapse of the plate panels adjacent to Section W (Fig. 2.23). The theoretical collapse strength for Test 2A was 7 per cent higher than the observed value, which suggests that the initial imperfections in the plate panels at the failed section were larger than those assumed in the analysis.

(ii) Test 2B:- After completion of the first test, the end bays of the model were stiffened (Fig. 2.28) and the model was loaded again. For the multi-span analysis three bays

were considered, that is, the span of the beam-column was assumed to be that between Sections C and U of the flange. Table 4.1b shows that the multi-span solution for Test 2B (case 1) is 6 per cent lower than the observed value. The deformation mode of the beam-column as predicted by the analysis was similar to that observed in the test (Fig. 2.30), the highly stressed regions being the tip of the stiffener outstand in bay I-O and the plate panel in bay O-U.

4.3.3 Model 4

Data relating to initial stiffener deflections in the compression flange of Model 4 is given in Table 2.3 while the average stress-strain curve for the plate panels is shown in Fig. 4.2. Since the average level of compressive residual stress in the flange plate panels was high (σ_R = 8.04 tonf/in^2, σ_R' = 0.562), the stress-strain curve shows a marked departure from the initial linear behaviour at an early stage in the loading history.

The comparisons between the theoretical and experimental values of the stiffened panel collapse strengths are given in Table 4.1c. The results from the single-span analysis show that the strength of the panel for failure by compression of the stiffener outstands (cases c and d) is significantly lower than the strength for failure by compression of the plate (cases a and b). Thus, in the multi-span analysis, compressive yielding of the tip of the stiffener in the end bay U-W, where the average initial stiffener deflection was $-\ell/660$ (towards the plate) occurred first; when the maximum load was reached, the plate panels in the adjacent bay were

also highly stressed. The analysis showed that adjacent bays of the beam-column deflected sympathetically in a mode similar to that observed during the test. Unfortunately, however, in the model the end bays of the compression flange were not strain-gauged and thus the extent to which the stiffeners were strained is not known.

Since the webs in Model 4 were significantly stronger than the flanges, the difference in yield stress being nearly 30 per cent, and also since the moment of inertia of the webs was about 17 per cent of the total inertia of the box section, the collapse strength of the compression flange was calculated allowing for the contribution of the webs to the total moment carrying capacity of the girder. From strain measured in the webs[59], it was noted that just before the maximum capacity of the girder was reached, the longitudinal strains in the webs at the flange/web junctions were close to the yield value; the collapse strength of the compression flange was thus evaluated on the basis of the measured strains, that is, the contribution of the webs to the moment capacity was considered as that causing yield in the extreme fibres of the webs.

Referring to Table 4.1c, it will be seen that the theoretical strength from the multi-span analysis in which the effect of eccentricity due to overall bending of the girder was included (case f), compares very well with the observed value, the theoretical strength being only 3 per cent lower.

4.3.4 Model 8

The compression flange of Model 8 had three bays. Average values of stiffener initial deflections for these bays are given in

Table 2.3. The average stress-strain curve for the plate panels is shown in Fig. 4.2. The level of compressive residual stress (σ_R) in the flange plate was 6.21 tonf/in^2 ($\sigma_R' = 0.346$) and thus as in Model 4 loss of stiffness of the plate panel, due to yielding under the combined effects of residual stress and applied stress, occurred at an early stage of loading.

Referring to Table 2.3, it will be seen that the average stiffener initial deflection in the end bay I-M was negative (towards the plate) and of greater magnitude than the average deflections (towards the stiffener) in the other two bays. In the multi-span analysis, the load-carrying capacity of the beam-column was reached due to compressive yielding in the tip of the stiffener outstand in bay I-M. The theoretical strengths of the stiffened panel for the various cases analysed are given in Table 4.1c. It will be seen that the result from the multi-span analysis (case f) is 11 per cent lower than the test value; a significant part of this difference can be attributed to the observed post-buckling behaviour of the compression flange. As discussed in Chapter 2 (Section 2.7) the compression flange of Model 8 sustained a load which was approximately equal to the elastic critical buckling load. The presence of stabilising membrane forces in the flange plate of the model was indicated by the increase in the level of transverse membrane strains as the ultimate state was reached.

4.3.5 Model 9

The compression flange in Model 9 was subjected to varying longitudinal compression due to the bending moment gradient. Thus, only the single-span analysis was undertaken for this model.

The initial imperfections assumed for the plate panel analysis, and the corresponding average stress-strain curve, are shown in Fig. 4.2. Results of the stiffened panel analysis are given in Table 4.1d.

The collapse strength of the compression flange of this model was determined in two ways as follows:

(i) The flange forces, P_{m1} and P_{m2}, corresponding to the maximum moment sustained by the girder were calculated using simple beam theory and $(P_m)_{test}$ was given by equation (4.2).

(ii) To take account of plasticity in the webs near the mid-span region, the collapse value of the flange force at the mid-span section, that is, P_{m1}, was computed with the assumption that yielding in the webs had spread to a depth of $0.4D^*$ from the flange (based on measured strains). The flange force at the cross-girder position P_{m2} was determined without considering any yielding of the webs. $(P_m)_{test}$ was then evaluated from equation (4.2).

It will be seen from Table 4.1d that the theoretical strength for the case when the stiffened panel was analysed as an eccentrically loaded member (case b) was 10 per cent lower than the observed value obtained by method (i), but the difference was only 4 per cent when the test value was evaluated with yielding in the webs allowed for in an approximate way (method (ii)).

However, while comparing the results for Model 9, the following factors must be borne in mind:

---

*D - depth of web

(a) The absence of a full-depth diaphragm at the position where the maximum bending moment occurred, that is, at mid-span, meant that the stiffened compression panels in the middle bay had an unusual stress gradient along the span. The observed values of collapse strength given in Table 4.1d represent the flange force at a distance of 0.4 ($\ell/2$) from the mid-span section.

(b) The flange forces are compared on an 'average' basis as though the stress distribution across the width of the stiffened flange was uniform, whereas in the test there was pronounced shear lag.

4.3.6 Model 10

Although the compression flange in Model 10 was sub-divided into three bays, the critical region of the flange was the centre bay; the end bays of the flange had additional longitudinal stiffeners so as to reduce the slenderness ratios of the plate panels (Fig. 2.75). Since a beam-column with varying cross-sectional geometry could not be considered in the analysis, a stiffened panel of constant cross-section, representing the flange panel in the middle bay, was considered for the multi-span analysis. The results obtained are given in Table 4.1d. The average stress-strain curves for the plate panels and the relevant initial imperfections are shown in Fig. 4.2.

Comparing the collapse strengths for case d (Table 4.1d) it is seen that the theoretical value is 15 per cent lower than the observed value. This significant difference in the collapse values is partly due to the post-buckling reserve in the flange (Section

2.9); also, by considering the plate/stiffener geometry in the end bays to be similar to that in the critical middle bay, the restraining influence of the increased stiffening in the end bays on the behaviour of the stiffened panel in the middle bay, was ignored.

CHAPTER 5

PARAMETRIC STUDY

5.0 GENERAL

In this chapter a systematic study on the behaviour of stiffened panels in compression is described. The study, which was based on the beam-column approach, covered a range of practical geometric parameters and its purpose was to investigate the influence of geometric initial imperfections and residual stresses on the strength of compression panels which are typical of those used in stiffened flanges of box girders. The analysis was carried out in two stages. In the first instance the behaviour of single-span pin-ended columns representing repeating sections of stiffener and associated plating in a single panel was established. The information obtained from this study was then used to assess the influence of continuity on the behaviour of two- and three-span continuous panels. For the multi-span panels, 'effective values' of stiffener initial deflections are derived. The effective deflections given in this study are based on a concept similar to that adopted in the Design Rules[32]; the effective stiffener initial deflection is defined as that value of initial bow in a single-span column which produces the same maximum strength as that predicted by the multi-span analysis.

5.1 STRESS-STRAIN DATA FOR PLATE PANELS

To allow for buckling of the flange plate panels, their stress-strain behaviour was described by average load-end shortening characteristics as derived from large-deflection elasto-plastic analysis[21]. This analysis used the dynamic relaxation technique to solve the finite difference form of the governing plate equations. In the post-elastic range the constitutive relationships were provided by the use of a single-layer yield function due to Ilyushin[17] in conjunction with the Prandtl-Reuss flow rule; it was assumed, therefore, that plasticity at any section occurred over the full depth of the plate. At the time this stiffened plate study was initiated, there were very few multi-layer solutions of the plate problem. Recently, an extensive set of multi-layer solutions[20] has become available. These results which have been compared by Frieze[19] show that both approaches predict similar behaviour up to peak load, but beyond this stage the behaviour is more conservatively predicted by the single-layer approach. The maximum difference in estimating the peak load by the two methods has been shown to be about $3\frac{1}{2}$ per cent and this occurs when the slenderness of the plate panel is such that the elastic critical buckling stress is close to yield stress. For other values of the slenderness ratios, the differences are less marked. The parametric study described in this chapter was based on Frieze's single-layer solutions for all the plate slenderness ratios considered.

5.1.1 Features of Plate Panels

The load-end shortening curves used were those derived for plate panels having the following features:

(i) aspect ratios (a/b) of unity,

(ii) edges simply supported and fixed against out-of-plane deflections,

(iii) unloaded edges constrained in-plane to remain straight but free to pull-in (this condition closely represents that in a multi-stiffened panel),

(iv) loaded edges held straight and displaced uniformly,

(v) material behaviour described by elastic perfectly plastic stress-strain curves,

(vi) doubly sinusoidal initial out-of-plane deflections, and

(vii) welding residual stresses represented by the idealised rectangular stress pattern, and assumed to be constant along the panel length.

5.1.2 Slenderness Range

The plate panel slenderness ratios adopted for this study were selected to represent the practical range of panels used in box girder bridge construction. The particular values of slenderness selected were β = 0.691, 1.037, 1.383 and 2.074, where β is the non-dimensionalised plate slenderness and is expressed as,

$$\beta = \frac{b}{t}\sqrt{\frac{\sigma_o}{E}} \qquad \ldots\ 5.1$$

For an elastic modulus (E) of 205000 N/mm^2 and a yield stress (σ_o) of 245 N/mm^2, that is for mild steel, the above β-values correspond to b/t-ratios of 20,30, 40 and 60 respectively.

5.1.3 Initial Imperfections

The values of initial out-of-plane deflections for the plate panels were chosen to correspond to the limiting values, both

minimum and maximum, given in the Interim Design and Workmanship Rules[32]. The non-dimensionalised values of initial deflection, δ_o' (= δ_o/t), are listed in Table 5.1. It will be seen that δ_o' is presented as a function of β^2 as this has been found[21,31] to be a more appropriate way of representing the initial deflections for the range of slenderness ratios considered. The minimum and maximum values of initial deflections assumed in the Rules correspond to δ_o' values of $0.044\ \beta^2$ and $0.174\ \beta^2$ respectively. The analysis of plate panels with $\beta = 0.691$ showed that for both levels of initial deflections, the average stress-strain curves were similar to the elastic perfectly plastic material stress-strain curve. Thus, for this particular slenderness ratio, the stress-strain data for the case of an initially stress-free plate was assumed to be of the bilinear form ($\delta_o' = 0$ and $\sigma_R' = 0$).

For $\beta = 2.074$ an additional level of initial deflection, $\delta_o' = 0.349\ \beta^2$ corresponding to twice the maximum value assumed in the Rules, was considered.

To study the influence of plate panel residual stress on column strength, average stress-strain curves corresponding to $\delta_o' = 0.174\ \beta^2$ and $\sigma_R' = 0.102$, were used. Data relating to the initial imperfections assumed in the plate panel analysis is given in Table 5.1; the corresponding average stress-strain curves are shown in Figs 5.1 to 5.4. These curves were obtained for $E = 205000$ N/mm^2 and $\sigma_o = 245$ N/mm^2.

5.2 STIFFENED PLATE PARAMETERS

For the stiffened plate analysis, the plate panels were assumed to be stiffened by longitudinal stiffeners of flat section. The stiffeners were proportioned such that the depth-to-thickness ratio (d/t_s) was always equal to 10. This assumption was made to ensure that the load-carrying capacity of the plate/stiffener cross-section was not limited by local instability of the stiffener outstand. In the column analysis, the stress-strain behaviour of the stiffener was assumed to be identical to the elastic perfectly plastic (bilinear) material stress-strain curve.

By choosing to keep d/t_s constant for all longitudinal stiffeners, the problem of proportioning the sizes of the plate and stiffener elements for any given b/t-ratio was thus reduced to that of selecting the ratio α (= stiffener area/plate area). For each plate panel slenderness ratio, three values of α were chosen; these were α = 0.2, 0.6 and 1.0. The values of h_f/r and h_s/r, which are the ratios of extreme fibre distances to the radius of gyration of the cross-section are listed in Table 5.2, for all the plate/stiffener geometries considered.

Throughout this study, the column slenderness ratio, ℓ/r, is referred to in its non-dimensionalised form λ, given by:

$$\lambda = \frac{\ell}{r} \cdot \frac{1}{\pi} \sqrt{\frac{\sigma_o}{E}} \qquad \ldots\ 5.2$$

(Note: $\lambda = 1$ when $\sigma_{cr} = \sigma_o$).

The behaviour of only those columns in the slenderness range $0 < \lambda \leq 1.3$ ($0 < \ell/r \leq 120$ for mild steel) was investigated.

5.2.1 Initial Out-of-plane Deflections

The magnitudes of the initial bow in the stiffeners were selected to cover the limiting values assumed in the Design Rules. Three levels of sinusoidal initial deflections were considered: Δ_o' = 1/1000, 1/750 and 1/500. The columns were analysed for both modes of initial deflections, that is, in the direction of stiffener outstand (considered positive) and away from it (negative).

5.2.2 Residual Stresses

To allow for the effects of plate panel residual stress σ_R' in the column analysis, the average plate stress-strain curve corresponding to the selected value of σ_R' was used. The ways by which residual stresses in the stiffener outstand can be incorporated into the study have been described in Chapter 3 (Section 3.1.2). However, due to the uncertainty of the nature of residual stress distribution over the depth of stiffener outstand, it was decided to exclude stiffener residual stresses from the parametric study. The extent to which column strength is affected by these stresses depends on the idealisation of the stress distribution. Table 5.3 illustrates the influence of the stiffener residual stresses on column strength, for one plate/stiffener geometry and λ-values of 0.33, 0.77 and 1.10 (ℓ/r ratios of 30, 70 and 100 for mild steel). It can be seen that the predicted strengths can vary significantly, in some cases by approximately 10 per cent, depending on the stress pattern assumed. For the examples given in Table 5.3, the residual stresses were obtained by the methods described in Section 3.1.2.

5.3 MOMENT-THRUST-CURVATURE RELATIONSHIPS

Figures 5.5 to 5.7 show typical moment-thrust-curvature relationships for the plate/stiffener cross-sections used in this study. The curves are presented in non-dimensionalised form for some selected values of axial loads. Figures 5.5a and 5.5b which relate to $\beta = 0.691$ and α-values of 0.2 and 1.0 show the curves for the case when the stress-strain behaviour is of the bilinear, elastic perfectly plastic form. It is seen from these figures that the curves for positive and negative curvatures exhibit different characteristics due to asymmetry of the cross-section. In particular, it will be noted that for positive curvatures the maximum moment on the cross-section (about the geometric centroid) does not occur for the zero axial thrust condition. It can be shown that the maximum moment will occur when the neutral axis coincides with the centroid of the cross-section; for an asymmetric cross-section this condition necessarily involves some axial load. When the curvatures are negative, the moment capacities will always decrease for increasing axial thrusts on the cross-section.

Figures 5.5a and 5.5b show also that the maximum moment for positive curvature occurs at a higher load for the lower α-value; but it will be seen that for any given axial load the difference in moment-carrying capacities for positive and negative curvatures is much greater for $\alpha = 0.2$ than for $\alpha = 1.0$.

Typical moment-thrust-curvature relationships for plate/stiffener combinations in which the plate panels are slender and buckling is accounted for by average stress-strain characteristics, are shown in Fig. 5.6 ($\beta = 1.383$, $\alpha = 0.6$) and Fig. 5.7 ($\beta = 2.074$,

$\alpha = 0.6$). The curves are given for plate panels with and without residual stresses, and $\delta_o' = 0.174\ \beta^2$. It will be seen that the curves reflect the features of the average stress-strain characteristics, Figs 5.3 and 5.4. In the case of initially stressed plate panels, the stress-strain curves show that once yield occurs due to the combination of applied stress and residual stress a reduction in stiffness occurs. A similar reduction can be observed in the moment-thrust-curvature curves.

One other feature that may be noted in Figs 5.6 and 5.7 is that the moment-curvature curves for non-zero axial thrusts do not pass through the origin. Thus, for zero curvature there is a moment about the geometric centroid of the cross-section. Where the initial slope of the average stress-strain curve of the plate panel is less than that of the stiffener stress-strain curve, that is, when axial load produces loss of stiffness in the plate panel, zero curvature will produce some moment (about the geometric centroid) even at low axial loads. If the stiffness of the plate panel deviates from that of the stiffener at higher strain levels, the non-zero moments for no curvature will occur at high axial loads. The influence of this feature on column behaviour is discussed in the following section.

5.4 ONE-SPAN COLUMNS

For the range of geometric and imperfection parameters described in Sections 5.1 and 5.2, column strength curves for single span pin-ended plate/stiffener columns have been obtained. All the curves are presented in their non-dimensionalised forms and give the

maximum strength (σ_m/σ_o) for varying column slenderness ratios (λ); the stress, σ_m, is the mean stress on the plate/stiffener cross-section at collapse.

The maximum strength of each plate/stiffener column was obtained by following the procedure described in Chapter 3. In the analysis of the column, the resultant thrust was assumed to act through the 'effective' centroid, that is, the location about which the moment on the cross-section was zero for zero curvature condition. This assumption was made in view of the use of different stress-strain characteristics for the component elements of the unsymmetrical section.

To illustrate the effects of assuming the geometric and 'effective' centroids as the positions of line of applied thrust, the maximum strength-slenderness curves for two cross-sections, $\beta = 0.691$, $\alpha = 0.6$ and $\beta = 1.383$, $\alpha = 0.6$ are shown, Table 5.4; the values correspond to $\delta_o' = 0.174\ \beta^2$ and $\sigma_R' = 0.102$. It will be seen that for $\beta = 0.691$, the differences in the predicted maximum loads occur for low slenderness ratios, that is, $\lambda < 0.6$ ($\sigma_m/\sigma_o > 0.85$) when the average stress-strain curve of the plate panel deviates from the initial elastic slope. For $\beta = 1.383$ the differences occur over the full range of slenderness considered, since the average stress-strain curve (Fig. 5.3) exhibits a reduced stiffness even at low strain values. Table 5.4 shows that for $\beta = 1.383$ and the initial deflection considered, that is, $\Delta_o' = + 1/750$, the maximum strength is about 5 per cent less for the 'fixed' centroid condition.

5.4.1 Load-Deflection Curves

Typical load-deflection curves for columns having the cross-sections and stress-strain data similar to those used to illustrate the moment-thrust-curvature relationships (Figs 5.5 to 5.7), are shown in Figs 5.8 and 5.10. For $\beta = 0.691$ (Figs 5.8 and 5.9) the curves are given for λ-values of 0.33, 0.77 and 1.10 corresponding, respectively, to ℓ/r-ratios of 30, 70 and 100 for mild steel. It may be seen that for $\lambda = 0.33$ the curves for both modes of bending (that is, for $\Delta_o' = + 1/750$ and $- 1/750$) are linear almost up to the peak loads. Beyond these points, the columns continue to deflect while maintaining the loads at levels close to the maximum attained. For $\lambda = 0.77$ and 1.10, the curves indicate significant losses in load-carrying capacities beyond the stages of maximum loads. In particular, it will be noted that the unloading branches show relatively greater losses in strength for $\alpha = 0.2$, Fig. 5.8, than for $\alpha = 1.0$, Fig. 5.9.

Figure 5.10 shows the load-deflection curves for columns with $\lambda = 0.77$ and β-values of 1.383 and 2.074 ($\alpha = 0.6$ in both cases). For the case when $\beta = 1.383$ the load-deflection curve corresponding to initially stress-free plate panel shows a marked drop in load-carrying capacity due to the rapid fall in plate panel stress after the attainment of peak stress (Fig. 5.3). However, when the plate panel is initially stressed, the load-carrying capacity of the column is reduced and the load-deflection curve does not exhibit a pronounced peak. The curves for $\beta = 2.074$ show a more gradual reduction in stiffness compared with those for $\beta = 1.383$.

5.4.2 Maximum Strength-Slenderness Curves

Maximum strength-slenderness curves for one-span columns are given in Figs 5.11 to 5.30. To show the influence of various parameters considered, the curves are grouped according to the parameter being studied. The effects on strength of varying the following parameters are illustrated:

(i) ratio of stiffener area to plate area, α, for a constant value of stiffener depth-to-thickness ratio of 10 and $\beta = 0.691$ (Figs 5.11a to 5.11c),

(ii) initial out-of-plane deflection of the stiffener, Δ_o' (Figs 5.12 to 5.23),

(iii) plate panel slenderness, β, for the selected levels of initial imperfections (Figs 5.24 to 5.26), and

(iv) plate panel initial imperfections, δ_o' and σ_R', for the selected values of β (Figs 5.27 to 5.30).

In Group (ii), column curves for $\alpha = 0.6$ are given only for those panels in which $\beta = 0.691$.

Groups (iii) and (iv) cover the full range of β, α and λ values with Δ_o' assuming the values + 1/750 and - 1/750.

The following observations relate to the results of one-span analyses:

(1) When $\beta = 0.691$ and the plate panel is initially stress-free, the effect of increasing stiffener area (note that $d/t_s = 10$ in all cases) is to reduce the difference in strength between the two modes of column failure, that is, failure by compression of the plate (Mode I) and compress-

ion of the stiffener (Mode II), for the same level of initial deflection Δ_o' (Fig. 5.11). It will be seen that for $\lambda < 1.0$, increasing α results in reduced load-carrying capacity for Mode I failure; for Mode II failure, the strength increases with α. This behaviour is explained by the large difference in moment-carrying capacities for Mode I and Mode II bending when α is low (Fig. 5.5).

(2) Figures 5.11a to 5.11c show that the maximum difference between Mode I and Mode II strength occurs in the vicinity of $\lambda = 0.85$. Beyond $\lambda = 1.0$, the strength in Mode I for $\alpha = 0.2$ falls below that for higher values of α. Referring to Table 5.2, it will be noted that the ratio h_s/r for $\alpha = 0.2$ is high and consequently when the axial thrust is low, tensile yielding of the stiffener outstand occurs first. For higher values of α, such tensile yielding will occur for $\lambda > 1.3$.

(3) Increasing the initial bow of the stiffener (Figs 5.12a to 5.12c and Fig. 5.32) results in a relatively greater reduction in strength for Mode II bending compared with that for Mode I, when α is low and $\lambda < 1.0$. For higher values of these ratios, the difference in imperfection sensitivity between the two modes of bending reduces.

(4) Except when the material stress-strain curve is used to describe the behaviour of plate panels, column strength values for $\lambda < 0.2$ are not given. This is because for columns which approach squash conditions, it would not be appropriate to assume that the behaviour of the plate

panels can be described by buckling stress-strain curves relating to more slender panels.

(5) Referring to Figs 5.1 to 5.4 it will be observed that the applied average strain at which the peak stress occurs varies for the different plate panels and depends on the level of initial imperfection. In the presence of residual stress, the peak average stress occurs when the applied average strain is greater than the yield strain, ε_o. As a result of this, it will be seen that the column strength curves converge to different limiting capacities as the slenderness ratio is reduced (e.g. 5.16a). For Mode I bending, that is, when the compressive strain in the plate panel is greater than that in the stiffener, the limiting strength corresponds to the condition of maximum stress in the plate panel and yield stress in the stiffener. For Mode II bending (compressive strain in the plate less than that in the stiffener), the limiting value occurs when both, the plate and stiffener are at yield strain. In this latter case, the maximum capacity of the plate panel cannot be mobilised since the load-carrying capacity of the column becomes limited by compressive yielding of the stiffener outstand.

(6) When the peak of the average stress-strain curve occurs at a strain value less than ε_o, as for $\beta = 2.074$ with $\delta_o' = 0.188$ and $\sigma_R' = 0$ (Fig. 5.4) the column curves again converge to different limits as λ is reduced. In this case, however, the limit for Mode II bending will be higher than that for Mode I.

(7) In the columns where the plate slenderness, β is greater than or equal to 1.037, varying the initial imperfection of the plate panel has a significant effect on column strength particularly when α is low. In the case of $\beta = 0.691$, the levels of plate panel initial bows considered in this study have very little effect on the average stress-strain behaviour when the panel is initially stress-free; thus,in such situations the strength of the column will be similar to that obtained by assuming that the plate panel follows the bilinear material stress-strain curve. However, in the presence of residual stress, the stiffness of the plate panel becomes reduced at an earlier stage of loading and thus the load-carrying capacity of the column can be reduced. Figures 5.27a to 5.27c show that residual stress can reduce the strength of columns in the slenderness range $0.5 < \lambda < 0.9$ by about 7 per cent.

(8) Where the material stress-strain curve is used to describe the behaviour of both, plate and stiffener, the column strength for Mode I bending will always be higher than that for Mode II bending if the stiffener initial bows in the two directions are equal in magnitude. However, where the capacity of the plate panel is reduced due to buckling, the strength of the column in Mode I can be lower than that in Mode II, when the proportion of stiffener area is high. Of course,Mode I strength can also be lower if the initial bow in this mode is of greater magnitude than that in Mode II. This implies that when the fabrication tolerances for the initial bows in the

two modes are different, as will usually be the case in practice (e.g. Design Rules[32]), the possibility of failure occurring in either mode must be investigated.

(9) The results of columns which had Mode I initial deflections showed that at $\lambda < 0.7$, collapse occurred soon after the mid-depth of the plate panel had reached maximum stress. The collapse of columns of similar slenderness but which had deflection in Mode II occurred when the loads were about 1.05 times those which initiated compressive yielding at the tips of stiffener outstands. At higher slenderness ratios, however, the load-carrying capacities of the columns were influenced mostly by the effective stiffnesses of the plate/stiffener combinations; thus, in such columns the maximum stresses in the plate panels were less than the peak stresses given by the average stress-strain curves, i.e. the columns approached the buckling conditions.

5.5 TWO-SPAN CONTINUOUS BEAM-COLUMNS

To study the effects of continuity on the strength of two-span continuous beam-columns, various modes of initial deflections in adjacent spans were considered (Figs 5.31a and 5.31b). In the analysis, the plate panels were assumed to be stocky with $\beta = 0.691$ and both δ_o' and σ_R' equal to zero. The stiffeners considered were of the same proportions as those used in the single-span study, that is, $d/t_s = 10$. The maximum strength-slenderness curves for beam-columns with $\alpha = 0.2$ and 1.0 are shown in Figs 5.31a and 5.31b respectively. The curves are given for the slenderness range $0 < \lambda \leqslant 1.3$. It should be noted here that the slenderness parameter, λ, for the two-span beam-column

refers to the span between cross-girders. In the analysis, the beam-columns were assumed to be pinned at the ends and laterally supported at the cross-girder positions by springs of large stiffnesses so that the deflections of the springs were small. The initial stiffener bow in each span was considered to be of sinusoidal form; the initial bows (Δ_o') towards the stiffener outstand, and away from it, were considered to be +1/750 and -1/750 respectively.

To show the influence of continuity of spans in the beam-columns, maximum strength-slenderness curves for single-span columns with Δ_o'-values of + 1/750 and - 1/750 are included in Figs 5.31a and 5.31b (Curves 1 and 2). Curves 3 relate to the situation when initial deflections are in the preferred buckling mode. In this case, failure of the beam-column is caused by compressive yielding in the stiffener outstand, in the span where deflections are towards the plate. However, due to the continuity of the unsymmetrical section, the beam-column strength is higher than the single-span strength (Curves 2).

In general, the maximum load-carrying capacity of a beam-column with a slenderness value λ in the range investigated will be reached when one of the following effects occurs in one or both of the span regions, depending upon the extent to which the initial stiffener bow in one span influences the column behaviour in the adjacent span:

(a) failure of the plate panel in compression

(b) compressive yielding in the stiffener outstand

(c) tensile yielding in the stiffener outstand.

Where the initial deflections in adjacent spans are such that the stiffener outstand at the cross-girder position is subjected

to greater compression than the plate, as in Curves 4 and 5, localised compressive yielding of the outstand will occur at this location. However, such yielding will not mark the limit of load-carrying capacity of the beam-column; with increasing load plastic deformations of the stiffener at the cross-girder location will increase and collapse of the beam-column will result only after failure of the plate or stiffener outstand occurs in one of the spans.

Of course, it is also possible to have localised compressive yielding of the plate at the cross-girder location when the initial deflections in the two adjacent spans are directed towards the plate and are of similar magnitudes. This mode of initial deflections was not considered in the present study.

Referring to Curves 4 in Figs 5.31a and 5.31b, it may be seen that at low slenderness ratios, the strength of the two-span beam-column is similar to that of the one-span column in which failure occurs in Mode I (Curves 1); this is because the limiting capacity of the beam-column is reached by failure of the plate in compression in the span where the initial deflection, Δ_o', is + 1/750. However, for higher values of the slenderness, λ, the strength is governed by compressive yielding in the stiffener outstands in the adjacent span. Hence where Mode II one-span column strength is significantly lower than Mode I strength, as in the case of $\alpha = 0.2$, the reduction in load-carrying capacity of the continuous beam-column is greater.

The effects of continuity on strength are greatest when adjacent spans have equal initial deflections, Curves 5, These curves show that in a slender beam-column ($\lambda > 1.2$ when $\alpha = 0.2$, and for $\lambda > 1.1$ when $\alpha = 1.0$) continuity of spans reduces the 'effective length' to the extent that

the failure stress is higher than the Euler stress for a single-span column. It should be noted, however, that under such conditions the strength of the continuous column is very sensitive to any variations in the initial bow (Fig. 5.32), that is, it is a highly unstable situation which could not be relied upon in design. Figure 5.32 shows the strength of the two-span beam-column for varying levels of initial deflections in one span (Δ'_{02}) when the initial deflection in the adjacent span is held constant (Δ'_{01} = + 1/750). It may be seen that when α = 1.0, the strength curve for λ = 1.10 has a cusp with a peak at $\Delta'_{01} = \Delta'_{02}$ = +1/750. When α = 0.2 and λ = 1.10 the behaviour of the beam-column for similar initial deflections in the two spans is influenced by tensile yielding in the outstands of longitudinal stiffeners; hence there is no distinctive cusp in the strength curve for this case.

5.5.1 Effective Stiffener Initial Deflections - Comparisons Based on Design Rules Formula

In the Design Rules[32], initial out-of-plane deflections in adjacent compression panels are accounted for by using the concept of 'effective initial deflections'. Empirical formulae for calculating these effective deflections in internal and end spans of a multi-span stiffened panel are given. For a two-span beam-column the effective deflections may be obtained by using the formula relating to an end span:

$$|\Delta'_{01}|_{eff} = \frac{3}{4}\Delta'_{01} - \frac{1}{4}\Delta'_{02} \qquad \ldots\ 5.3$$

Results obtained by using the above formula are compared in Figs 5.33a to 5.33c with those derived from the two-span analysis;

the latter values were obtained from strength-initial deflection curves for two-span beam-columns in conjunction with similar curves for one-span pin-ended columns (Fig. 5.32). The comparisons given in Figs 5.33 are for three selected values of slenderness ratio: λ = 0.33, 0.77 and 1.10; in each case β = 0.691 with δ_o' and σ_R' equal to zero. It can be seen that the comparison is satisfactory in only one case, viz. λ = 0.77 where α = 1.0. It is interesting to note that at λ = 0.77 the analytically derived effective deflections for similar levels of positive initial deflections in the two adjacent spans are larger when α = 0.2; reference to Fig. 5.32 will show that when the initial deflections, Δ_{o1}' and Δ_{o2}', are of the same order of magnitude, the strengthening effect of continuity is less when α = 0.2 since at this value of α the outstand of the stiffener near the cross-girder region undergoes larger plastic deformations due to compressive yielding.

Although the comparison of effective deflections is less satisfactory at λ = 0.33 (Fig. 5.33a), the differences in predicted strength will not be very significant as, at low slenderness ratio, the column is less sensitive to initial deflections, Fig. 5.32. For the slender beam-column, that is when λ = 1.10, the empirical formula of the Design Rules is generally unsatisfactory (Fig. 5.33c) when Δ_{o2}' is positive as the strength in this case is often governed by compressive yielding of the stiffener outstand in the span where the initial deflection is of lesser magnitude.

5.5.2 Alternative Values for the Empirical Coefficients in the Effective Deflection Formula for an End Span

The empirical formula (5.3) can be written in a general form as:

$$|\Delta'_{o1}|_{eff} = C_1 \cdot \Delta'_{o1} - C_2 \cdot \Delta'_{o2} \qquad \ldots\ 5.4$$

The coefficients C_1 and C_2 in the above formula represent the slopes of the lines of effective deflections such as those shown in Fig. 5.33. Figures 5.34a and 5.34b show that by assuming the values $C_1 = 0.8$ and $C_2 = 0.2$, the comparison between the empirically based and analytically derived effective deflections for $\lambda = 0.33$ and 0.77 is improved for similar levels of initial deflections in the adjacent spans. But for small values of Δ'_{o2} that is, in the transition zone where the collapse mode changes (from plate failure in one span to compressive yielding of the stiffener outstand in the other) the formula underestimates the effective deflections; the empirical formula of the Design Rules[32] also tends to underestimate the deflections in the transition zone but the differences are of lesser magnitude.

Figure 5.34c shows the comparisons for $\lambda = 1.10$. The effective deflections are given for two cases: $C_1 = 2/3$, $C_2 = 1/3$ and $C_1 = C_2 = 1/2$. It should be noted that in the latter case, the critical effective deflection will always be the one which is negative. The analytical effective deflections shown in the figure indicate the tendency to approach the effective values obtained for $C_1 = C_2 = 1/2$. Thus for slender beam-columns, it would seem that the coefficients $C_1 = C_2 = 1/2$ could be used provided that a minimum effective deflection is also specified so that the effective value

does not reduce to zero when the initial deflections in the two spans are similar.

5.6 THREE-SPAN CONTINUOUS BEAM-COLUMNS

Maximum strength-slenderness curves for three-span beam-columns with various modes of initial deflections are shown in Figs 5.35a and 5.35b. The proportions of plate panels and stiffeners considered in the three-span study were the same as those used in the two-span analysis. For comparison, curves for one-span columns (Curves 1 and 2) are also given in Fig. 5.35. It will be seen that due to continuity the strength of the three-span beam-column for sympathetic initial deflections in adjacent spans, that is, deflections equal in magnitude but alternating in direction (Curves 3 and 4), is higher than the strength of the one-span column in which failure occurs by compression of the stiffener outstand (Curves 2). However, when $\lambda > 0.8$ the difference in strength is only marginal. The maximum influence occurs when $\alpha = 0.2$ and the slenderness λ is low; this is because when $\alpha = 0.2$, the column strength for Mode I bending is considerably higher than that for Mode II bending and hence the stiffening effect of continuity is relatively greater than that for $\alpha = 1.0$. Curves 4 show lower strength than Curves 3 since the former curves relate to the situation when the outer spans fail in the weaker mode, that is, by compression of the stiffener outstands.

When the outer spans have zero initial deflections (Curves 6 and 7) the strength of the beam-column is significantly higher than that given by Curves 3 and 4. Comparing Curves 4 and 6 it will be seen that reducing the negative initial bow of the stiffener to zero

in the outer spans, results in a substantial increase in the load-carrying capacity; the high sensitivity of the beam-column to negative initial deflections, particularly for $\lambda > 0.4$ is well illustrated in Fig. 5.36 which shows the maximum strength of the beam-column for varying levels of initial deflections in the outer-spans (Δ'_{o2}) when the initial deflection in the middle span is held constant at $\Delta'_{o1} = + 1/750$.

It is interesting to note that when the initial deflections in all three spans are equal ($\Delta'_{o1} = \Delta'_{o2} = + 1/750$), Curves 5 in Figs 5.35a and 5.35b, although the maximum strength values are higher than those for one-span columns (Curves 1), they never exceed the Euler values as they did in two-span beam-columns (Curves 5, Figs 5.31a and 5.31b). This important difference in behaviour can be explained by considering the nature of symmetry in the two systems. In the two-span case with deflections of equal magnitude and direction conditions of symmetry dictate that adjacent spans must deflect equally and in the same direction thus, in effect, achieving an 'encastré-type' condition over the cross-girders. In contrast, in the three-span beam-column, although symmetry still exists the outer spans are restrained differently from the middle span and consequently do not have to deflect equally or indeed in the same direction. The restraining effects in the three-span beam-column are therefore less than those in the two-span case.

Curve 5, Fig. 5.35a, which relates to the beam-column with $\alpha = 0.2$ shows a sudden drop in load-carrying capacity at $\lambda \simeq 0.97$, as failure of the beam-column beyond this slenderness value is influenced by compressive yielding in the stiffener outstand in the

middle span. When $\lambda > 0.97$ the effects of continuity cause the middle span to deflect towards the plate and as the column is weaker in this direction, the load sustained by the beam-column is reduced. For values of λ up to 0.97 the beam-column can sustain deflections in the same direction in all three spans; this is aided by localised compressive yielding in the stiffener outstands at the cross-girder positions. However, as the slenderness ratio is increased, such yielding is reduced and the beam-column can then no longer maintain deflections in the same direction in all three spans. With $\alpha = 1.0$, Curve 5 (Fig. 5.35b) does not show a sudden drop in strength since the difference between Mode I and Mode II strength is not as large as that for $\alpha = 0.2$; also when $\alpha = 1.0$, yielding of the stiffener outstands at the cross-girder regions is not as extensive as in the case of $\alpha = 0.2$.

5.6.1 Effective Stiffener Initial Deflections - Comparisons Based on the Design Rules Formulae

As in the two-span beam-column effective initial deflections obtained by using the empirical formulae given in the Design Rules, are compared (Figs 5.37a to 5.37c) with the values derived analytically from Fig. 5.36. For the three-span beam-column, the formula for calculating the effective deflections in the outer spans is the same as that for a two-span beam-column (equation 5.3); the deflection in the middle span is calculated from the formula relating to internal spans which is as follows:

$$|\Delta'_{o(s)}|_{eff} = -\frac{1}{4}\Delta'_{o(s-1)} + \frac{1}{2}\Delta'_{o(s)} - \frac{1}{4}\Delta'_{o(s+1)} \quad \ldots\ 5.5$$

where $|\Delta'_{o(s)}|_{eff}$ is the effective initial deflection of the stiffener in the internal span, s.

The comparisons of effective initial deflections for the three selected values of column slenderness, viz. λ = 0.33, 0.77 and 1.10 (Figs 5.37a to 5.37c) show similar features to those observed in Figs 5.33a to 5.33c for two-span beam-columns. However, it is interesting to note that whereas in the two-span beam-column the maximum strengthening effect of continuity always occurred when $\Delta'_{o1} = \Delta'_{o2} = +\ 1/750$, in the three-span beam-column such an effect occurs when the initial deflections in the outer spans (Δ'_{o2}) are less than the initial deflection in the middle span ($\Delta'_{o1} = +\ 1/750$); Fig. 5.36 shows that the maximum strength is achieved when Δ'_{o2} is about 1/2 Δ'_{o1}. In general, it will be seen that for positive initial deflections, the empirical formula contained in the Design Rules overestimates the effects of continuity.

5.6.2 Alternative Values for the Empirical Coefficients in the Effective Deflection Formula for an Internal Span

Expressing equation 5.5 in the general form similar to that given for an end span (equation 5.4) we have:

$$|\Delta'_{o(s)}|_{eff} = -\ C_4 \cdot \Delta'_{o(s-1)} + C_3\ \Delta'_{o(s)} - C_4\ \Delta'_{o(s+1)} \quad \ldots\ 5.6$$

When λ = 0.33 or 0.77, the values of the coefficients C_3 and C_4 that give better estimates of the effective initial deflections are 0.6 and 0.2 respectively. The comparisons between effective deflections obtained from the empirical formula using the above values for the coefficients and effective deflections derived analytically are shown in Figs 5.38a and 5.38b. The deflections shown for the outer spans were obtained from equation 5.4 using C_1 = 0.8 and C_2 = 0.2.

As in the two-span beam-column, the coefficients (C_3 and C_4) assumed for $\lambda = 0.33$ and 0.77 do not give a satisfactory comparison when the beam-column is slender ($\lambda = 1.10$). Figure 5.38c shows that at $\lambda = 1.10$, the differences in the effective deflections are reduced if the following values are assumed for the coefficients:

$$C_1 = \frac{2}{3}, \quad C_2 = \frac{1}{3}; \qquad C_3 = \frac{1}{3}, \quad C_4 = \frac{1}{3}$$

It should be noted that the use of the above coefficients for $\lambda = 1.10$ leads to the situation where the critical span is always the one with a negative value of effective deflection. Thus, for the beam-columns referred to in Fig. 5.38c the above coefficients must be considered as the limiting values, since there is a small range of Δ'_{02} where the analytical values of effective deflections are positive.

5.7 EFFECTIVE STIFFENER INITIAL DEFLECTIONS WHEN AVERAGE STRESS-STRAIN CURVES ARE USED TO DESCRIBE PLATE BEHAVIOUR

The effective initial deflections which were discussed in the foregoing sections related to beam-columns with stocky plate panels ($\beta = 0.691$) and it was assumed that the plate panel behaviour can be represented by the bilinear elastic-perfectly plastic stress-strain curve. To investigate how the results would compare when the average stress-strain behaviour of the plate was different from the bilinear material characteristic, effective initial deflections for the stiffened compression panels of Models 2, 4, 8 and 10 were evaluated by the Design Rules formulae[32]. The collapse strengths obtained by the multi-span analyses, and single-span analyses using

effective initial deflections, are compared in Table 5.5. Note that the strengths shown are those derived for axially loaded panels; the influence of eccentricity of loading on the effective values of initial deflections has not been investigated. Except in the case of Model 8, where the stiffeners were slender ($\ell/r = 114.5$), the strengths obtained by using effective initial deflections are similar to those given by the multi-span analyses. For Model 8, the comparison is better when the modified formula, equation 5.4 with $C_1 = C_2 = \frac{1}{2}$, is used.

CHAPTER 6

CONCLUSIONS

6.0 CONCLUSIONS FROM TEST RESULTS

(1) *Initial Stiffener Geometrical Imperfections:* Measurements of initial deflection profiles indicated that the compression flanges of the models had both modes of longitudinal stiffener deformations, that is, deflection in the direction of stiffener outstand and away from it. Only in one model (Model 10) were the stiffener deflections clearly in the preferred buckling mode, that is, alternate inward and outward deflections in adjacent bays. In the compression flange of Model 4, the longitudinal stiffeners exhibited a nearly sympathetic deformation mode, while in all other models the stiffeners deflected in a more random way over several bays, although stiffeners in any one bay generally deflected in the same direction. The deformations of stiffeners in the direction of stiffener outstands were generally within the tolerances prescribed in the Design Rules[32]; deformations in the direction of the plate often exceeded the specified tolerances.

(2) *Initial Plate Geometrical Imperfections:* Initial deflections of compression flange plate panels were determined in Models 1, 2, 9 and 10, in which the plate panels were slender ($b/t \simeq 49$). Except at a few locations, the plate panels between stiffeners bowed inwards, towards stiffener outstands, with amplitudes well within the maximum values allowed in the Design Rules.

(3) *Effect of Initial Imperfections on Failure Mode:* The compression flanges of those models that were subjected to uniform bending moments failed in modes generally following the initially deflected shapes. In the point load tests, the influence of initial deformation patterns on the collapse modes, was not so clear.

(4) *Failure Modes:* Except in Models 8 and 10, observations from the tests indicated that compression flange collapse was preceded by failure of the plate either by buckling or yielding rather than failure of the outstand. However, in Model 4, as the longitudinal stiffeners in the end bay were outwards, that is, away from the outstands, it is possible that yielding in the tips of outstands initiated the collapse of the compression flange. There is no strain data to confirm the behaviour; the remark is based on observations from theoretical studies which indicated that the stiffened panel was weaker in the end bay. In Models 8 and 10, yield was first observed in the stiffener outstands.

(5) *Failure by Stiffener Outstand Yielding:* By restricting the depth-to-thickness ratio (d/t_s) of the stiffeners to values of 6 (Model 8) and 8.8 (Model 10) the possibility of torsional buckling of the stiffeners was greatly reduced. In fact, at collapse the maximum compressive strains in the stiffeners were several times the yield values, while the stiffeners remained almost straight.

(6) *Effects of Residual Stresses on Failure:* The effect of residual stresses on the collapse of compression flange plate panels of stocky proportions (Models 4 and 8) was very small. The results of Model 4 showed that almost the full squash capacity of the flange

plate was realised despite the presence of high residual stresses. However, residual stresses did influence the overall behaviour of the models by causing earlier departure from linearity in the load-deflection relationships. The non-linearity occurred approximately when the sum of the applied and residual compressive strains in the compression flange plate reached the yield strain value.

(7) *Overall Stiffnesses of Models under Service Loads:* In the early stages of loading when the models were generally elastic, the stiffnesses of the constant moment girders were estimatedvery satisfactorily from simple bending theory on the basis of gross section properties. For the centrally loaded models the beam theory also predicted satisfactory values for the stiffness when deformations due to shear and shear lag were included. To allow for these effects, effective widths[63] of flanges were used in the inertia calculations. The contributions of shear deformations of the webs were also included in the deflection calculations.

(8) *Overall Stresses in Models under Service Loads:* In the elastic range, measured longitudinal stresses in the compression flange compared very well with stresses predicted from simple beam theory; the theoretical values were derived using gross section properties when the moment on the girder was constant, and on the basis of effective flange widths[63] for shear lag when the girder was subjected to a moment gradient.

(9) *Stress Concentrations in Box Girders:* From the strain data collected for each model, it was observed that local increases in the longitudinal strains occurred at the girder corners wherever

transverse stiffeners were situated. These stress concentrations were caused by the restriction imposed by the transverse members on the Poisson's contraction or expansion. Local curvatures in the plane of the flange plates produced edge strains which were of the same sign as the primary longitudinal strains in the flange and were superimposed upon them.

(10) *Post-buckling Behaviour of Stiffened Flanges:* Evidence of post-buckling reserve in the longitudinally stiffened compression flanges was provided by the results of tests on Models 8 and 10. In Model 8 where the longitudinal stiffeners were slender (ℓ/r = 114.5), the compression flange was able to sustain its critical buckling load, in spite of the high level of residual stresses and pronounced initial stiffener deflections. The presence of membrane action was confirmed by the significant increase in the level of transverse tensile membrane strains in the plate at loads approaching the peak values.

(11) *Post-buckling in Flanges in which Failure is Preceded by Stiffener Yielding:* Strain data collected from the tests on Model 10 also indicated the development of significant transverse membrane strains. Even though the compression flange in Model 10 failed by compressive yielding of the stiffener outstands, its capacity was 10 per cent higher than that of Model 2, where failure was by compression of the plate. Furthermore, the stiffeners in Model 10 were slender (ℓ/r = 75.4) compared with those in Model 2 (ℓ/r = 53.6) while the plate panels in the two models were of similar slenderness. This indicates that the compression flange in Model 10 had some post-buckling reserve; it should be noted though that the outer bays of the flange in Model 10 had additional longitudinal stiffening and thus the centre bay had some additional restraint.

(12) *Overall Elasto-Plastic Stiffness of Box Models:* Although in Models 8 and 10 failure occurred by compression of the stiffener outstands, the unloading branches of the load-deflection curves do not exhibit rapid fall-off in load. The capacity of the model to shed the load gradually (rather than suddenly as reported in isolated stiffened panel tests[50]) can be attributed to the post-buckling stiffness of the compression flange. The ability of the flange to retain much of its load-carrying capacity may be attributed largely to the presence of longitudinal stiffeners of stocky cross-section.

(13) *Effects of Shear Lag on Collapse:* The results of Models 1 and 2 showed that even with the presence of shear and shear lag at the position of maximum bending moment under point load condition, about 6 per cent higher capacity was achieved in Model 1 when the moment at the position of maximum curvature was compared with the moment achieved in the pure bending test on Model 2. A similar comparison for Models 9 and 10 showed that the maximum moment in the point load test (Model 9) was 12 per cent higher than the uniform moment sustained by Model 10. It may therefore be concluded that in these models shear lag had no weakening effect on moment-carrying capacity.

(14) *Redistribution of Flange Forces in Boxes Subjected to Shear Lag:* The test on Model 9, in which shear lag was very pronounced, showed that after the highly loaded edge panels had yielded, the panels continued to maintain their resistance until the strength of less highly loaded panels was mobilised. The ultimate strength of the entire stiffened panel was thus not so much dependent on

yielding of the highly loaded panels adjacent to the webs. The redistribution of stresses in this case was possible because the stiffeners were stocky (d/t_s = 8.8) and consequently, the flange plate was able to take fairly high compressive strains of values much greater than the yield strain value. It would appear, therefore, that in such a situation if it can be assumed that there is no loss in panel strength due to any interaction between panels, it would be reasonable to assess the ultimate capacity of a stiffened panel by aggregating the strength of individual panels.

To determine the effect of shear lag on the collapse strength of the stiffened compression flange of Model 9, another model, Model 10, of similar geometry and material properties was tested with the stiffened flange panels subjected to uniform longitudinal compression. It was hoped that the results obtained would provide a basis for comparison. However, as the initial deflections in Model 10 were such that they favoured failure of the critical centre bay by compression of the stiffener outstands, Model 10 does not provide the necessary datum for comparison, although it does provide a lower bound to the strength in pure bending. Thus, until results of a plate-initiated failure in a model similar to Model 10 become available, an accurate assessment of the effects of shear lag in Model 9 cannot be made.

(15) *Further Evidence of the Effects of Shear Lag on Collapse:* The results of Models 1 and 9 showed that the compression flange capacity in Model 9 was about 8 per cent higher. This was so despite the fact that the flange plate panels in the two models were of similar slenderness, and the stiffeners in Model 9 were more slender. These results indicate, therefore, that the pronounced

shear lag in Model 9 did not have any significant effect on the load-carrying capacity. However, there are two other factors which must also be considered, as they may have influenced the collapse behaviour of the flanges. These are:-

(a) Failure of the compression flange panels in Model 1 occurred almost simultaneously with failure of the slender web panels in shear. Although these failures did not occur at the same section it is possible that the two collapse modes interacted and influenced the strength of the model.

(b) In Model 9, the initial bows of longitudinal stiffeners were considerably smaller than those in Model 1. Also, the centre longitudinal stiffener in Model 9 was observed to deflect outwards, almost up to the maximum load. This may have had some stiffening effect on the panel.

6.1 CONCLUSIONS RELATING TO COMPARISONS BETWEEN TESTS AND THEORY

(16) *Point Loaded Models:* For both, Models 1 and 9, strengths of the stiffened compression flange as predicted by the beam-column analysis were within 5 per cent of the observed values; in the case of Model 1 the theoretical strength was higher, probably because the moment-carrying capacity of the girder was reduced due to the buckling of the web panels.

(17) *Influence of Shear Lag on Collapse:* The good correlation between the theoretical and experimental stiffened panel strength

for Model 9 suggests that shear lag did not have any significant effect on the ultimate capacity of the compression flange.

(18) *Pure Bending Tests on Models with Stockily Stiffened Flanges:* The beam-column analyses of the compression flanges of Models 2 and 4 (pure bending tests) predicted both, the collapse mode and the ultimate stiffened panel strength, very satisfactorily; for both models the collapse strengths were conservatively predicted, the difference being 6 per cent for Model 2 and 3 per cent for Model 4.

(19) *Pure Bending Tests on Models with Flanges using Slender Stiffeners:* In the case of Models 8 and 10, which were also pure bending tests, the beam-column analysis predicted the correct collapse modes but the collapse strengths were somewhat lower than the observed values, 11 per cent for Model 8 and 15 per cent for Model 10. These differences can be attributed to the post-buckling reserve in the flanges. In Model 10, the behaviour of the compression flange was further influenced by the increased longitudinal stiffening in the end bays.

(20) *Comparisons Between Theory and Other Methods:* The collapse strengths of the stiffened flanges were also obtained by IDAR[69] and BS153[1]. Generally, both the methods gave very conservative estimates of the collapse strengths.

6.2 CONCLUSIONS FROM THEORETICAL PARAMETRIC STUDY

(21) *Range of Parametric Study:* A parametric study on the ultimate load behaviour of plate/stiffener beam-columns has been presented. The parameters covered plate panels with slenderness values (β) of

0.691, 1.037, 1.383 and 2.074; these values correspond to b/t-ratios of 20, 30, 40 and 60 respectively for mild steel. The column slenderness ratios (λ) were varied between 0 and 1.3 (that is, $0 < \ell/r < 120$ for mild steel). The levels of initial imperfections chosen for the analyses were related to the values considered in the Design Rules[32].

The stiffeners considered were those of flat section with depth-to-thickness ratios (d/t_s) of 10, so that their stress-strain behaviour could be assumed to be that of the material. The proportion of stiffener area to plate area (α) was varied; the ratios considered were $\alpha = 0.2$, 0.6 and 1.0.

(22) *Comparisons Between Two Modes of Failure for Single-Span Panel:* The results of plate/stiffener columns with $\beta = 0.691$ and in which the stress-strain behaviour for the plate was assumed to be of bi-linear elasto-plastic form, showed that for given values of column slenderness, λ and initial stiffener bow, Δ_o, the strength of the column for Mode II failure (compression of the stiffener outstand) was less than that for Mode I failure (compression of the plate). The difference in strength was greater for the lower value of α.

(23) *Effect of Plate Buckling on Failure in Single-Span Panels:* In the columns where the capacities of the plate panels were reduced due to buckling - which was allowed for by using an average stress-strain curve as derived from Frieze's elasto-plastic large-deflection analysis[21], instead of the material stress-strain curve - the column strength for Mode I failure was not necessarily higher than that for Mode II; the limiting strength depended on both, α and the

level of the initial stiffener bow, Δ_o. Thus, in practice, where the fabrication tolerances for the initial bows in the two modes may be different (as in the Design Rules[32]), the possibility of failure occurring in either mode must be investigated.

(24) *Failure by Tensile Yielding of the Stiffener Outstand:* Failure of the column can also be caused by tensile yielding in the stiffener outstand occurring first; such yielding will occur when the slenderness value λ is high (approximately greater than 1.0), and the distance of the extreme fibre of the stiffener, from the centroid, is considerably greater than that of the plate.

(25) *Effect of Residual Stresses on Single Panel Strength:* In the presence of residual stress, the average stress-strain curve of the plate panel showed a reduction in stiffness once yielding had occurred due to the combination of applied stress and residual stress; thus at $\beta = 0.691$, the load-carrying capacities of columns were affected most in the medium slenderness range ($0.5 < \lambda < 0.9$), the maximum reduction being about 7 per cent. When the plate panels were slender, the initial stresses also had a detrimental effect on plate strength, and hence on column strength.

(26) *Failure Criteria for Two Modes in Single Panels:* The analyses of columns with initial bows in the direction of the stiffener outstand (Mode I) indicated that for $\lambda < 0.7$, collapse of the columns occurred soon after the plate panels had reached their maximum stresses (as given by the average stress-strain curves); when failure was by compression of the stiffener (Mode II), the maximum load reached was approximately 1.05 times the load which initiated yielding in the tip of the stiffener.

(27) *Effect of Continuity on Strength in Multi-Span Panels:* The results of multi-span analyses showed that the effects of continuity on the maximum load-carrying capacity are not necessarily strengthening due to the difference in behaviour between Mode I and Mode II collapse. In a two-span beam-column, the strengthening effect of continuity was greatest when the initial bows in the two spans were equal. However, in a three-span beam-column the maximum strength did not occur when initial deflections in all the spans were equal, as the restraining effects in the middle span were not similar to those in the outer spans; from the cases analysed in this study it was noted that the maximum strength occurred when the initial bow in the middle span was approximately half that in the outer spans.

(28) *Use of 'Effective Imperfections' to Relate Multi-Span to Single-Span Failure:* From the maximum strengths obtained for single-span and multi-span beam-columns, effective initial stiffener deflections (that is, initial deflections which in single-span column analyses would give the same strength as the multi-span analyses), were derived. The effective deflections so obtained were then compared with the values given by the Design Rules formulae[32]. The results indicated that for columns of medium slenderness ($0.5 < \lambda < 0.9$) the Design Rules would give satisfactory values for the effective initial deflections. However, for more slender columns or, for stocky columns with similar initial deflections in the adjacent spans, the effective values given by the Rules will be less satisfactory. In such cases, alternative values for the empirical coefficients assumed in the Design Rules formulae are suggested.

(29) *'Effective Imperfections' in Multi-Span Panels with Plates using Average Stress-Strain Curves:* In the parametric study, the beam-columns considered for the purpose of comparing analytically derived effective initial deflections with empirically based values, were those in which the behaviour of the plate panels was described by the bilinear material stress-strain curve. A few beam-columns in which plate panel behaviour was described by average stress-strain curves, were also analysed; the data used in the analysis was that relating to the compression flanges of the box girder models. The effective initial deflections derived for these cases also compared well with the values given by the empirical formulae.

(30) The thesis has presented the results of several tests on box girder models, fabricated on a realistic scale, in which the attention has been focussed on the ultimate strength of the stiffened compression flange. An inelastic column analysis approach has been presented which predicts satisfactorily the behaviour of the tests and which has been used to study in detail the parameters controlling the behaviour of compression flanges. Both the theoretical and experimental data presented should provide a sound basis against which any design rules can be confidently calibrated.

6.3 SUGGESTIONS FOR FUTURE WORK

During the course of the research work described in this thesis some test programmes on the ultimate load behaviour of stiffened compression panels were initiated, the results of which have recently become available. It would be useful to compare these experimental

results with the theoretical values given by the present analysis. Such an exercise would help provide a basis for formulating simplified design rules from the theoretical data.

With regard to the analytical work, there are certain other aspects on which more information is needed. The stiffened compression panels analysed in the present study were those which would be classified as lightly welded panels; the study could, therefore, be extended to cover other levels of residual stresses which are likely to be encountered in practice.

Information is also needed on the behaviour of stiffened panels with longitudinal stiffeners other than those of the flat type; the computer program written for the present analysis can be used to analyse a column of any cross-section in which biaxial or torsional effects can be ignored.

For multi-span stiffened panels, the effects of eccentricity of loading (due to overall bending) on continuity also need investigation, so that effective imperfections under such loading condition can be established. The study, as described in this thesis, on the derivation of effective stiffener initial deflections was concerned mainly with compression panels whose stres-strain behaviour was described by the material stress-strain characteristic. More work is needed to check the applicability of the Design Rules empirical formulae in situations where the plate panels are slender and buckling of the plate is accounted for by the use of an average stress-strain curve, instead of the material characteristic.

Finally, the work on the grillage approach could be continued to examine in a systematic way, the forces on the transverse beams, the influence of flexibility of the beams on overall behaviour and the effects of lateral loading on the total load-carrying capacity of the grillage.

REFERENCES

1. British Standard 153, Specification for steel girder bridges, British Standards Institution, London.

2. German Standard DIN 1073, Stählerne Strassenbrücken: Berechnungsgrundlagen, Deutscher Normenausschus, Beuth-Vertrieb, Berlin.

3. Committee of Inquiry into the basis for design and method of erection of steel box girder bridges. Report of the Committee, Department of the Environment, London 1973.

4. Dowling, P.J. Strength of steel box girder bridges. Journal of the Structural Division, ASCE, Vol. 101, No. ST9, Proc. Paper 11550, September 1975.

5. Dowling, P.J. Some approaches to the non-linear analysis of plated structures. Symposium on Non-Linear Techniques and Behaviour in Structural Analysis. T.R.R.L., Crowthorne, Berks., U.K., 11-12 December 1974.

6. Bleich, F. Buckling strength of metal structures. McGraw-Hill Book Company, New York, 1952.

7. Timoshenko, S.P. and Gere, J.M. Theory of elastic stability. Second Edition. McGraw-Hill Book Company, New York, 1961.

8. Bulson, P.S. The stability of flat plates. Chatto and Windus, London, 1970.

9. Column Research Committee of Japan (Edited by) Handbook of Structural Stability. Corona Publishing Ltd., Tokyo, 1971.

10. Levy, S. Bending of rectangular plates with large deflections. National Advisory Committee for Aeronautics Report 737, 1942.

11. Coan, J.M. Large-deflection theory for plates with small initial curvature, loaded in edge compression. Journal of Applied Mechanics, Vol. 18, June 1951.

12. Falconer, B.H. and Chapman, J.C. Compressive buckling of stiffened plates. The Engineer, Vol. 195, Nos 5080 and 5081, 5 and 12, June 1953.

13. Abdel-Sayed, G. Effective width of thin plates in compression. Journal of the Structural Division, ASCE, Vol. 95, No. ST10, Proc. Paper 6837, October 1969.

14. Moxham, K.E. Theoretical prediction of the strength of welded steel plates in compression. Cambridge University Report CUED/C - Struct/TR.2, 1971.

15. Crisfield, M.A. Large-deflection elasto-plastic buckling analysis of plates using finite elements. T.R.R.L. Report LR593, Crowthorne, Berks., U.K., 1973.

16. Crisfield, M.A. Collapse analysis of box girder components using finite elements. Symposium on Non-Linear Techniques and Behaviour in Structural Analysis. T.R.R.L., Crowthorne, Berks., U.K., 11-12 December 1974.

17. Ilyushin, A.A. Plasticite. Editions Eyrolles, Paris, 1956.

18. Mendelson, A. Plasticity: Theory and application. The Macmillan Company, New York, 1968.

19. Frieze, P.A. Ultimate load behaviour of steel box girders and their components. Ph.D. Thesis, University of London, October 1975.

20. Harding, J.E. The behaviour of bolted splice panels and aspects of stress redistribution in the collapse analysis of box girder components. Ph.D. Thesis, University of London, May 1975.

21. Frieze, P.A., Dowling, P.J. and Hobbs, R.E. Steel box girders. Parametric study on plates in compression. Engineering Structures Laboratories, Civil Engineering Department, Imperial College, London. CESLIC Report BG39, January 1975.

22. Davidson, H.L. Post-buckling behaviour of long rectangular plates. Fritz Engineering Laboratory Report No. 248.15, June 1965.

23. Ractliffe, A.T. The strength of plates in compression. Ph.D. Thesis, Cambridge University, October 1966.

24. Moxham, K.E. Buckling tests on individual welded steel plates in compression. Cambridge University Report CUED/C-Struct/TR.3, 1971.

25. Dwight, J.B. A possible design procedure for stiffened compression panels. Journal of the Australian Institute of Steel Construction, Vol. 9, No. 3, 1975.

26. Dwight, J.B. Use of Perry formula to represent the new European Strut-Curves. Cambridge University Report CUED/C-Struct/TR.30, 1972.

27. Murray, N.W. Analysis and design of stiffened plates for collapse load. The Structural Engineer, Vol. 53, No. 3, March 1975.

28. Horne, M.R. and Narayanan, R. An approximate method for the design of stiffened steel compression panels. Proc. Institution of Civil Engineers, Part 2, Vol. 59, September 1975.

29. Massonnet, Ch. and Maquoi, R. New theory and tests on the ultimate strength of stiffened box girders. Paper 9. Proceedings, International Conference on Steel Box Girder Bridges, The Institution of Civil Engineers, London, February 1973.

30. Pflüger, A. About the buckling problem of the anisotropic rectangular plate (in German), Ingenieur-Archiv, Berlin, 1947.

31. Faulkner, D. A review of effective plating to be used in the analysis of stiffened plating in bending and compression. Journal of Ship Research, Vol. 19, No. 1, March 1975.

32. Committee of Inquiry into the basis for design and method of erection of steel box girder bridges. Report of the Committee - Appendix 1. Interim design and workmanship rules, Department of the Environment, London 1973.

33. Chatterjee, S. and Dowling, P.J. Proposed design rules for longitudinal stiffeners in compression flanges of box girders. Engineering Structures Laboratories, Civil Engineering Department, Imperial College, London. CESLIC Report BG40, March 1975.

34. Rubin, H. Longitudinally stiffened and compressed plates of box girders. ECCS Commission 8, Working Group 3 Document.

35. Djahani, P. Large-deflection analysis of discretely stiffened plates subjected to transverse and/or in-plane loading. M.Sc. Thesis, University of London, August 1974.

36. Djahani, P. Large-deflection elasto-plastic analysis of discretely stiffened plates subjected to transverse and/or in-plane loading. Ph.D. Thesis (to be submitted).

37. Moan, T. and Söreide, T. Analysis of stiffened plates considering non-linear material and geometric behaviour using finite elements. Paper presented at the World Congress on Finite Element Methods in Structural Mechanics, Bournemouth, 12-17 October 1975.

38. Ostapenko, A. and Lee, T. Tests on longitudinally stiffened plate panels subjected to lateral and axial loading. Fritz Engineering Laboratory Report No. 248.4, Lehigh University, August 1960.

39. Kondo, J. Ultimate strength of longitudinally stiffened plate panels subjected to combined axial and lateral loading. Fritz Engineering Laboratory Report No. 248.13, Lehigh University, August 1965.

40. Koiter, W.T. The effective width of flat plates for various longitudinal edge conditions at loads far beyond buckling load. National Luchtvaartlaboratorium, Netherlands, Report S287, 1943 (In Dutch).

41. Tsuiji, T. Strength of longitudinally stiffened plate panels with large b/t. Fritz Engineering Laboratory Report No. 248.14, Lehigh University, June 1965.

42. Vojta, J. and Ostapenko, A. Design curves for longitudinally stiffened plate panels with large b/t. Fritz Engineering Laboratory Report No. 248.19, Lehigh University, August 1967.

43. Rutledge, D.R. and Ostapenko, A. Ultimate strength of longitudinally stiffened plate panels (large and small b/t, general material properties). Fritz Engineering Laboratory Report No. 248.24, September 1968.

44. Parsanejad, S. Ultimate strength analysis of plate grillages under combined loads using a grid model. Ph.D. Thesis, Lehigh University, 1972.

45. Mittleman, M.L. A theoretical and experimental investigation in connection with steel box girders. M.Sc. Thesis, University of London, December 1971.

46. Virdi, K.S. and Dowling, P.J. Failure loads of composite columns in biaxial bending. Engineering Structures Laboratories, Civil Engineering Department, CESLIC Report CC2, September 1971.

47. Virdi, K.S. Inelastic column behaviour. Ph.D. Thesis, University of London, November 1973.

48. Little, G.H. Local and flexural failure in steel compression members. Ph.D. Thesis, Cambridge University, April 1974.

49. Dorman, A.P. and Dwight, J.B. Tests on stiffened compression plates and plate panels. Paper 5. Proceedings, International Conference on Steel Box Girder Bridges, The Institution of Civil Engineers, London, February 1973.

50. Horne, M.R. and Narayanan, R. (i) Ultimate load capacity of longitudinally stiffened panels; (ii) further tests on the ultimate load capacity of longitudinally stiffened panels. Simon Engineering Laboratories, University of Manchester, 1974.

51. Smith, C.S. Compressive strength of welded steel ship grillages. Trans. R.I.N.A., Vol. 117, (Spring Meeting) 1975.

52. Dibley, J.E. and Manoharan, A. Experimental behaviour of a two-span continuous box girder. Paper 8. Proceedings, International Conference on Steel Box Girder Bridges, The Institution of Civil Engineers, London, February 1973.

53. Guile, P.J.D. and Dowling, P.J. Steel box girders, progress reports 1. Engineering Structures Laboratories, Civil Engineering Department, Imperial College, London. CESLIC Reports: BG1, July 1971 (Model 1); BG3, Nov. 1971 (Model 2); BG5, Feb. 1972 (Model 4): BG18, Nov. 1972 (Model 8).

54. Guile, P.J., Moolani, F.M. and Dowling, P.J. Steel box girders, Models 9 and 10 - progress report 1. Engineering Structures Laboratories, Civil Engineering Department, Imperial College, London. CESLIC Report BG33, February 1975.

55. Panel for Standard Practices for Testing. Report of the Working Group on long-term research into steel box girder bridges. Department of the Environment, June 1975.

56. Rao, N.R., Lohrmann, M. and Tall, L. Effect of strain rate on the yield stress of structural steels. Journal of Materials, Vol. 1, No. 1, American Society for Testing and Materials, March 1966.

57. Mittleman, M.L. and Dowling, P.J. Steel box girders, Model 1 - progress report 2. Engineering Structures Laboratories, Civil Engineering Department, Imperial College, London. CESLIC Report BG4, January 1972.

58. Frieze, P.A. and Dowling, P.J. Steel box girders, Model 2 - progress report 2. Engineering Structures Laboratories, Civil Engineering Department, Imperial College, London. CESLIC Report BG11, June 1972.

59. Moolani, F.M. and Dowling, P.J. Steel box girders, progress reports 2. Engineering Structures Laboratories, Civil Engineering Department, Imperial College, London. CESLIC Reports: BG8, March 1972 (Model 4); BG19, May 1973 (Model 8); BG34, August 1975 (Models 9 and 10).

60. Moffatt, K.R. Finite element analysis of box girder bridges. Ph.D. Thesis, University of London, January 1974.

61. Dowling, P.J., Chatterjee, S., Frieze, P.A. and Moolani, F.M. Discussion on Paper 6, Experimental and predicted collapse behaviour of rectangular steel box girders, Session B, Proceedings, International Conference on Steel Box Girder Bridges, The Institution of Civil Engineers, London, February 1973.

62. Moffatt, K.R. and Dowling, P.J. Shear lag in steel box girder bridges. The Structural Engineer, Vol. 53, London, October 1975.

63. Moffatt, K.R. and Dowling, P.J. Parametric study on the shear lag phenomenon in steel box girder bridges. Engineering Structures Laboratories, Civil Engineering Department, Imperial College, London, CESLIC Report BG17, September 1972.

64. Dwight, J.B. and Moxham, K.E. Welded steel plates in compression. The Structural Engineer, Vol. 47, London, February 1969.

65. Dibley, J.E. and Disney, P.L. The measurement of residual stresses and initial imperfections on the Cleddau Bridge. CIRIA Project RP/183 Report, 1974.

66. Rao, N.R., Estuar, F.R. and Tall, L. Residual stresses in welded shapes. Welding Journal, Vol. 43, Part 7, 1964.

67. Kamtekar, A.G. and Dwight, J.B. Thames Barrier Project - Welding stresses in rising sector gates. Cambridge University Report CUED/C-Struct/TR.36, 1973.

68. Owens, G.W., Guile, P.J.D. and Dowling, P.J. Thames Barrier - Steel model of a rising sector gate; supplementary residual stress study. Engineering Structures Laboratories, Civil Engineering Department, Imperial College, London. CESLIC Report TB3, July 1975.

69. Committee of Inquiry into the basis for design and method of erection of steel box girder bridges. Appendix A - Interim design appraisal rules, Department of the Environment, September 1971.

70. Chatterjee, S. and Dowling, P.J. Steel box girders, progress reports 3. Engineering Structures Laboratories, Civil Engineering Department, Imperial College, London. CESLIC Reports: BG7, May 1972 (Model 1); BG9, May 1972 (Model 2); BG10, June 1972 (Model 4); BG21, December 1972 (Model 8).

NOTATION

a	Plate length in the longitudinal direction
b	Width of plate panel
B	Span of cross-girder
C_1, C_2	Empirical coefficients in formula for evaluating effective stiffener initial deflection
d	Depth of stiffener outstand
e	Eccentricity of applied thrust on plate/stiffener column
E	Modulus of Elasticity
E_r	Error function showing difference between y_r and Y_r
E_{ij}	Error function showing difference between Δ_{ij} and ω_{ij}
f_{st}	Flexibility influence coefficients for transversals in grillage
F_s	Spring reaction at support s
F_{ij}	Force in grillage at the intersection of ith longitudinal with jth transversal
h	Distance of a cross-section element from reference axis a-a (along outer surface of plate)
h_c, h_f	Distance of extreme fibre of flange plate from centroid of plate/stiffener combination
h_n	Distance of neutral axis of plate/stiffener combination from reference axis a-a (along outer surface of plate)
h_s	Distance of extreme fibre of stiffener from centroid of plate/stiffener combination
H	Distance between centroidal axis of plate/stiffener combination and neutral axis of box girder
I_T	Moment of intertia of cross-girder and assumed effective width of flange plate, about the centroidal axis (of combination) parallel to the plate

K_s	Spring constant at support s
ℓ	Spacing of cross-girders
L	Length of multi-span beam-column ($= \Sigma\ell$)
M	Bending moment
M_E	M due to external loads
M_I	Moment due to internal forces
$(M_E)_r$	Total external moment at node r
$(M_I)_r$	Moment due to internal forces at node r
$(M_L)_r$	Bending moment, at node r, due to lateral forces
n	Total number of segments along length of column
N	Number of panels in multi-span beam-column
N_L	Number of longitudinals (or beam-columns) in grillage
N_T	Number of transversals in grillage
P	Axial force in plate/stiffener column, or applied load on model as defined in figures relating to Chapter 2
P_i	Axial force on ith longitudinal
P_m	Force in plate/stiffener column at collapse
P_{m_1}	Force in plate/stiffener column at collapse, at mid-span of compression flange (for point load tests)
P_{m_2}	Force in plate/stiffener column at collapse, in middle bay of compression flange at cross-girder position (for point load tests)
$(P_m)_{theory}$	Collapse value of force in plate/stiffener column of compression flange, as predicted by present theory
$(P_m)_{test}$	Collapse value of force in plate/stiffener column of compression flange, as derived from test results
P_o	Squash load of plate/stiffener column
r	Radius of gyration of plate/stiffener cross-section with respect to centroidal axis parallel to plate, *or* Node (or station) along length of column

R_A, R_B	Support reactions at ends A and B of beam-column
S_i^L	Slope of end thrust versus end-shortening curve for ith longitudinal
t	Thickness of plate
t_s	Thickness of stiffener outstand
w_r	Computed value of W_r
W_r	Component of function Y_r, relating to internal moment $(M_I)_r$
x_r	Distance of node r from end of column
y_r	Deflection of column at node r
y_{or}	Initial deflection of column at node r
Y_r	Function representing computed deflection at node r
z_s, z_t	Distances, from one end of transversal, of intersection locations s and t in grillage
α	Ratio of stiffener area to plate area in plate/stiffener cross-section
β	Plate non-dimensionalised slenderness ratio (= $b/t\sqrt{\sigma_o/E}$)
γ	Shear strain
γ_y	Shear yield strain
δA	Area of cross-section element
δ_o	Amplitude of doubly-sinusoidal initial deformation in plate panel
δ_o'	$= \delta_o/t$
δP	Force in a cross-section element
δx	Distance between nodes along length of column
δy_r	Error correction for the assumed deflection y_r
Δ, δ	Deflections as defined on figures relating to Chapter 2
Δ_o	Amplitude of sinusoidal initial stiffener bow
Δ_o'	$= \Delta_o/\ell$

Δ_s Deflection of spring at support s

Δ_y Incremental deflection used to obtain rate of change of computed deflections with respect to assumed deflections

Δ_{o1}, Δ_{o2} Amplitudes of initial stiffener bows in spans 1 and 2 respectively

Δ_{o1}', Δ_{o2}' $= \Delta_{o1}/\ell$, Δ_{o2}/ℓ

$\Delta_{o(s)}$ Amplitude of initial stiffener bow in span s

$\Delta_{o(s)}'$ $= \Delta_{o(s)}/\ell$

$|\Delta_o|_{eff}$ Effective value of stiffener initial bow (Δ_o replaced by Δ_{o1}, Δ_{o2}, or $\Delta_{o(s)}$ for spans 1, 2 or s respectively)

$|\Delta_o'|_{eff}$ $= |\Delta_o|_{eff}/\ell$ (Δ_o' replaced by Δ_{o1}', Δ_{o2}' or $\Delta_{o(s)}'$ for spans 1, 2, or s respectively)

ΔL End-shortening of beam-column (or longitudinal)

ΔL^o End displacement in grillage

ΔL_i End-shortening of ith longitudinal

ΔP Load increment for plate/stiffener column

ΔP_i End thrust correction for grillage (constant end displacement case)

Δ_{ij} Deflection of ith longitudinal of grillage, at intersection with jth transversal

ε Longitudinal strain

ε_a Strain in extreme fibre of plate (at reference axis a-a)

ε_c Longitudinal strain at centroid of plate/stiffener combination

ε_o, ε_y Yield strain (ε_y on figures relating to Chapter 2)

ε_R Residual strain

ε_T Total strain in a cross-section element (i.e. including ε_R)

η, η_s Width of residual stress tension block as proportion of plate thickness (defined in Fig. 3.1); s denotes stiffener

θ_c Rotation of tangent to the initial deflection curve of beam-column, at the location of a cusp

λ	Column non-dimensionalised slenderness ratio ($= \frac{\ell}{r} \cdot \frac{1}{\pi} \sqrt{\sigma_o/E}$)
ξL	Accuracy for adjusting end-shortening in grillage with constant end displacement
ξP	Accuracy of ultimate load for plate/stiffener column
ξy	Accuracy of column deflections
σ	Longitudinal stress
σ_{cr}	Euler stress for plate/stiffener column
σ_m	Mean stress on the plate/stiffener column at collapse
σ_n	Nominal mid-plane compression flange plate stress in model calculated using gross section properties and simple beam theory (at mid-span for point load tests)
σ_o	Yield stress
σ_R	Average compressive residual stress in the plate
σ'_R	$= \sigma_R/\sigma_o$
σ_{RF}	Additional residual stress in the flange plate (as defined in Fig. 3.1); $\sigma'_{RF} = \sigma_{RF}/\sigma_o$
σ_{RS}	Residual stress in the tip of stiffener outstand; $\sigma'_{RS} = \sigma_{RS}/\sigma_o$
ϕ	Curvature
ϕ_r	Curvature at node r, due to applied loading
ϕ_{or}	Initial curvature at node r
χ_r	Component of function Y_r, relating to moment due to lateral forces, $(M_L)_r$
ψ	Effective width ratio for shear lag
ω_{sj}	Deflection of jth transversal of grillage at intersection with longitudinal at location s

Model No.	Cross section of model Dimensions, in.	Component	Nominal size, in	t^*, in	σ_o tonf/sq.in	E tonf/sq.in
1	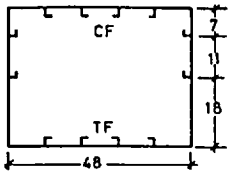	C F	3/16	0·195	16·0	13000
		T F	3/16	0·195	16·0	13000
		W	1/8	0·133	17·7	13900
		L S	2× 5/8 × 3/16 L	–	21·3	13000
		T S	3× 2 × 1/4 L	–	20·3	12600
		D	1/4	–	16·5	12900
2	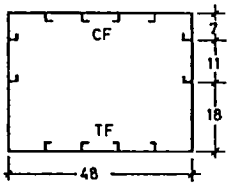	C F	3/16	0·192	19·3	13500
		T F	3/16	0·192	19·3	13500
		W	1/8	0·133	13·7	14000
		L S	2× 5/8 × 3/16 L	–	17·9	12400
		T S	3 × 2 × 1/4 L	–	20·1	12700
4	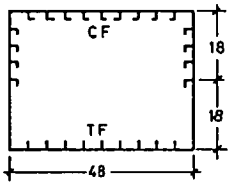	C F	3/16	0·198	14·3	13400
		T F	3/16	0·195	14·0	13500
		W	3/16	0·196	18·2	13900
		LS(CF)LS(W)	2× 5/8 × 3/16 L	–	18·6	12900
		LS(TF)	2× 1/4 Flat	–	19·7	12900
		TS	4× 2 1/2 × 1/4 L	–	19·7	13400
8	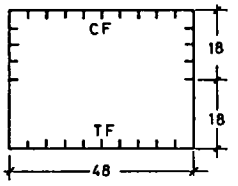	C F	3/16	0·186	17·9	13500
		T F	3/16	0·184	23·7	13500
		W	1/8	0·125	16·3	14000
		L S	1 1/2 × 1/4 Flat	–	20·2	13600
		T S	3 × 1/4 Flat	–	19·0	13500
9	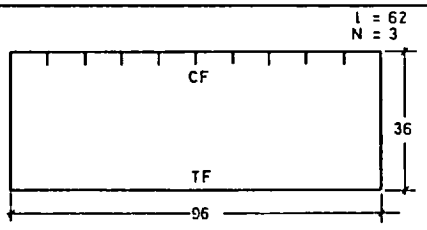	C F	3/16	0·192	21·6	13300
		T F	1/4	0·268	20·4	13900
		W	1/2	0·500	18·0	13500
		L S	2 3/4 × 5/16 Flat	0·312	18·5	13300
		T S	5× 3 × 3/8 L	–	18·7	13200
10	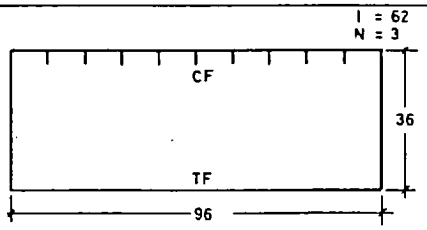	C F	3/16	0·194	21·7	13400
		T F	1/4	0·242	22·0	13700
		W	1/2	0·500	18·0	13500
		L S	2 3/4 × 5/16 Flat	0·312	18·5	13300
		T S	5 × 3 × 3/8 L	–	18·7	13200

TF Tension flange
W Web
D Diaphragm
l Spacing of cross-girders
C F Compression flange
L S Longitudinal stiffener
T S Transverse stiffener
LS(CF) Longitudinal stiffener on compression flange
LS(TF) Longitudinal stiffener on tension flange
LS(W) Longitudinal stiffener on web
N Number of bays along span of model.
t^* Measured thickness

Table 2.1
Principal Dimensions of Models and Properties of Materials

Model	Type of Test	Critical Components	b/t or b/t_w+	ℓ/r†	α	d/t_s	h_f/r	h_s/r
1	Point Load	(a) Largest web panels (b) Compression flange plate panels	135.3 48.8	53.8	0.25	-	0.60	3.21
2	Pure bending	Compression flange plate panels	49.6	53.6	0.25	-	0.60	3.19
4	Pure bending	Compression flange stiffeners*	24.0	44.7	0.49	-	0.74	2.43
8	Pure bending	Compression flange stiffeners*	25.6	114.5	0.42	6	0.76	2.96
9	Point load	Compression flange plate panels and stiffeners*	49.3	75.4	0.47	8.8	0.69	2.89
10	Pure bending	Compression flange plate panels and stiffeners*	48.8	75.6	0.47	8.8	0.69	2.90

*Stiffener considered as the flange plate and longitudinal stiffener acting together.

†Slenderness ratio for plate/stiffener column with the flange plate considered to be fully effective.

+t_w - thickness of web plate.

Table 2.2 Critical Components of the Models and Relevant Parameters

Model	Panel	Average Stiffener Initial Deflection in Panel	Maximum Stiffener Initial Deflection in Model	Maximum Plate Panel Initial Deflection in Model	Average Longitudinal Residual Strain* μstrain	Average Transverse Residual Strain* μstrain	Fabrication Tolerances (Design Rules)	
							Plate Panel Initial Deflection	Stiffener Initial Deflection
1	D-I'	+ ℓ/3100	+ ℓ/1550	b/380	-150	-415	b/70	+ ℓ/900 (Towards Stiffener Outstand)
	I'-O	- ℓ/7150	- ℓ/1630					
2	A-C	- ℓ/2000	+ ℓ/2280	b/330	-250	-	b/70	
	C-I	- ℓ/5280						
	I-O	- ℓ/3200						
	O-U	- ℓ/9250	- ℓ/1450					
	U-W	- ℓ/1680						
4	A-C	- ℓ/1050	+ ℓ/690	n.m.	-600	-	-	- ℓ/1200 (Away from Stiffener Outstand)
	C-I	+ ℓ/1950						
	I-O	+ ℓ/2280						
	O-U	+ ℓ/4920	- ℓ/510					
	U-W	- ℓ/660						
8	A-E	+ ℓ/1770	+ ℓ/930	n.m.	-460	-15	-	
	E-I	+ ℓ/1500						
	I-M	- ℓ/950	- ℓ/610					
9	A-E	+ ℓ/15900	+ ℓ/2700	b/360	-275	+25	b/75	
	E-Q	- ℓ/7560	- ℓ/1475					
	Q-U	+ ℓ/23850						
10	A-E	+ ℓ/4950	+ ℓ/925	b/315	-255	+45	b/75	
	E-Q	- ℓ/1480	- ℓ/1000					
	Q-U	+ ℓ/2760						

*Residual strain in plate panels (negative sign indicates compression)

n.m. not measured.

b = spacing of longitudinal stiffeners.

ℓ = spacing of cross-girders.

Table 2.3 Initial Imperfections in the Compression Flanges of the Models

λ	$\Delta_o' = +1/400$			$\Delta_o' = -1/600$		
	$(\frac{P_m}{P_o})^*$	$(\frac{P_m}{P_o})^\dagger$	$\frac{P_m^*}{P_m\dagger}$	$(\frac{P_m}{P_o})^*$	$(\frac{P_m}{P_o})^\dagger$	$\frac{P_m^*}{P_m\dagger}$
0.33	0.962	0.972	0.99	0.877	0.903	0.97
0.65	0.910	0.914	0.99	0.743	0.755	0.98
0.98	0.742	0.746	0.99	0.552	0.561	0.98
1.10	0.439	0.441	0.99	0.388	0.392	0.99

*Maximum strength as obtained by Virdi[47].

†Maximum strength from present analysis.

Note:- The maximum strength values given were obtained using the following data:

β = 2.468 (stress-strain curves assumed to be bilinear for both, the plate and stiffener)

α = 0.3

d/t_s = 8

σ_R = 0

σ_o = 340 N/mm^2

E = 200700 N/mm^2

Table 3.1 Comparison Between Maximum Strength Values Given by Virdi[47] and those Obtained from Present Analysis

Model	Case	Single-Span Analysis			Test P_m/P_o	$\frac{(P_m)_{theory}}{(P_m)_{test}}$
		Δ_o, in	e, in	P_m/P_o		
1 (First Test)	a	+ℓ/3100	0	0.729	0.652	1.12
	b	+ℓ/3100	0.019	0.712		1.09
1 (Second Test)	c	+ℓ/1000†	0	0.712	0.652	1.09
	d	+ℓ/1000†	0.019	0.698		1.07
1 (Final Test)	e	+ℓ/470*	0	0.674	0.632	1.07
	f	+ℓ/470*	0.019	0.654		1.04

†Stiffener Initial Deflections for Second Test

*Stiffener Initial Deflections for Final Test

Table 4.1 Model 1. Experimental and Theoretical Strengths for the Compression Flange

Model	Case	Single-Span Analysis			Multi-Span Analysis		Test P_m/P_o	$\frac{(P_m)_{theory}}{(P_m)_{test}}$
		Δ_o, in	e, in	P_m/P_o	e, in	P_m/P_o		
2 Test 2A (5 Bays)	a	+ $\ell/2280^{\dagger}$	0	0.733	-	-	0.690	1.06
	b	+ $\ell/2280^{\dagger}$	0.019	0.707	-	-		1.02
	c	- $\ell/1680^{\dagger}$	0	0.732	-	-		1.06
	d	- $\ell/1680^{\dagger}$	0.019	0.740	-	-		1.07
	e	-	-	-	0	0.744		1.08
	f	-	-	-	0.019	0.741		1.07
2 Test 2B (3 Bays)	g	+ $\ell/580$	0	0.662	-	-	0.690	0.96
	h	+ $\ell/580$	0.019	0.647	-	-		0.94
	i	- $\ell/1430$	0	0.661	-	-		0.96
	j	- $\ell/1430$	0.019	0.701	-	-		1.01
	k	-	-	-	0	0.659		0.96
	l	-	-	-	0.019	0.646		0.94

†Maximum value of stiffener initial deflection

Stiffener initial deflections for Test 2B:- Panel C-I : $\Delta_o = -\ell/8000$ in

I-O : $\Delta_o = -\ell/1430$ in

O-U : $\Delta_o = +\ell/580$ in

Table 4.1b Model 2. Experimental and Theoretical Strengths for the Compression Flange

Model	Case	Single-Span Analysis			Multi-Span Analysis		Test P_m/P_o	$\frac{(P_m)_{theory}}{(P_m)_{test}}$
		Δ_o, in	e, in	P_m/P_o	e, in	P_m/P_o		
4	a	+ ℓ/1950	0	0.964	-	-	0.856	1.13
	b	+ ℓ/1950	0.028	0.946	-	-		1.11
	c	- ℓ/660	0	0.780	-	-		0.91
	d	- ℓ/660	0.028	0.832	-	-		0.97
	e	-	-	-	0	0.808		0.94
	f	-	-	-	0.028	0.828		0.97
8	a	+ ℓ/1500	0	0.471	-	-	0.541	0.87
	b	+ ℓ/1500	0.012	0.455	-	-		0.84
	c	- ℓ/950	0	0.426	-	-		0.79
	d	- ℓ/950	0.012	0.447	-	-		0.83
	e	-	-	-	0	0.470		0.87
	f	-	-	-	0.012	0.482		0.89

Table 4.1c Models 4 and 8. Experimental and Theoretical Strengths for the Compression Flanges

Model	Case	Single-Span Analysis (Span E-Q)		Multi-Span Analysis		Test P_m/P_o	$\frac{(P_m)_{theory}}{(P_m)_{test}}$
		e, in	P_m/P_o	e, in	P_m/P_o		
9	a	0	0.720	-	-	0.740+	0.97
	b	0.038	0.663	-	-		0.90
	a	0	0.720	-	-	0.689*	1.04
	b	0.038	0.663	-	-		0.96
10	a	0	0.638	-	-	0.763	0.84
	b	0.039	0.672	-	-		0.88
	c			0	0.680		0.89
	d			0.039	0.651		0.85

Δ_o-values after initial tests:-

Model 9, Panel E-Q: $+\ell/6900$ in
Model 10, Panel A-E: $+\ell/990$ in
E-Q: $-\ell/420$ in
Q-U: $+\ell/960$ in

+Value obtained from simple bending theory with webs assumed to be elastic

*Value obtained by considering the webs to be partially plastic at mid-span (see test, Section 4.3.5)

Table 4.1d Models 9 and 10. Experimental and Theoretical Strengths for the Compression Flanges.

Model	P_m/P_o			
	BS153[1]	IDAR[69]	Present Theory	Test
1 (First Test) 1 (Final Test)	0.578	0.632	0.712 0.654	0.652 0.632
2 (Test 2A) 2 (Test 2B)	0.625	0.752	0.741 0.646	0.690 0.690
4	0.784	0.559	0.828	0.856
8	0.408	0.403	0.482	0.541
9	0.542	0.514*	0.663	0.689
10	0.502	0.547*	0.651	0.763

*Values given by the Design Rules[32].

Table 4.2 Comparisons of Compression Flange Strengths

β (b/t)	$\sigma'_R = 0$				$\sigma'_R = 0.102$
	Out-of-plane Deformations, δ'_o				
		$0.044\beta^2$	$0.174\beta^2$	$0.349\beta^2$	$0.174\beta^2$
0.691 (20)	0	0.021	0.083	-	0.083
1.037 (30)	-	0.047	0.188	-	0.188
1.383 (40)	-	0.083	0.333	-	0.333
2.074 (60)	-	0.188	0.750	1.500	0.750

Notes: The b/t-ratios given in brackets are for mild steel
σ_R is non-dimensionalised using $\sigma_o = 245$ N/mm^2.

Table 5.1 Initial Imperfections of Plate Panels

β (b/t)	α = 0.2		α = 0.6		α = 1.0	
	h_f/r	h_s/r	h_f/r	h_s/r	h_f/r	h_s/r
0.691 (20)	0.704	3.940	0.786	2.640	0.899	2.278
1.037 (30)	0.651	3.985	0.758	2.654	0.877	2.287
1.383 (40)	0.619	4.011	0.741	2.662	0.864	2.292
2.074 (60)	0.578	4.041	0.721	2.671	0.848	2.298

Notes: The b/t-ratios given in brackets are for mild steel. The longitudinal stiffeners considered are flats with d/t_s ratios of 10.

Table 5.2 Extreme Fibre Distances (as ratios of radii of gyration) of Plate-Stiffener Columns

λ	σ_m/σ_o					
	$\Delta_o' = +1/750$			$\Delta_o' = -1/750$		
	$\sigma_R' = 0.102$ $\eta_s = 0$	$\sigma_R' = 0.102$ η_s, σ_{RS}' } Method 'A'	$\sigma_R' = 0.102$ η_s, σ_{RS}', σ_{RF}' } Method 'B'	$\sigma_R' = 0.102$ $\eta_s = 0$	$\sigma_R' = 0.102$ η_s, σ_{RS}' } Method 'A'	$\sigma_R' = 0.102$ η_s, σ_{RS}', σ_{RF}' } Method 'B'
0.33	0.700	0.698	0.671	0.625	0.627	0.573
0.77	0.657	0.655	0.621	0.538	0.548	0.487
1.10	0.527	0.527	0.506	0.414	0.423	0.384

Notes: The above strength values relate to $\beta = 2.074$, $\delta_o' = 0.750$ and $\alpha = 0.2$.

Method 'A' - A separately self-equilibrating residual stress pattern for the stiffener outstand (Fig. 3.1b): $\eta_s = 0.22$, $\sigma_{RS}' = 0.041$ (tensile).

Method 'B' - Residual stress pattern in which flange plate area is included for establishing equilibrium (Fig. 3.1c): $\eta_s = 2.5$, $\sigma_{RS}' = 0.105$, $\sigma_{RF}' = 0.038$.

Table 5.3 Effect of Stiffener Residual Stresses on Column Strength

λ	σ_m/σ_o			
	$\delta_o' = 0.174\beta^2$; $\sigma_R' = 0.102$			
	$\beta = 0.691$		$\beta = 1.383$	
	'Fixed' Centroid	'Effective' Centroid	'Fixed' Centroid	'Effective' Centroid
0.22	0.978	0.983	0.809	0.856
0.33	0.958	0.969	0.794	0.844
0.44	0.931	0.951	0.774	0.817
0.66	0.854	0.854	0.719	0.752
0.77	0.811	0.811	0.685	0.721
0.99	0.705	0.705	0.599	0.636
1.10	0.635	0.635	0.549	0.580

Notes: (i) The strength values shown are for one-span columns with $\alpha = 0.6$ and $\Delta_o' = +1/750$.

(ii) 'Fixed' centroid cases refers to the condition when the line of resultant thrust passes through the geometric centroid of the cross-section.

Table 5.4 Effect on Column Strength of Varying the Position of Line of Resultant Thrust

Model	Panel	Δ_o, in	P_m/P_o Single-Span Analysis	$\lvert\Delta_o\rvert_{eff}$, in	P_m/P_o Single-Span Analysis	P_m/P_o Multi-Span Analysis
2 Test 2A	U-W O-U	- ℓ/1680 - ℓ/9250	0.732 0.756	- ℓ/2385 + ℓ/5785	0.746 0.743	0.744
2 Test 2B	O-U I-O	+ ℓ/580 - ℓ/1430	0.662 0.661	+ ℓ/680 - ℓ/1330	0.668 0.658	0.659
4	U-W O-U	- ℓ/660 + ℓ/4920	0.780 0.971	- ℓ/840 + ℓ/2700	0.797 0.967	0.808
8	I-M I-M	- ℓ/950 - ℓ/950	0.426 0.426	- ℓ/1045 - ℓ/1160*	0.433 0.441	0.470
10	E-Q	- ℓ/420	0.638	- ℓ/590	0.670	0.680

Note: Except where indicated otherwise, $\lvert\Delta_o\rvert_{eff}$ calculated by the Design Rules[32] formulae.

*Effective stiffener deflection given by equation 5.4, with $C_1 = C_2 = 1/2$.

Table 5.5 Comparison Between Strength as Predicted by Multi-Span Analysis and Strength Obtained from Single-Span Analysis Using Effective Initial Stiffener Deflections

APPENDIX A

GRILLAGE ANALYSIS

A.1 GENERAL

In the method described in Chapter 3 the beam-column was assumed to be supported at the cross-girder positions by springs representing the stiffnesses of cross-girders. By idealising the stiffened plate in this manner, the analysis involved considering only one beam-column consisting of a stiffener and associated width of plating. If, however, the springs are replaced by discrete transverse beams consisting of transverse stiffeners and effective widths of flange plating, the stiffened plate can be represented by a grillage model as shown in Fig. A.1. Assuming that the transverse beam behaviour is known a treatment similar in principle to that used for the beam-column problem can be applied to the grillage model. In this appendix a solution procedure for the grillage analysis is described.

A.2 FURTHER ASSUMPTIONS

The following assumptions for the grillage analysis are additional to those already made in Chapter 3 for the beam-column analysis.

(1) There is no deflection or shear interaction between any adjacent beam-columns, that is, the effects of continuity of the plate are not considered.

(2) The effect of transverse stiffening can be allowed for by considering effective transverse beams, consisting of transverse stiffeners and some effective widths of flange plating. In general, the width of plating acting with the stiffener varies. For the analysis, any constant value of effective width may be adopted.

(3) Each beam-column is treated as a uniaxially compressed member with applied lateral loading, if any. The beam-columns along the longitudinal edges of the stiffened panel are analysed in the same way as those located inwards. Thus the analysis applies only to uniaxially compressed panels.

A.2 SOLUTION PROCEDURE

Figure A.1 shows a general grillage with N_L longitudinals and N_T transversals. The longitudinals are considered to be pin-ended and subjected to end thrust P in the same way as the isolated beam-columns analysed earlier. It is also assumed that the longitudinals are continuous over the transversals so that at intersections they deflect equally. The transversals are treated as either simply supported or encastré beams subjected to forces at the positions where they intersect with the longitudinal members. The response of the transverse beams can be considered on the basis of either small deflection elastic beam theory or elasto-plastic beam theory. In most practical stiffened plates subjected to end thrust only, the elastic theory may be adequate in representing the transverse beam behaviour. However, in those grillages where

directly applied lateral loading is significant plastic deformations of the transverse beams may need to be considered.

The steps involved in the computations are now given.

A.2.1 Equilibrium Shapes of the Longitudinals

After all initial data, that is, cross-sectional data, overall geometry, initial imperfections, etc. is specified, the values of forces at the intersections are guessed and equilibrium shapes of the N_L longitudinals subjected to end thrust P are determined separately in much the same way as for any laterally loaded isolated beam-column with no spring supports. The intersection reactions in this case are considered as the unknown quantities, the solutions for which are sought in the main iteration scheme. The process of establishing equilibrium shapes of the longitudinals forms a secondary iteration scheme. Thus, in the first stage of the solution, the values of forces $\{F_{ij}\}$ at the intersections are guessed and the corresponding deflections of the longitudinals at these locations, $\{\Delta_{ij}\}$ are found. The suffices i and j denote the intersection of ith longitudinal with jth transversal.

A.2.2 Deflections of Transverse Beams

For the present study, it is assumed that the transverse beams behave elastically and that their deflections under lateral loads can be evaluated from simple beam bending theory. The flexural rigidity of any transverse beam is computed with an assumed effective width of the flange plate and elastic value of Young's Modulus for the material. With the transverse beam properties

known, deflections of the transversals can be determined for any given loads and end support conditions.

In general, the deflections $\{\omega_{sj}\}$ for the jth transversal and intersection locations s are given by,

$$\{\omega_{sj}\} = - [f_{st}]_j \{F_{tj}\} \qquad s = 1, N_L \qquad t = 1, N_L \qquad \text{.... A.1}$$

where $\{F_{tj}\}$ are the intersection forces considered as equal in magnitude and opposite in direction to the forces assumed to act on the longitudinals, and $[f_{st}]_j$ is the flexibility influence coefficient matrix for transversal j.

The influence coefficients $(f_{st})_j$ for simply supported or encastré transverse beams of flexural rigidities $(EI_T)_j$ are given by the following relations:-

(a) Simply supported case:

For $t \geq s$,

$$(f_{st})_j = \frac{z_s (B - z_t)}{6B (EI_T)_j} \left[2B (B - z_s) - (B - z_t)^2 - (B - z_s)^2\right] \qquad \text{.... A.2}$$

where B and z are as defined in Fig. A.1. For $t < s$, the coefficients are found from symmetry of the matrix $[f_{st}]_j$.

(b) Encastré case:

For $t \geq s$,

$$(f_{st})_j = \frac{z_s^2 (B - z_t)^2}{6B (EI_T)_j} \left[3Bz_t - 3Bz_s z_t - (B - z_t) z_s\right] \qquad \text{.... A.3}$$

The note under equation A.2 applies in this case as well.

A.2.3 Deflection Compatibility at Intersections of Longitudinals with Transversals

From the deflections of longitudinals and transversals obtained as outlined in Sections A.2.1 and A.2.2 respectively, conditions of deflection compatibility may be written for the $N_L \times N_T$ intersections. Thus:

$$E_{ij}(F_{k\ell}) = \Delta_{ij} - \omega_{ij} = 0 \qquad \begin{matrix} i = 1, N_L \ (k = 1, N_L) \\ j = 1, N_T \ (\ell = 1, N_T) \end{matrix} \qquad \ldots\ldots \text{A.4}$$

where E_{ij} is an error function which depends on the assumed forces $\{F_{k\ell}\}$, and represents the lack of deflection compatibility at the intersection ij.

The above equations are similar in form to equations 3.22 and hence are also suitable for solution by the Newton-Raphson iterative numerical method described in Chapter 3. The unknowns in equations A.4 are the intersection forces $\{F_{k\ell}\}$ and consequently the Jacobian matrix in this case is evaluated about the assumed solution vector $\{\bar{F}_{k\ell}\}$. The correction terms $\{\delta\bar{F}_{k\ell}\}$ are then obtained by satisfying the following necessary conditions for convergence:

$$\{E_{ij}(\bar{F}_{k\ell})\} + \left[\frac{\partial E_{ij}(F_{k\ell})}{\partial F_{k\ell}}\right]_{F_{k\ell}=\bar{F}_{k\ell}} \cdot \{\delta\bar{F}_{k\ell}\} = 0 \qquad \ldots\ldots \text{A.5}$$

It should be noted that the above conditions relate to a general grillage which need not have any symmetry about its longitudinal or transverse axis. However, where symmetry does exist, advantage may be taken to simplify the computations involved.

In addition, since the process of establishing equilibrium shapes of the longitudinals does not involve springs but some assumed values of intersection forces, the Jacobian matrix of equation 3.25 is always a banded matrix in the grillage analysis. Hence by taking advantage of this feature, the computations can be further simplified.

A.3 ULTIMATE LOAD CAPACITY OF THE GRILLAGE

In the analysis procedure described in Sections A.2.1 to A.2.3, the grillage was assumed to be in uniform compression, that is, each longitudinal was subjected to end thrust P. Under such loading conditions, the ultimate load of the grillage is determined by following the procedure described in Section 3.3 for an isolated beam-column. The effects of any constant or proportional lateral loading on the grillage can be considered in the same way as for the beam-column.

By making some modifications in the computational procedure, it is possible also to obtain a solution for the uniform displacement condition, that is, when the loaded edges remain straight. The steps involved in such an analysis are described in the following section.

A.4 GRILLAGE WITH CONSTANT END DISPLACEMENT

When a grillage is loaded such that it undergoes constant end-shortening across its full width, the corresponding distribution of end thrust is not uniform. Thus, in the first instance, the analysis procedure described in earlier sections has to be

modified to cater for the varying end thrust. The solution for the constant end displacement condition is then achieved by systematically adjusting the end thrust on each longitudinal until the resulting end-shortenings of all longitudinals are the same.

As an initial step in the solution procedure, the end thrusts P_i (i=1, N_L) on the longitudinals are assumed and the equilibrium shape of the grillage is established. The total end-shortenings ΔL_i(i=1, N_L) which include in-plane displacements due to both curvature and axial straining, are then evaluated by using the expressions given in Appendix C.

The criteria adopted for adjusting the end thrusts so that the end-shortenings of all longitudinals approach the same value, are as follows:

(a) The total end thrust P^* on the grillage does not change. Thus, for any adjusted end thrust distribution P_i, we have,

$$P^* = \sum_{i=1}^{N_L} P_i \qquad \ldots\ \text{A.6}$$

(b) The end thrust correction ΔP_i for the ith longitudinal is given by,

$$\Delta P_i = S_i^L \, (\Delta L^o - \Delta L_i) \qquad \ldots\ \text{A.7}$$

where S_i^L is the slope of the end thrust versus end-shortening curve, in the vicinity of thrust P_i (Fig. A.2) and ΔL^o is the constant end displacement for the entire grillage.

Now, from equation A.6 it follows that the sum of all end thrust corrections must be zero, that is,

$$\sum_{i=1}^{N_L} \Delta P_i = \sum_{i=1}^{N_L} S_i^L (\Delta L^o - \Delta L_i) = 0 \qquad \ldots\ \text{A.8}$$

Hence,

$$\Delta L^o = \frac{\sum_{i=1}^{N_L} S_i^L \cdot \Delta L_i}{\sum_{i=1}^{N_L} S_i^L} \qquad \ldots\ \text{A.9}$$

With ΔL^o evaluated, the end thrust corrections are obtained from equation A.7 and the procedure of establishing the deflected shape of the grillage is repeated with the adjusted values of end thrusts P_i. In each cycle of this iterative procedure, ΔL^o is calculated. The constant displacement condition for the grillage is assumed to be achieved when the following condition is satisfied for each longitudinal:

$$\left[\frac{\Delta L^o - \Delta L_i}{\Delta L^o}\right] < \xi L \qquad \ldots\ \text{A.10}$$

where ξL is a specified small quantity representing the accuracy to which the end-shortenings of the longitudinals must be adjusted.

Having established one equilibrium condition for the grillage, the total thrust on the grillage is incremented and another equilibrium shape for constant end displacement is attempted. This incremental procedure is carried through until the ultimate load of the grillage is reached.

A.5 EXAMPLE OF GRILLAGE ANALYSIS

To illustrate the application of the grillage approach to the inelastic analysis of stiffened compression panels, a grillage representing panels E-I and I-M of the compression flange of Model 8 was chosen as an example. Details of the plate/stiffener geometry and data relating to the stress-strain behaviour of the plate panels were the same as those used in the beam-column analysis described in Chapter 4.

The grillage consisted of nine pin-ended beam-columns which were supported at their mid-spans by a transverse beam representing the cross-girder and a width of flange plating equal to B/8 on each side of the cross-girder. The initial deflections of the stiffened panels were assumed to be of sinusoidal form; the deflections were such that the average value for each bay was the value given in Table 2.3. The grillage was analysed for two conditions, namely, uniform end thrust and uniform end displacement conditions; Fig. A.3 shows the variation of end displacement (end-shortening) and of axial thrust across the flange width for these two cases. With constant axial thrust, the maximum load-carrying capacity of the grillage was reached when failure occurred in the central beam-column, that is, the beam-column with maximum initial curvature. However, when the axial thrusts on the beam-columns were adjusted so as to achieve uniform end-shortening, the load was redistributed from the inner beam-columns to the outer ones, and at collapse the axial thrust on the outermost member was 1.2 times that on the central one; the total load on the grillage in this case was 5 per cent more than that attained under constant axial thrust. The analysis indicated that the process of

adjusting axial thrusts to achieve similar end-shortenings (variation of less than one per cent) in the beam-columns, was generally accomplished within 3 iteration cycles.

Since in the grillage example considered the initial bow in the transverse direction was assumed to be of sinusoidal form, the initial deflections in the inner parts of the grillage were of greater magnitudes than the deflections assumed (in Chapter 4) in the analysis of the individual beam-column; hence the lower value for the ultimate capacity of the grillage. For the same reason, the example grillage does not adequately represent the test grillage of Model 8. Nevertheless, the example has helped test the method of analysis which could now be applied to study such aspects of stiffened panel behaviour as, forces on cross-girders, the influence of flexibility of the cross-girders and the behaviour of grillages subjected to combined axial thrust and lateral loading.

APPENDIX B

CURVATURE AT THE LOCATION OF A CUSP IN THE INITIAL SHAPE OF THE BEAM-COLUMN

Let the cusp in the initial shape of the beam-column occur at node r. Then for any assumed values of initial deflections, the slopes of the tangents to the right and left of node r, denoted by θ_c^R and θ_c^L respectively, may be determined from the following forward and backward difference formulae:

$$\theta_c^R = \frac{(-3y_{or} + 4y_{or+1} - y_{or+2})}{2\delta x} \quad .... \quad (B.1)$$

$$\theta_c^L = -\frac{(-3y_{or} + 4y_{or-1} - y_{or-2})}{2\delta x} \quad .... \quad (B.2)$$

where y_{or}, y_{or+1} ... are initial deflections at nodes r, r+1 ... etc.

Denoting the total rotation of the tangent to the initial deflection curve at r by θ_c $(= \theta_c^R - \theta_c^L)$, and considering continuity of rotations at the node, the applied curvature at r can be evaluated from the expression,

$$\phi_r = -\frac{(y_{r-1} - 2y_r + y_{r+1})}{\delta x^2} + \frac{\theta_c}{\delta x} \quad .... \quad (B.3)$$

APPENDIX C

END-SHORTENING OF THE BEAM-COLUMN

Let the end-shortening of the beam-column due to curvature alone be denoted by ΔL^B. Then, for small displacements, we have,

$$\Delta L^B = \frac{1}{2} \int_0^L \left(\frac{dy}{dx}\right)^2 \cdot dx \qquad \ldots\ (C.1)$$

The axial shortening of the beam-column, ΔL^C, under the action of applied loading is given by,

$$\Delta L^C = \int_0^L \varepsilon_c \cdot dx \qquad \ldots\ (C.2)$$

where ε_c is the strain at the centroid of the plate/stiffener assembly. Denoting the end-shortening due to initial curvature by ΔL^I, the total end-shortening of the beam-column under load is,

$$\Delta L = \Delta L^B + \Delta L^C - \Delta L^I \qquad \ldots\ (C.3)$$

For any given load, after the equilibrium shape of the beam-column has been established, ΔL can be evaluated using numerical integration procedures.

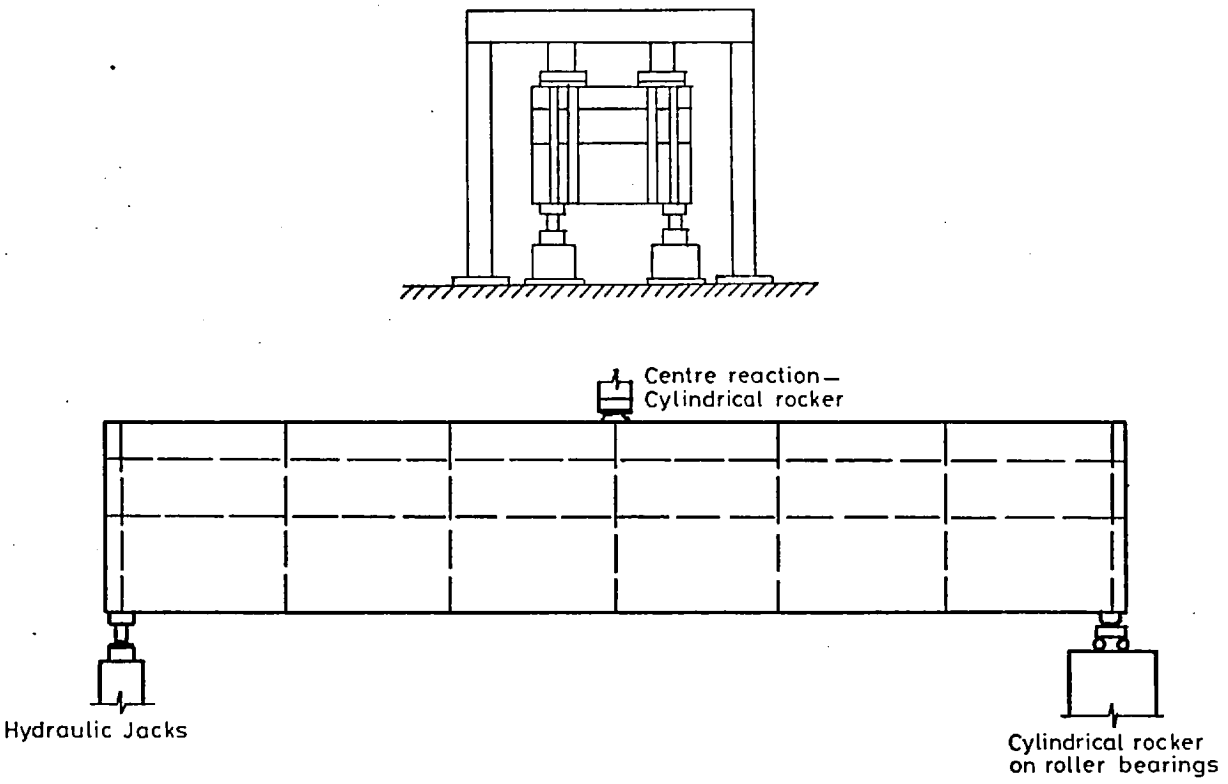

TEST RIG FOR MODEL 1. INSERT SHOWS TRANSVERSE LOCATIONS OF JACKS AND CENTRAL BEARINGS.

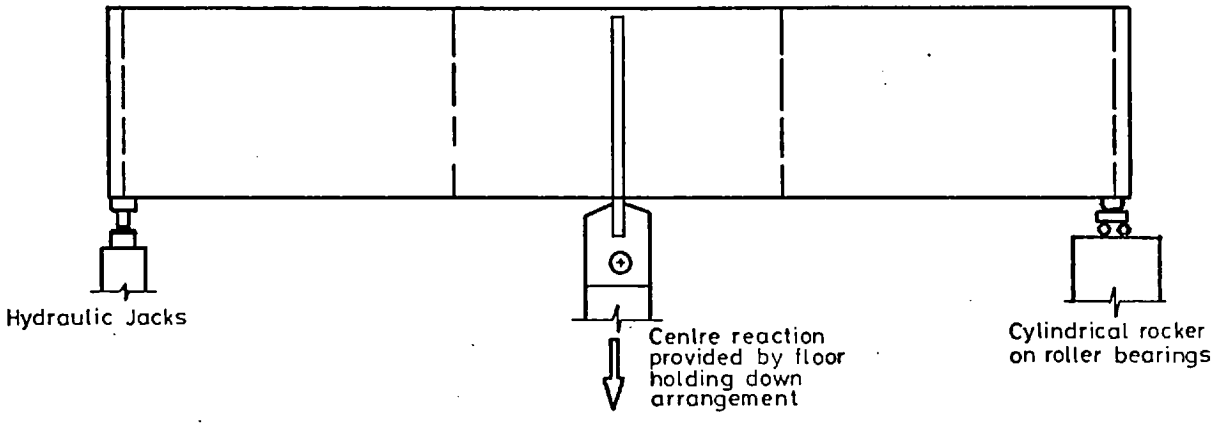

TEST RIG FOR MODEL 9 (SHEAR LAG TEST)

Fig. 2.1 Diagrams of Rigs used for Point Load Tests

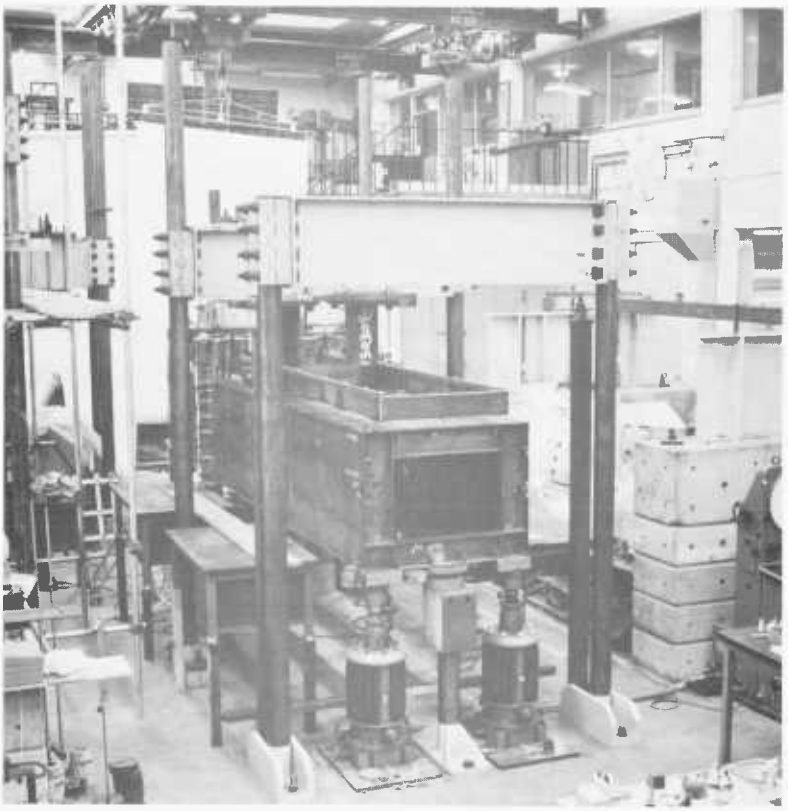

Fig. 2.2. Model 1 - a general view of the model and the test rig.

Fig. 2.3. Model 9 - showing the centre support arrangement.

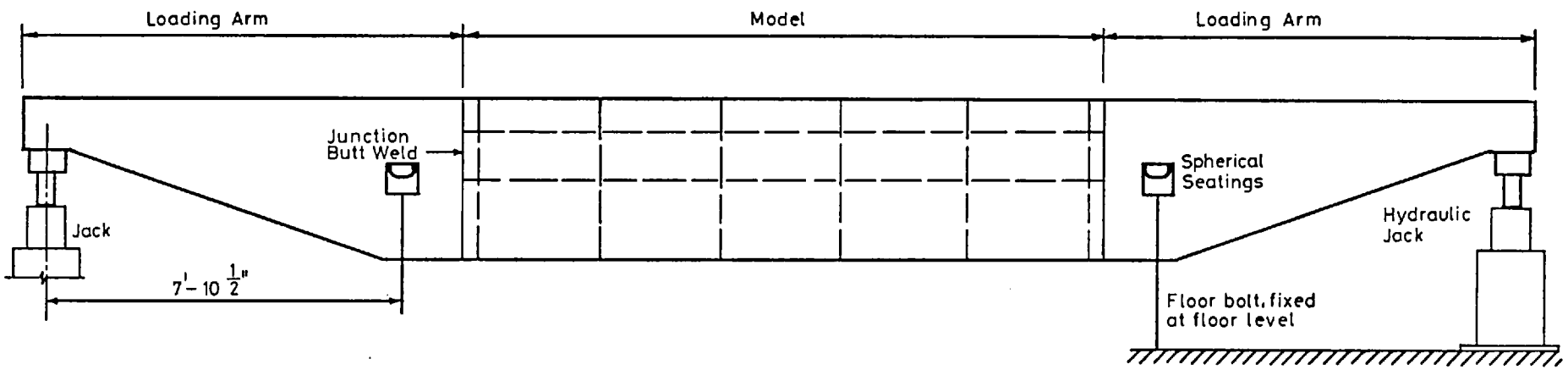

Fig. 2.4 Diagram of Rig used to Apply Pure Moment on Models 2,4 & 8

(Model 10 was loaded in a similar way, but the loading arms and the holding-down arrangement were modified details of which are given in Fig 2.6 Lever arm for Model 10 was 7'-9")

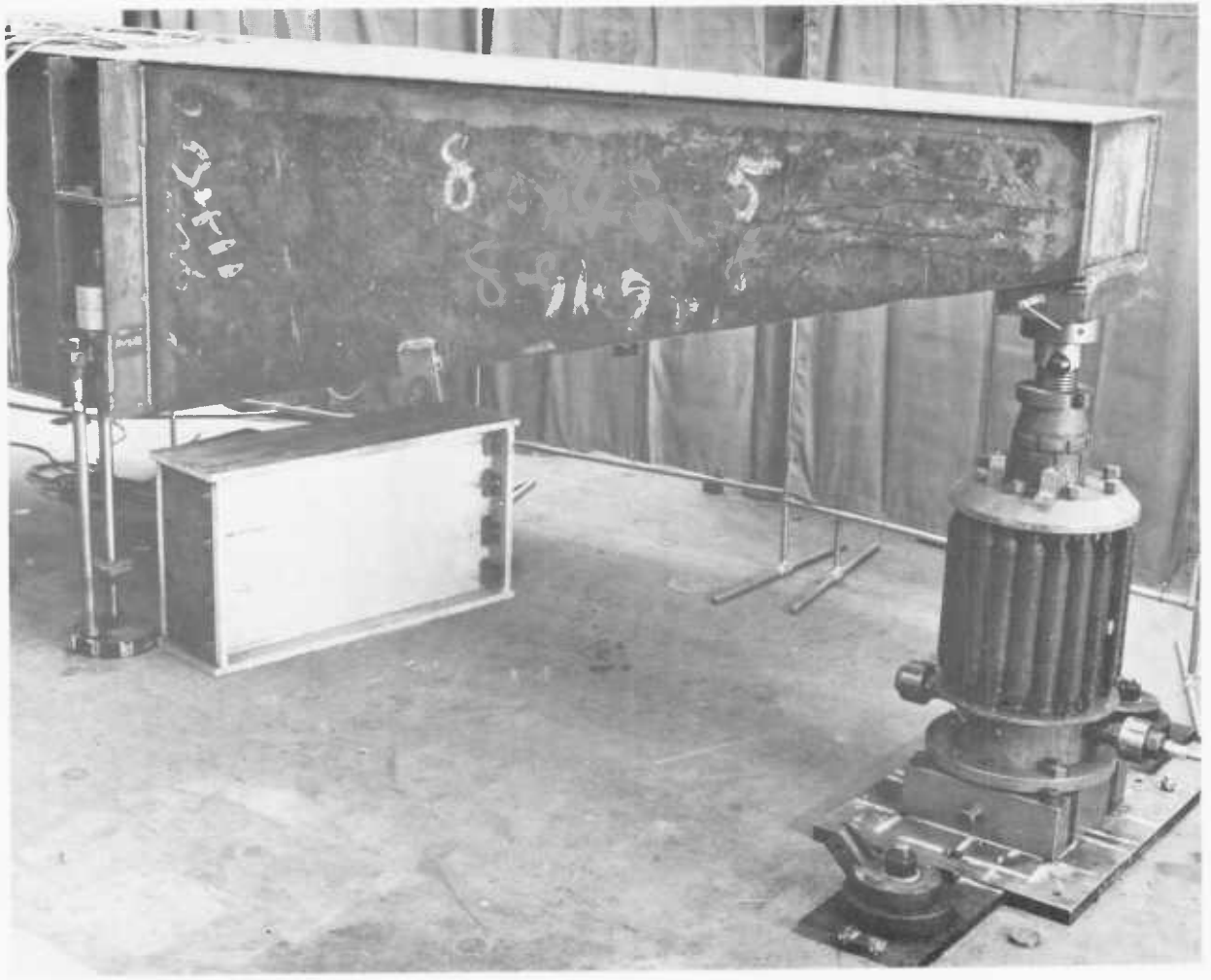

Fig. 2.5. End loading unit used for Models 2, 4 and 8. The 100 ton Amsler hydraulic jack and the holding-down bolt at model/loading unit junction can also be seen.

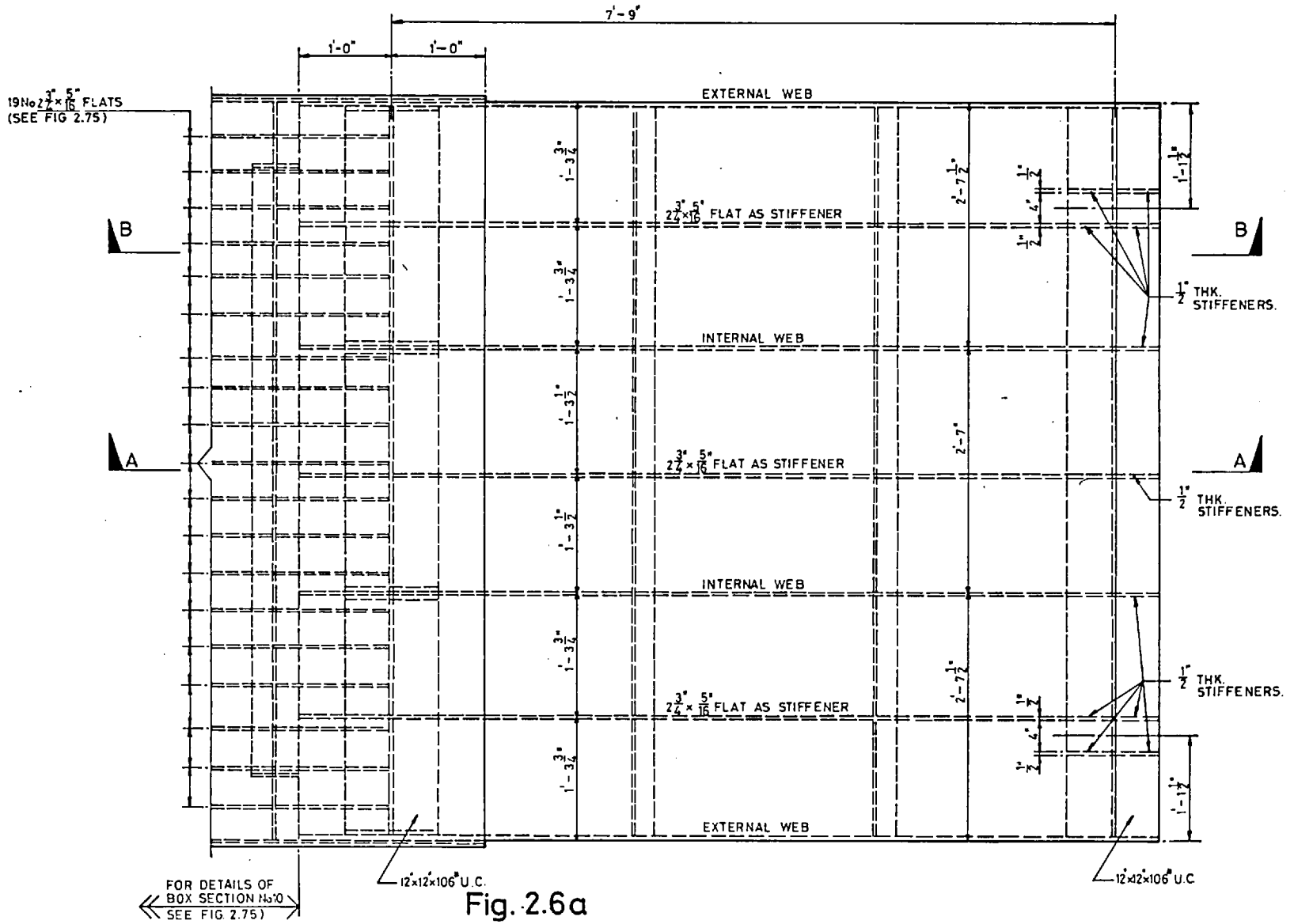

Fig. 2.6a

Model 10: Plan of End Loading Unit

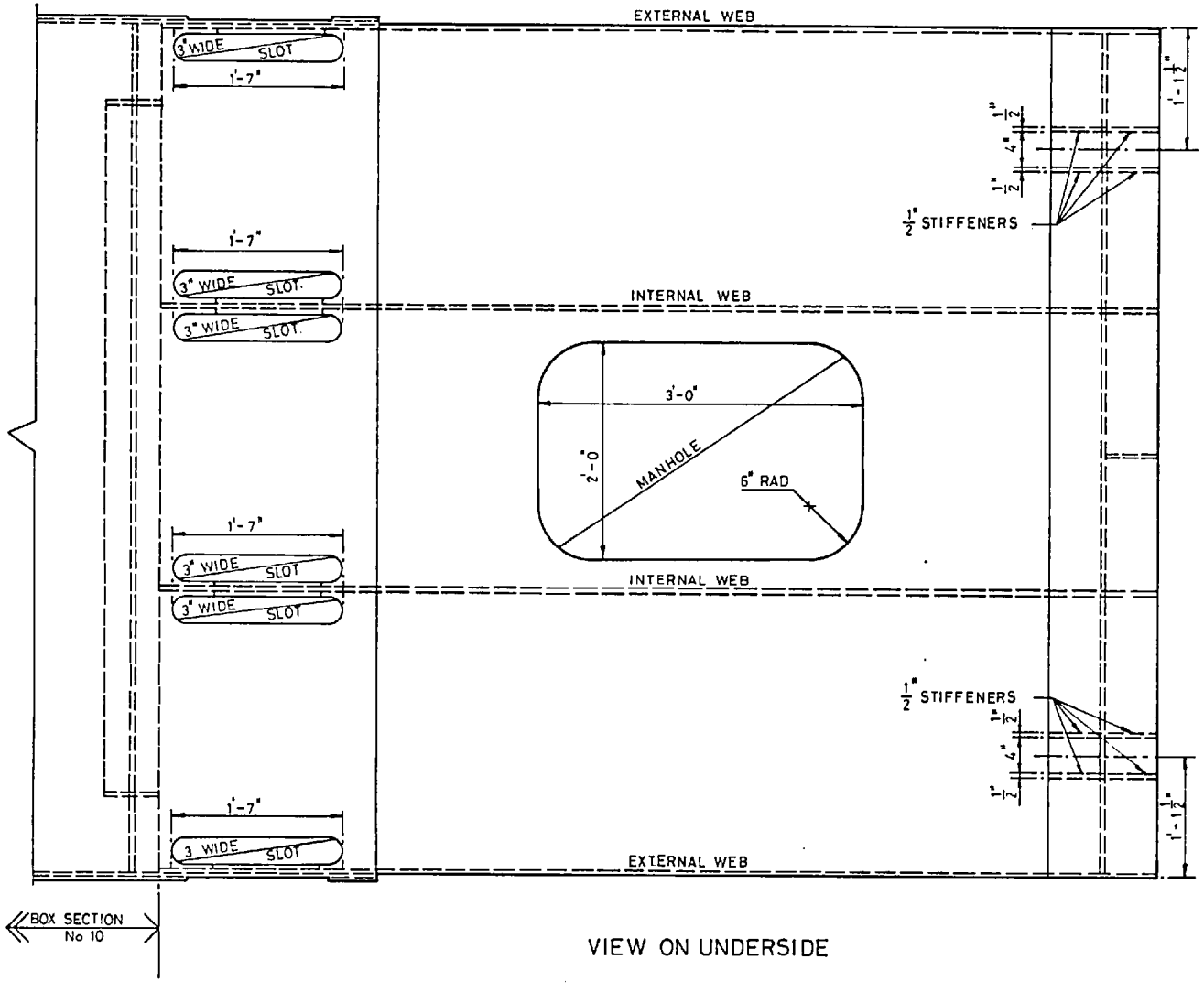

VIEW ON UNDERSIDE

Fig. 2.6b Model 10: End Loading Unit

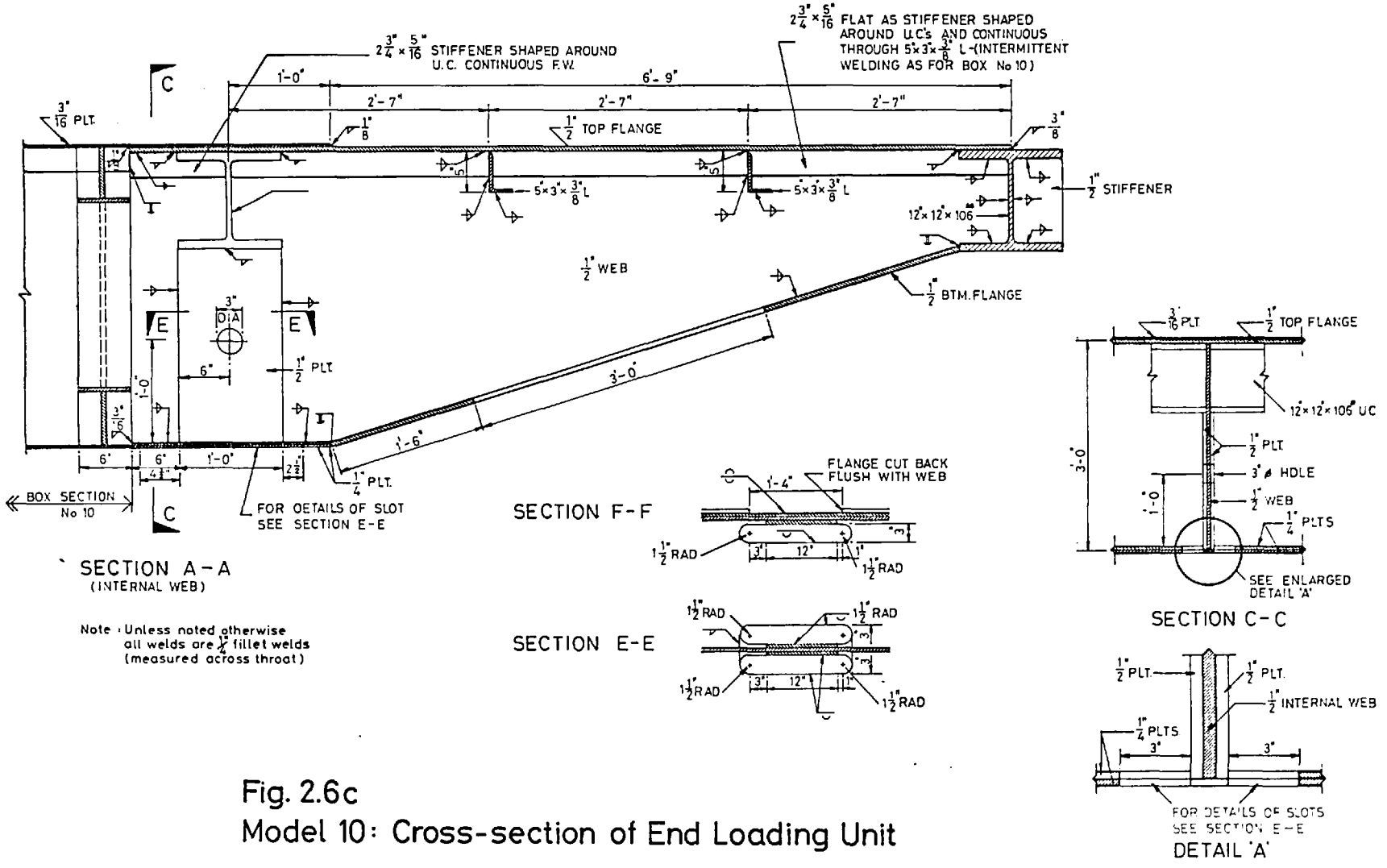

Fig. 2.6c
Model 10: Cross-section of End Loading Unit

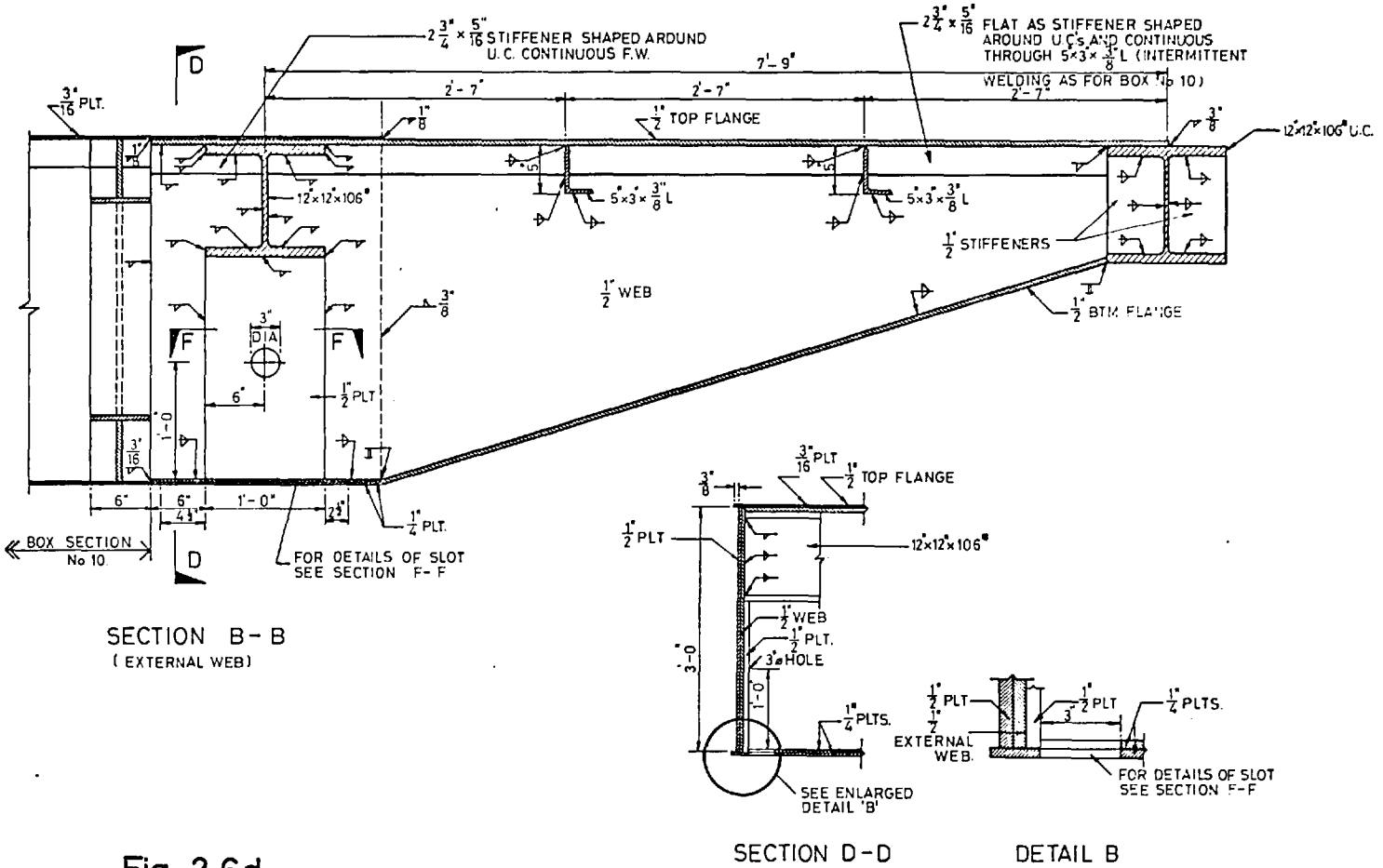

Fig. 2.6d
Model 10: Cross-section of End Loading Unit

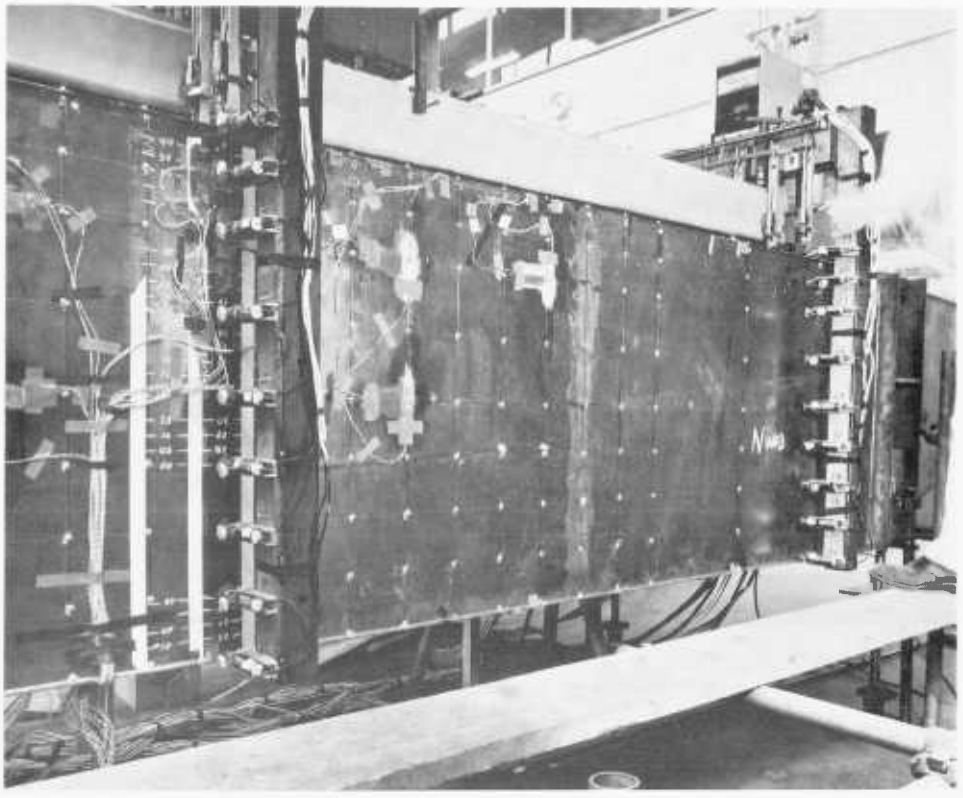

Fig. 2.7. A view of the deflection rig for Models 2, 4 and 8.

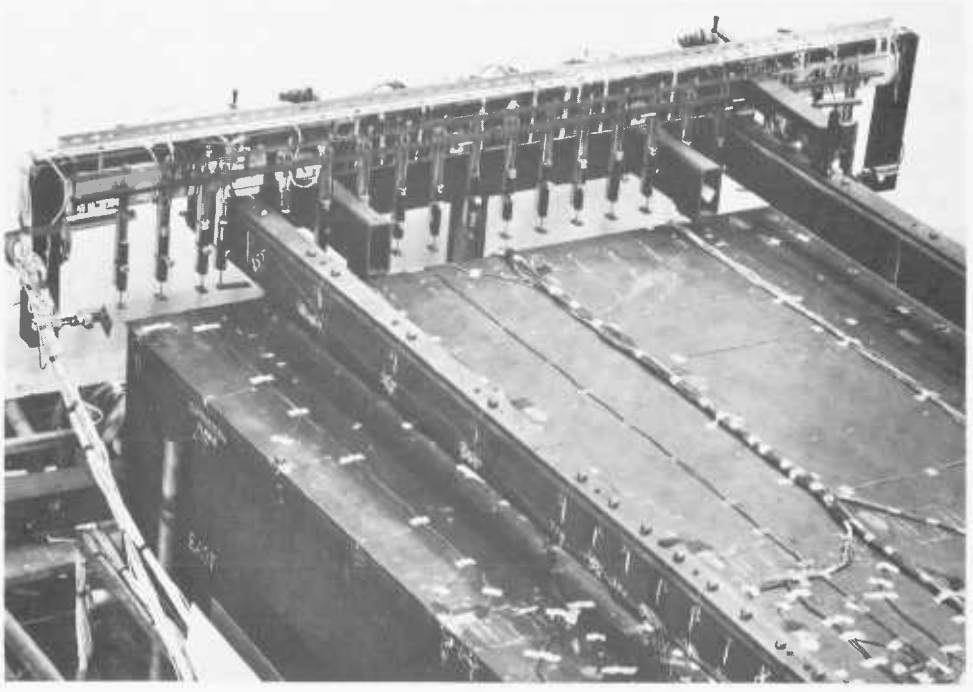

Fig. 2.8. A close-up view of the deflection frame used for Models 9 and 10.

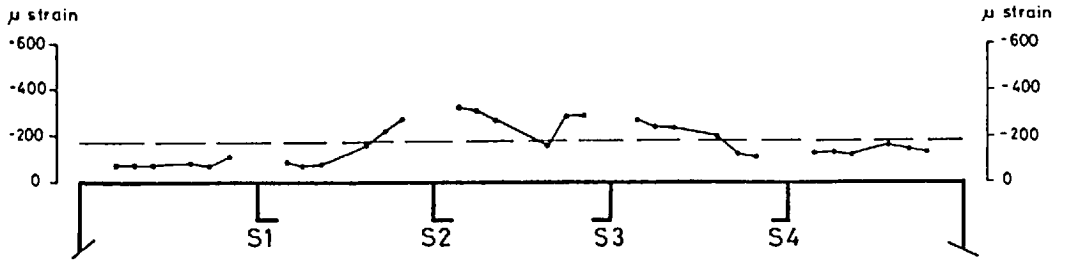

Model 1.

(Cross-section 8ins from Mid - span, between Sections H&I)

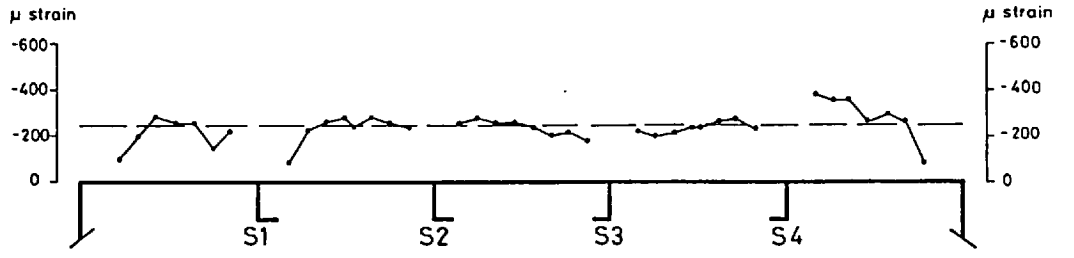

Model 2.
(mid-span)

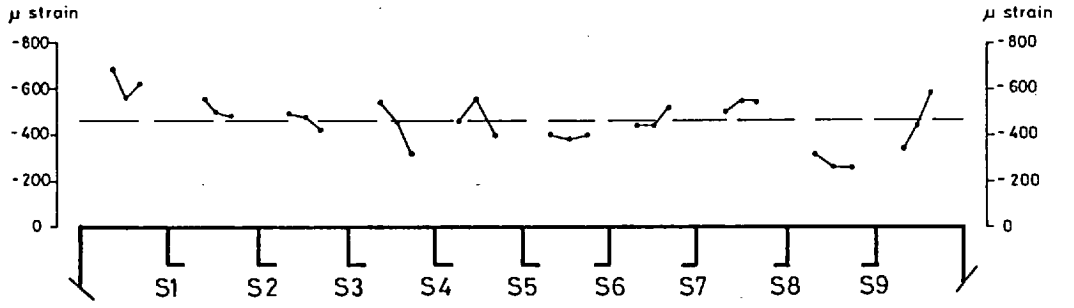

Model 4.
(mid-span)

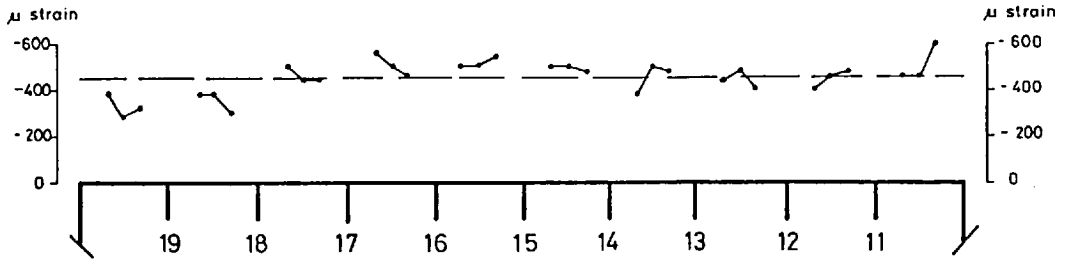

Model 8.

(Cross-section 12 ins from Cross - girder I, between Sections H & I)

KEY
• Mid-plate residual strain
——Average residual strain

Fig. 2.9a Measured Residual Strains

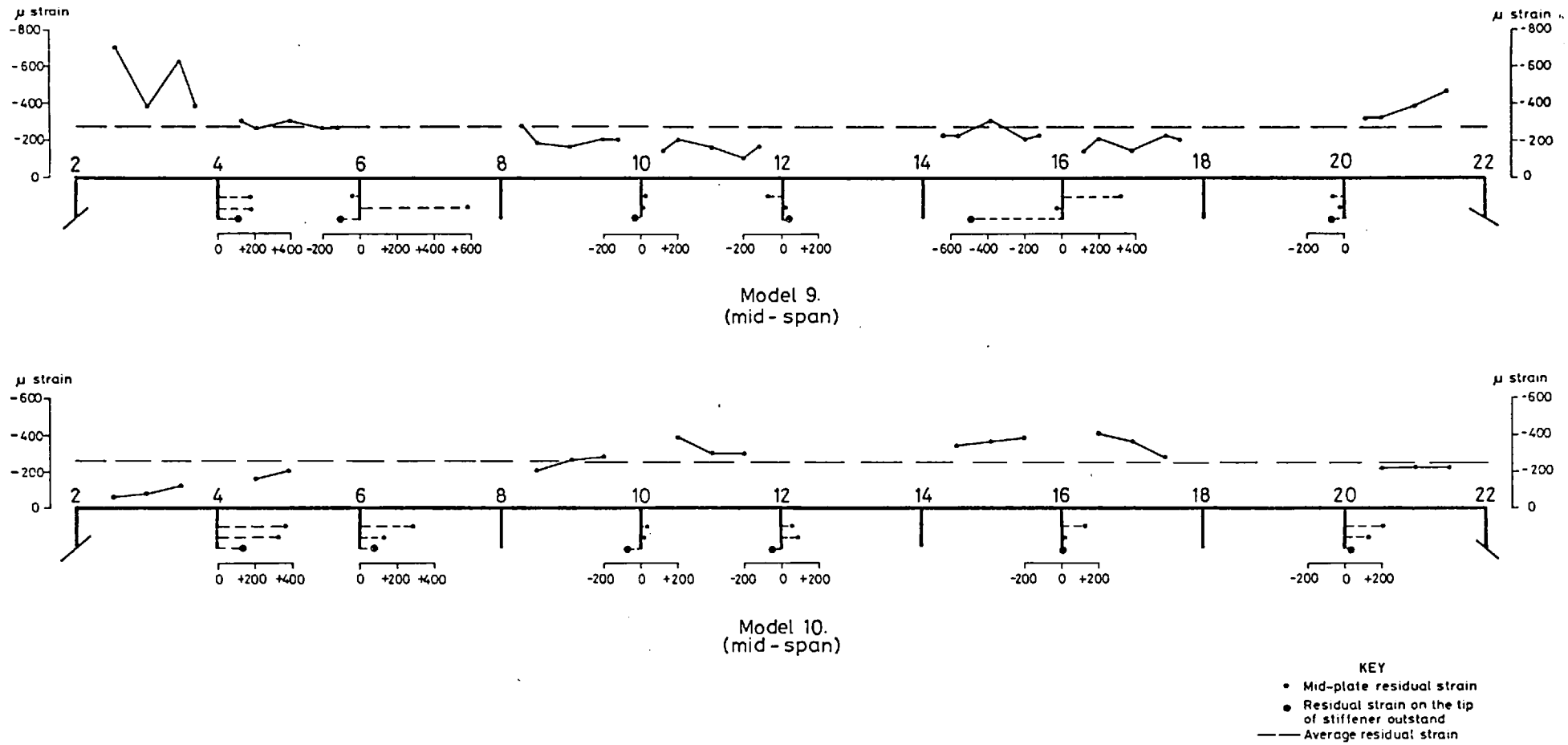

Fig. 2.9b Measured Residual Strains

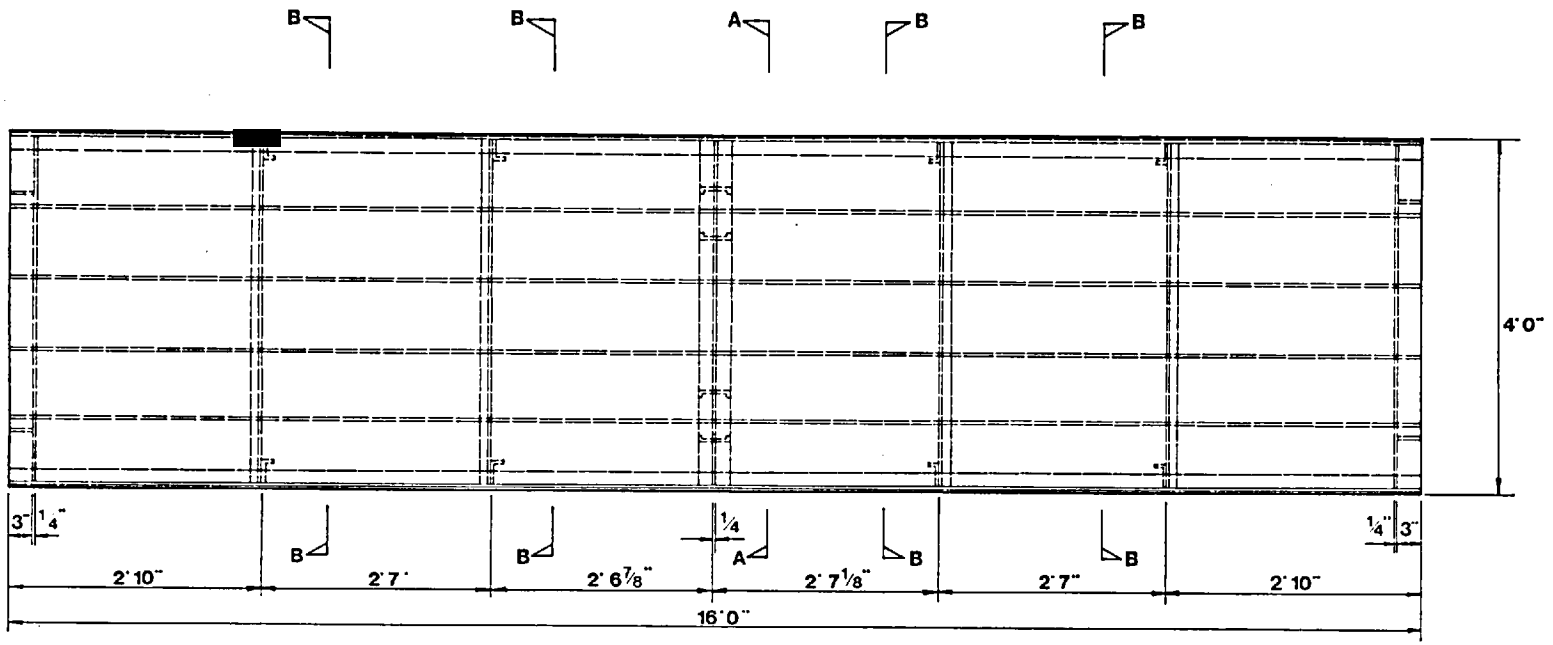

PLAN ON TOP

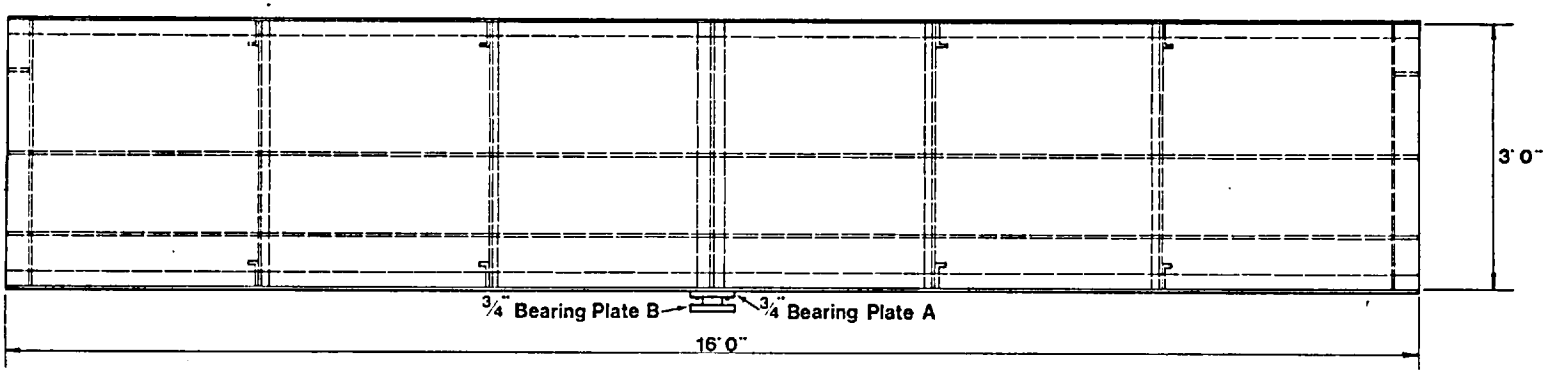

SIDE ELEVATION

Fig. 2.10a Model 1 : Plan and Elevation

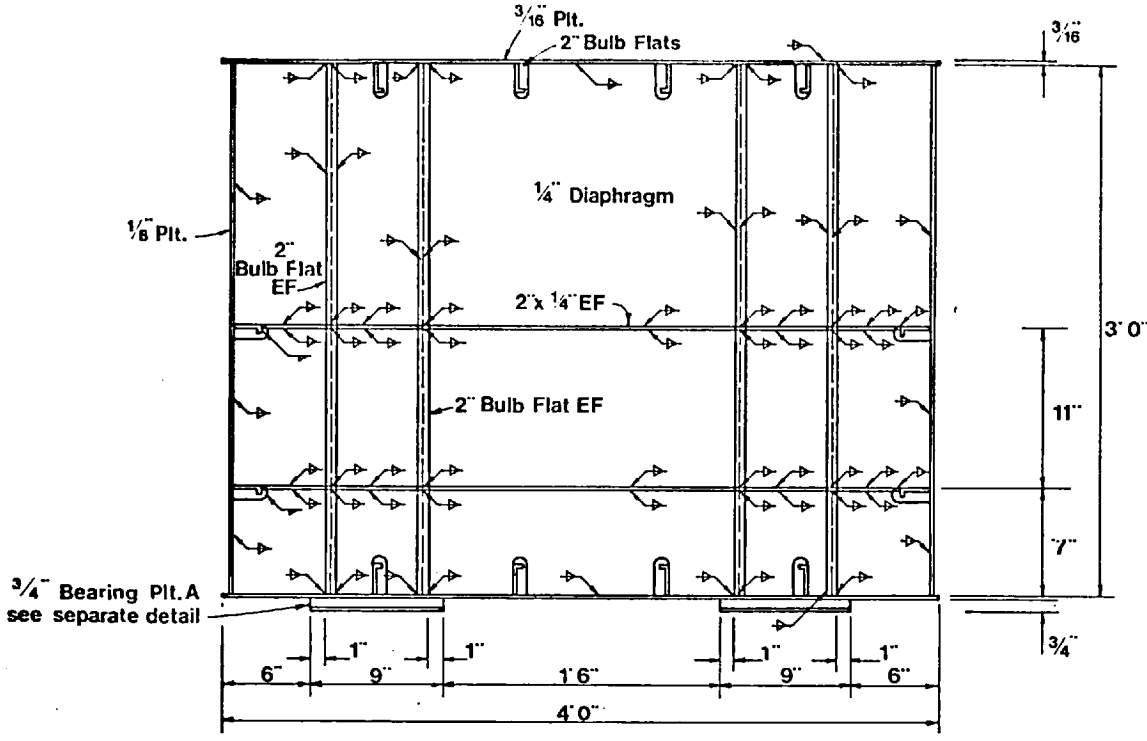

SECTION A-A

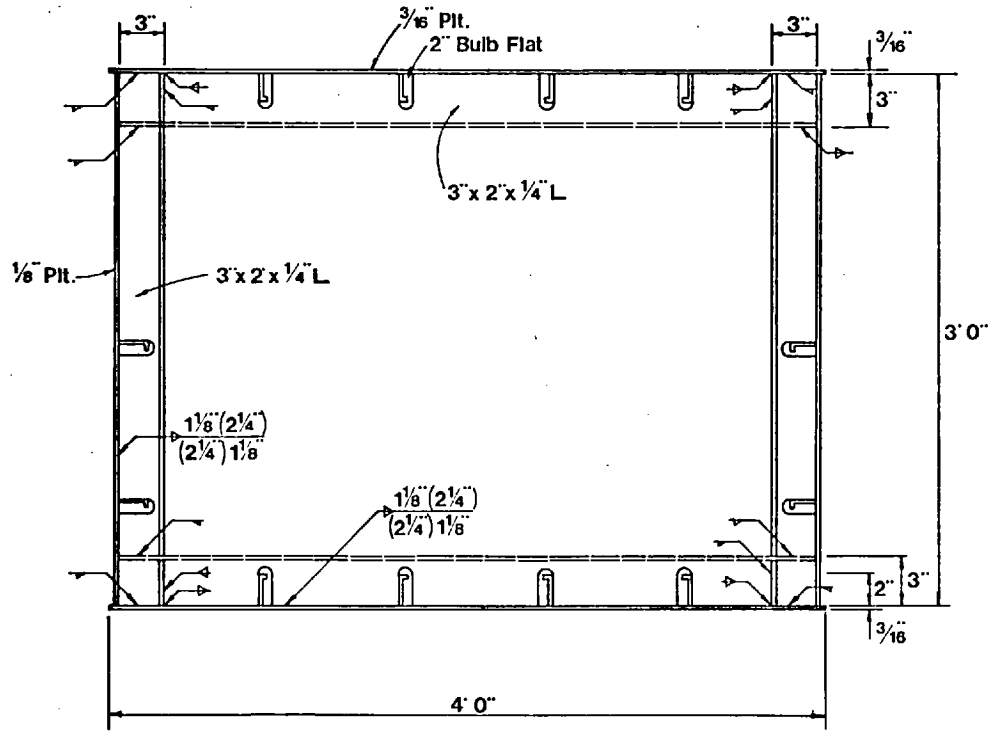

SECTION B-B

Fig. 2.10b
Model 1: Details of Diaphragm and Internal Cross-frame

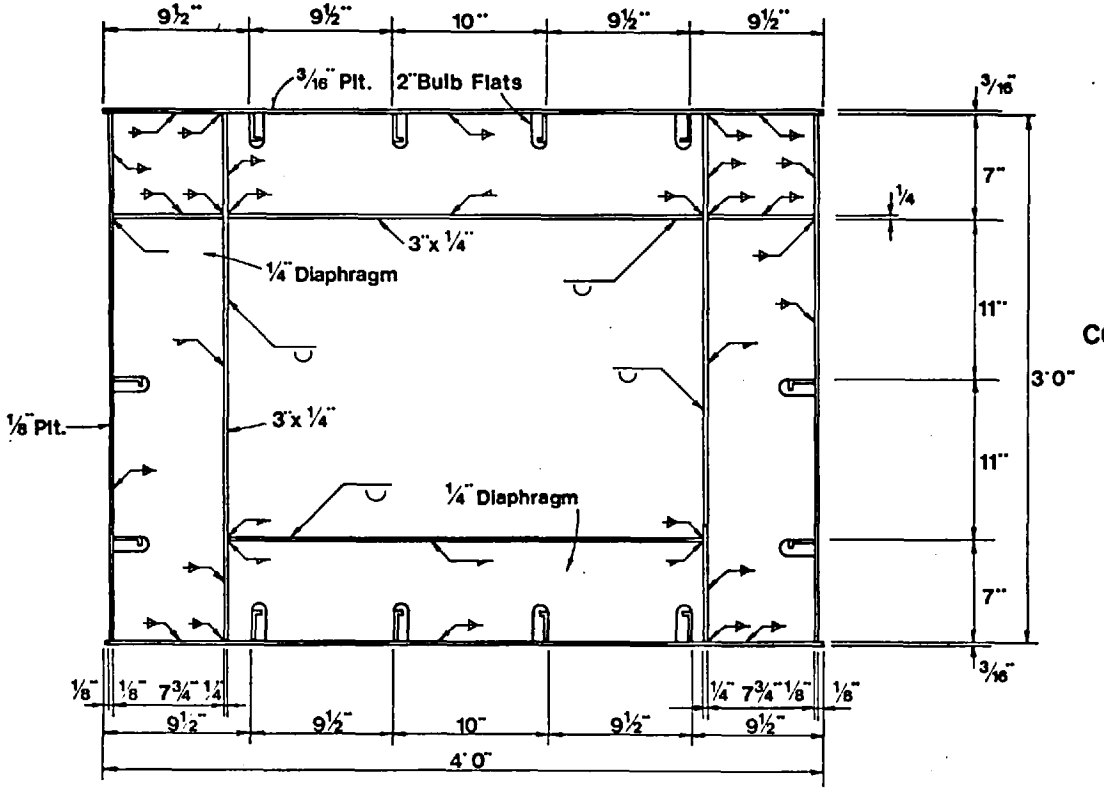

END ELEVATION

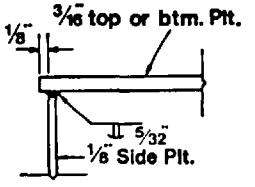

WELDING DETAIL AT CORNER OF BOX GIRDER

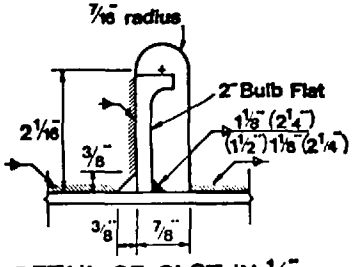

DETAIL OF SLOT IN 1/4" DIAPHRAGM AND 3½"x2½"x¼" ANGLE

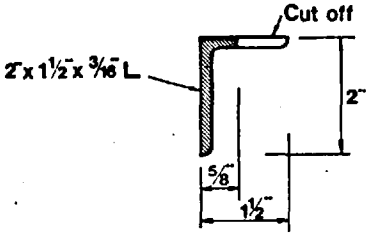

DETAIL OF 2" BULB FLAT

Fig. 2.10c Model 1: End Cross-frame

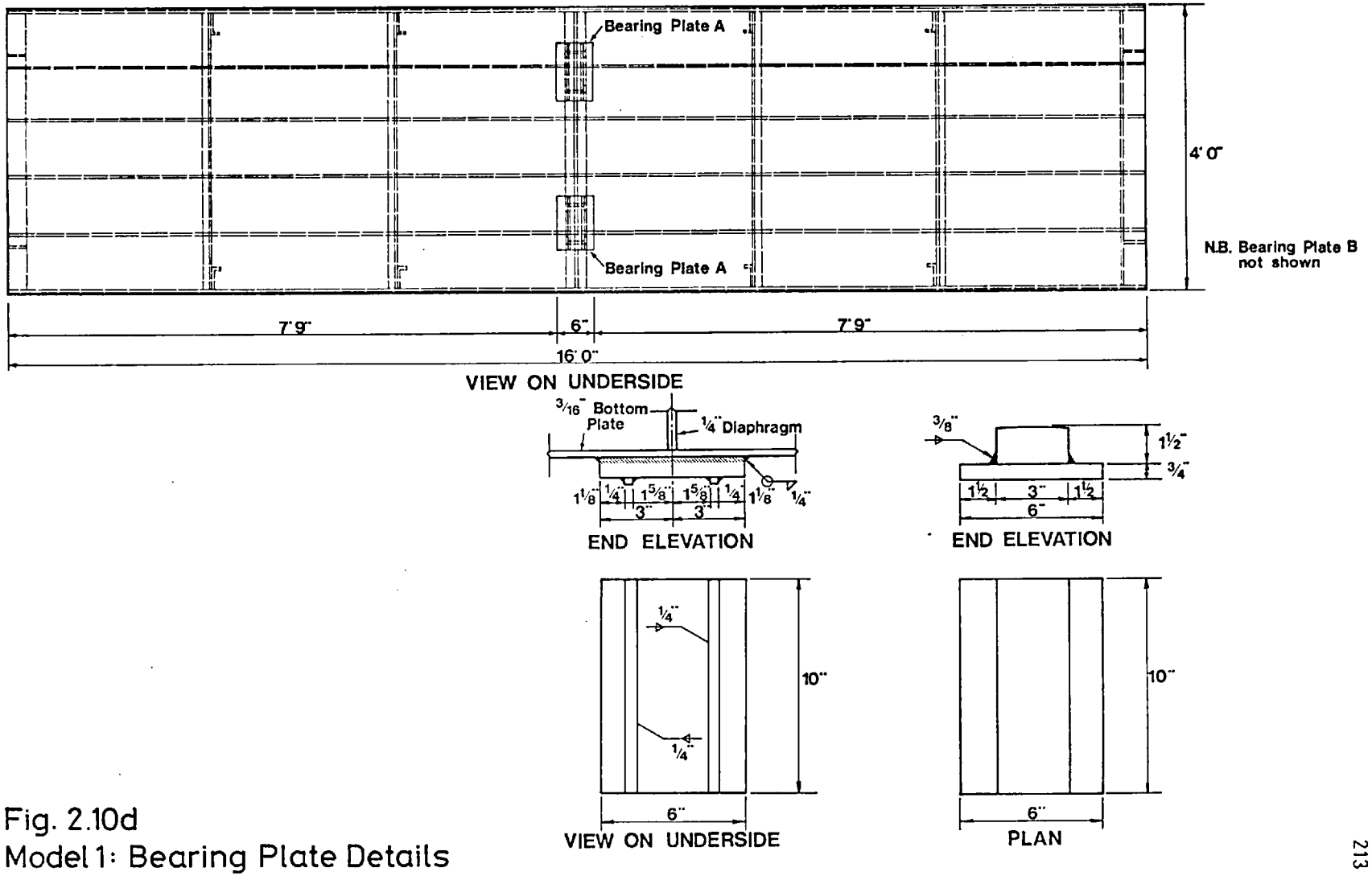

Fig. 2.10d
Model 1: Bearing Plate Details

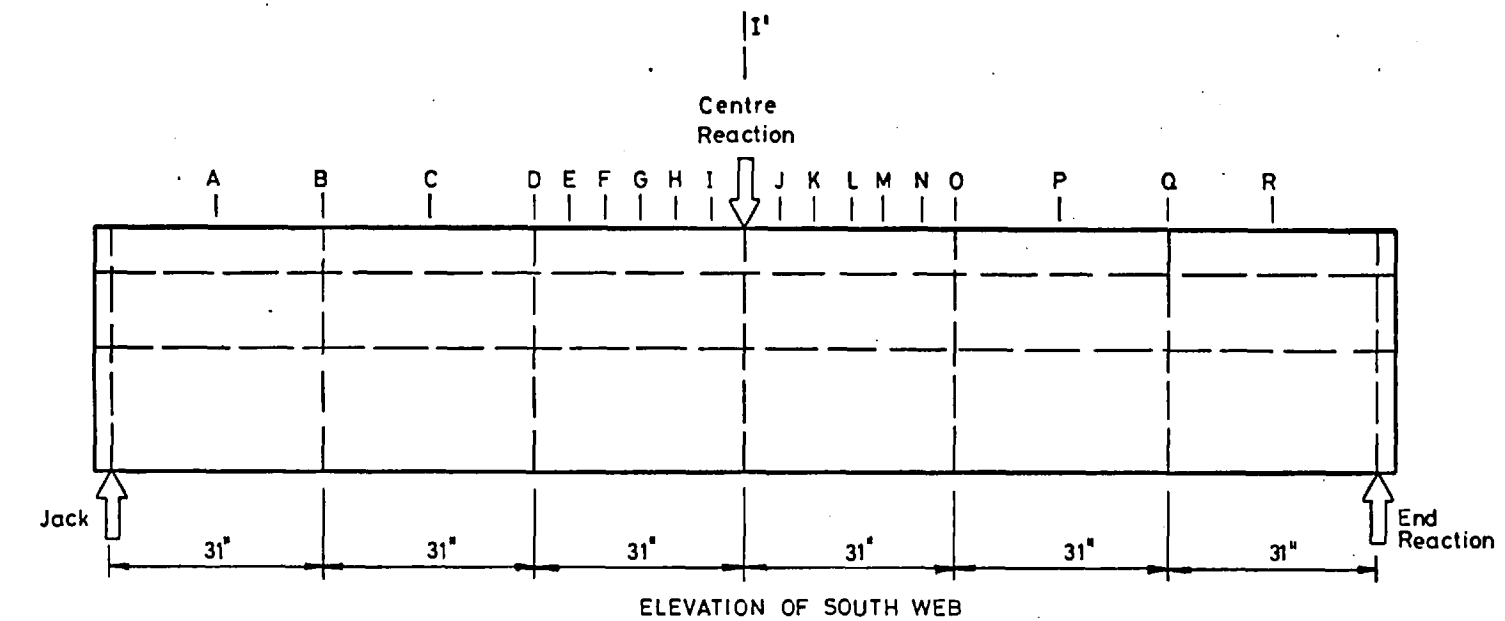

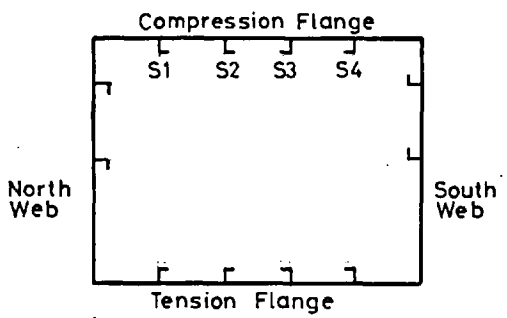

Note :
Letters A to R indicate locations along the model All grid lines within panels are at equal distances.

Fig. 2.11 Model 1: Details of Reference Grid

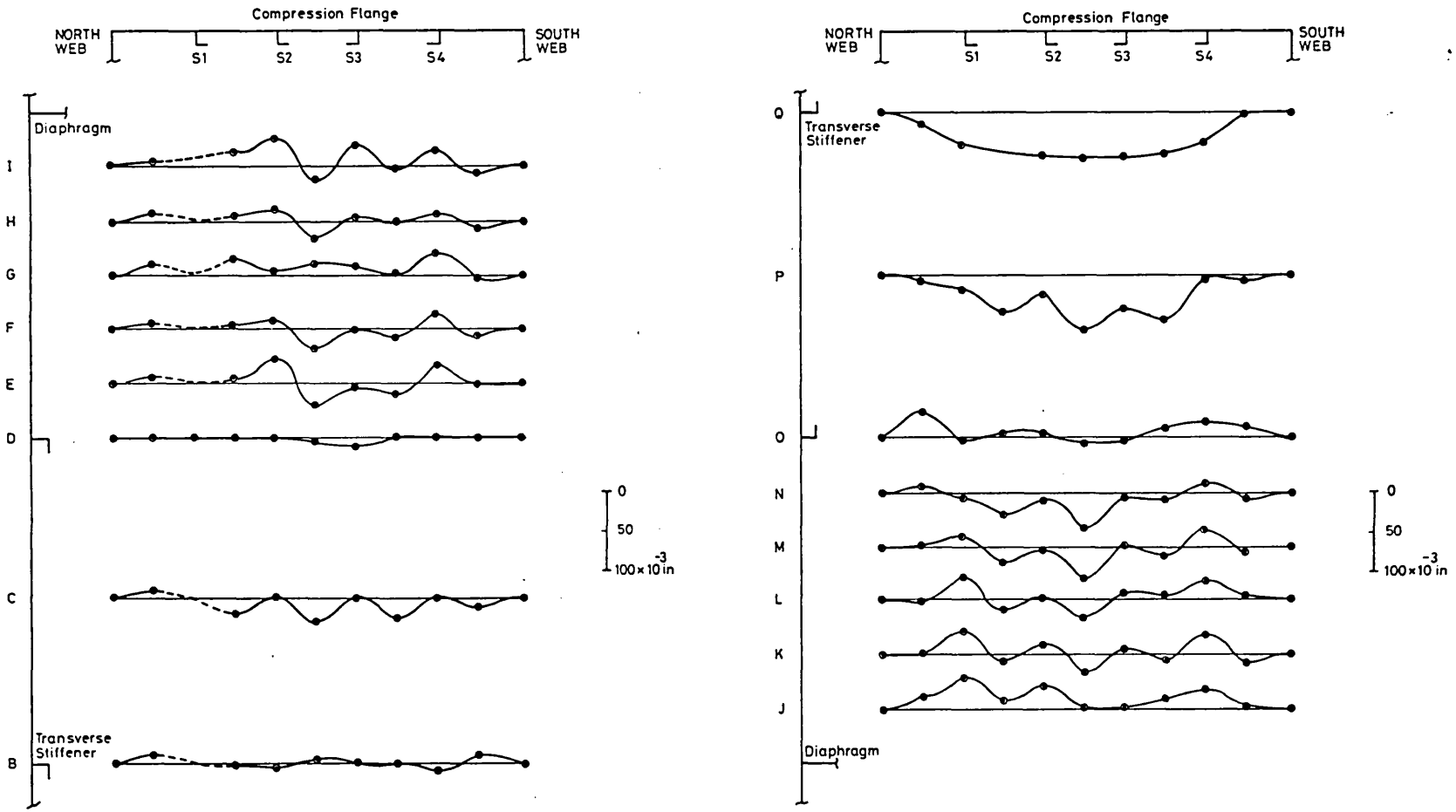

Fig. 2.12 Model 1: Transverse Initial Deflection Profiles of Compression Flange

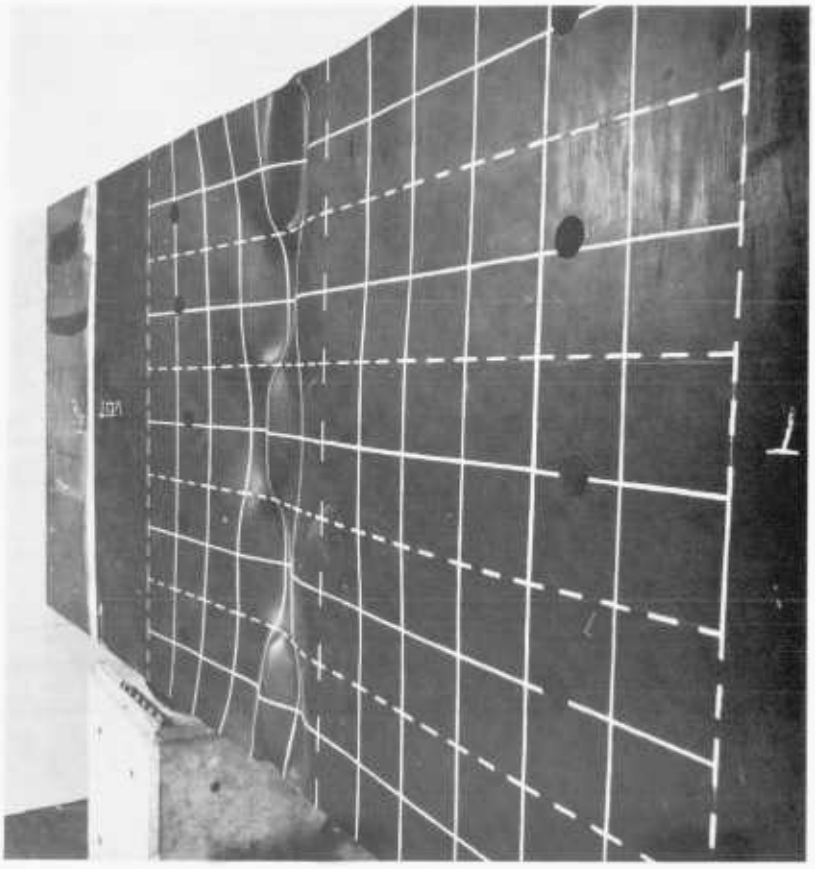

Fig. 2.13. Model 1 - showing the compression flange after collapse. The positions of diaphragm and stiffeners are indicated by dashed lines.

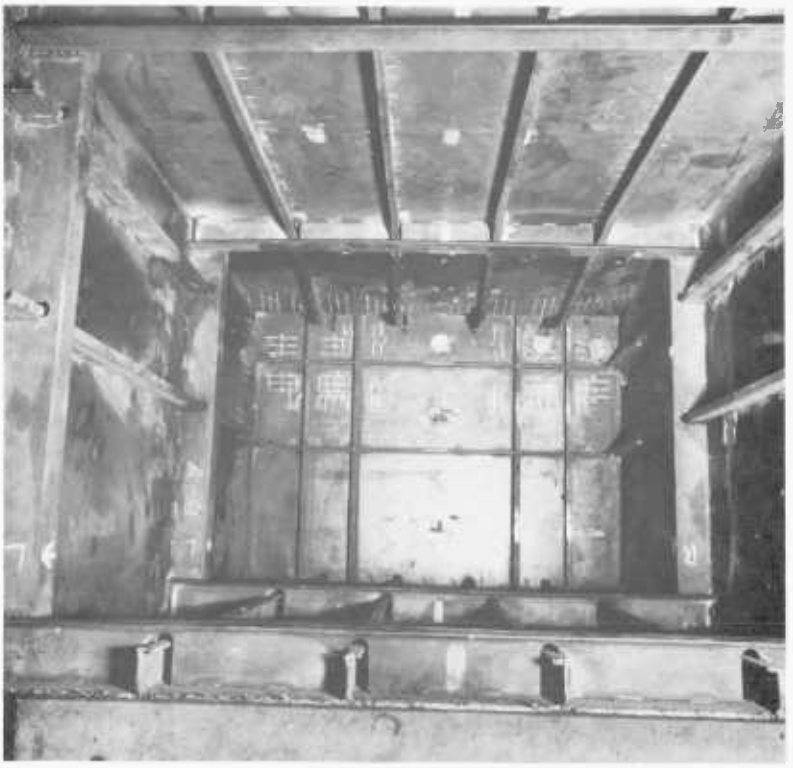

Fig. 2.14. Model 1 - an inside view of the model (from end A). Note the deflected shape of longitudinal stiffeners of the compression flange in the panel nearest to the central diaphragm and the lateral buckling in the next panel.

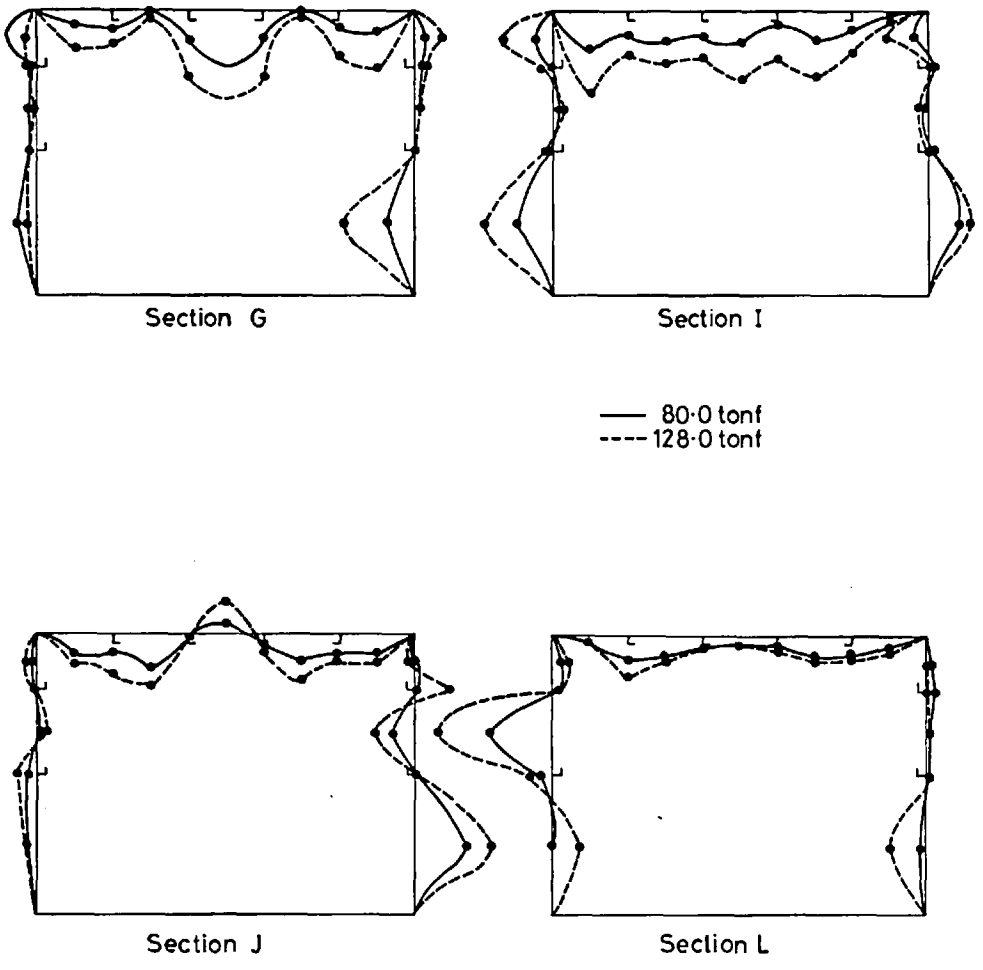

Transverse Deflections (Relative to Initial Shape)

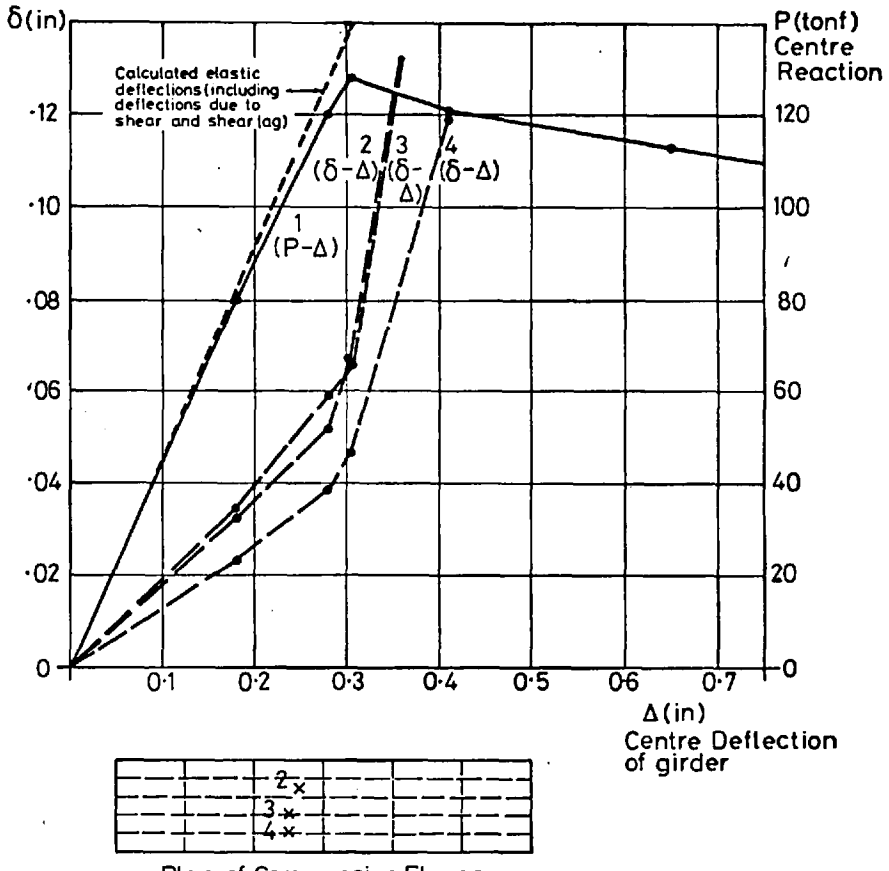

Plan of Compression Flange

CURVE 1. Load-deflection relationship

CURVE 2. Plate panel out-of-plane deformation at location 2.

CURVE 3. Stiffener out-of-plane deflection at location 3.

CURVE 4. Stiffener out-of-plane deflection at location 4.

Fig. 2.15 Model 1: Deflections

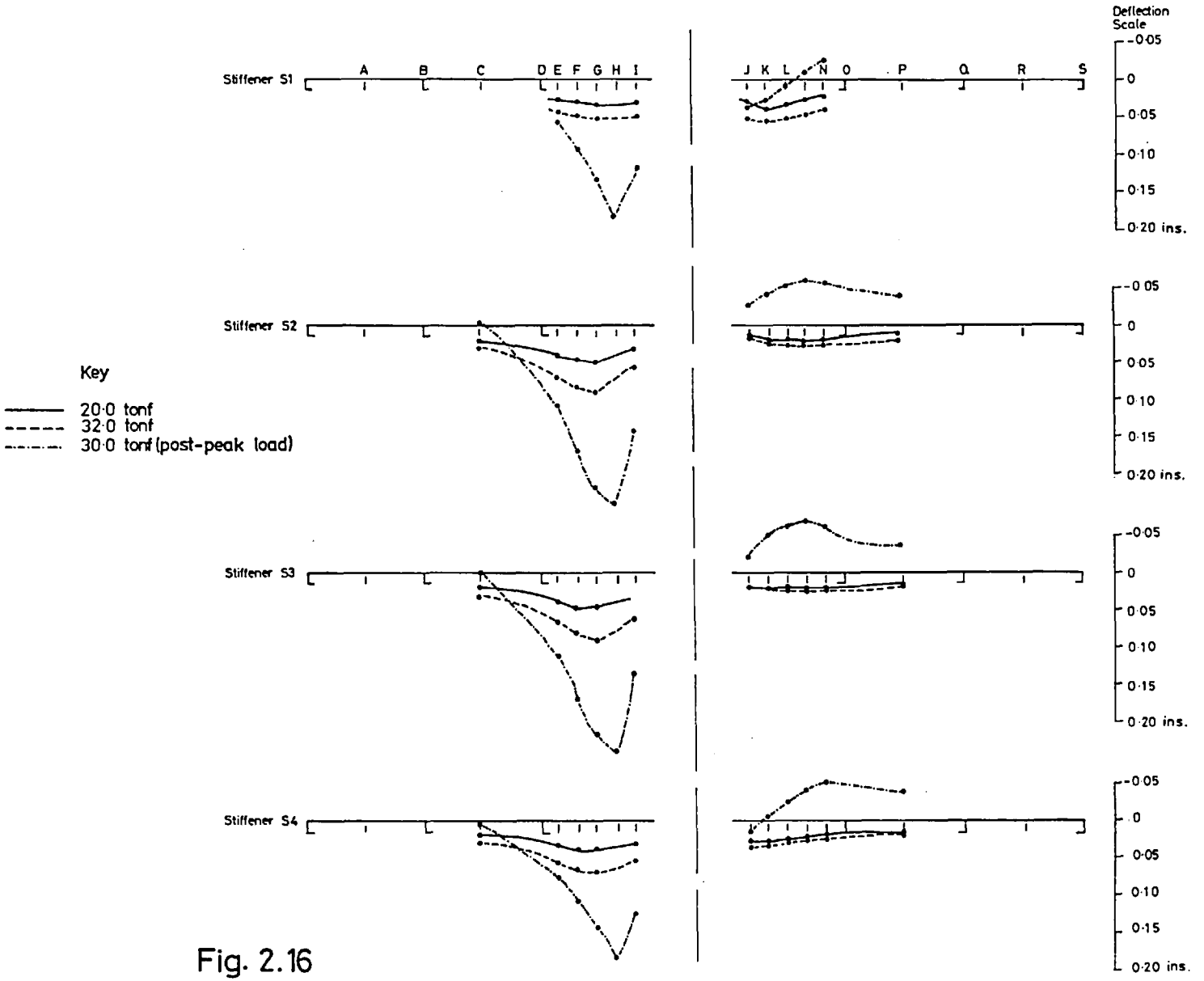

Fig. 2.16
Model 1: Deflections of Longitudinal Stiffeners (Relative to Initial Shape)

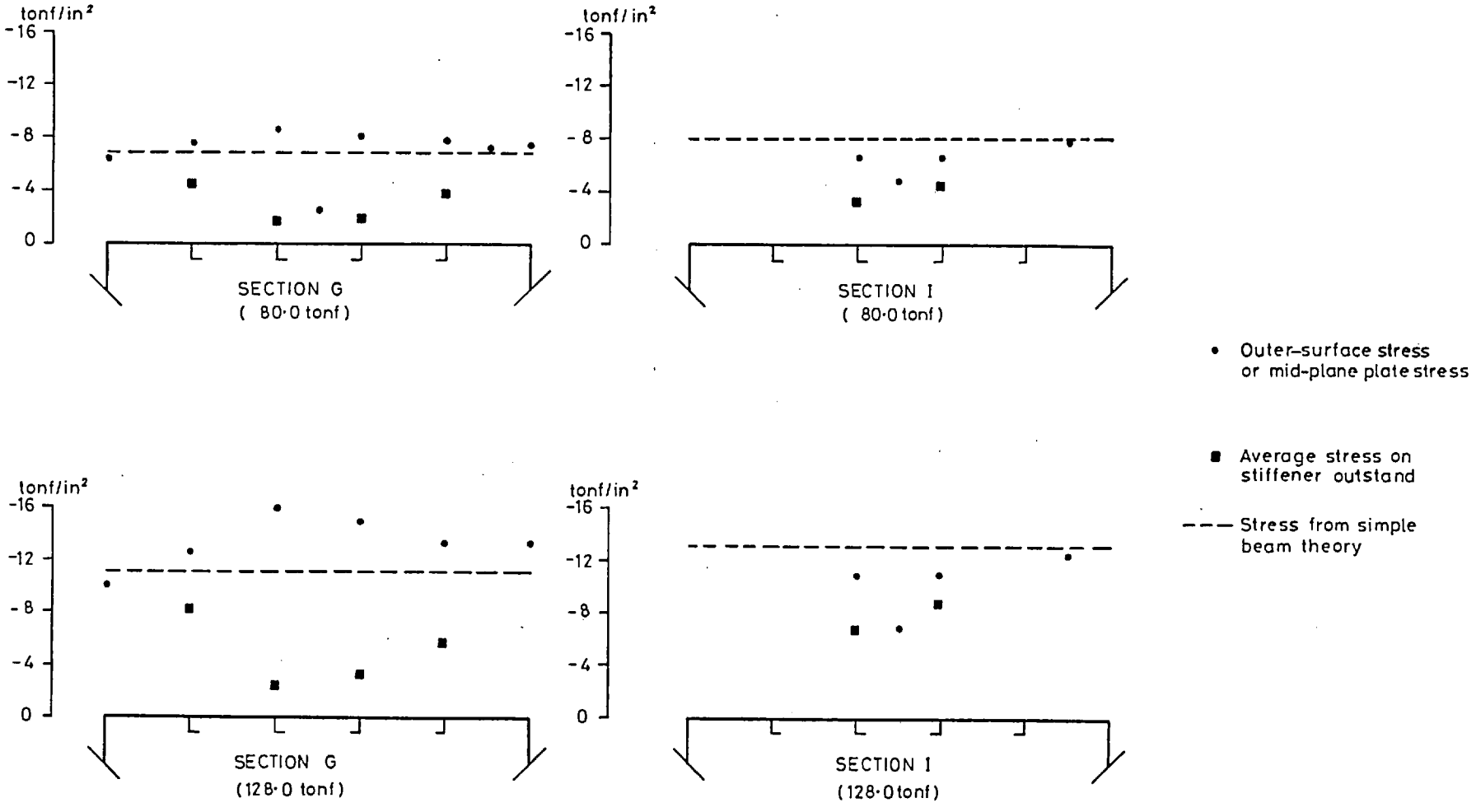

Fig. 2.17 Model 1. Distributions of Longitudinal Stresses in the Compression Flange at Cross-Sections Indicated.

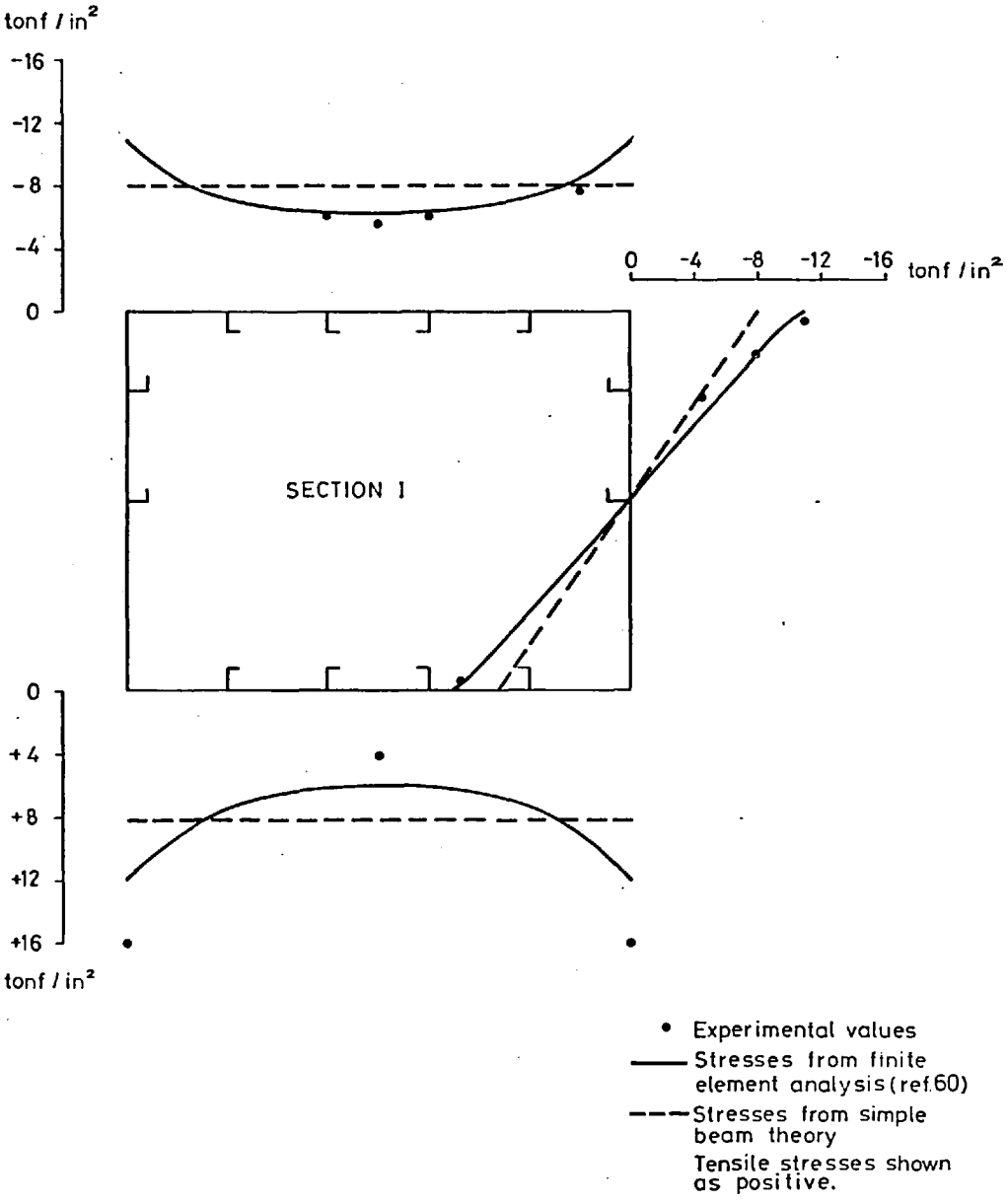

Fig. 2.18
Model 1: Distribution of Longitudinal Stresses at Cross-Section I ($5\frac{1}{16}$ in from mid-span) for Model Under Total Centre Point Load of 80·0 tonf

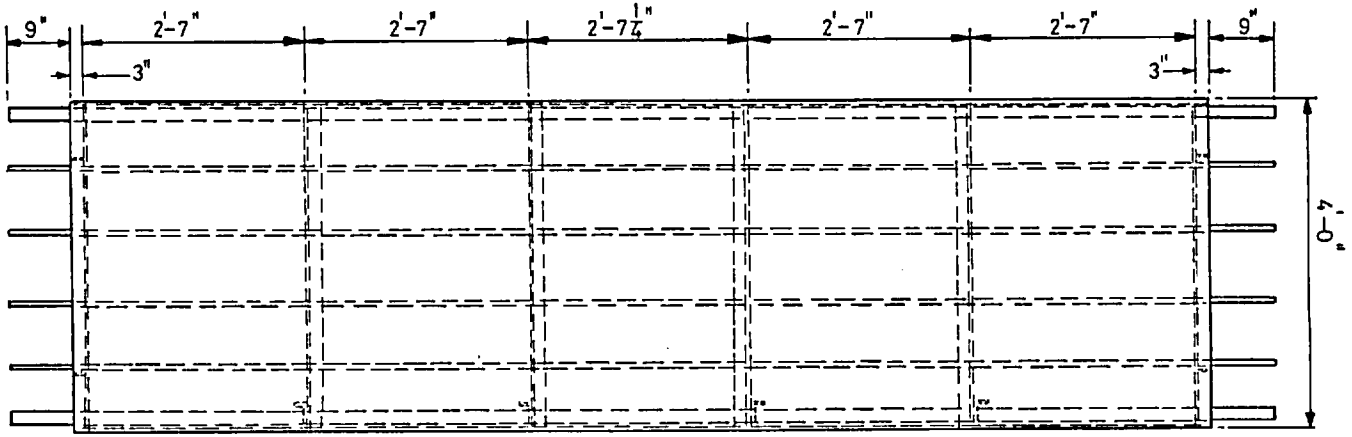

PLAN OF COMPRESSION FLANGE

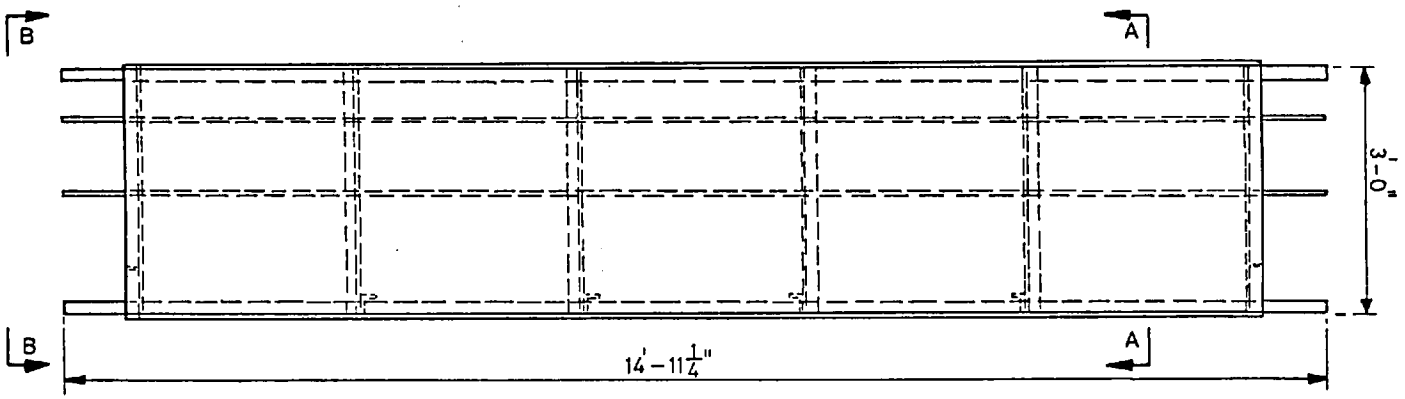

SIDE ELEVATION

Fig. 2.19a Model 2: Plan and Elevation

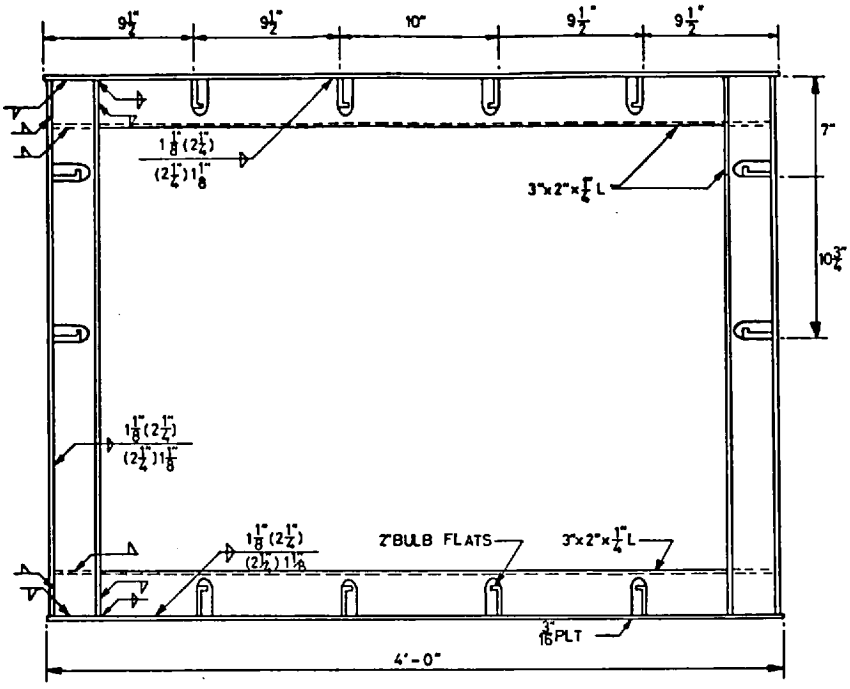

SECTION A-A

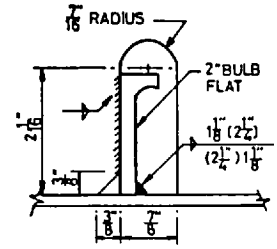

DETAIL OF SLOT IN $4" \times 2\frac{1}{2}" \times \frac{1}{4}"$ AND $\frac{1}{4}"$ DIAPHRAGMS

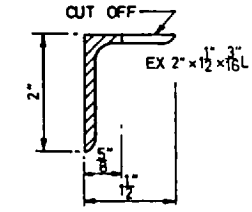

note: Bulb flat shown shaded.

DETAIL OF 2" BULB FLAT

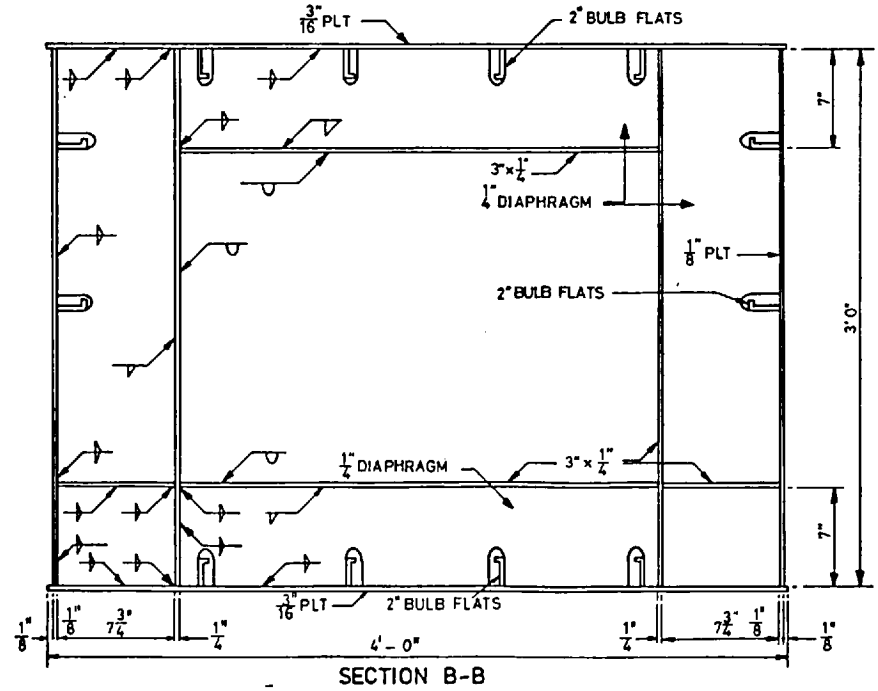

SECTION B-B

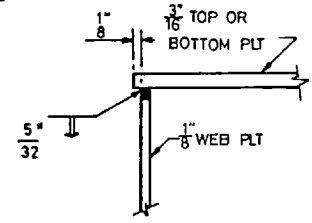

WELDING DETAIL AT CORNER OF BOX GIRDER

Fig. 2.19b
Model 2: Cross-sections

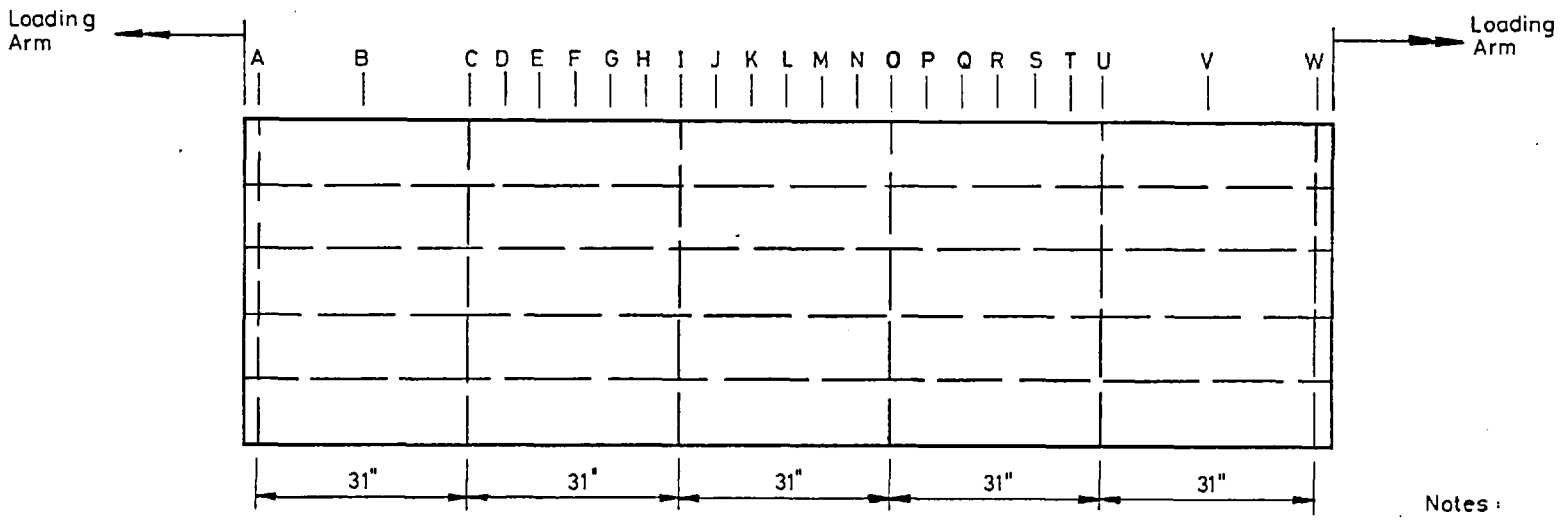

PLAN OF MODEL 2. COMPRESSION FLANGE

Notes :

1. Overall plan dimensions of Model 4 similar to Model 2.
2. Letters A to W indicate locations along the model. All grid lines within panels are at equal distances.

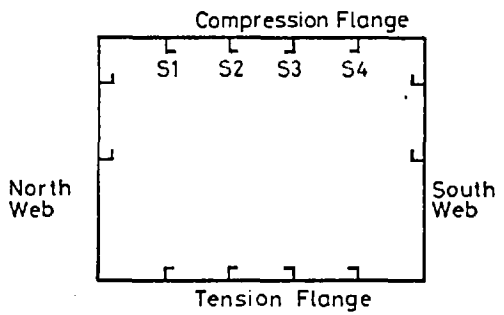

CROSS-SECTION OF MODEL 2
(viewed from end A)

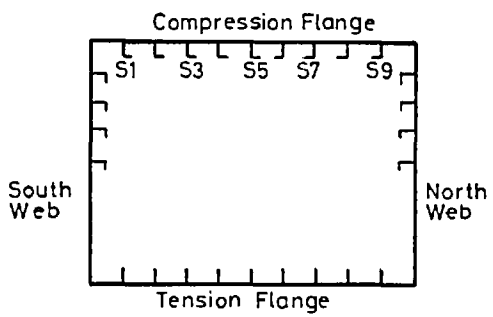

CROSS-SECTION OF MODEL 4.
(viewed from end A)

Fig. 2.20 Models 2 and 4. Details of Reference Grid.

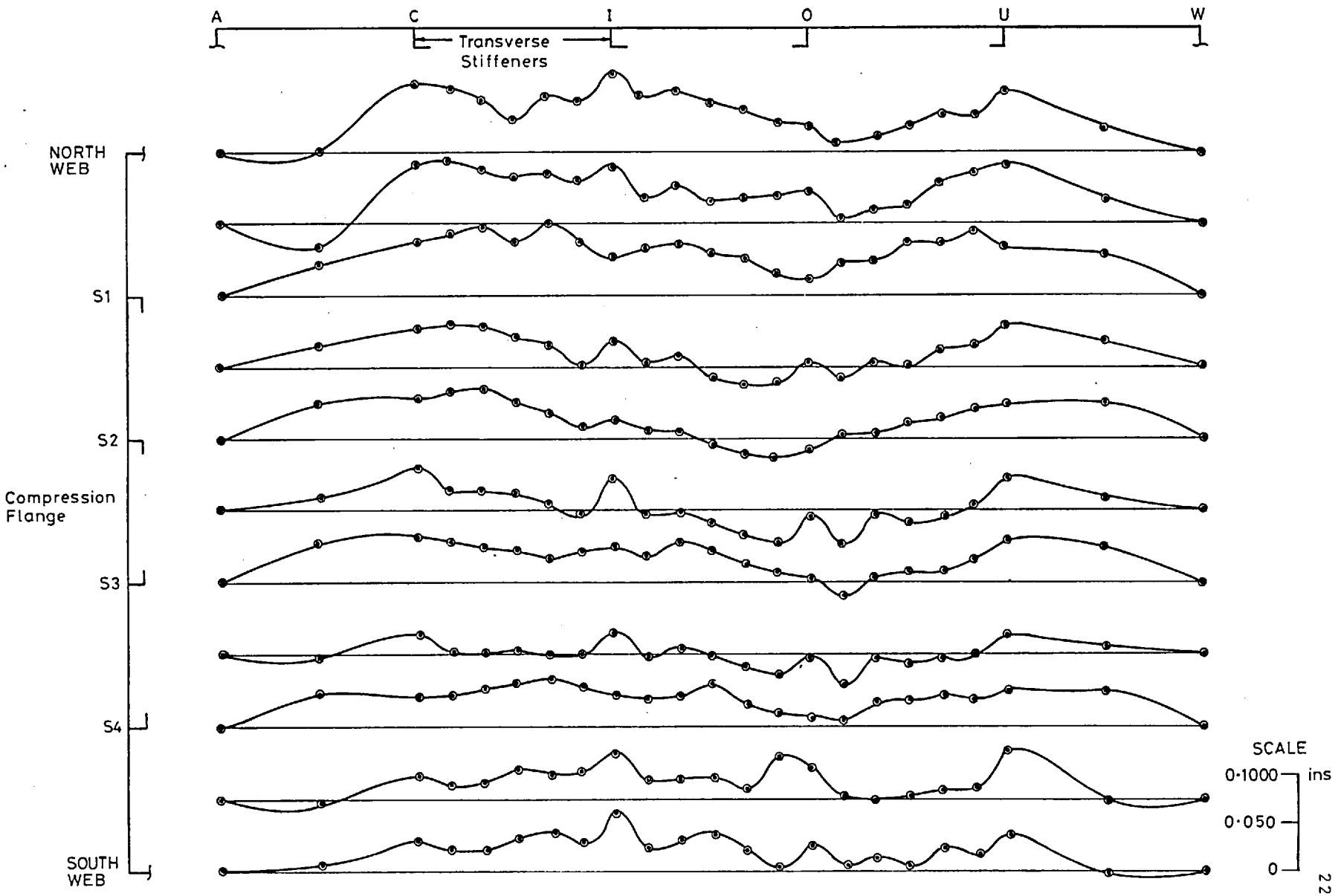

Fig. 2.21a Model 2: Longitudinal Initial Deflection Profiles of Compression Flange

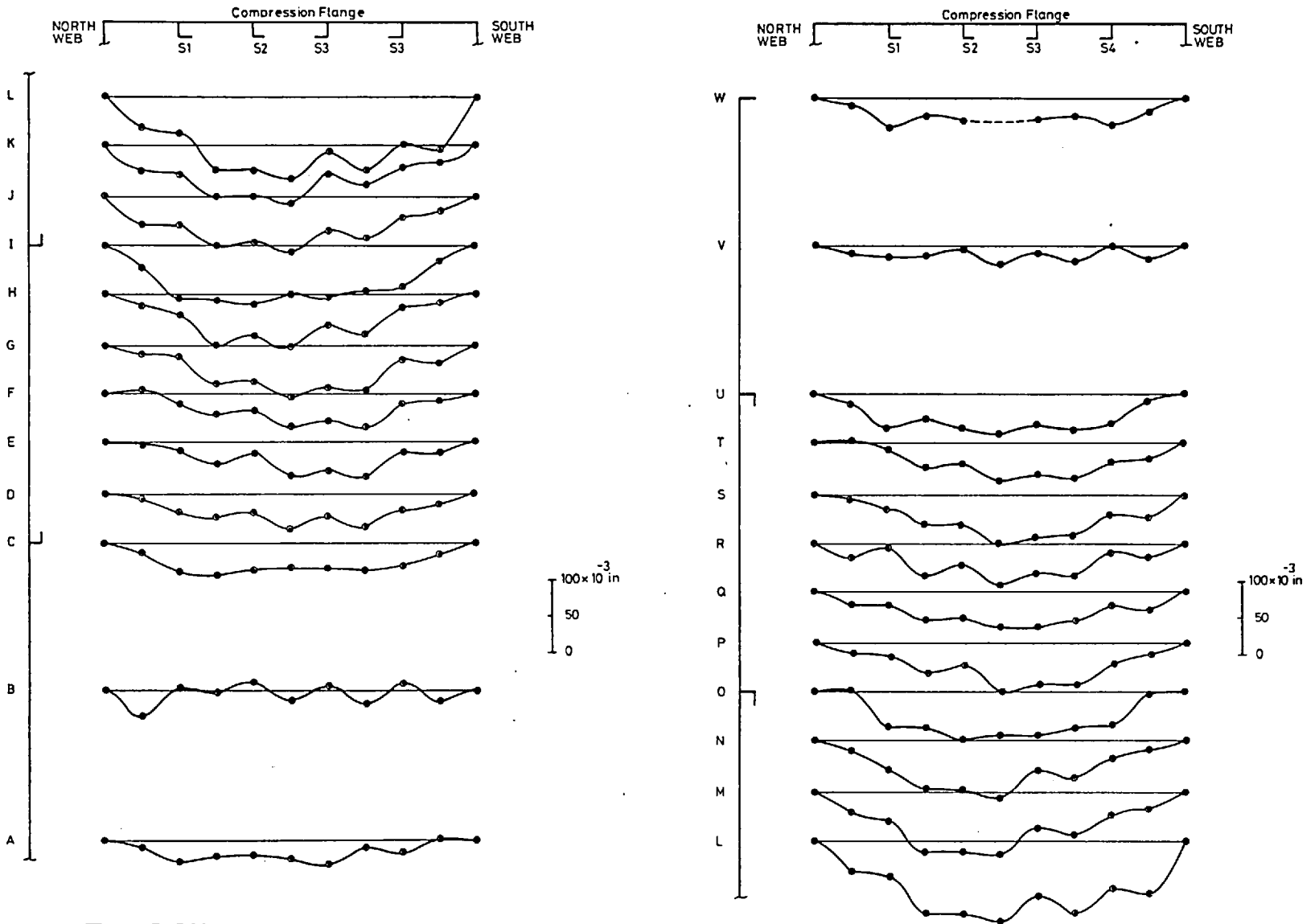

Fig. 2.21b
Model 2: Transverse Initial Deflection Profiles of Compression Flange

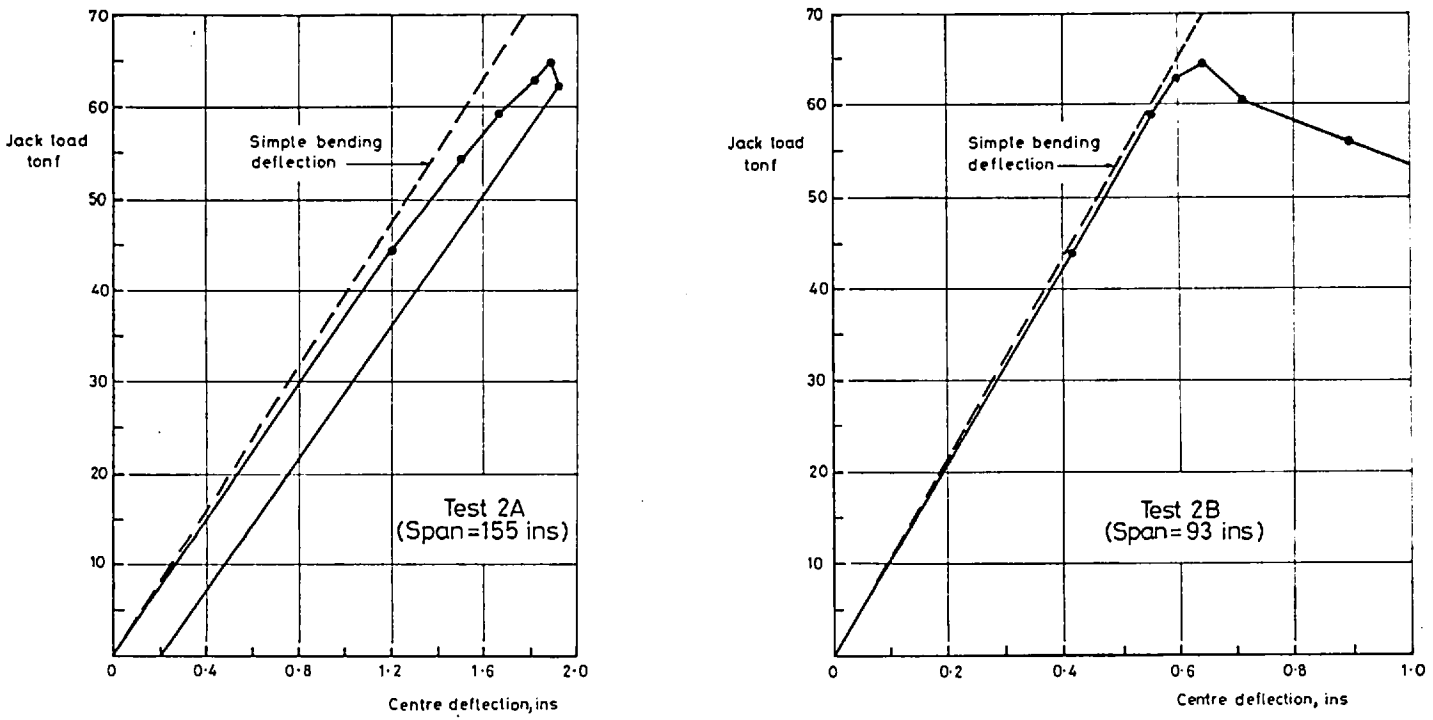

Fig. 2.22 Model 2: Load-Deflection Curves

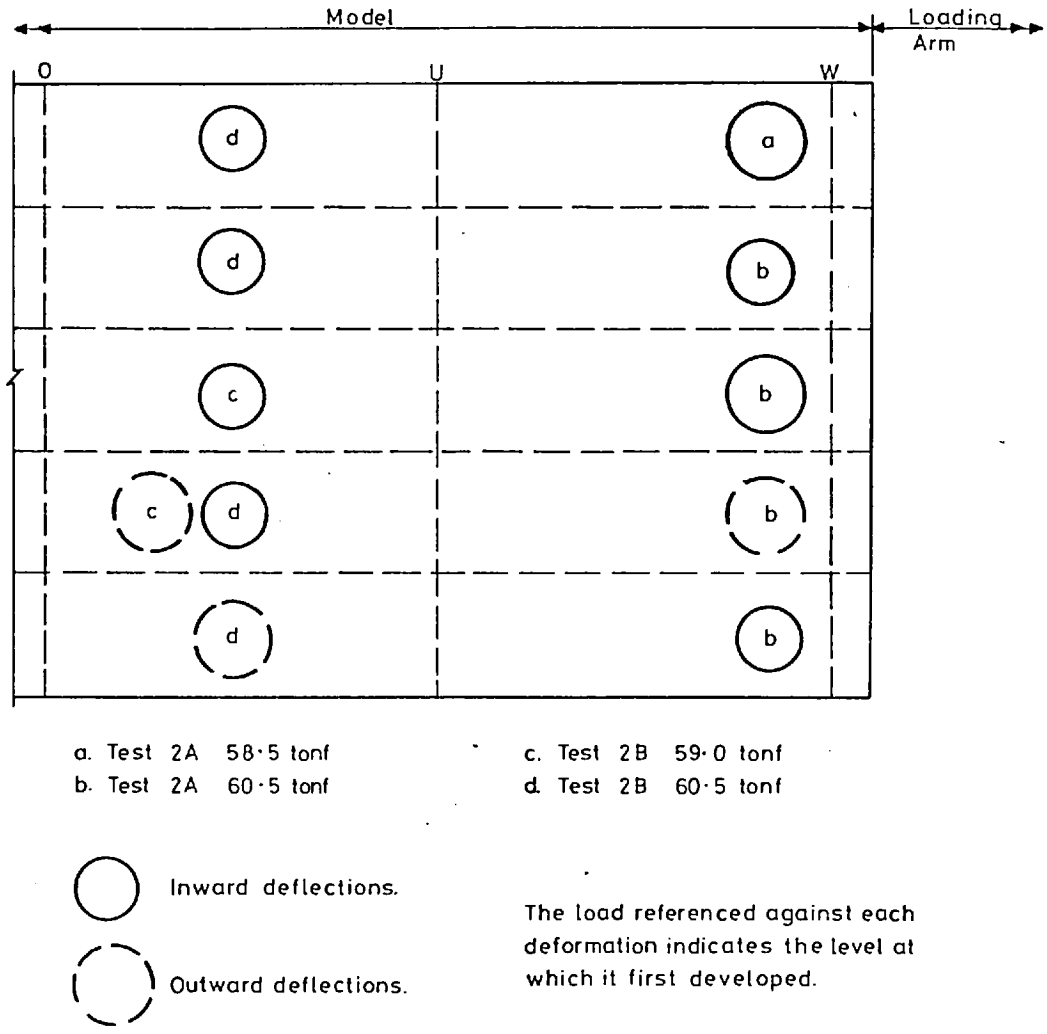

Fig. 2.23 Model 2. Development of Compression Flange Plate Panel Buckles.

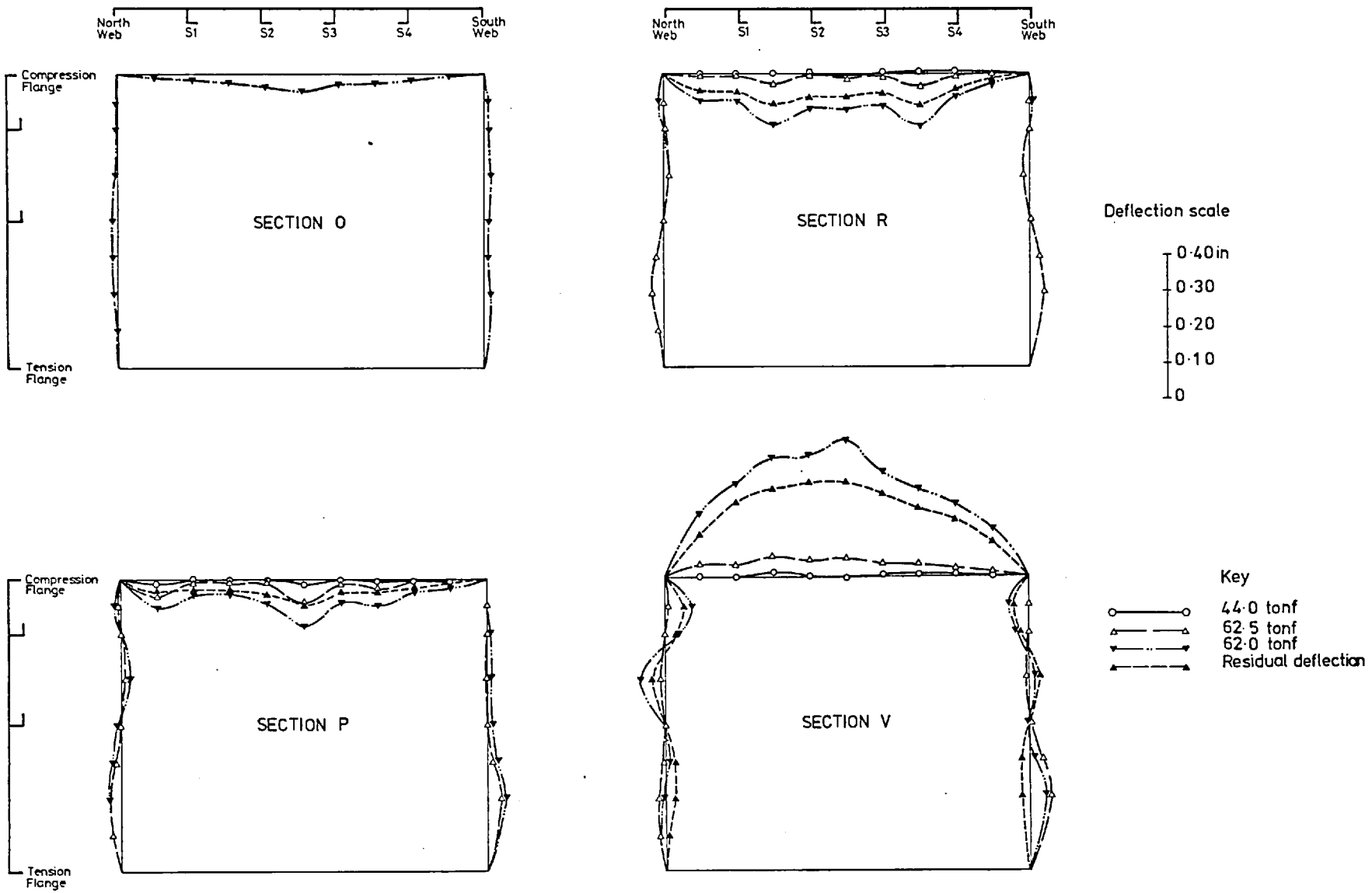

Fig. 2.24
Test 2A: Transverse Deflections (Relative to Initial Shape)

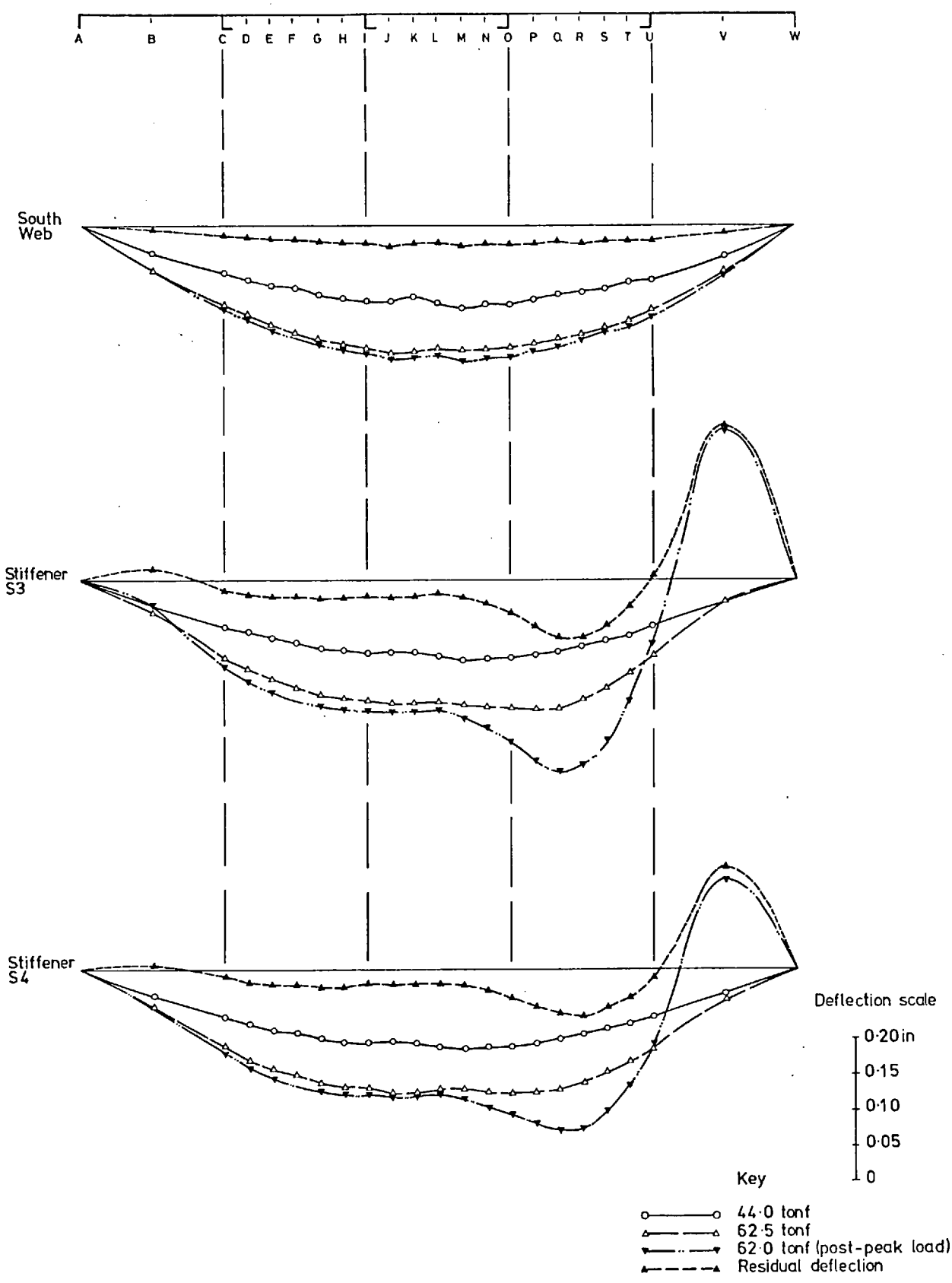

Fig. 2.25
Test 2A: Longitudinal Deflections (Relative to Initial Shape)

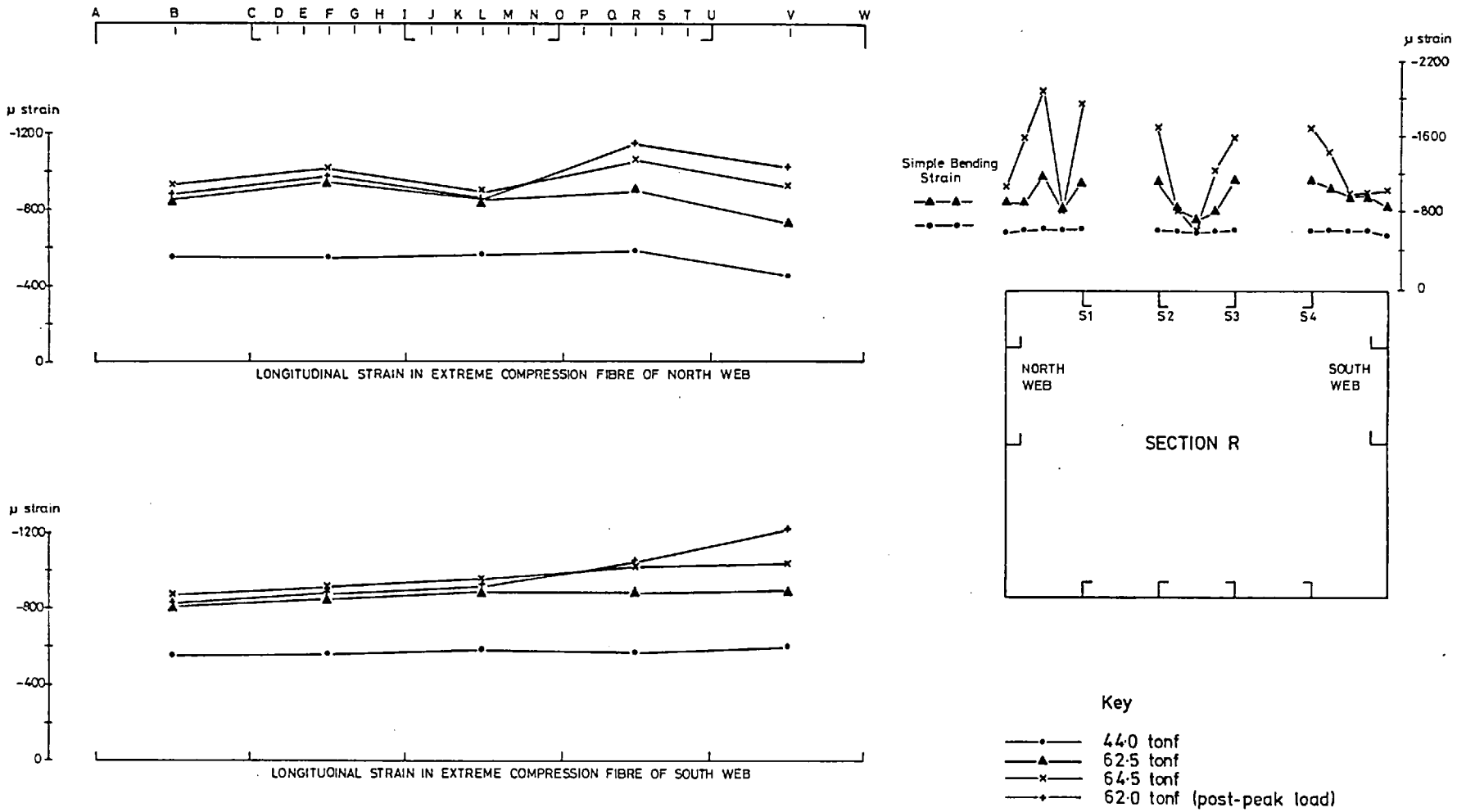

Fig. 2.26 Test 2A: Longitudinal Strains

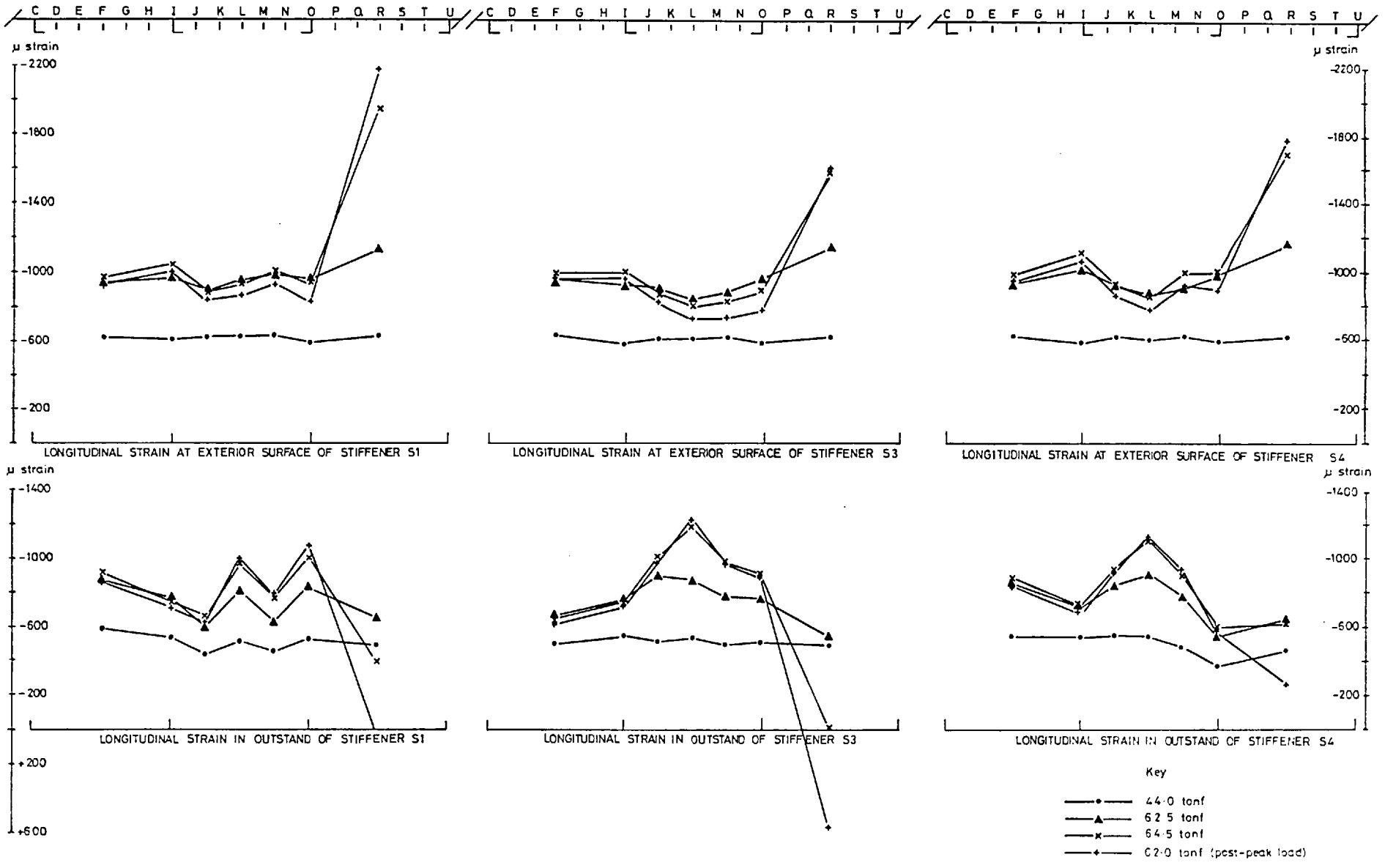

Fig. 2.27 Test 2A: Longitudinal Strains in Stiffeners S1 S3 and S4

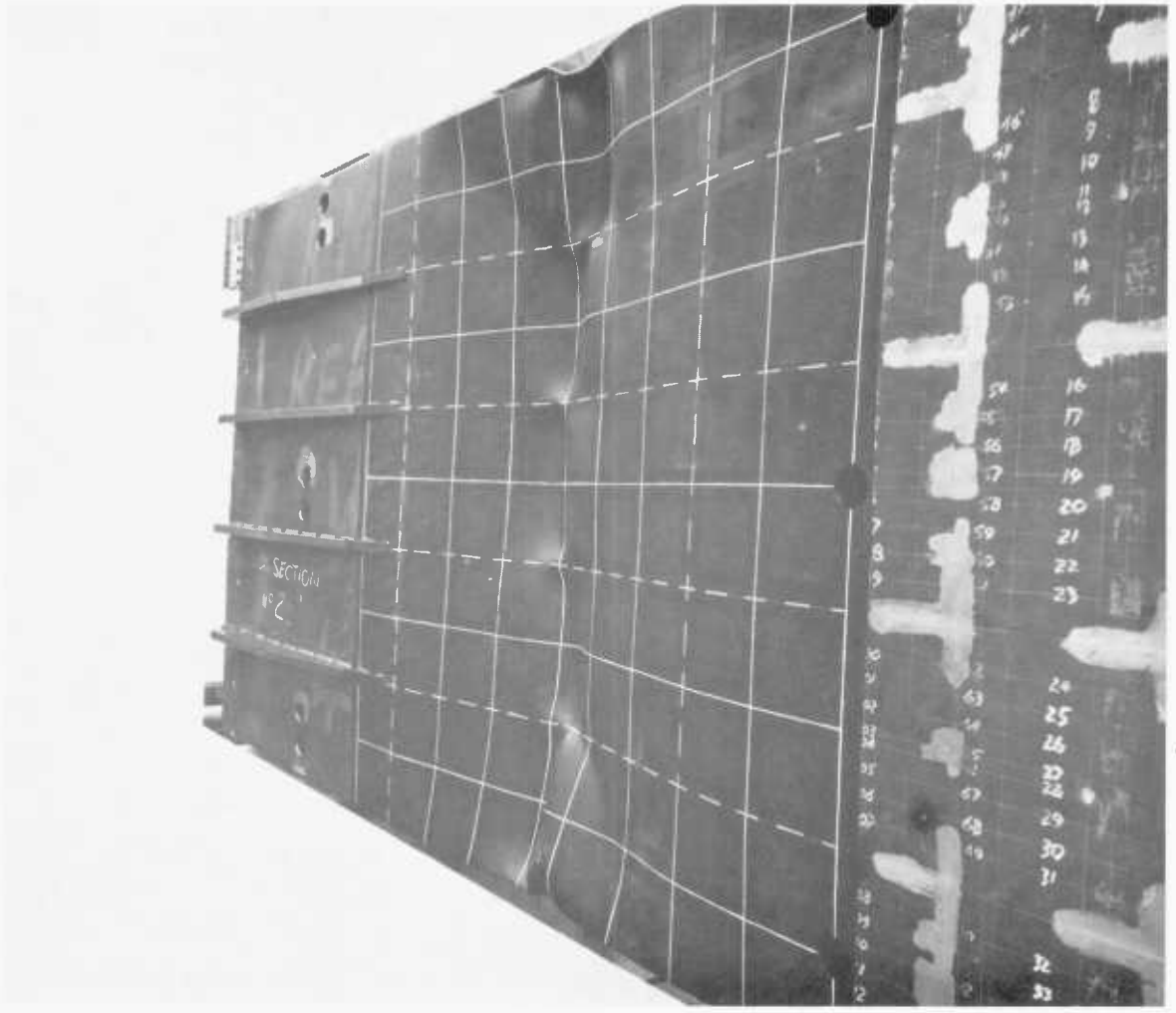

Fig. 2.28. Model 2 - showing buckles in the compression flange after the second collapse test (Test 2B). After first collapse (Test 2A) in the panel adjacent to the end cross-frame, this bay was stiffened as shown. Stiffener locations are indicated by dashed lines.

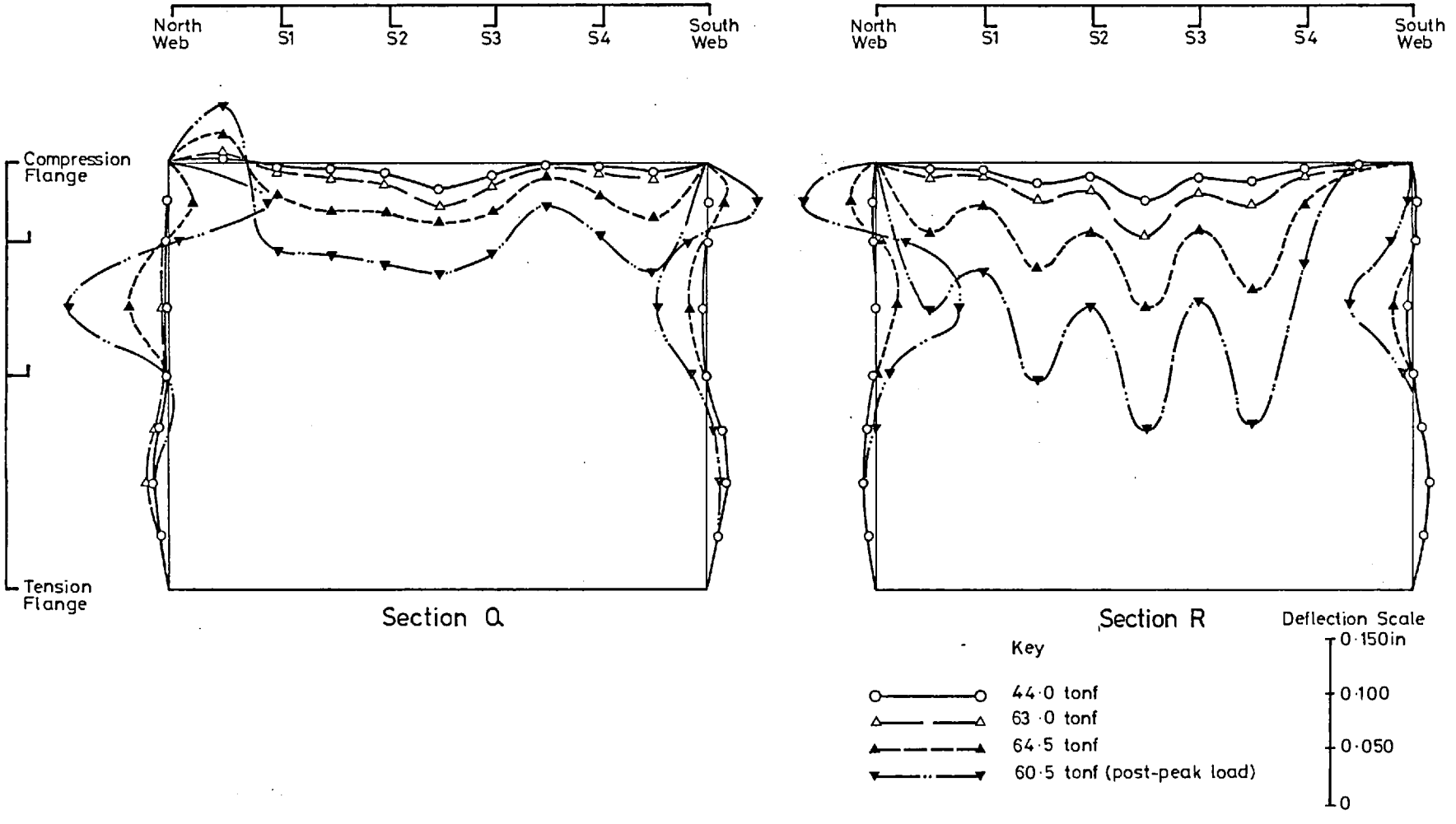

Fig. 2.29 Test 2B: Transverse Deflections (Relative to Initial Shape)

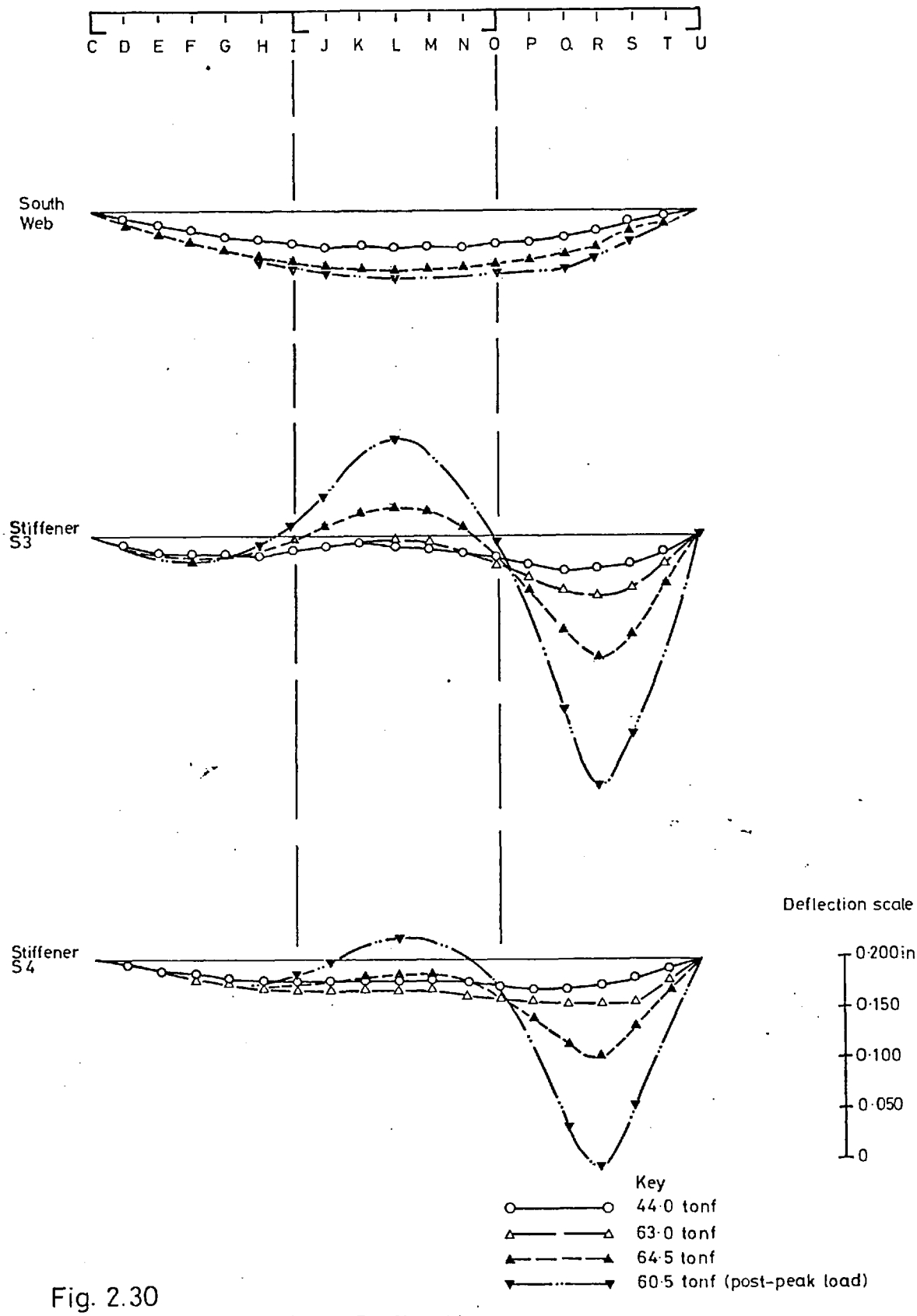

Fig. 2.30
Test 2B: Longitudinal Deflections (Relative to Initial Shape)

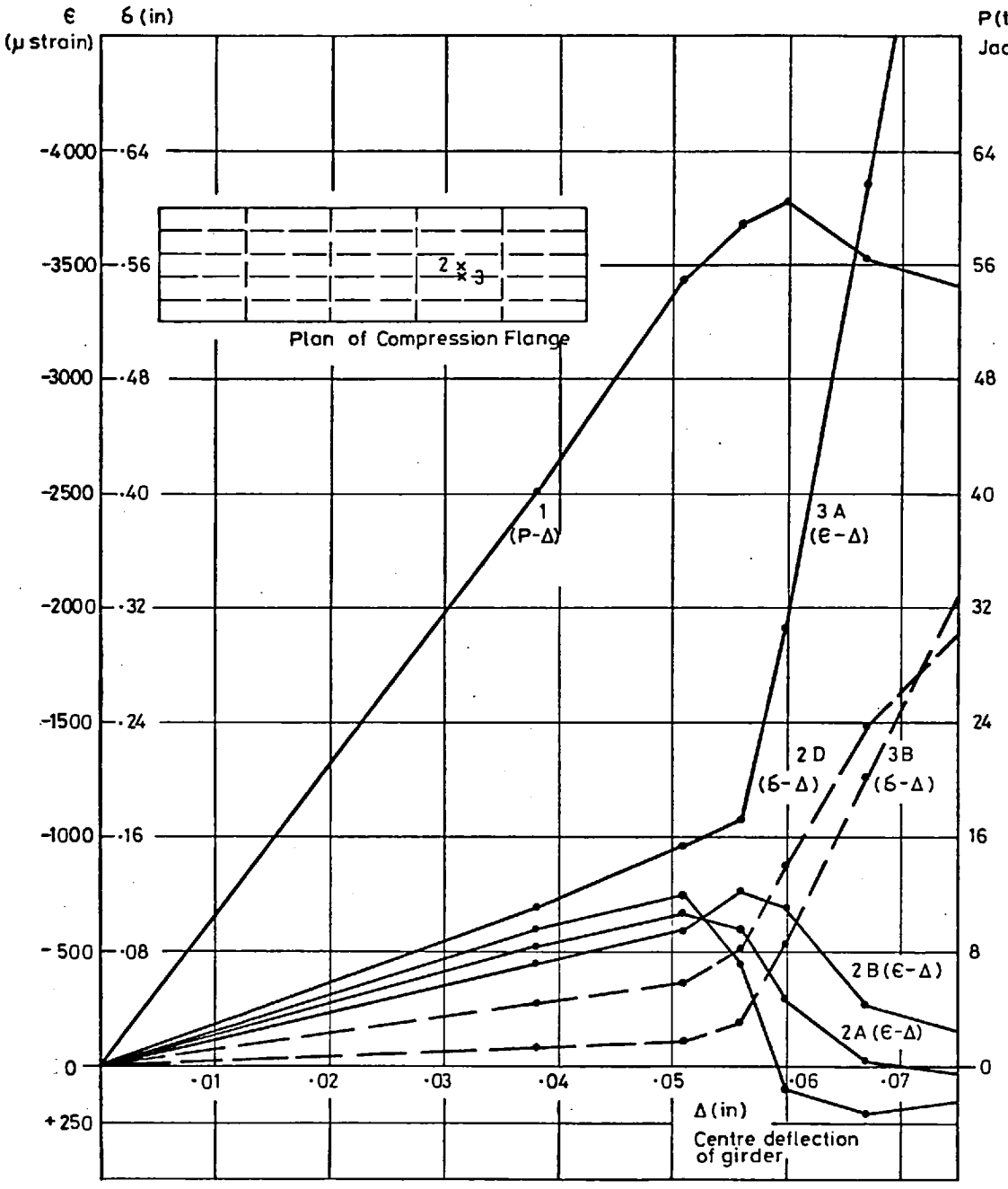

CURVE 1 OVERALL LOAD-DEFLECTION RELATIONSHIP
CURVE 2A MID-PLANE STRAIN AT LOCATION 2.
CURVE 2B INNER SURFACE STRAIN AT LOCATION 2.
CURVE 2C OUTER SURFACE STRAIN AT LOCATION 2
CURVE 2D PLATE PANEL OUT-OF-PLANE DEFORMATION AT LOCATION 2
CURVE 3A MID-PLANE STRAIN AT LOCATION 3
CURVE 3B STIFFENER OUT-OF-PLANE DEFLECTION AT LOCATION 3

Note : DATUM LOAD WAS 4·0 tonf. THUS TOTAL LOAD ON MODEL IS (P+4) tonf

Fig. 2.31 Model 2. Growth of Deflections and Strains with Load.

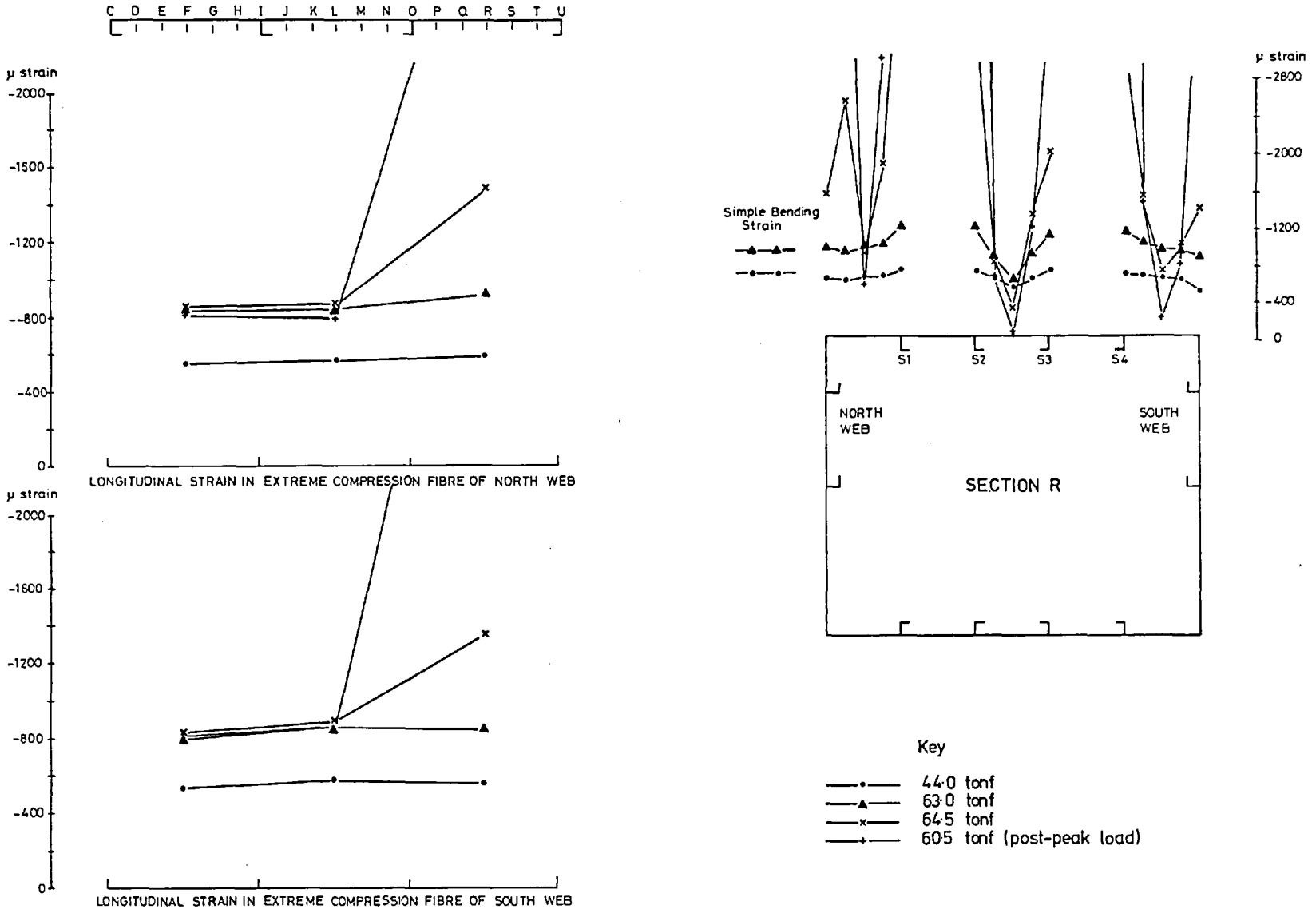

Fig. 2.32 Test 2B: Longitudinal Strains

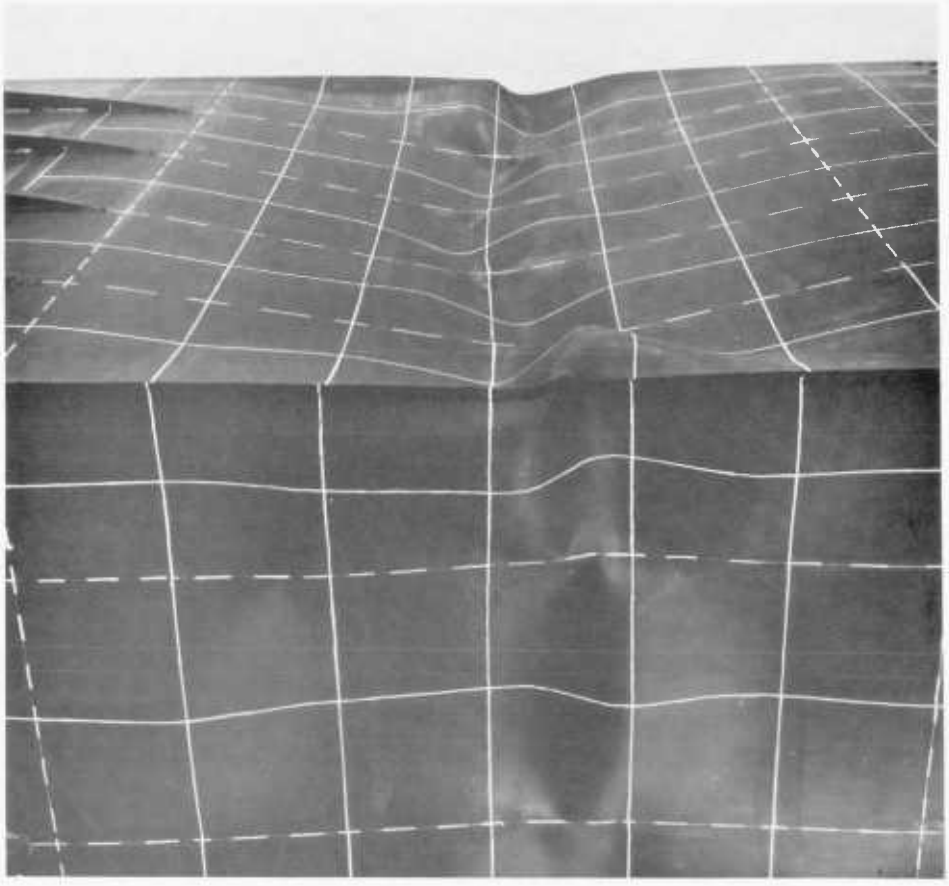

Fig. 2.33a. Model 2 - a close-up view showing the mid-span regions of the compression flange and north web, after Test 2B.

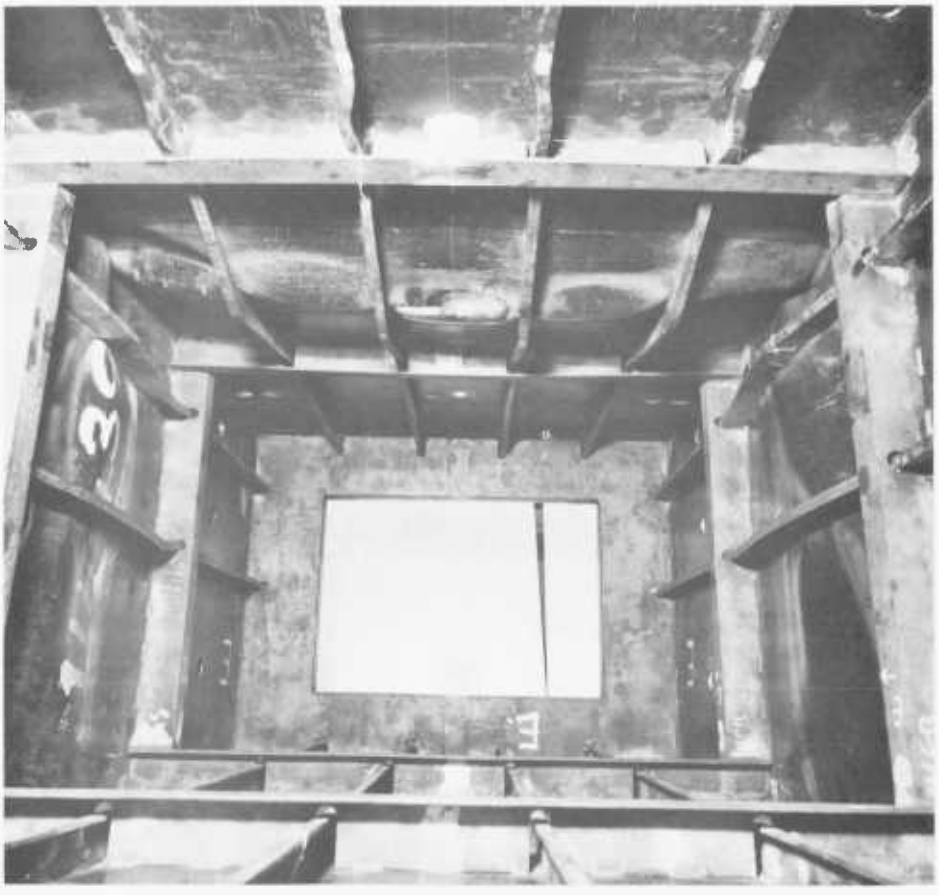

Fig. 2.33b. Model 2 - showing the interior of the model (from end C) after collapse. Note the lateral buckling of longitudinal stiffeners close to the transversals, in the bay adjacent to the critical one.

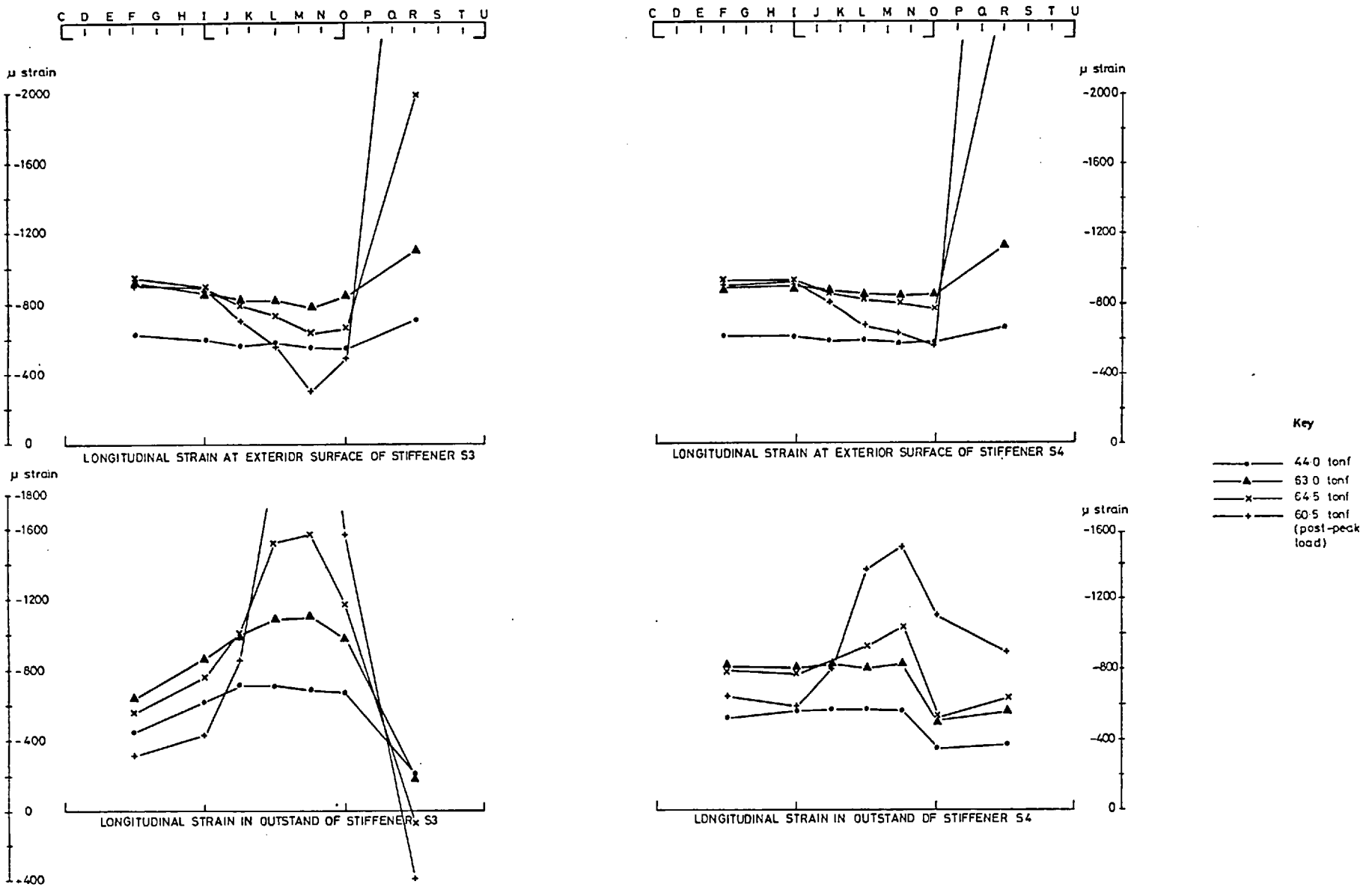

Fig. 2.34 Test 2B: Longitudinal Strains in Stiffeners S3 and S4

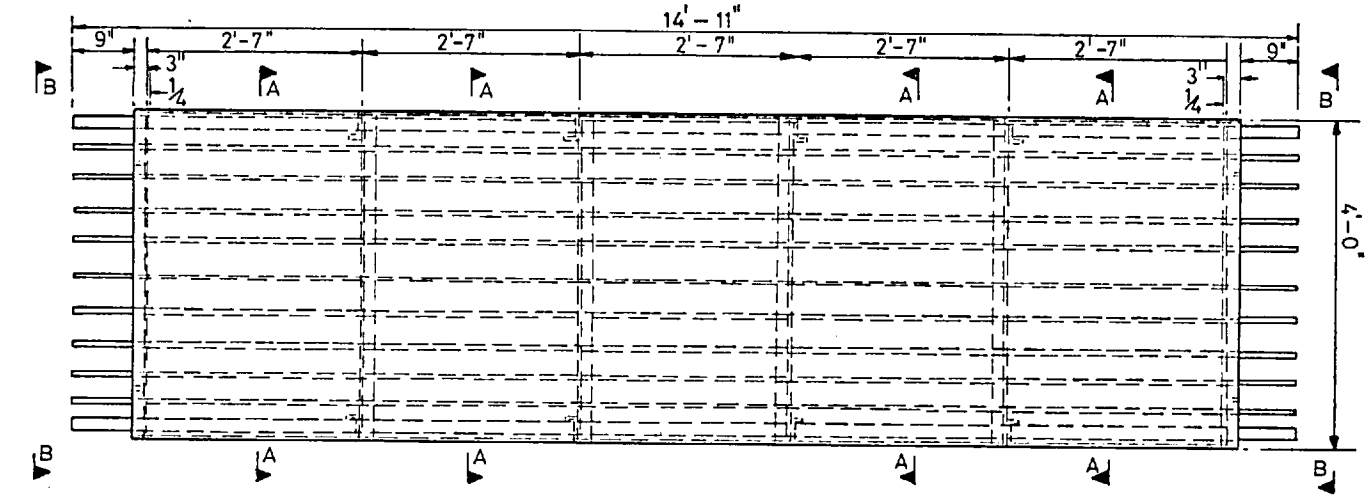

PLAN OF COMPRESSION FLANGE

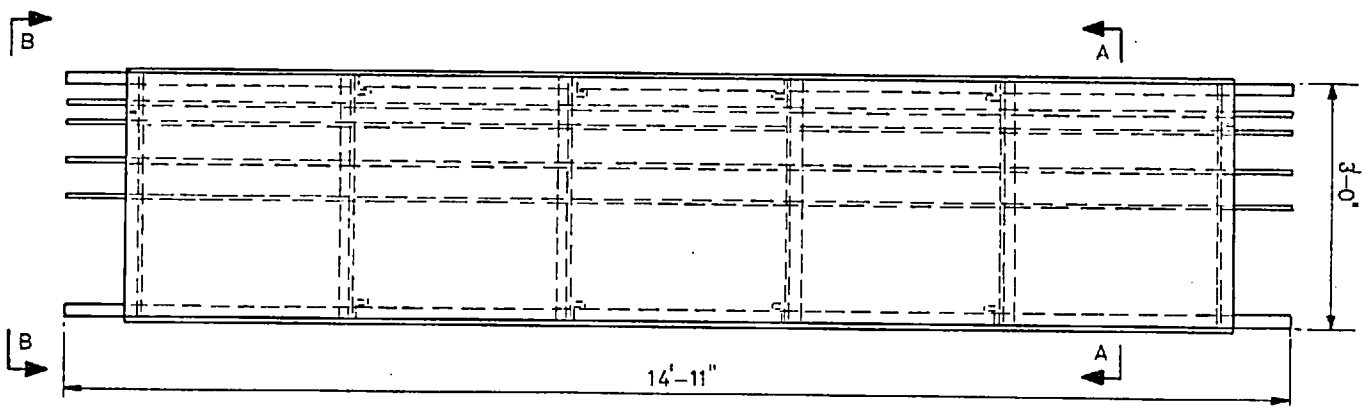

SIDE ELEVATION

Fig. 2.35a Model 4: Plan and Elevation

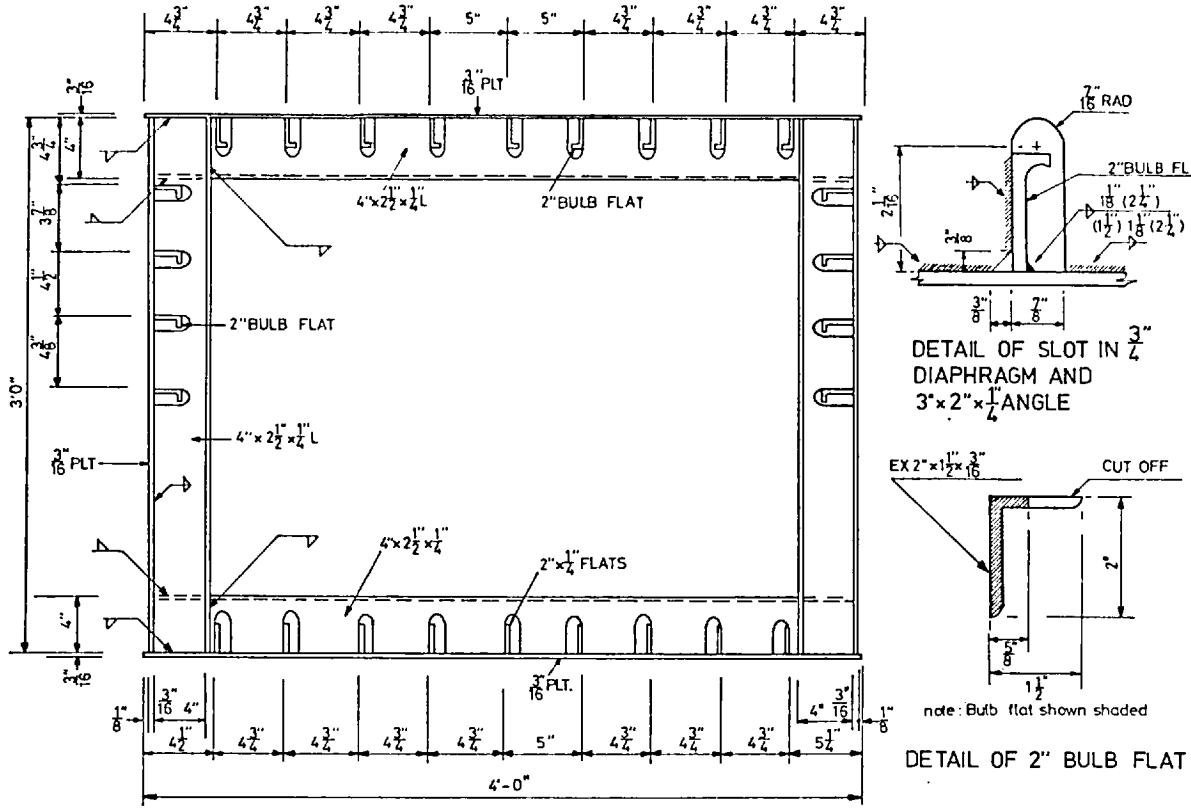

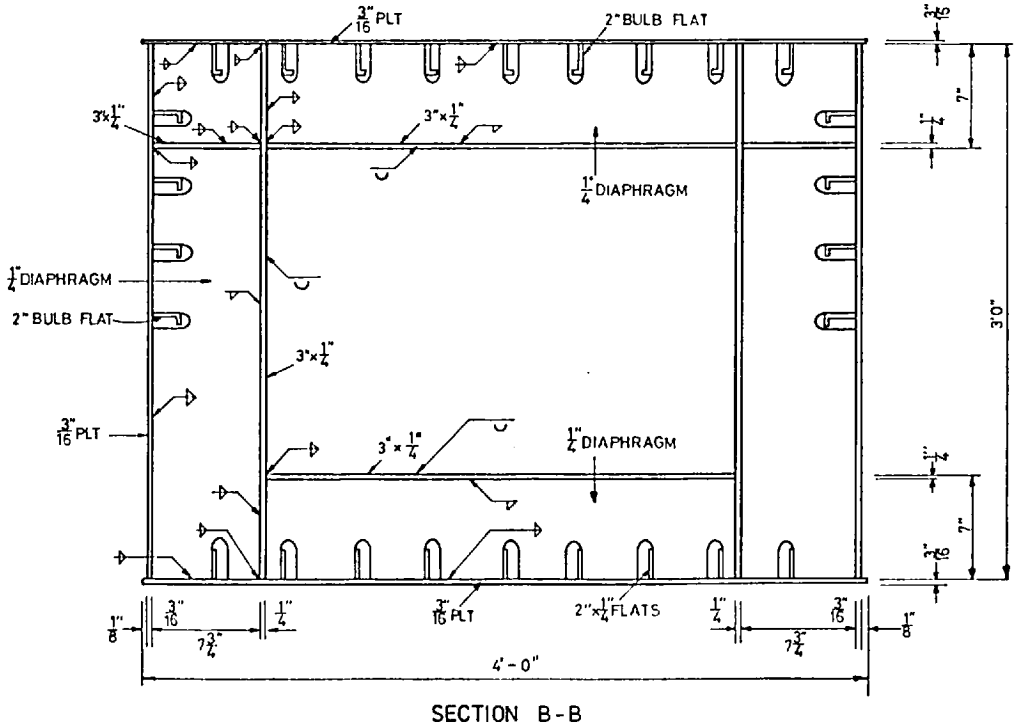

Fig. 2.35b Model 4: Cross-sections

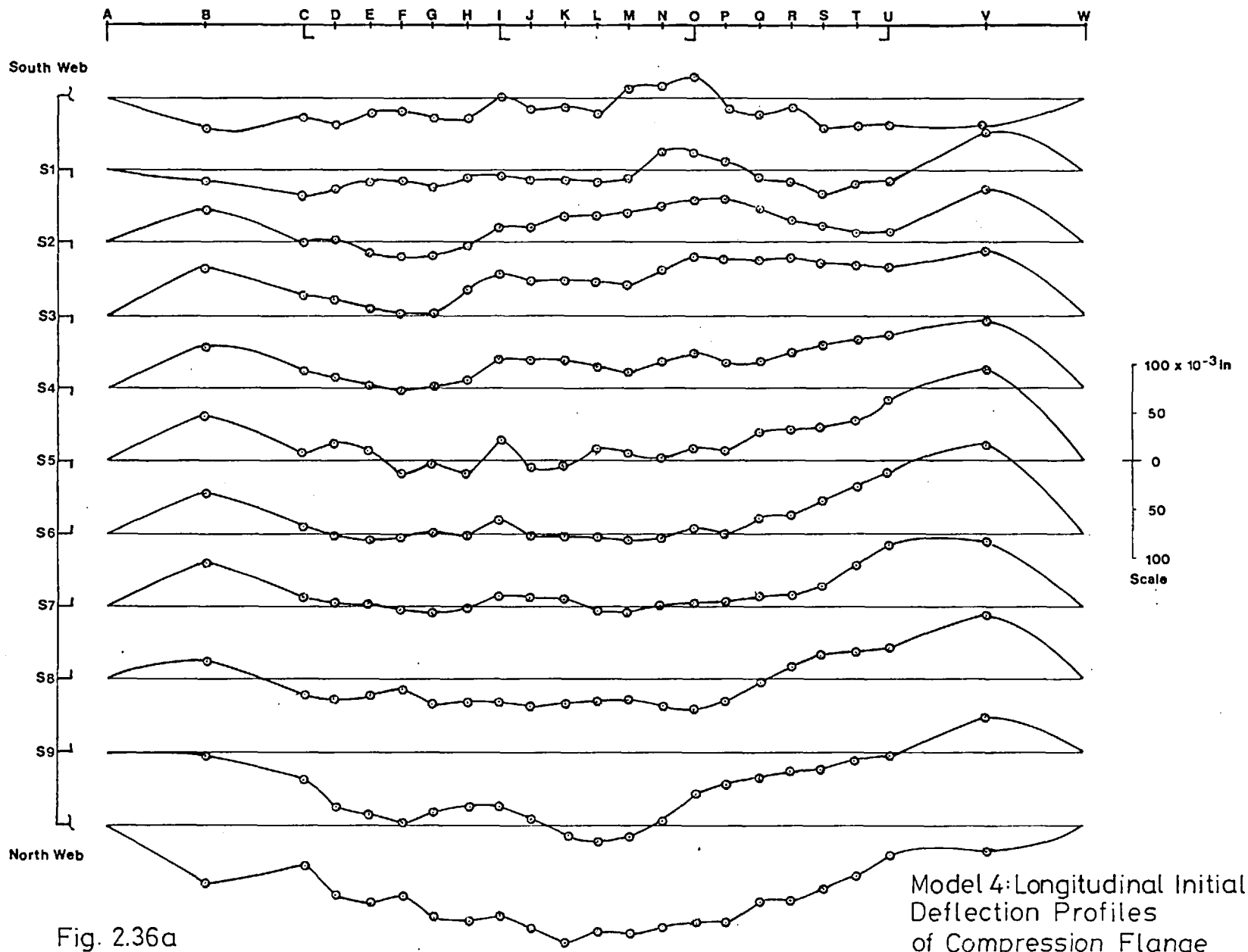

Fig. 2.36a

Model 4: Longitudinal Initial Deflection Profiles of Compression Flange

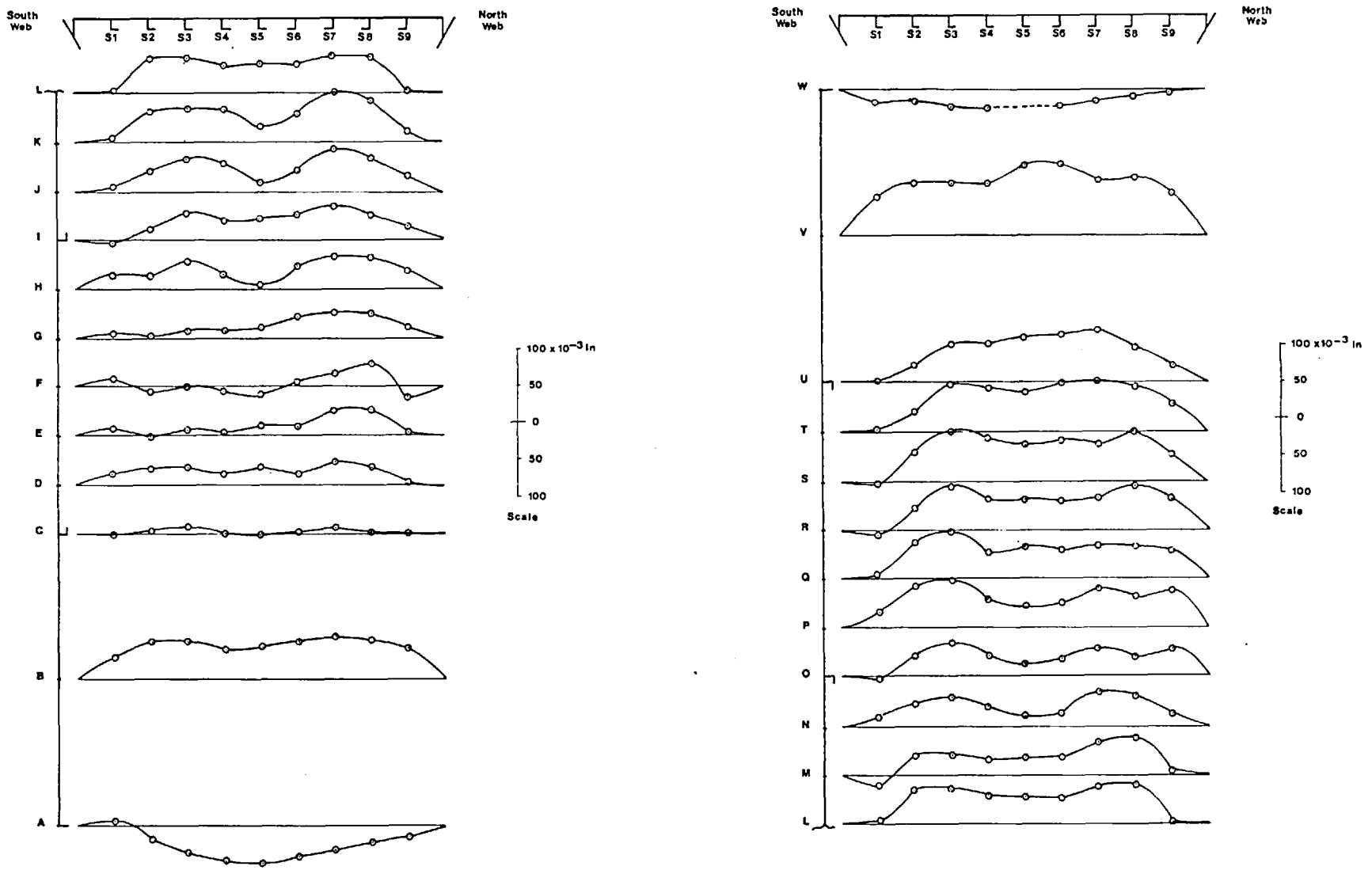

Fig. 2.36b
Model 4: Transverse Initial Deflection Profiles of Compression Flange

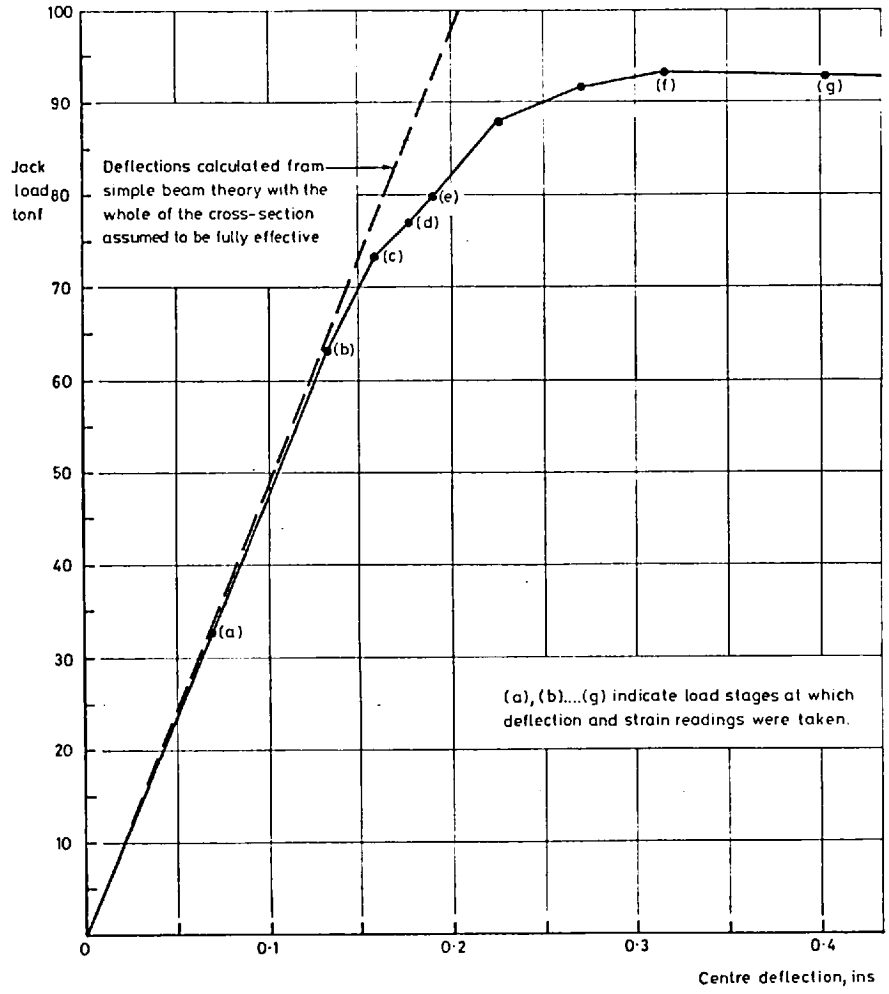

Fig. 2.37
Model 4: Load-Deflection Curve

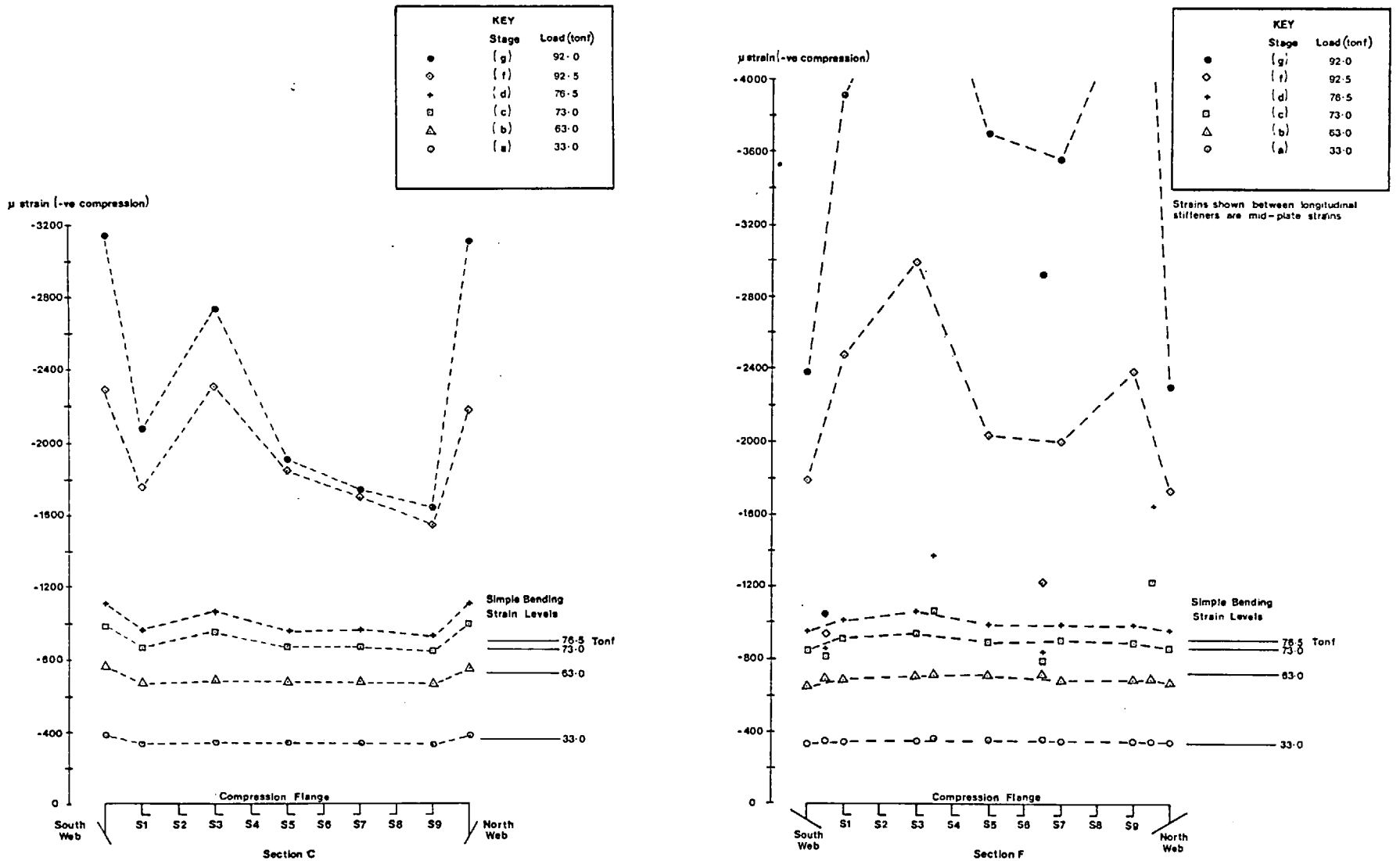

Fig. 2.38a Model 4: Longitudinal Strains at Sections C and F

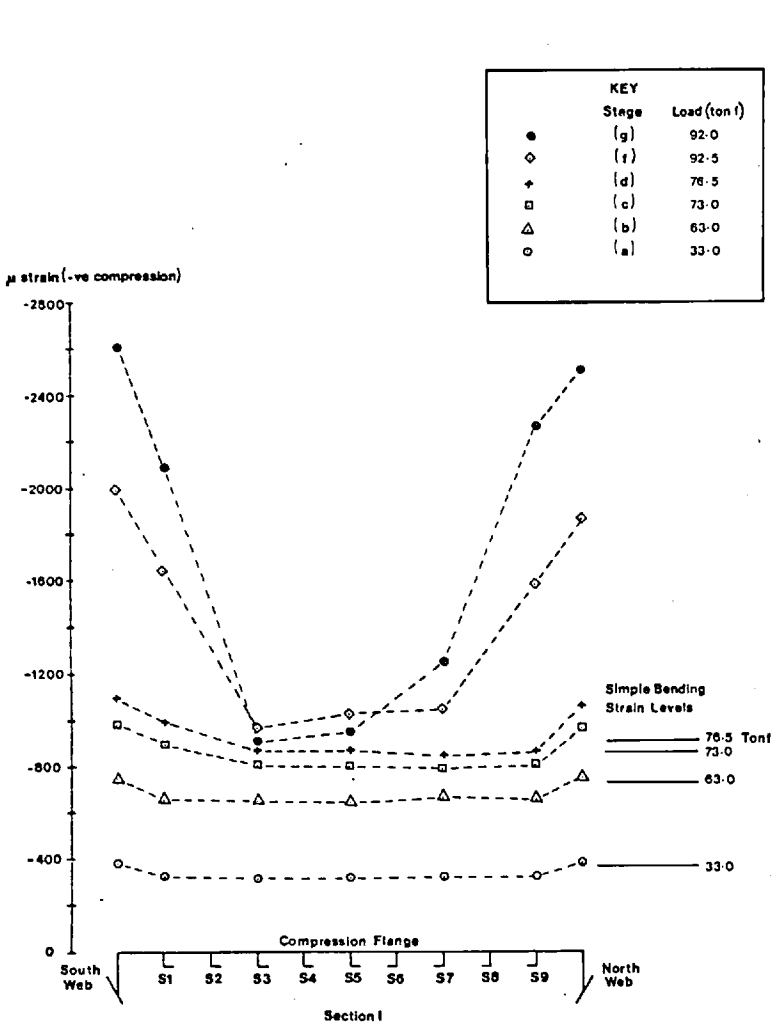

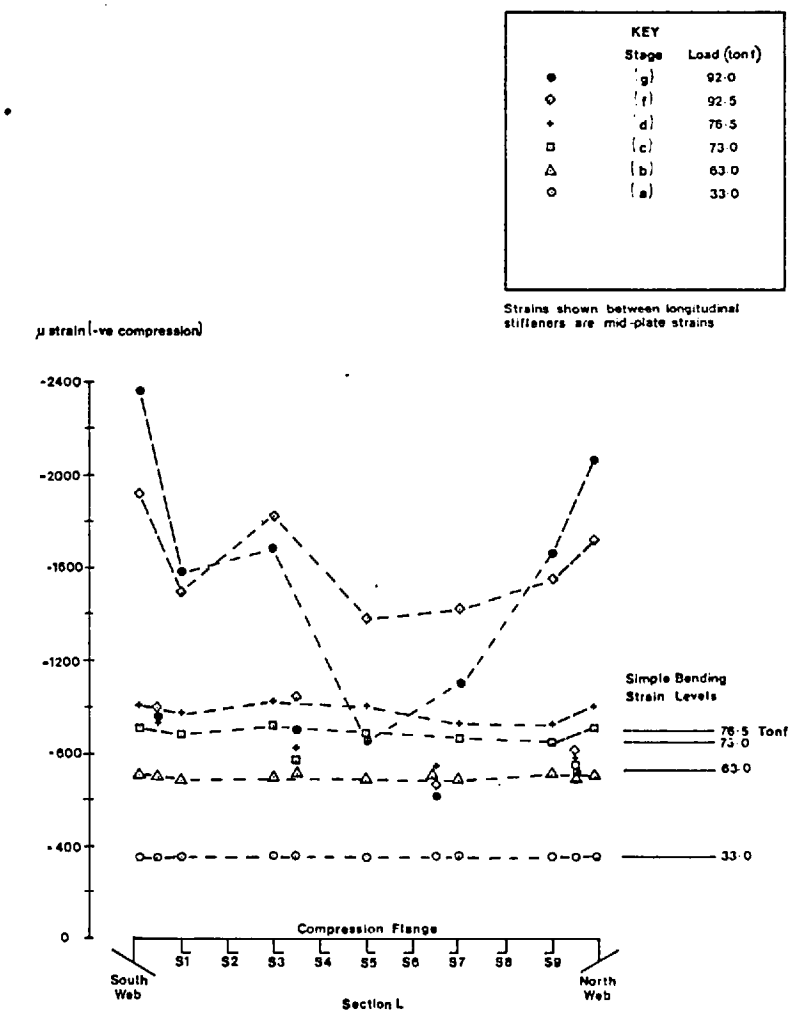

Fig. 2.38b Model 4 : Longitudinal Strains at Sections I and L

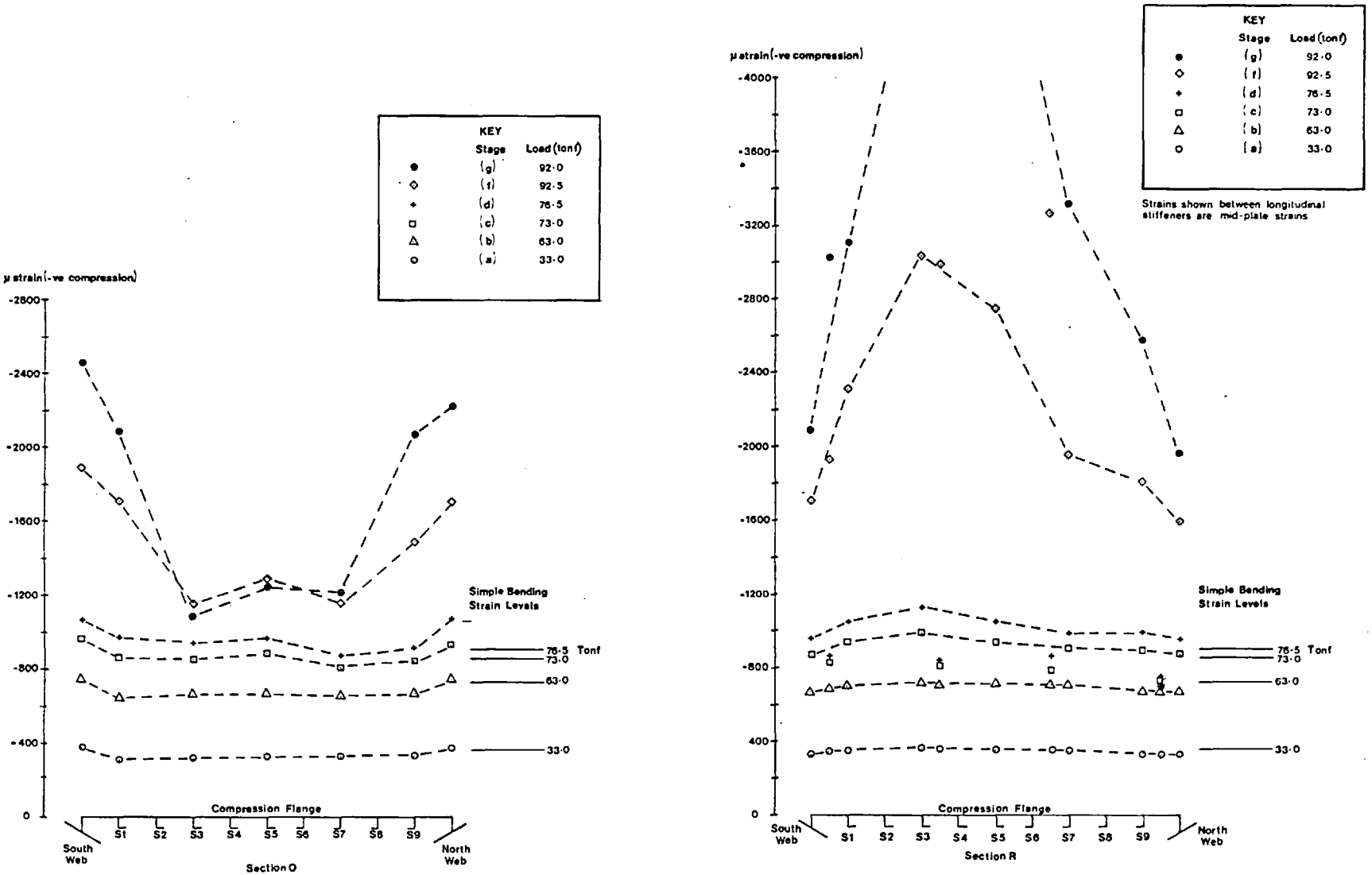

Fig. 2.38c Model 4: Longitudinal Strains at Sections O and R

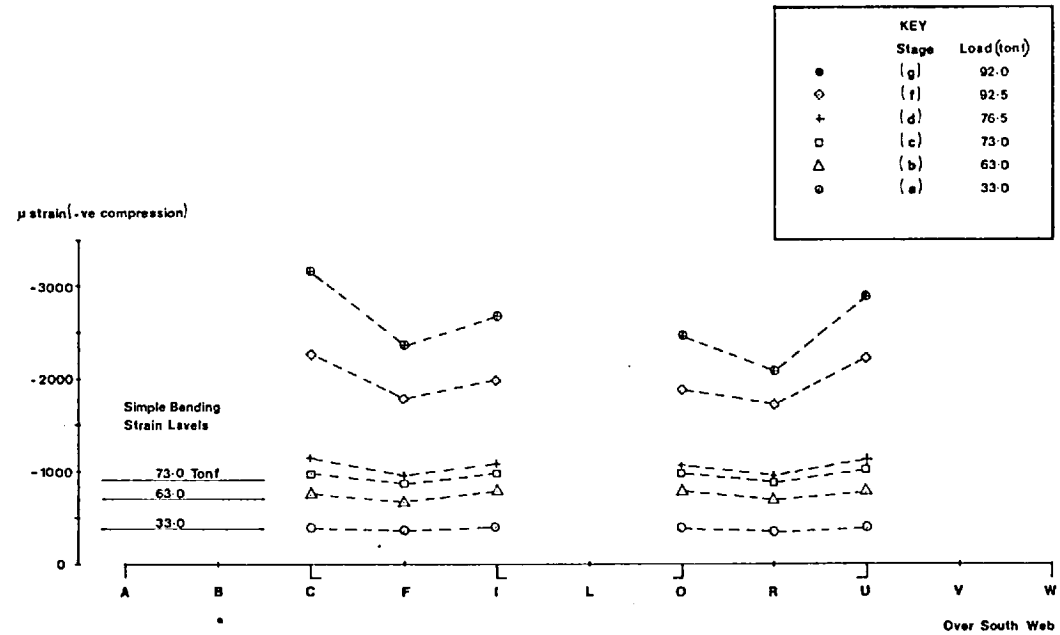

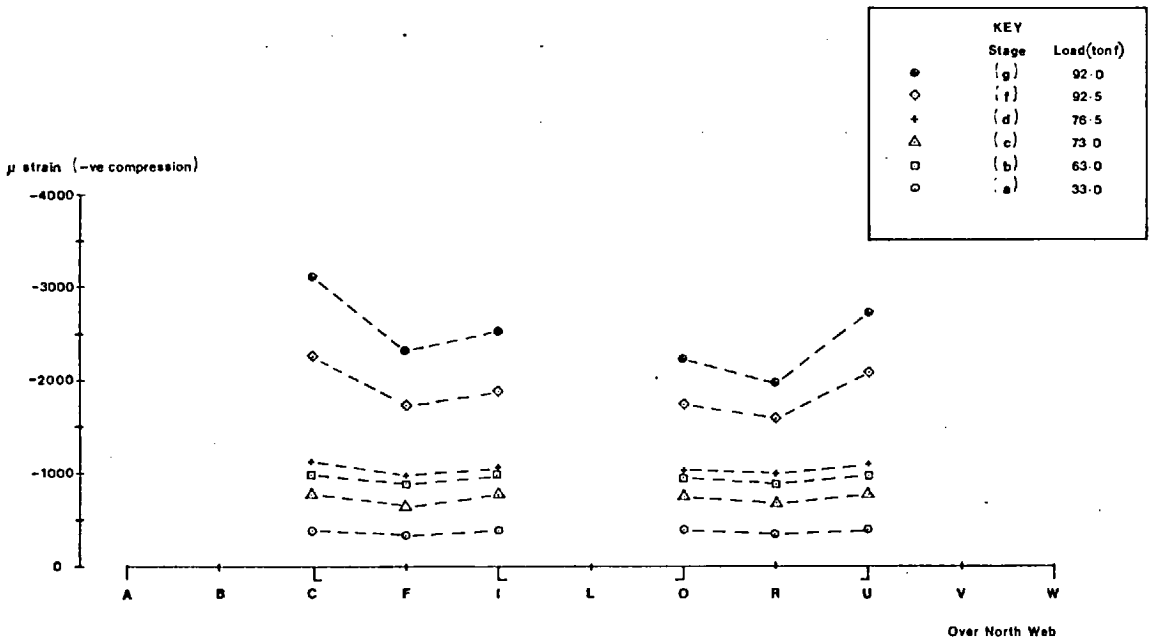

Fig. 2.39a Model 4: Longitudinal Strain in Compression Flange at its Junctions with Webs

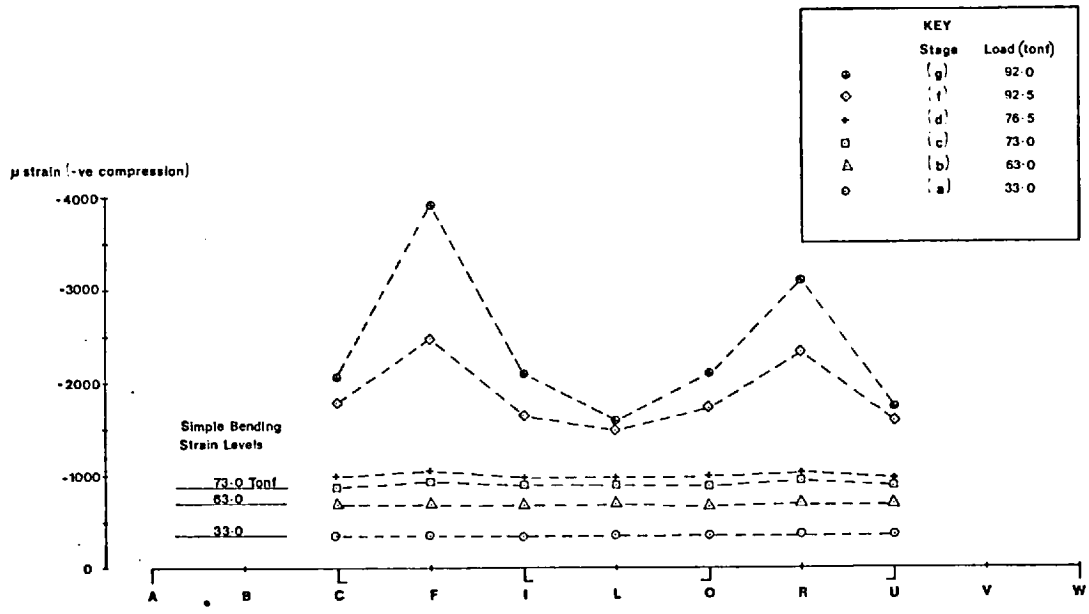

Fig.46 Longitudinal Outer-surface Strain in Compression Flange Along Line of Stiffener S1

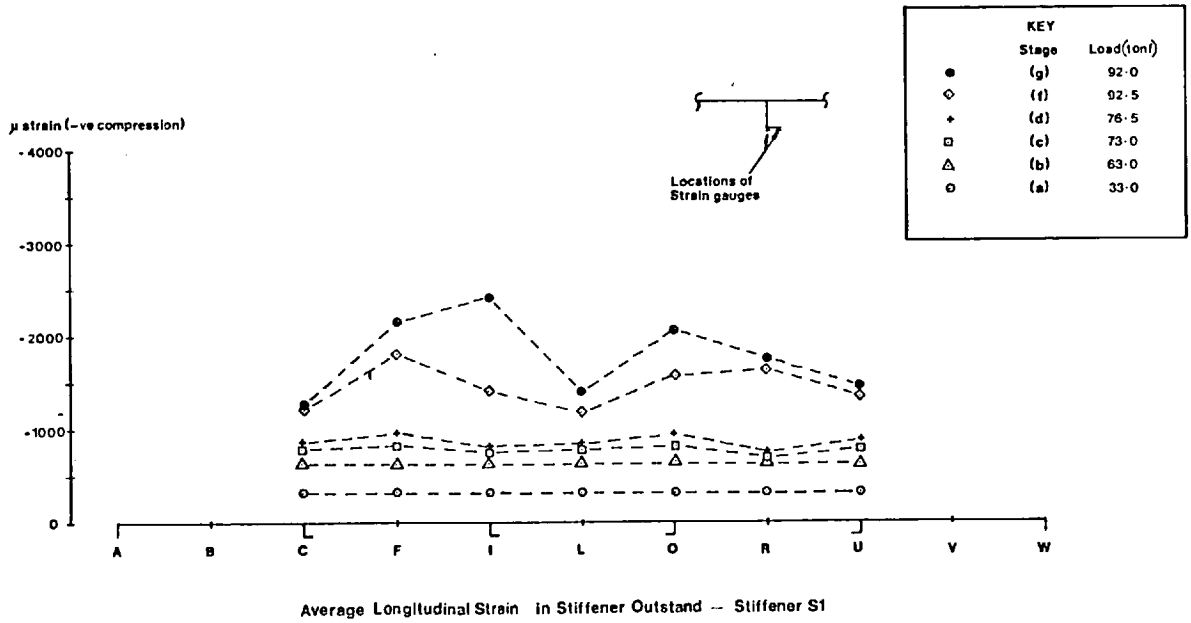

Average Longitudinal Strain in Stiffener Outstand -- Stiffener S1

Fig. 2.39b Model 4: Strain in Stiffener S1

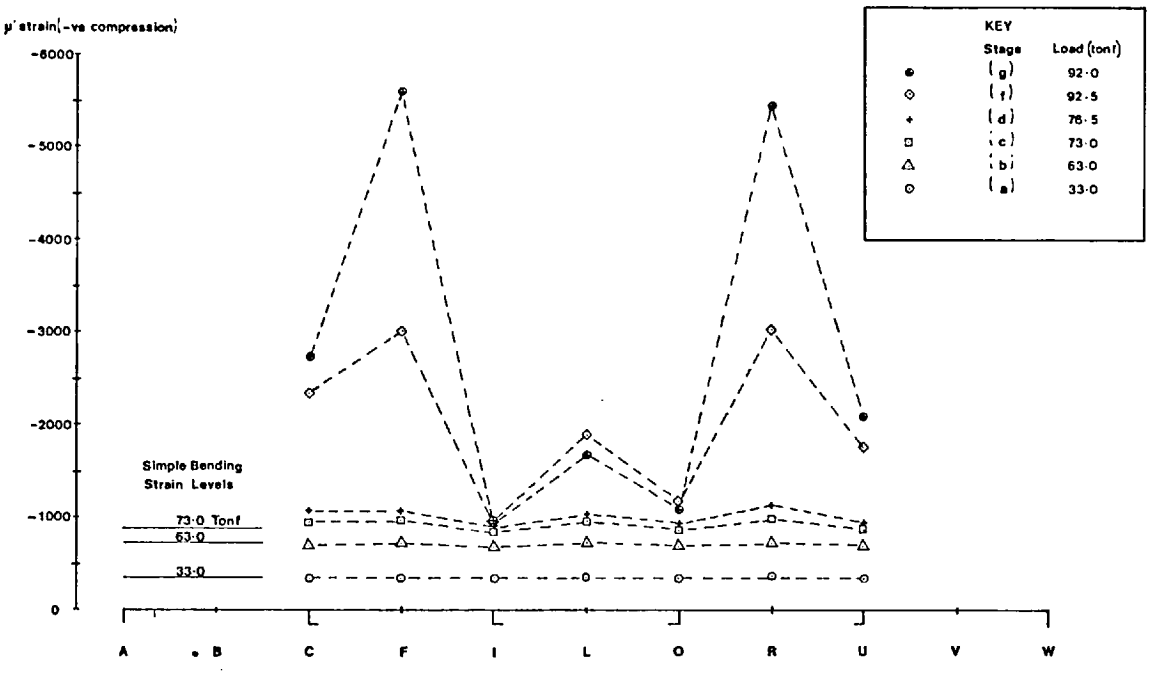

Longitudinal Outer – surface strain in Compression Flange Along Line of Stiffener S3

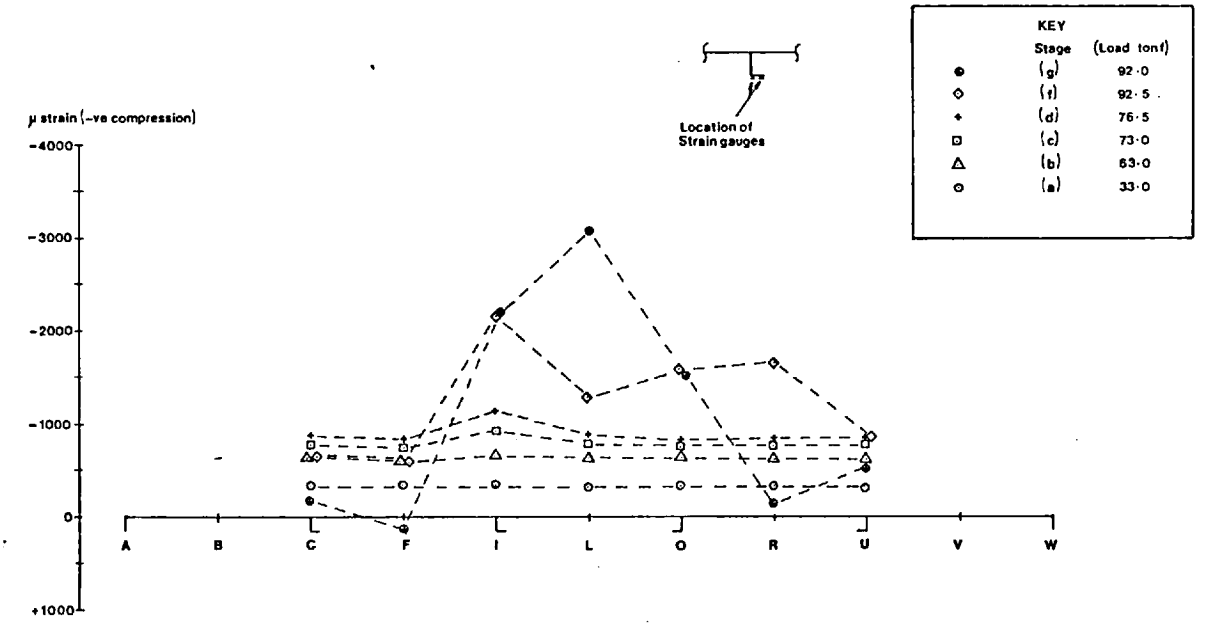

Average Longitudinal Strain in Stiffener Outstand – Stiffener S3

Fig. 2.39c Model 4: Strain in Stiffener S3

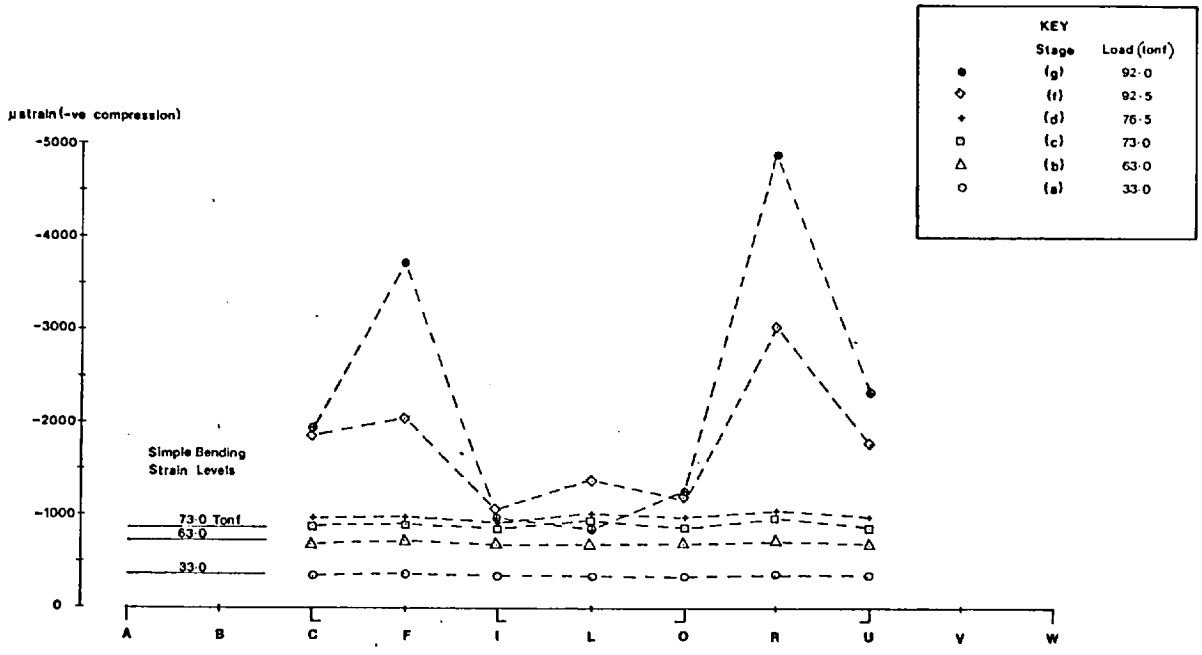

Longitudinal Outer – surface strain in Compression Flange Along Line of Stiffener S5

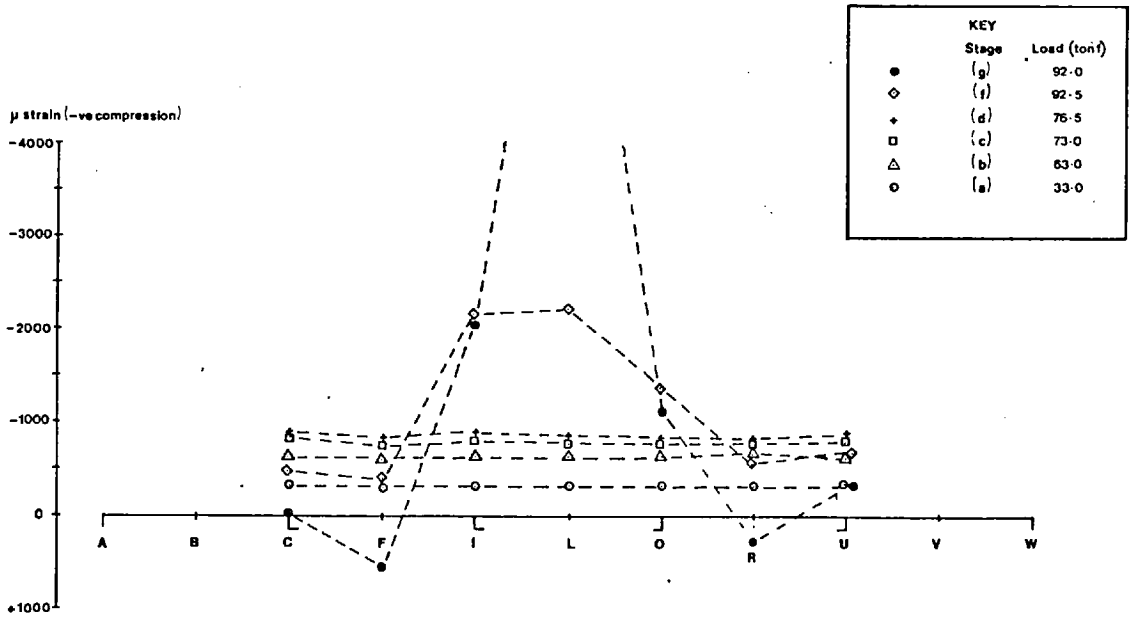

Average Longitudinal Strain In Stiffener Outstand – Stiffener S5

Fig 2.39d Model 4: Strain in Stiffener S5

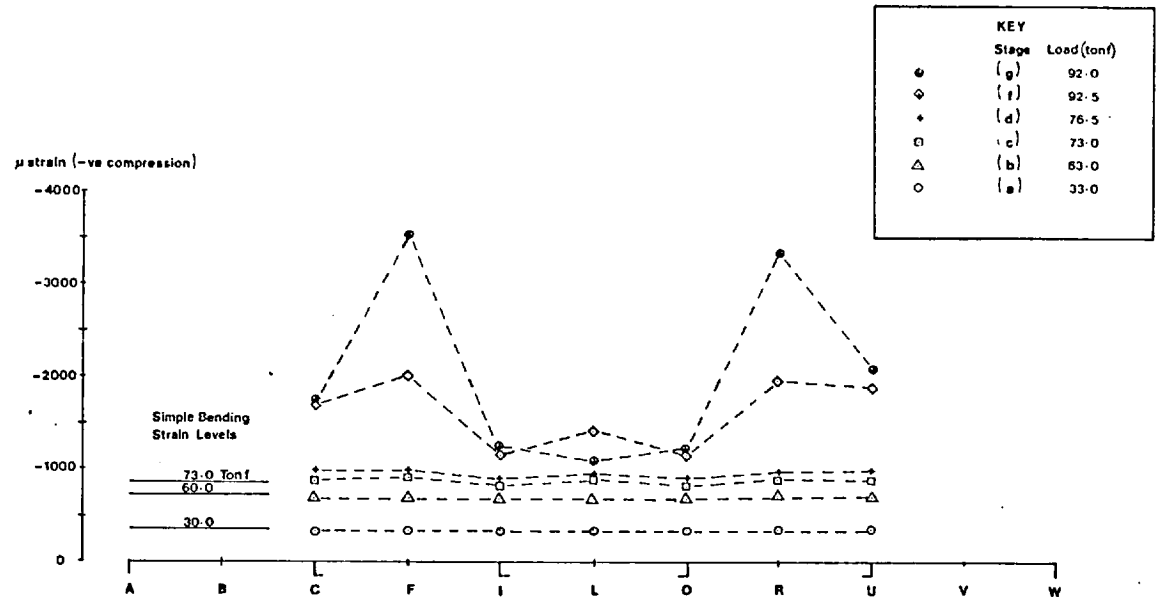

Longitudinal Outer – surface strain in Compression Flange Along Line of Stiffener S7

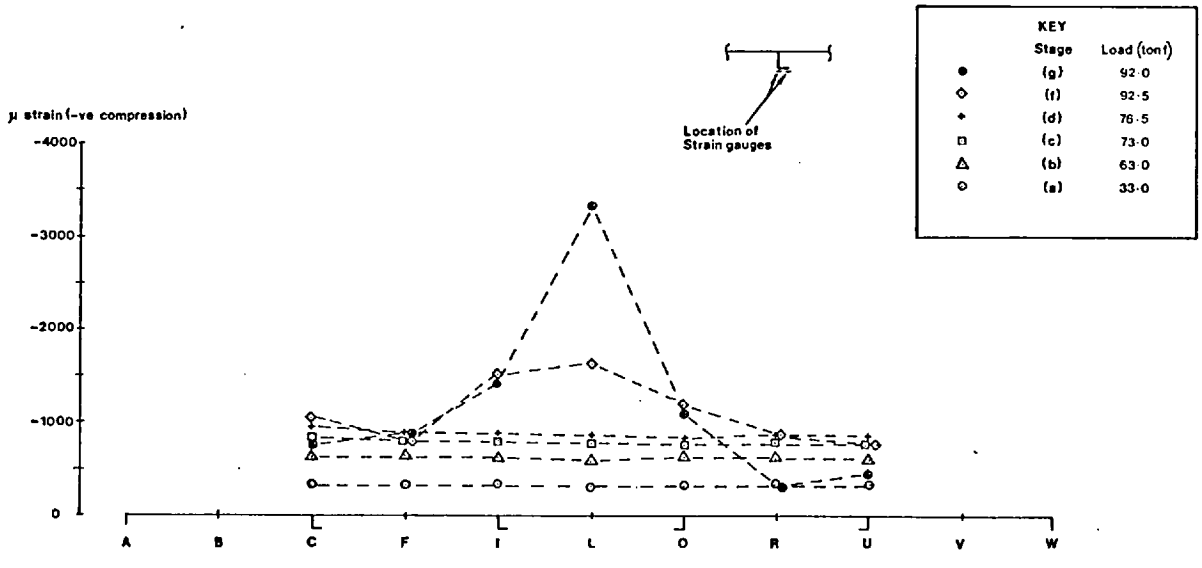

Average Longitudinal Strain In Stiffener Outstand — Stiffener S7

Fig. 2.39e Model 4: Strain in Stiffener S7.

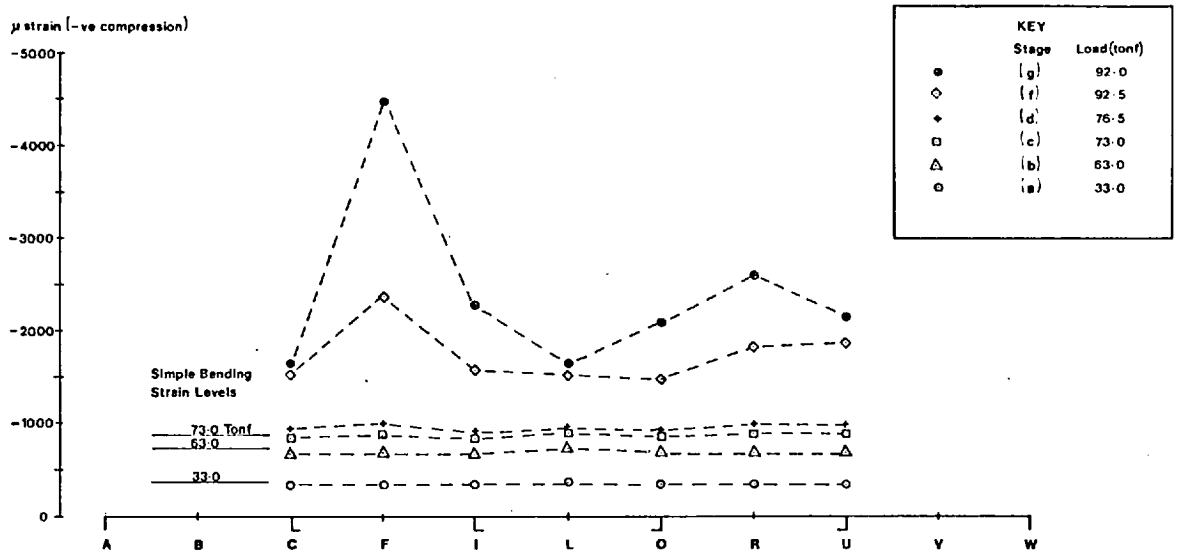

Longitudinal Outer – surface strain in Compression Flange Along Line of Stiffener S9

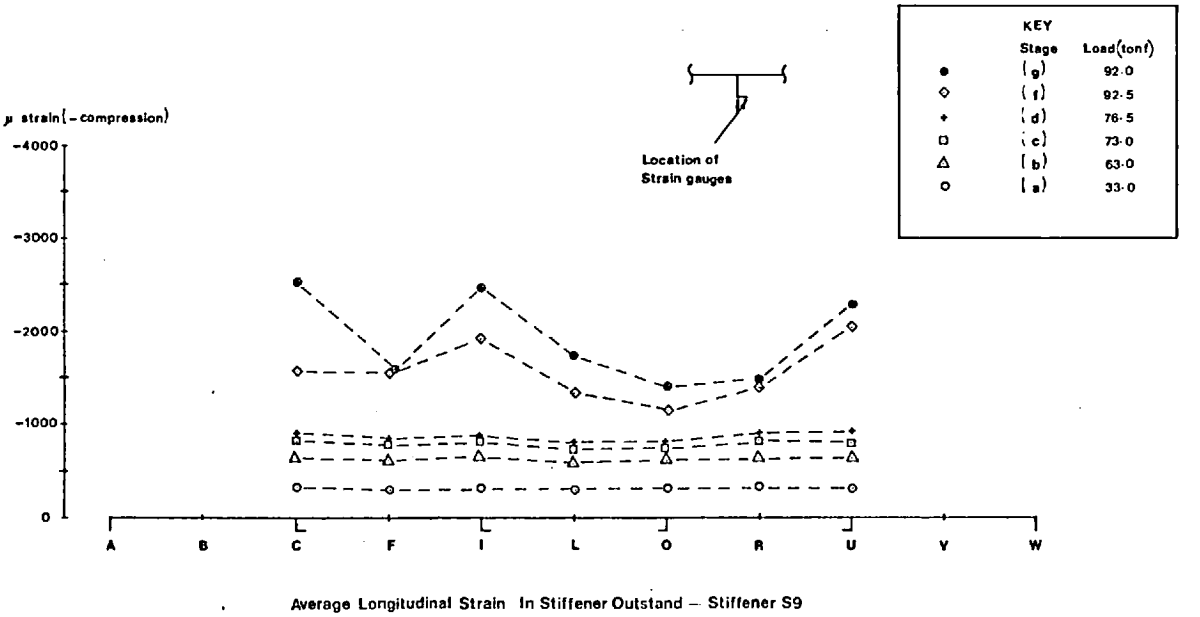

Average Longitudinal Strain In Stiffener Outstand – Stiffener S9

Fig. 2.39f Model 4: Strain in Stiffener S9

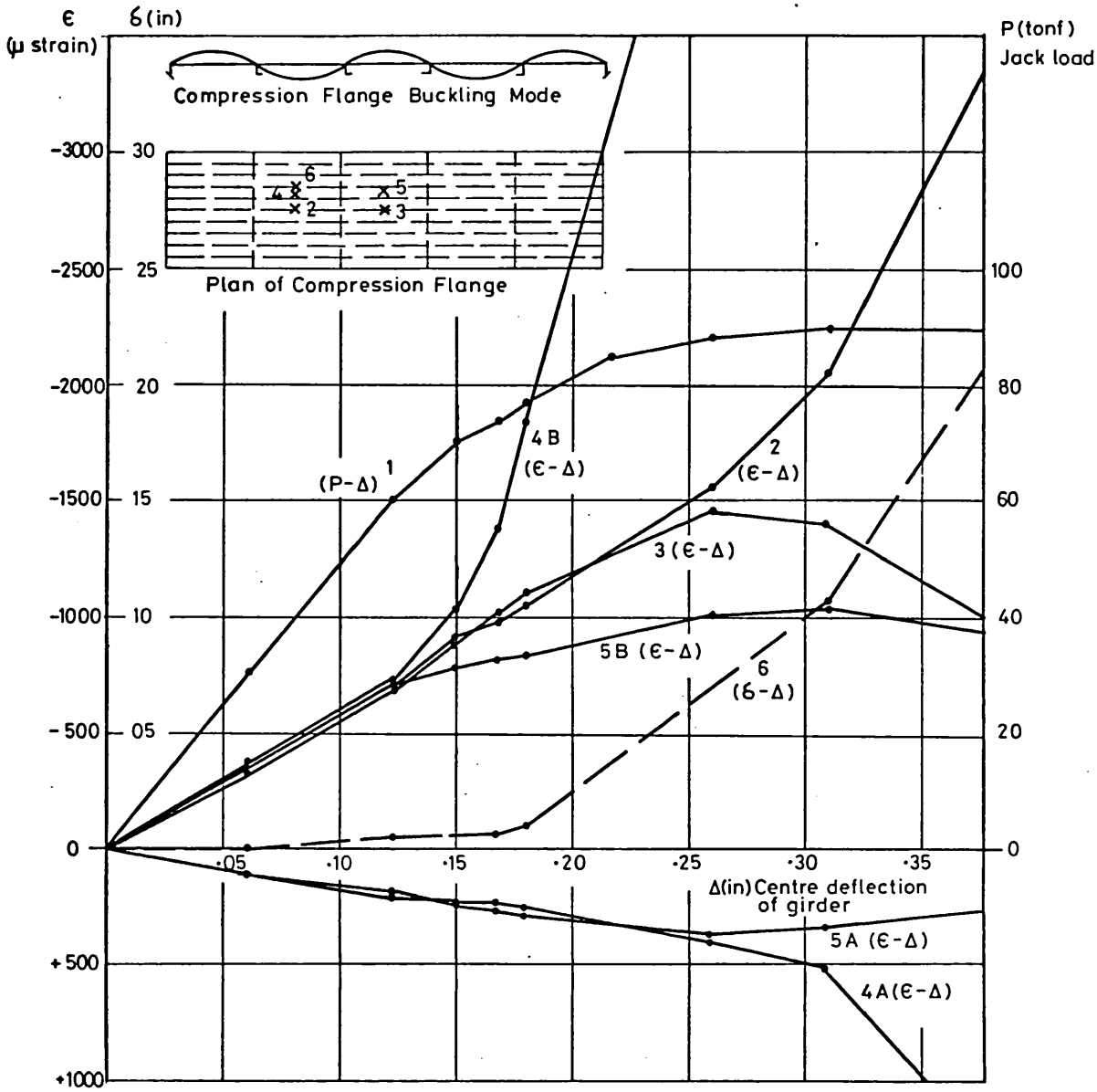

CURVE 1 OVERALL LOAD - DEFLECTION RELATIONSHIP
CURVE 2 MID-PLANE STRAIN AT LOCATION 2
CURVE 3 MID-PLANE STRAIN AT LOCATION 3
CURVE 4A TRANSVERSE MID-PLANE STRAIN AT LOCATION 4
CURVE 4B MID-PLANE STRAIN AT LOCATION 4
CURVE 5A TRANSVERSE MID-PLANE STRAIN AT LOCATION 5
CURVE 5B MID-PLANE STRAIN AT LOCATION 5
CURVE 6 STIFFENER OUT-OF-PLANE DEFLECTION AT LOCATION 6

Note : DATUM LOAD WAS 3 tonf. THUS TOTAL LOAD ON MODEL IS (P+3) tonf

Fig. 2.40 Model 4. Growth of Deflections and Strains with Load.

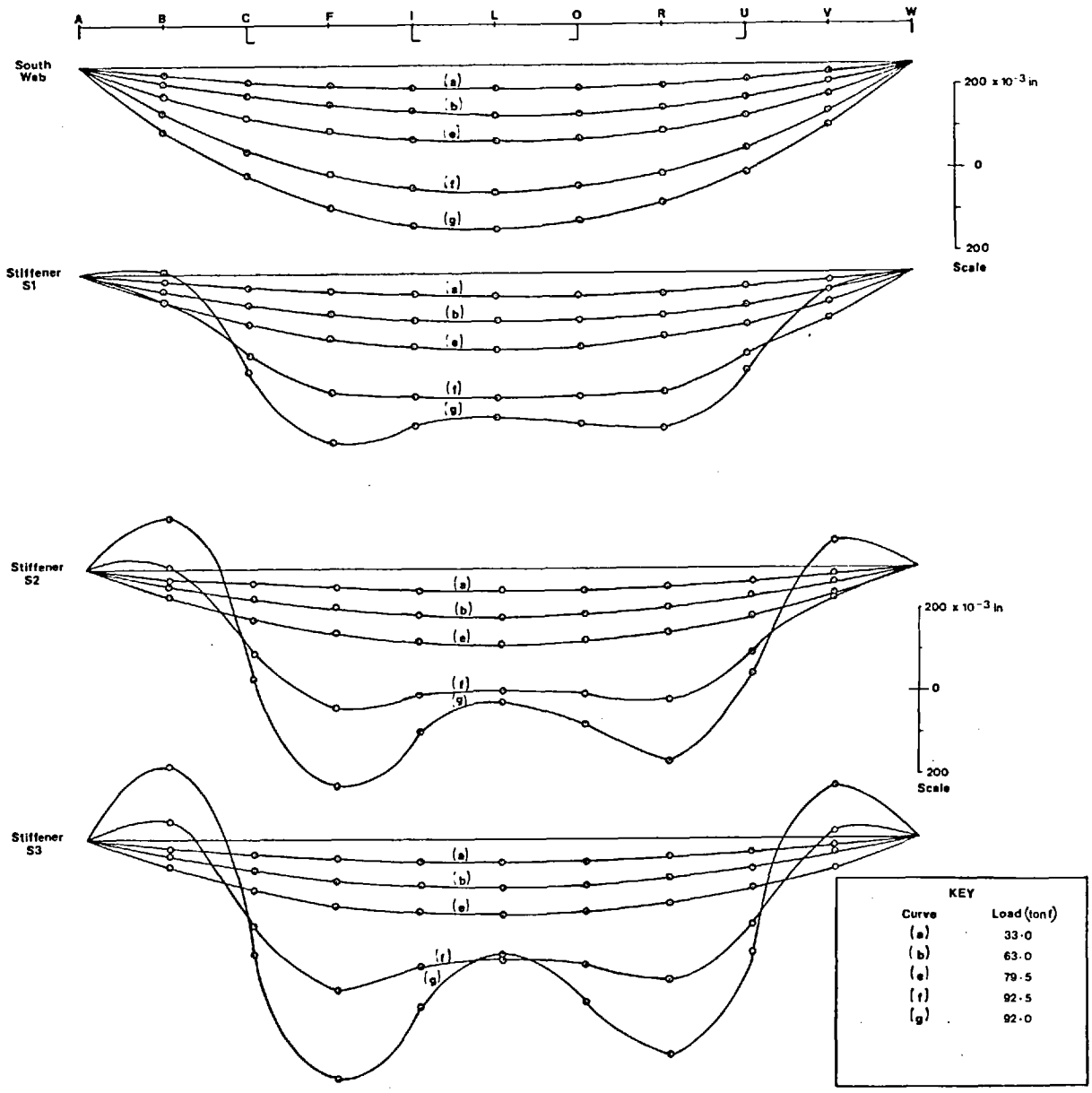

Fig. 2.41a Model 4: Longitudinal Deflections (Relative to Initial Shape)

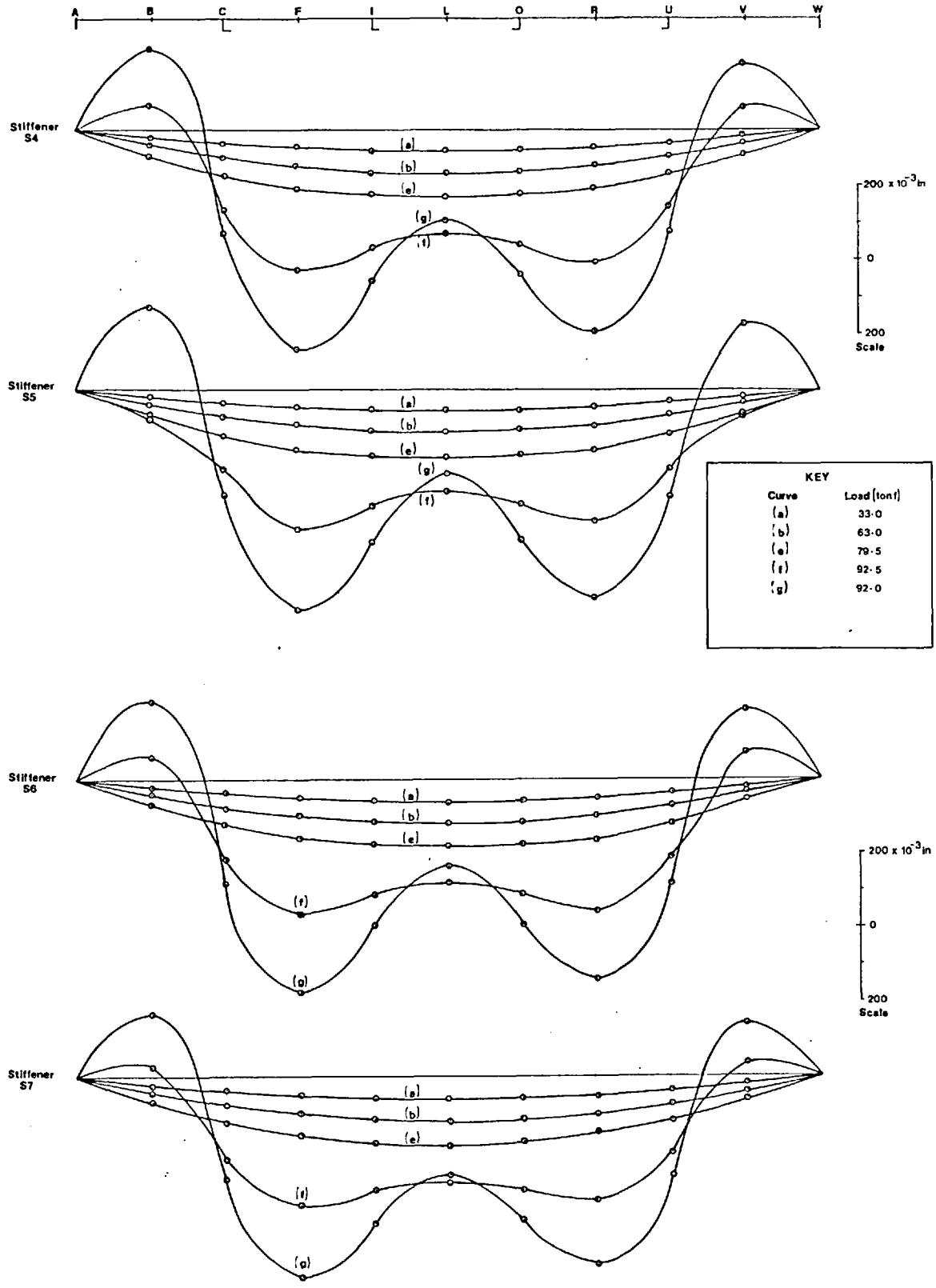

Fig. 2.41b Model 4: Longitudinal Deflections (Relative to Initial Shape)

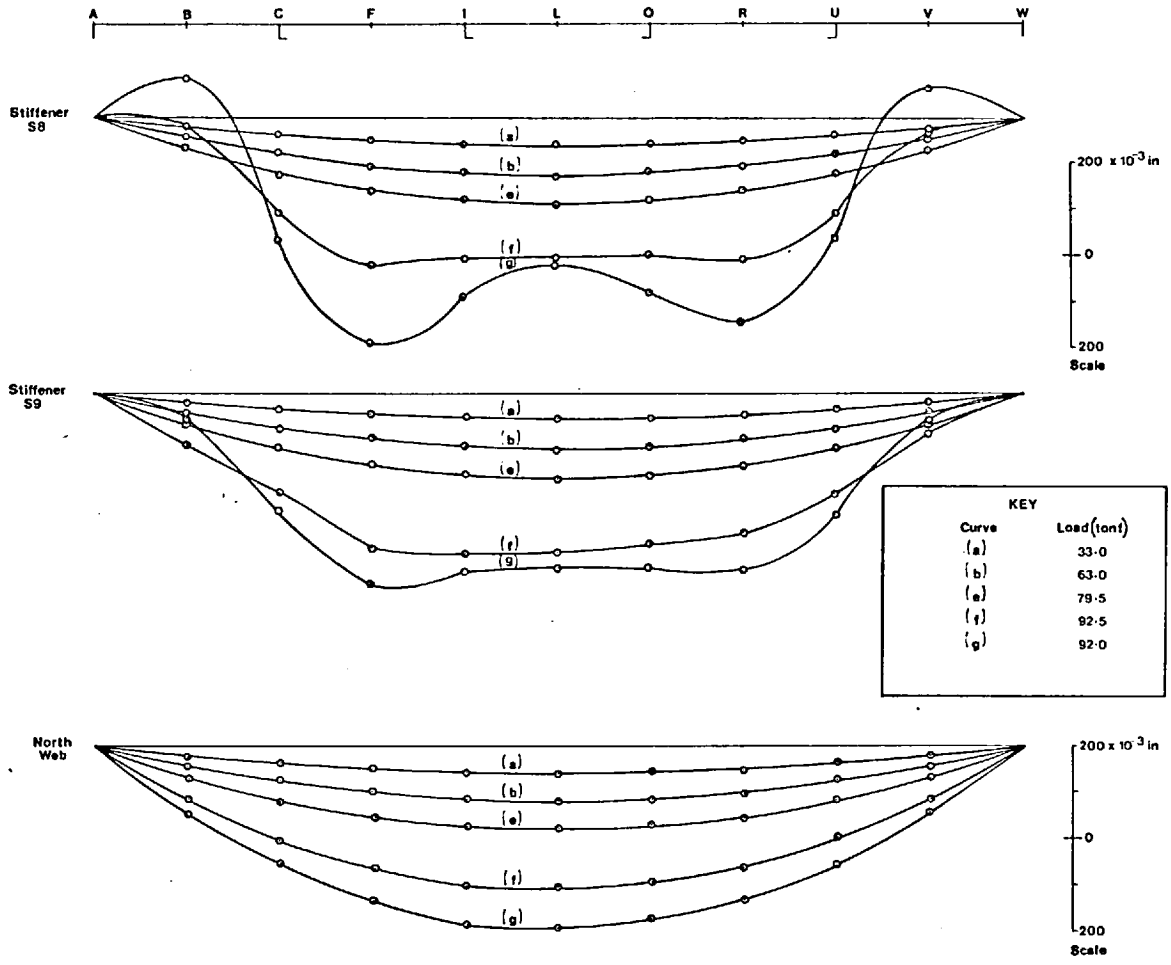

Fig. 2.41c Model 4: Longitudinal Deflections.

(Relative to Initial Shape)

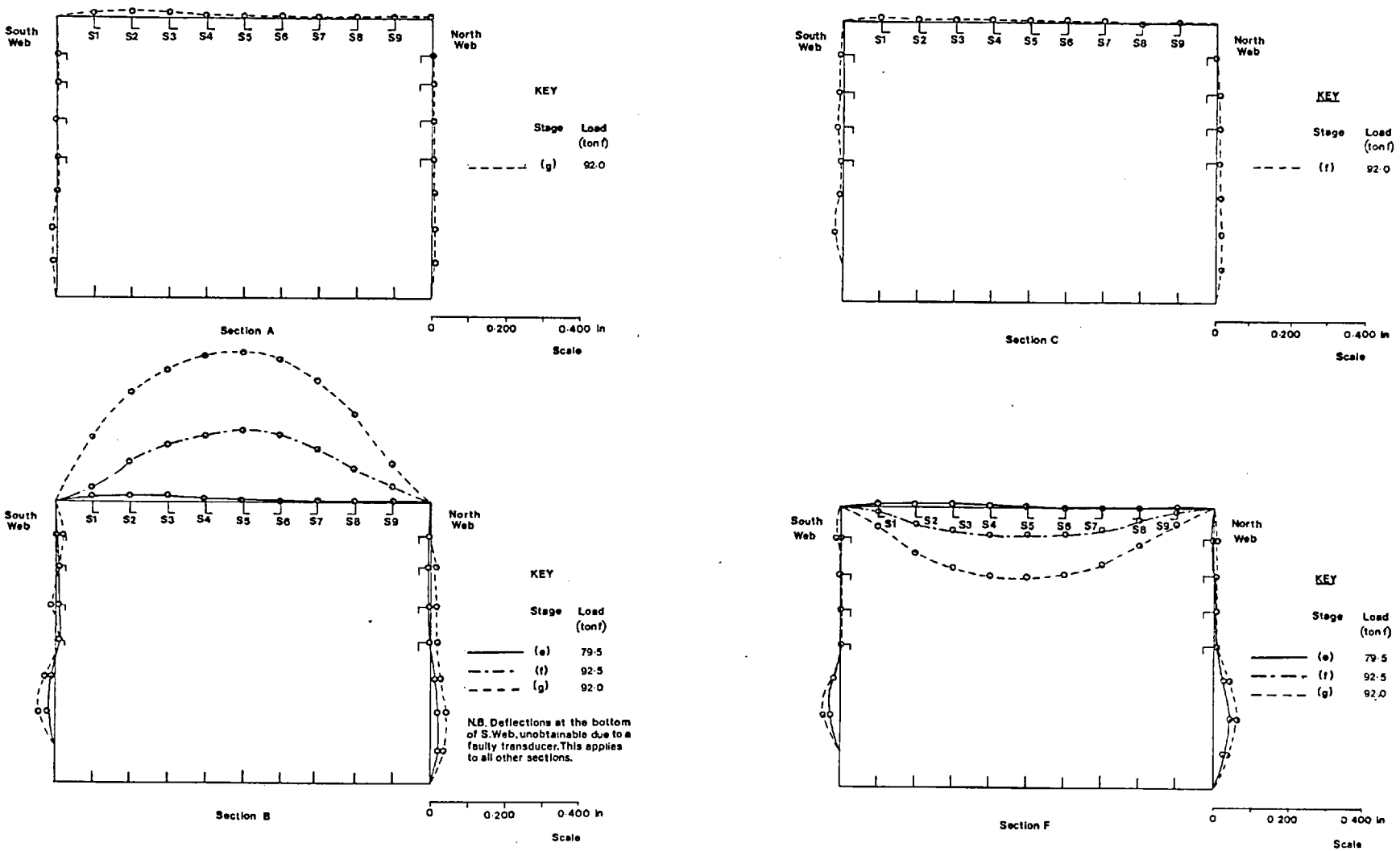

Fig. 2.42a Model 4: Transverse Deflections (Relative to Initial Shape)

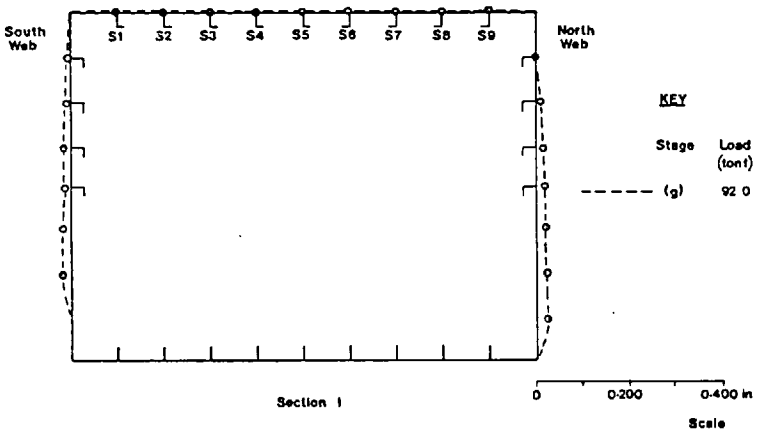

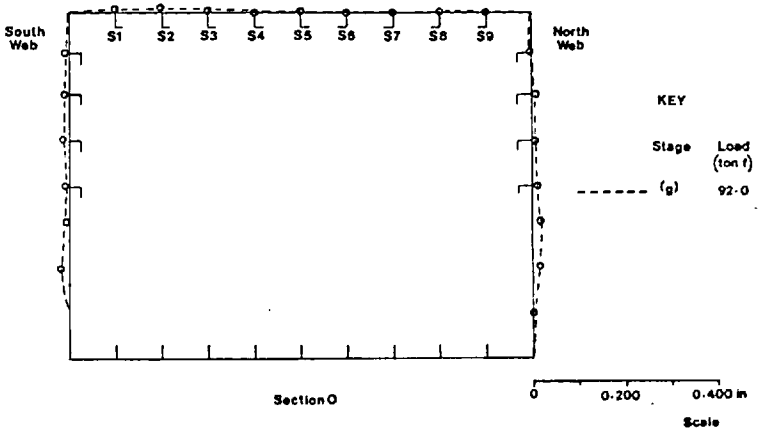

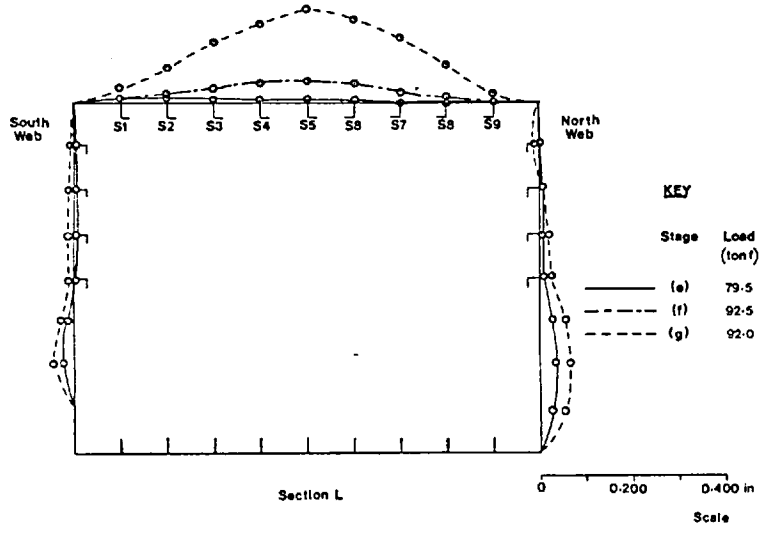

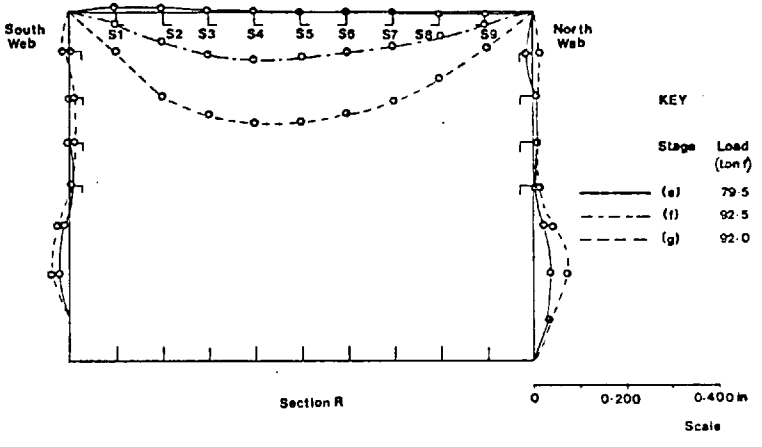

Fig. 2.42b Model 4: Transverse Deflections (Relative to Initial Shape)

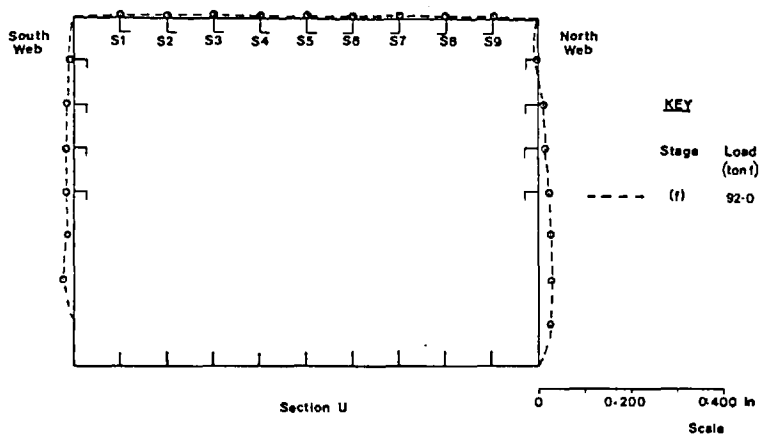

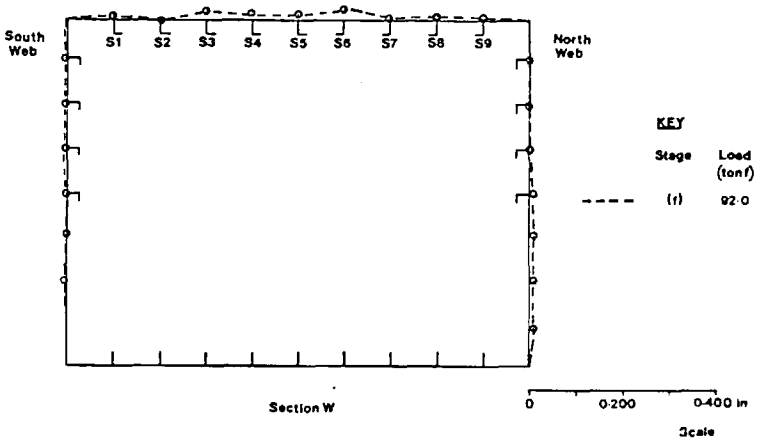

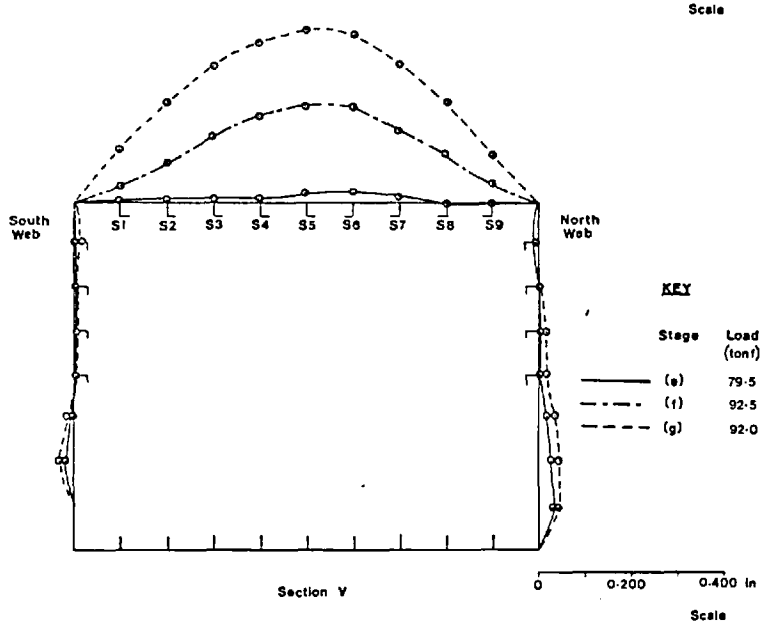

Fig. 2.42c Model 4: Transverse Deflections (Relative to Initial Shape)

Fig. 2.43a. Model 4 - showing part of the compression flange after the test to failure. Stiffener locations are indicated by dashed lines.

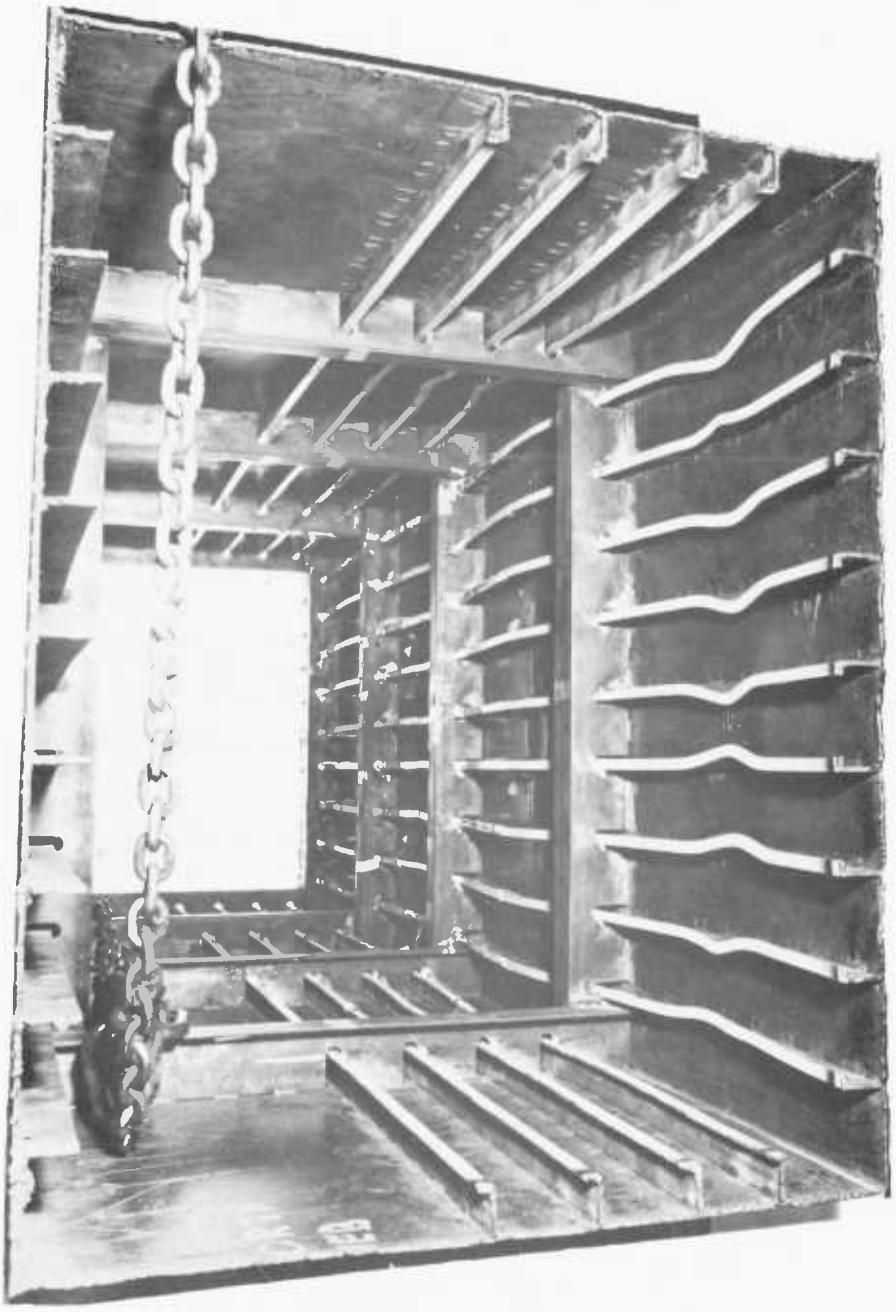

Fig. 2.43b. Model 4 - an interior view of the model (from end A) after failure.

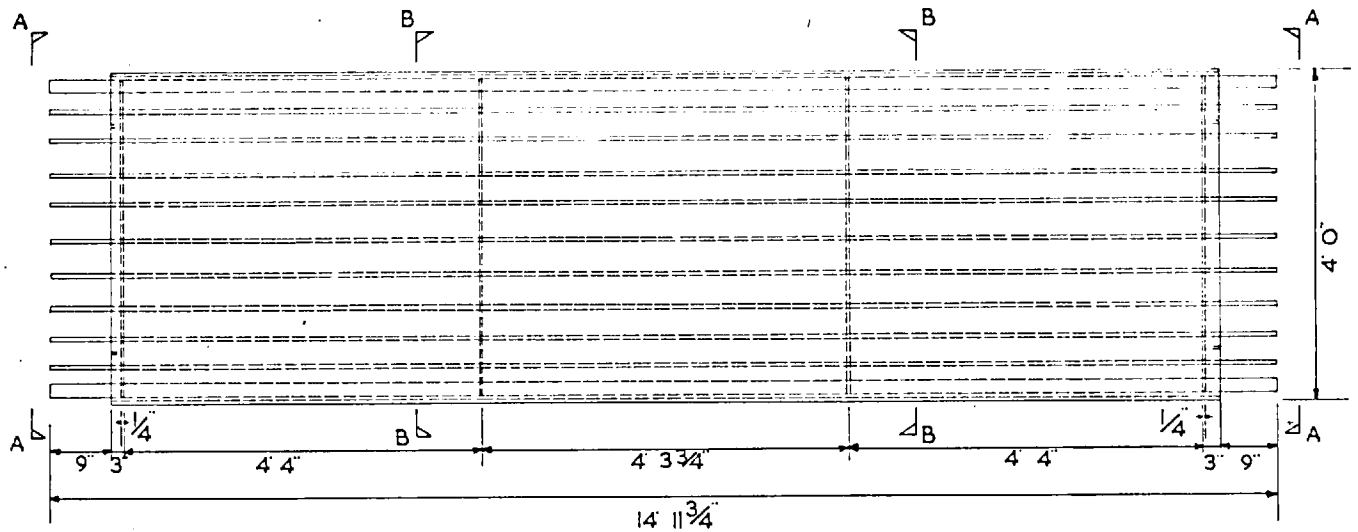

PLAN OF COMPRESSION FLANGE

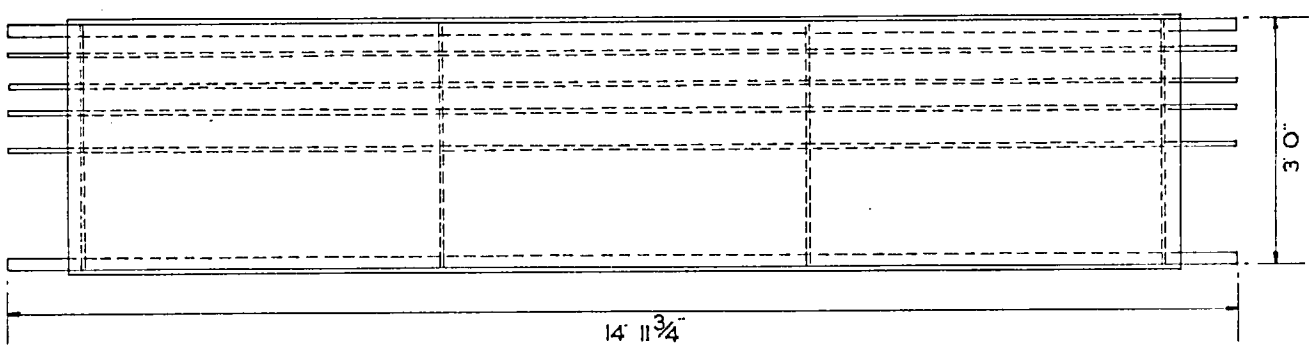

SIDE ELEVATION

Fig. 2.44a Model 8 : Plan and Elevation

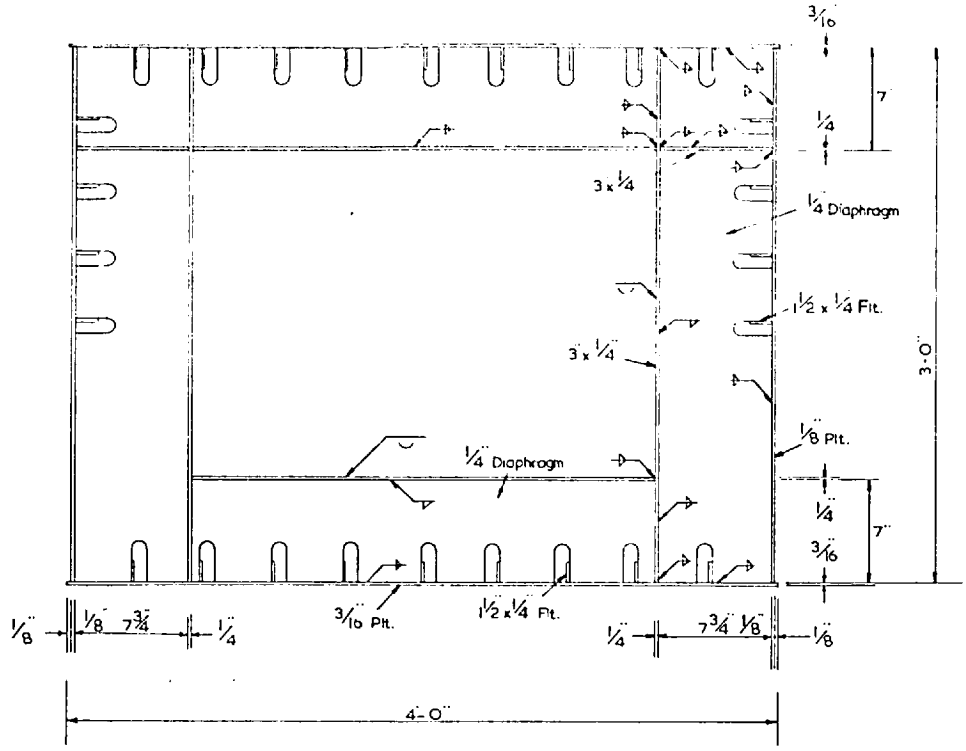

SECTION A-A

NOTES :

1. Unless noted otherwise all welds are 1/8" fillet welds (measured across throat).
2. 1 1/2" x 1 1/4" Flats are continuous throughout the length of the model

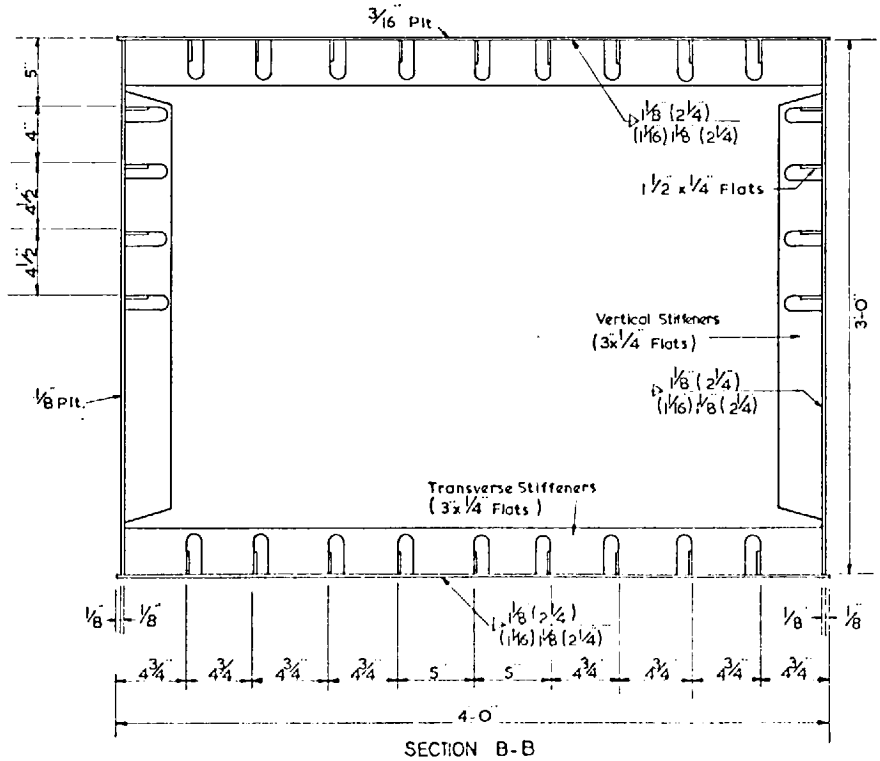

SECTION B-B

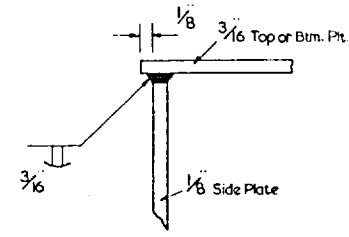

WELDING DETAIL AT CORNER OF BOX GIRDER

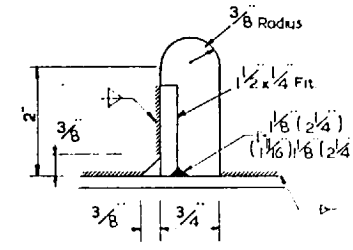

DETAIL OF SLOT IN 1/4 DIAPHRAGM, VERTICAL AND TRANSVERSE STIFFENERS

Fig. 2.44b Model 8: Cross-sections

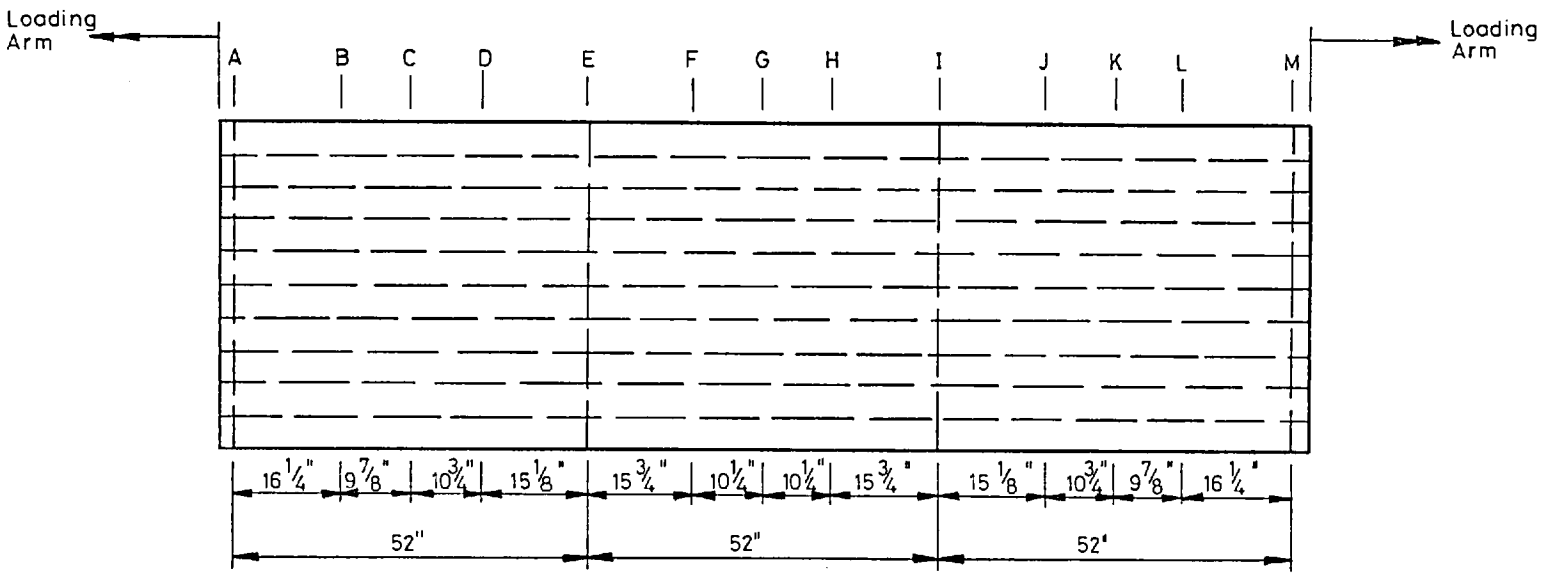

PLAN OF COMPRESSION FLANGE

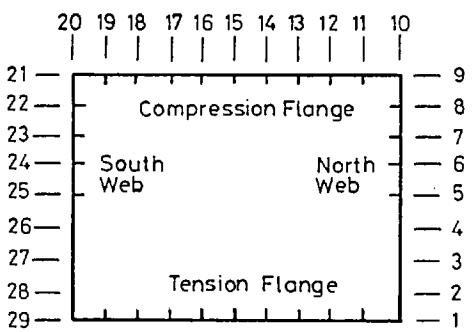

CROSS SECTION OF MODEL 8.
(viewed from end A)

Note :
Letters A to M indicate locations along the model

Fig. 2.45 Model 8. Details of Reference Grid

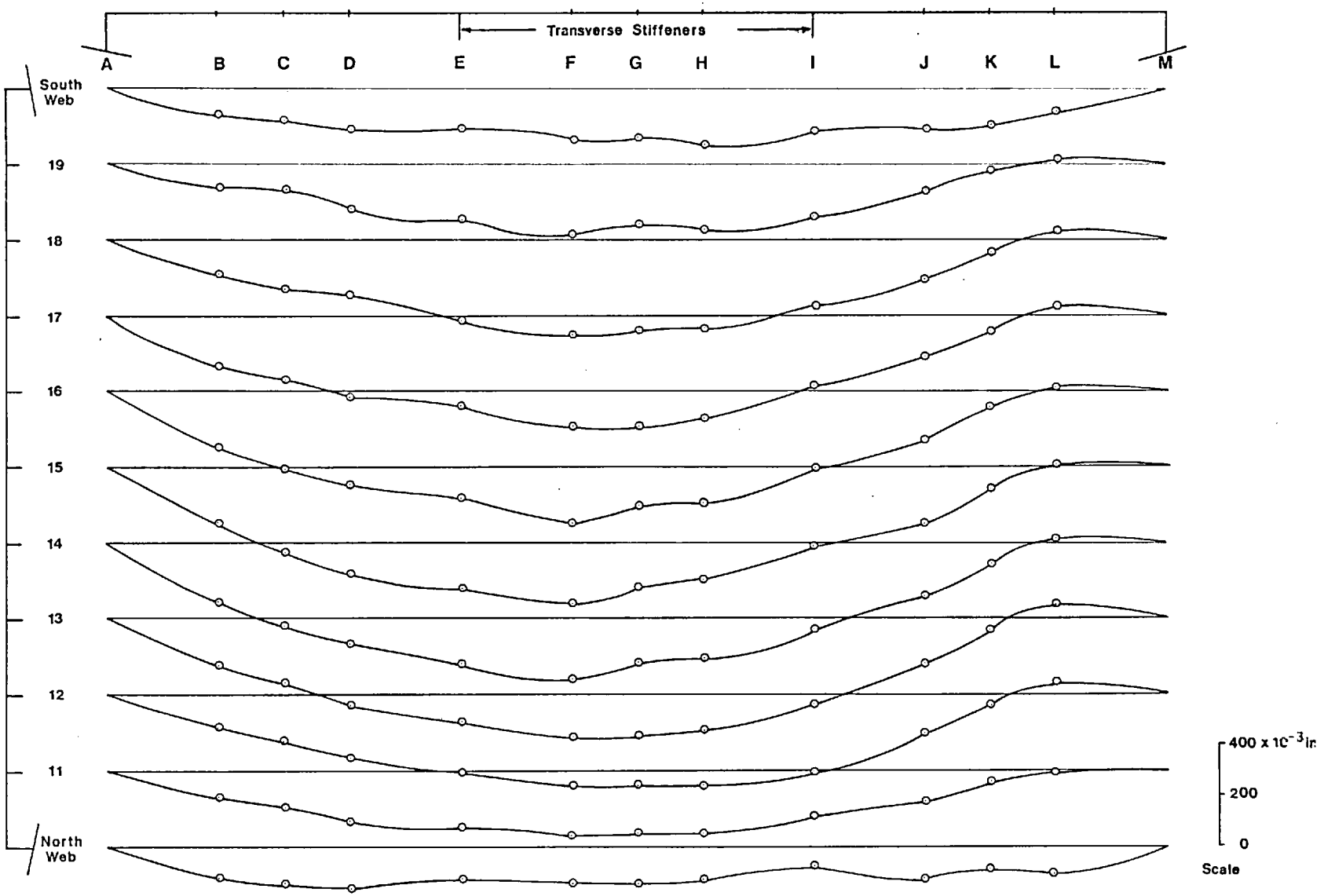

Fig. 2.46a Model 8 : Longitudinal Initial Deflection Profiles of Compression Flange

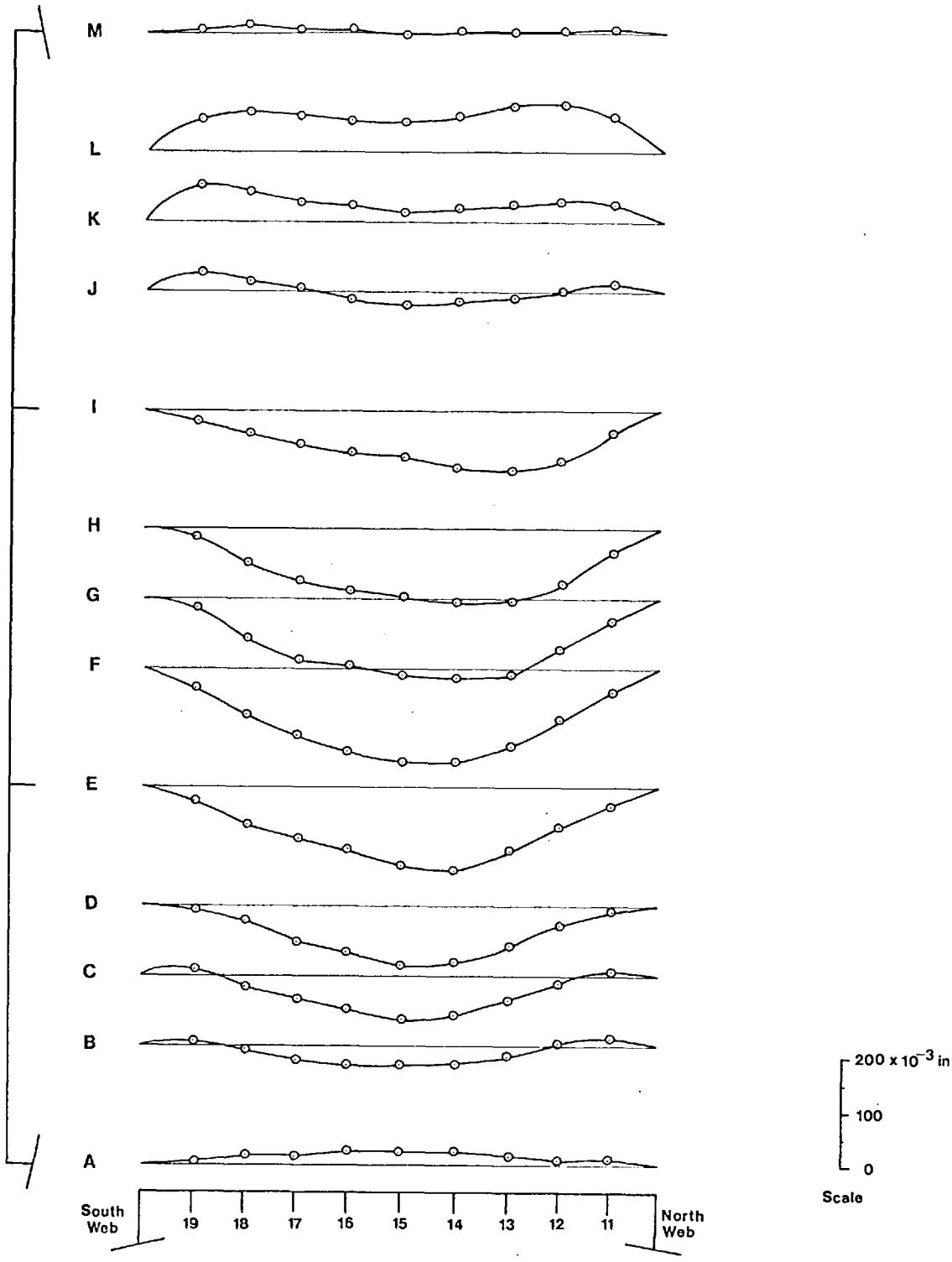

Fig. 2.46b
Model 8: Transverse Initial Deflection Profiles of Compression Flange

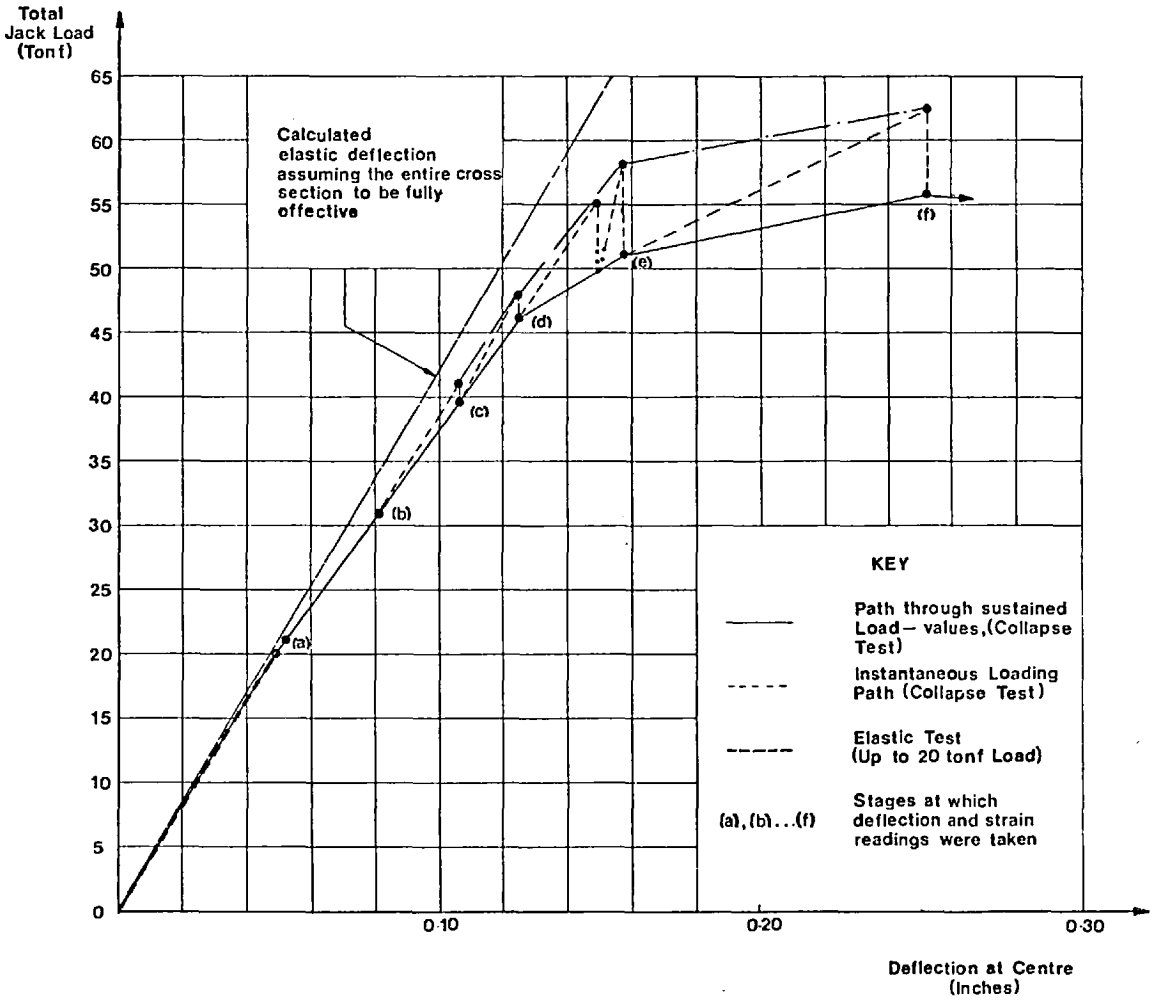

Fig. 2.47 Model 8: Load-Deflection Curve

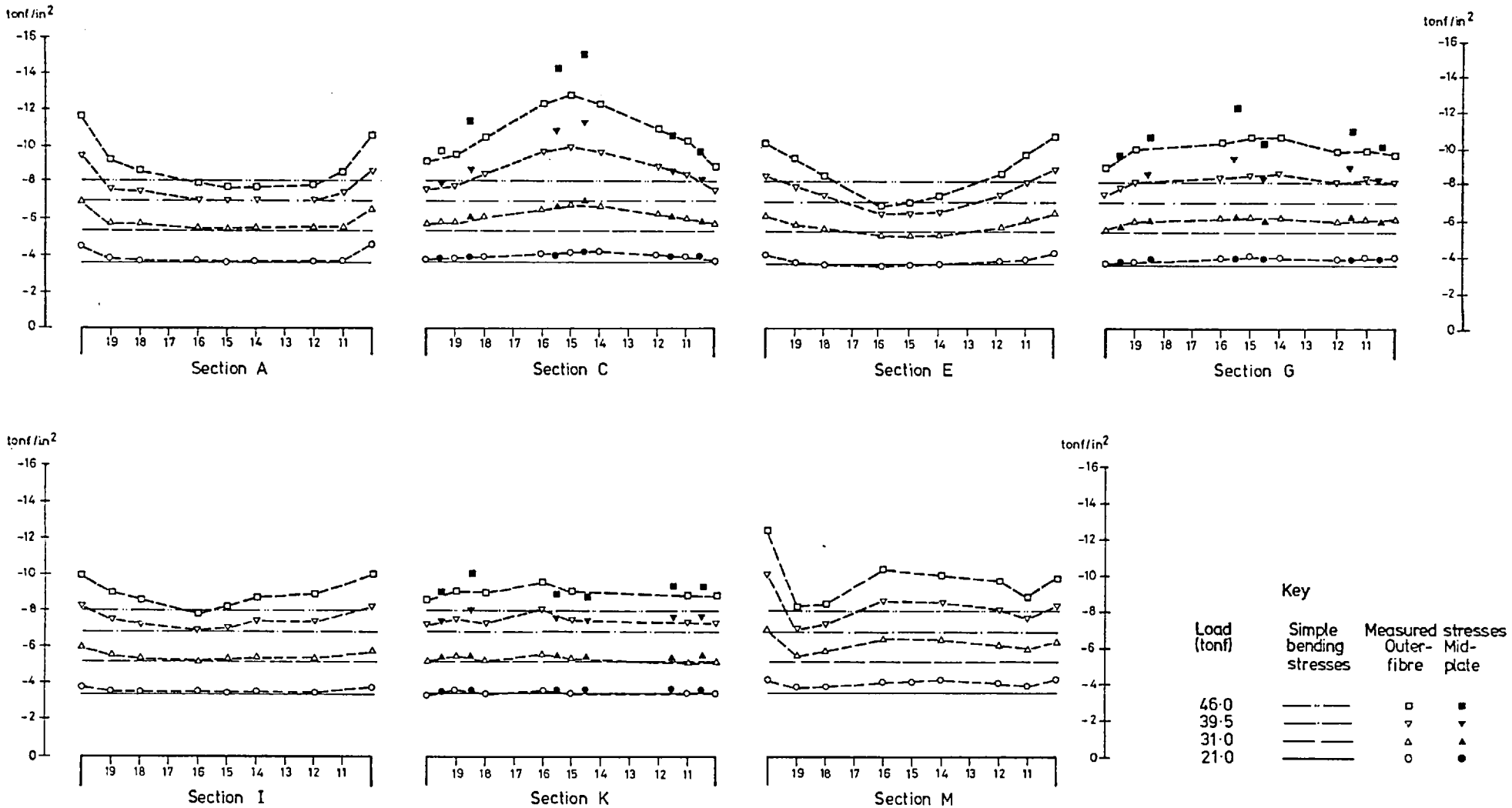

Fig. 2.48
Model 8: Comparison of Theoretical and Measured Compression Flange Longitudinal Stresses.

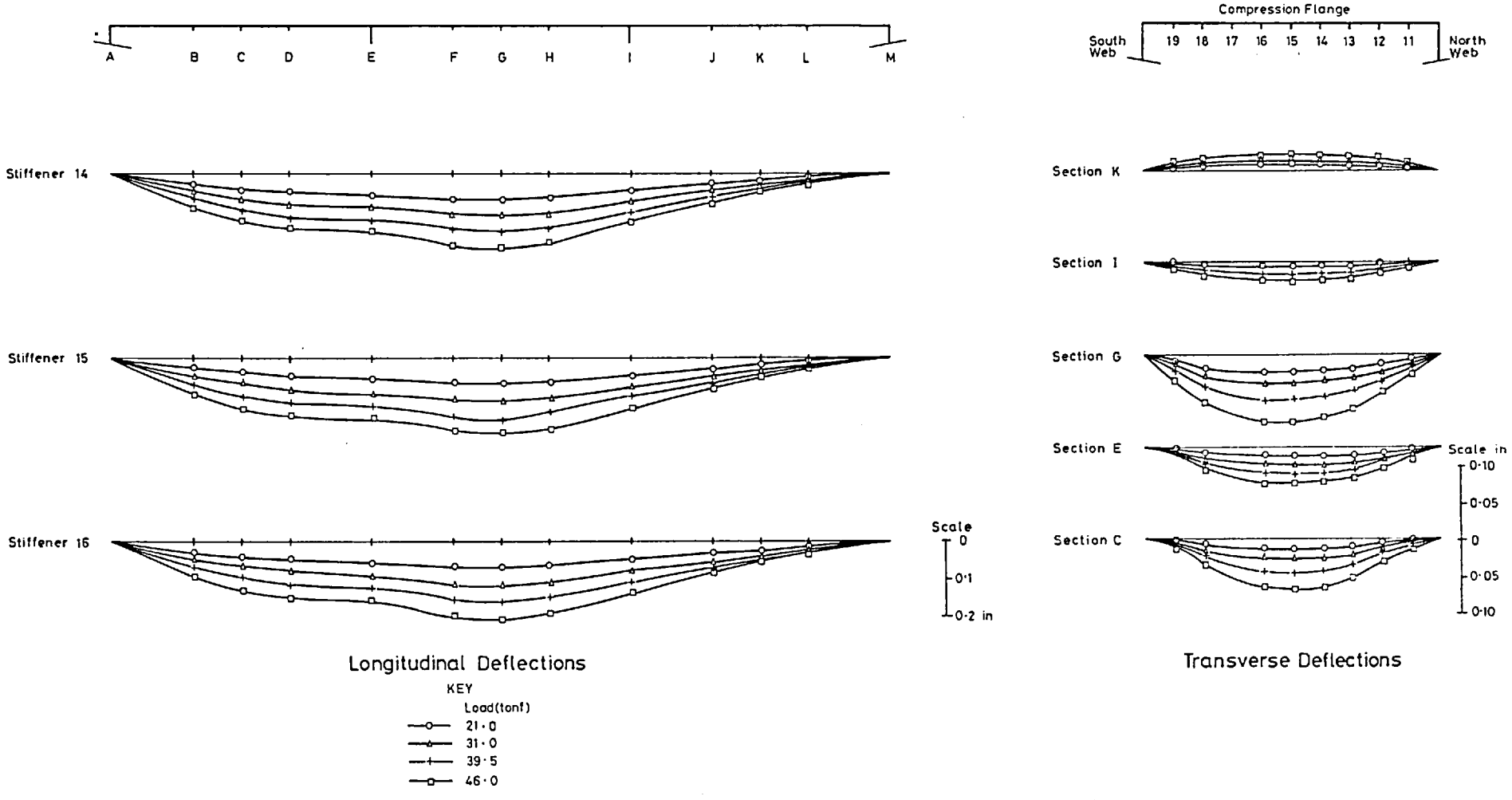

Fig. 2.49a Model 8: Deflections of Compression Flange (Relative to Initial Shape)

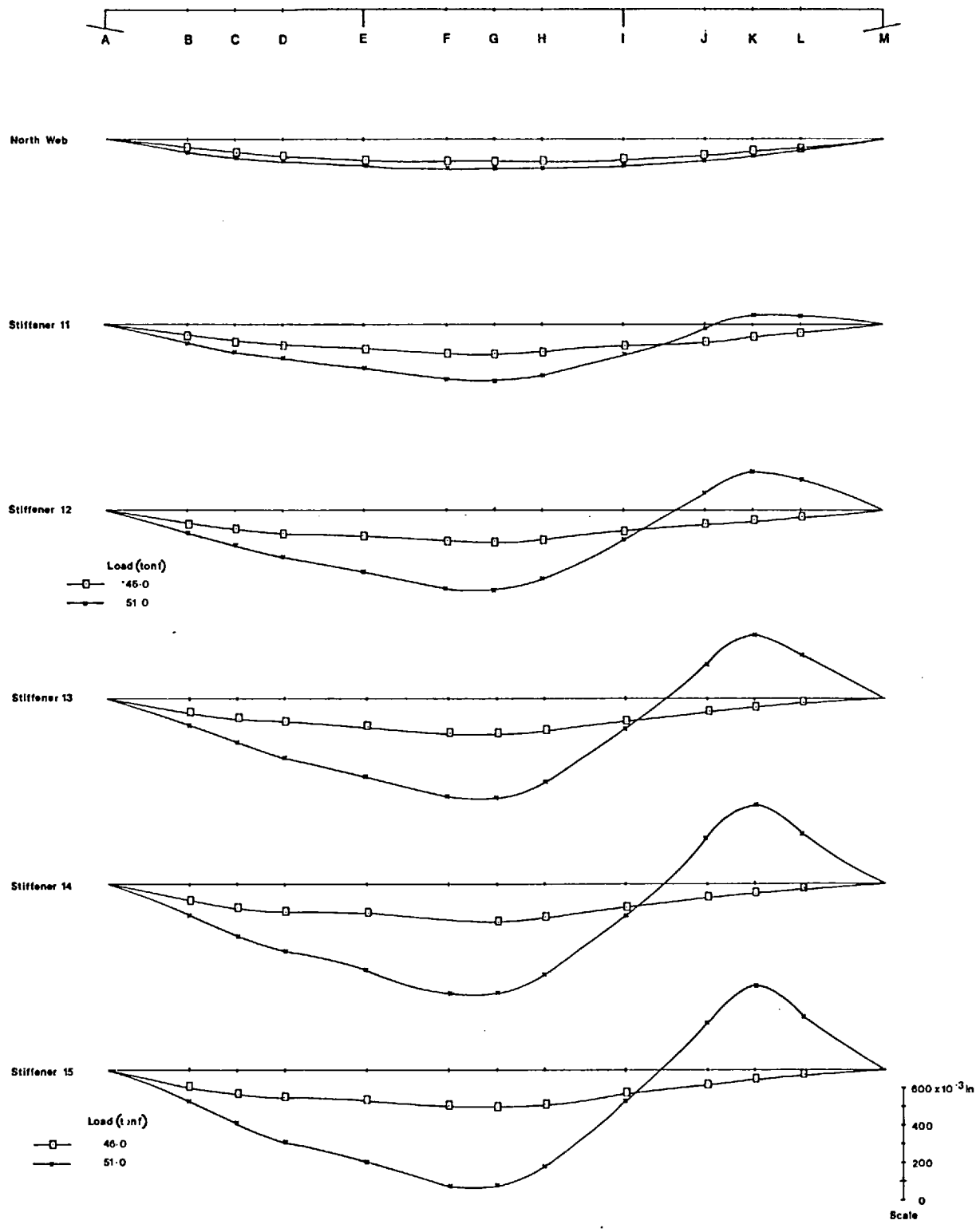

Fig. 2.49b Model 8: Longitudinal Deflections (Relative to Initial Shape)

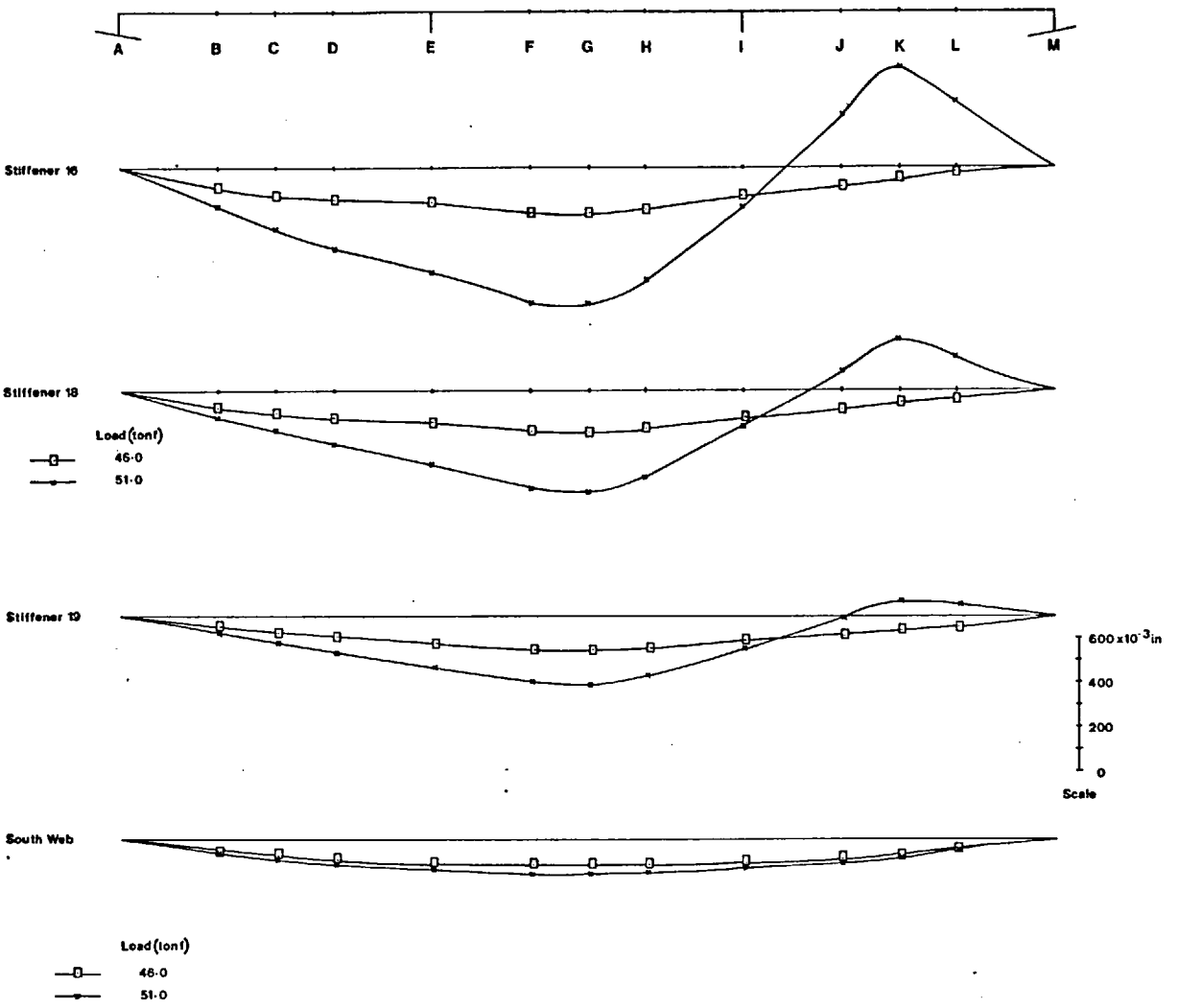

Fig. 2.49c Model 8: Longitudinal Deflections (Relative to Initial Shape)

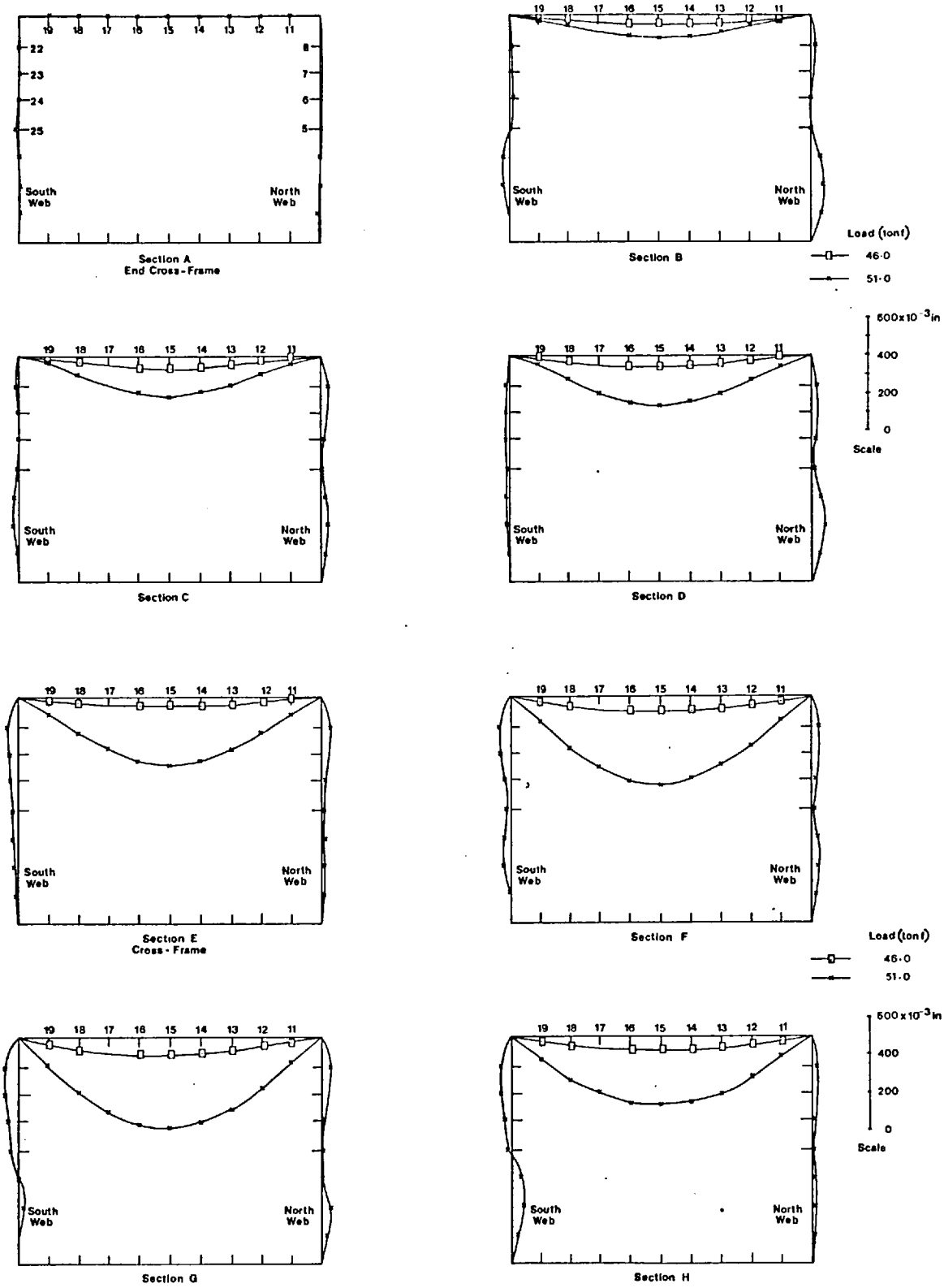

Fig. 2.50a Model 8: Transverse Deflections (Relative to Initial Shape)

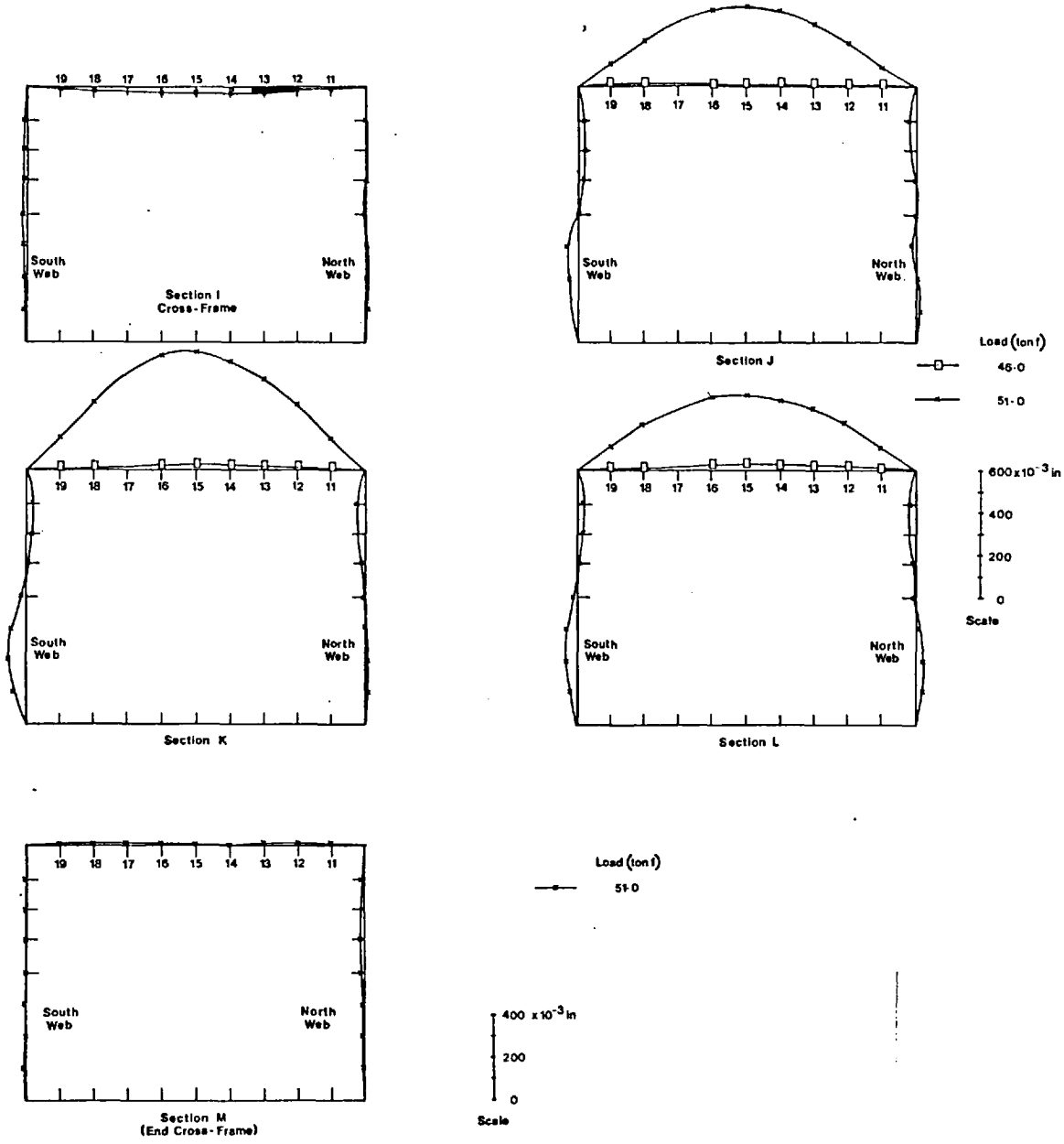

Fig. 2.50b Model 8: Transverse Deflections (Relative to Initial Shape)

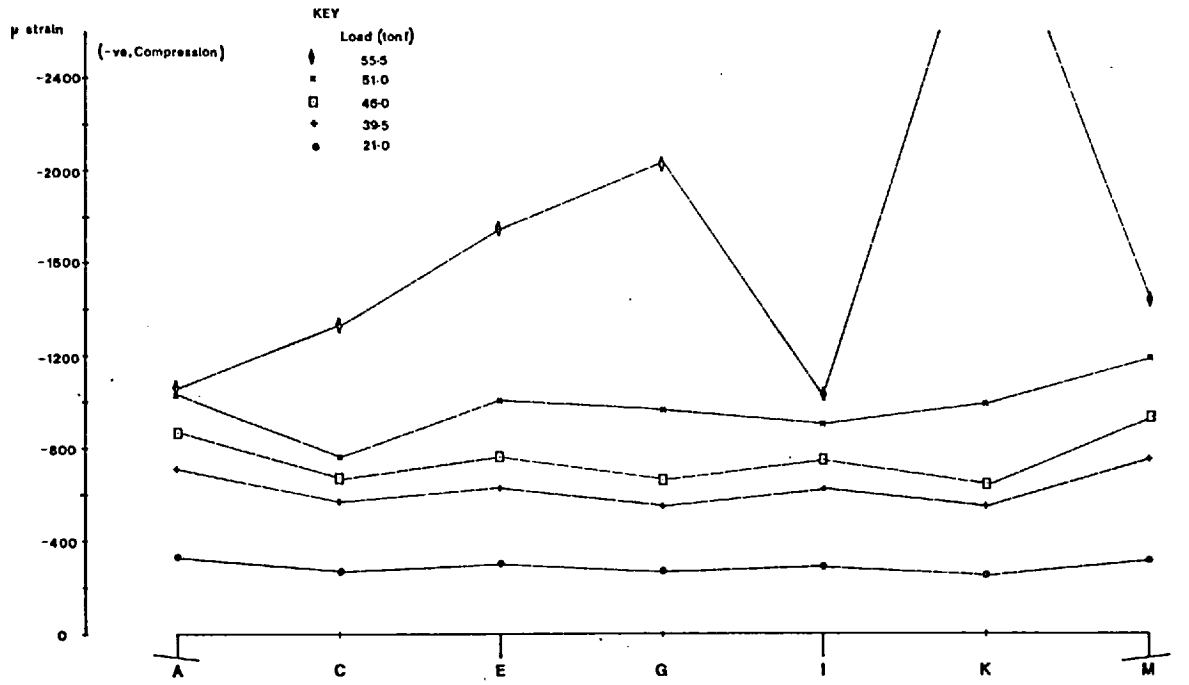

Longitudinal Outer Surface Strain in Compression Flange over South Web

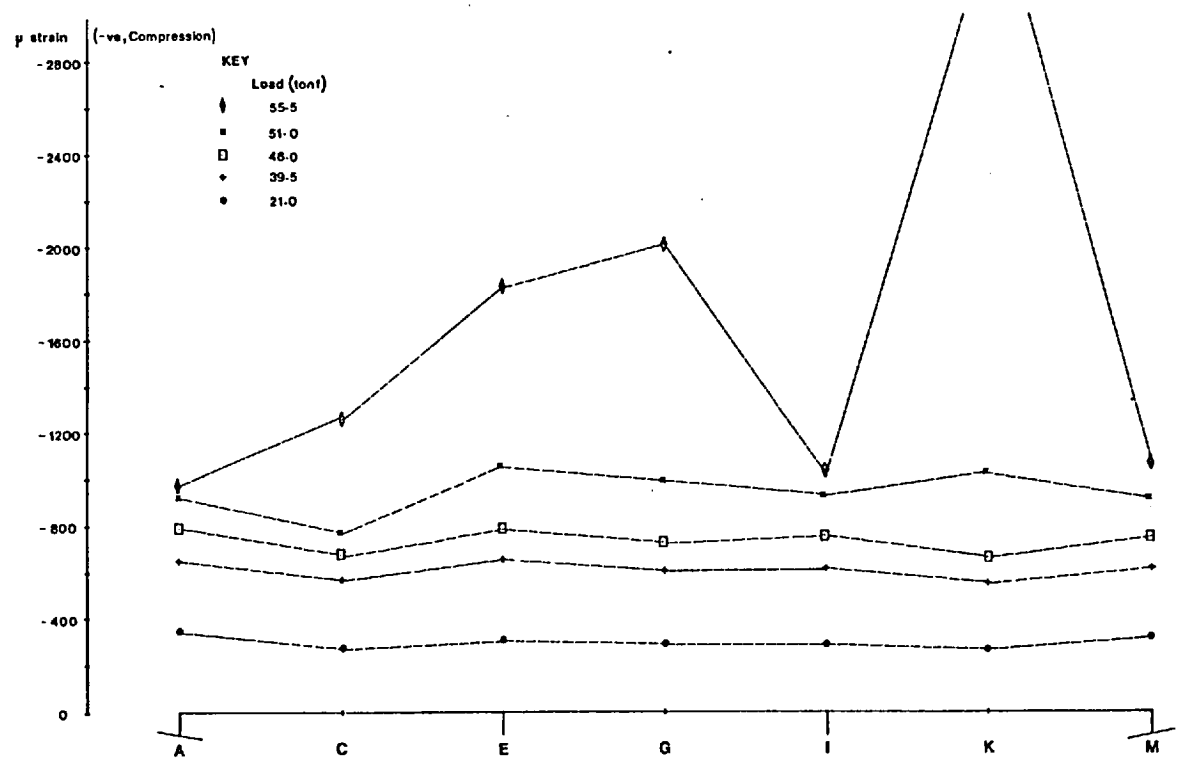

Longitudinal Outer Surface Strain in Compression Flange Over North Web

Fig. 2.51a Model 8: Longitudinal Strain in Compression Flange at its Junctions with Webs.

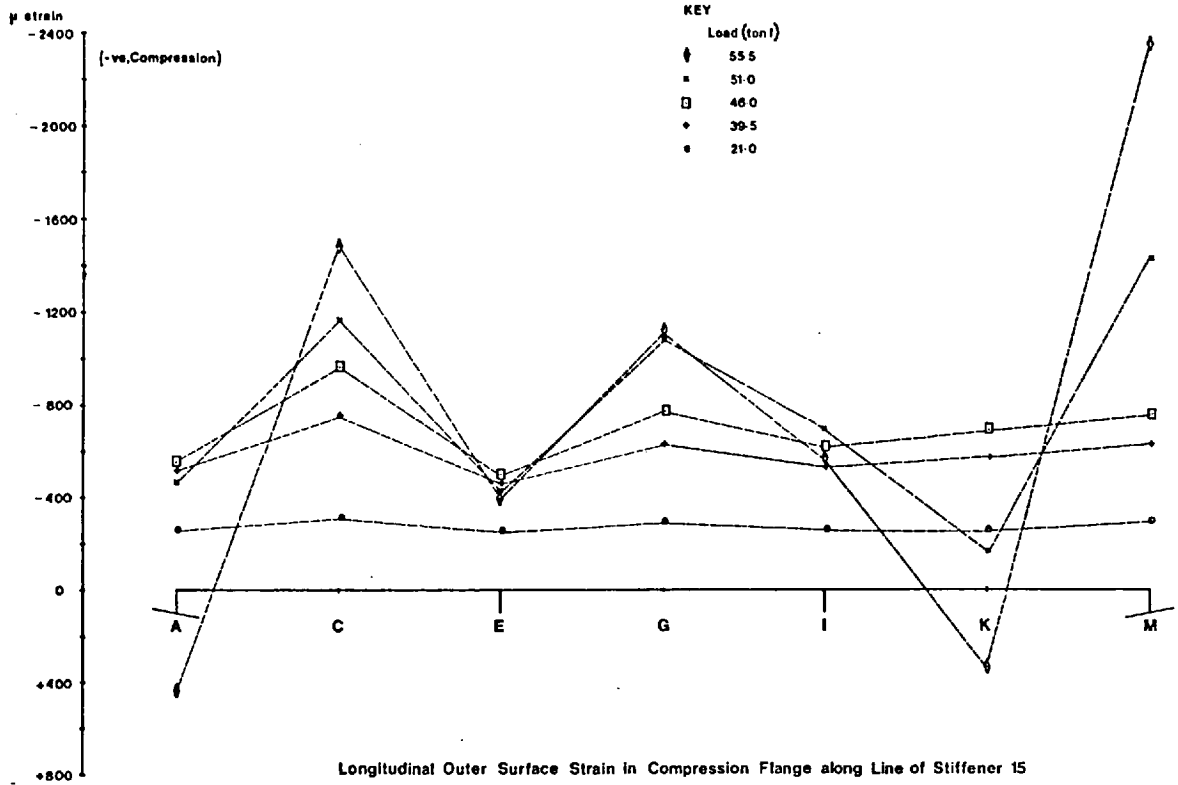

Longitudinal Outer Surface Strain in Compression Flange along Line of Stiffener 15

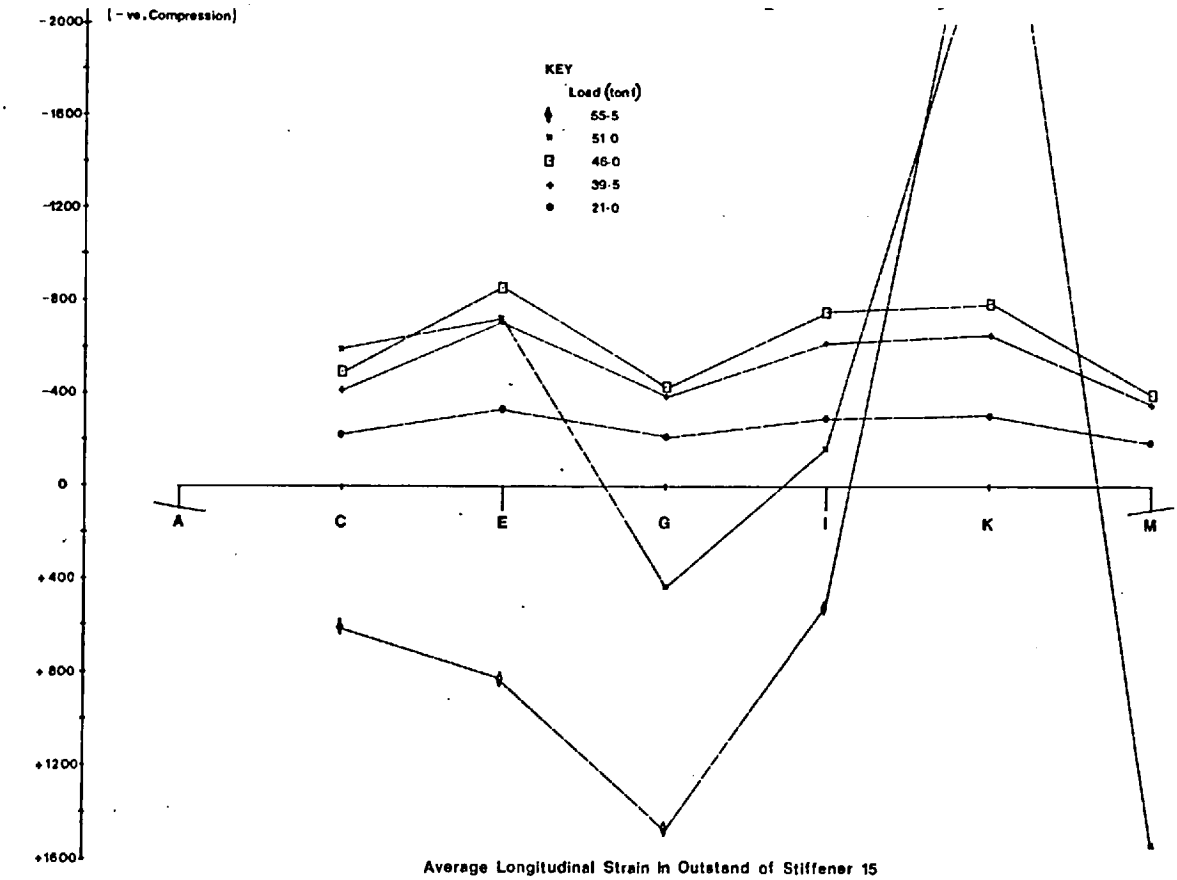

Average Longitudinal Strain in Outstand of Stiffener 15

Fig. 2.51b Model 8: Strain in Stiffener 15

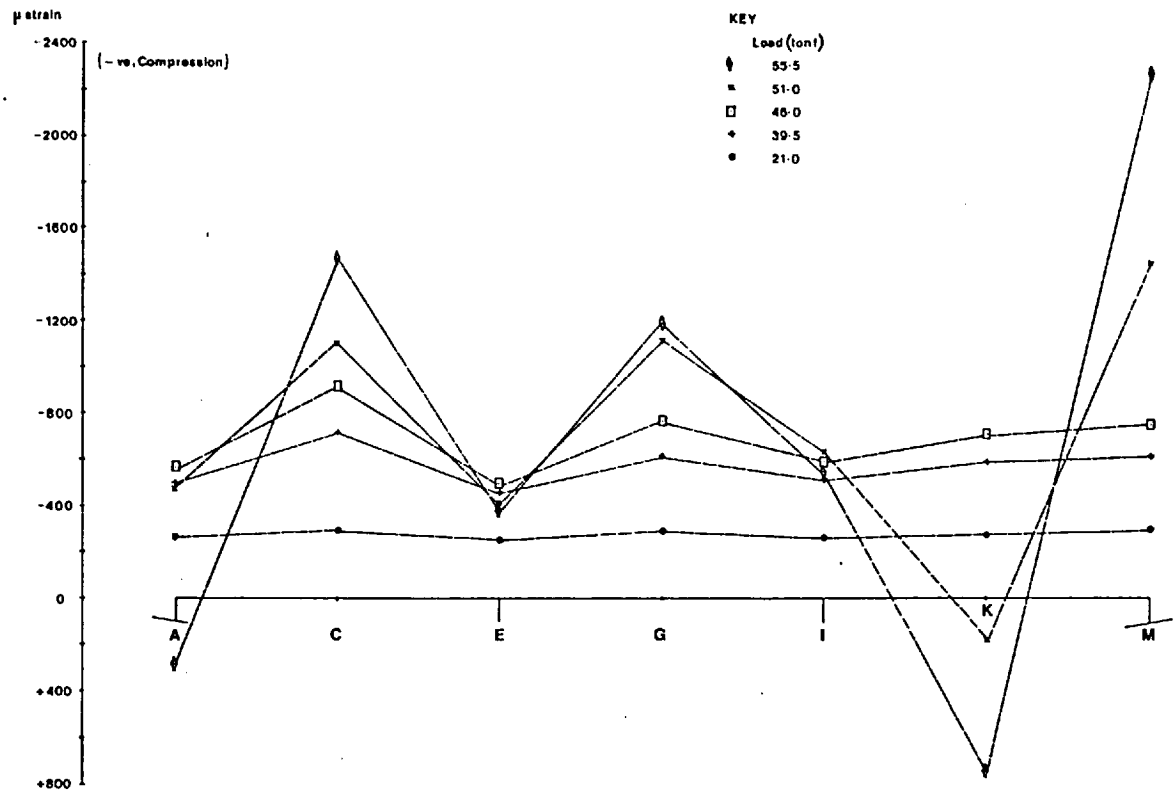

Longitudinal Outer Surface Strain in Compression Flange along Line of Stiffener 16

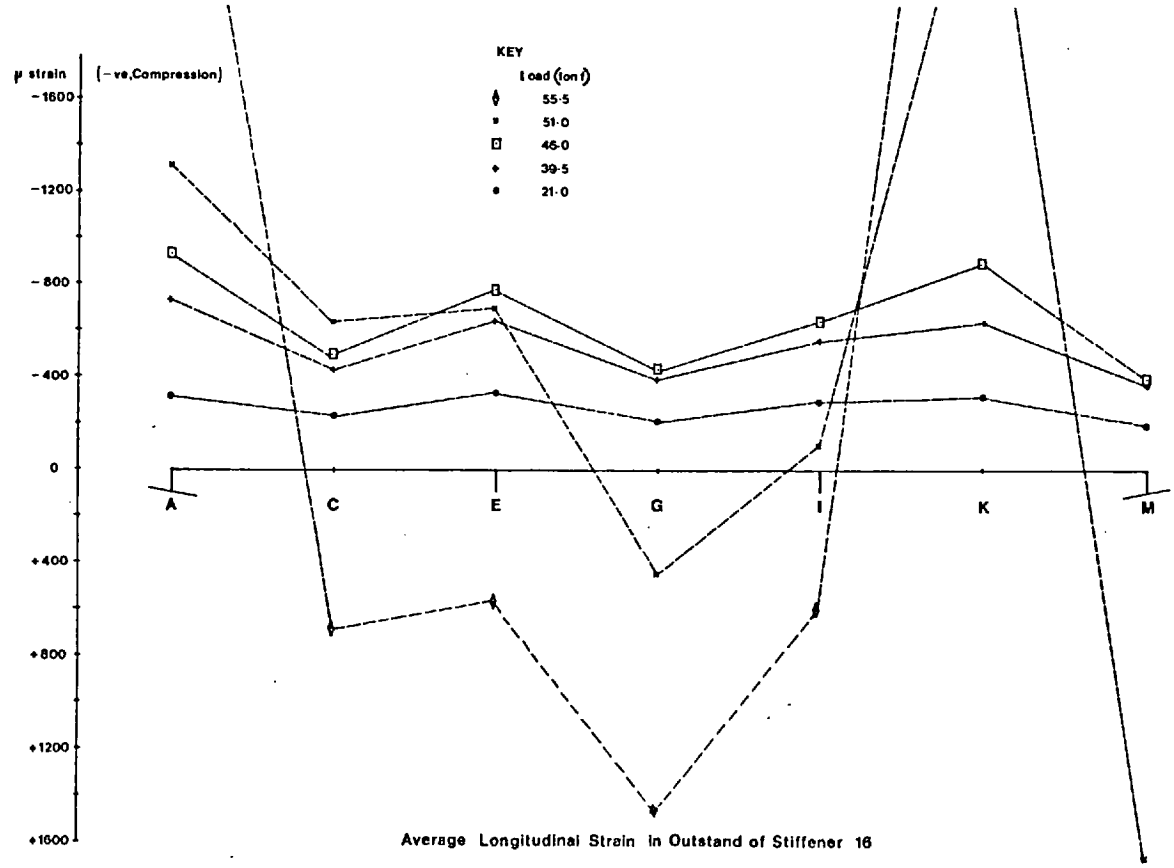

Average Longitudinal Strain in Outstand of Stiffener 16

Fig. 2.51c Model 8: Strain in Stiffener 16

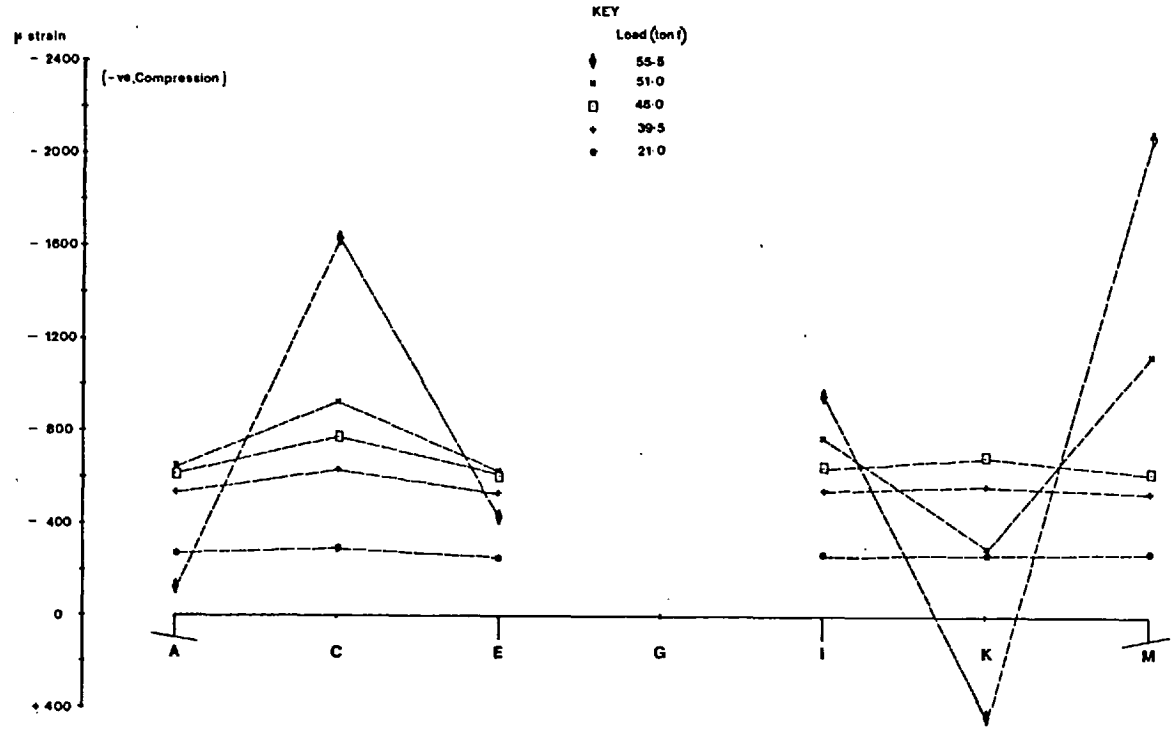

Longitudinal Outer Surface Strain in Compression Flange along Line of Stiffener 18

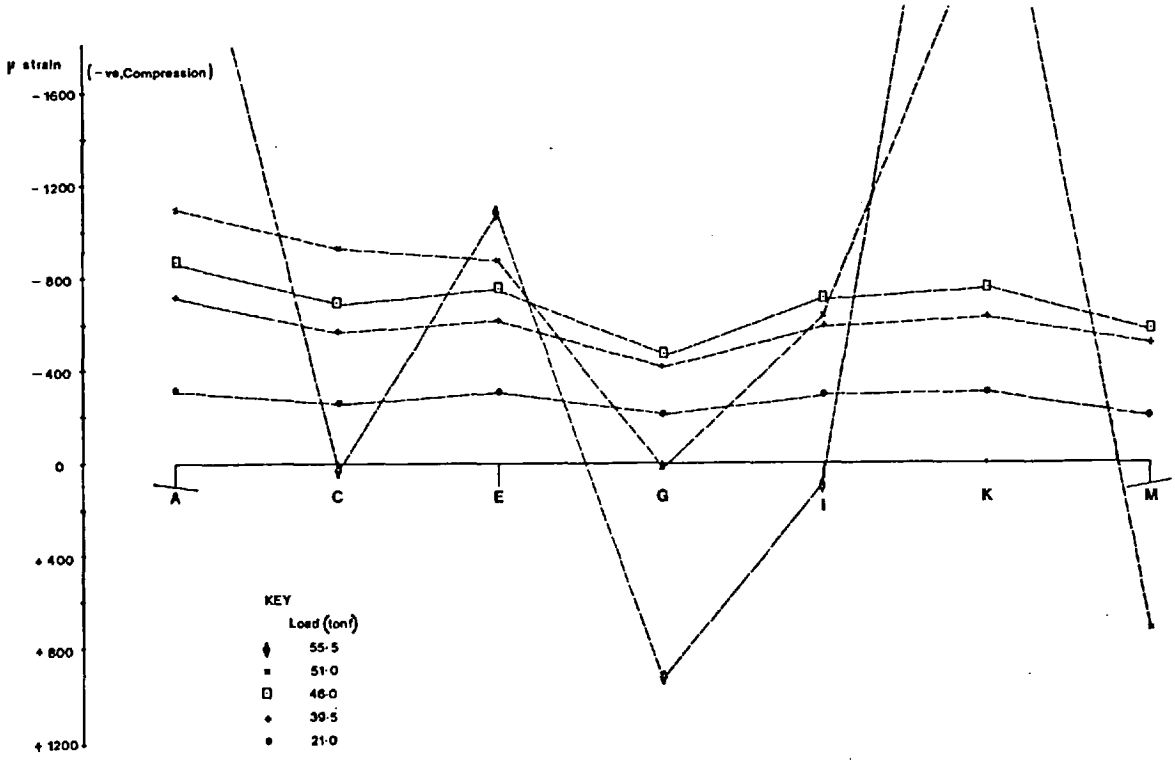

Longitudinal Strain in Outstand of Stiffener 18

Fig. 2.51d Model 8: Strain in Stiffener 18

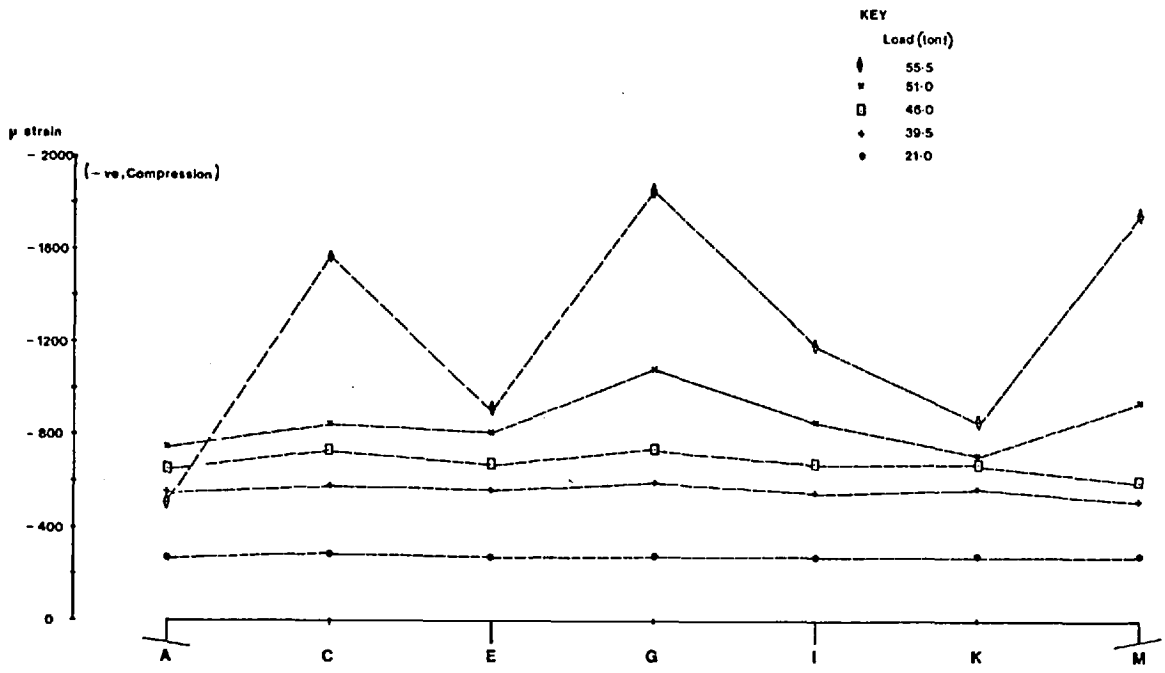

Longitudinal Outer Surface Strain in Compression Flange along Line of Stiffener 19

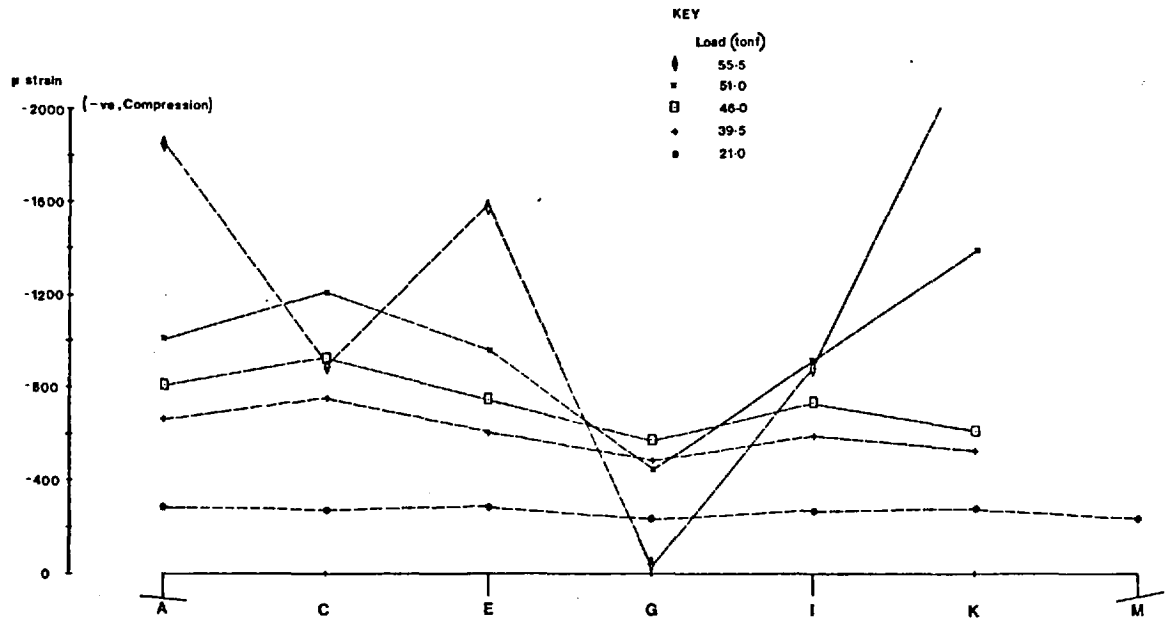

Average Longitudinal Strain in Outstand of Stiffener 19

Fig. 2.51e Model 8: Strain in Stiffener 19

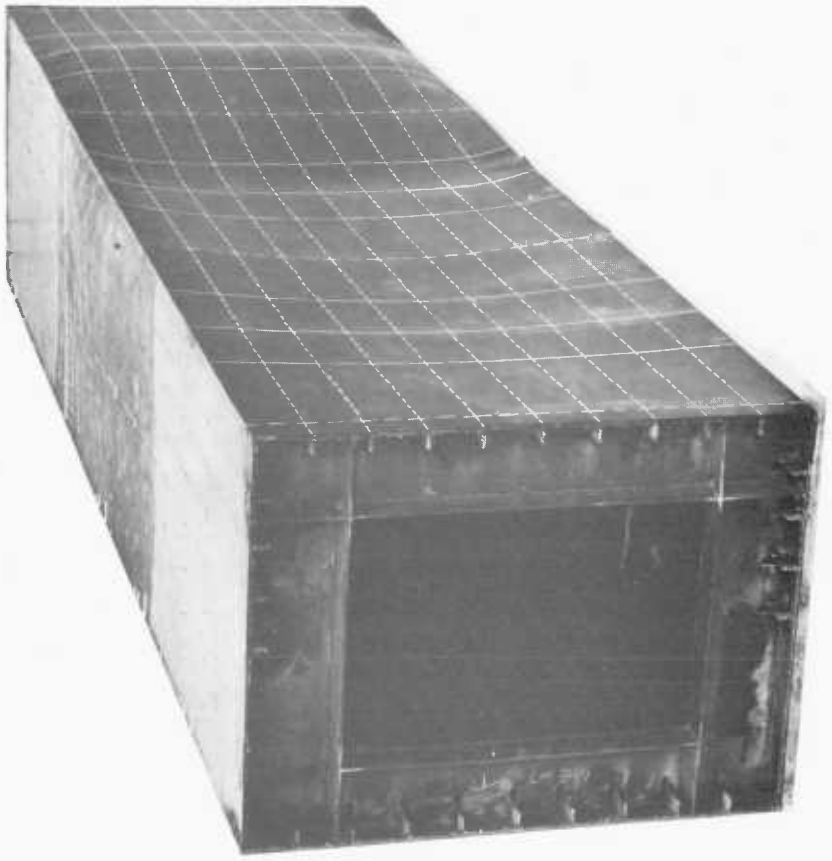

Fig. 2.52a. Model 8 - after the collapse test.

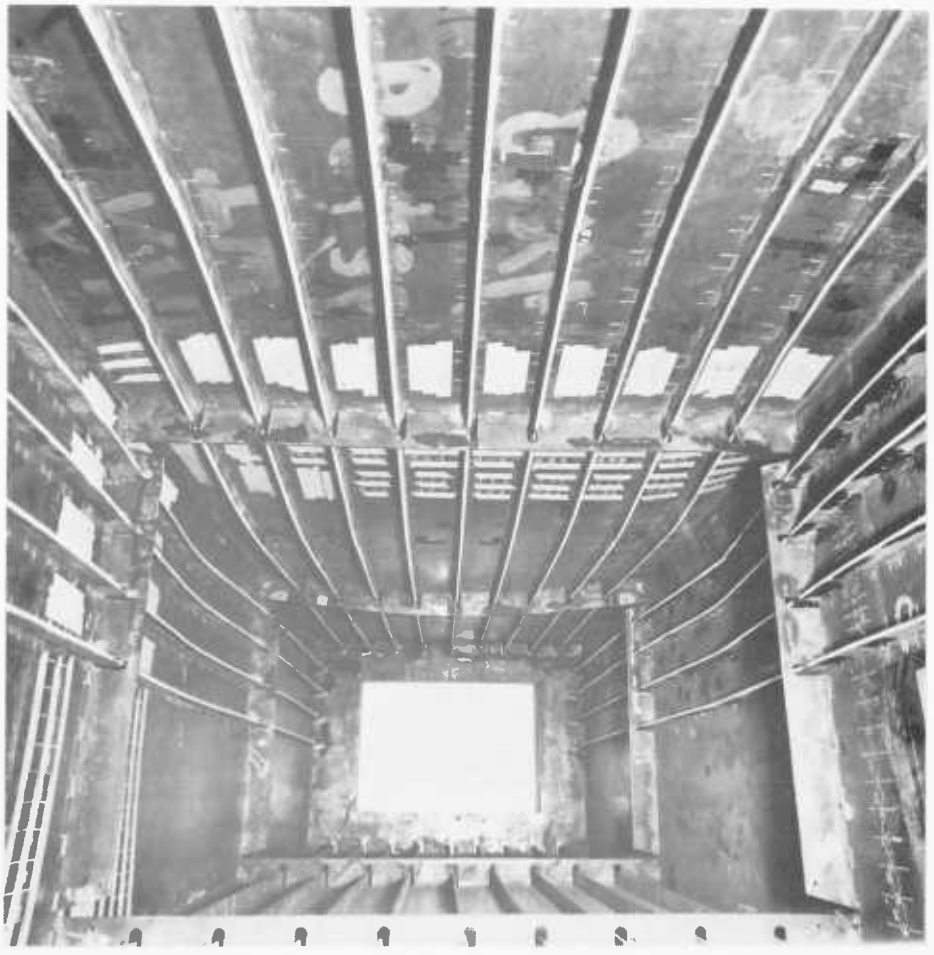

Fig. 2.52b. Model 8 - showing the inside of the model (from end M) after failure. The compression flange is at the top of the picture. Although the deflections in bay I-M were outwards, the longitudinal stiffeners exhibit very little lateral deflections.

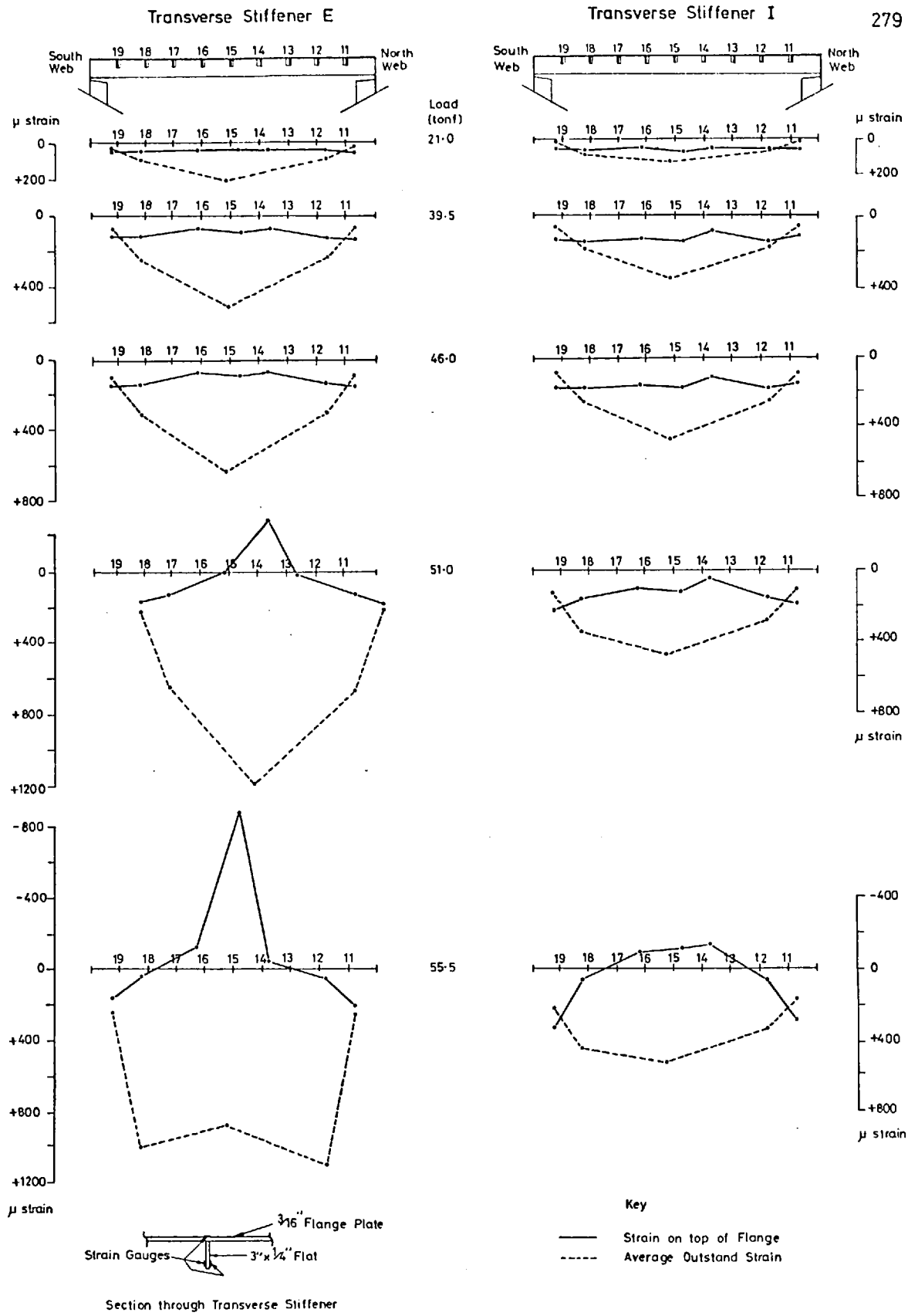

Fig. 2.53 Model 8: Transverse Strains at Sections E and I

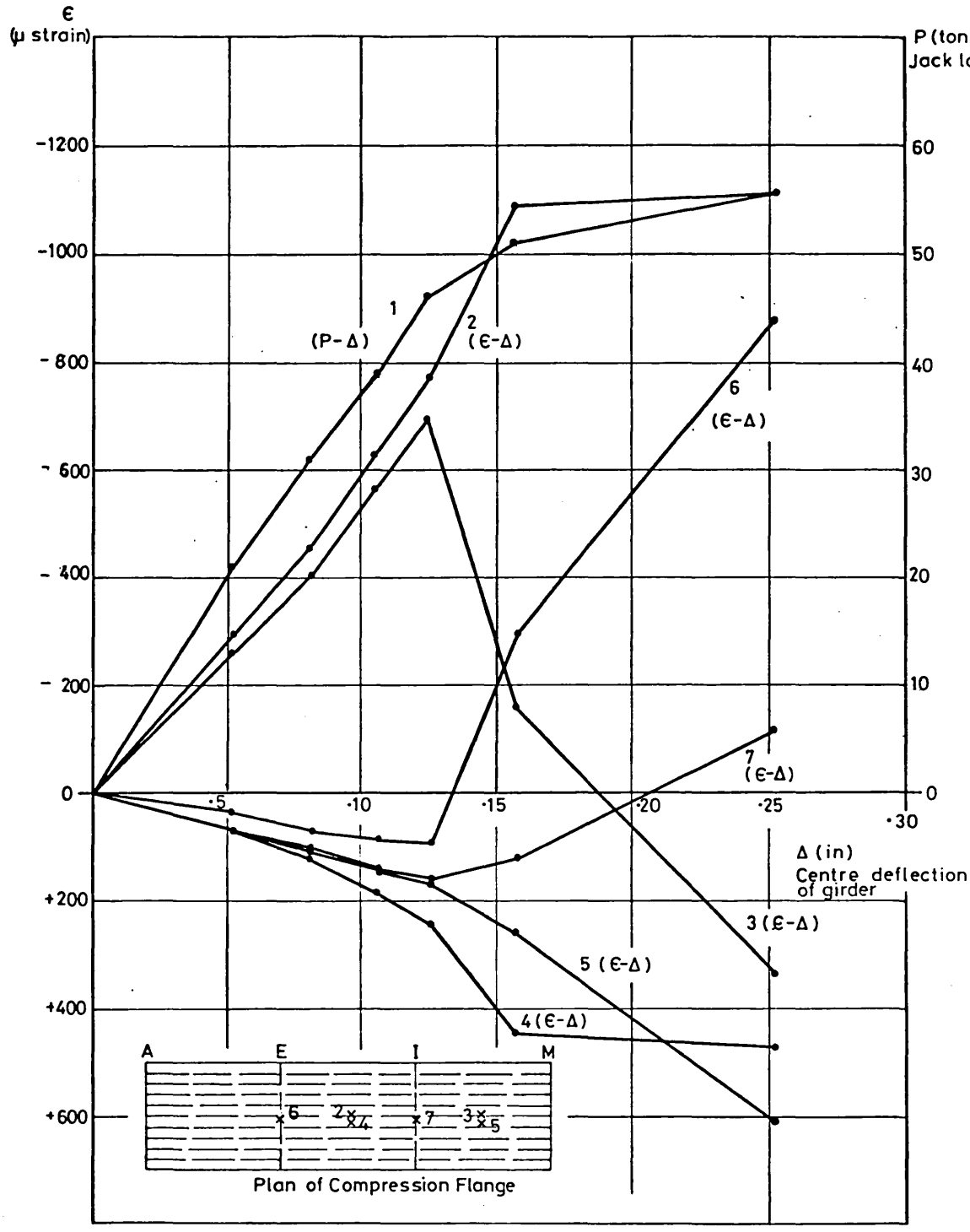

CURVE 1 OVERALL LOAD-DEFLECTION RELATIONSHIP
CURVE 2 MID-PLANE STRAIN AT LOCATION 2
CURVE 3 MID-PLANE STRAIN AT LOCATION 3
CURVE 4 TRANSVERSE MID-PLANE STRAIN AT LOCATION 4
CURVE 5 TRANSVERSE MID-PLANE STRAIN AT LOCATION 5
CURVE 6 TRANSVERSE MID-PLANE STRAIN AT LOCATION 6
CURVE 7 TRANSVERSE MID-PLANE STRAIN AT LOCATION 7

Fig. 2.54 Model 8. Growth of Deflections and Strains with Load.

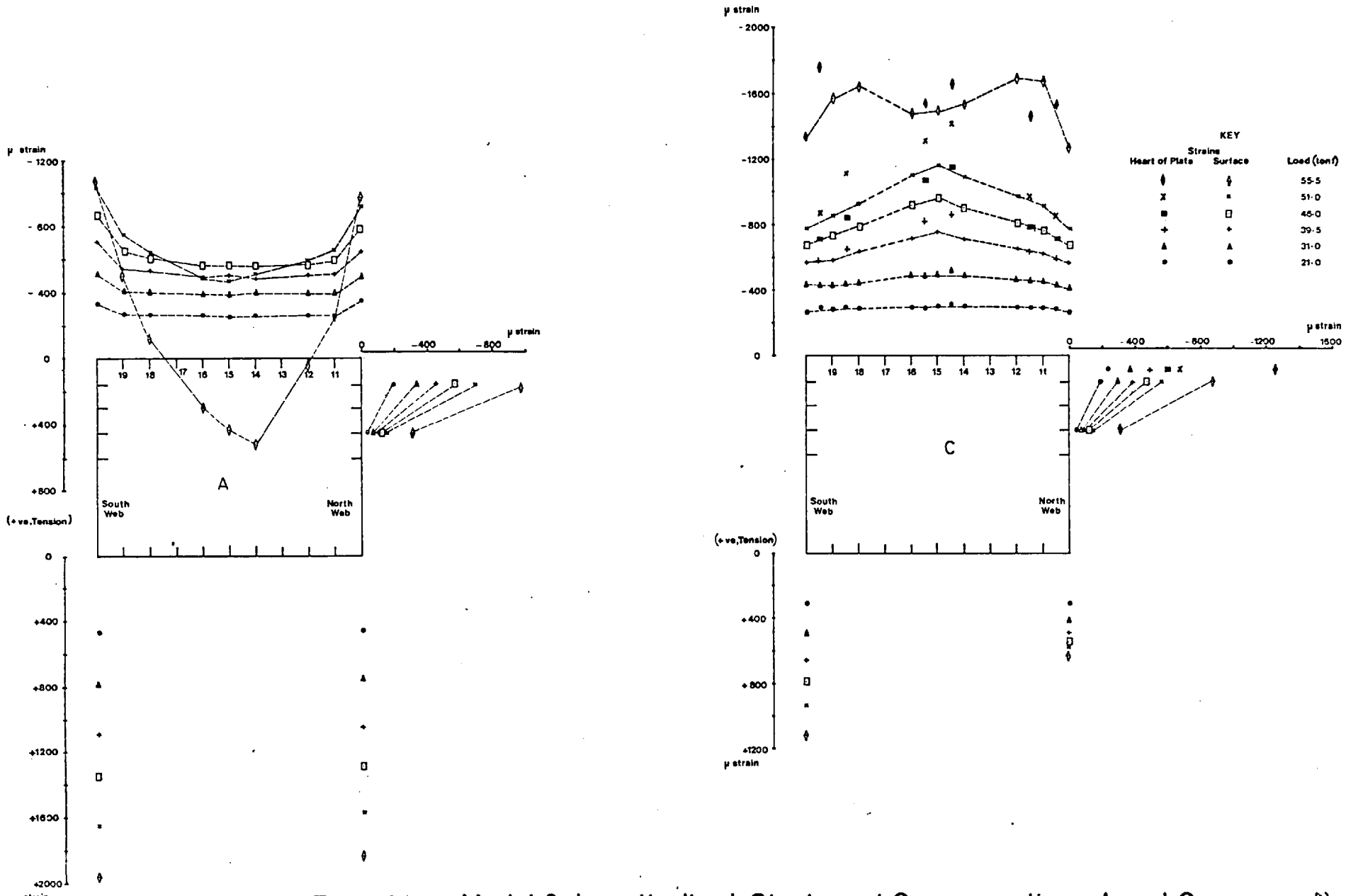

Fig. 2.55a Model 8: Longitudinal Strains at Cross-sections A and C

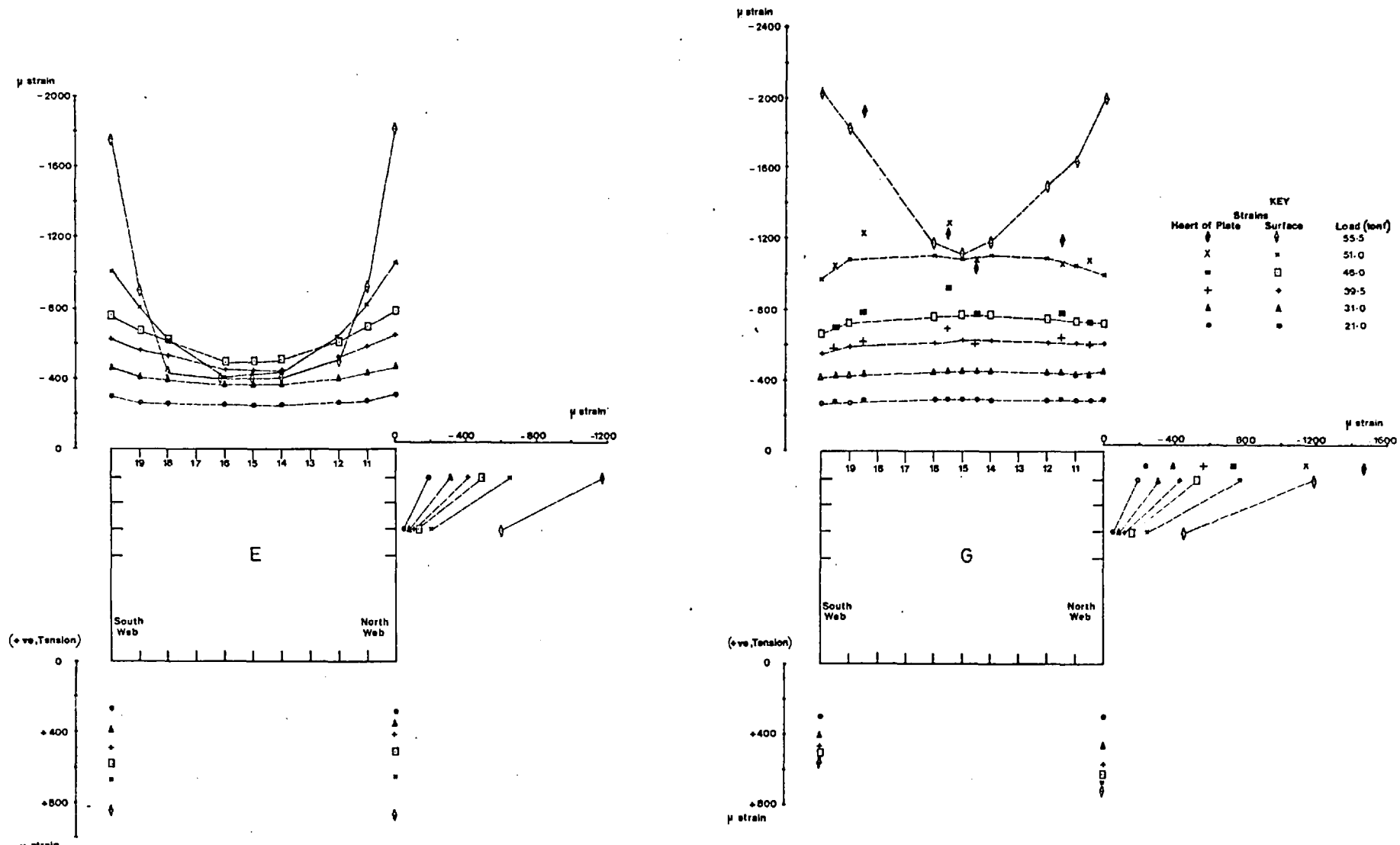

Fig. 2.55b Model 8: Longitudinal Strains at Cross-sections E and G

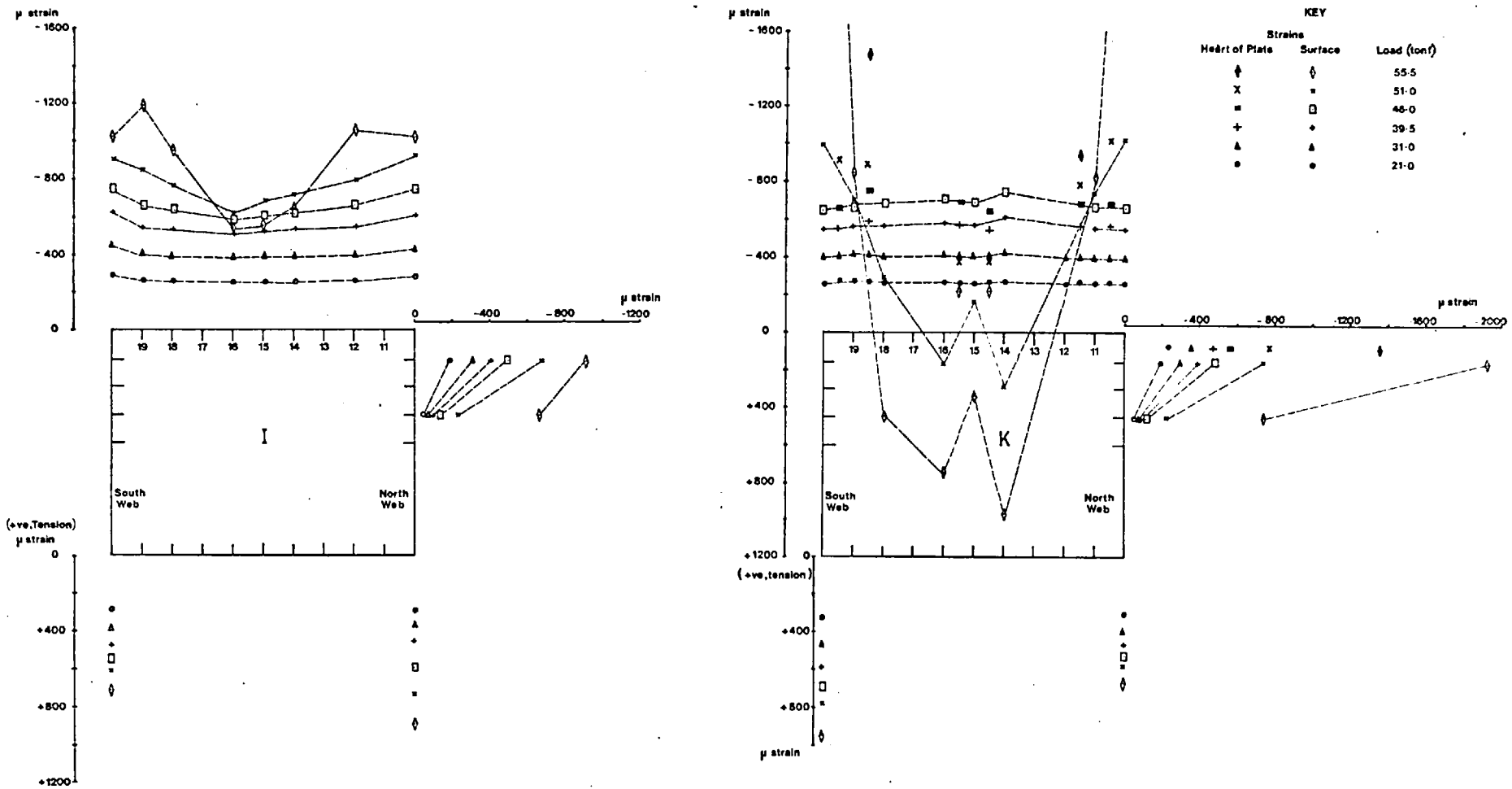

Fig. 2.55c Model 8: Longitudinal Strains at Cross-sections I and K

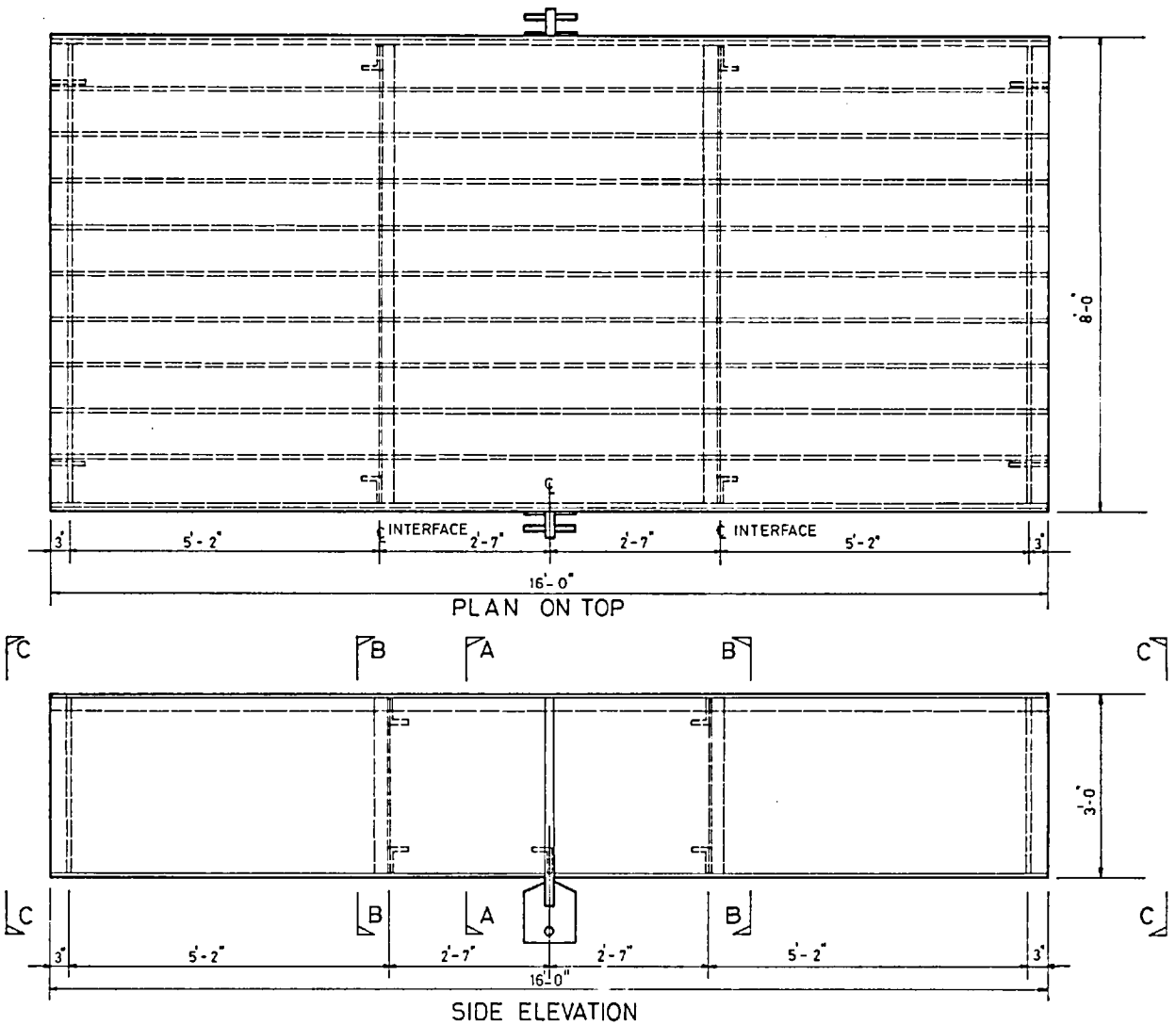

Fig. 2.56a Model 9 : Plan and Elevation

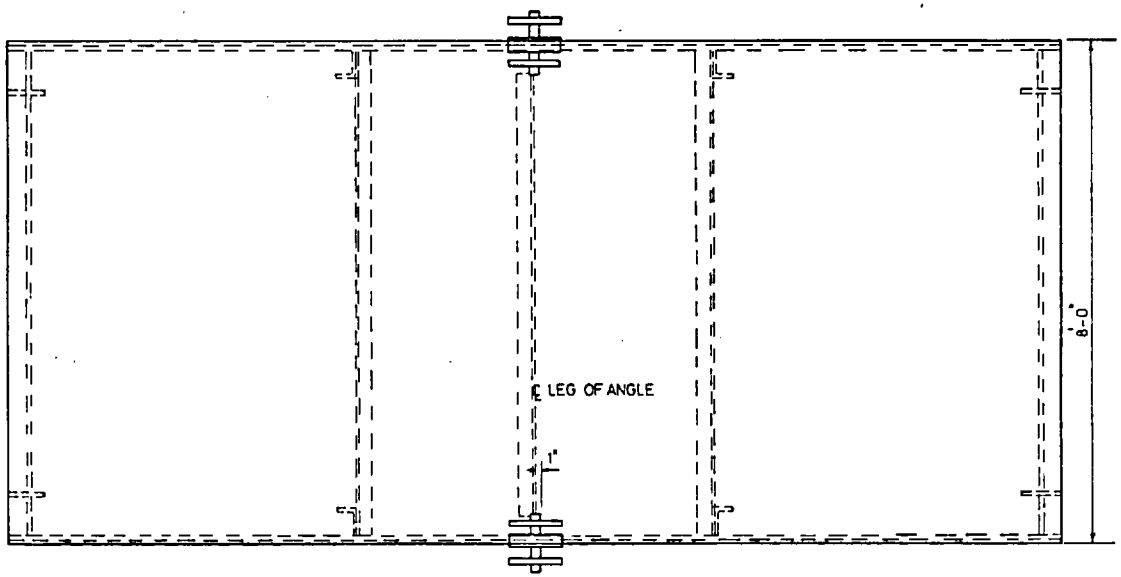

VIEW ON UNDERSIDE

Fig. 2.56b
Model 9 : View on Underside

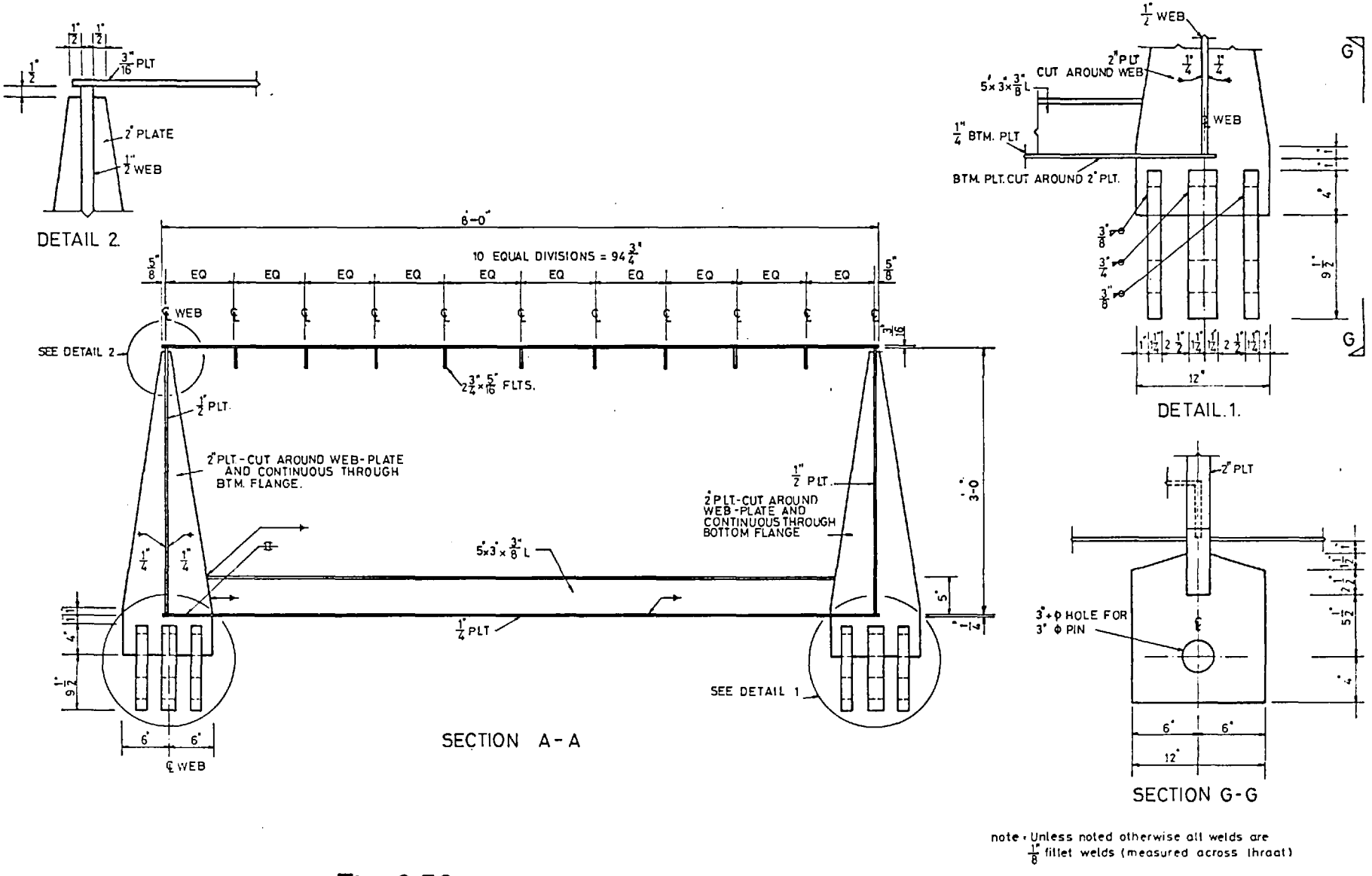

Fig. 2.56c
Model 9 : Cross-section and Details of Loading Lugs

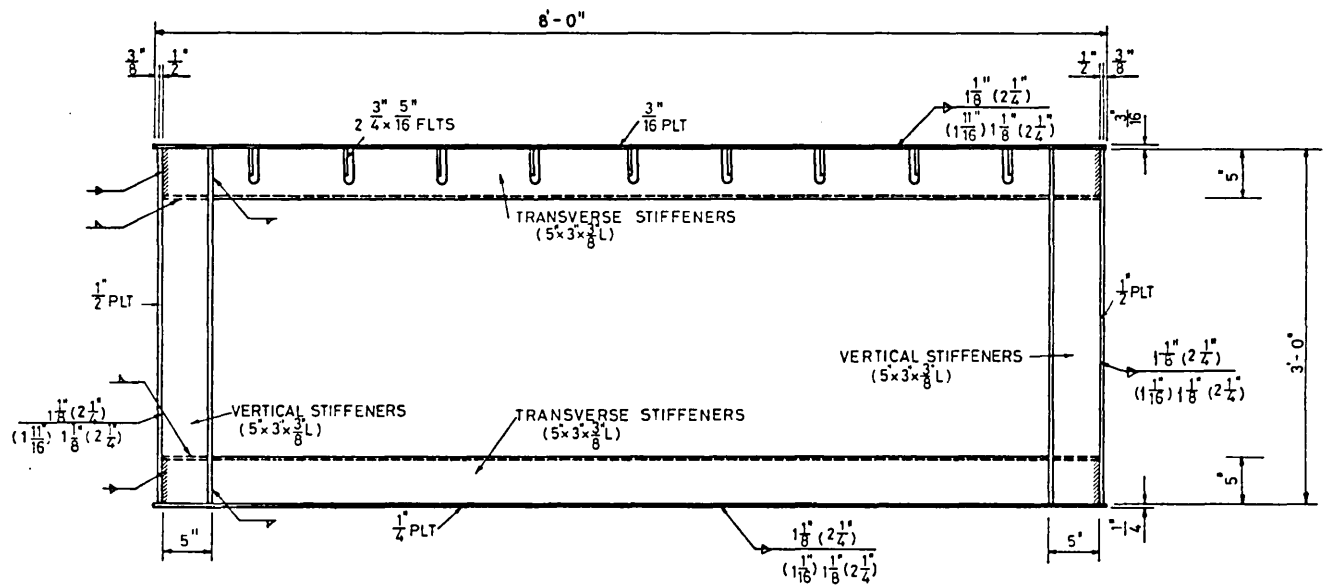

note : For location of $2\frac{3}{4}"\times\frac{5}{16}"$ FLTS see section A-A

SECTION B-B

Fig. 2.56d
Model 9 : Details of Internal Cross-frame

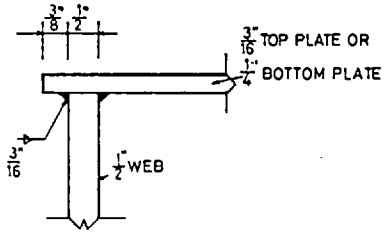

note : Remaining three corners are similar

WELDING DETAIL AT
CORNER OF BOX.

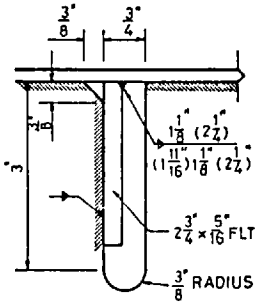

DETAIL OF SLOT IN
TRANSVERSE STIFFENERS

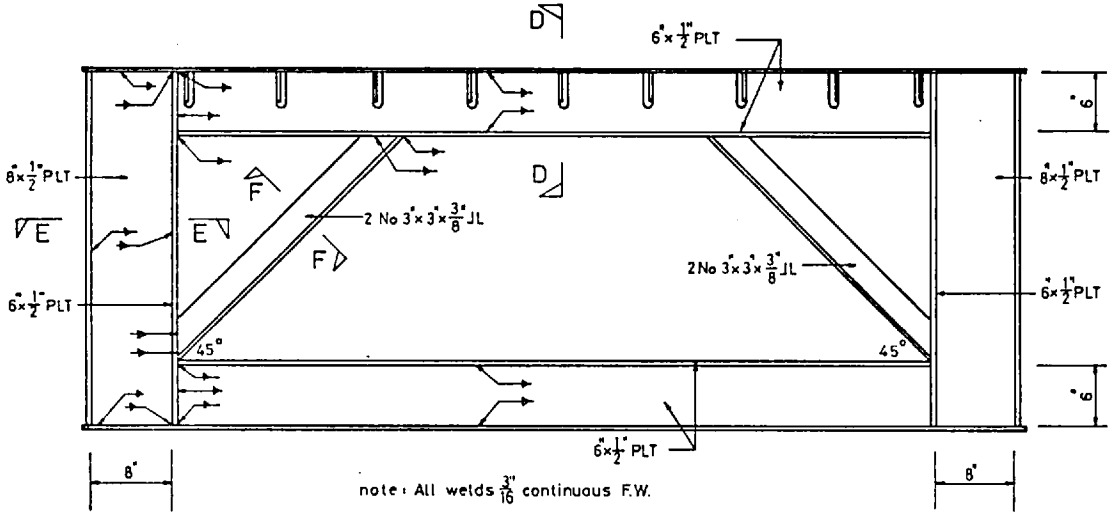

ELEVATION C-C

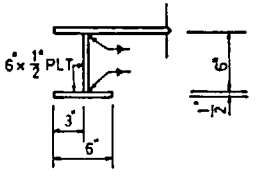

SECTION D-D

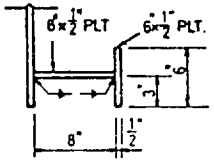

SECTION E-E

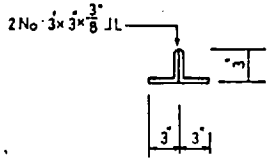

SECTION F-F

Fig. 2.56e Model 9 : Details of End Cross-frame

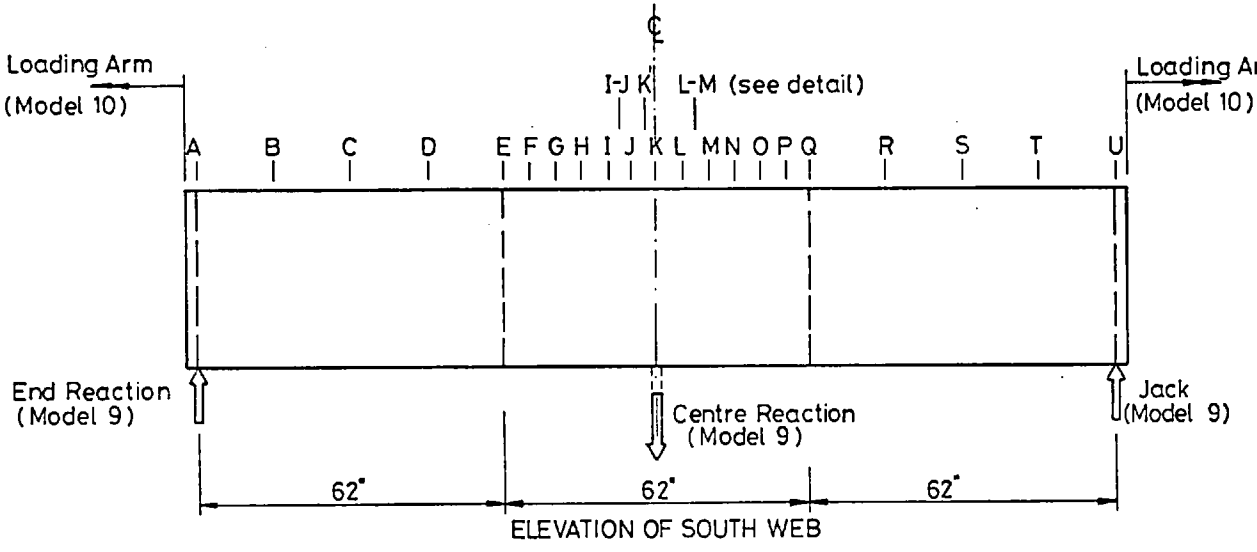

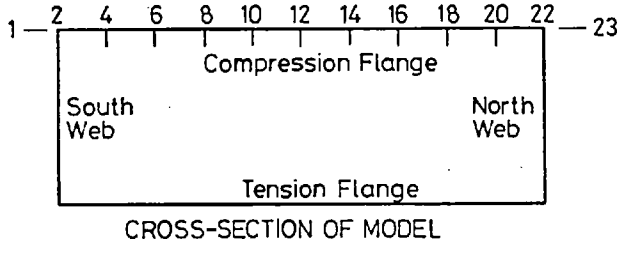

Notes
1. Letters A to U indicate locations along the model. Unless indicated otherwise all grid lines within panels are at equal distances.
2. Locations 3,5,.... to 21 (not shown) are midway between longitudinal stiffeners.

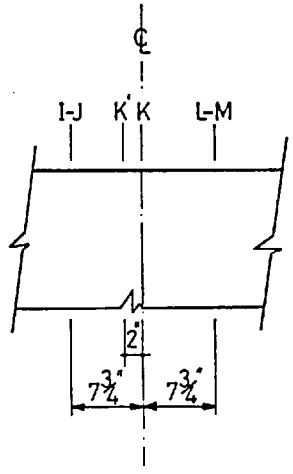

Detail showing dimensions of additional grid lines for strain measurements. Line K' applies to web of model 9 only.

Fig. 2.57
Models 9 and 10. Details of Reference Grids

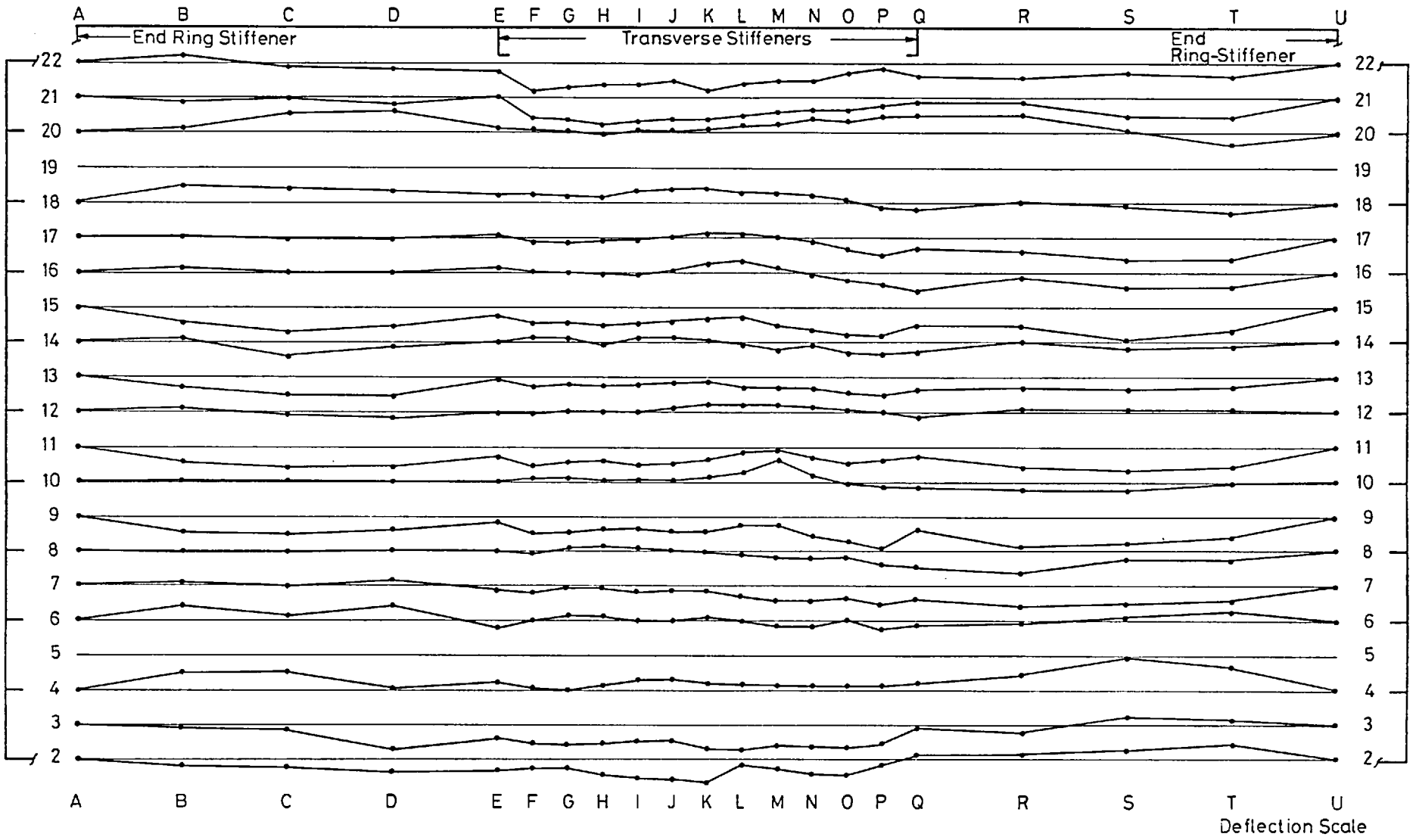

Fig. 2.58a
Model 9 : Longitudinal Initial Deflection Profiles of Compression Flange.

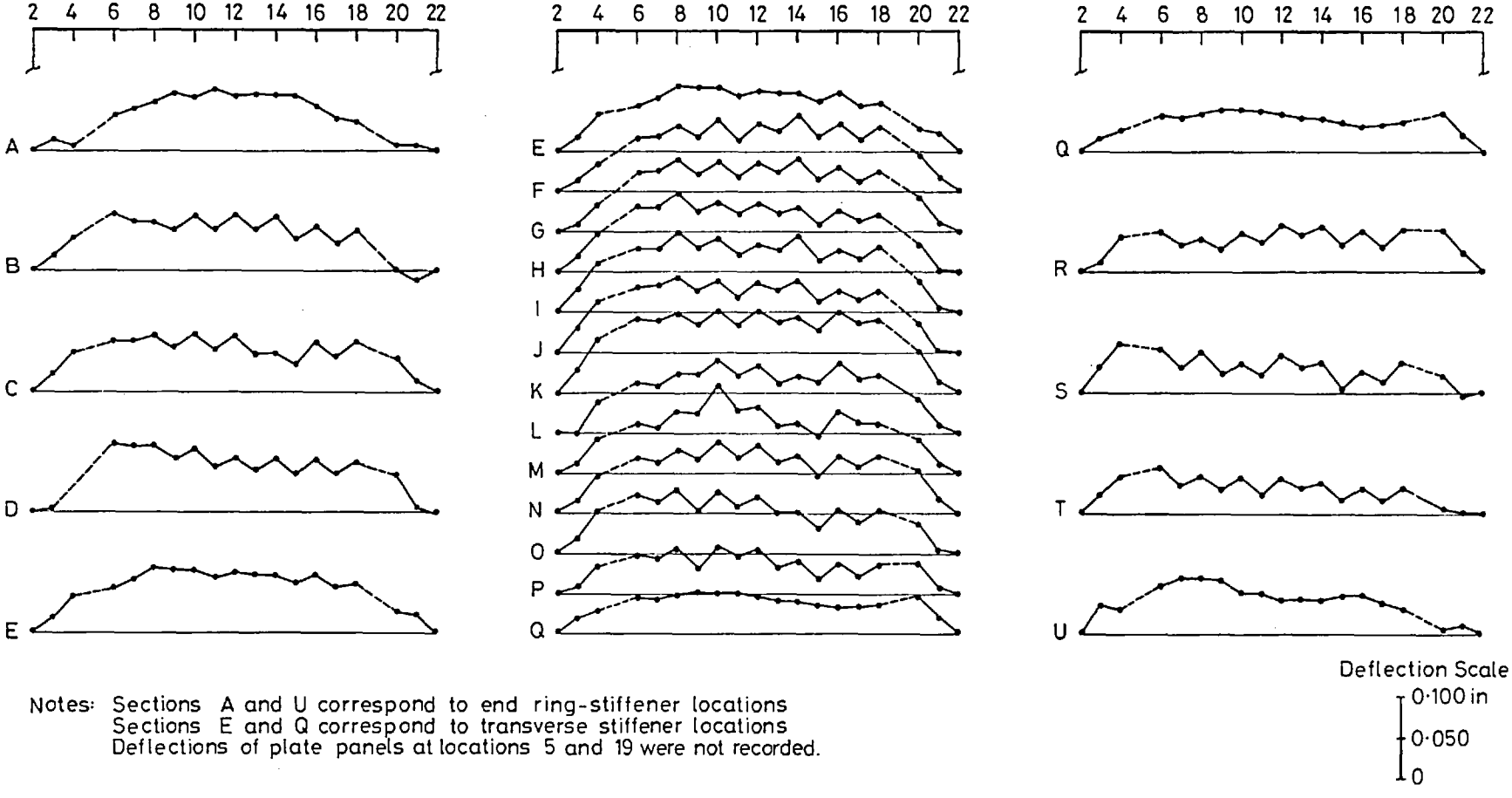

Notes: Sections A and U correspond to end ring-stiffener locations
Sections E and Q correspond to transverse stiffener locations
Deflections of plate panels at locations 5 and 19 were not recorded.

Fig. 2.58b
Model 9 : Transverse Initial Deflection Profiles of Compression Flange

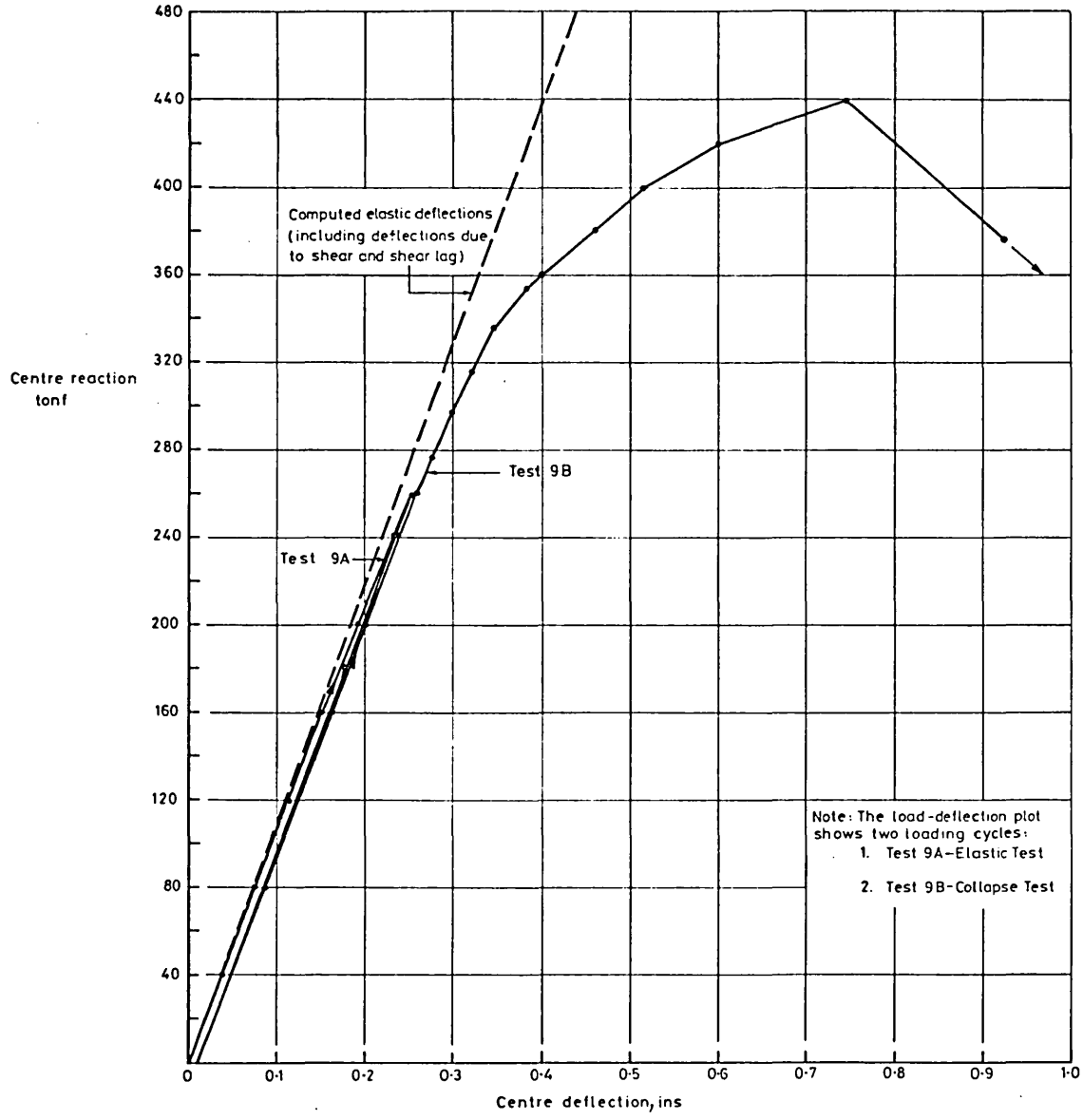

Fig. 2.59
Model 9: Load-Deflection Curves

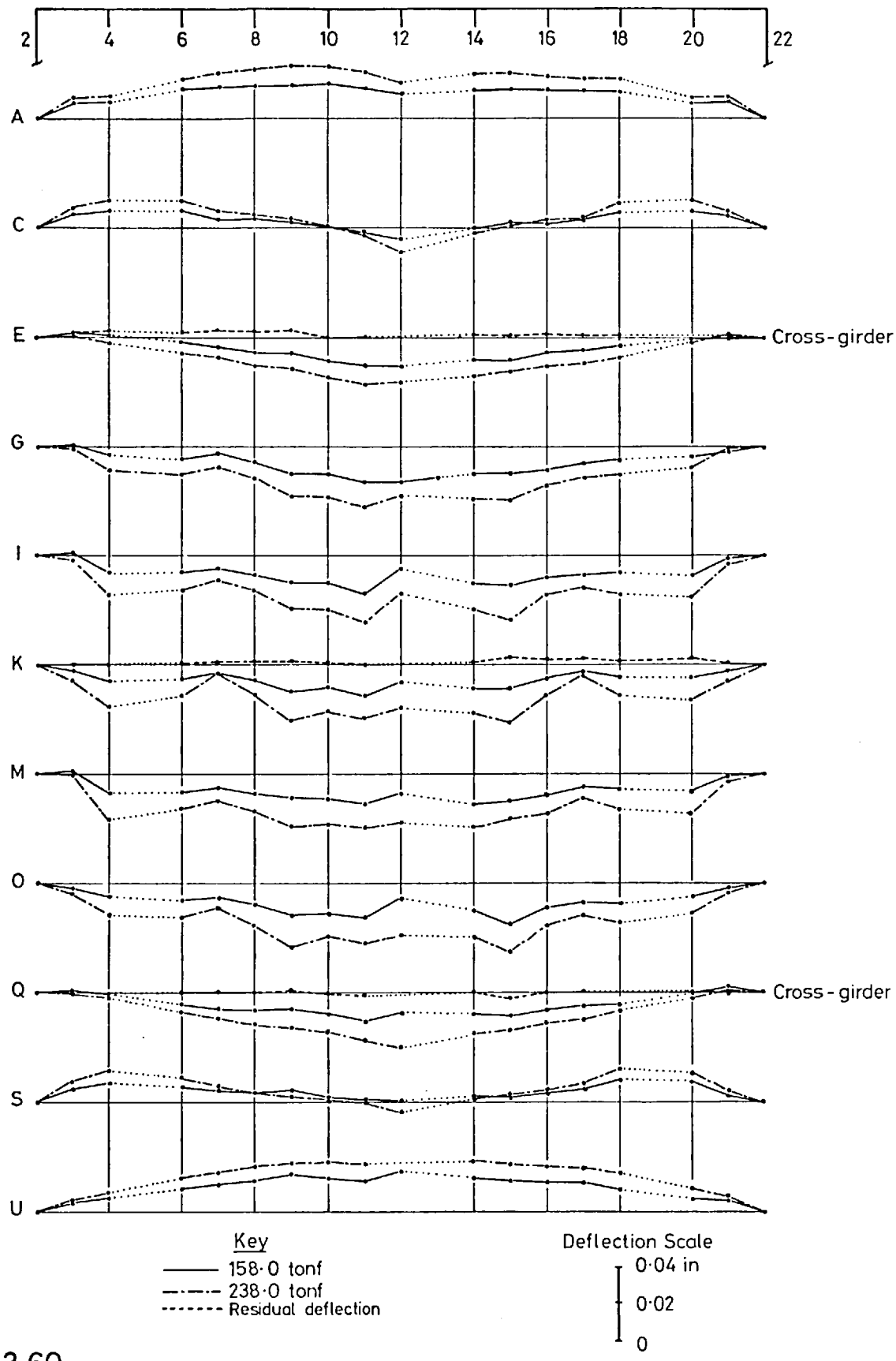

Fig. 2.60
Test 9A: Relative Transverse Deflections of Compression Flange

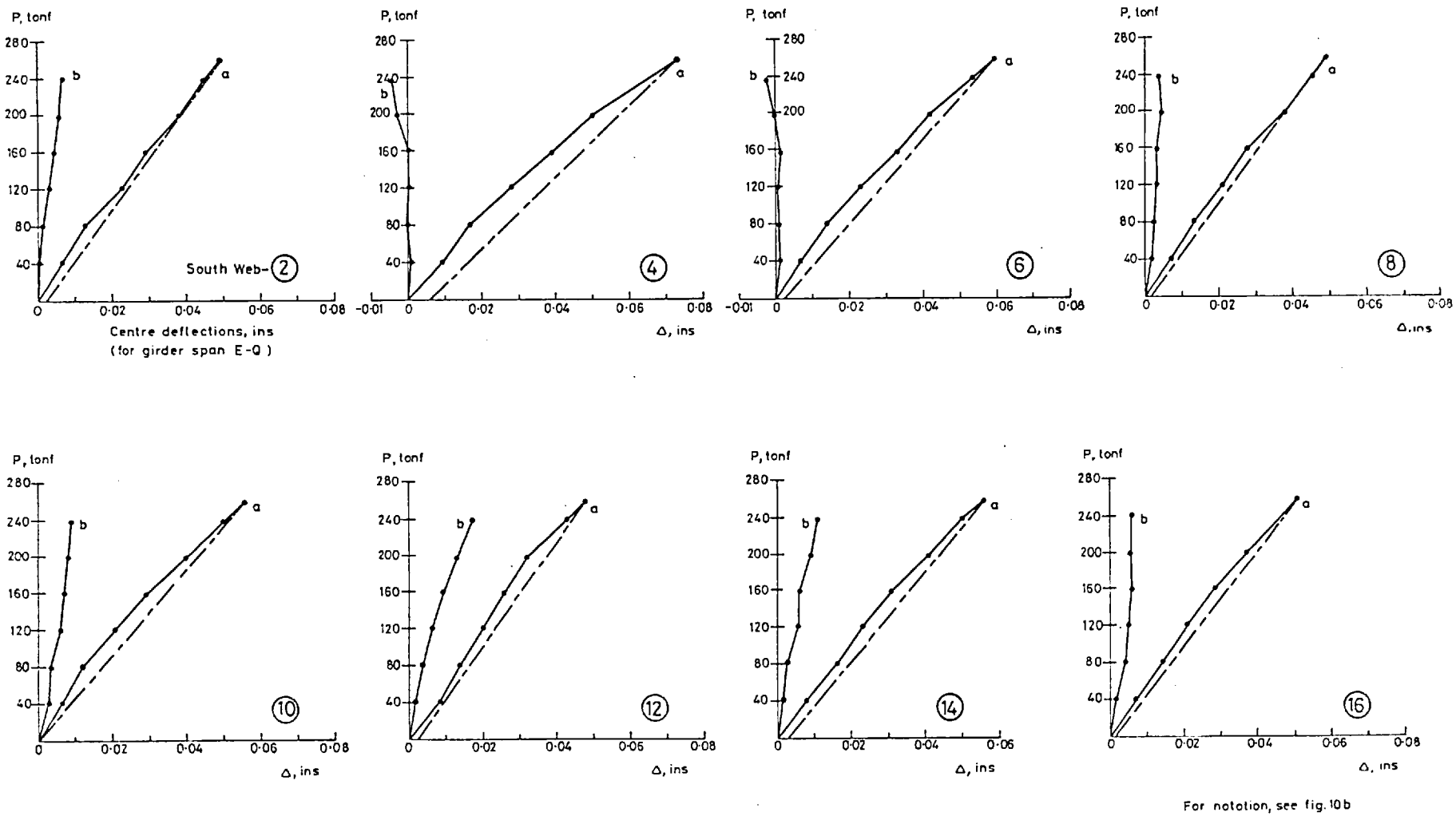

Fig. 2.61a
Test 9A: Out-of-plane Deflections of Longitudinal Stiffeners

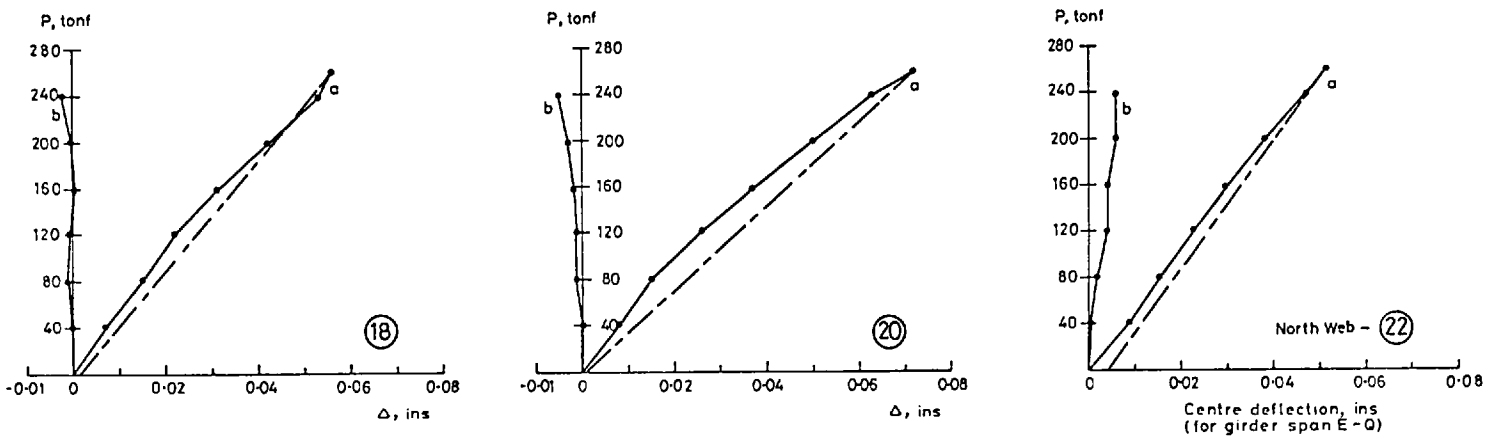

Fig. 2.61b
Test 9A: Out-of-plane Deflections of Longitudinal Stiffeners

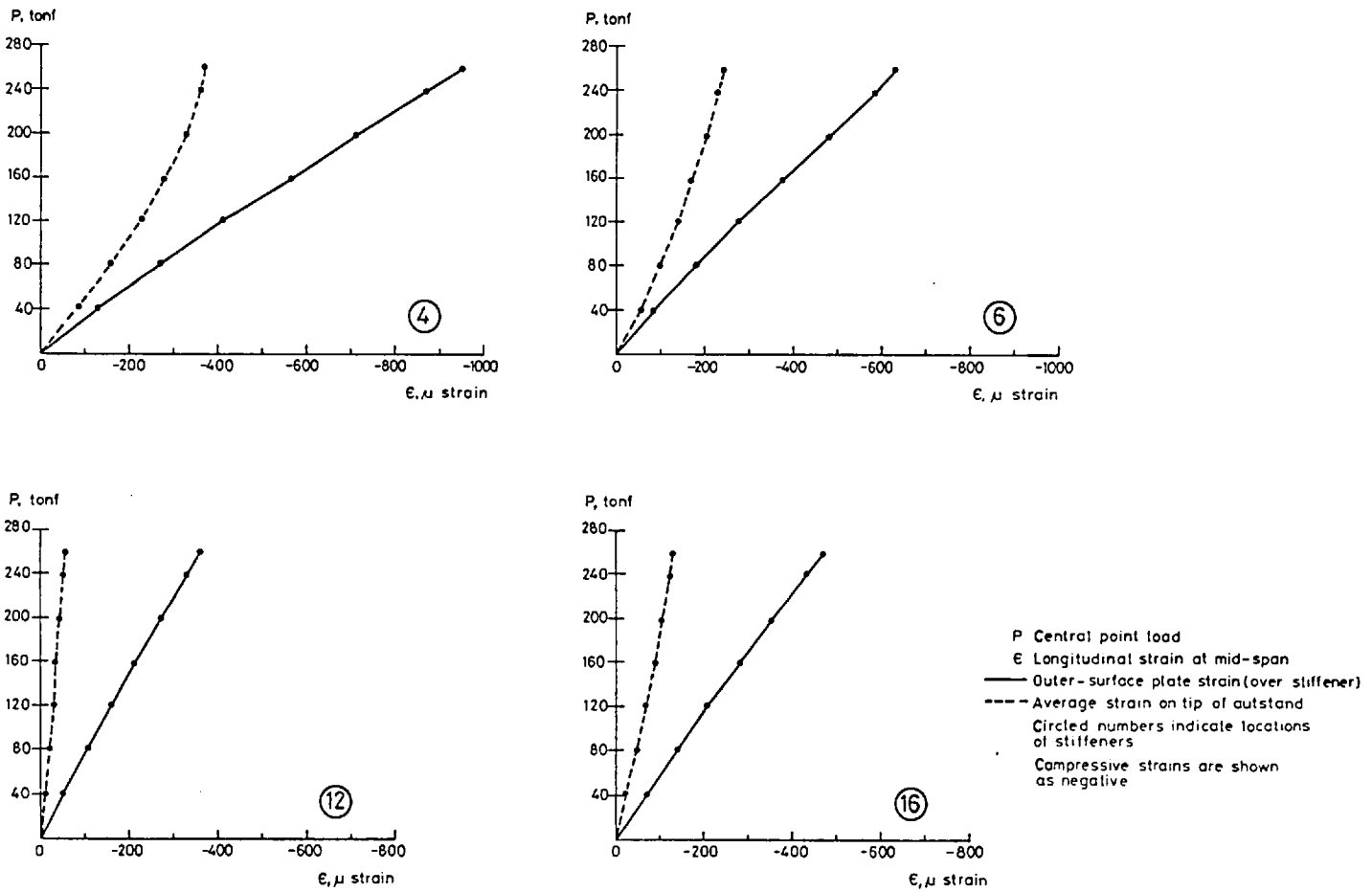

Fig. 2.62
Test 9A: Strain in Longitudinal Stiffeners

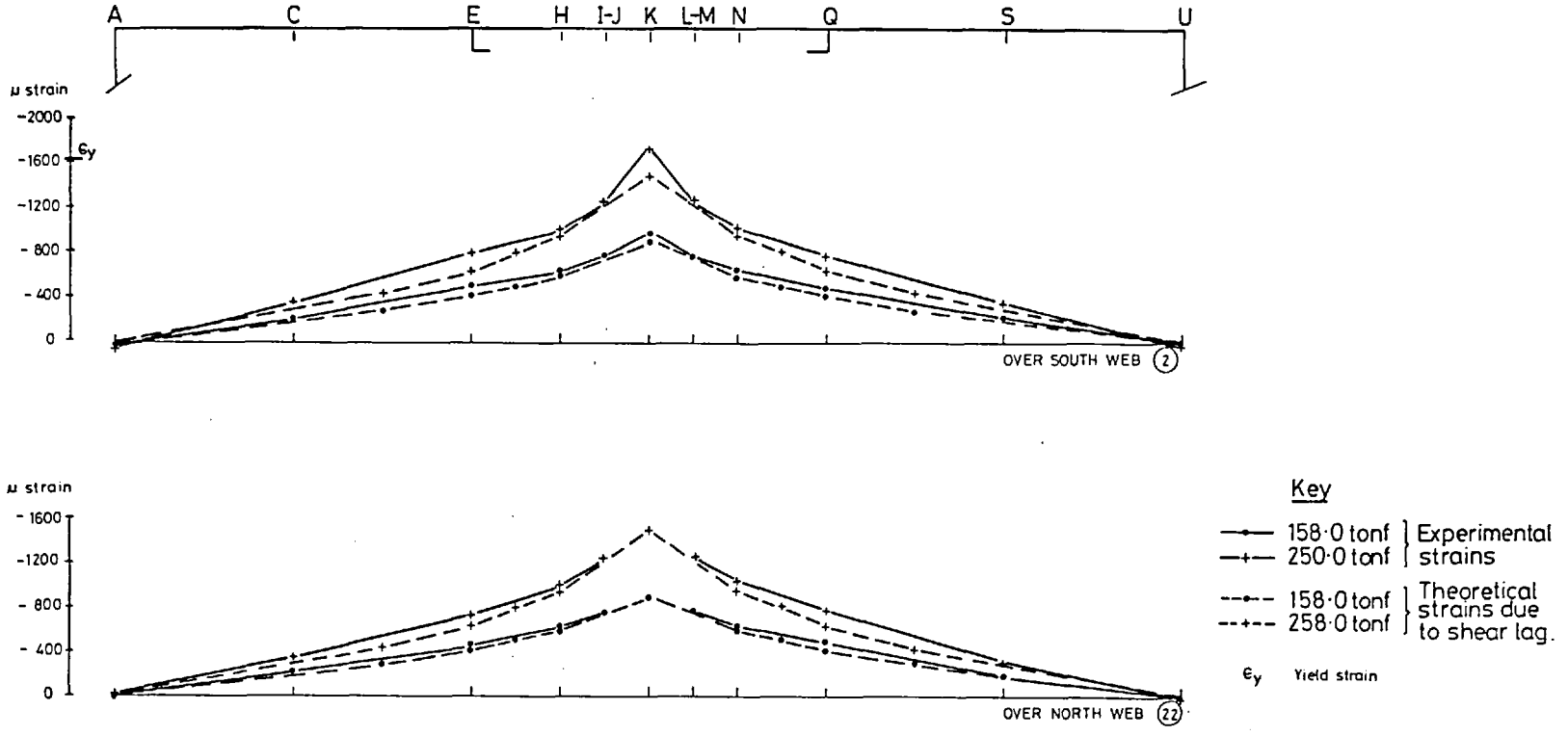

Fig. 2.63a
Test 9A: Longitudinal Strain in Compression Flange at its Junctions with Webs

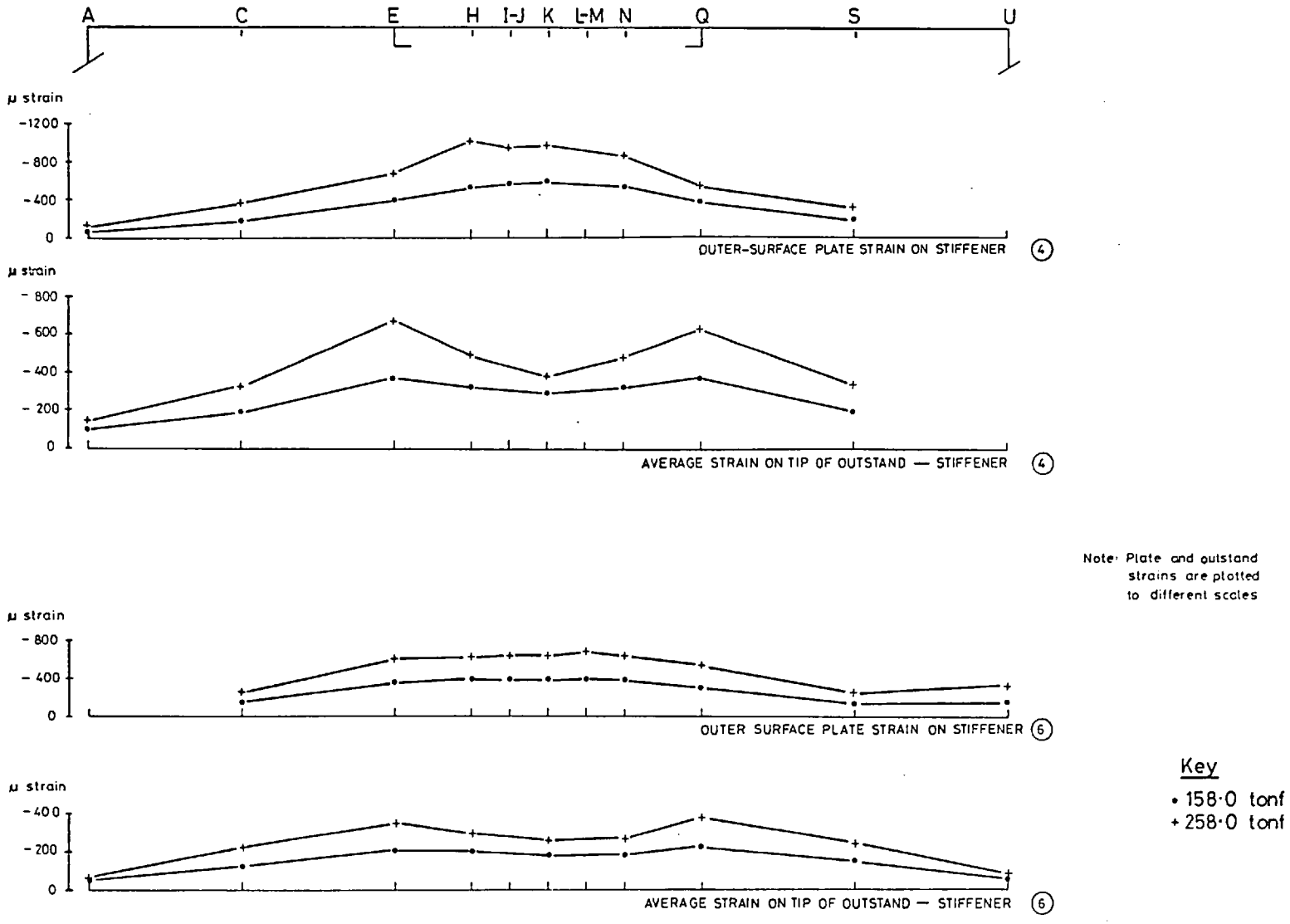

Fig. 2.63b
Test 9A: Longitudinal Strain in Compression Flange Stiffeners ④ and ⑥

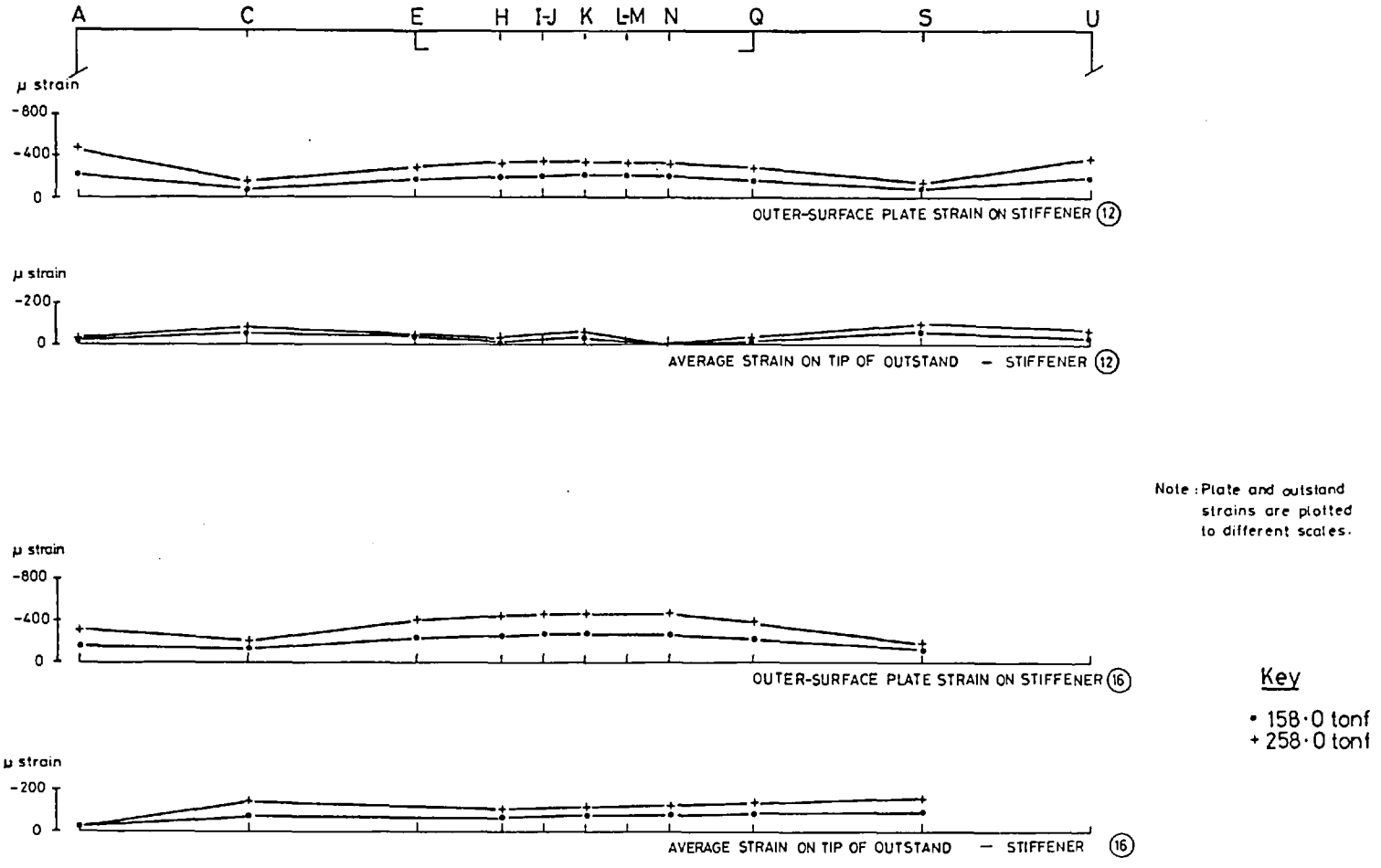

Fig. 2.63c
Test 9A: Longitudinal Strain in Compression Flange Stiffeners (12) and (16)

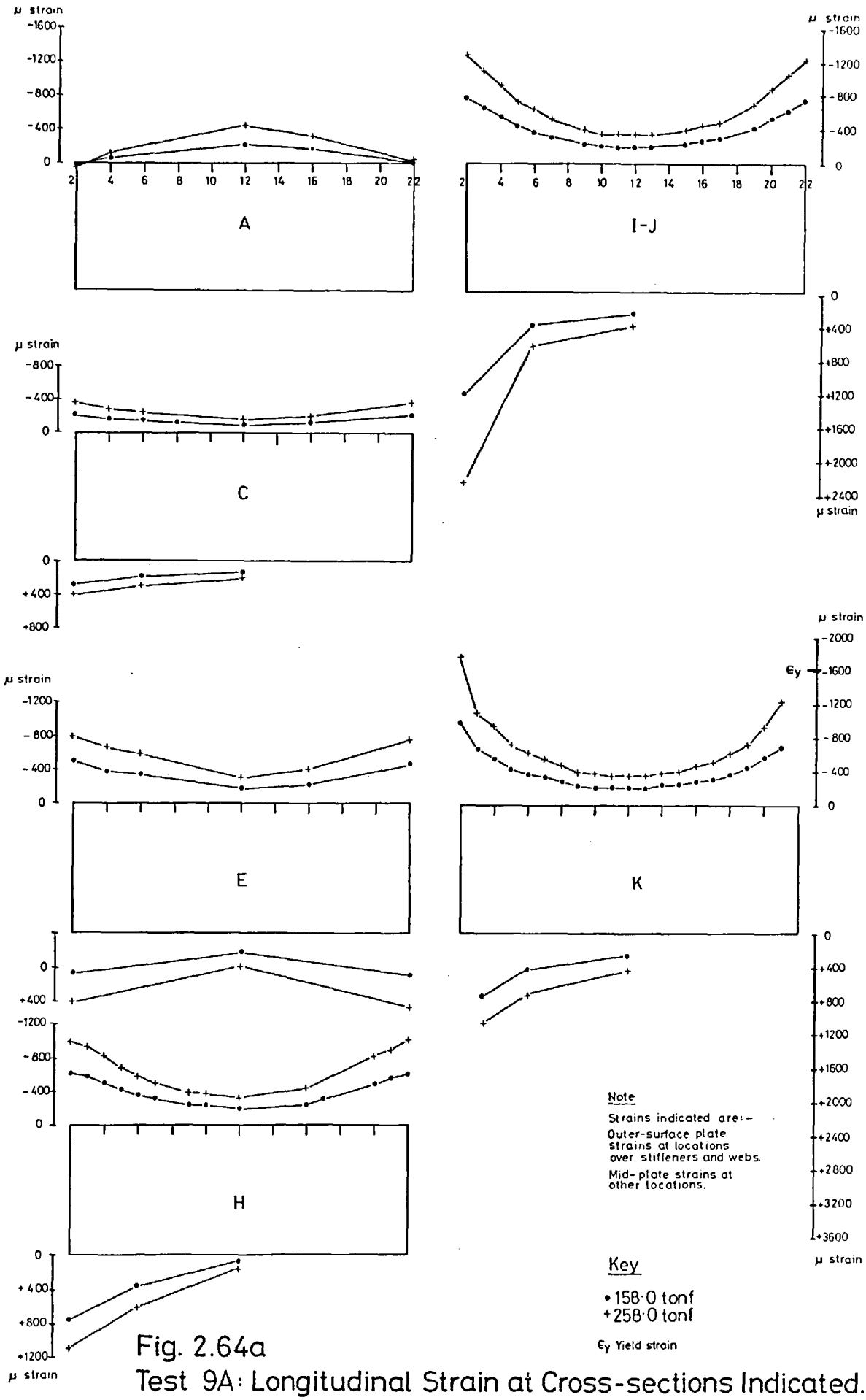

Fig. 2.64a
Test 9A: Longitudinal Strain at Cross-sections Indicated.

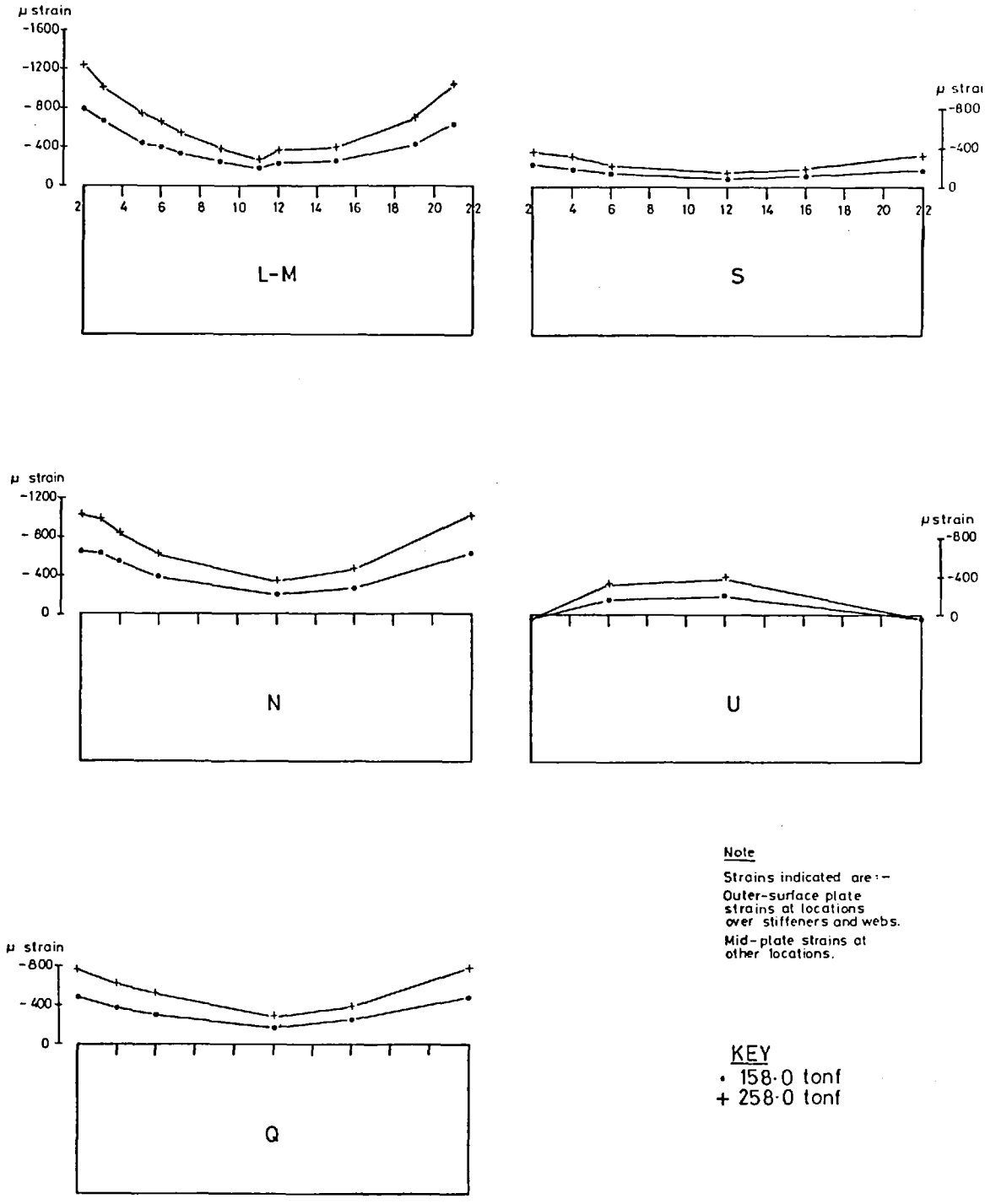

Fig. 2.64b
Test 9A: Longitudinal Strain at Cross-sections Indicated

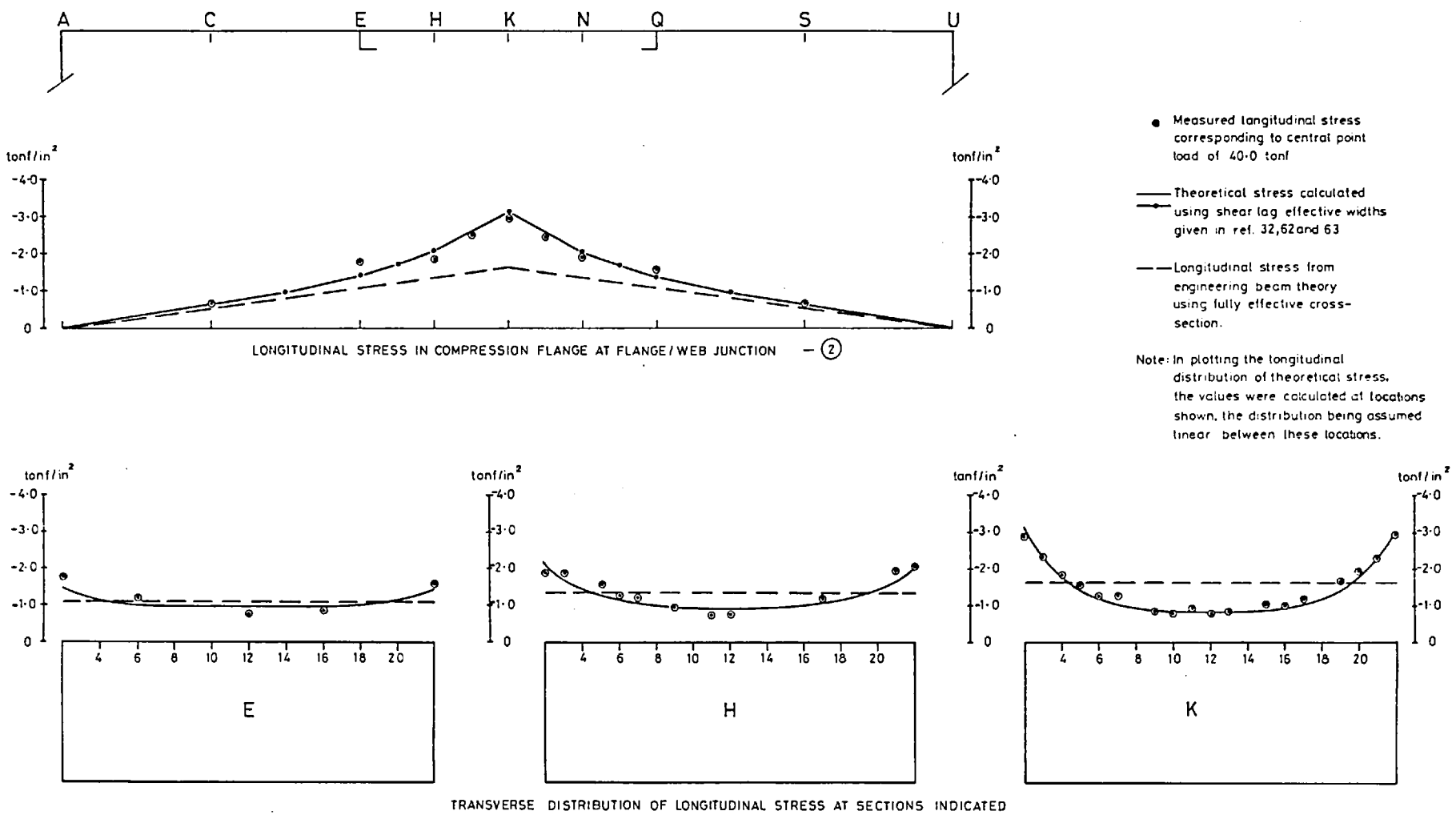

Fig. 2.65
Test 9A: Comparison of Theoretical and Measured Longitudinal Stresses in Compression Flange.

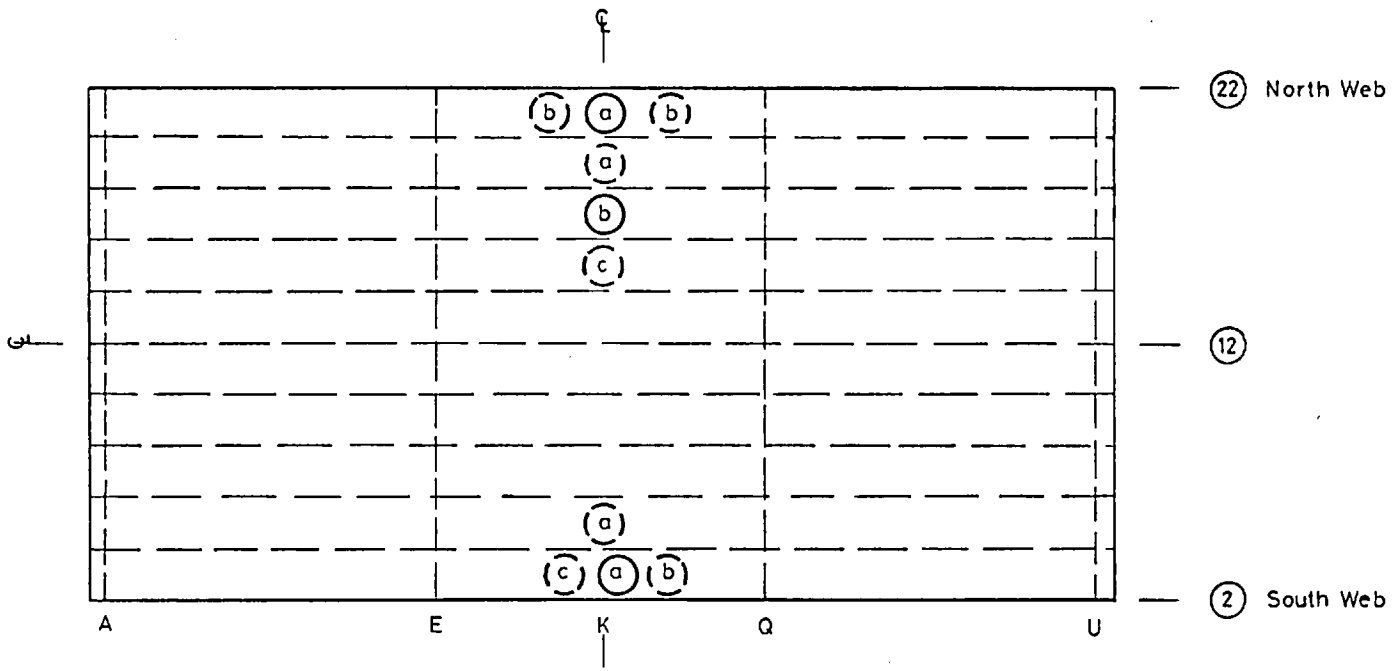

Fig. 2.66
Test 9B: Development of Compression Flange Plate Panel Buckles

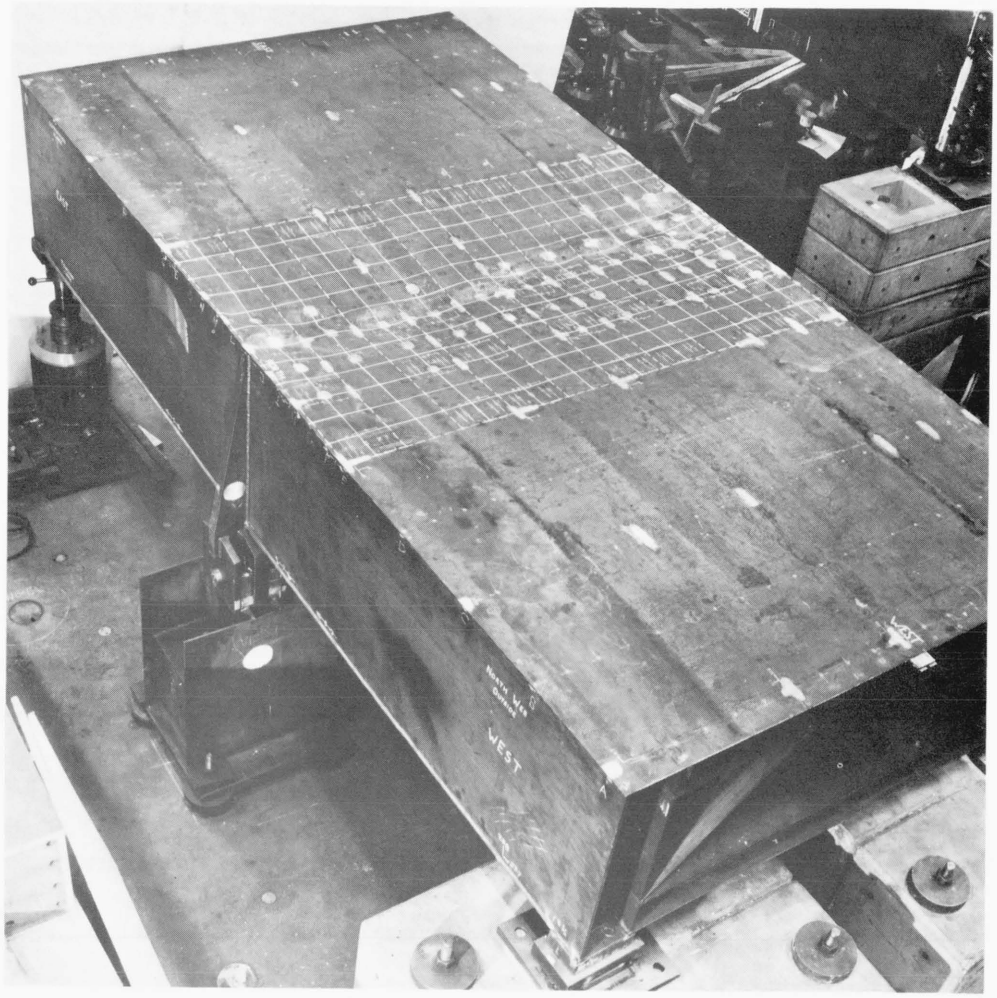

Fig. 2.67a. Model 9 - after the collapse test (Test 9B). Stiffener locations are indicated by dashed lines.

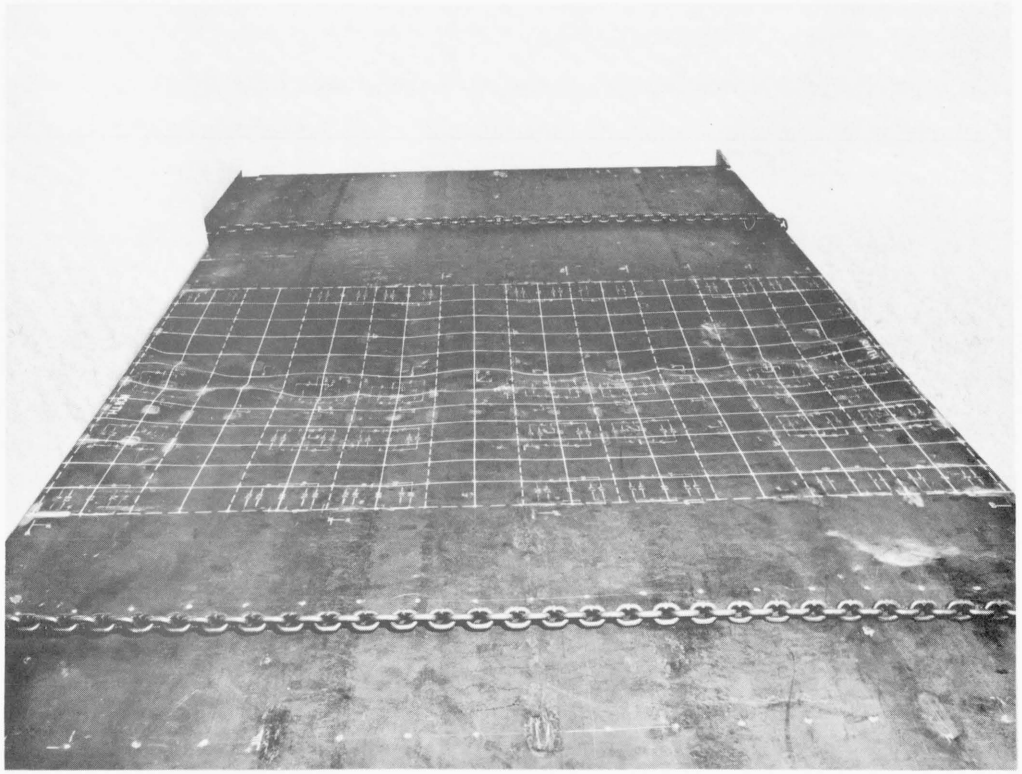

Fig. 2.67b. Model 9 - showing the compression flange (from end A) after collapse. Stiffener locations are indicated by dashed lines.

Fig. 2.67c. Model 9 - an inside view of the model (from end A) after collapse.

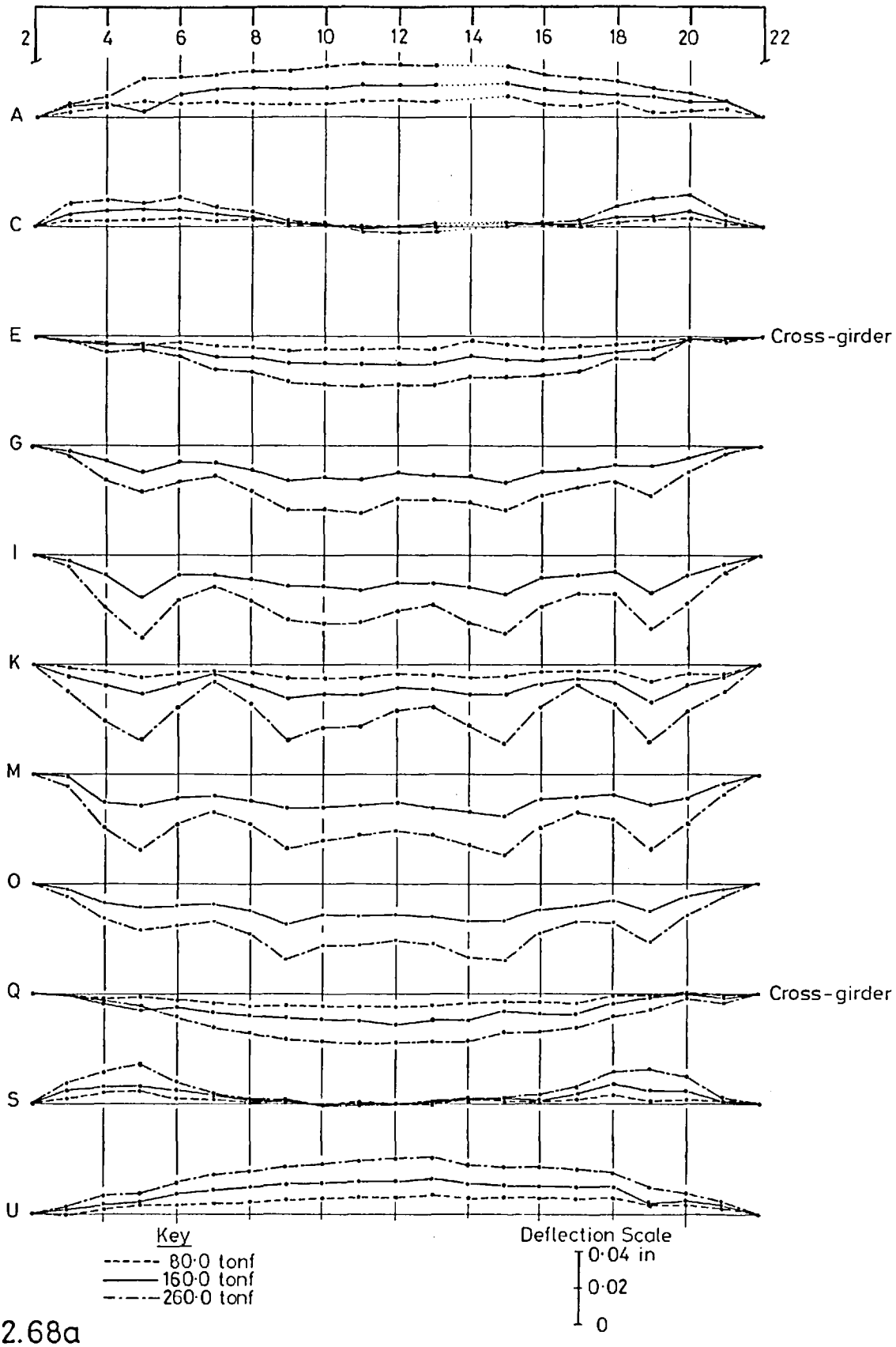

Fig. 2.68a
Test 9B: Relative Transverse Deflections of Compression Flange

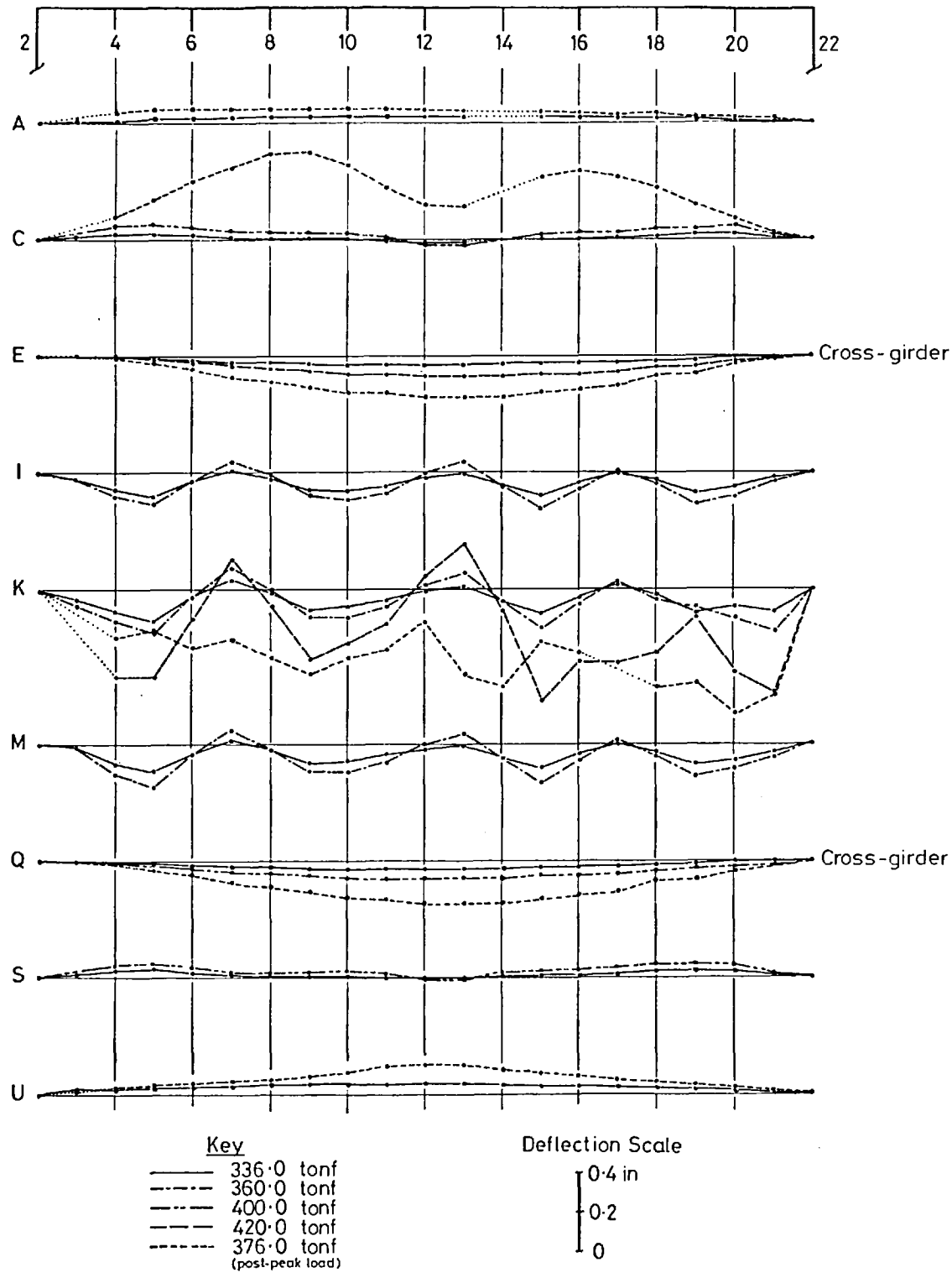

Fig. 2.68b
Test 9B Relative Transverse Deflections of Compression Flange

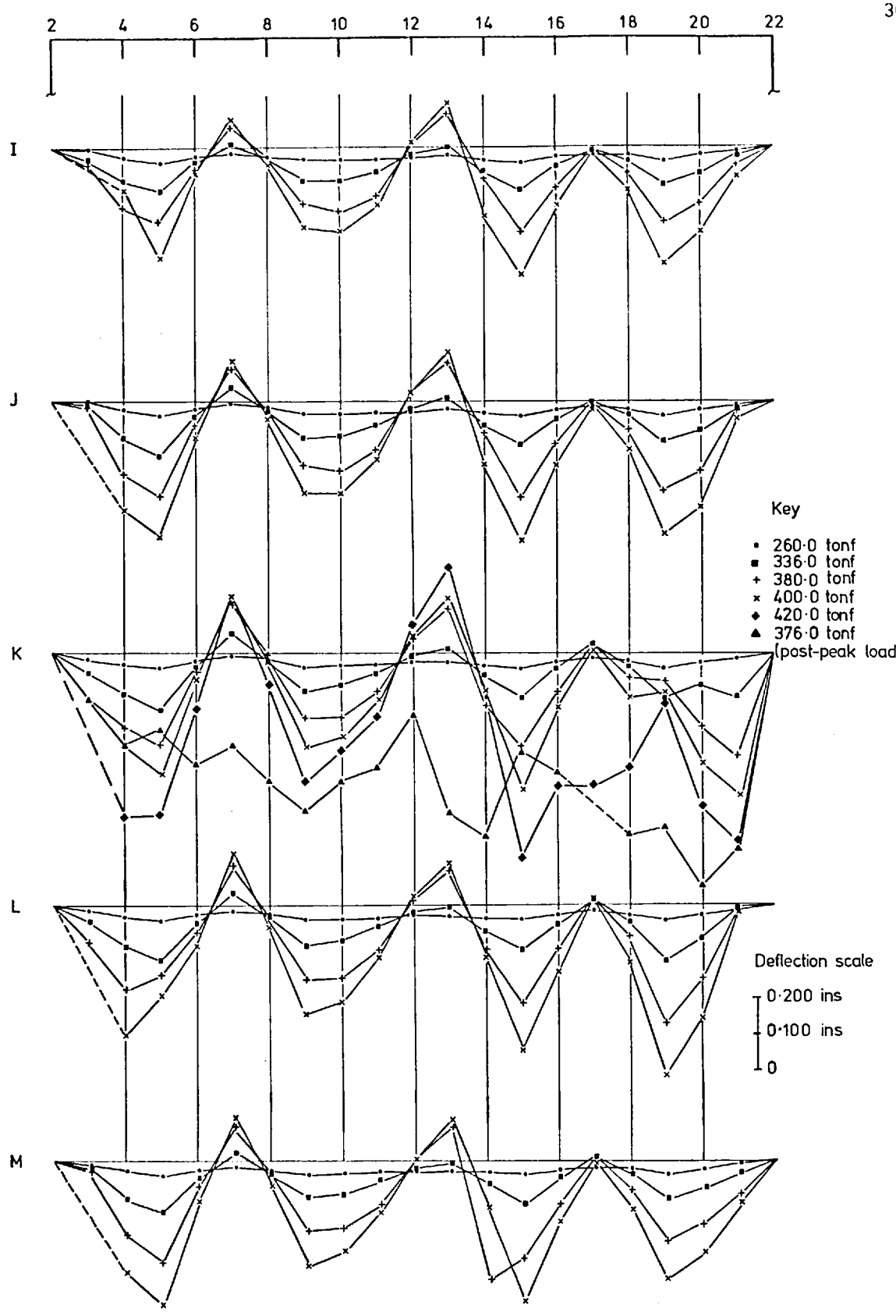

Fig.. 2.68c
Test 9B: Relative Transverse Deflections of Compression Flange

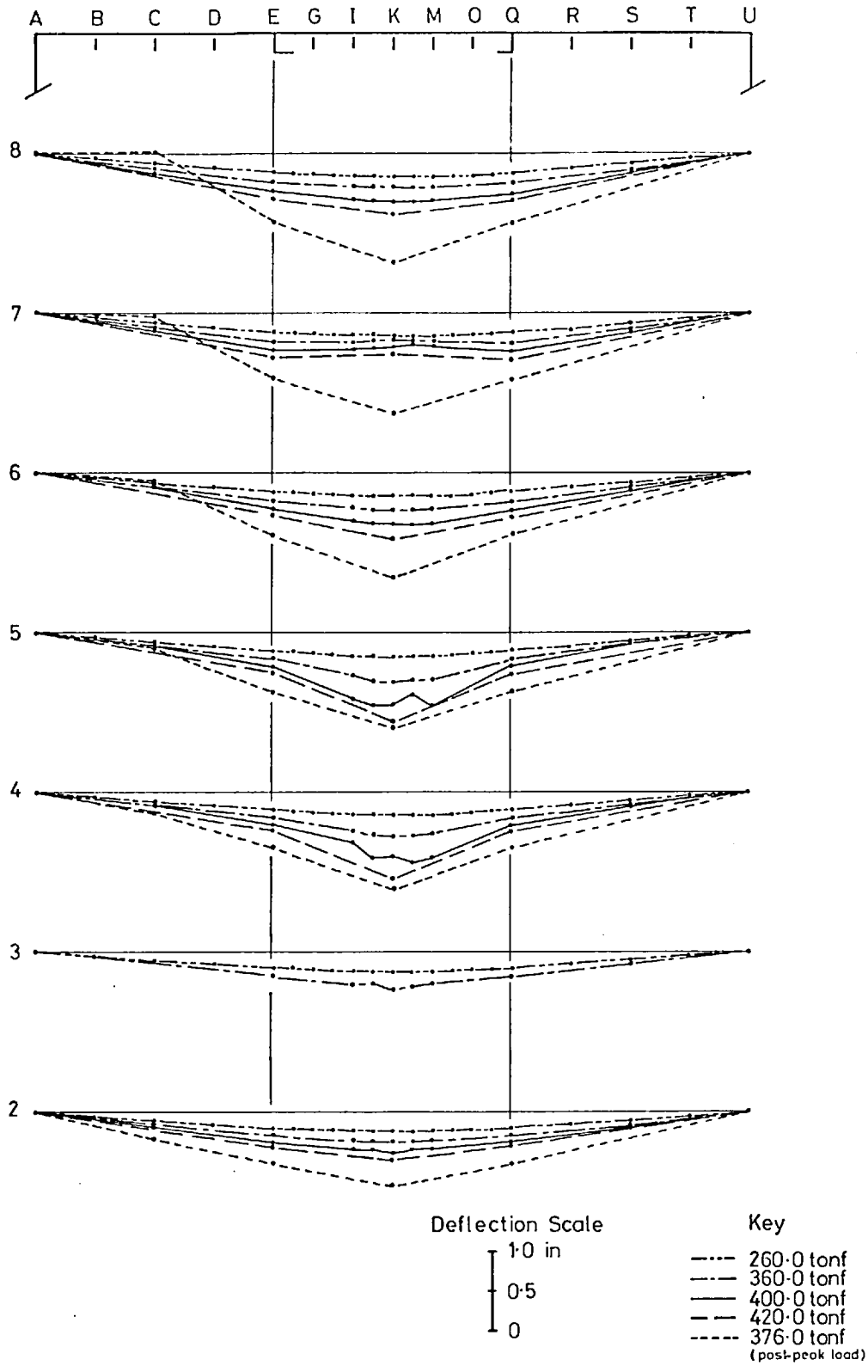

Fig. 2.69a
Test 9B: Relative Longitudinal Deflections of Compression Flange

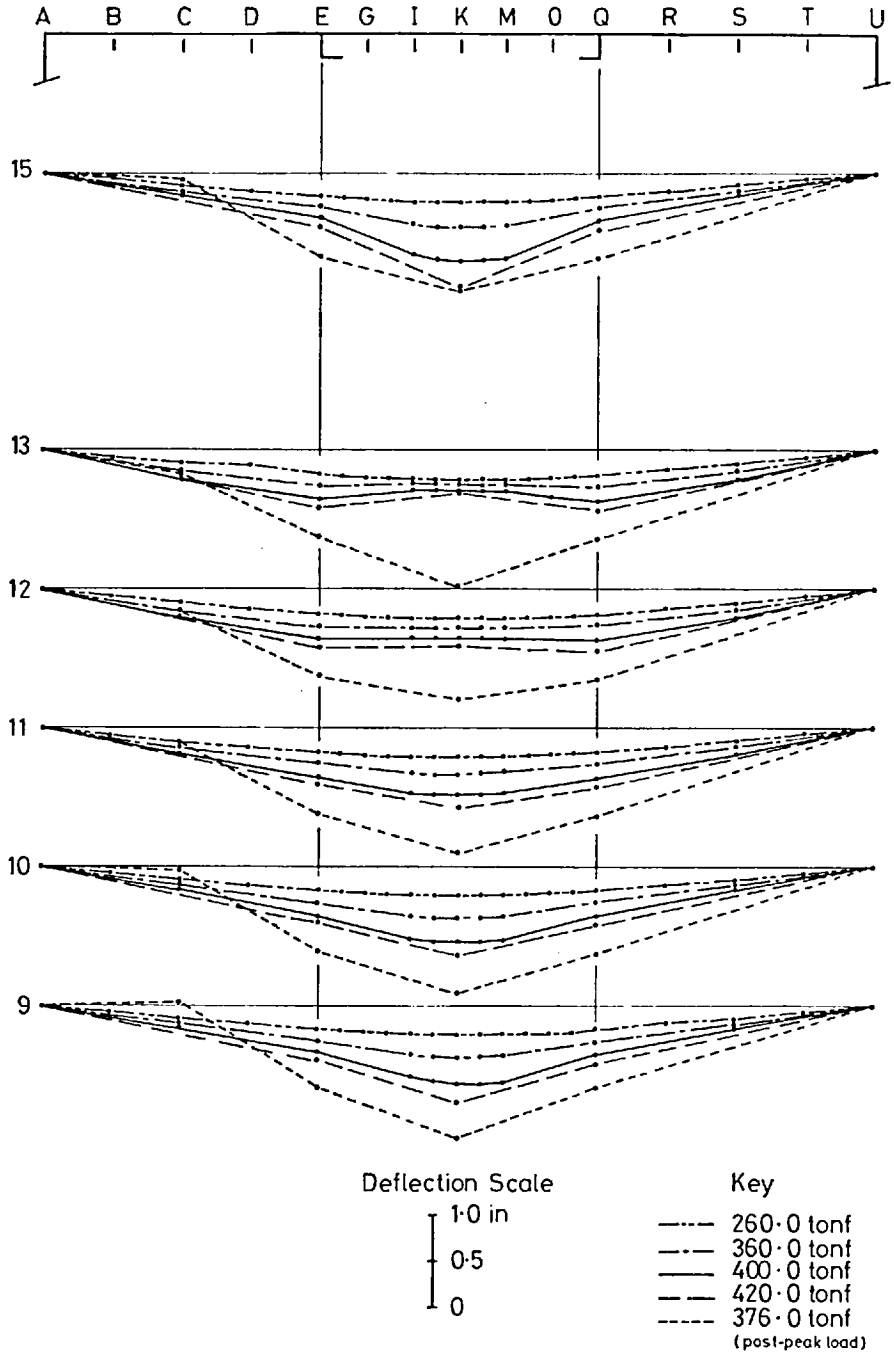

Fig. 2.69b
Test 9B: Relative Longitudinal Deflections of Compression Flange

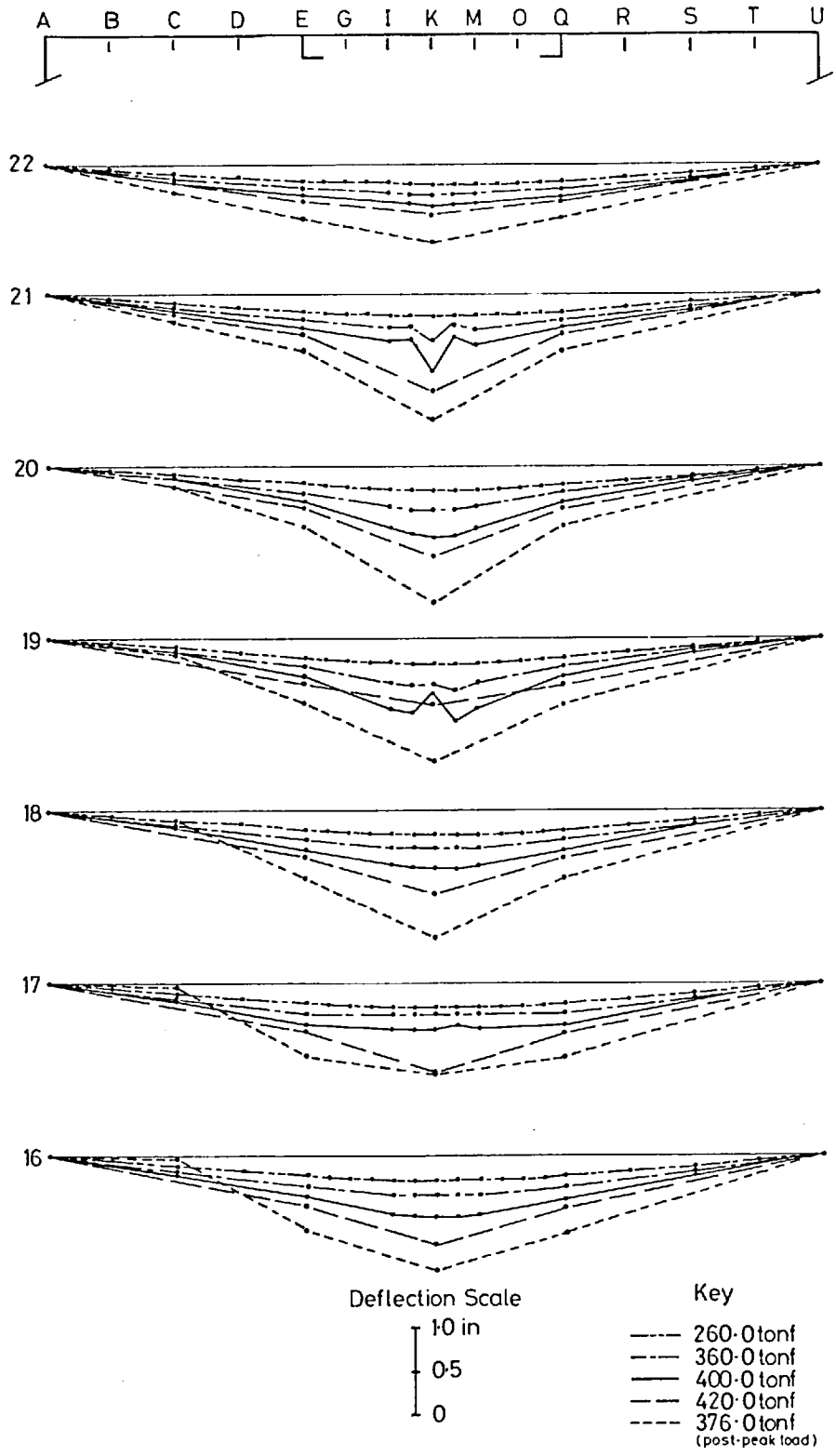

Fig. 2.69c
Test 9B: Relative Longitudinal Deflections of Compression Flange

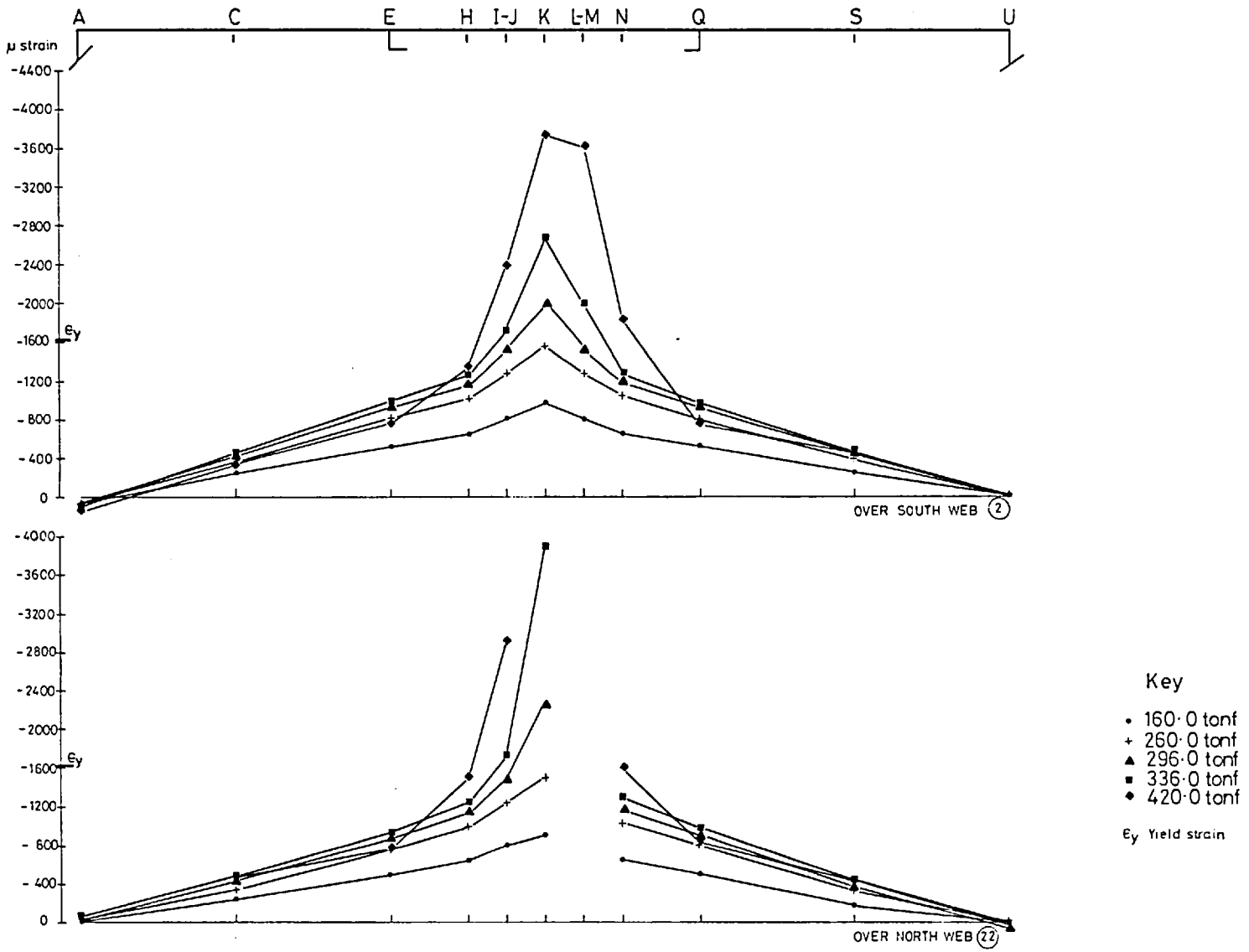

Fig. 2.70a
Test 9B: Longitudinal Strain in Compression Flange at its Junctions with Webs

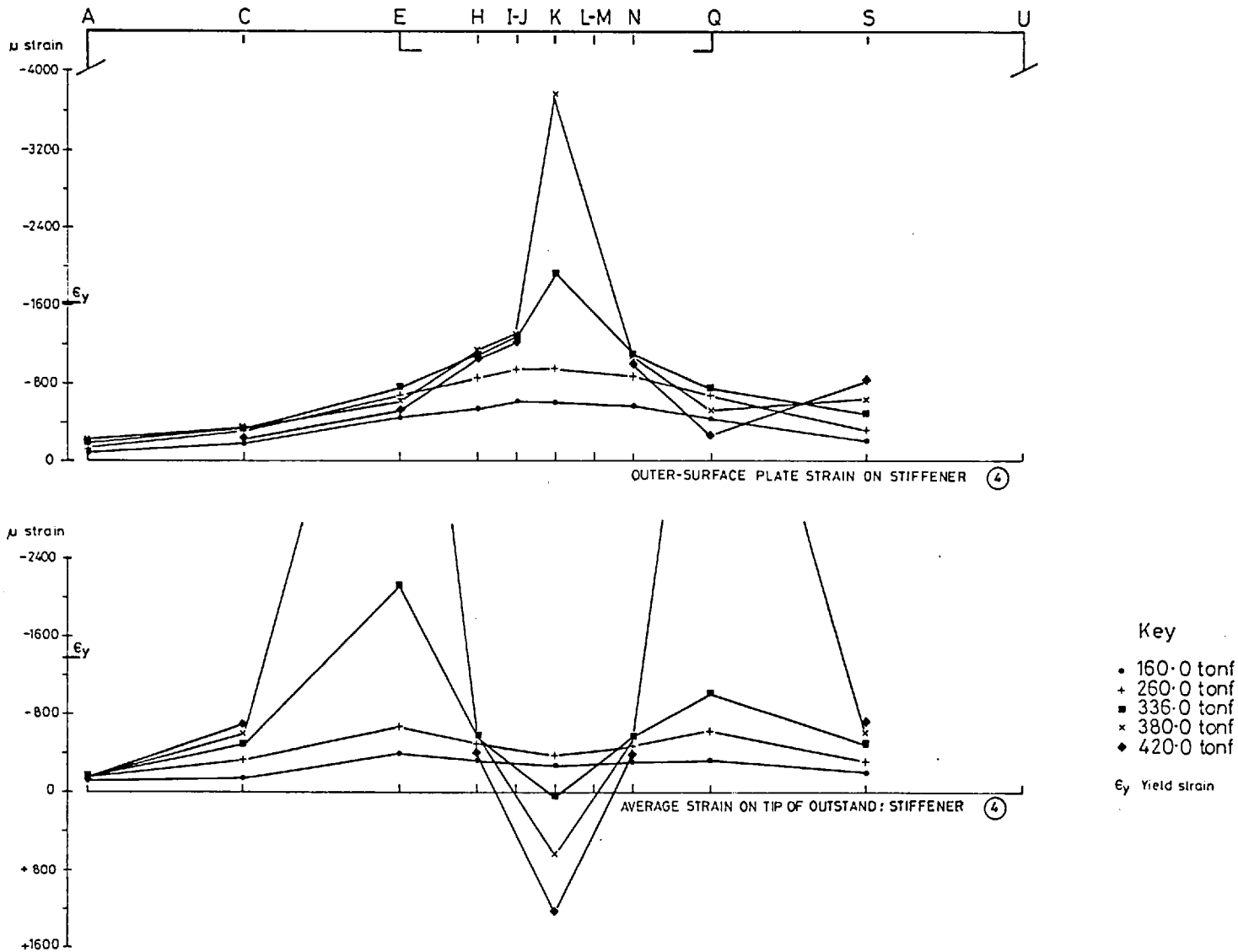

Fig. 2.70b
Test 9B: Longitudinal Strain in Compression Flange Stiffener ④

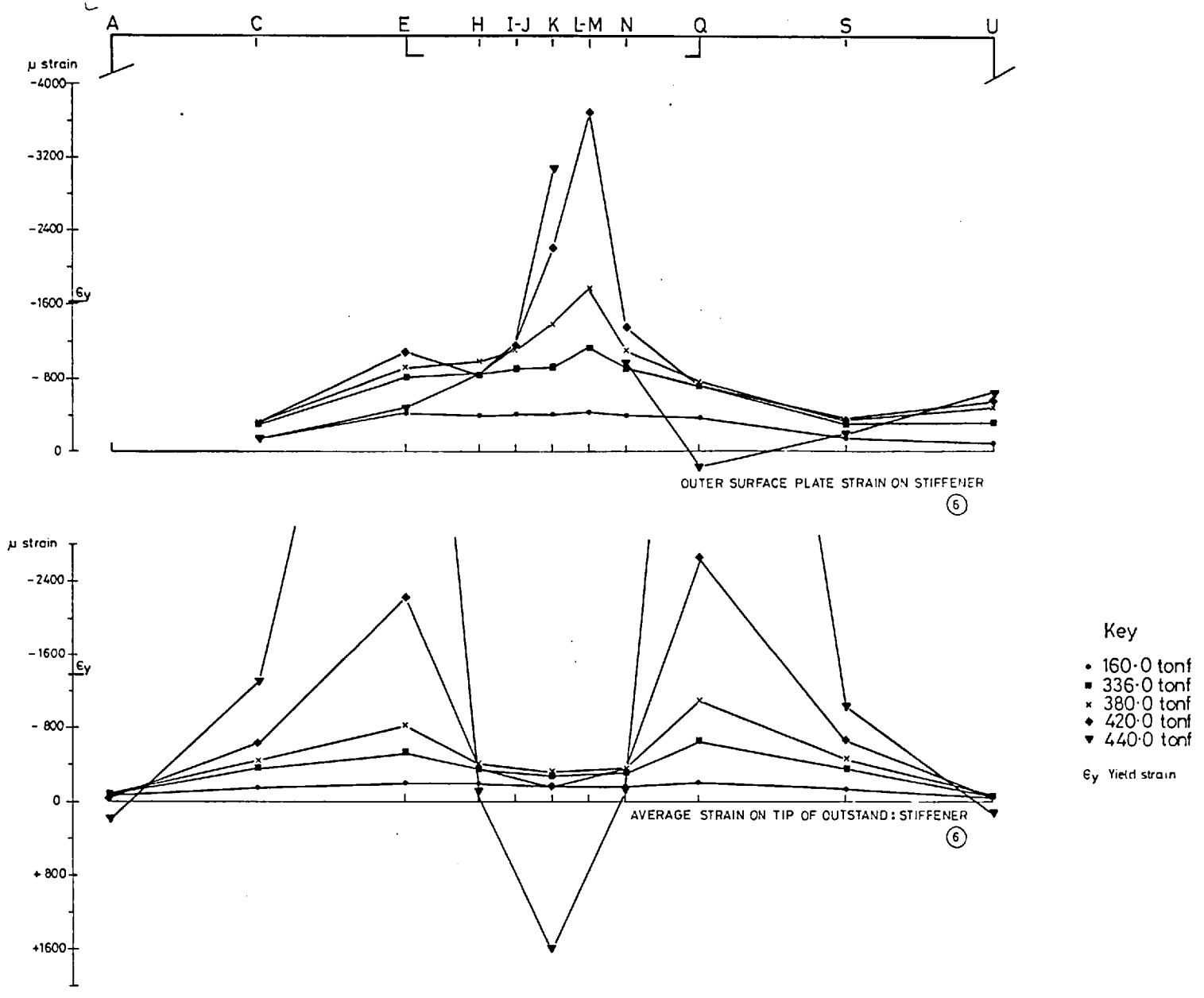

Fig. 2.70c
Test 9B: Longitudinal Strain in Compression Flange Stiffener ⑥

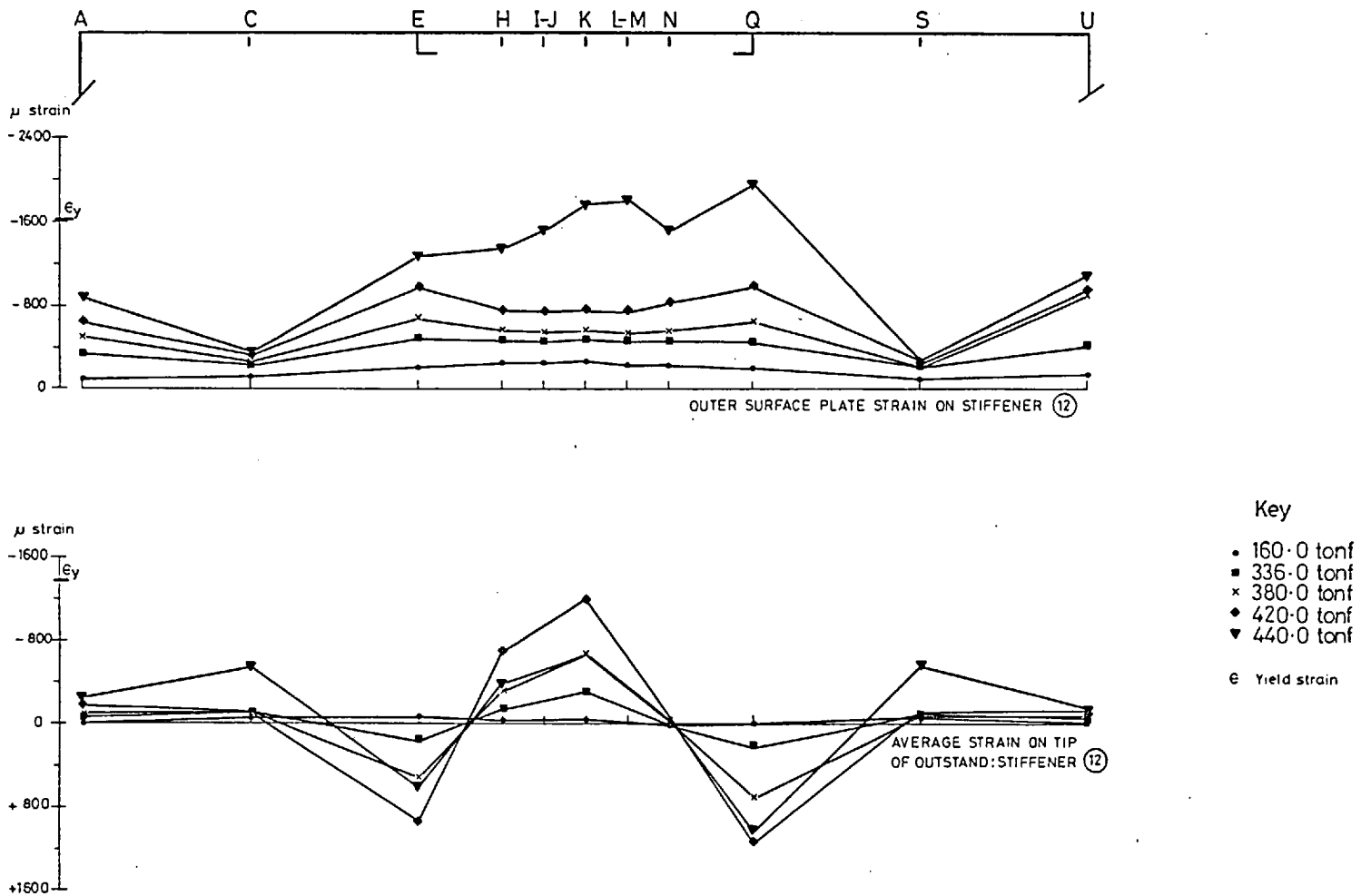

Fig. 2.70d
Test 9B: Longitudinal Strain in Compression Flange Stiffener (12)

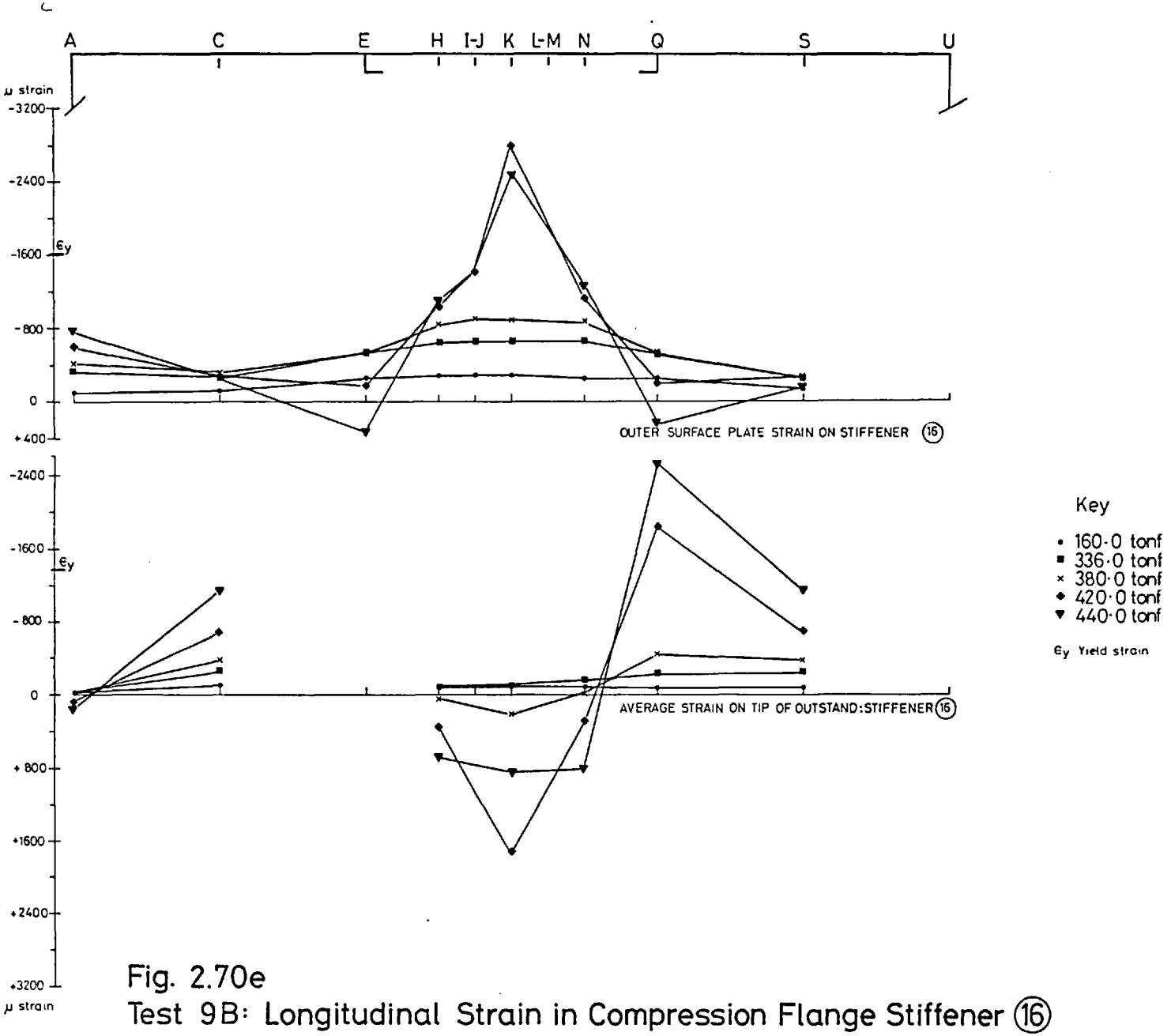

Fig. 2.70e
Test 9B: Longitudinal Strain in Compression Flange Stiffener (16)

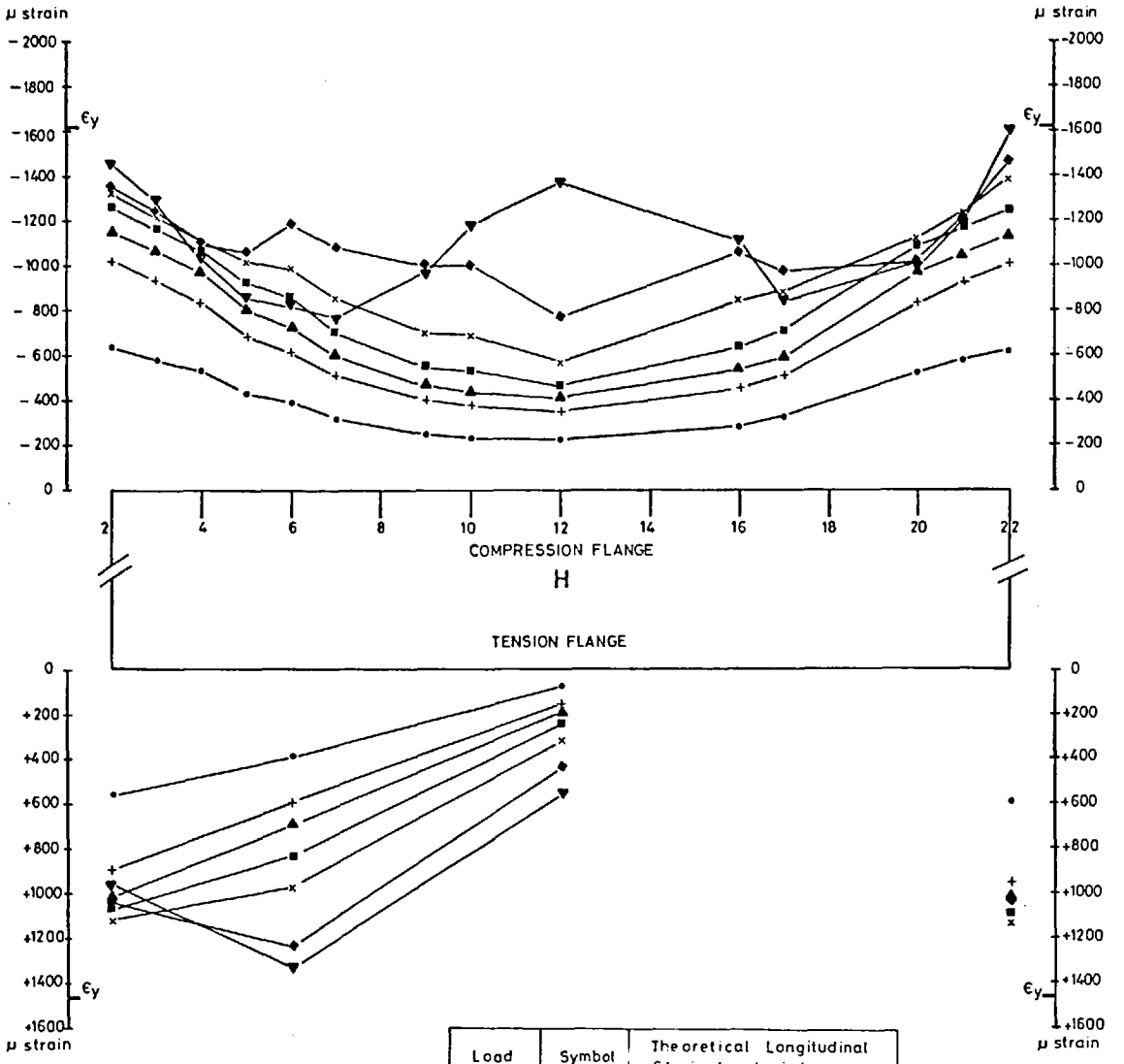

Load tonf	Symbol	Theoretical Longitudinal Strain (μ strain)	
		ϵ_{max}	ϵ_n
160	•	- 610	- 410
260	+	- 990	- 665
296	▲	-1130	- 760
336	■	-1280	- 860
380	×	-1450	- 975
420	◆	-1600	-1075
440	▼	-1680	-1130

Note

Strains indicated are:-
Outer-surface plate strains at locations over stiffeners and webs.
Mid-plate strains at other locations.

ϵ_y Yield strain

ϵ_{max} Theoretical shear lag strain in compression flange plate at flange/web junction

ϵ_n Longitudinal strain in compression flange plate from simple beam theory

Fig. 2.71a
Test 9B: Longitudinal Strain at Cross-section H
($15\frac{1}{2}$ in from mid-span)

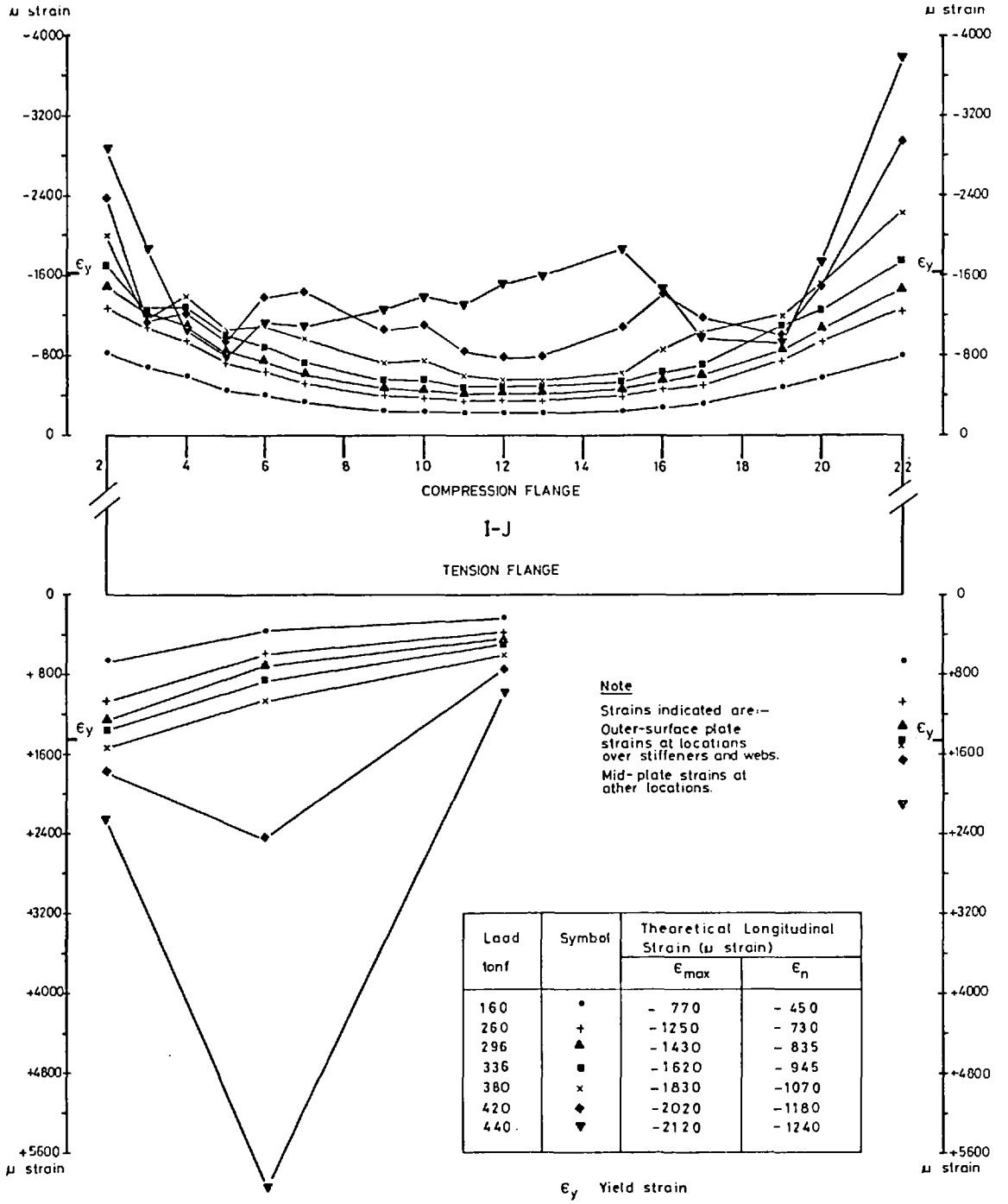

Load tonf	Symbol	Theoretical Longitudinal Strain (μ strain)	
		ϵ_{max}	ϵ_n
160	•	- 770	- 450
260	+	-1250	- 730
296	▲	-1430	- 835
336	■	-1620	- 945
380	×	-1830	-1070
420	◆	-2020	-1180
440	▼	-2120	- 1240

ϵ_y Yield strain

ϵ_{max} Theoretical shear lag strain in compression flange plate at flange/web junction

ϵ_n Longitudinal strain in compression flange plate from simple beam theory

Fig. 2.71b
Test 9B: Longitudinal Strain at Cross-section I-J
($7\frac{3}{4}$ in from mid-span)

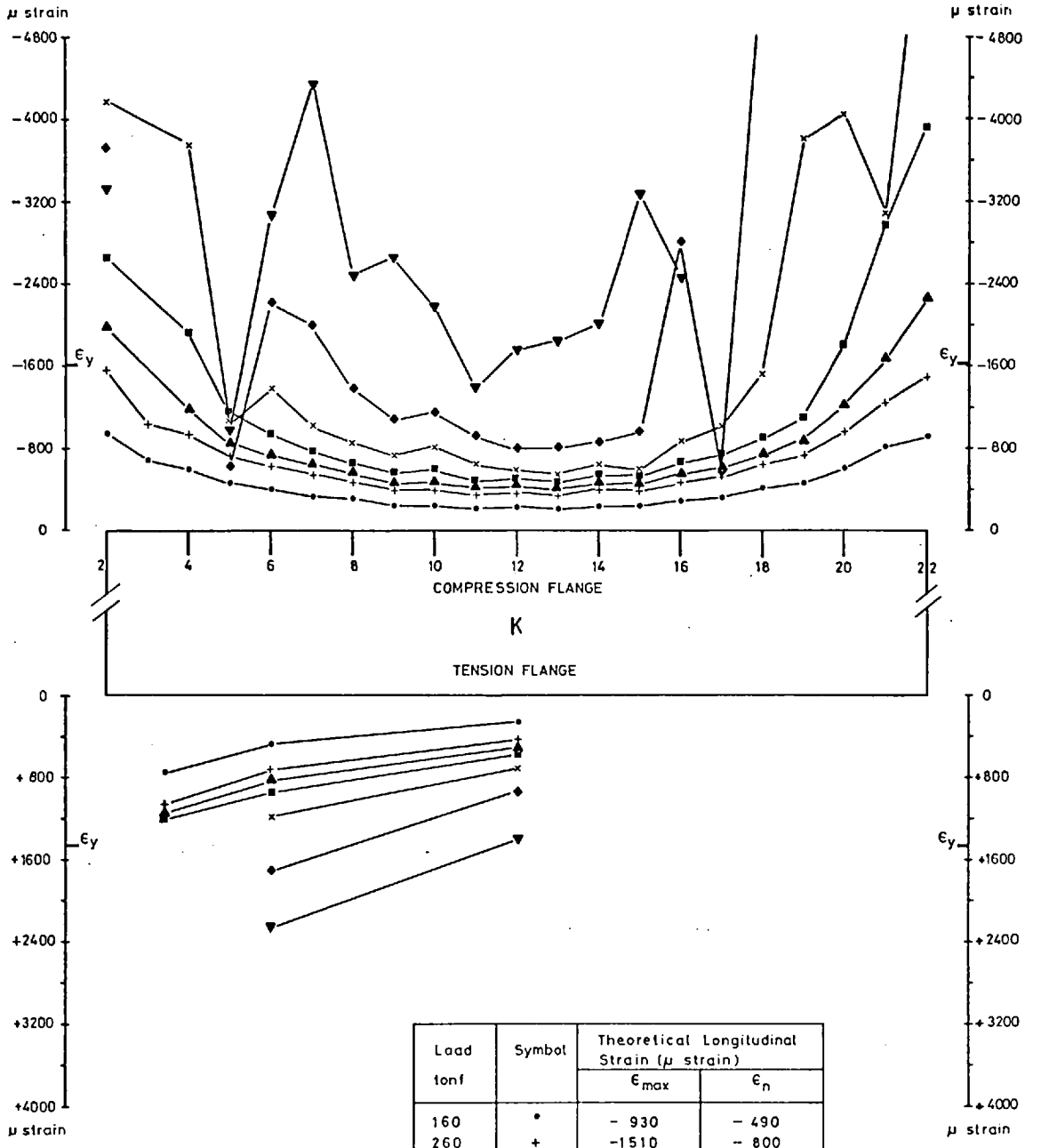

Load tonf	Symbol	Theoretical Longitudinal Strain (μ strain)	
		ϵ_{max}	ϵ_n
160	•	- 930	- 490
260	+	-1510	- 800
296	▲	-1730	- 910
336	■	-1960	-1030
380	×	-2210	-1170
420	◆	-2440	-1290
440	▼	-2560	-1350

Note

Strains indicated are:-

Outer-surface plate strains at locations over stiffeners and webs.

Mid-plate strains at other locations.

ϵ_y Yield strain

ϵ_{max} Theoretical shear lag strain in compression flange plate at flange/web junction

ϵ_n Longitudinal strain in compressian flange plate from simple beam theory

Fig. 2.71c
Test 9B: Longitudinal Strain at Mid-span

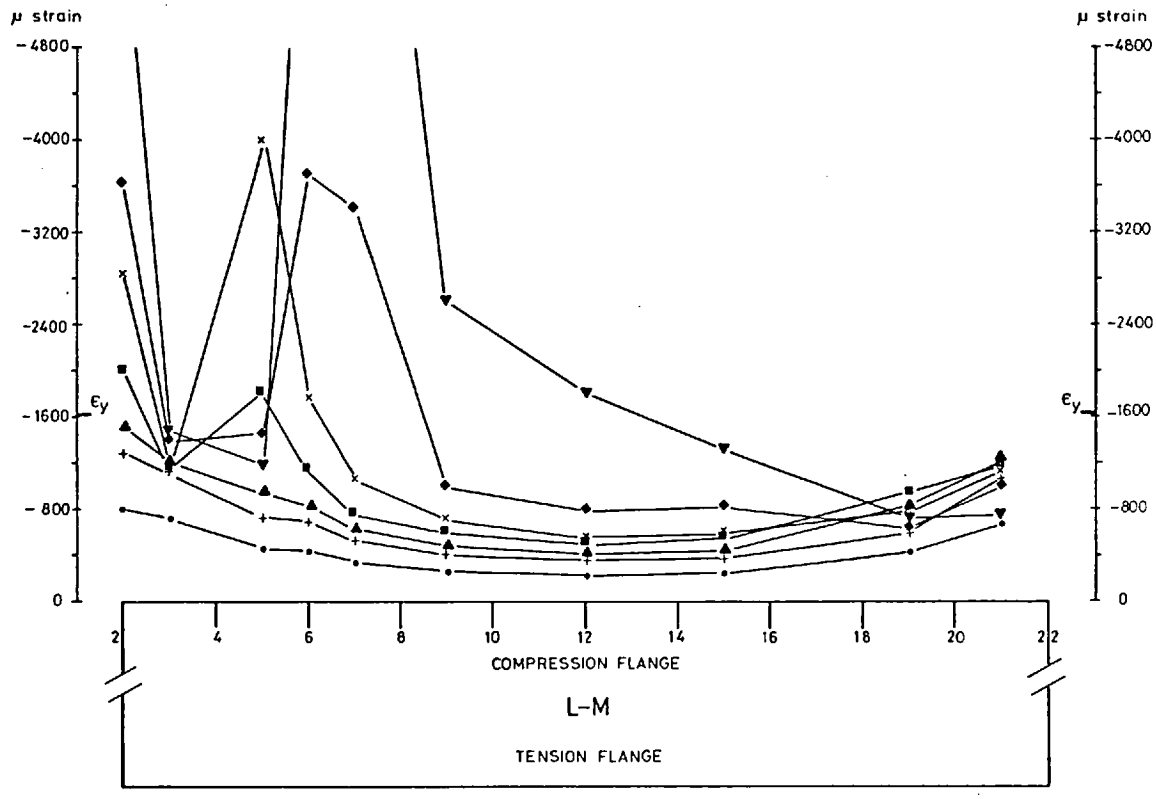

Load tonf	Symbol	Theoretical Longitudinal Strain (μ strain) ϵ_{max}	ϵ_n
160	•	- 770	- 450
260	+	-1250	- 730
296	▲	-1430	- 835
336	■	-1620	- 945
360	×	-1830	-1070
420	◆	-2020	-1180
440	▼	-2120	-1240

Note

Strains indicated are:-
Outer-surface plate strains at locations over stiffeners and webs
Mid-plate strains at other locations.

ϵ_y Yield strain

ϵ_{max} Theoretical shear lag strains in compression flange plate at flange/web junction

ϵ_n Longitudinal strain in compression flange plate from simple beam theory

Fig. 2.71d
Test 9B: Longitudinal Strain at Cross-section L-M ($7\frac{3}{4}$ in from mid-span)

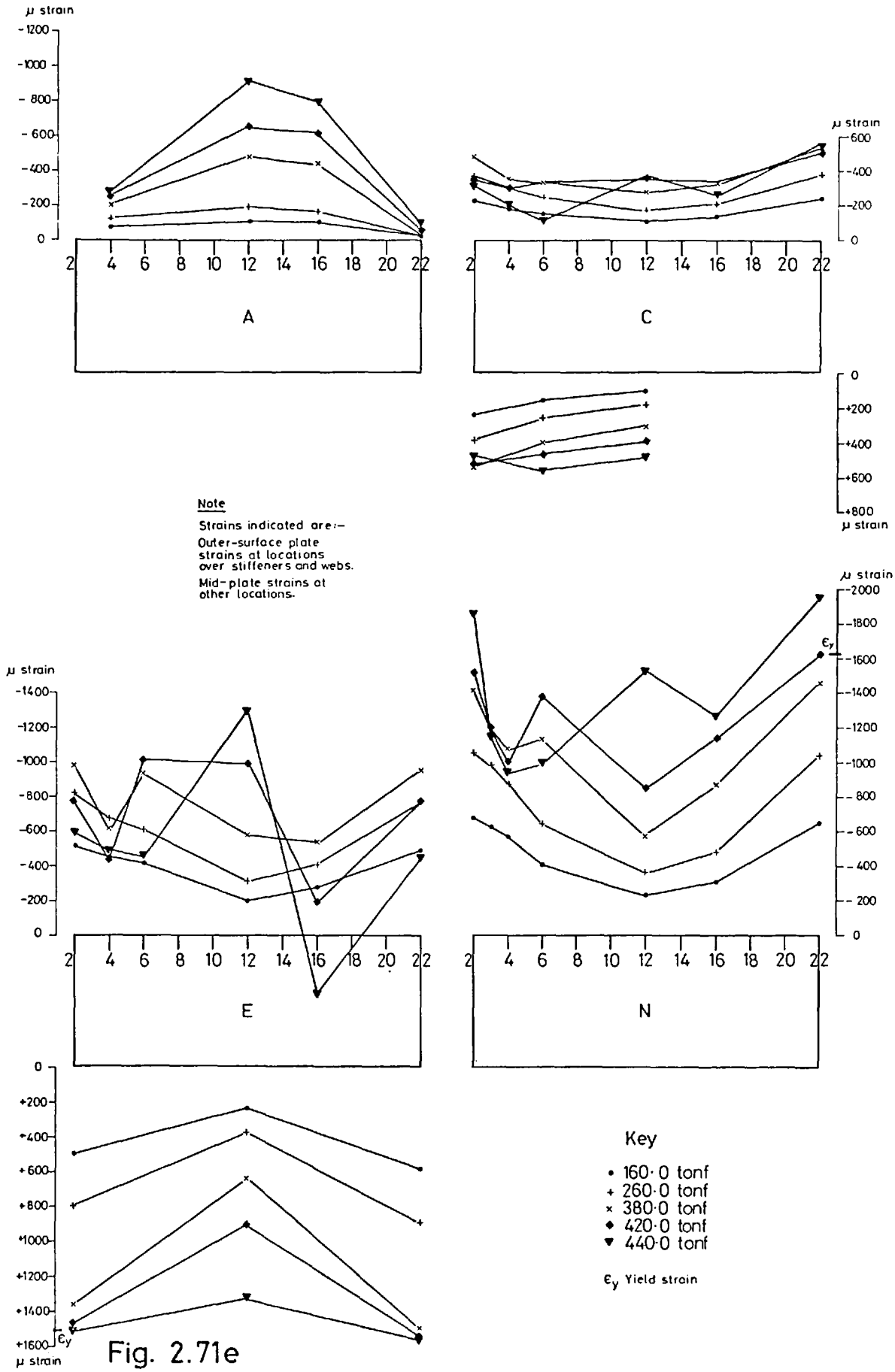

Fig. 2.71e
Test 9B: Longitudinal Strain at Cross-sections Indicated

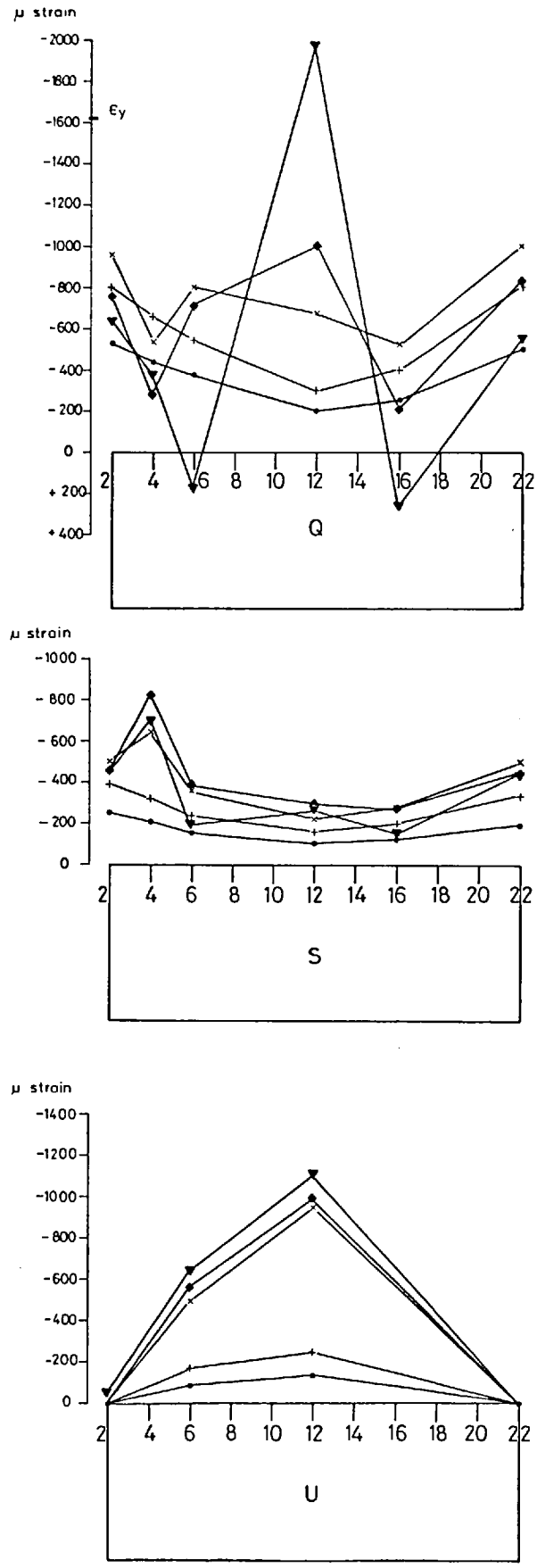

Key

- 160·0 tonf
- 260·0 tonf
- 380·0 tonf
- 420·0 tonf
- 440·0 tonf

Note

Strains indicated are:-
Outer-surface plate strains at locations over stiffeners and webs.
Mid-plate strains at other locations.

Fig. 2.71f
Test 9B: Lonigitudinal Strain at Cross-sections Indicated

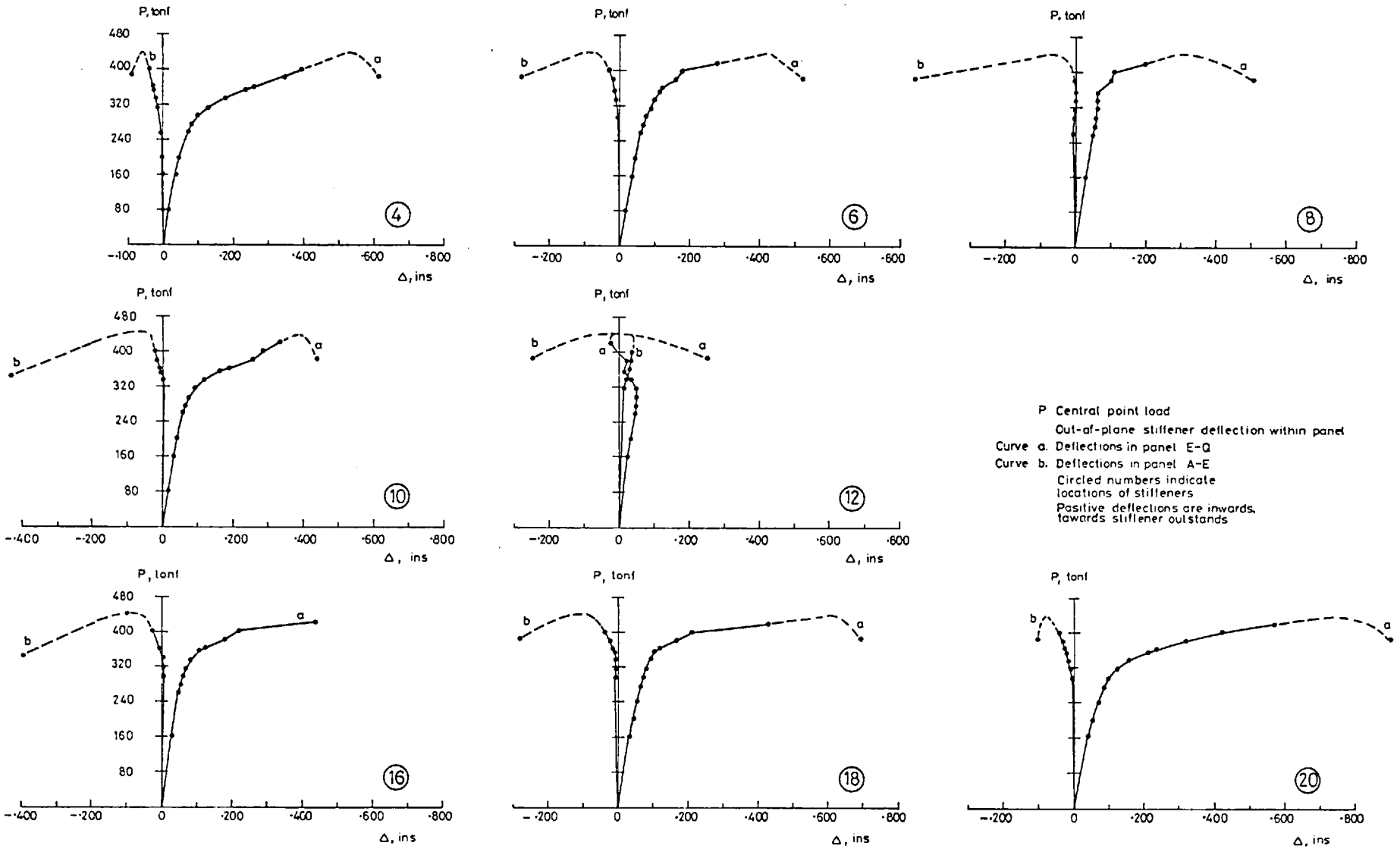

Fig. 2.72
Test 9B: Out-of-plane Deflections of Longitudinal Stiffeners

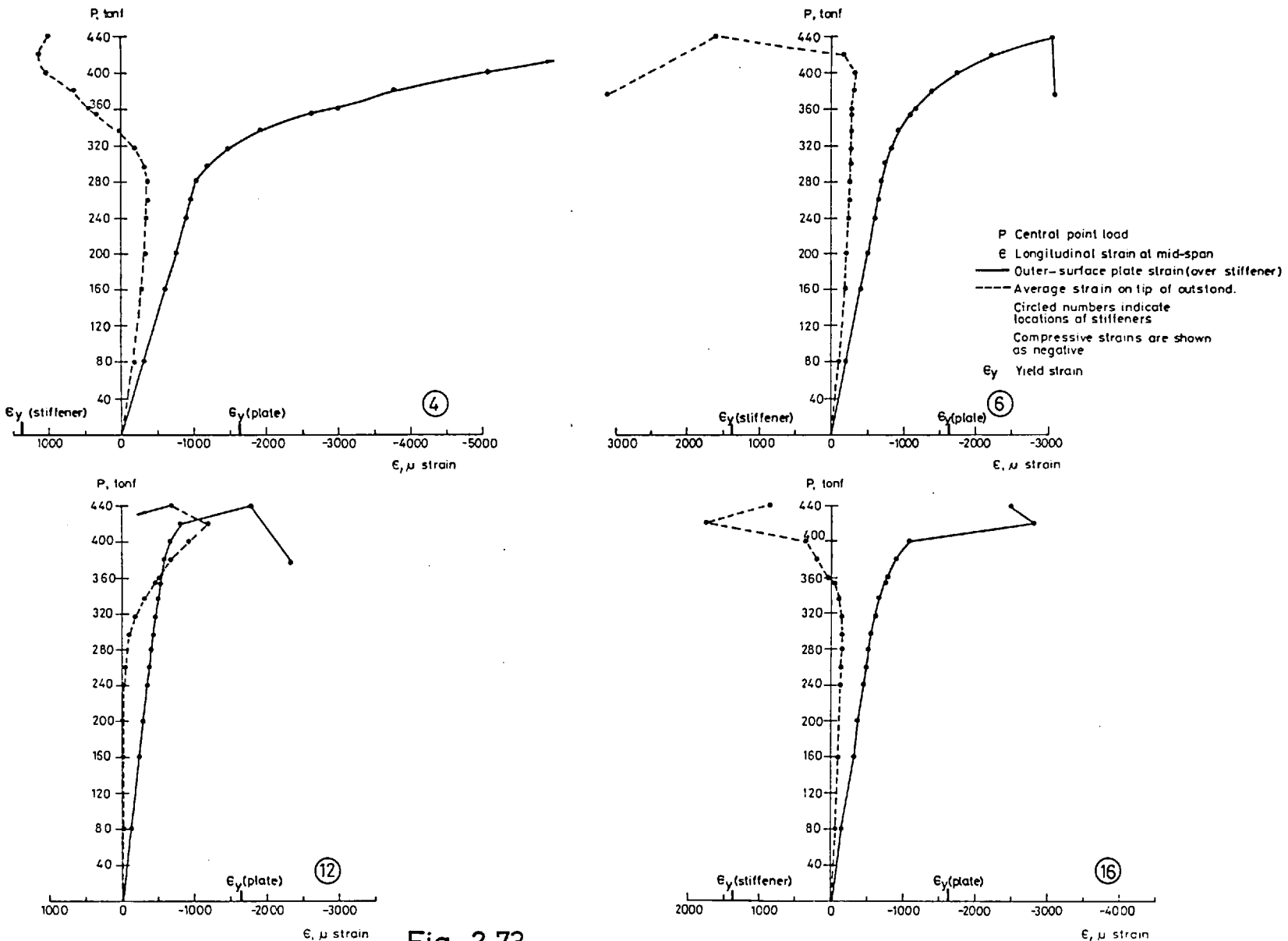

Fig. 2.73
Test 9B: Strain in Longitudinal Stiffeners

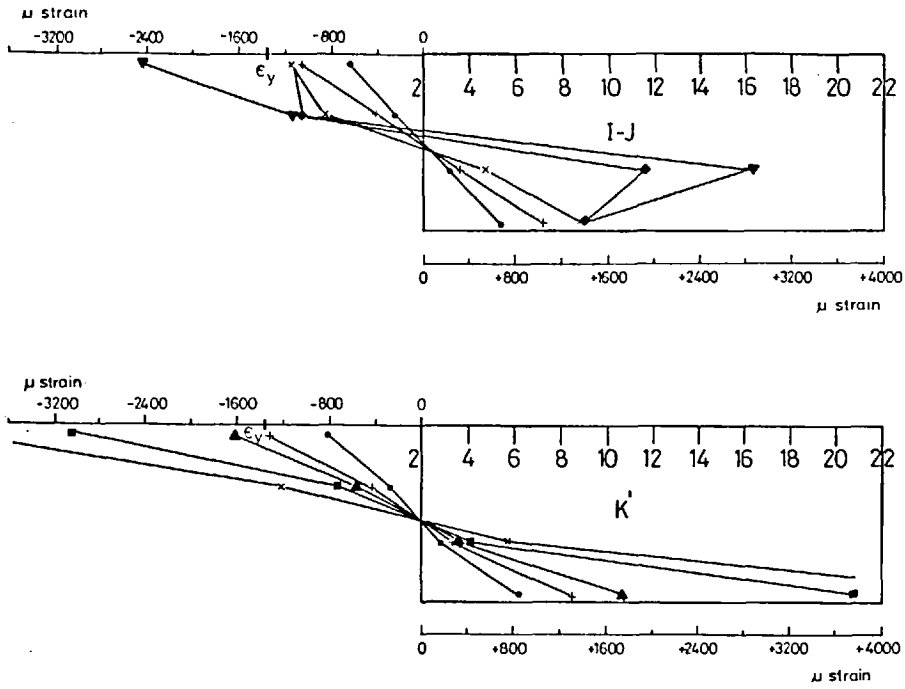

Mid-plane Longitudinal Strains in South Web at Sections I-J and K'

ϵ_y – Yield strain

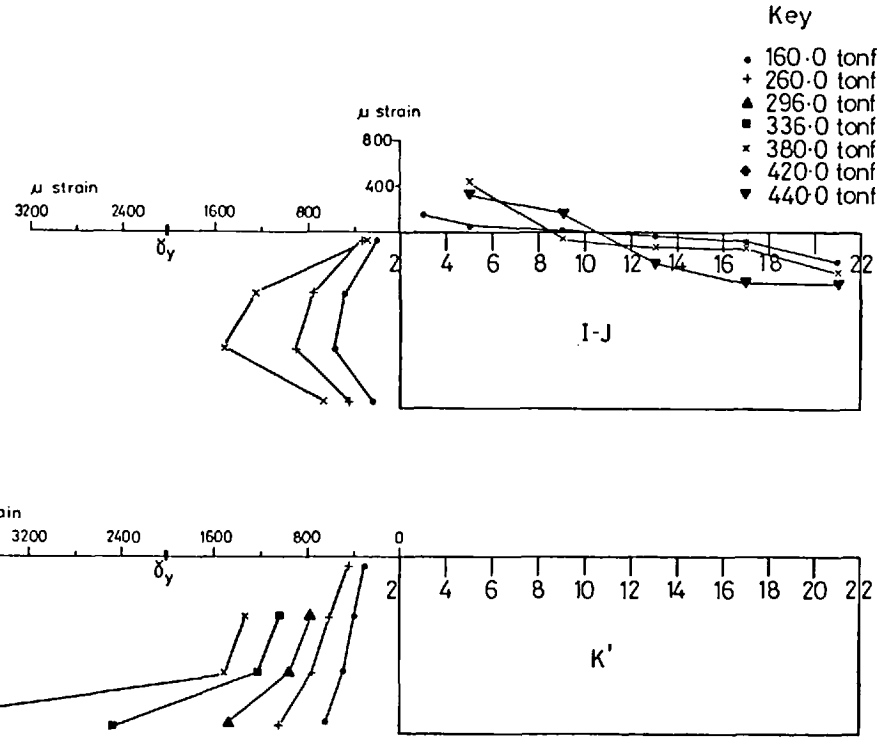

Mid-plane Shear Strains at Section I-J and K'

δ_y – Shear yield strain

Fig. 2.74
Test 9B: Longitudinal and Shear Strains at Cross-sections I-J and K'

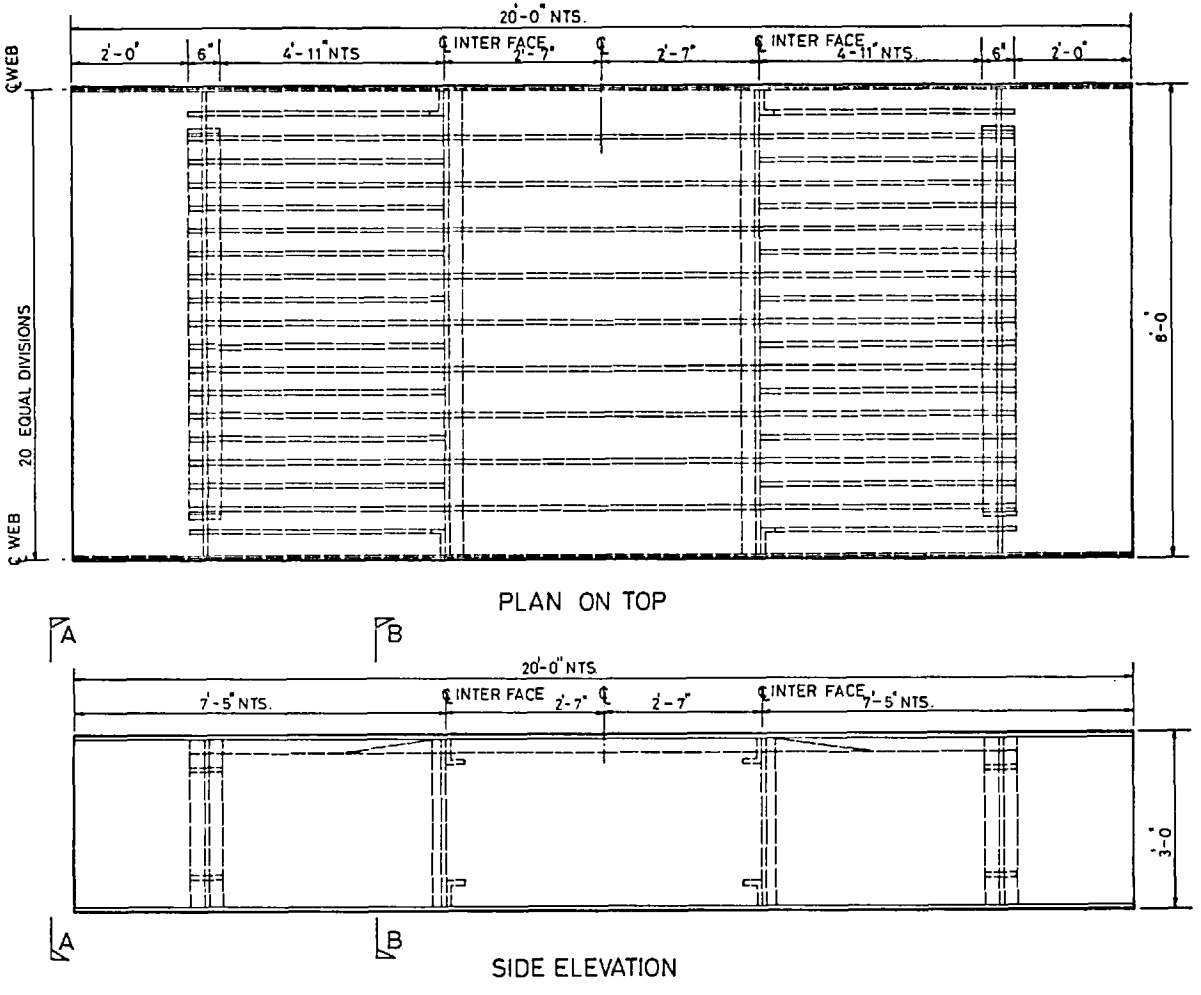

Fig. 2.75a
Model 10 : Plan and Elevation

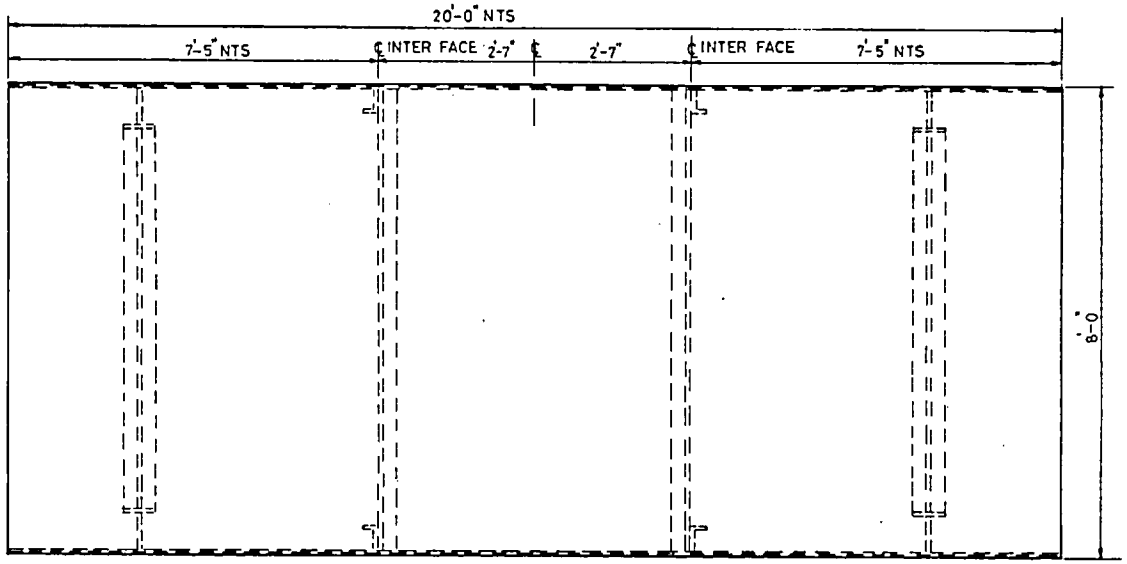

VIEW ON UNDERSIDE

Fig. 2.75b
Model 10 : View on Underside

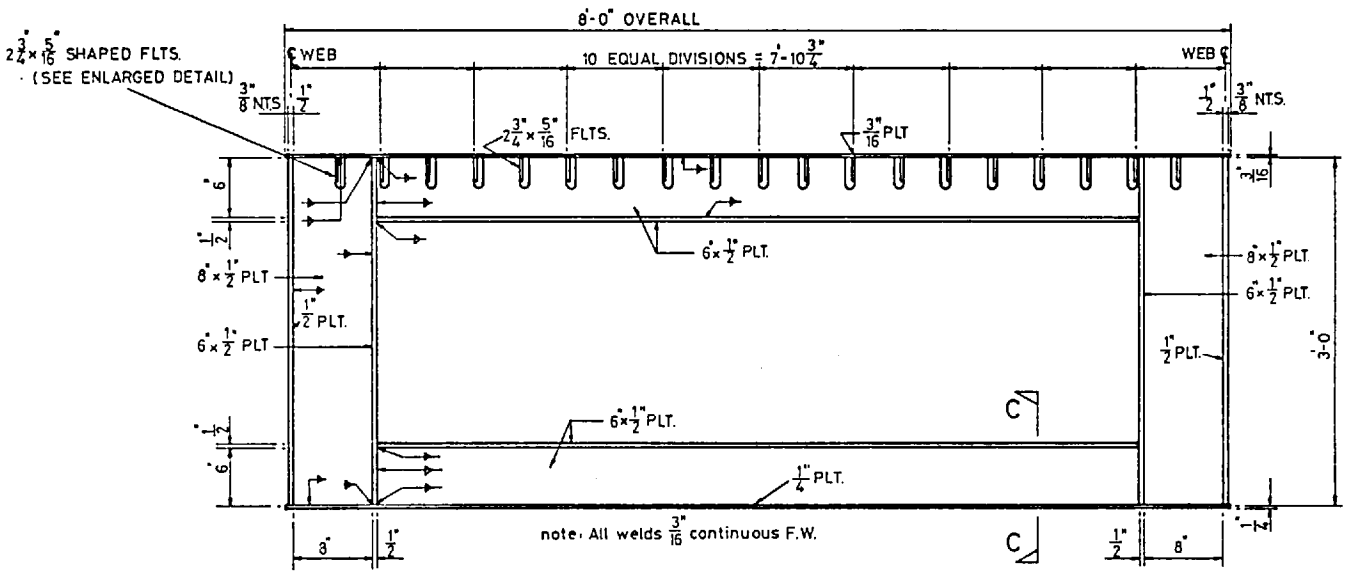

SECTION A- A

Fig. 2.75c
Model 10 : Details of End Cross-frame

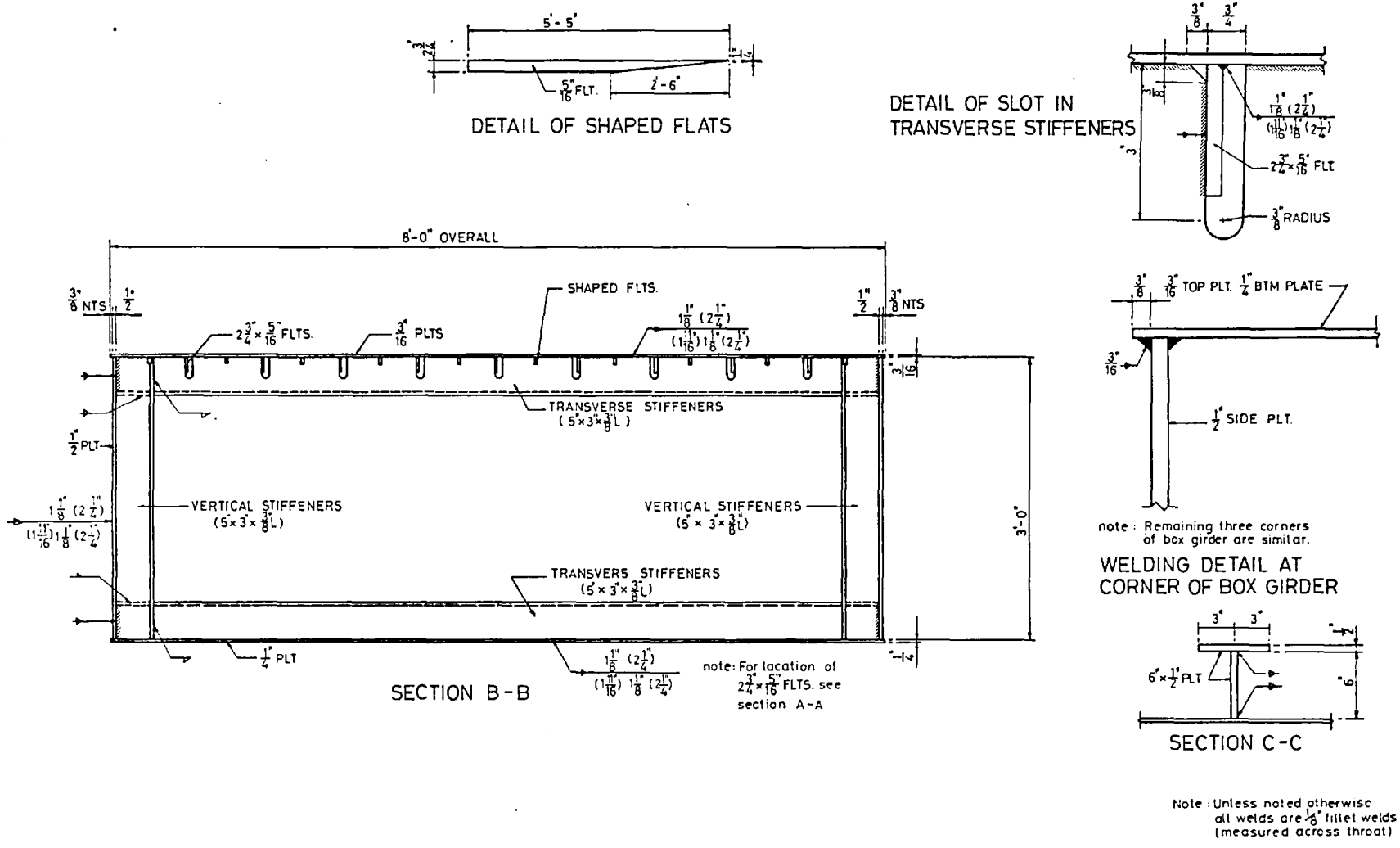

Fig. 2.75d
Model 10: Internal Cross-frame and Other Cross-sectional Details

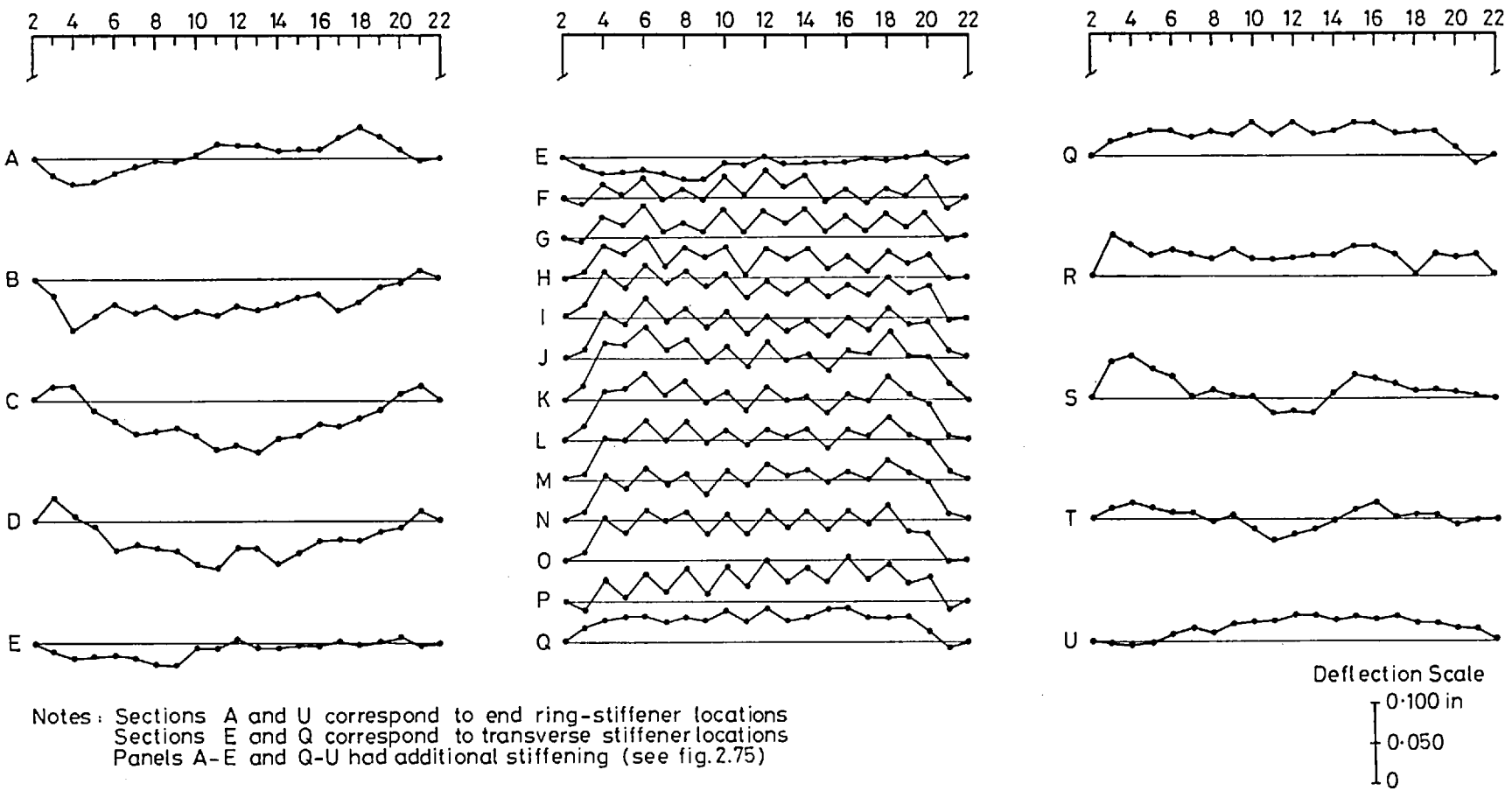

Notes : Sections A and U correspond to end ring-stiffener locations
Sections E and Q correspond to transverse stiffener locations
Panels A-E and Q-U had additional stiffening (see fig. 2.75)

Fig. 2.76a
Model 10 : Transverse Initial Deflection Profiles of Compression Flange

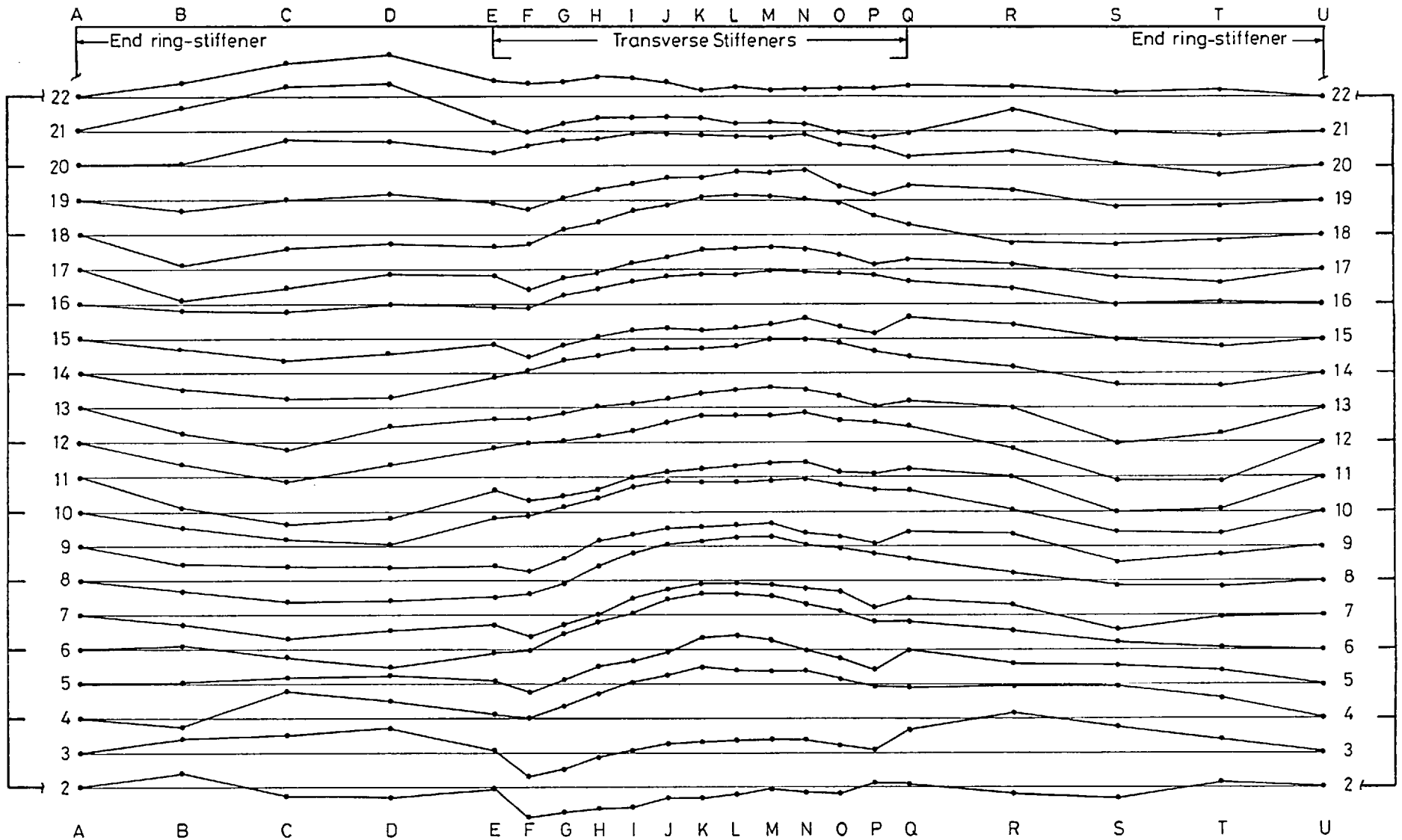

Note: Panels A-E and Q-U had additional stiffening (see fig. 2.75)

Fig. 2.76b
Model 10: Longitudinal Initial Deflection Profiles of Compression Flange

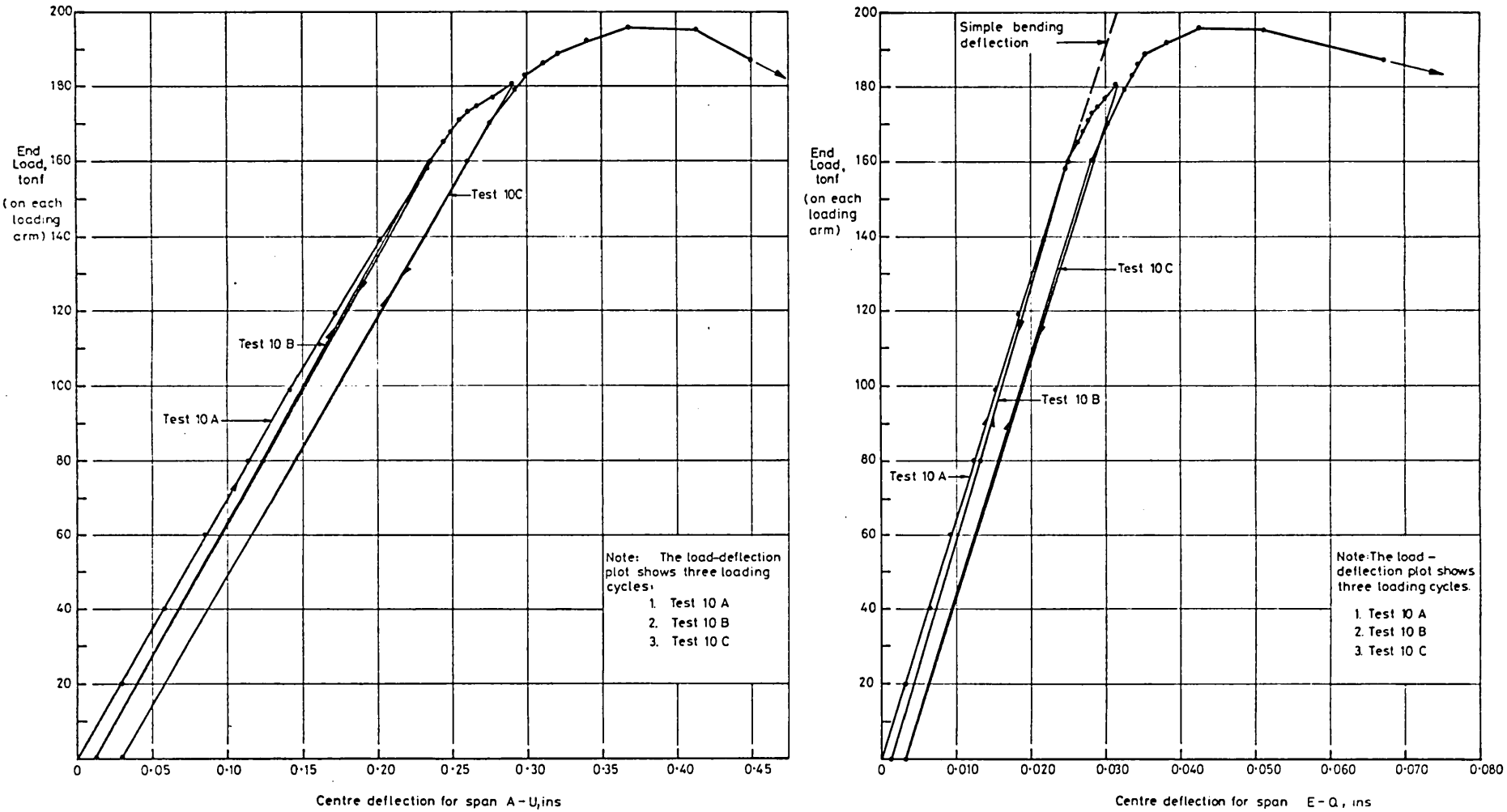

Fig. 2.77
Model 10: Load – Deflection Curves

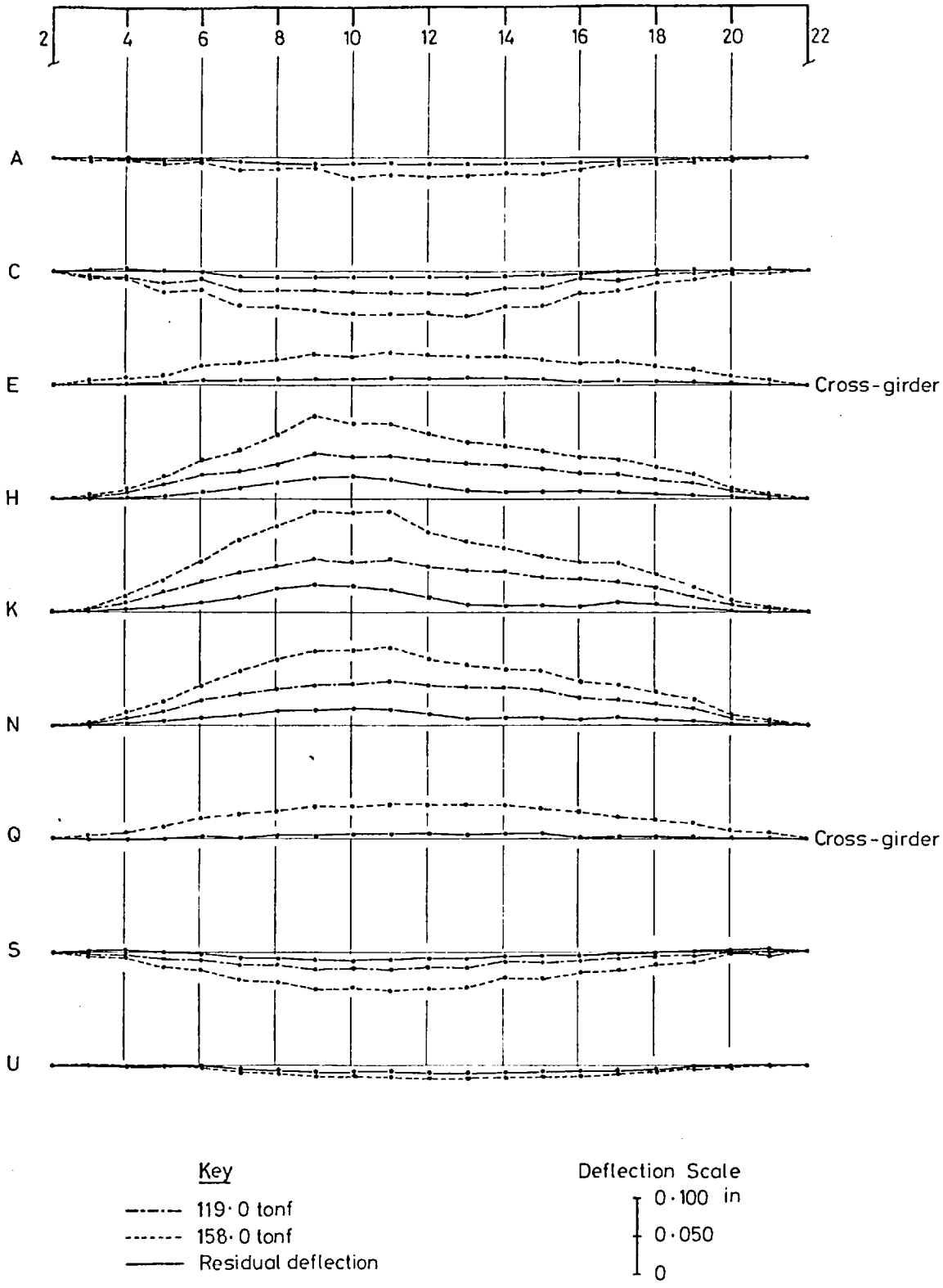

Fig. 2.78
Test 10 A: Relative Transverse Deflections of Compression Flange

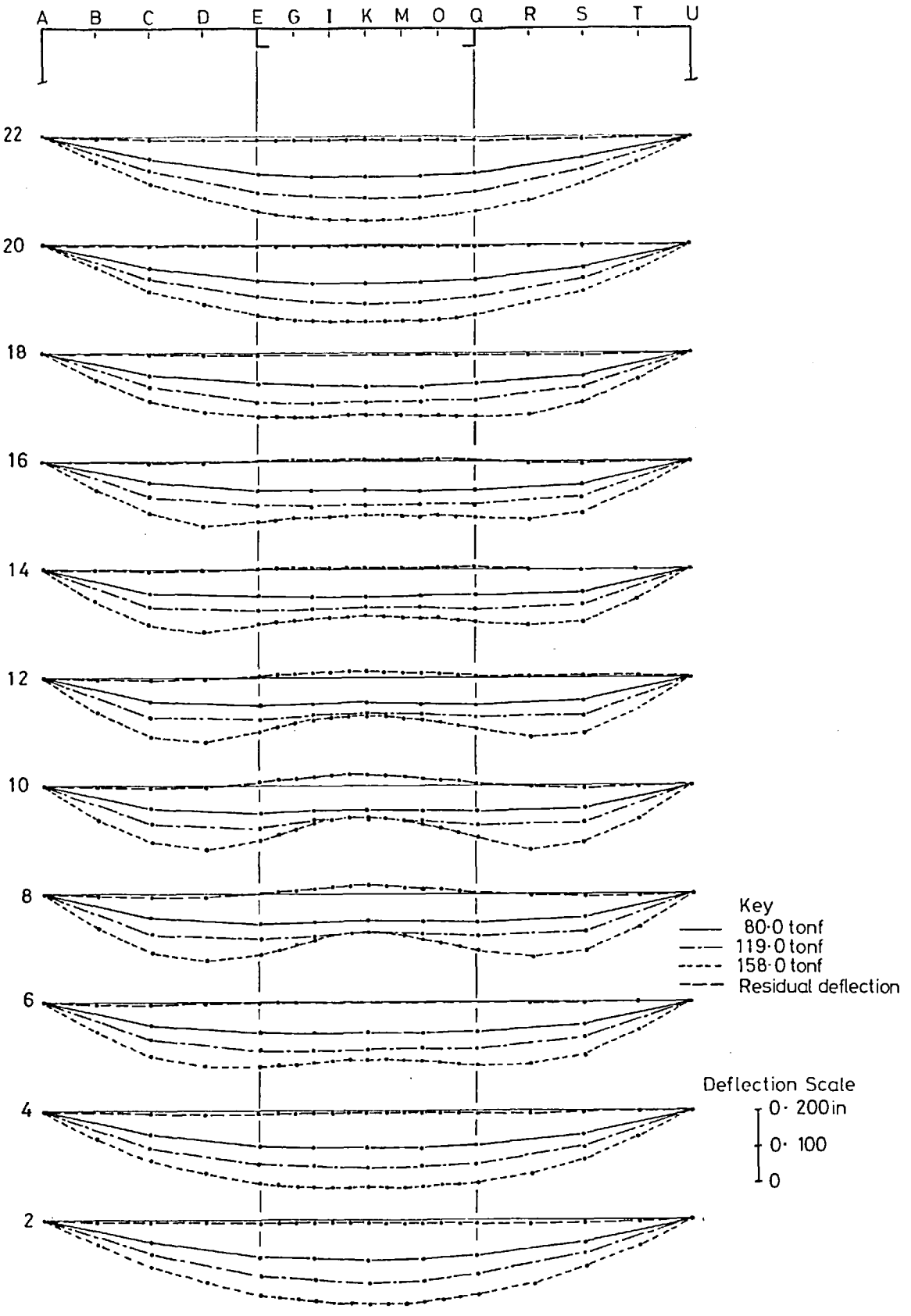

Fig. 2.79
Test 10 A: Relative Longitudinal Deflections of Compression Flange

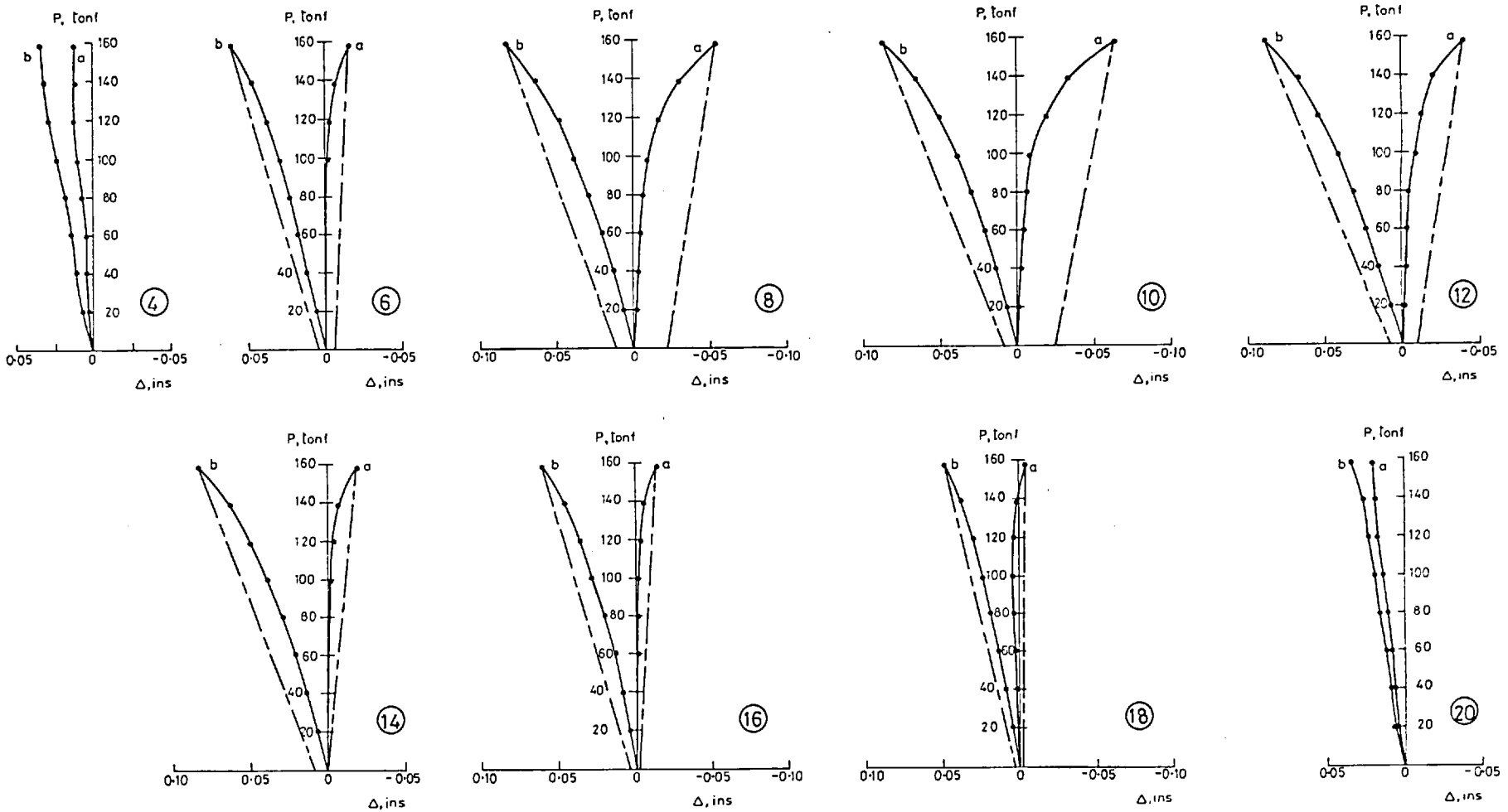

P Load on each loading arm
Δ Out-of-plane stiffener deflection within panel
Circled numbers indicate stiffener locations
Curve a. Deflections in panel E-Q
Curve b. Deflections in panel A-E
Positive deflections are inwards, towards stiffener outstands

Fig. 2.80a
Test 10A: Out-of-plane Deflections of Longitudinal Stiffeners

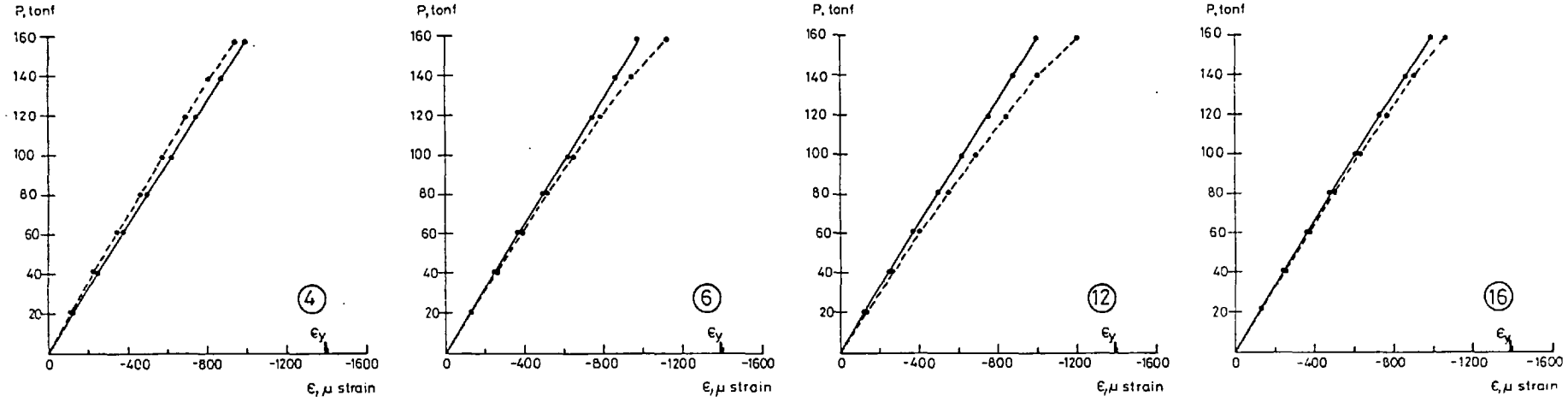

Fig. 2.80b
Test 10A: Strain in Longitudinal Stiffeners

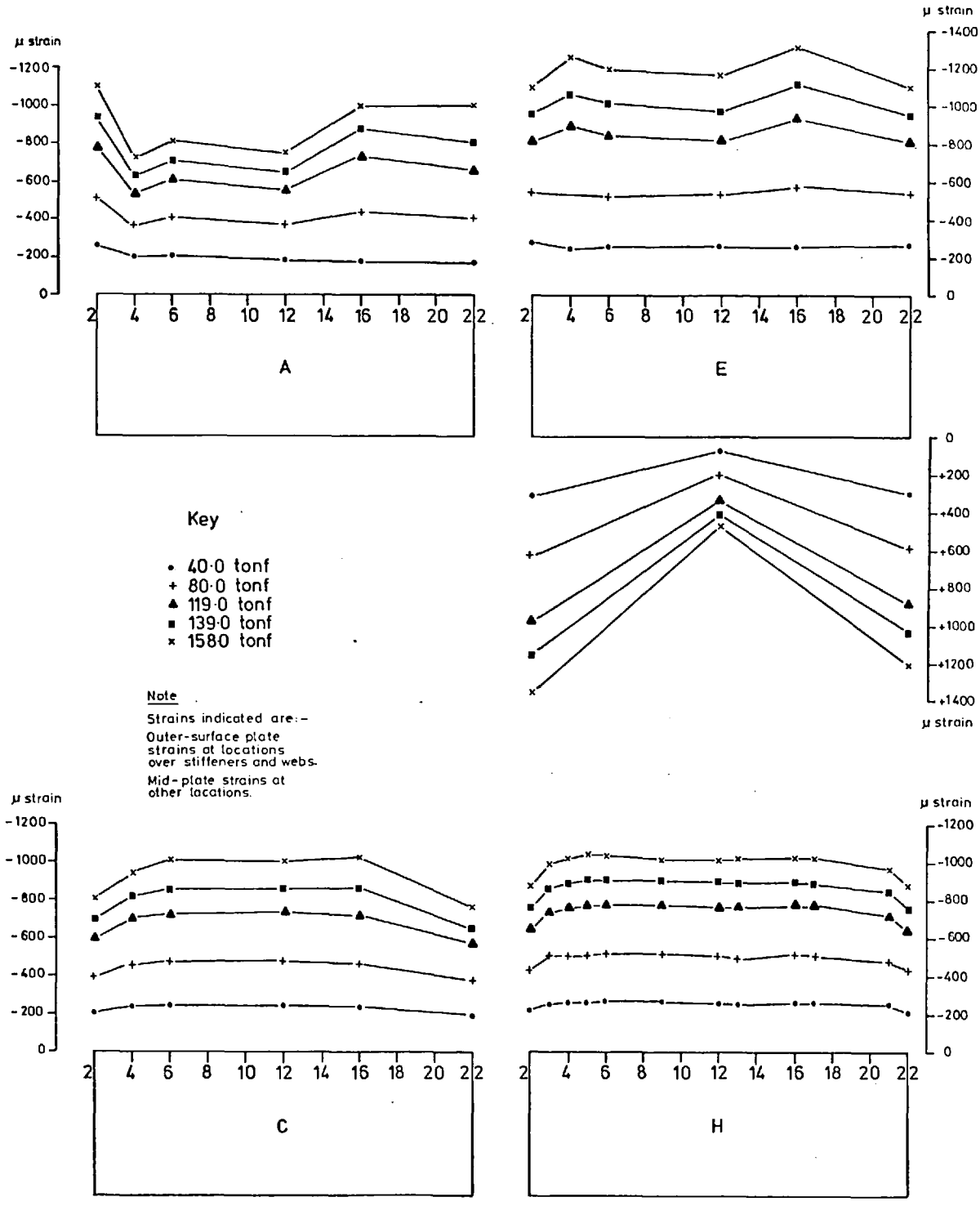

Fig. 2.81a
Test 10 A: Longitudinal Strain at Cross-sections Indicated

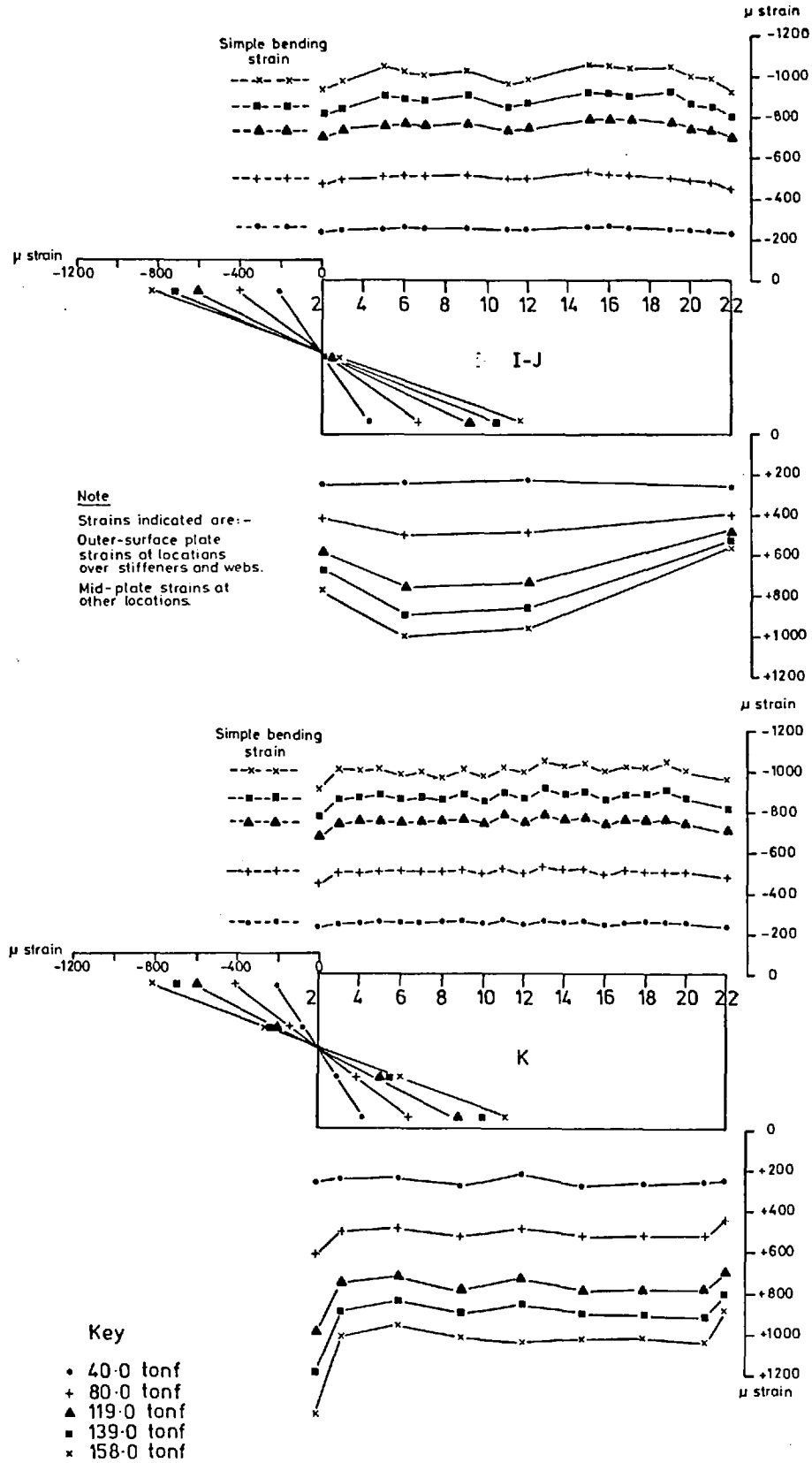

Fig. 2.81b
Test 10 A: Longitudinal Strain at Cross-sections I-J and K

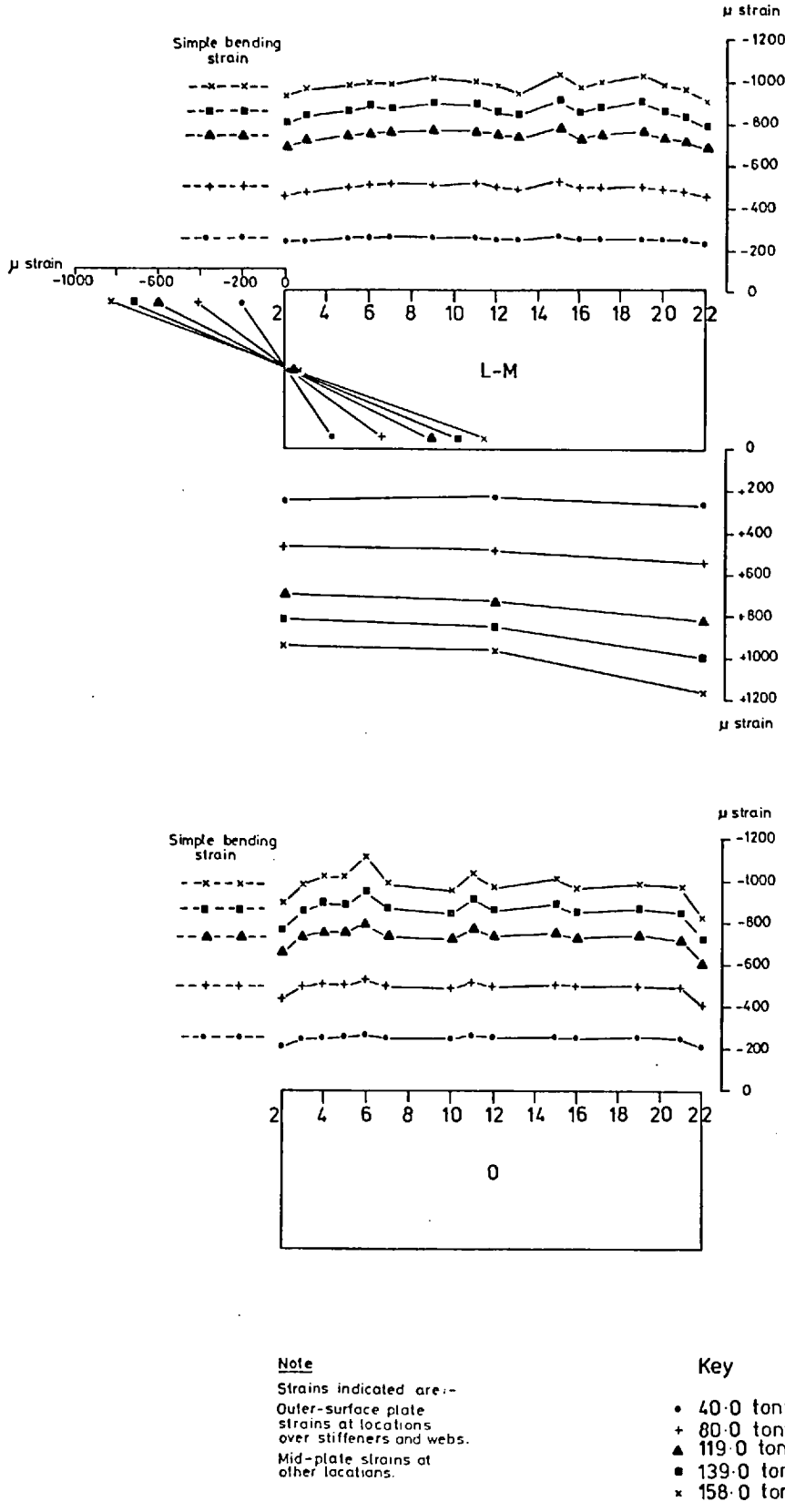

Note

Strains indicated are:-

Outer-surface plate strains at locations over stiffeners and webs.

Mid-plate strains at other locations.

Key

- 40·0 tonf
+ 80·0 tonf
▲ 119·0 tonf
■ 139·0 tonf
× 158·0 tonf

Fig. 2.81c
Test 10 A: Longitudinal Strain at Cross-sections L-M and 0

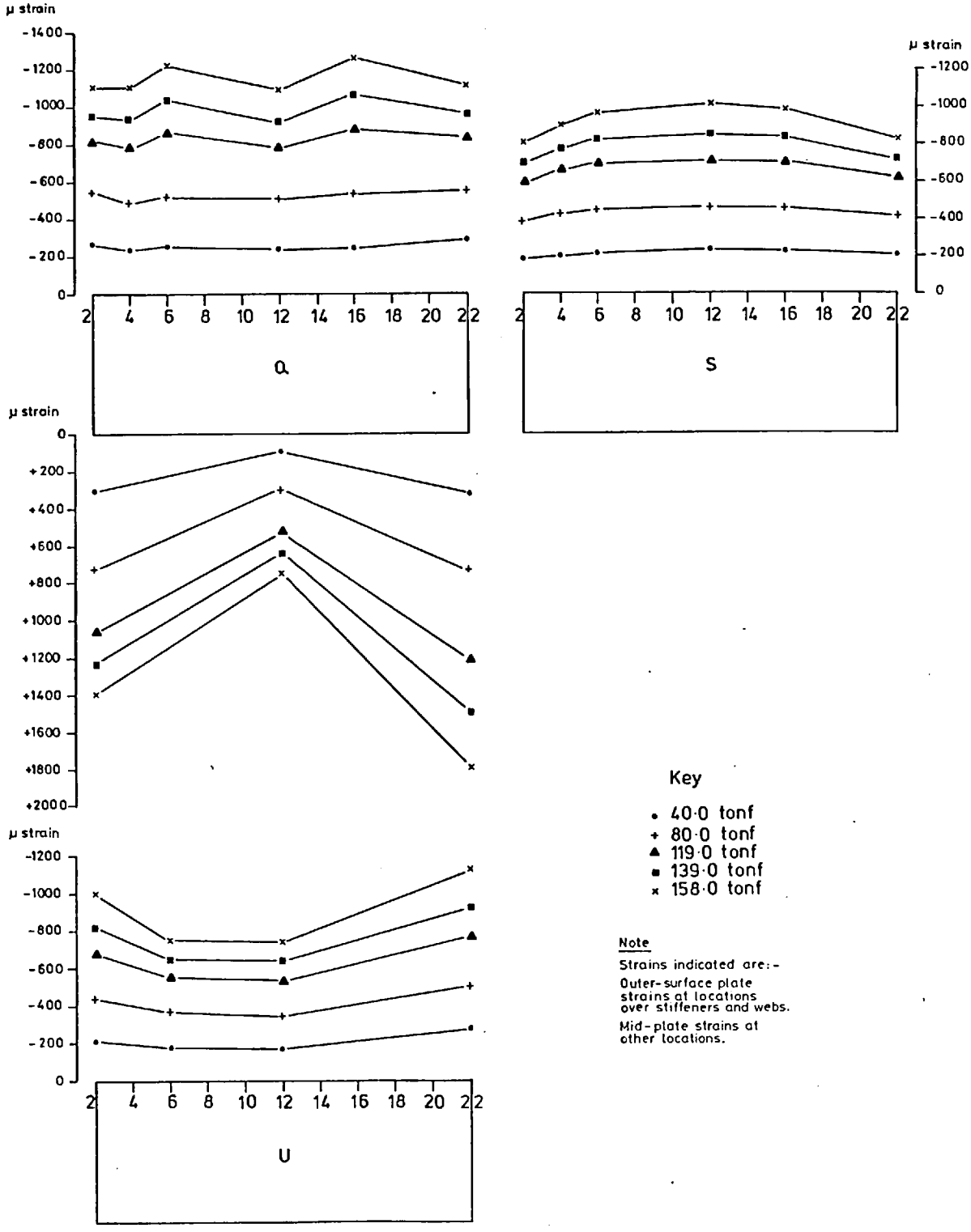

Fig. 2.81d
Test 10 A : Longitudinal Strain at Cross-sections Indicated

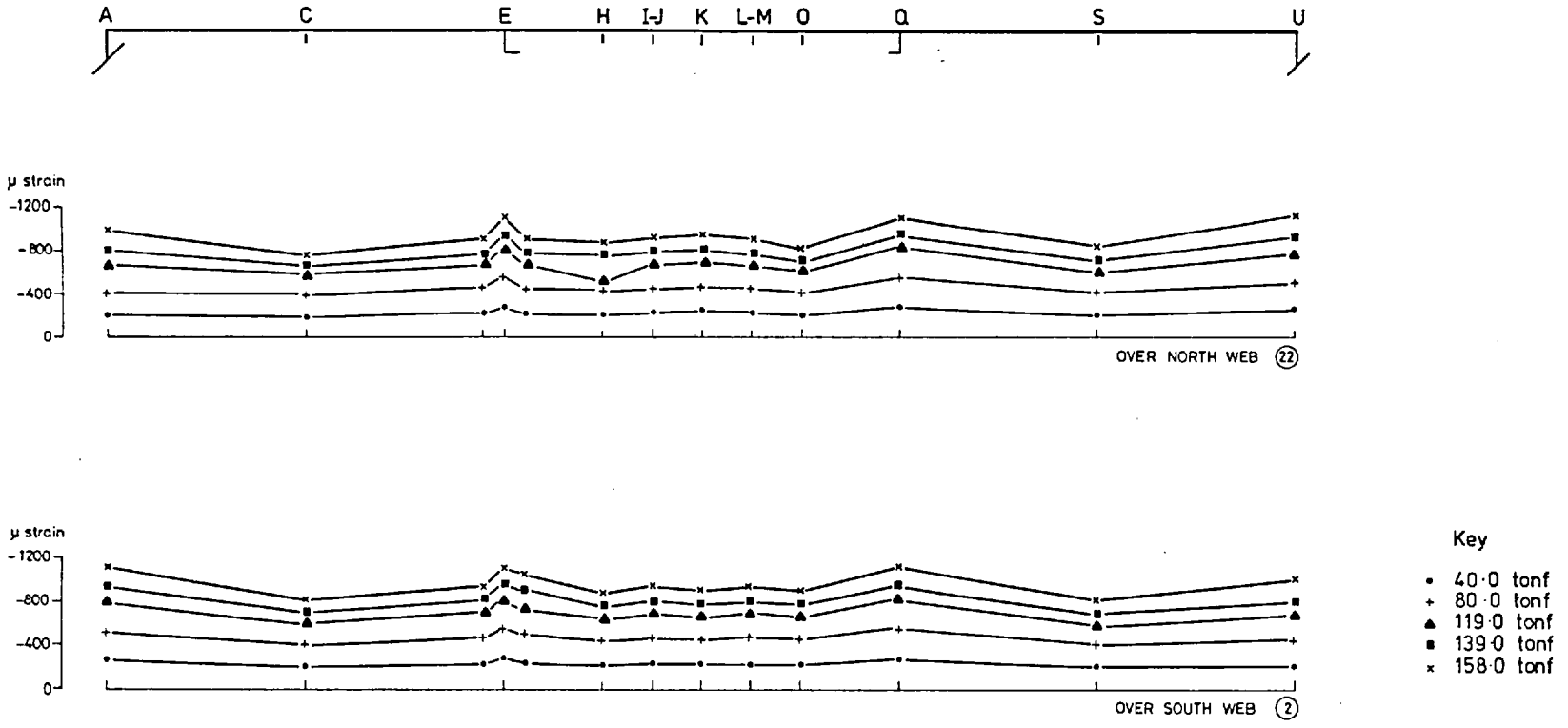

Fig. 2.82a
Test 10A: Longitudinal Strain in Compression Flange at its Junctions with Webs

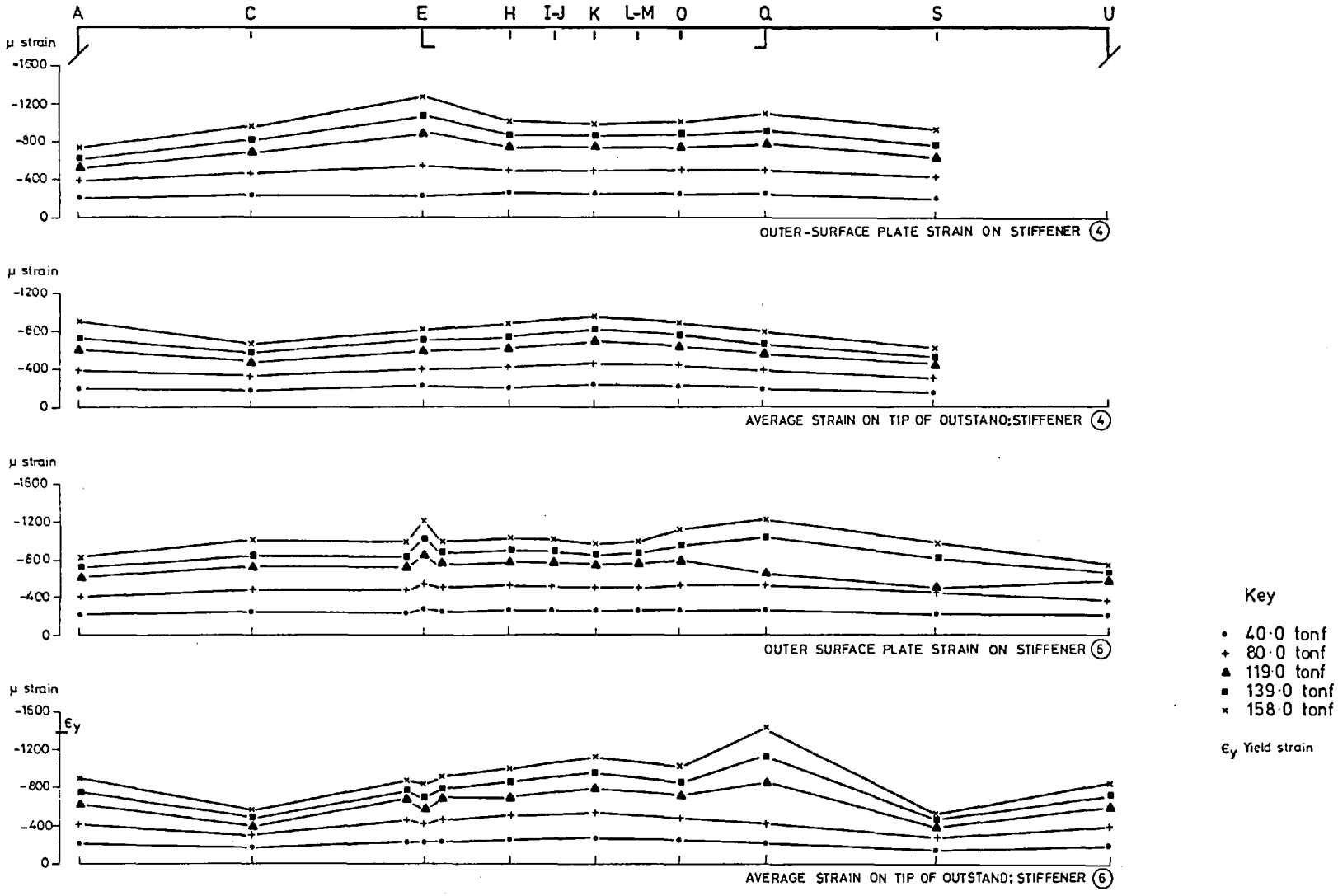

Fig. 2.82b
Test 10 A: Strain in Stiffeners ④ and ⑥

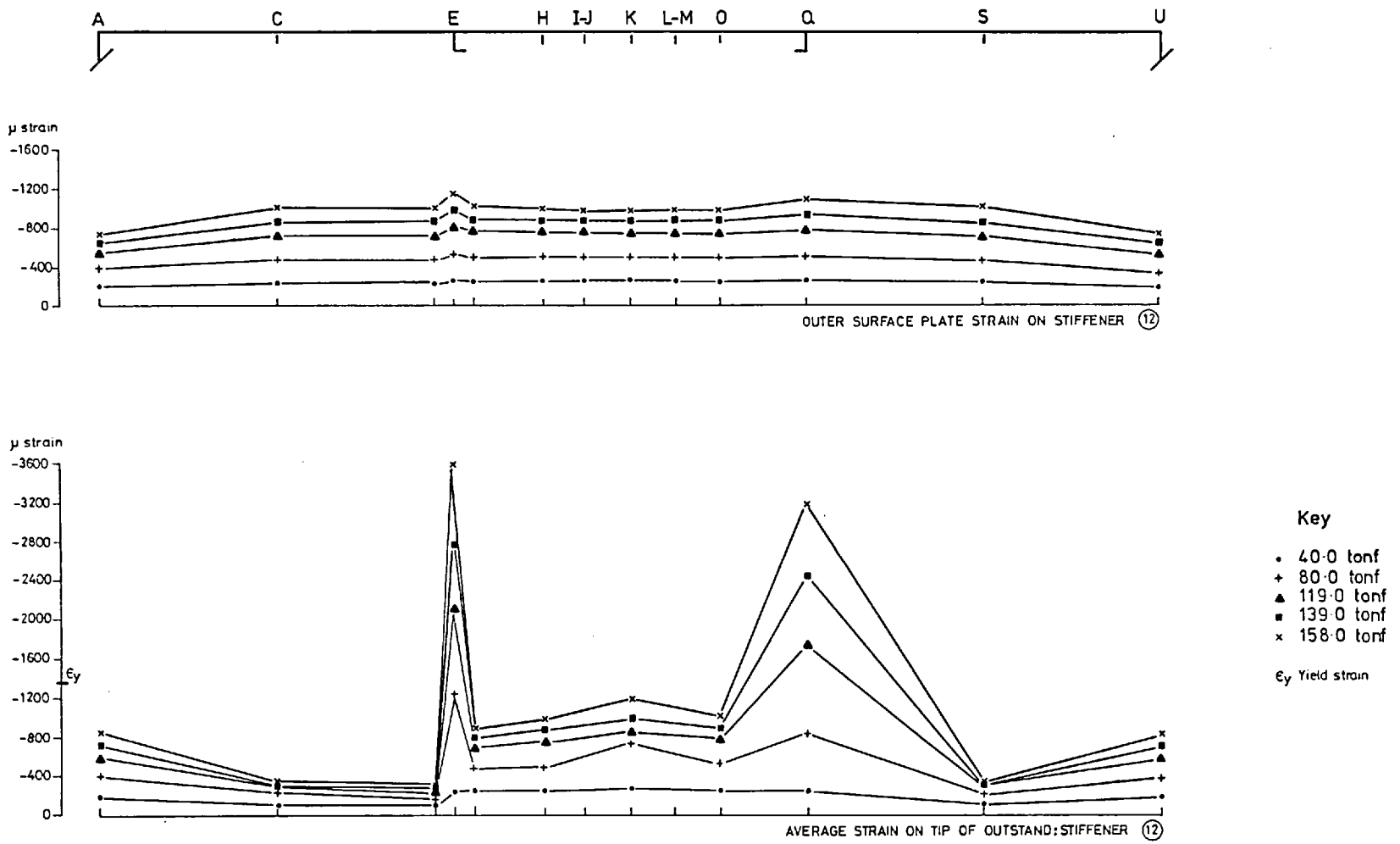

Fig. 2.82c
Test 10A: Strain in Stiffener (12)

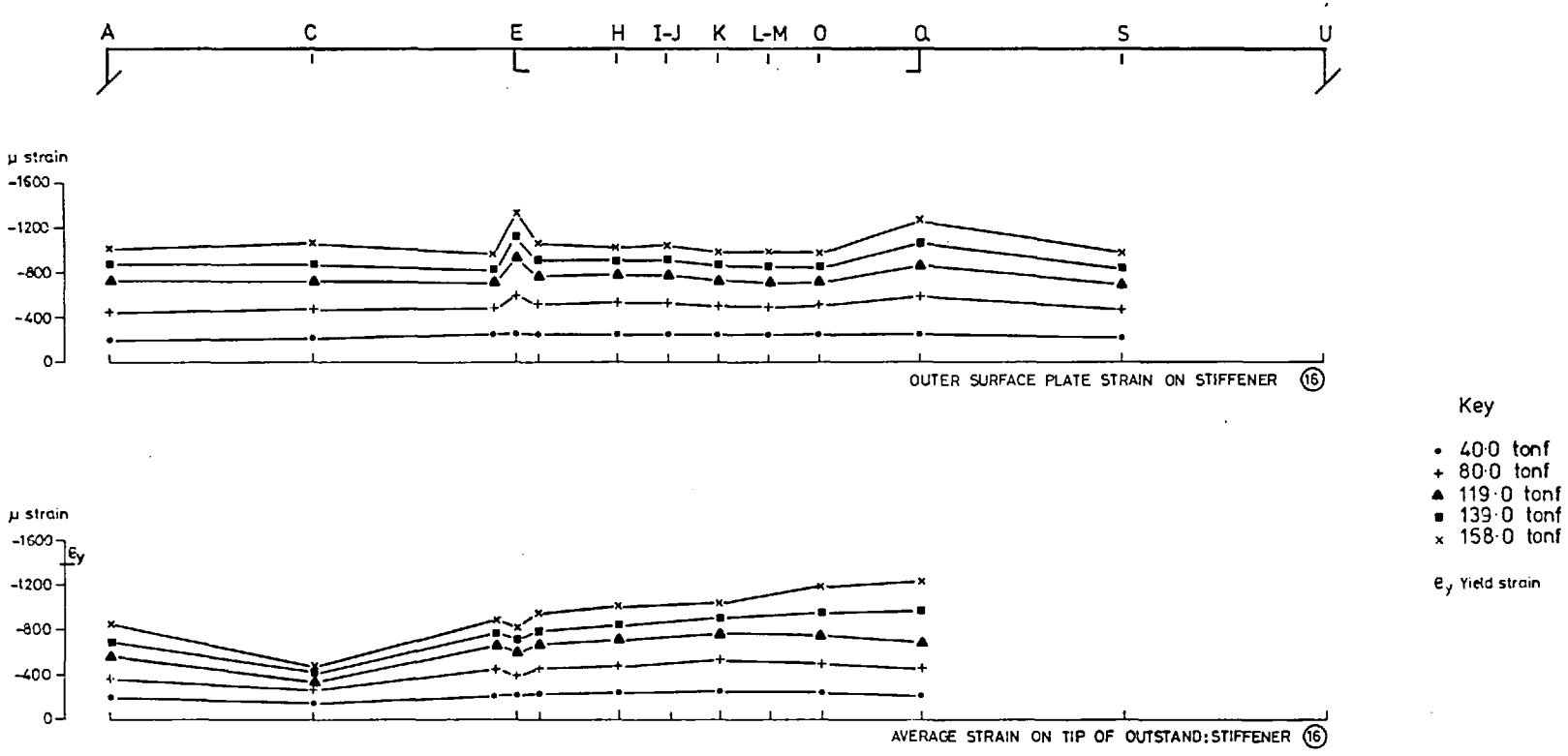

Fig. 2.82d
Test 10A: Strain in Stiffener (16)

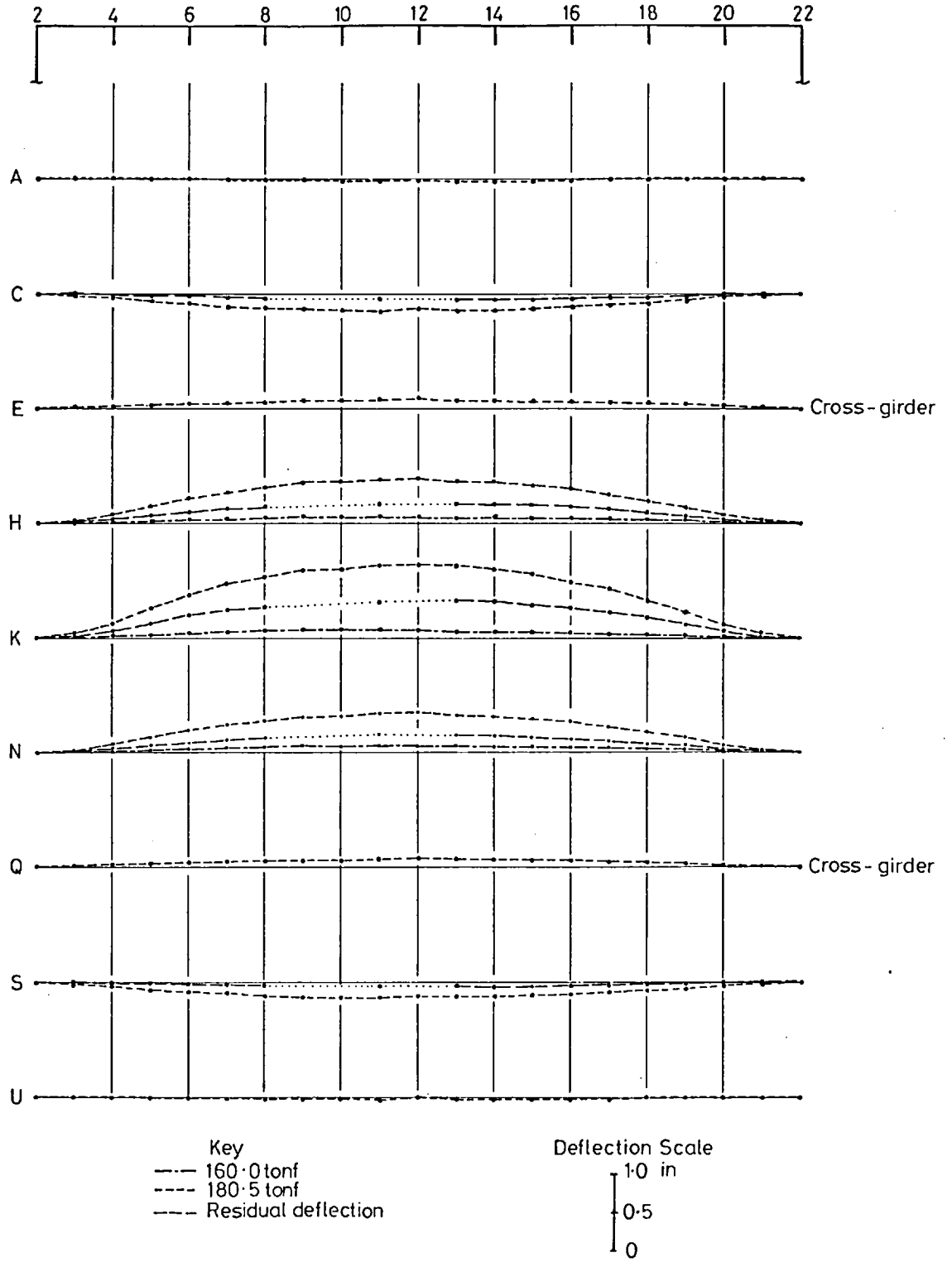

Fig. 2.83
Test 10 B: Relative Transverse Deflections of Compression Flange

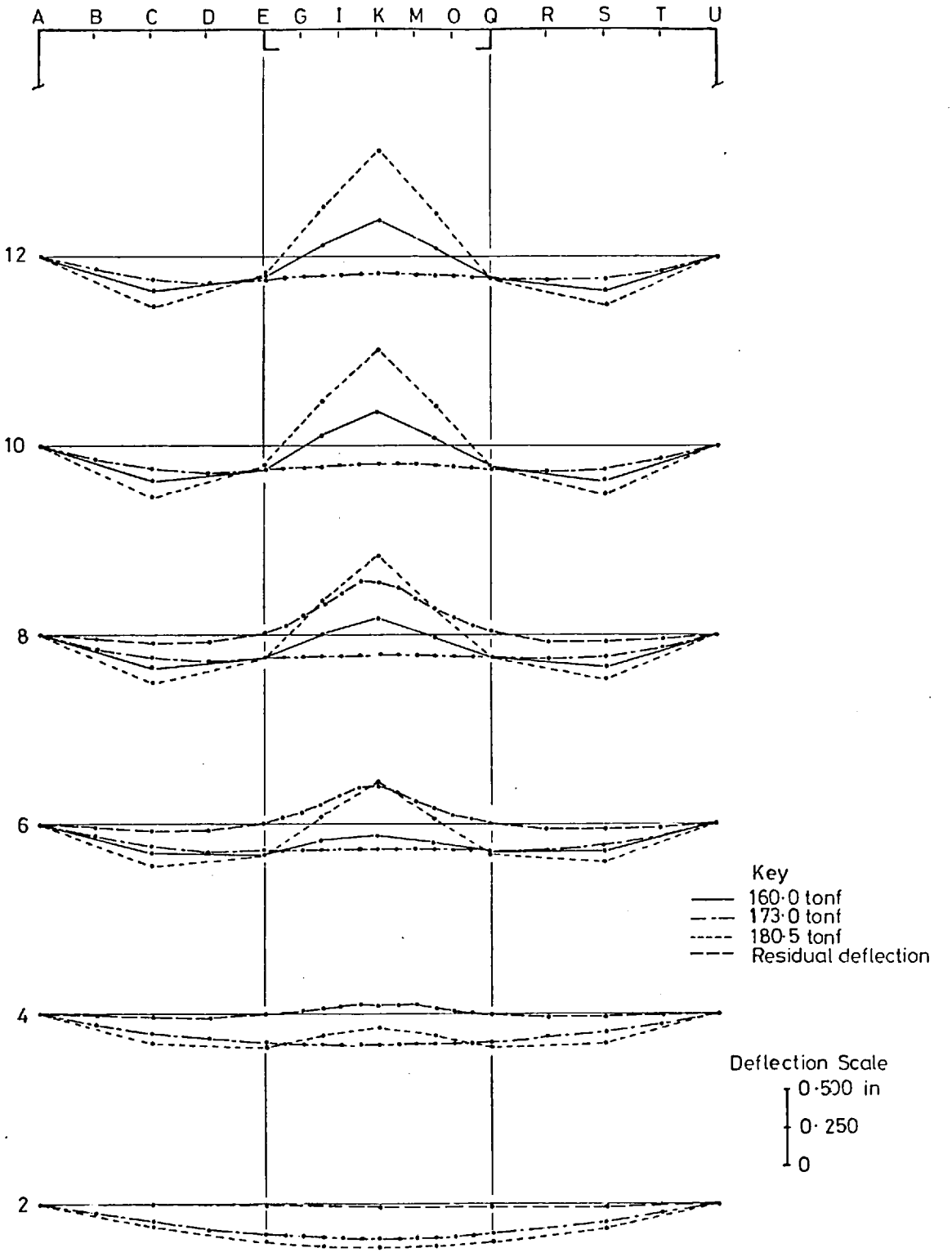

Fig. 2.84a
Test 10 B: Relative Longitudinal Deflections of Compression Flange

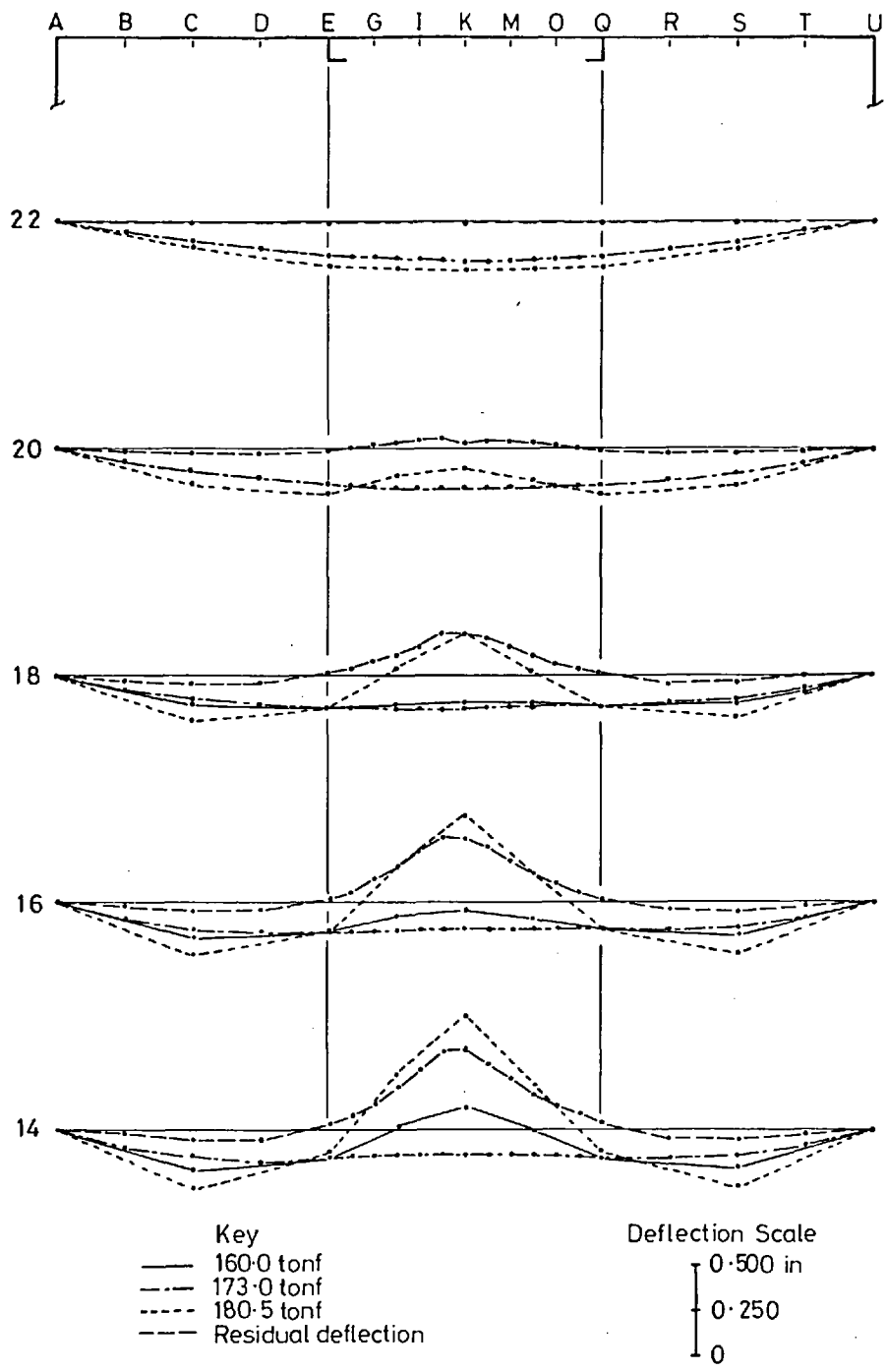

Fig. 2.84b
Test 10 B: Relative Longitudinal Deflections of Compression Flange

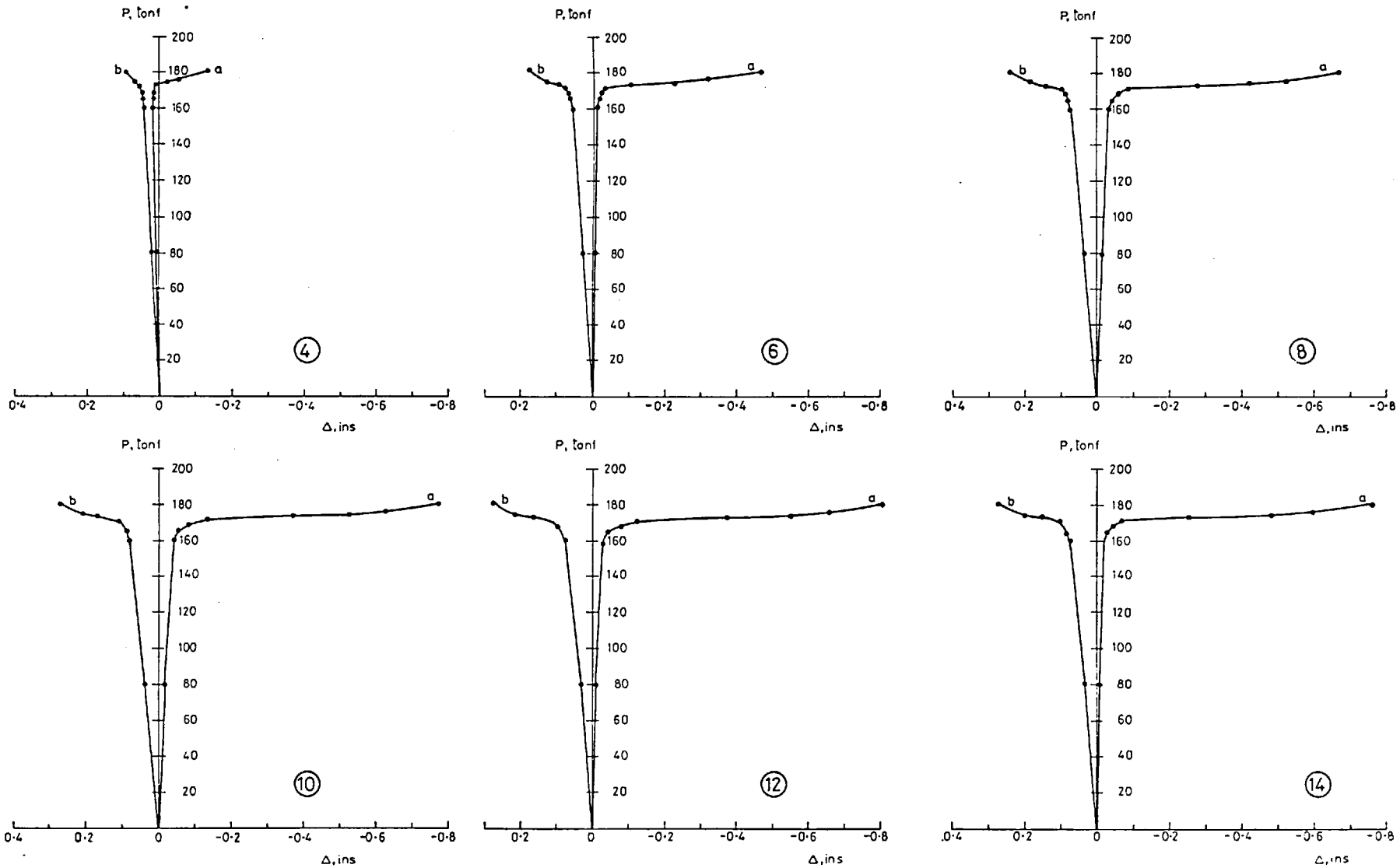

(For notion, see fig 23b)

Fig. 2.85a
Test 10 B: Out-of-plane Deflections of Longitudinal Stiffeners

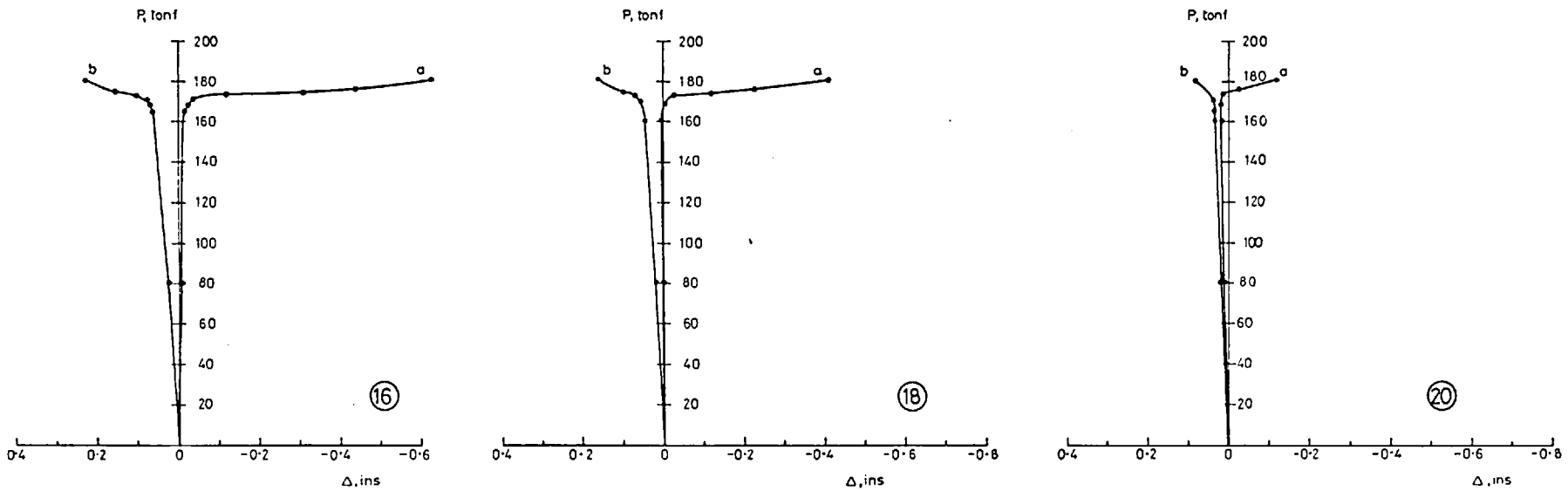

P Load on each loading arm
Δ Out-of-plane stiffener deflection within panel
Circled numbers indicate stiffener locations
Curve a. Deflections in panel E-Q
Curve b. Deflections in panel A-E
Positive deflections are inwards, towards stiffener outstands

Fig. 2.85b
Test 10 B: Out-of-plane Deflections of Longitudinal Stiffeners

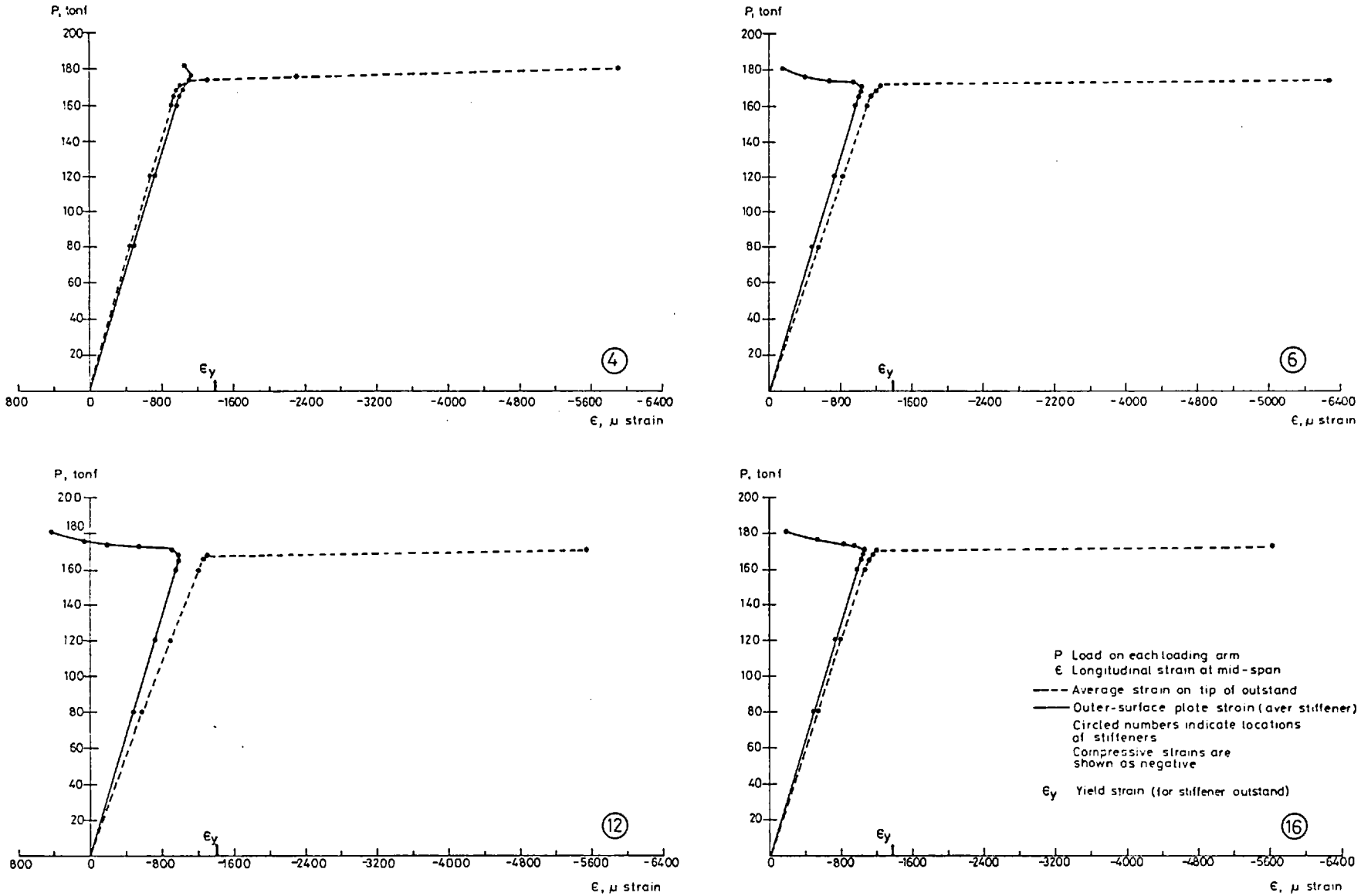

Fig. 2.86
Test 10 B: Strain in Longitudinal Stiffeners

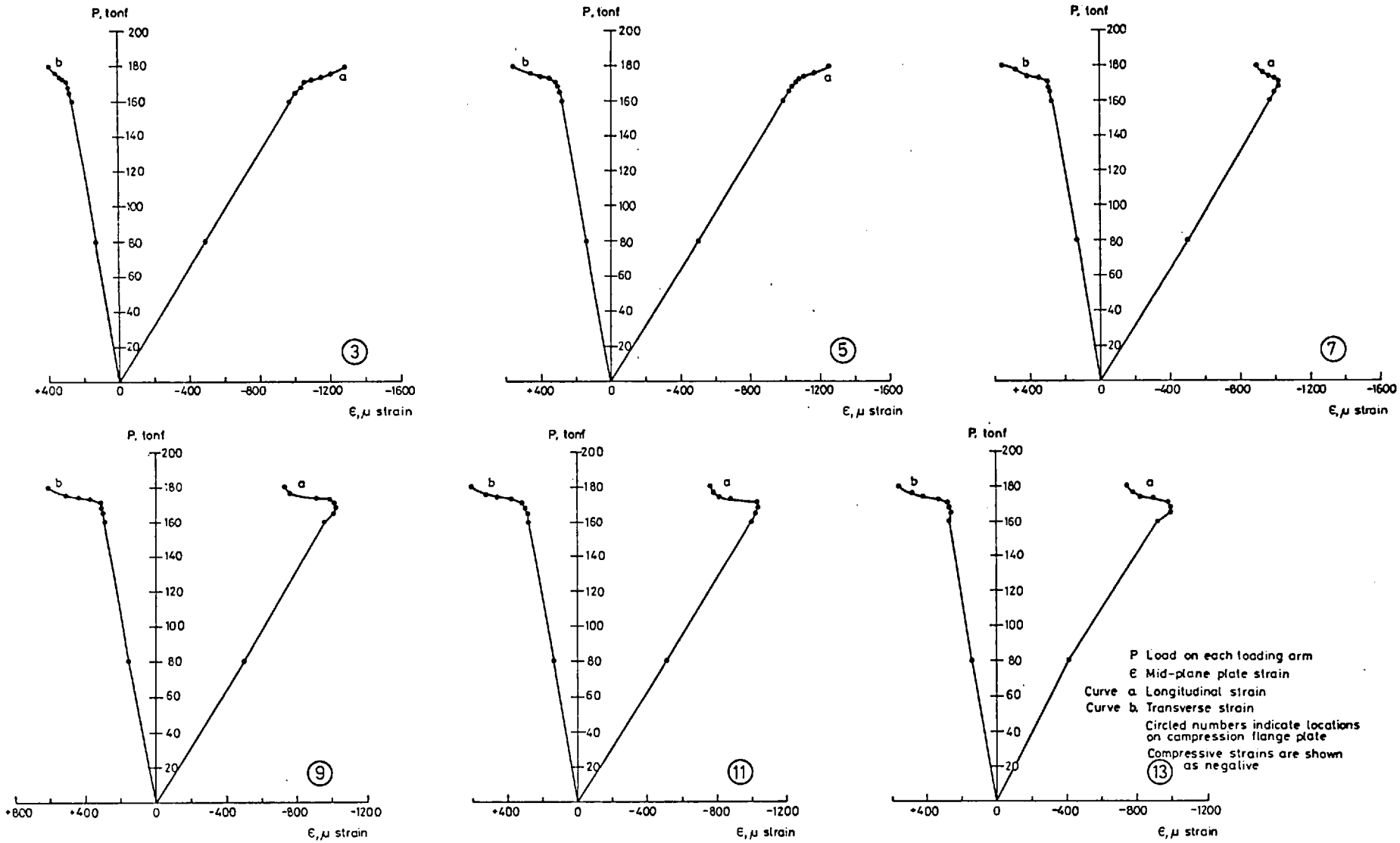

Fig. 2.87
Test 10B: Longitudinal and Transverse Mid-plate Strains at Mid-span

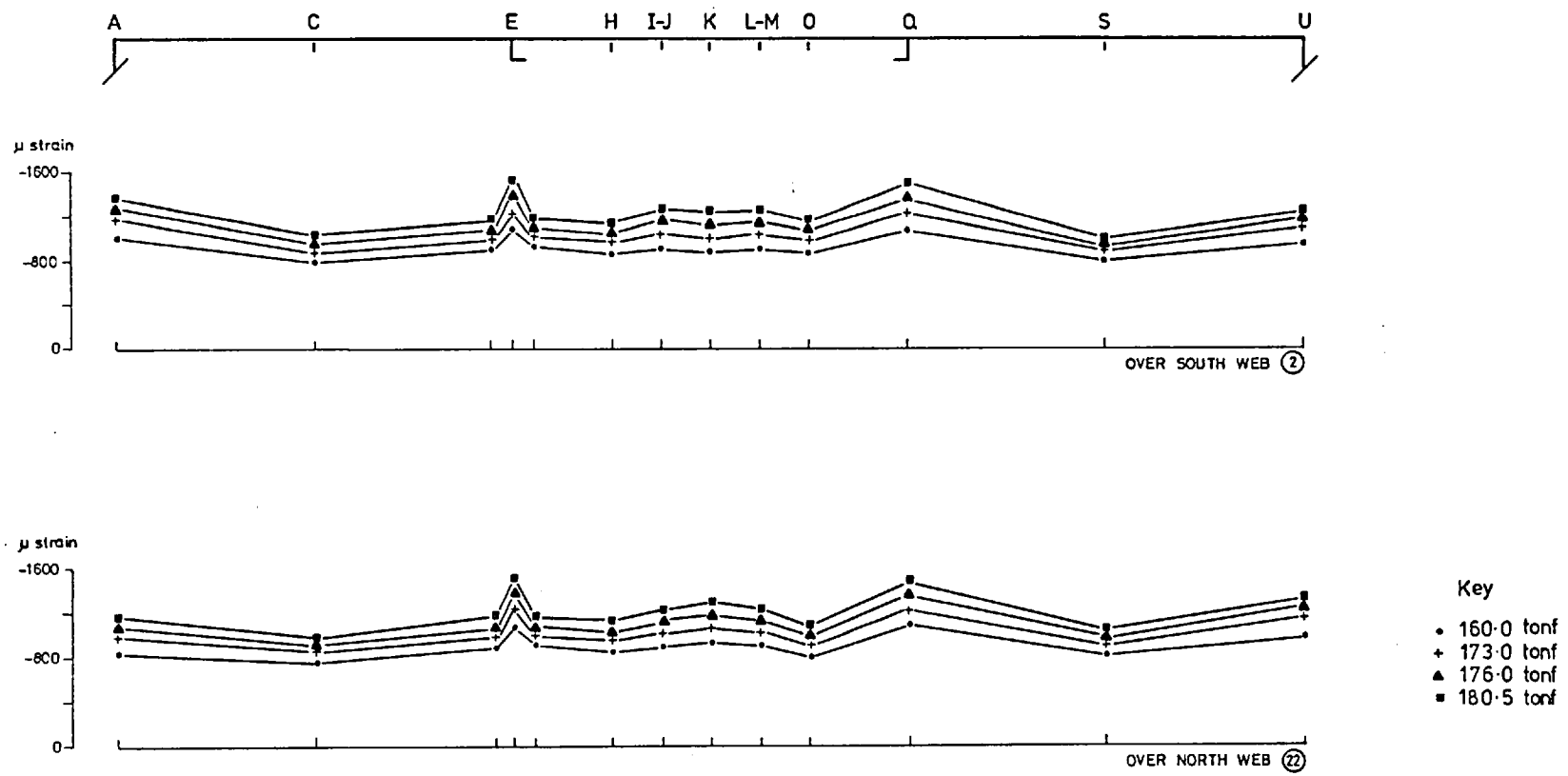

Fig. 2.88a
Test 10B: Longitudinal Strain in Compression Flange at its Junctions with Webs

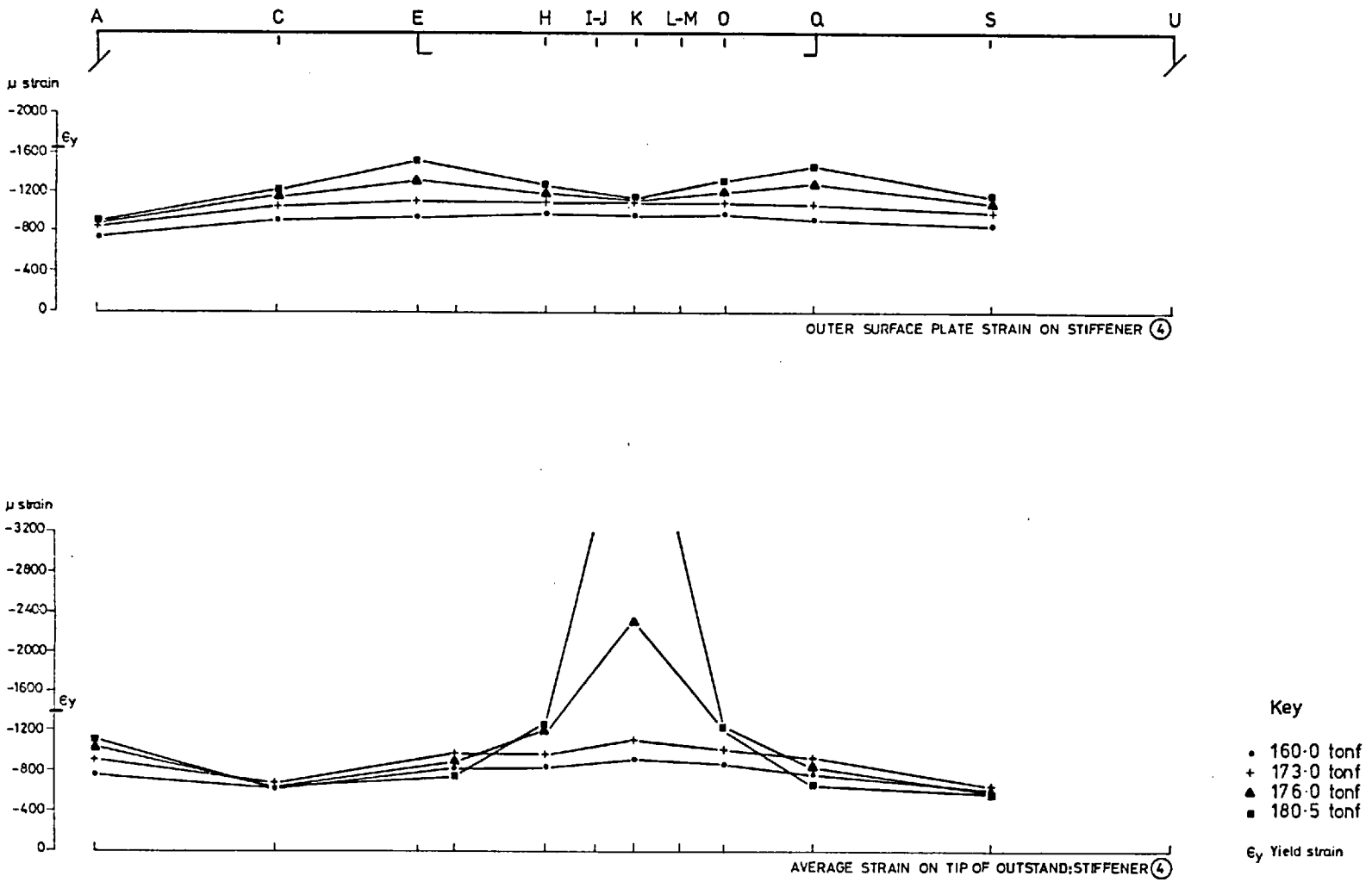

Fig. 2.88b
Test 10 B : Strain in Stiffener (4)

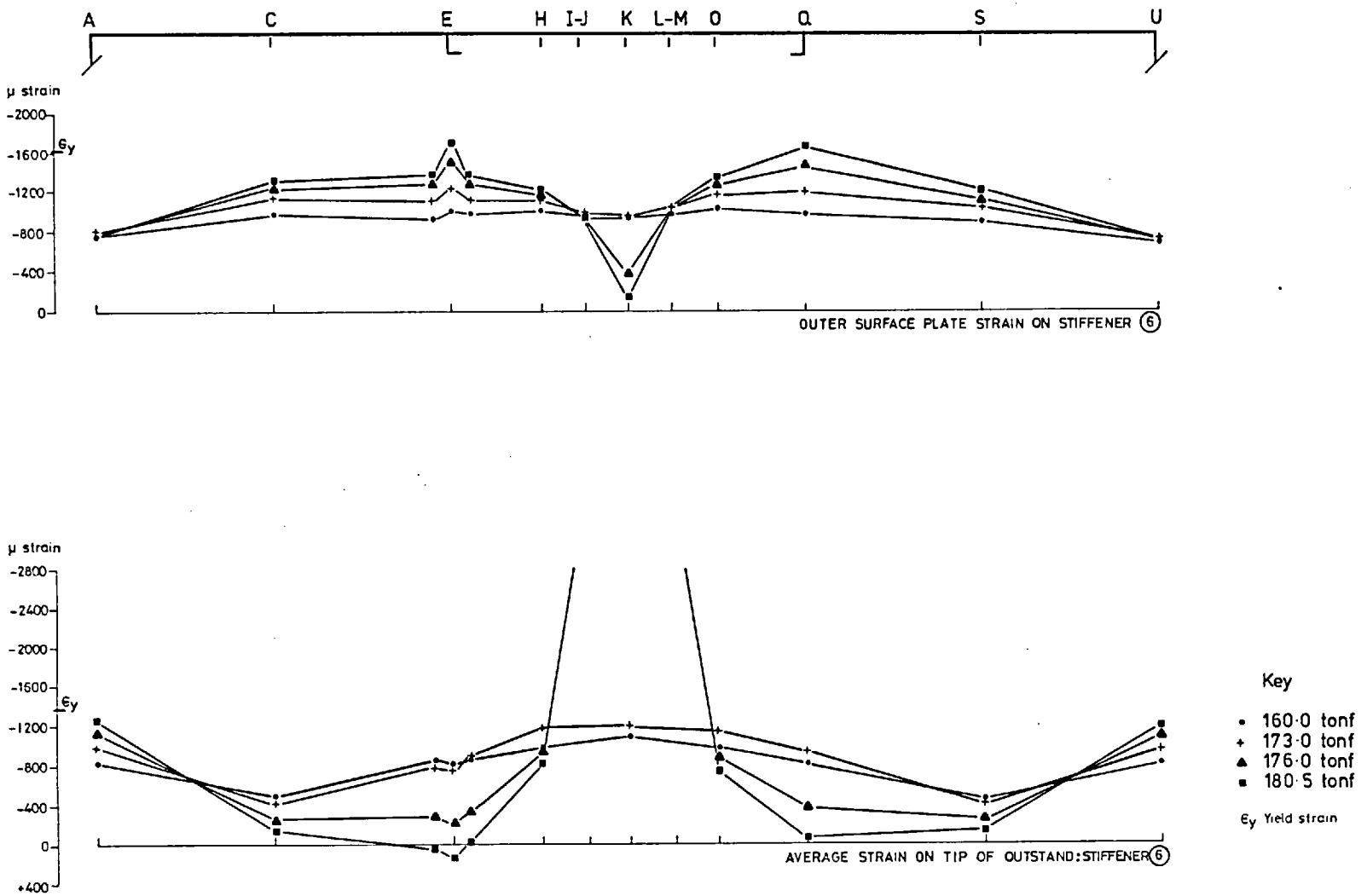

Fig. 2.88c
Test 10B: Strain in Stiffener ⑥

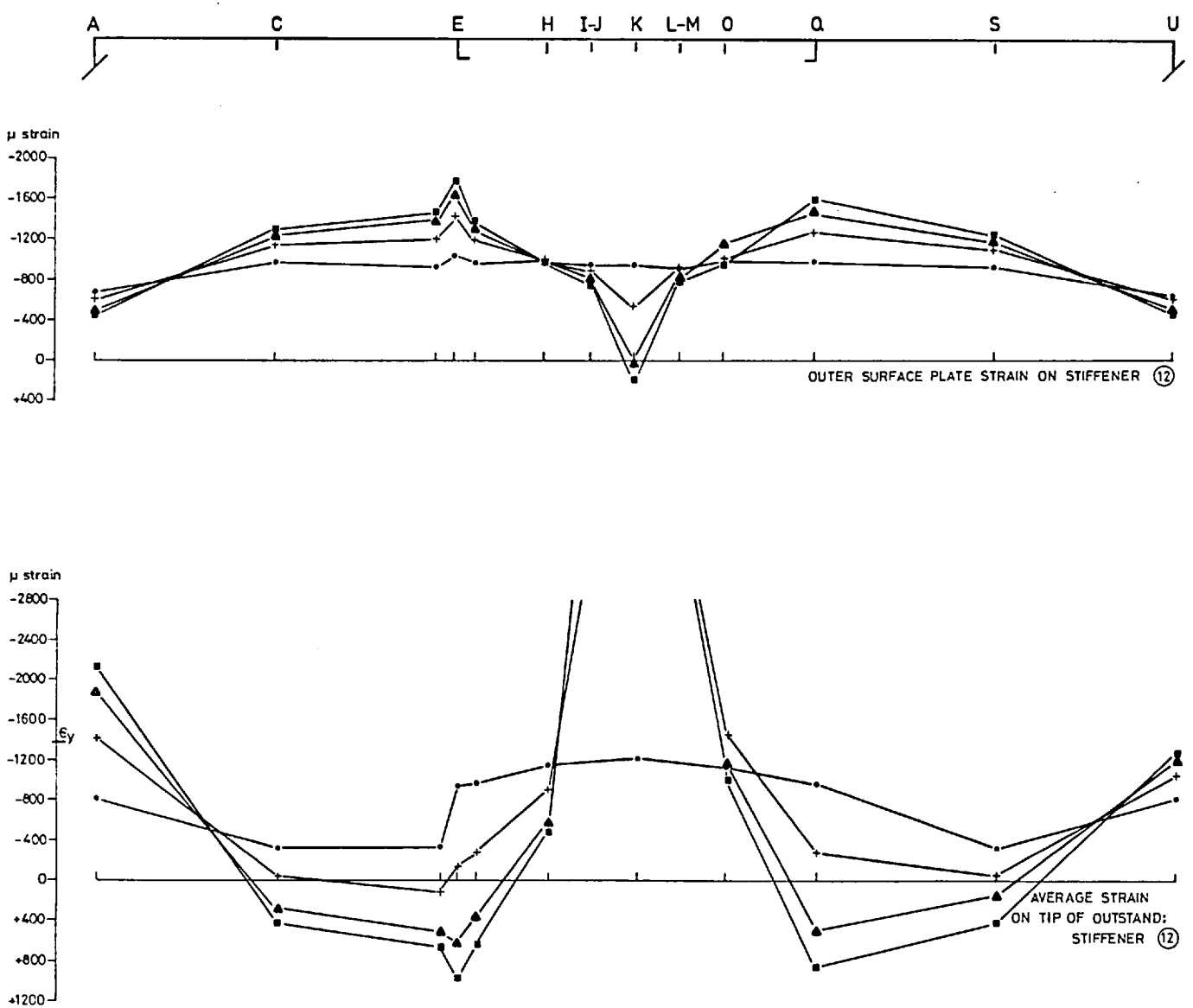

Fig. 2.88d
Test 10 B : Strain in Stiffener (12)

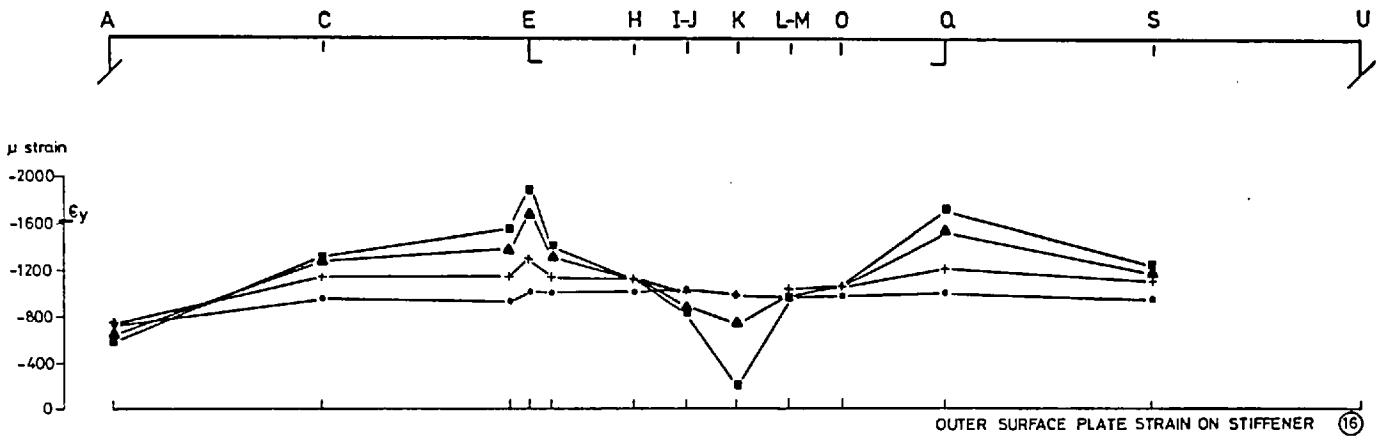

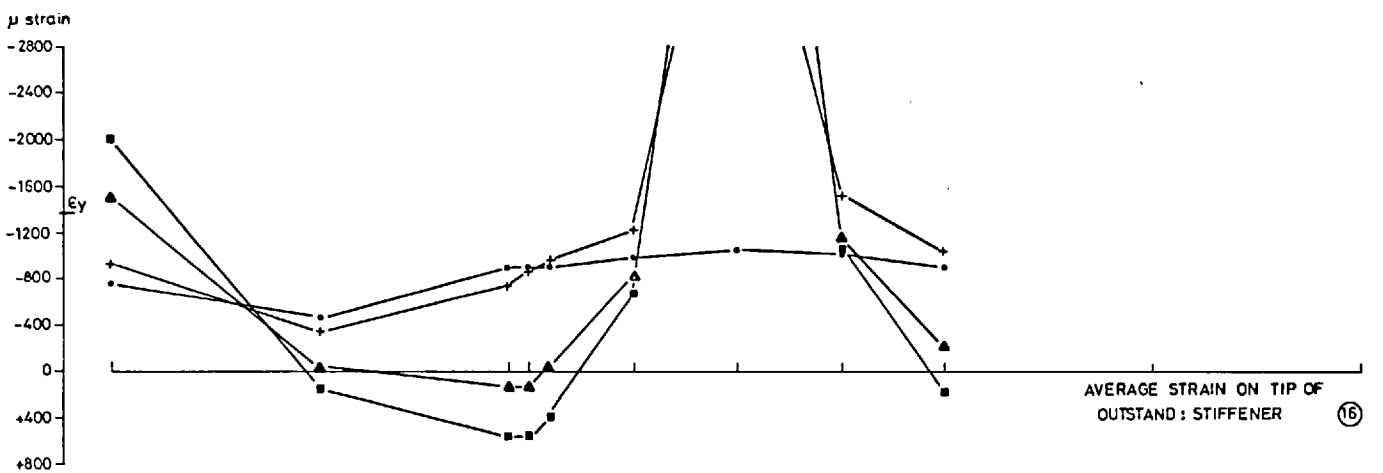

Key

- 160·0 tonf
+ 173·0 tonf
▲ 176·0 tonf
■ 180·5 tonf

εy Yield strain

Fig. 2.88e
Test 10B: Strain in Stiffener (16)

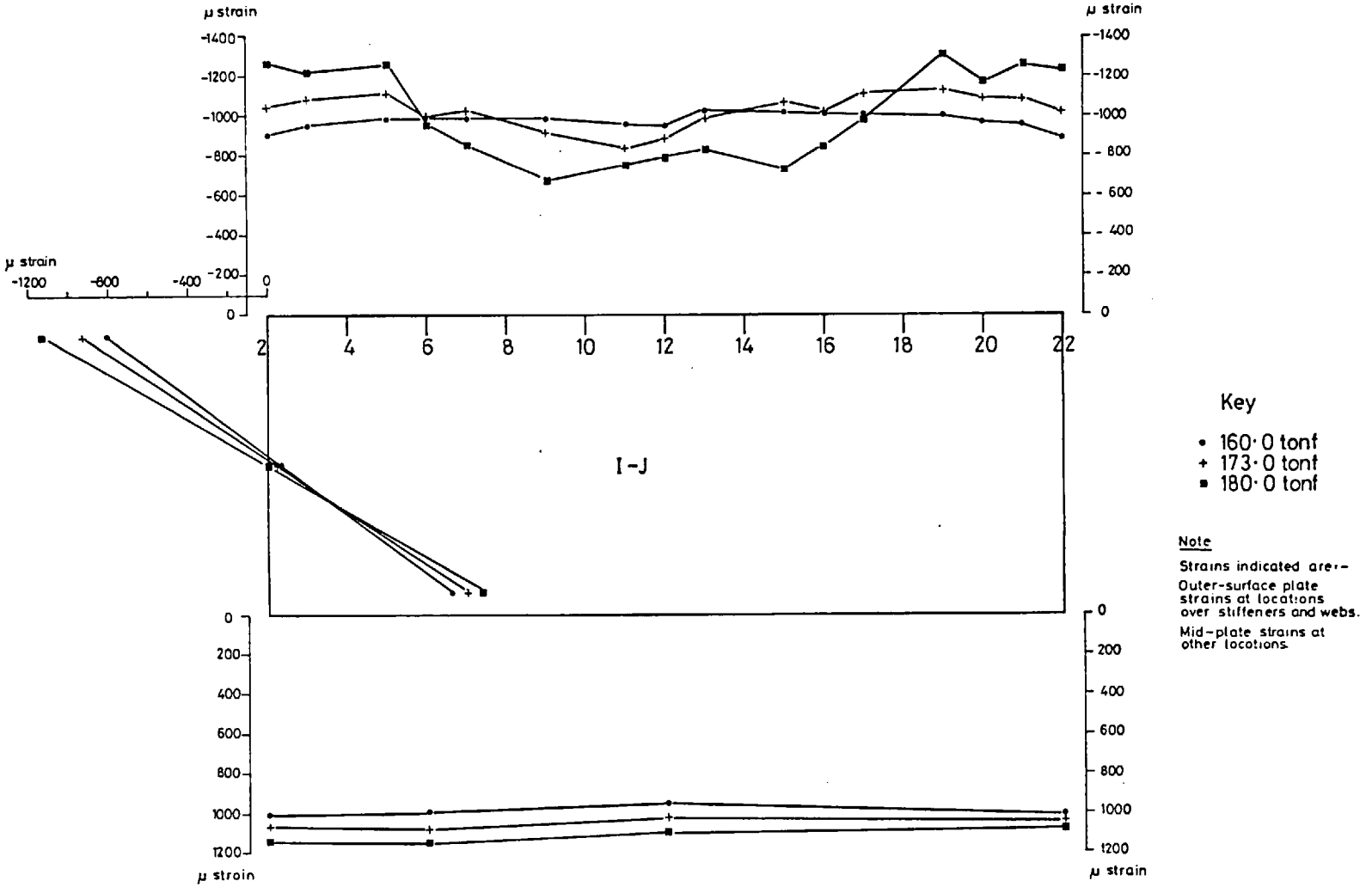

Fig. 2.89a
Test 10 B: Longitudinal Strain at Cross-section I-J
($7\frac{3}{4}$ in from mid-span)

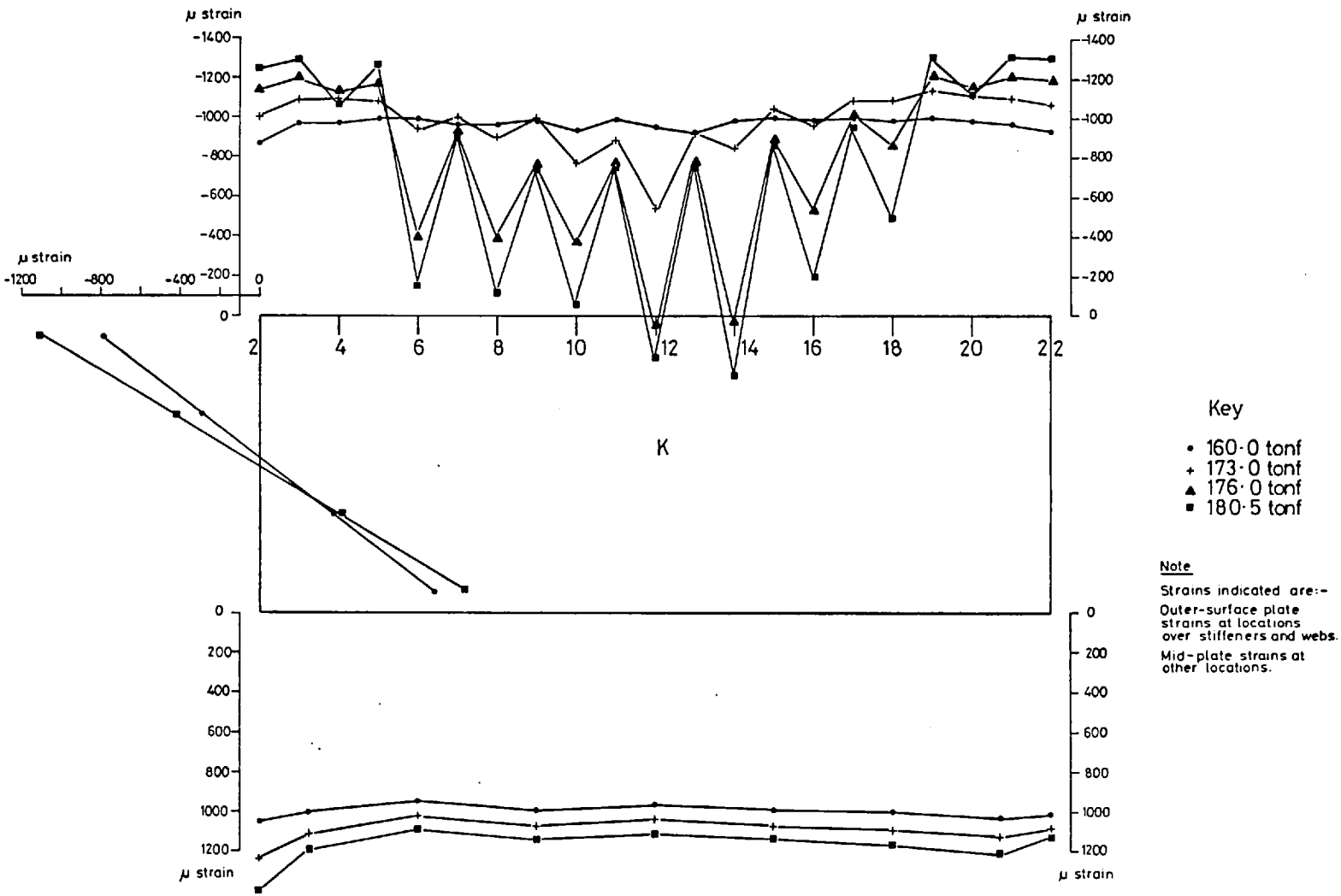

Fig. 2.89b
Test 10B: Longitudinal Strain at Mid-span

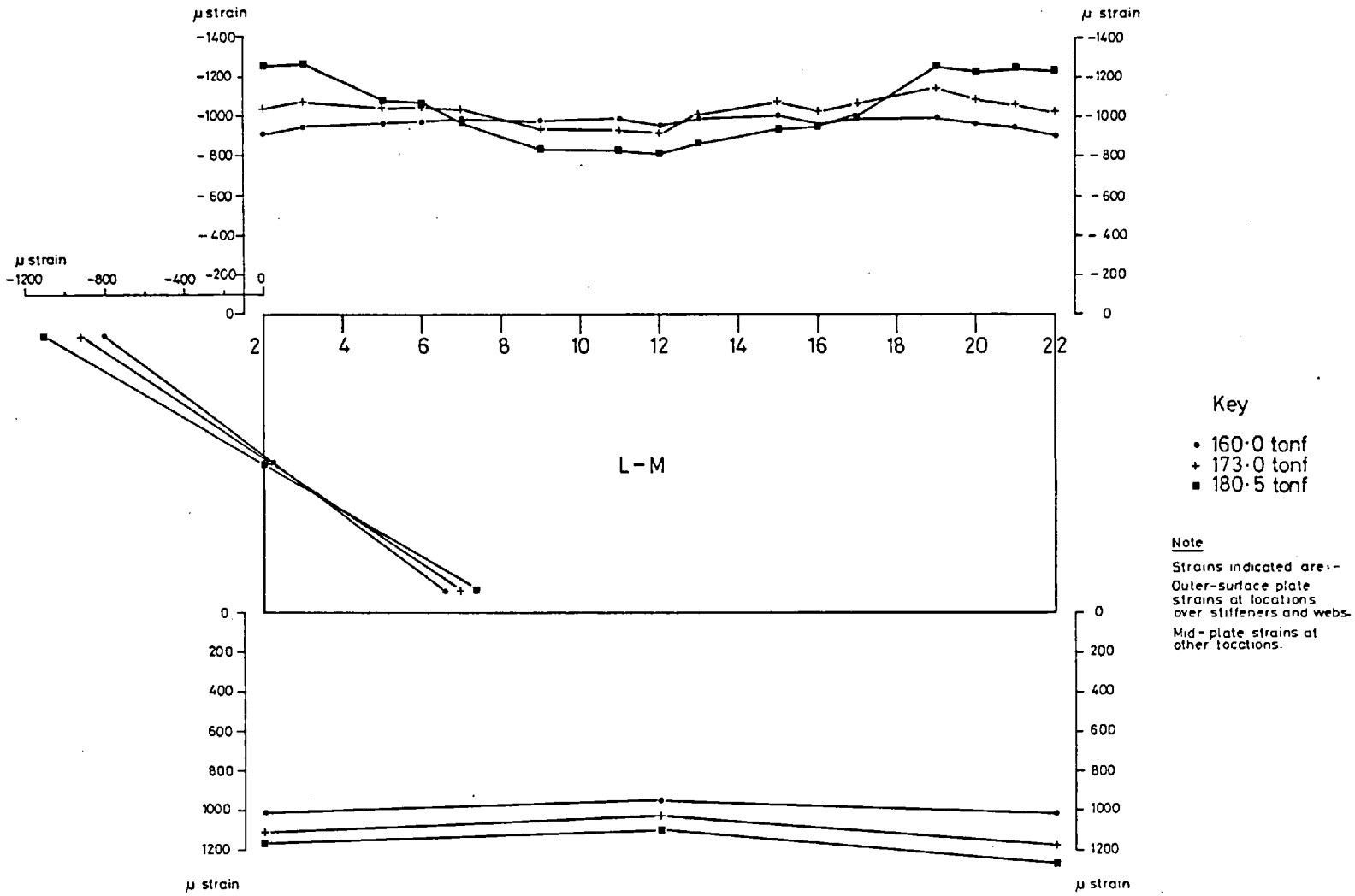

Fig. 2.89c
Test 10B: Longitudinal Strain at Cross-section L-M
($7\frac{3}{4}$ in from mid-span)

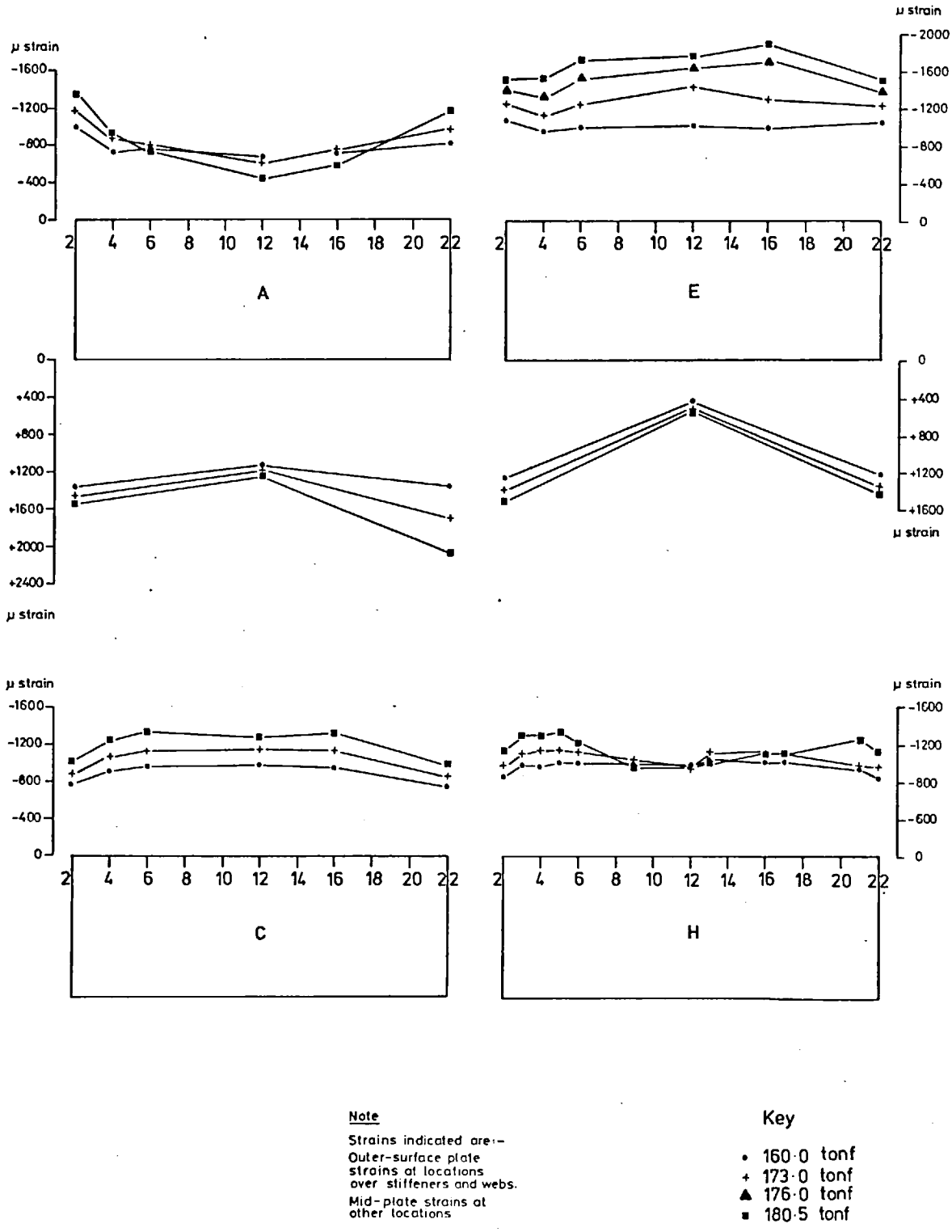

Fig. 2.89d
Test 10 B: Longitudinal Strain at Cross-sections Indicated

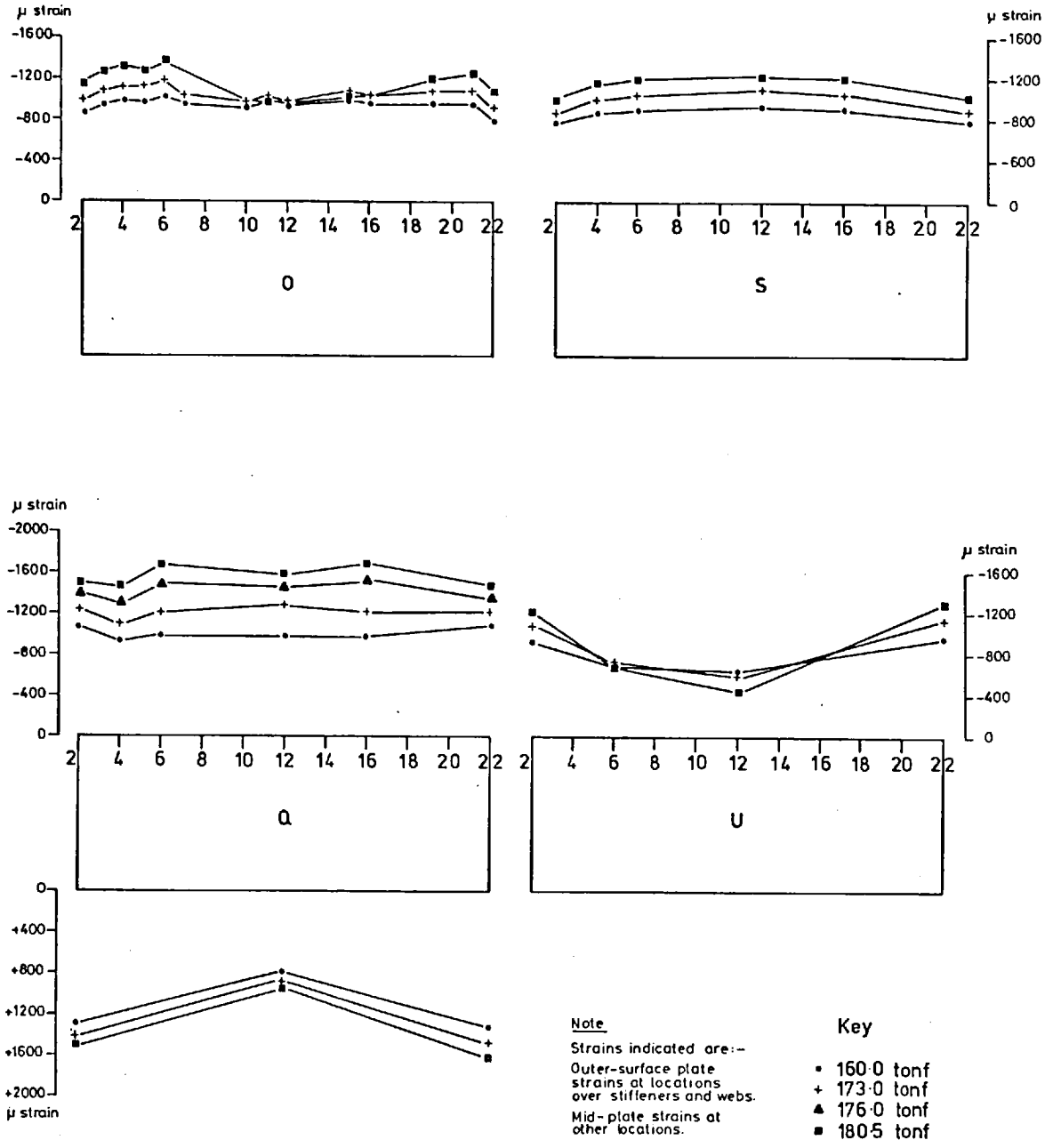

Fig. 2.89e
Test 10 B: Longitudinal Strain at Cross-sections Indicated

Fig. 2.90a. Model 10 - a view of the model after the collapse test (Test 10C). Stiffener locations are indicated by dashed lines.

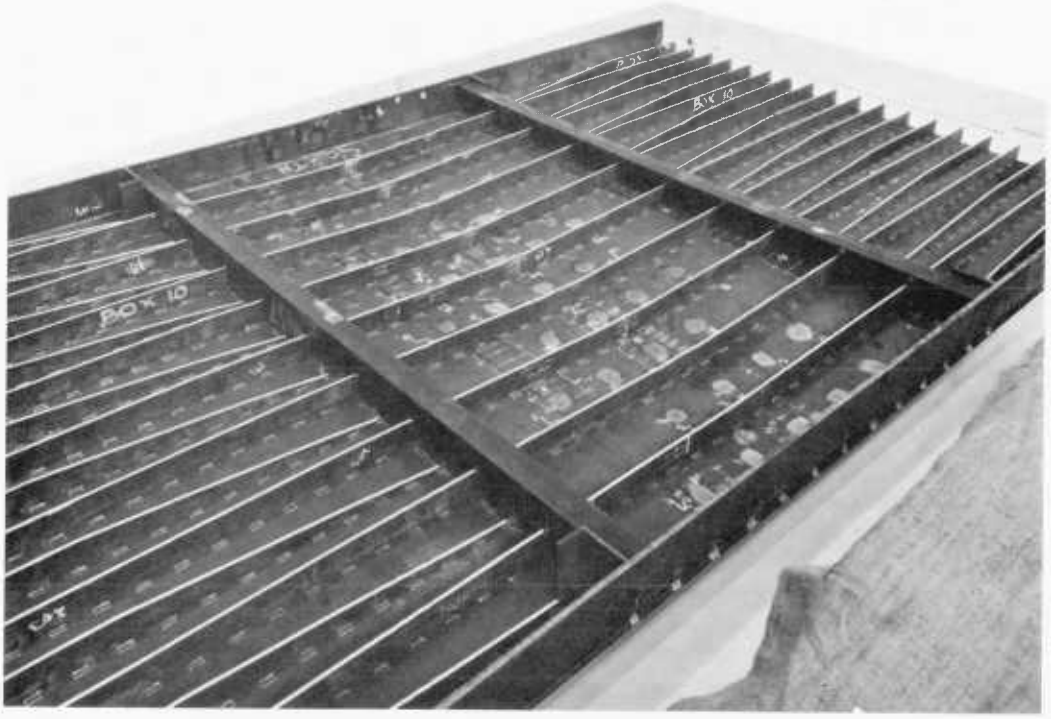

Fig. 2.90b. Model 10 - showing the compression flange (cut-off from the model) after the collapse test.

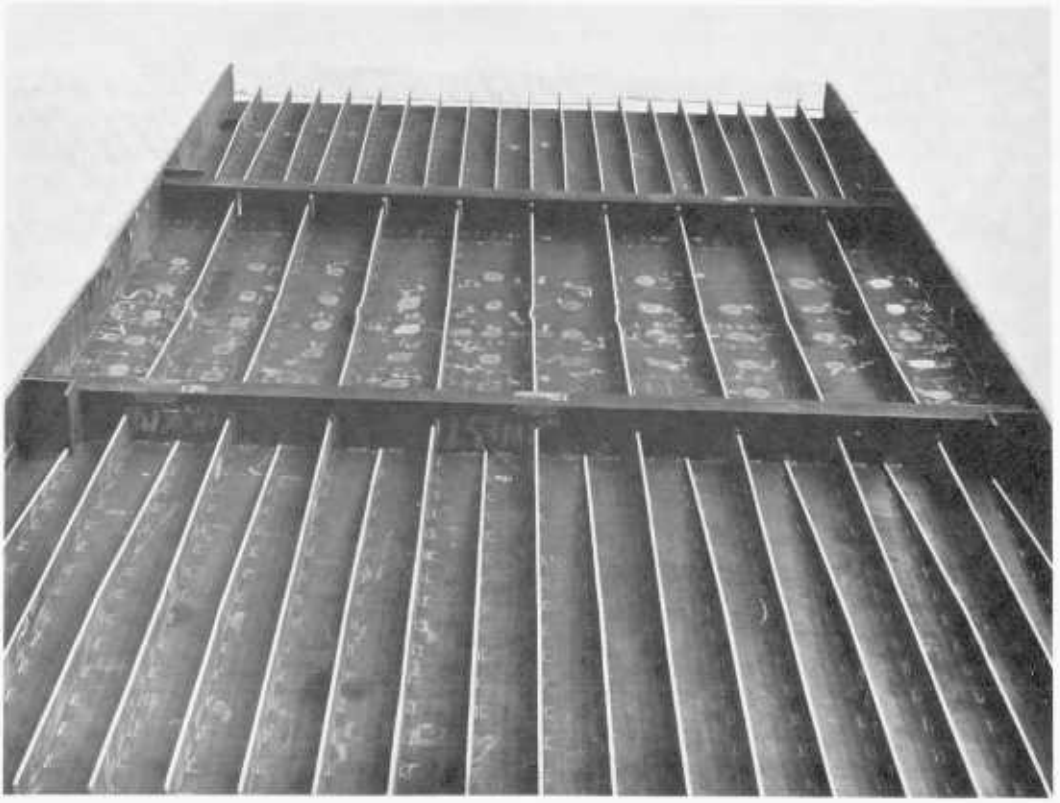

Fig. 2.90c. Model 10 - the compression flange after collapse, showing the lateral deflections of longitudinal stiffeners. The deflections became amplified (as seen above) after large deformations were applied to the model.

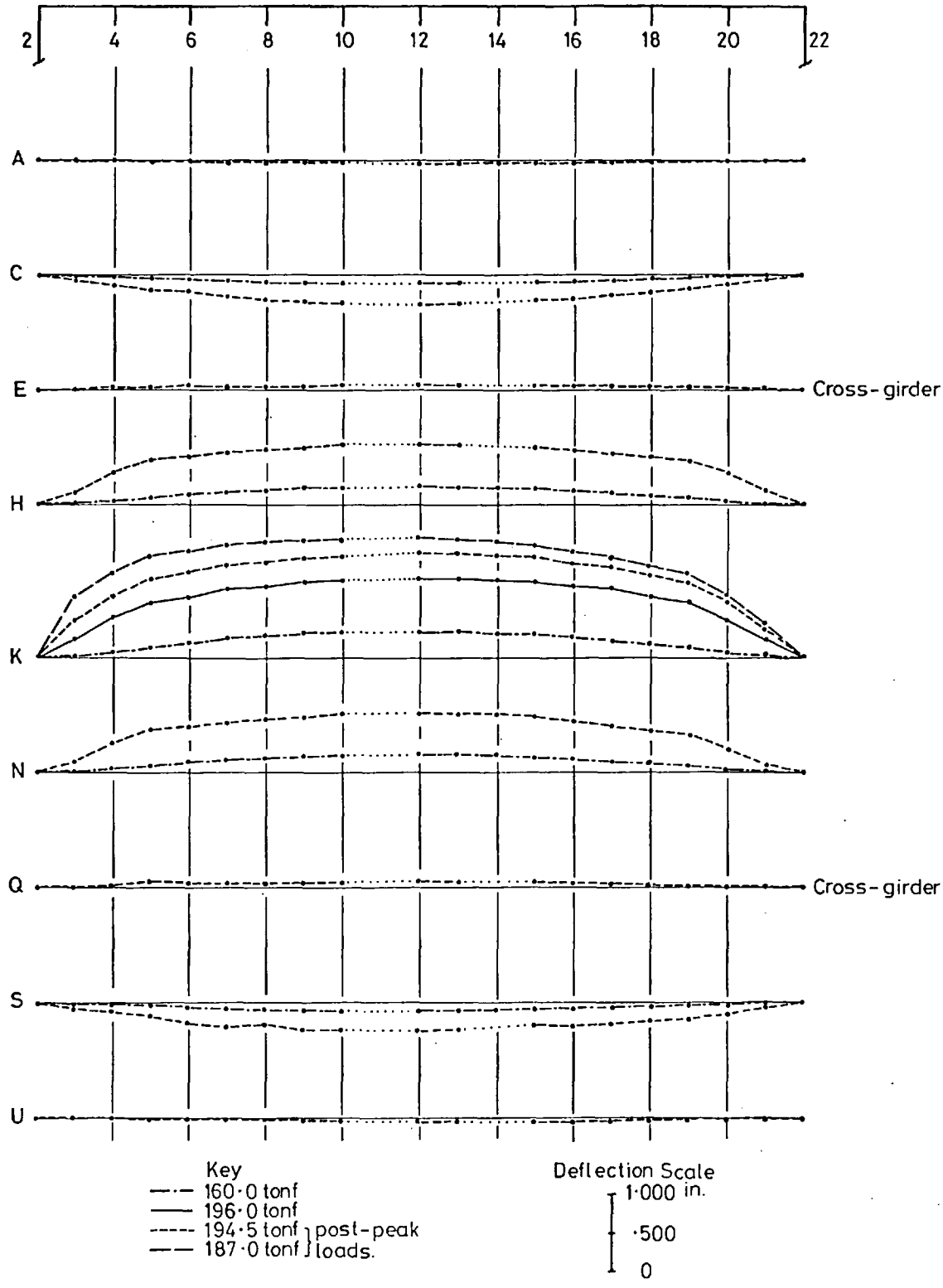

Fig. 2.91
Test 10C: Relative Transverse Deflections of Compression Flange

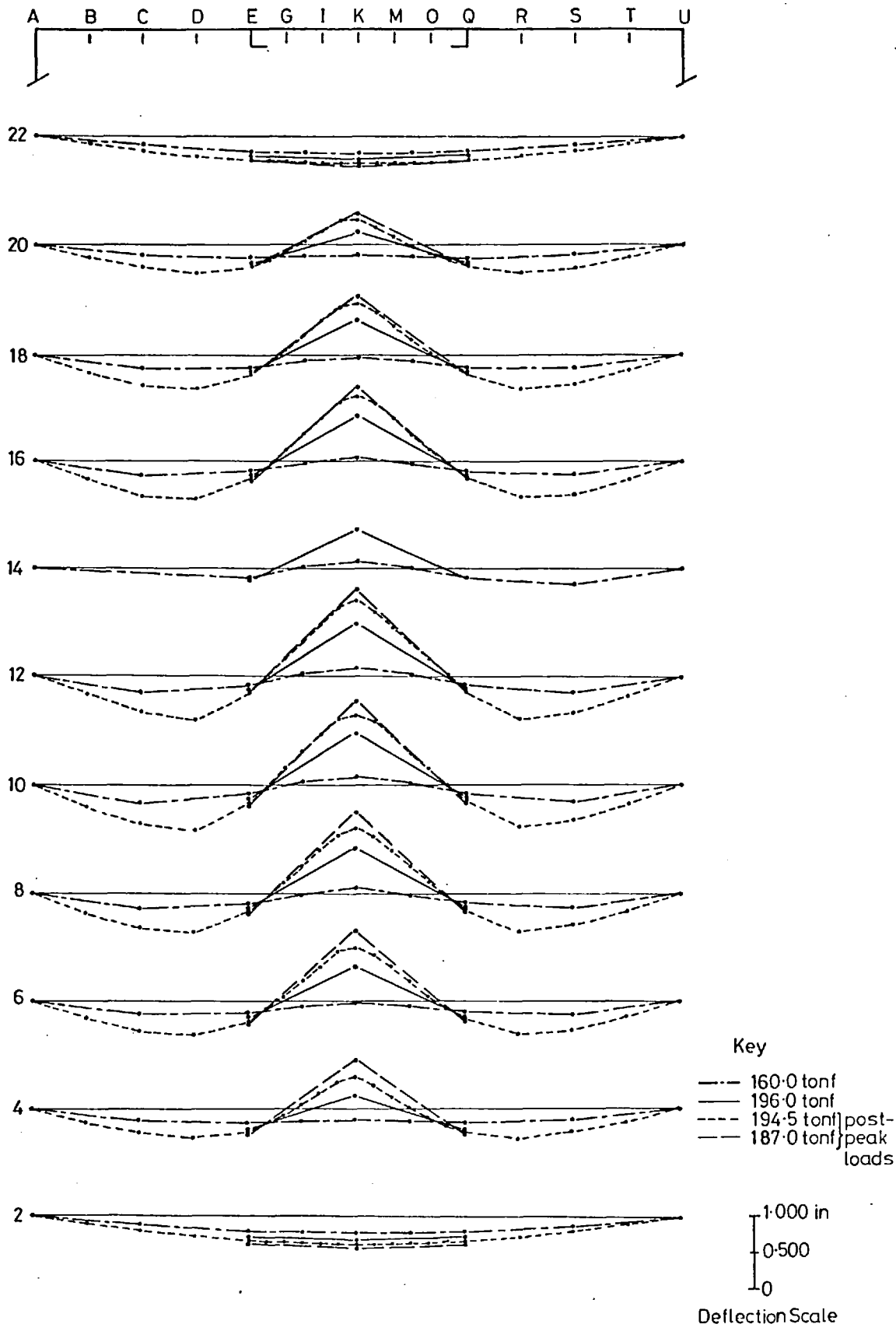

Fig. 2.92
Test 10 C : Relative Longitudinal Deflections of Compression Flange

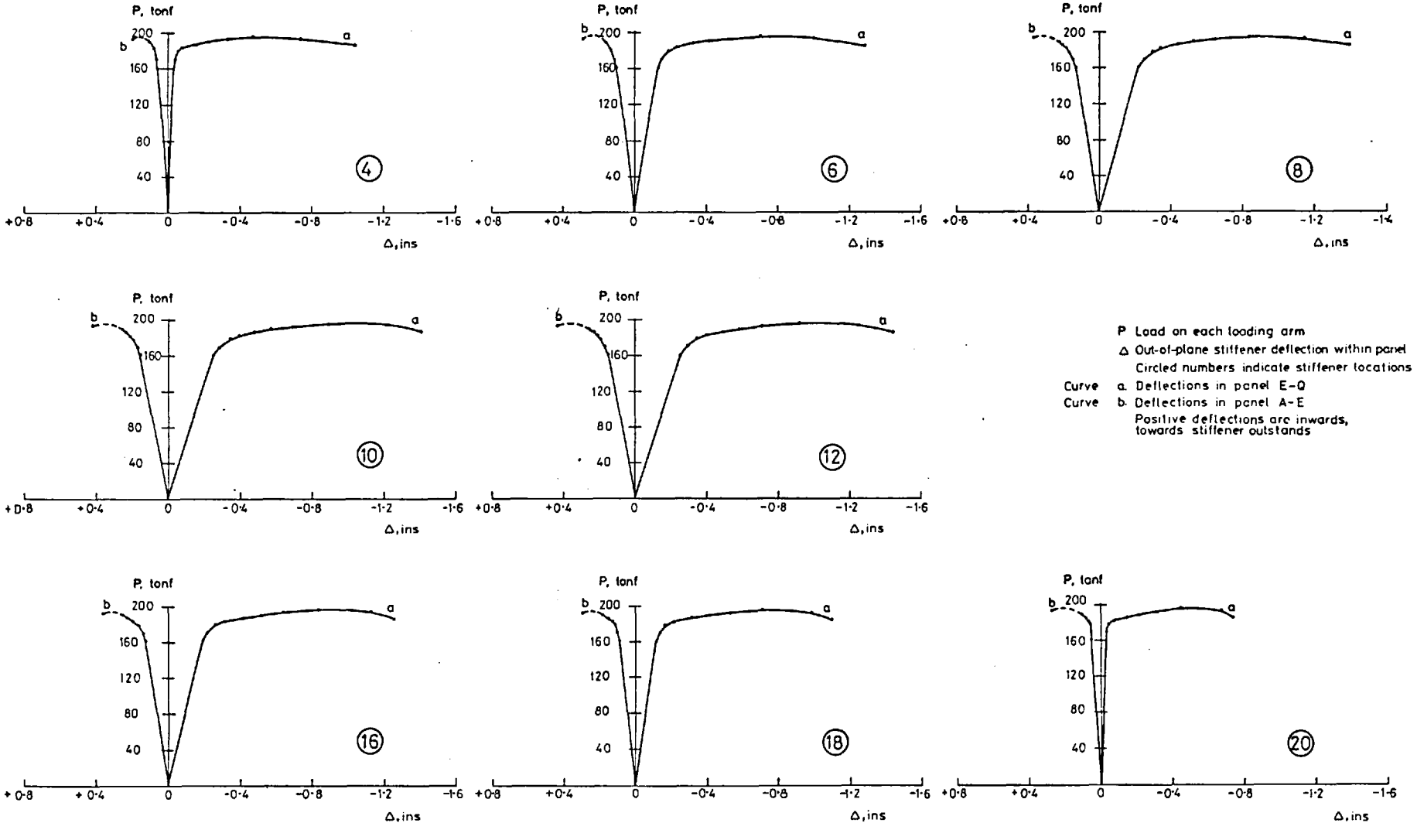

Fig. 2.93
Test 10C: Out - of - plane Deflections of Longitudinal Stiffeners

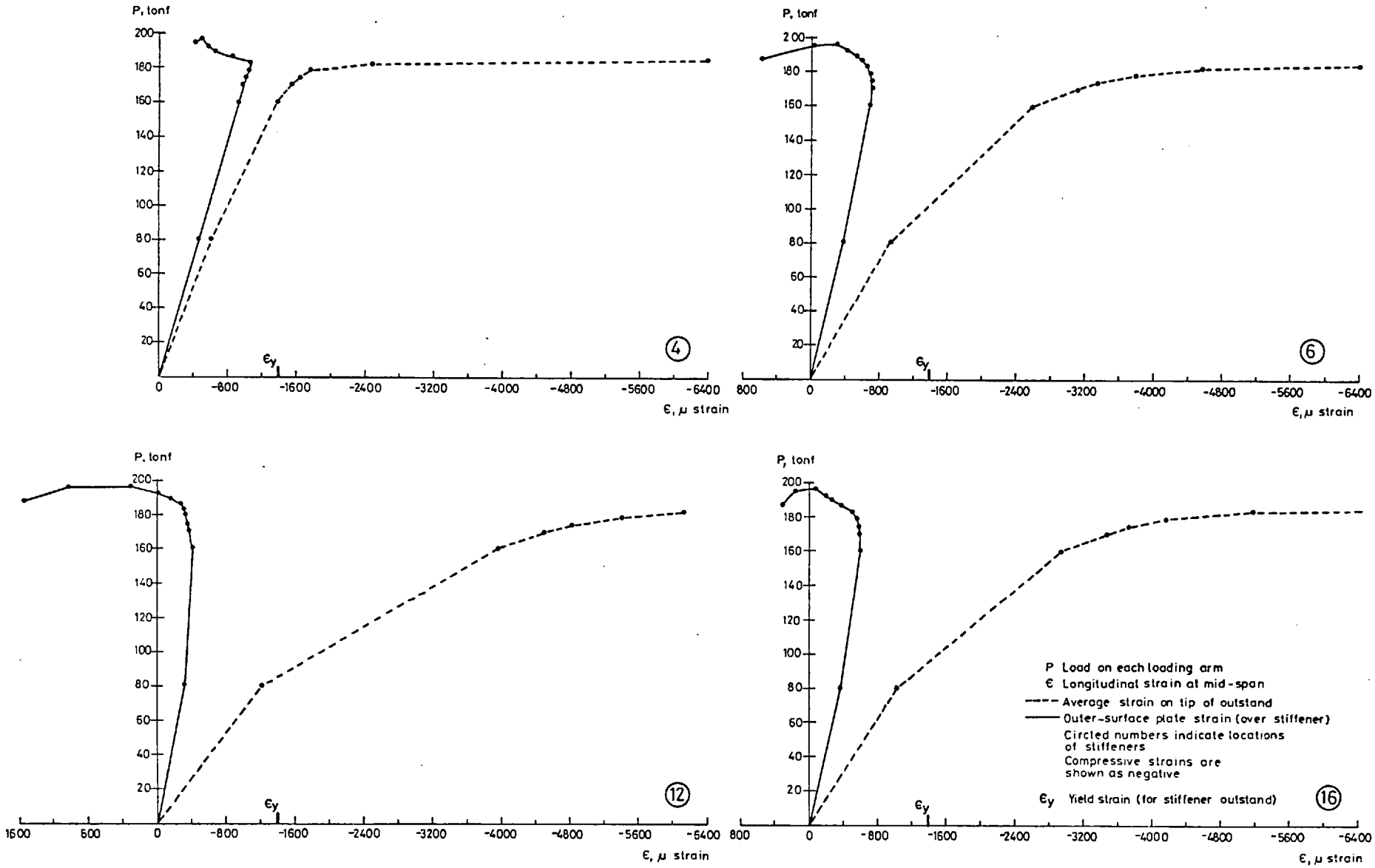

Fig. 2.94
Test 10 C : Strain in Longitudinal Stiffeners

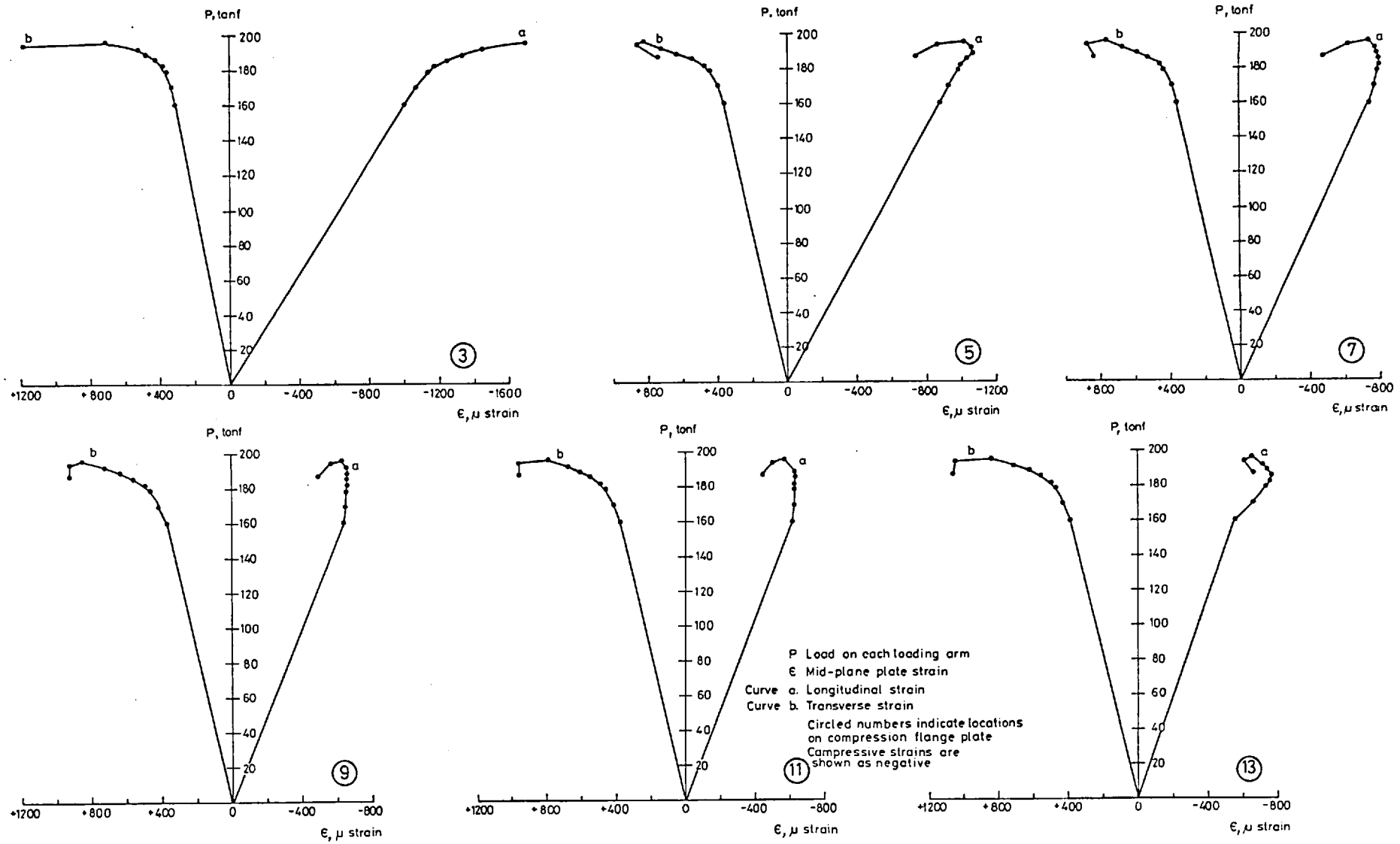

Fig. 2.95
Test 10 C: Longitudinal and Transverse Mid-plate Strains at Mid-span

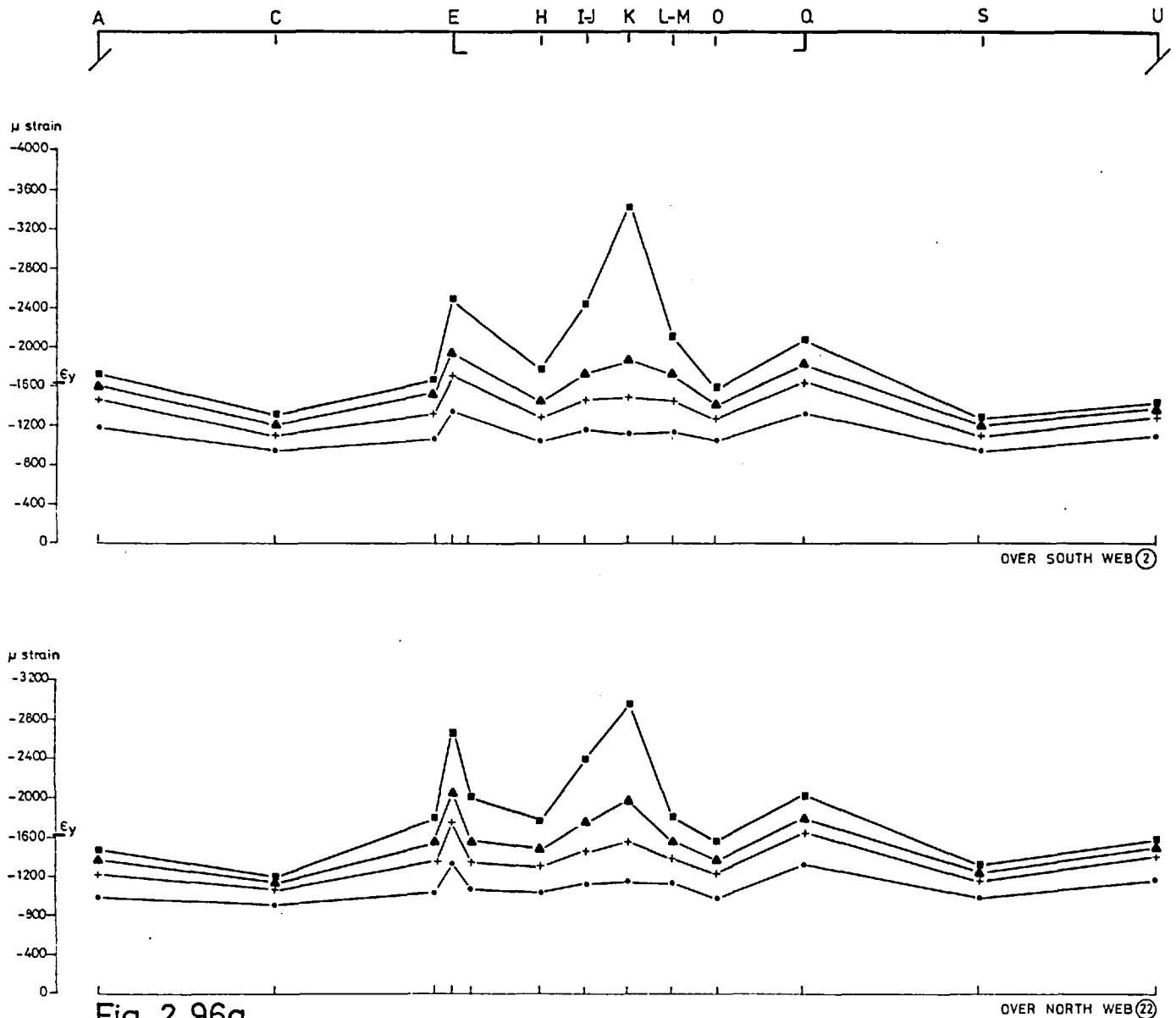

Fig. 2.96a
Test 10 C: Longitudinal Strain in Compression Flange at its Junctions with Webs

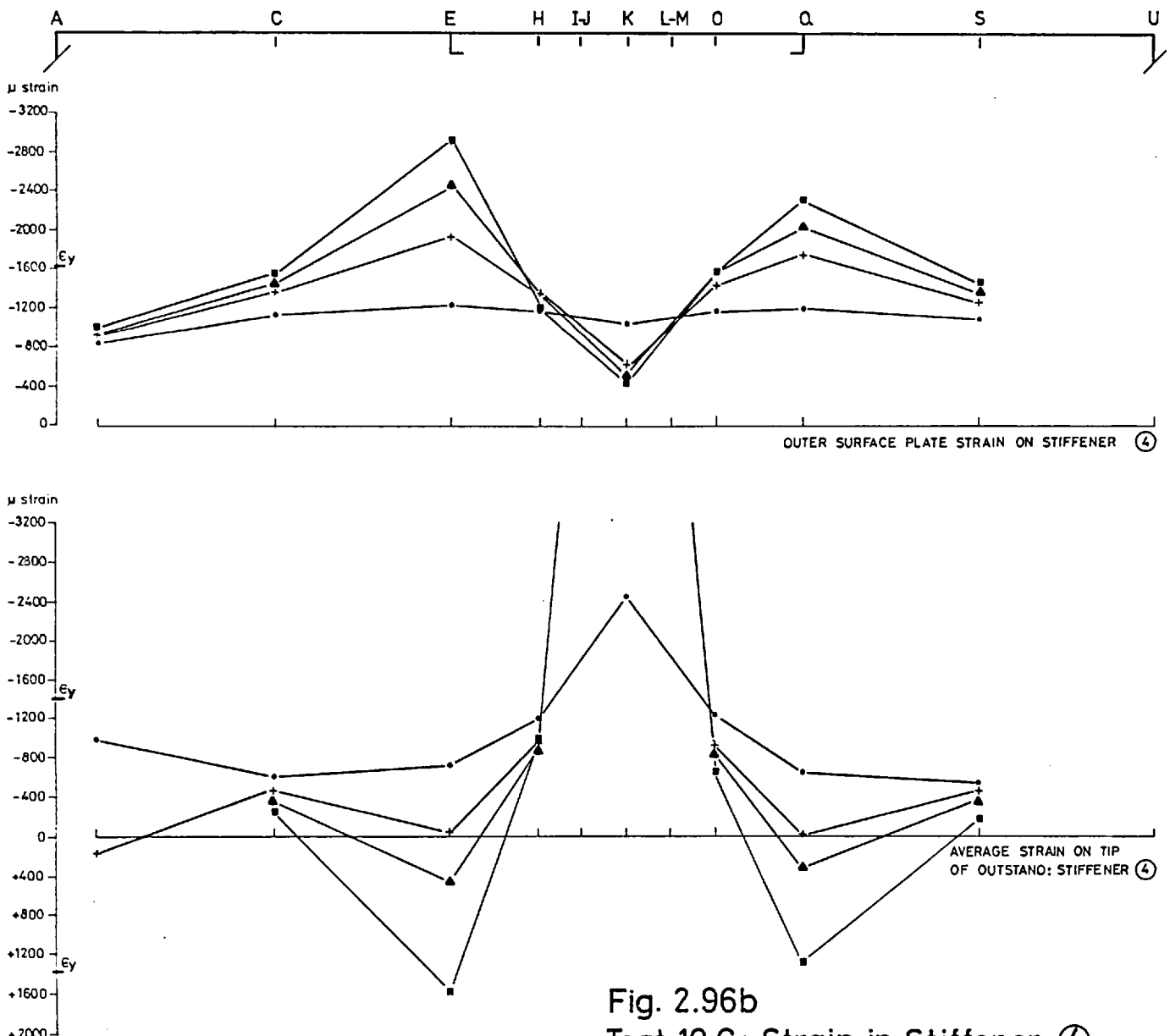

Fig. 2.96b
Test 10 C : Strain in Stiffener ④

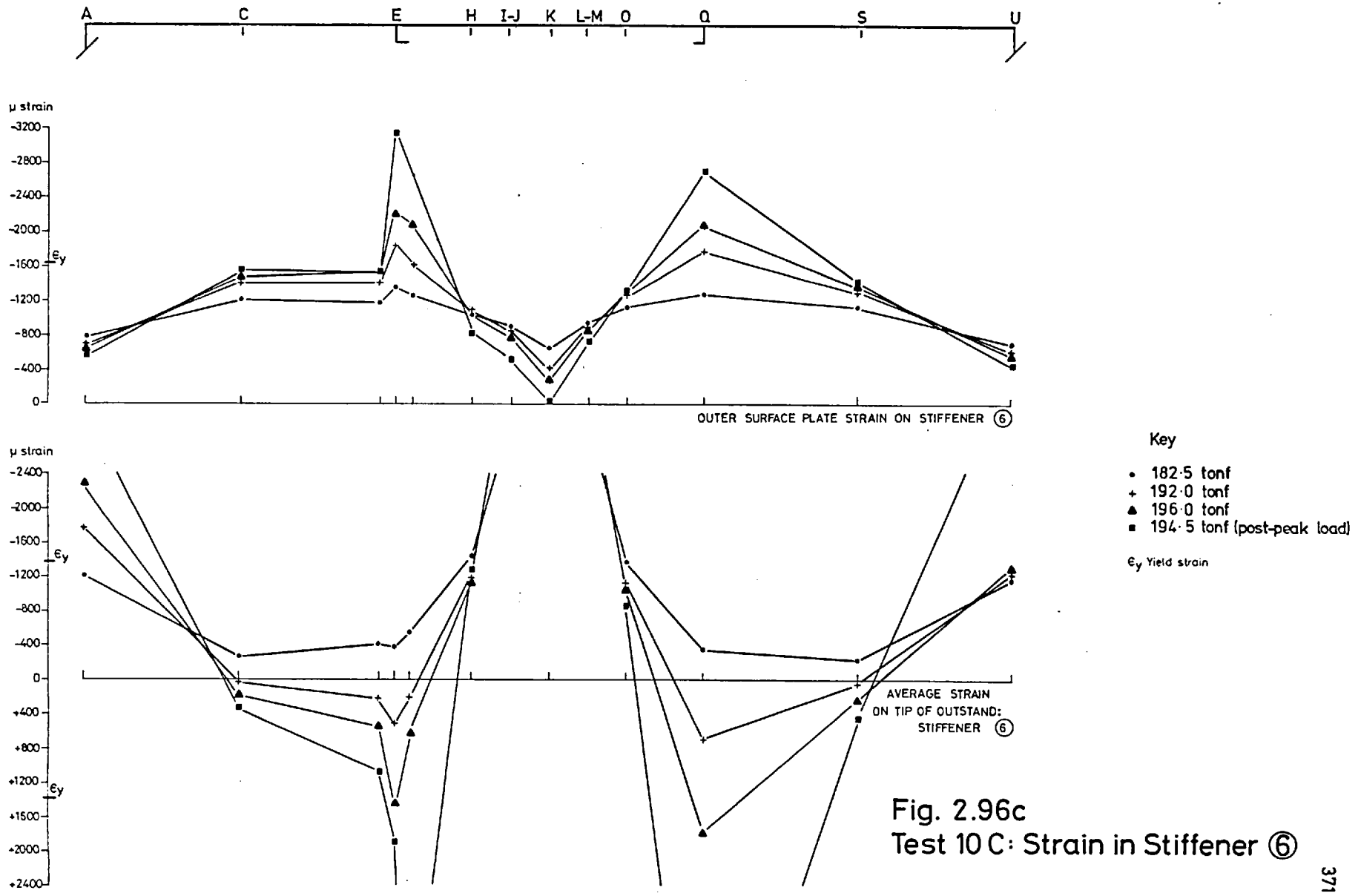

Fig. 2.96c
Test 10 C: Strain in Stiffener ⑥

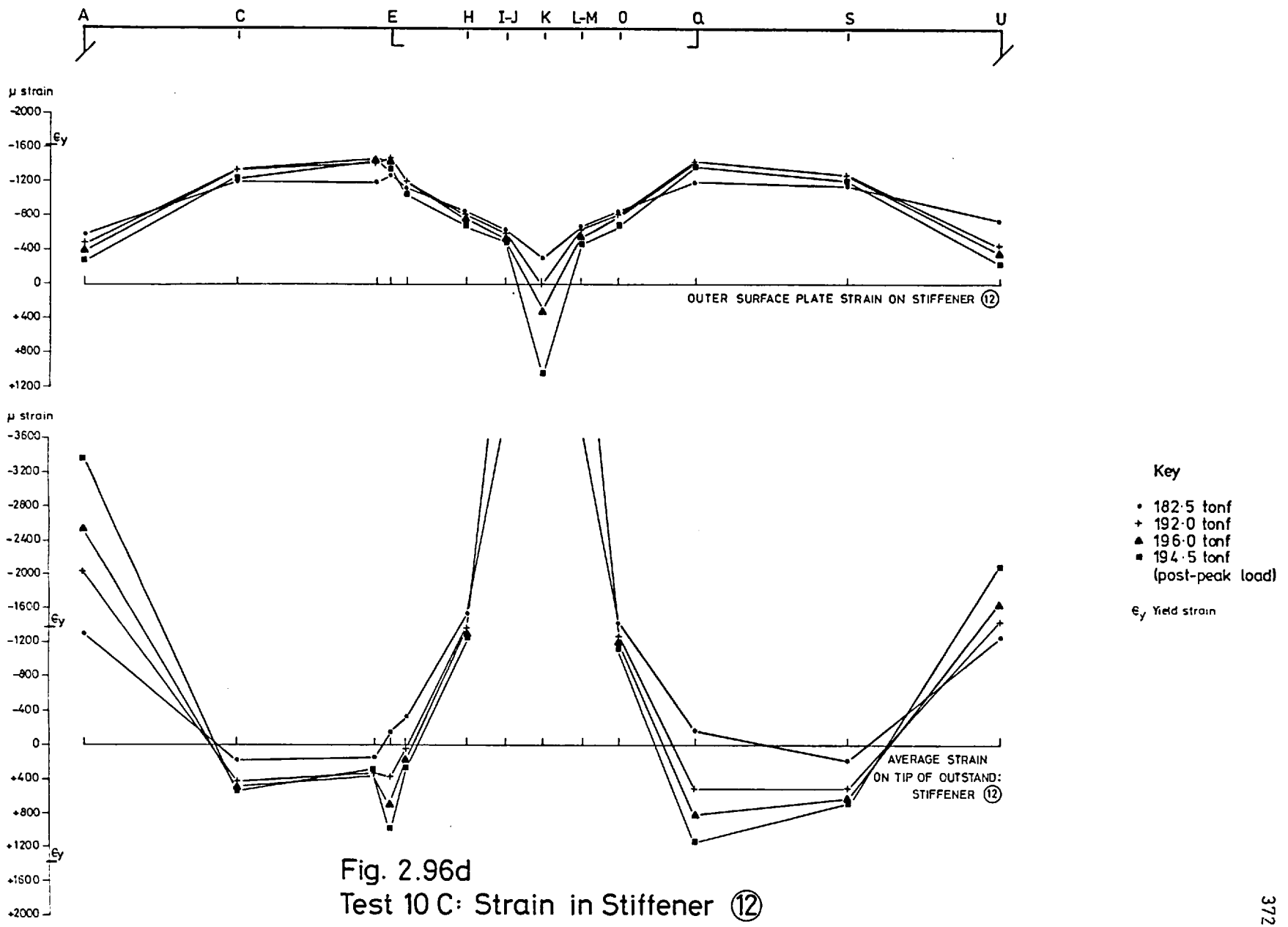

Fig. 2.96d
Test 10 C: Strain in Stiffener (12)

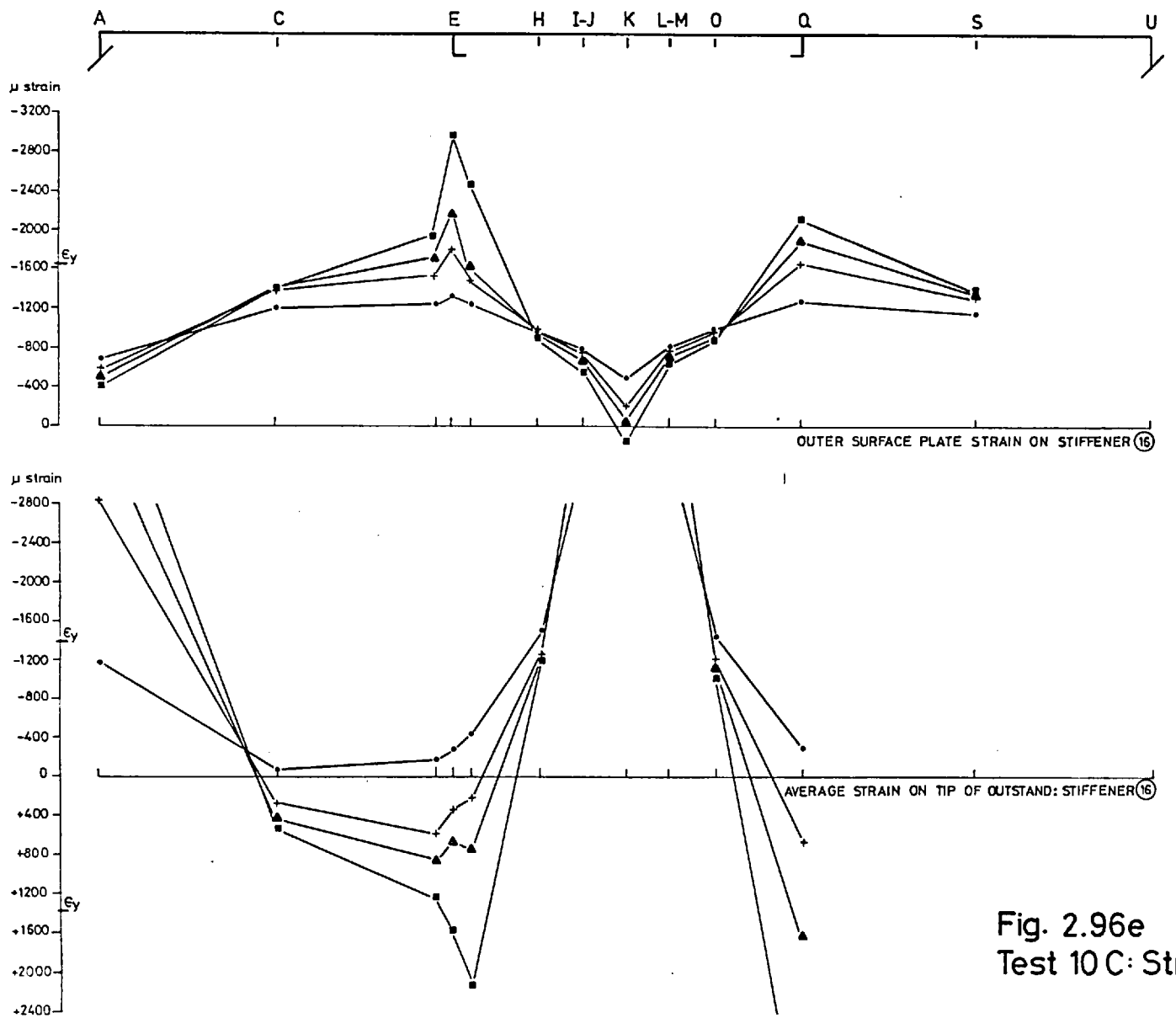

Key

- 182.5 tonf
- 192.0 tonf
- 196.0 tonf
- 194.5 tonf (post-peak load)

ϵ_y Yield strain

Fig. 2.96e
Test 10 C: Strain in Stiffener (16)

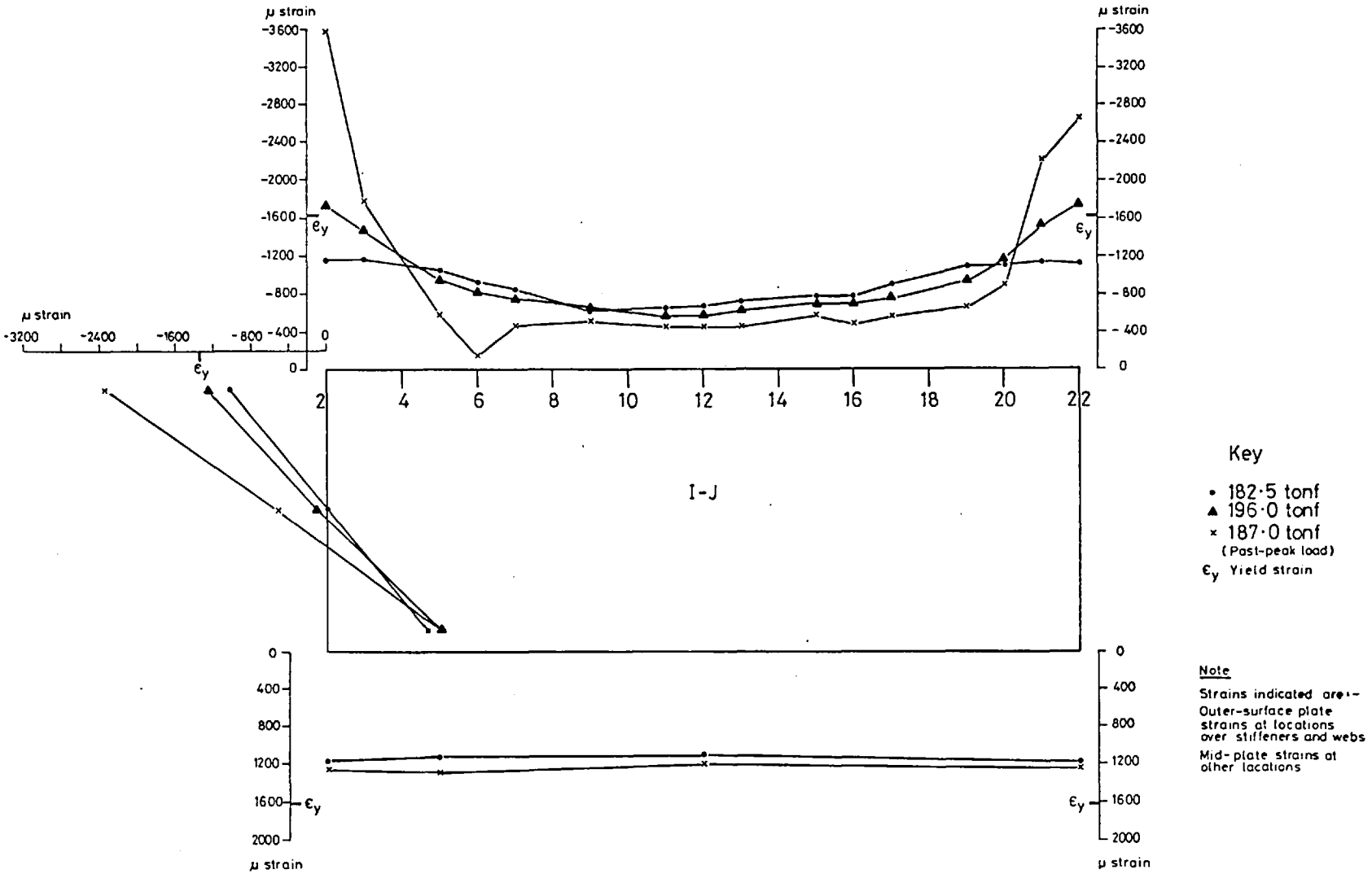

Fig. 2.97a
Test 10 C: Longitudinal Strain at Cross-section I-J
($7\frac{3}{4}$ in from mid-span)

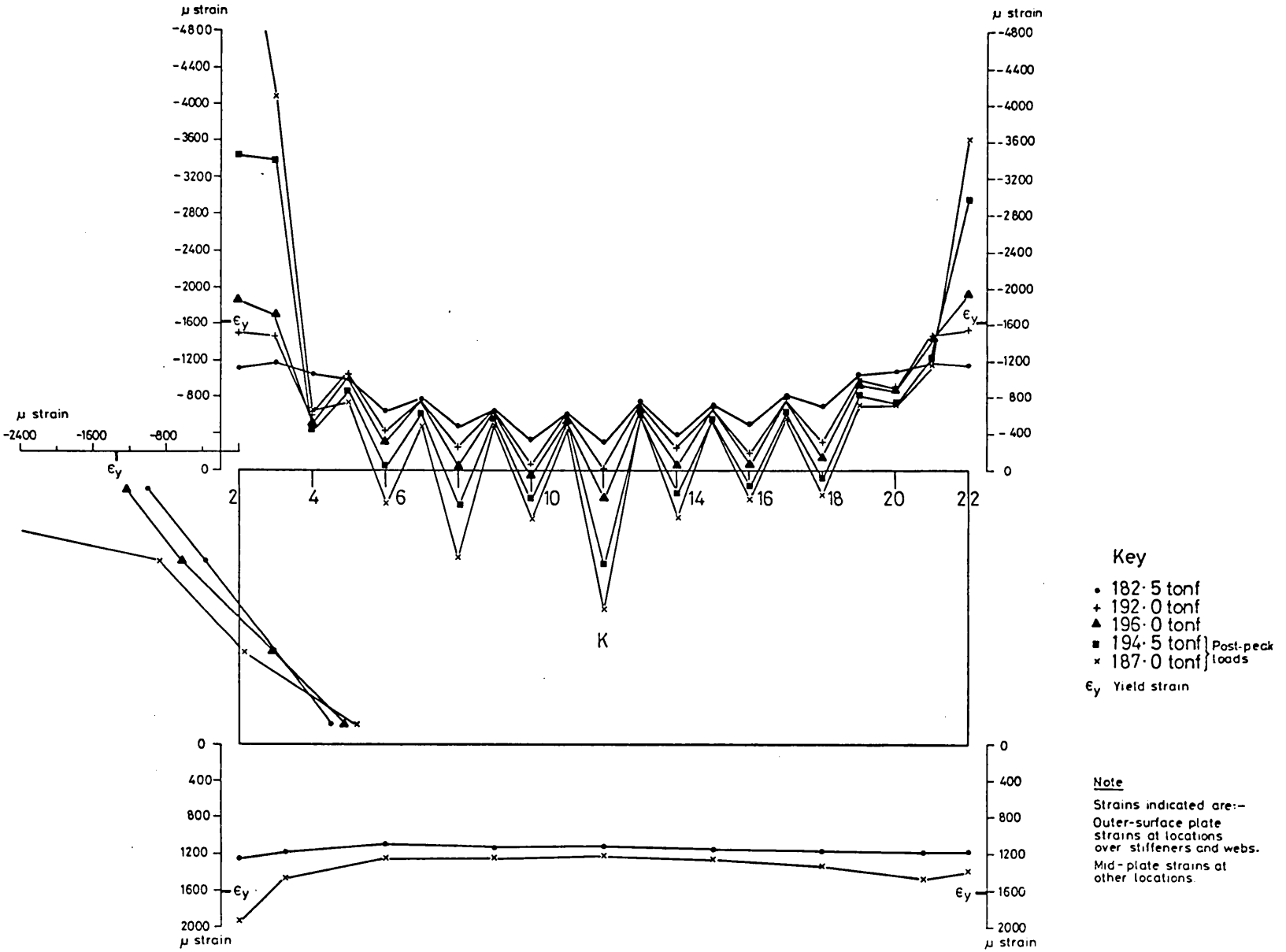

Fig. 2.97b
Test 10 C: Longitudinal Strain at Mid-span

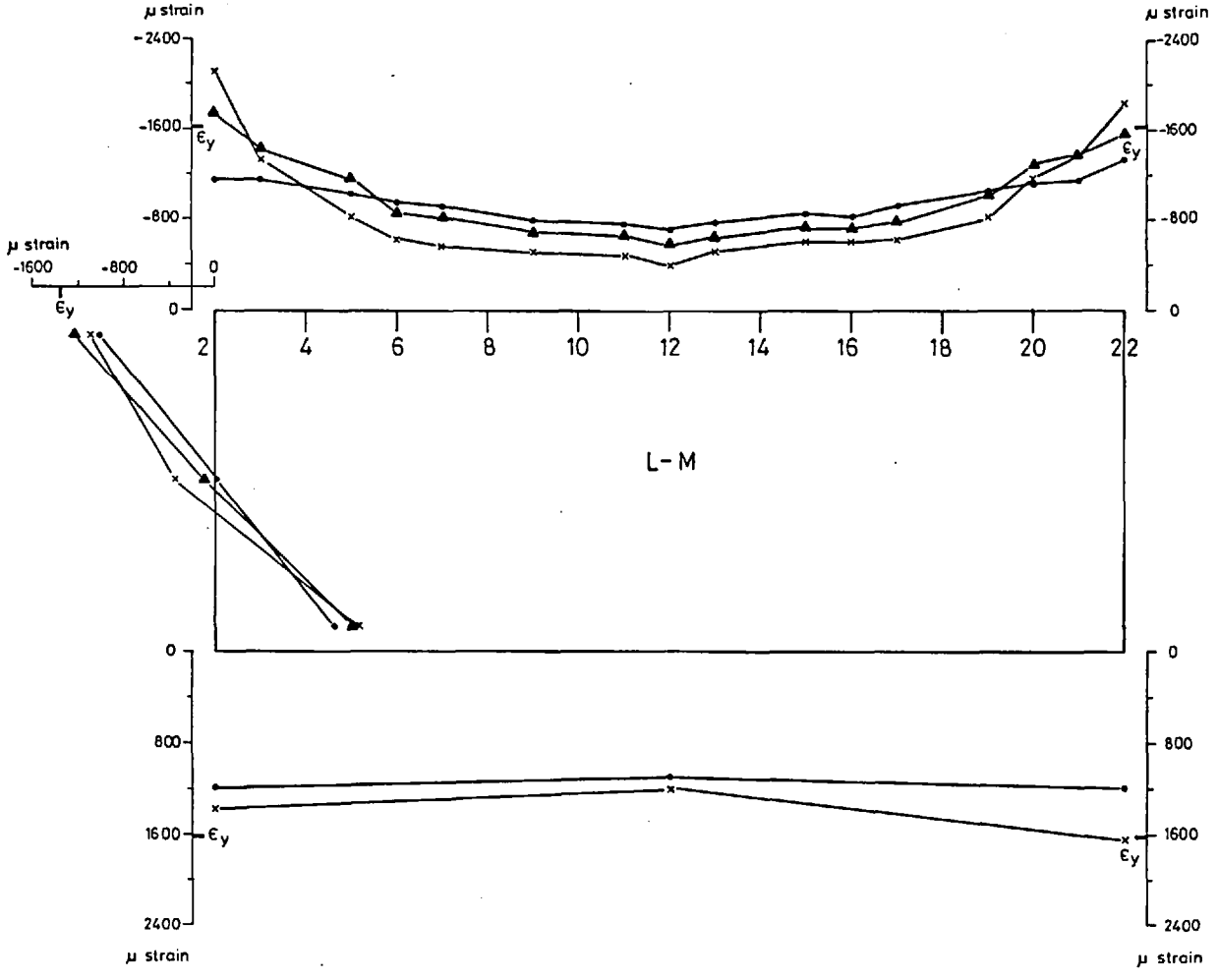

Key

- 182·5 tonf
- ▲ 196·0 tonf
- × 187·0 tonf (Post-peak load)

ϵ_y Yield strain

Note

Strains indicated are:—
Outer-surface plate strains at locations over stiffeners and webs.
Mid-plate strains at other locations.

Fig. 2.97c
Test 10C: Longitudinal Strain at Cross-section L-M
(7¾ in from mid-span)

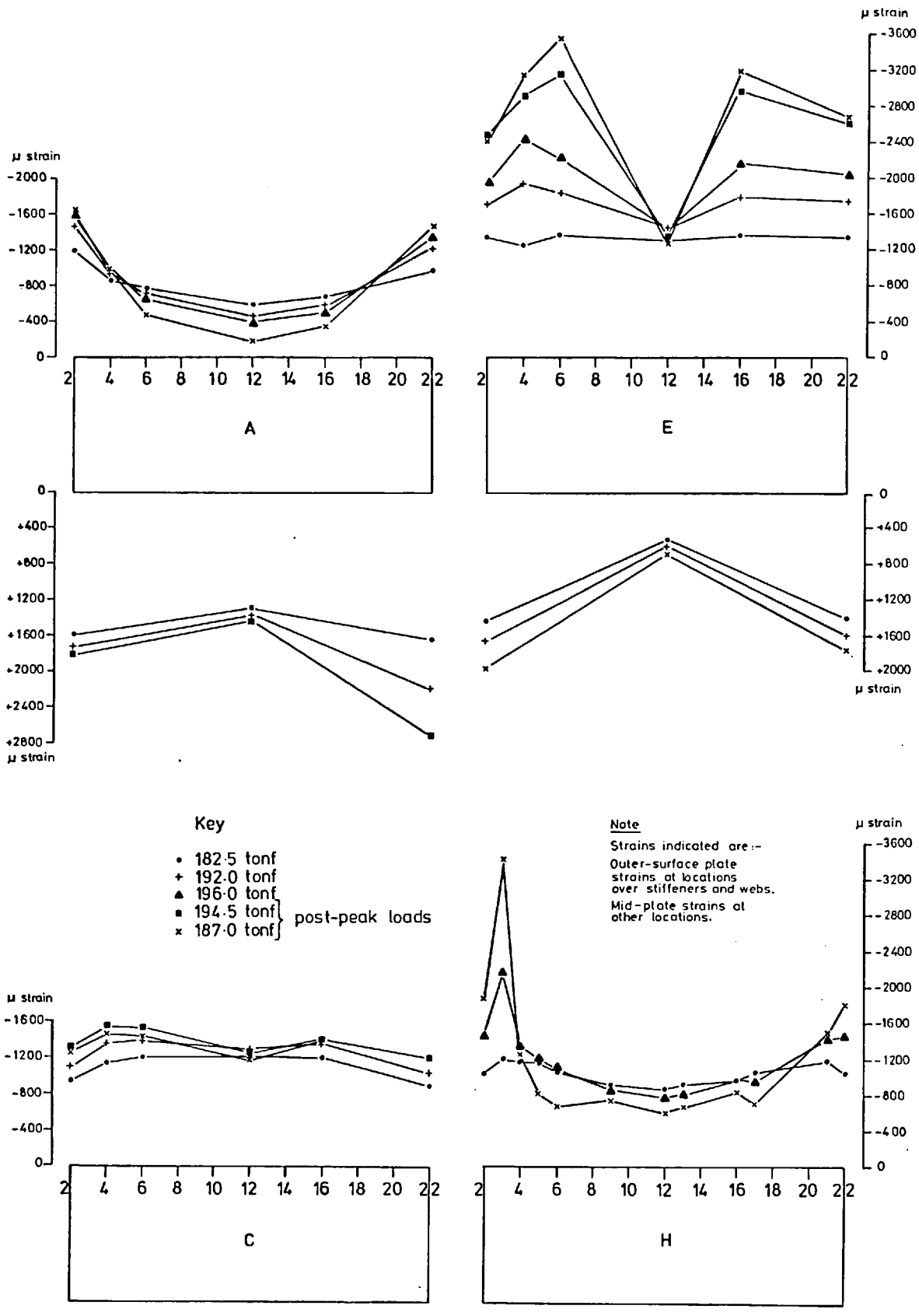

Fig. 2.97d
Test 10 C: Longitudinal Strain at Cross-sections Indicated

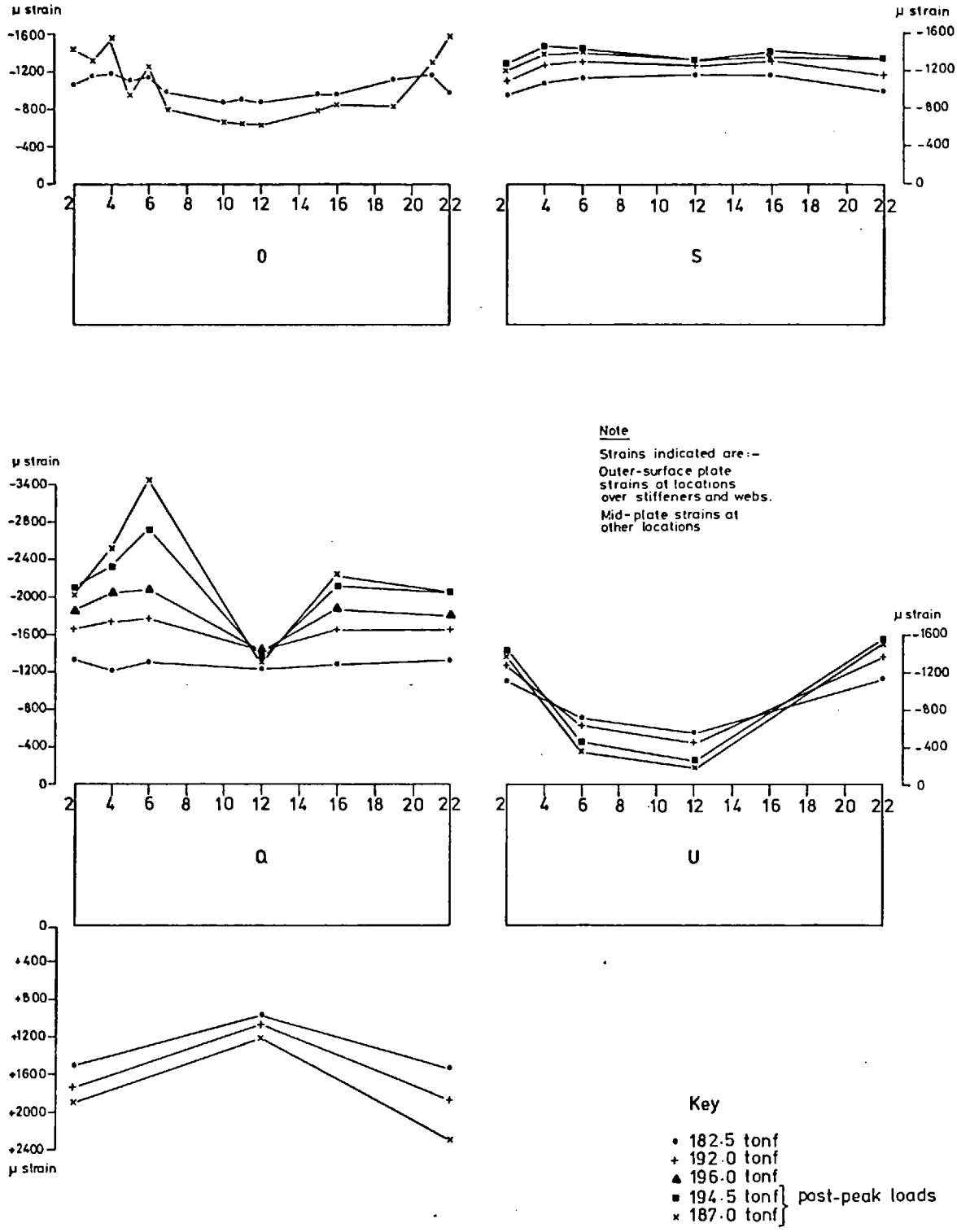

Fig. 2.97e
Test 10 C: Longitudinal Strain at Cross-sections Indicated

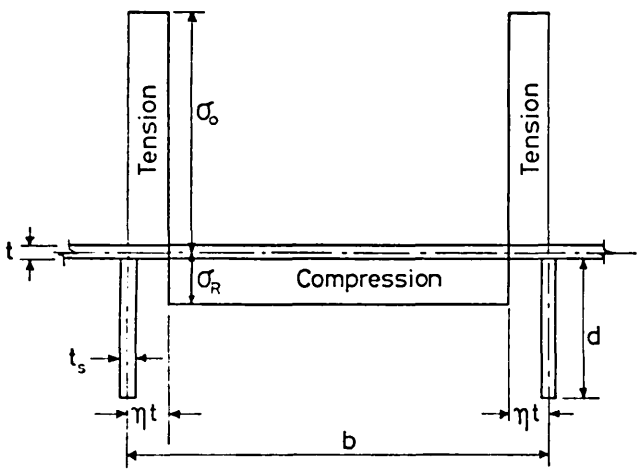

(a) Idealised residual stress distribution for the flange plate.

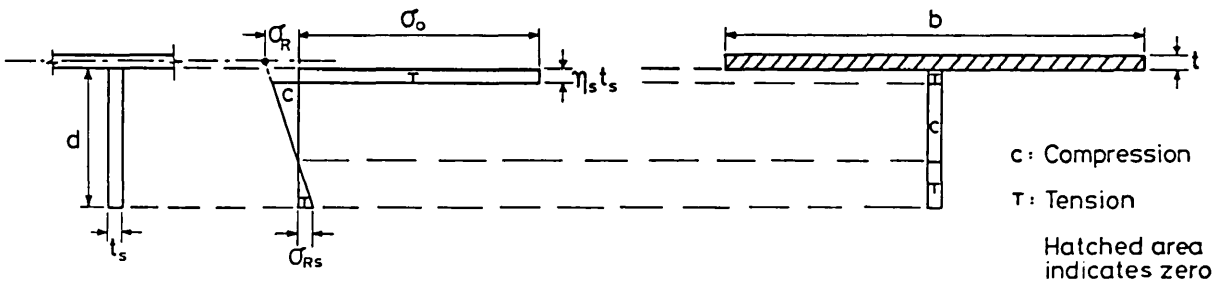

(b) A self-equilibrating residual stress pattern for the stiffener outstand. (considered separate from the plate)

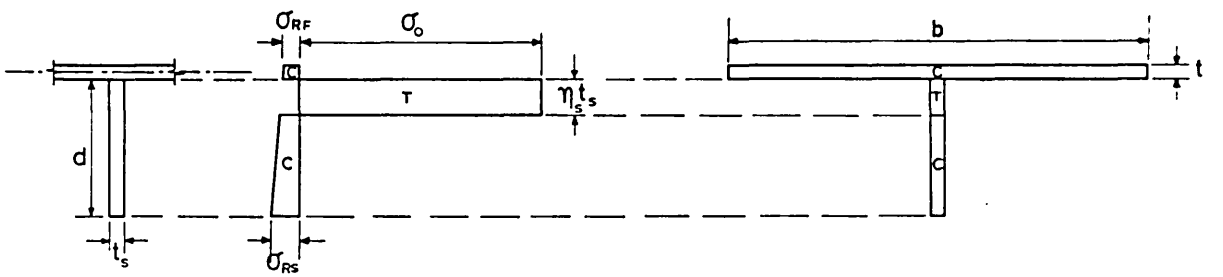

(c) Residual stress pattern for the stiffener outstand with plate area included for establishing equilibrium.

Fig 3.1 Idealised Residual Stress Patterns

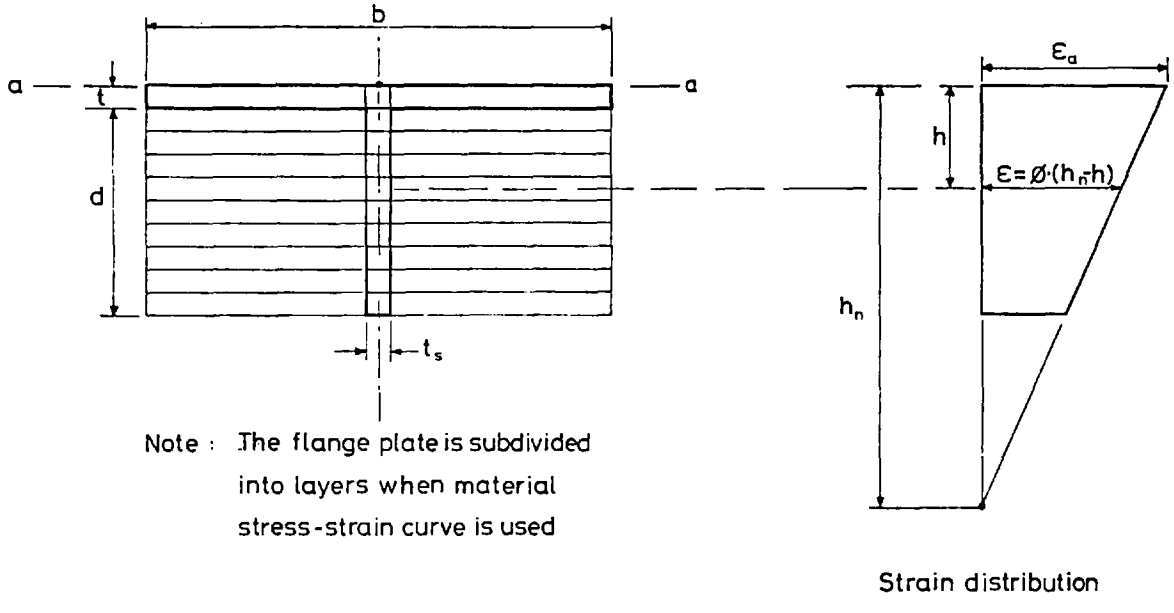

Fig3.2 Idealisation of Cross-section

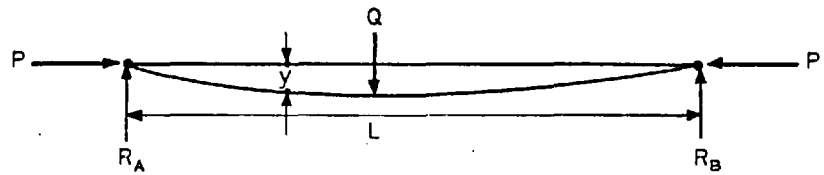

(a) SINGLE-SPAN BEAM-COLUMN

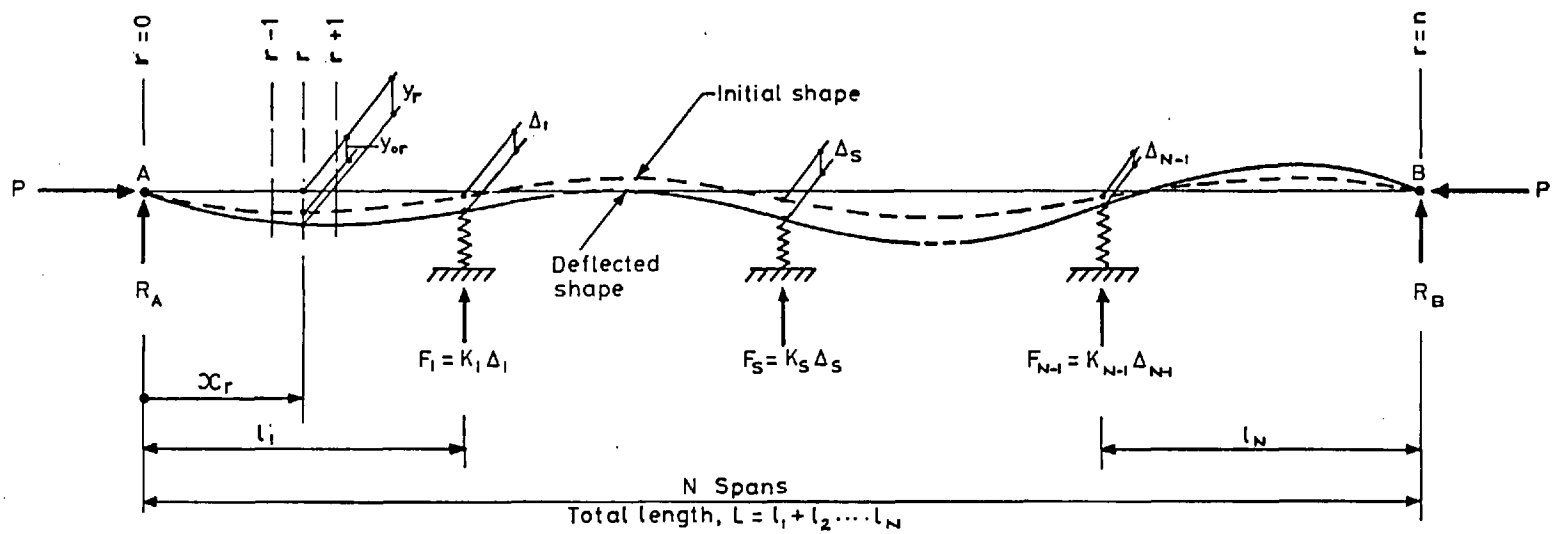

(b) MULTI-SPAN BEAM-COLUMN

Fig 3.3 Beam-column Deflections and Forces

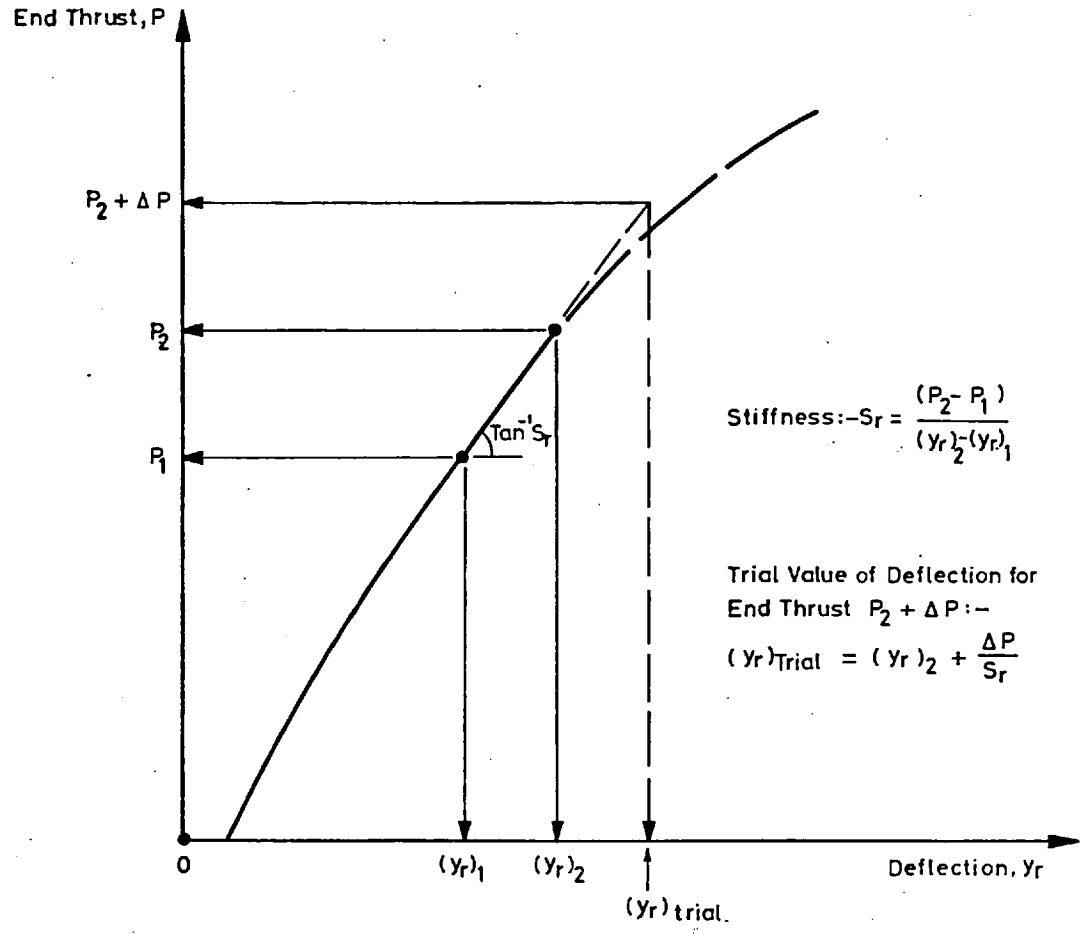

Fig 3.4 Estimation of Deflection Values for a Trial Value of End Thrust.

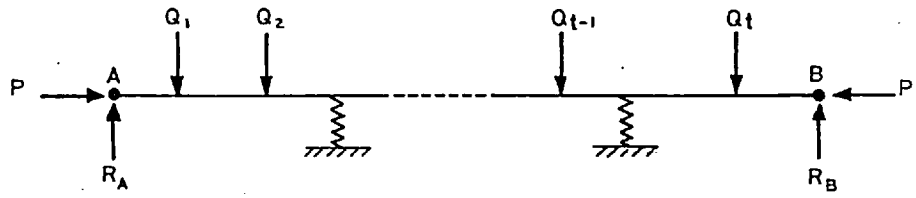

(a) CONCENTRATED LATERAL LOADS

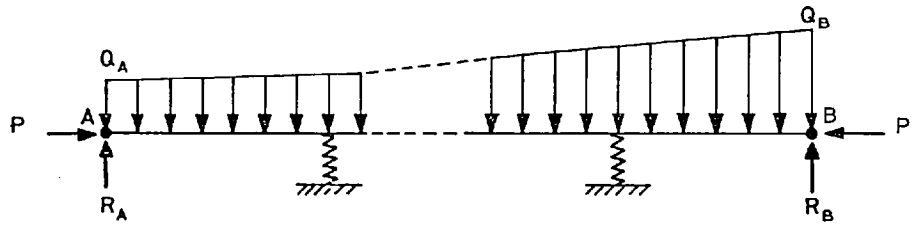

(b) UNIFORMLY VARYING DISTRIBUTED LOADING

Fig 3.5 Lateral Loading on Beam-Columns

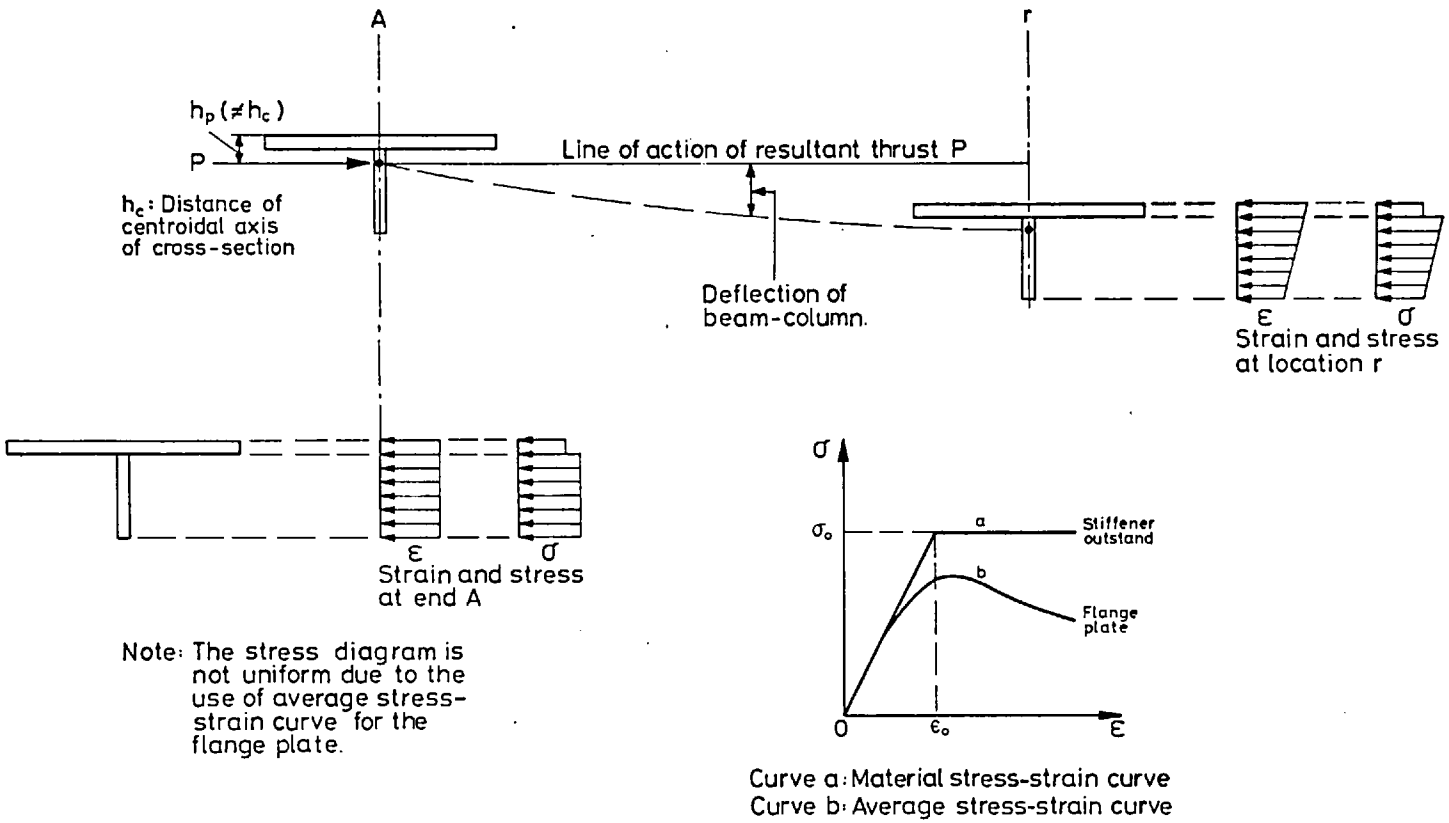

Fig.3.6 Resultant Thrust Line

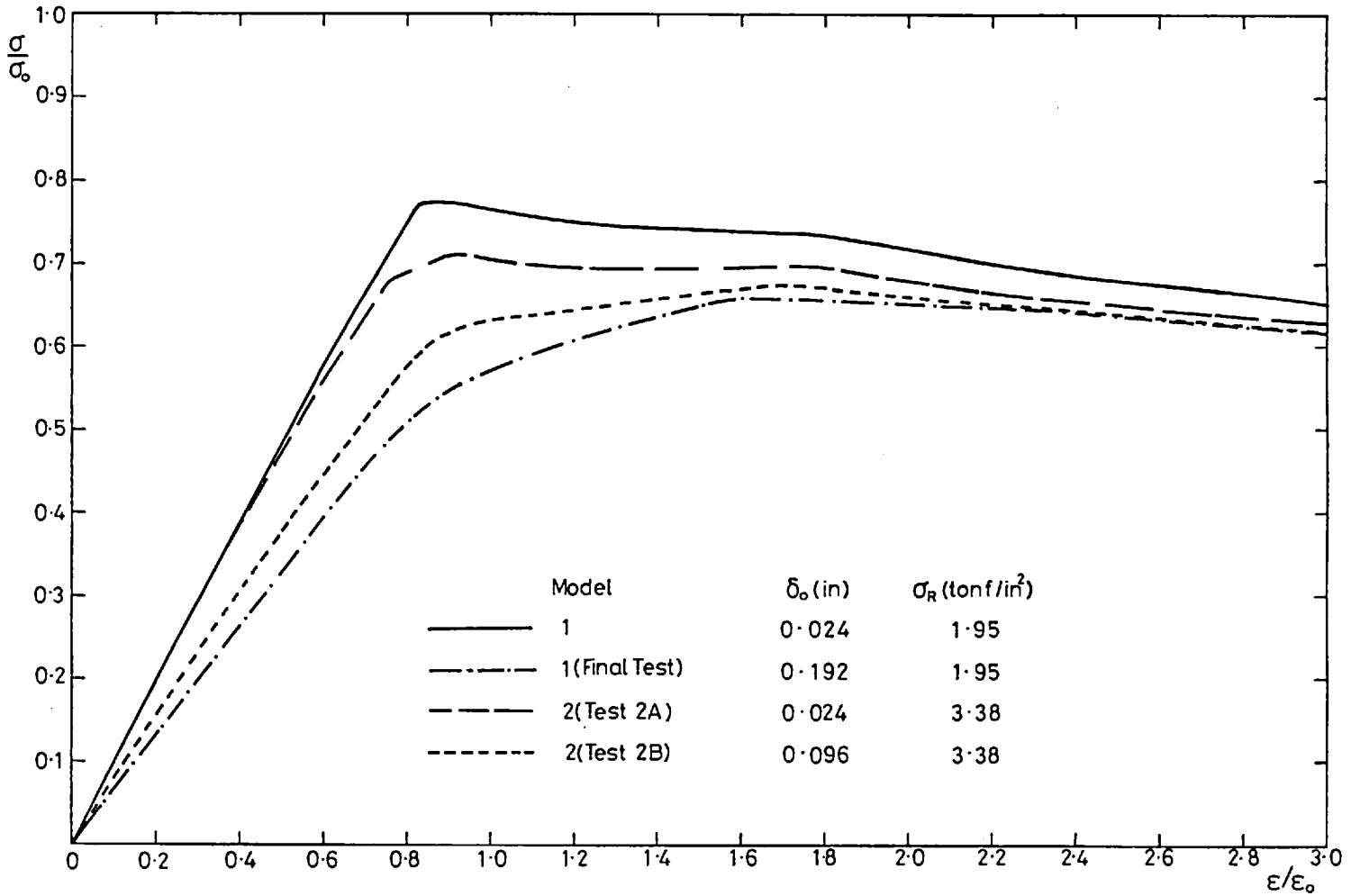

Fig.4.1 Average Stress-Strain Curves for Compression Flange Plate Panels (Models 1 and 2)

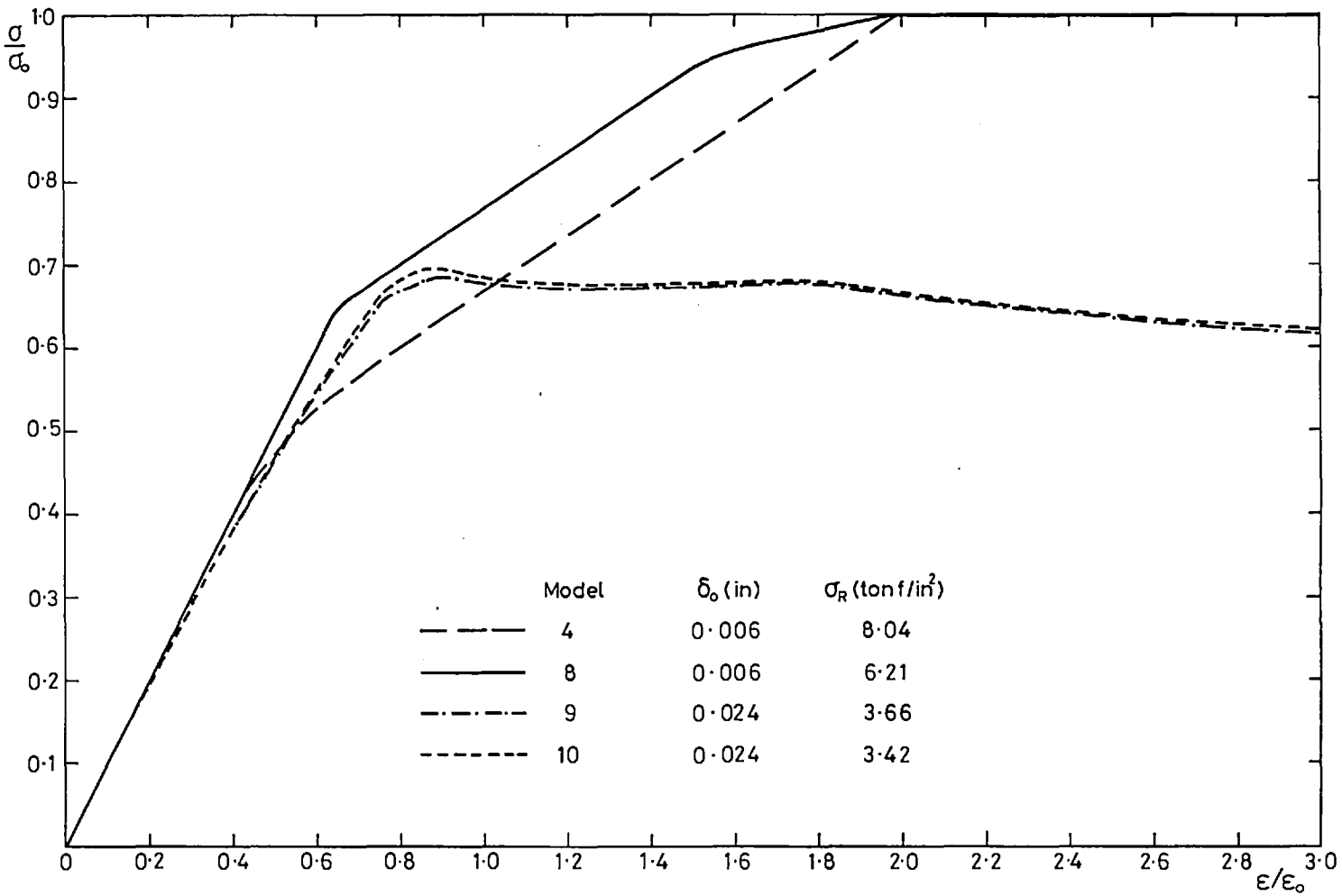

Fig.4.2 Average Stress-Strain Curves for Compression Flange Plate Panels (Models 4, 8, 9 and 10)

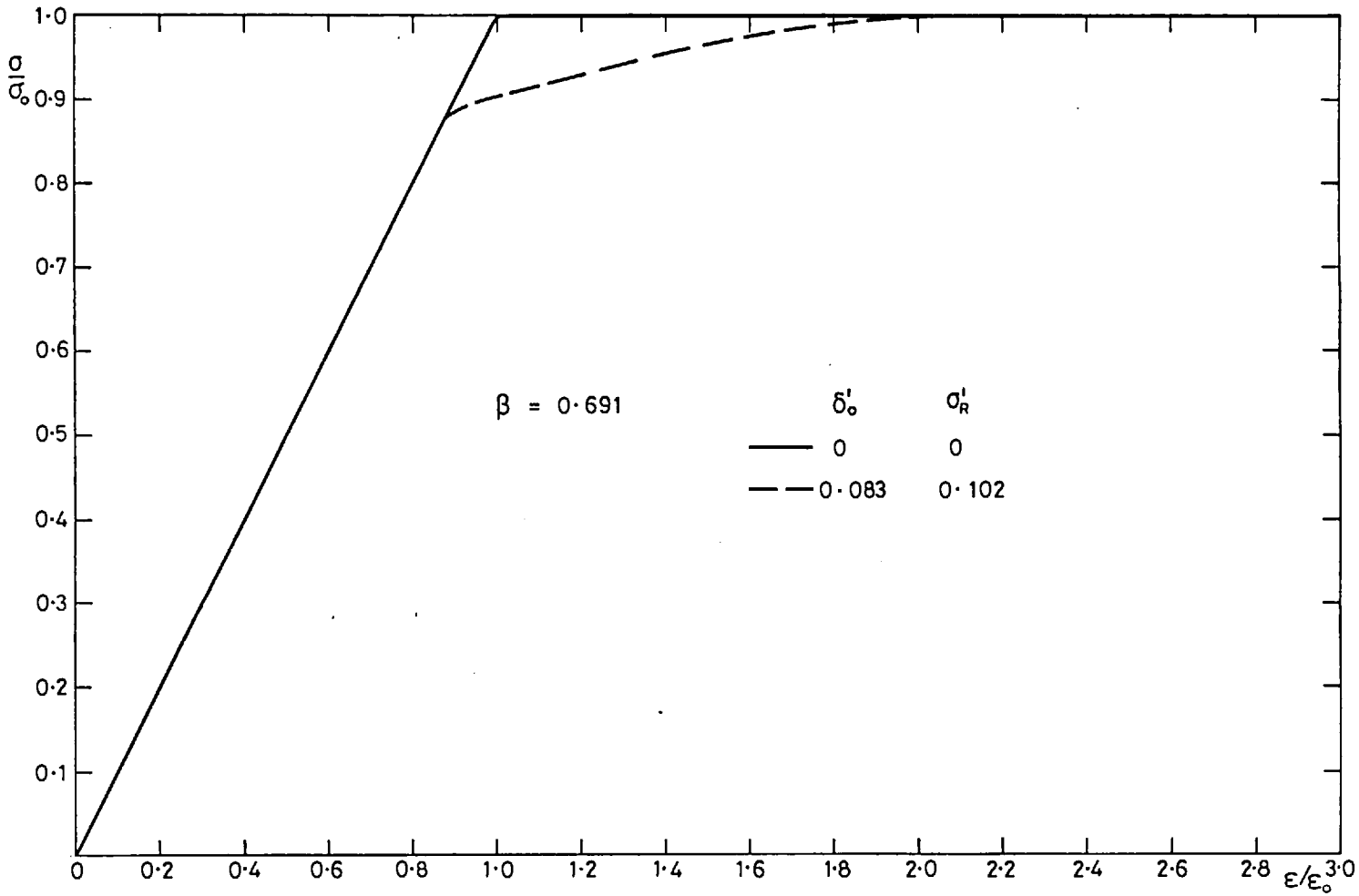

Fig. 5.1 Average Stress-Strain Curves for Plate in Compression with Constrained Edges.

Effect of Varying Initial Imperfections

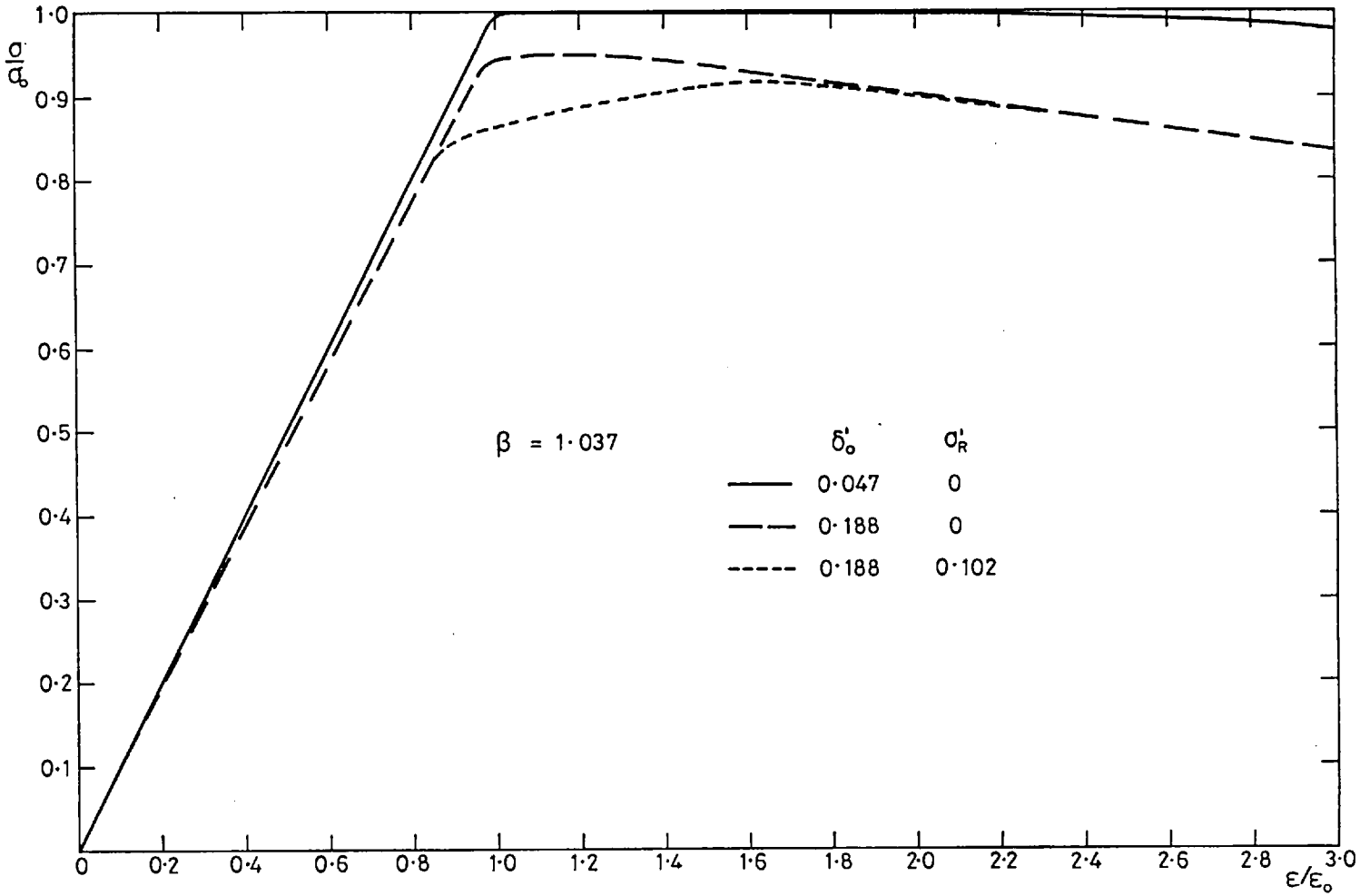

Fig. 5.2 Average Stress-Strain Curves for Plate in Compression with Constrained Edges.
Effect of Varying Initial Imperfections

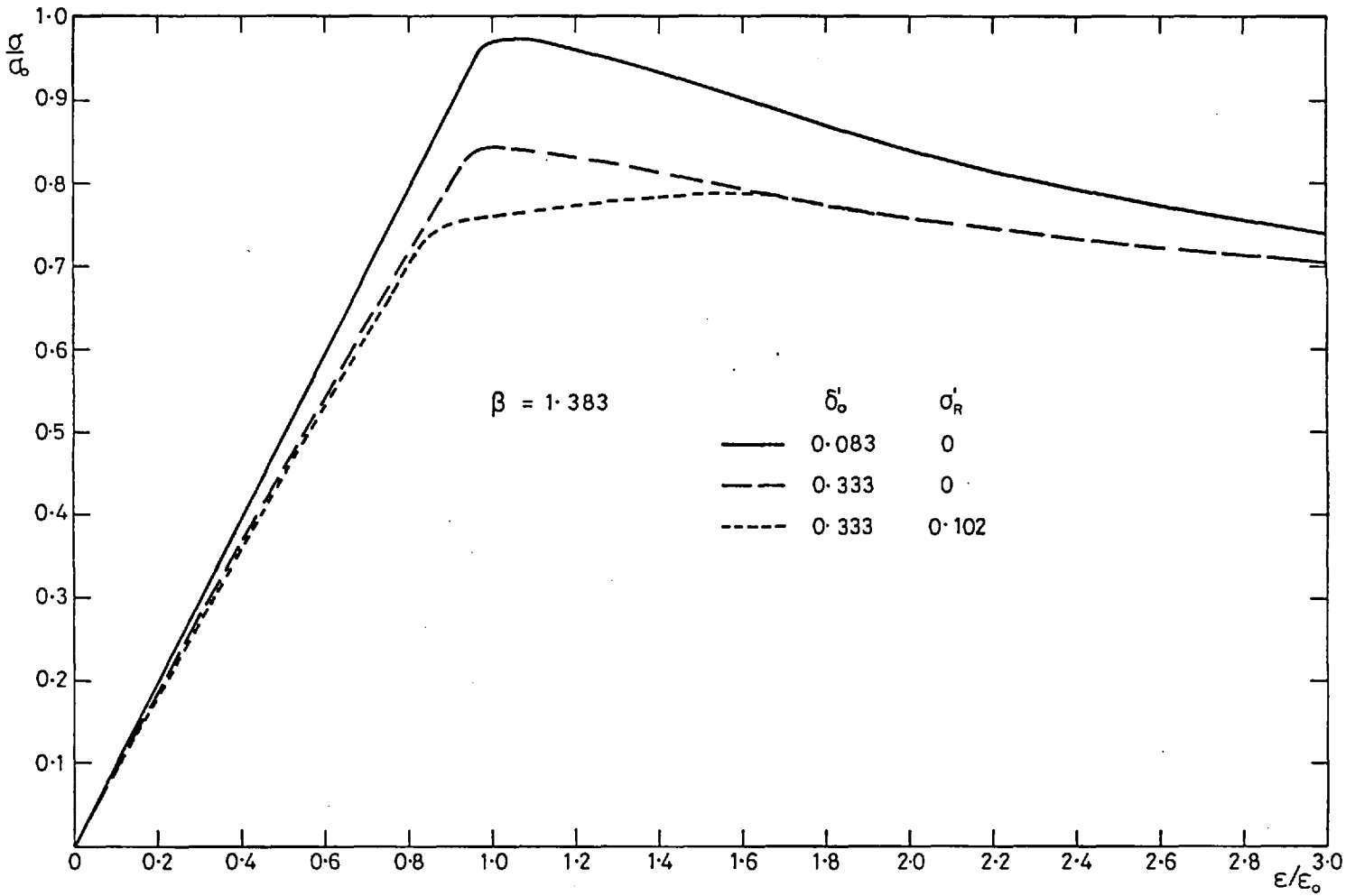

Fig. 5.3 Average Stress-Strain Curves for Plate in Compression with Constrained Edges.
Effect of Varying Initial Imperfections.

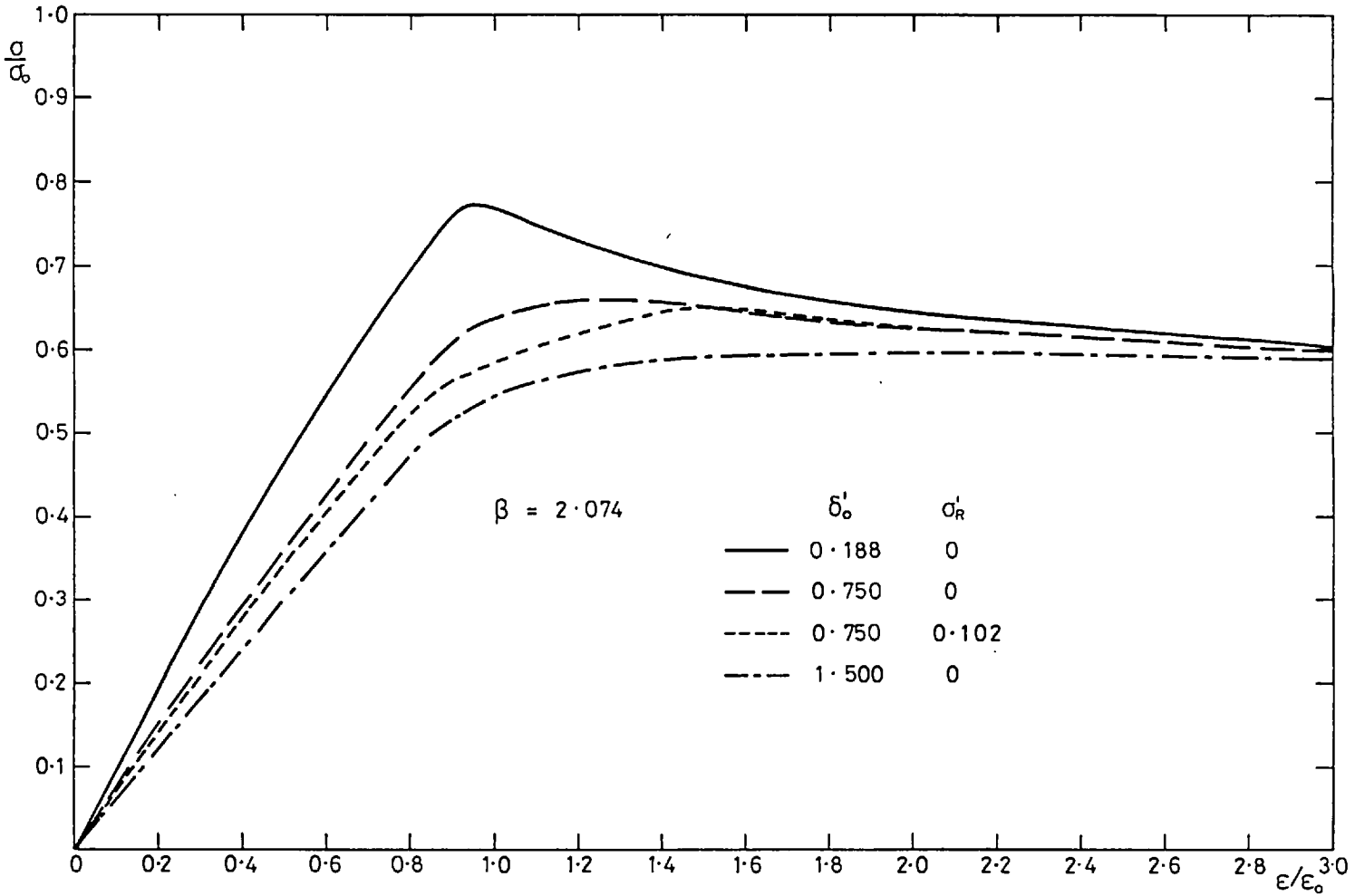

Fig. 5.4 Average Stress-Strain Curves for Plate in Compression with Constrained Edges.

Effect of Varying Initial Imperfections

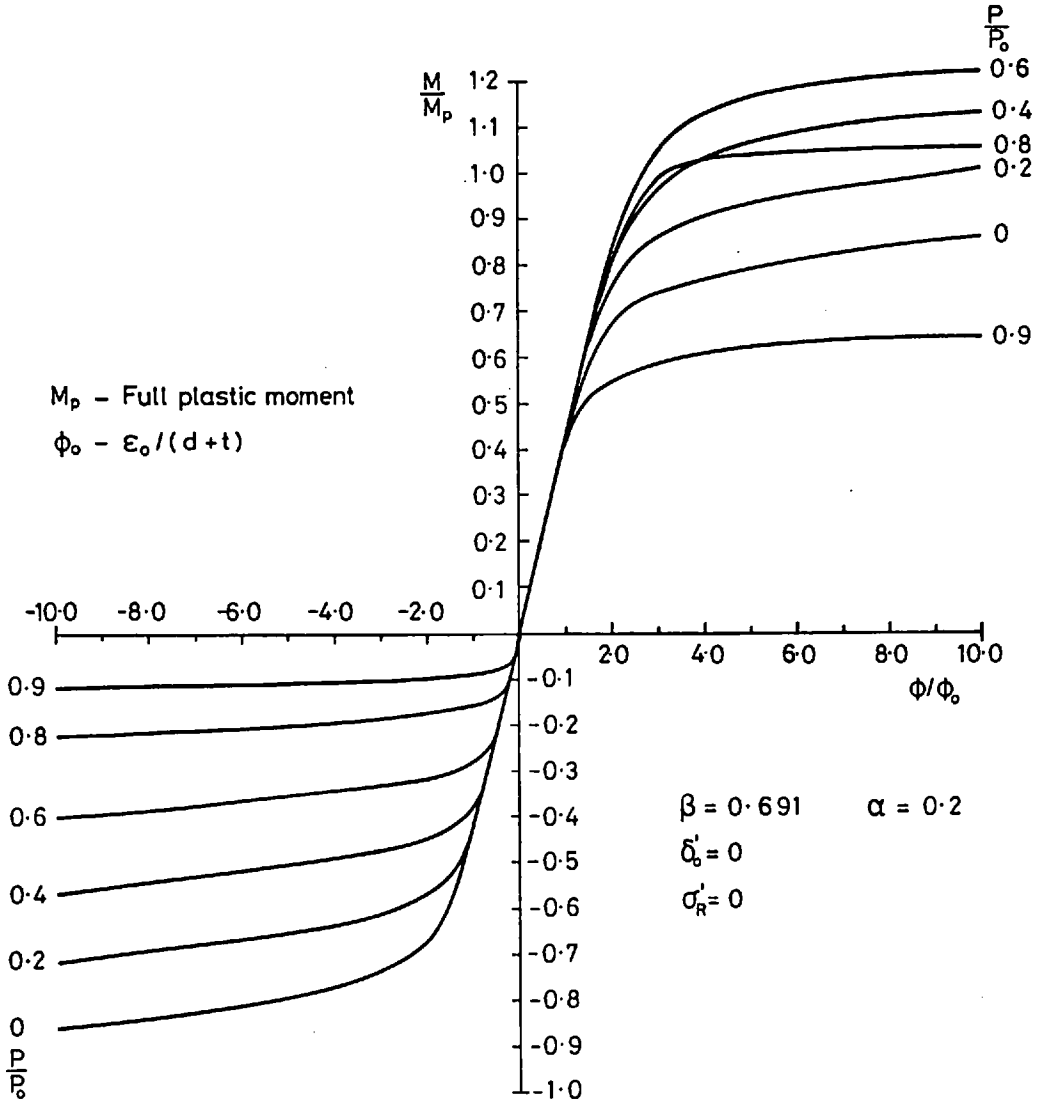

Fig. 5.5a Moment-Thrust-Curvature Relationships

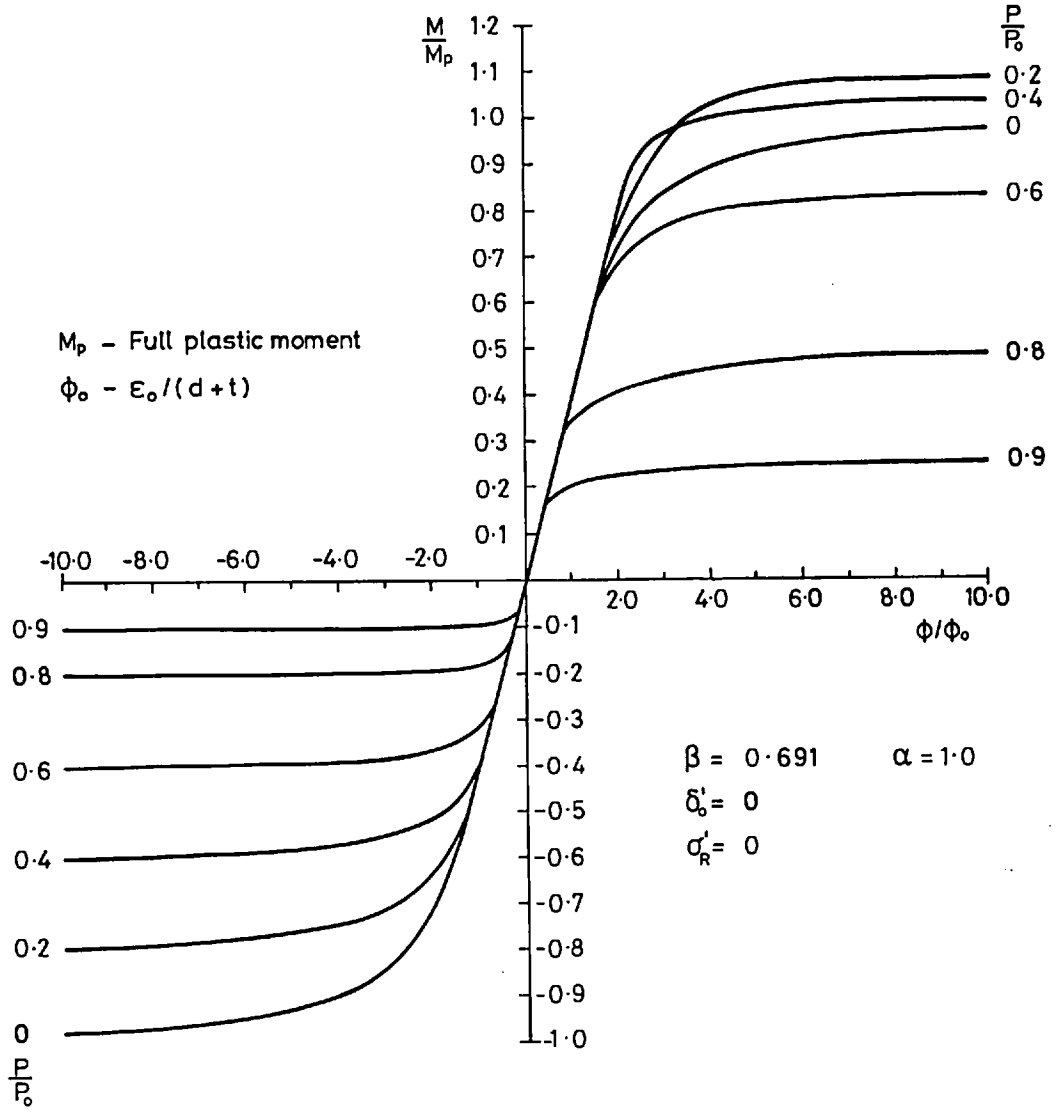

Fig. 5.5b Moment – Thrust – Curvature Relationships

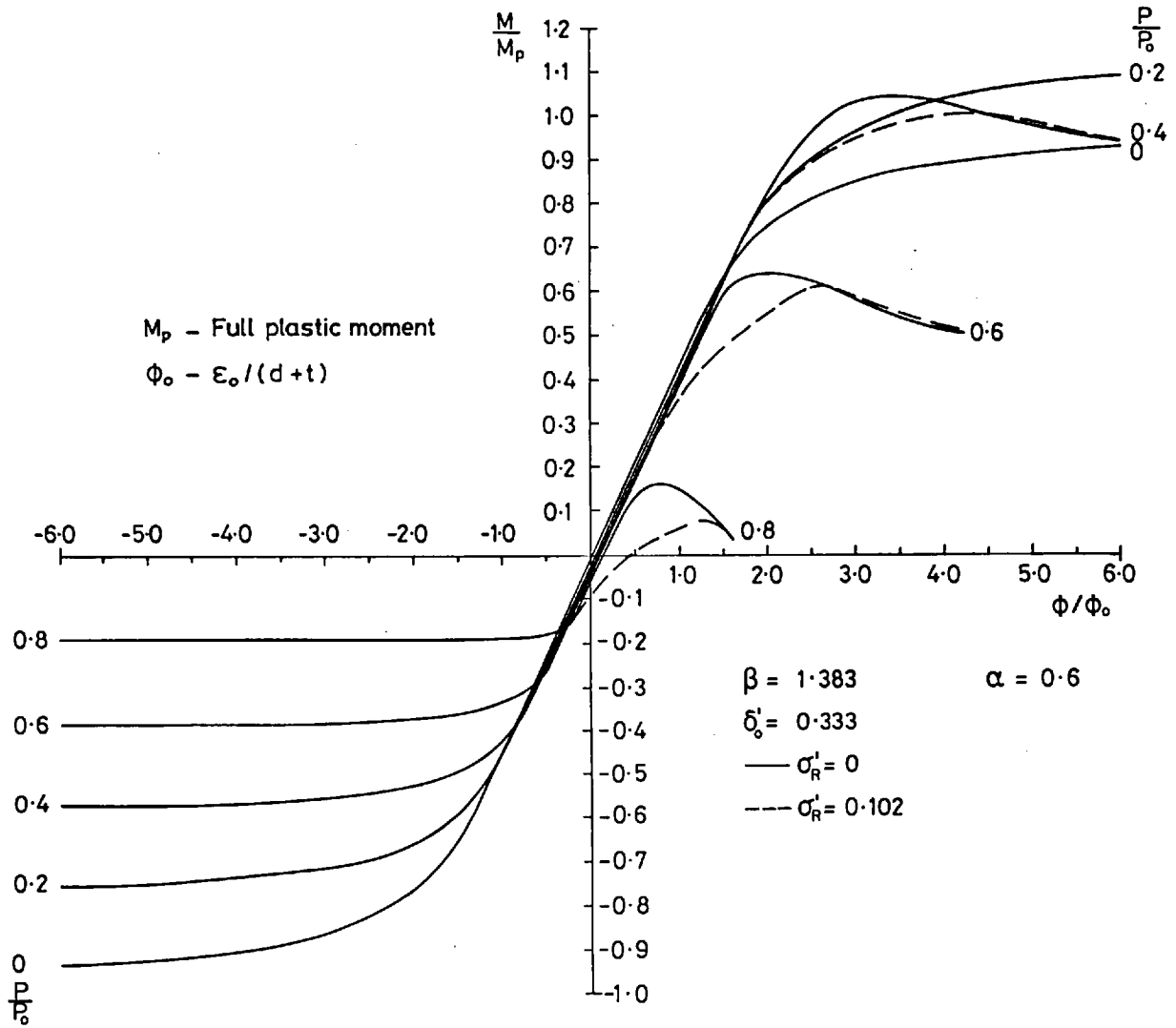

Fig. 5.6 Moment – Thrust – Curvature Relationships

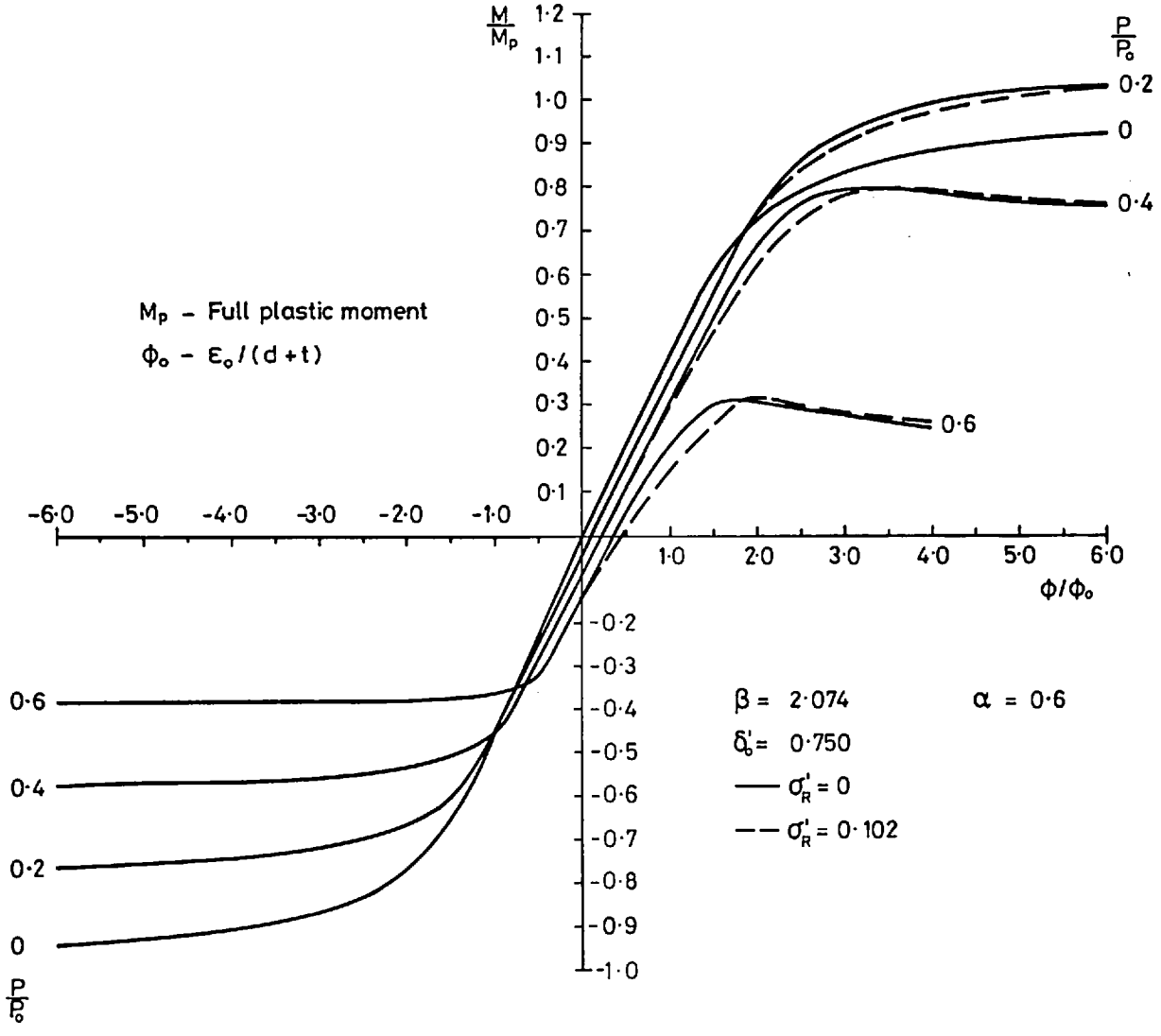

Fig. 5.7 Moment – Thrust – Curvature Relationships

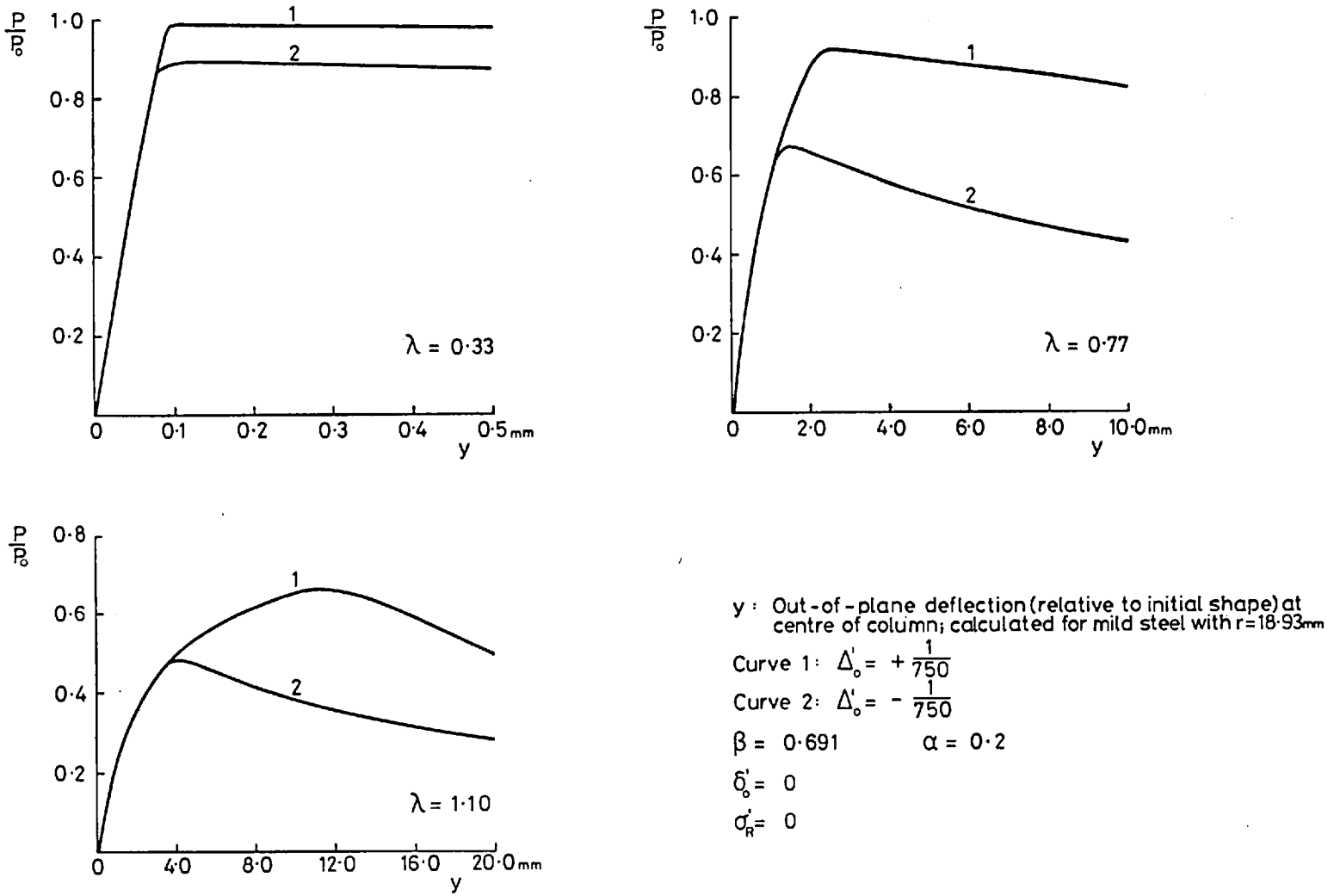

y : Out-of-plane deflection (relative to initial shape) at centre of column; calculated for mild steel with r=18·93mm

Curve 1: $\Delta_o' = +\frac{1}{750}$

Curve 2: $\Delta_o' = -\frac{1}{750}$

$\beta = 0{\cdot}691$ $\alpha = 0{\cdot}2$

$\delta_o' = 0$

$\sigma_R' = 0$

Fig. 5.8 Load-Deflection Curves for One-Span Columns.

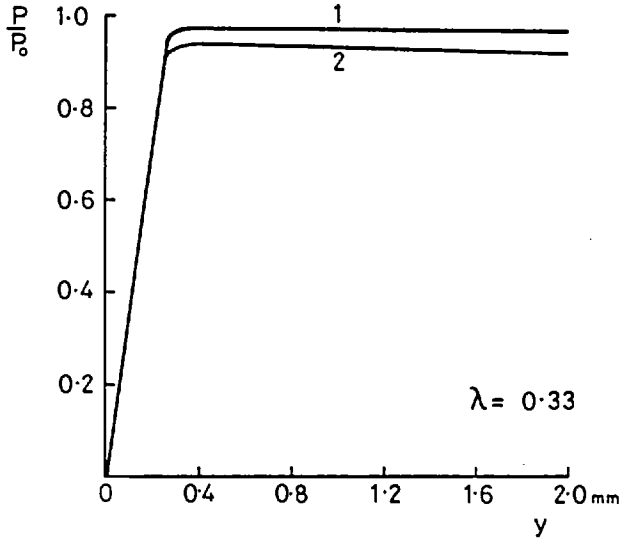

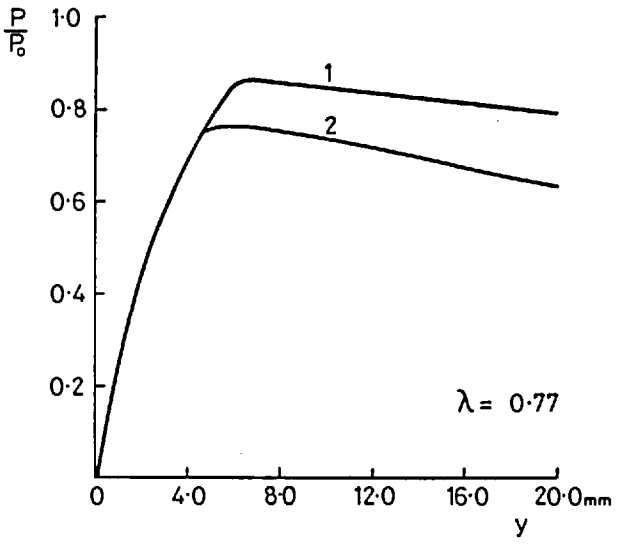

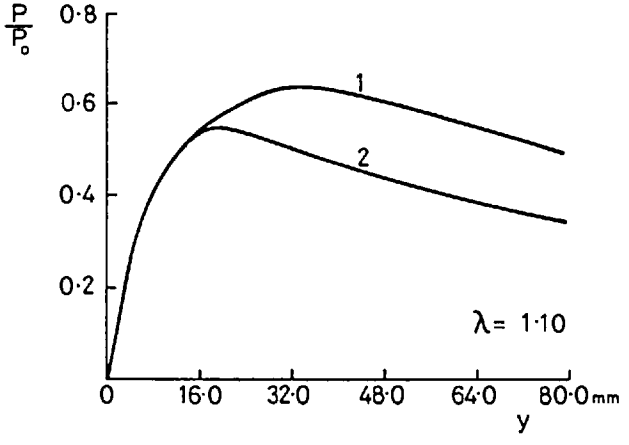

y : Out-of-plane deflection (relative to initial shape) at centre of column; calculated for mild steel with r = 57·18mm

Curve 1 : $\Delta_o' = + \frac{1}{750}$

Curve 2 : $\Delta_o' = - \frac{1}{750}$

$\beta = 0 \cdot 691$ $\alpha = 1 \cdot 0$

$\delta_o' = 0$

$\sigma_R' = 0$

Fig. 5.9 Load - Deflection Curves for One - Span Columns

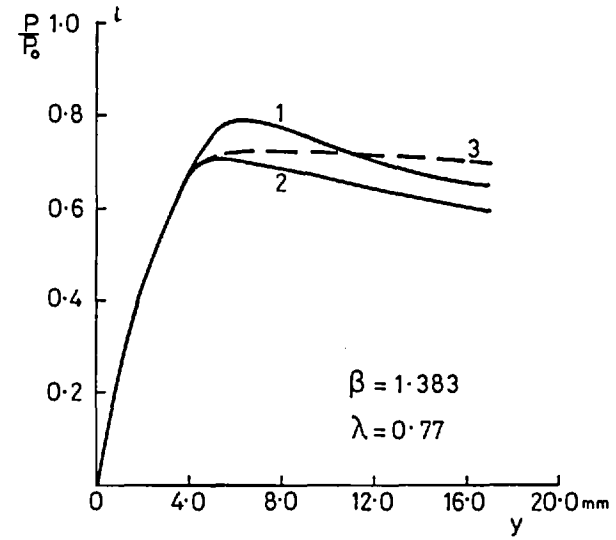

Curve	Δ_o'	δ_o'	σ_R'
1	$+\frac{1}{750}$	0·333	0
2	$-\frac{1}{750}$	0·333	0
3	$+\frac{1}{750}$	0·333	0·102

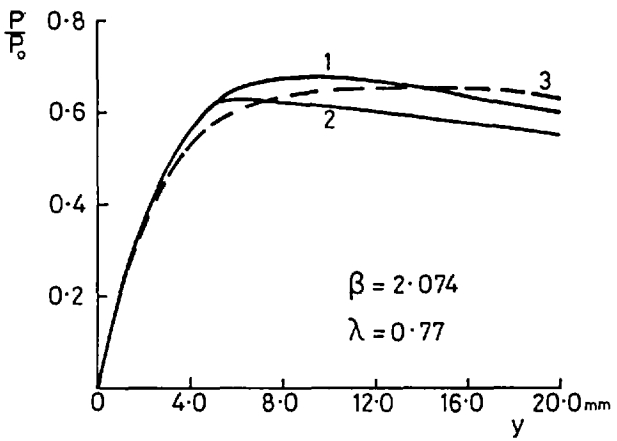

y : Out-of-plane deflection (relative to initial shape) at centre of column; calculated for mild steel with
r = 58·16mm (β = 1·383)
r = 70·67mm (β = 2·074)

Curve	Δ_o'	δ_o'	σ_R'
1	$+\frac{1}{750}$	0·750	0
2	$-\frac{1}{750}$	0·750	0
3	$+\frac{1}{750}$	0·750	0·102

Fig. 5.10 Load - Deflection Curves for One-Span Columns.

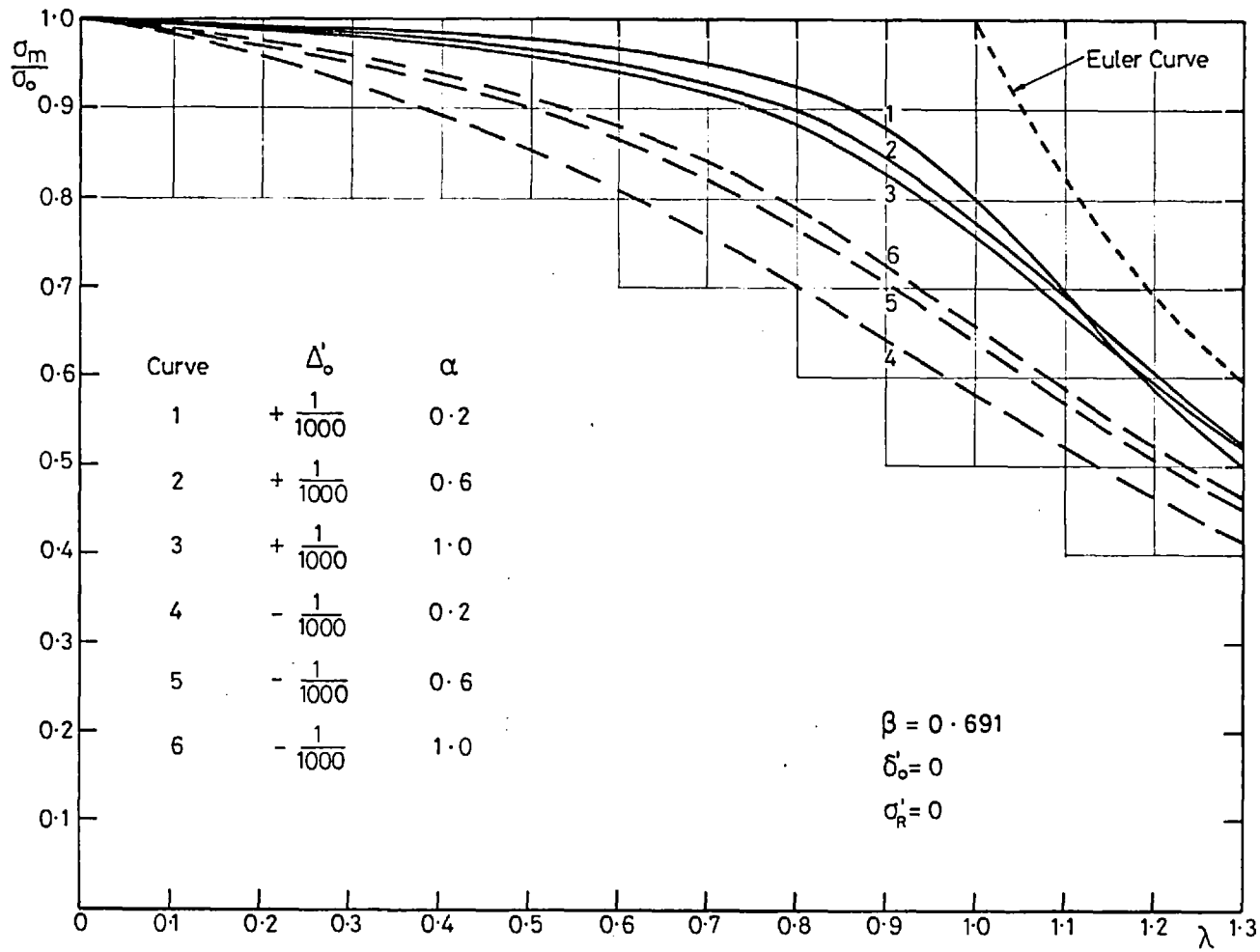

Fig. 5.11a Maximum Strength–Slenderness Curves for One-Span Columns

Effect of Varying Stiffener Area

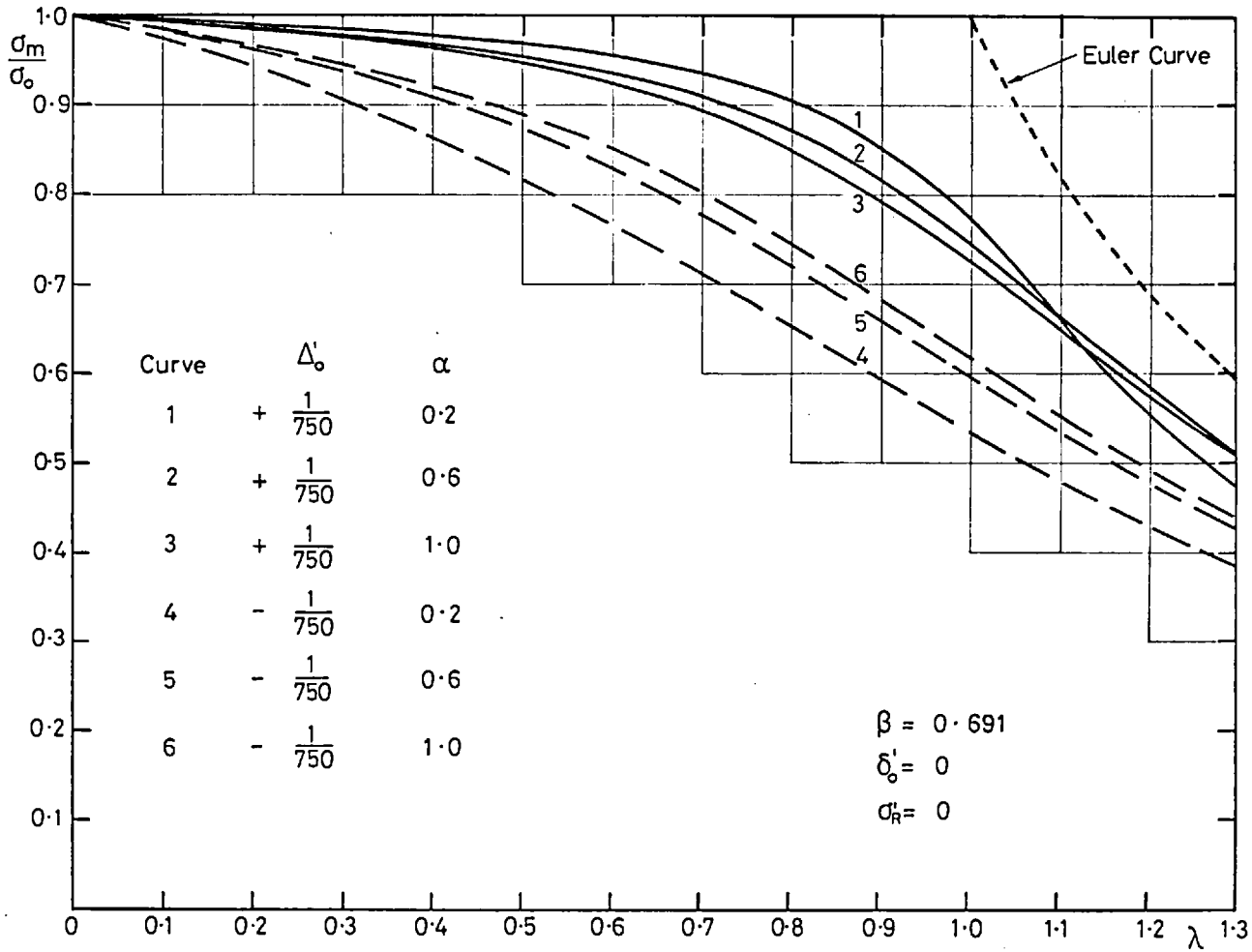

Fig. 5.11b Maximum Strength-Slenderness Curves for One-Span Columns

Effect of Varying Stiffener Area

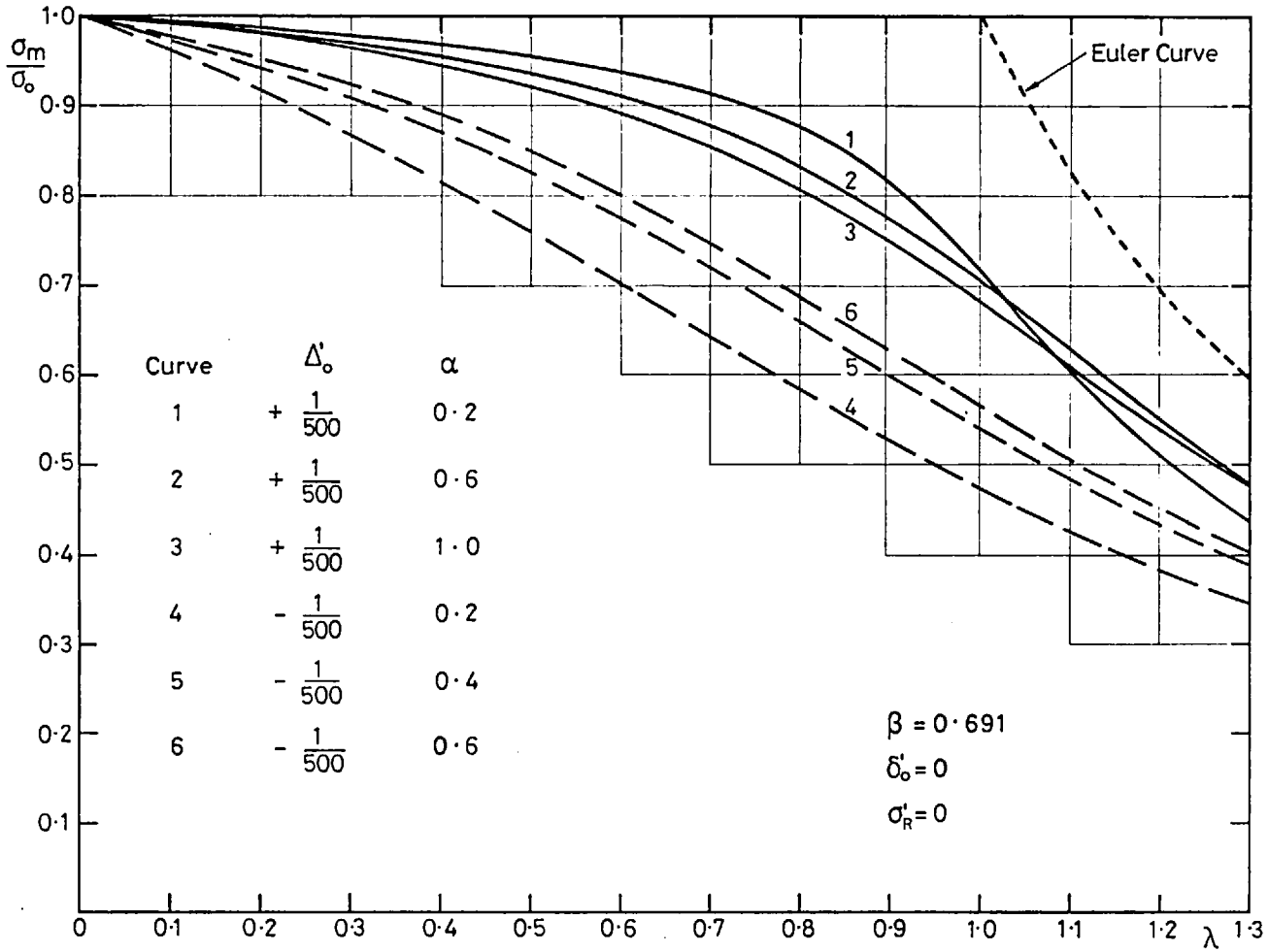

Fig. 5.11c Maximum Strength-Slenderness Curves for One-Span Columns

Effect of Varying Stiffener Area

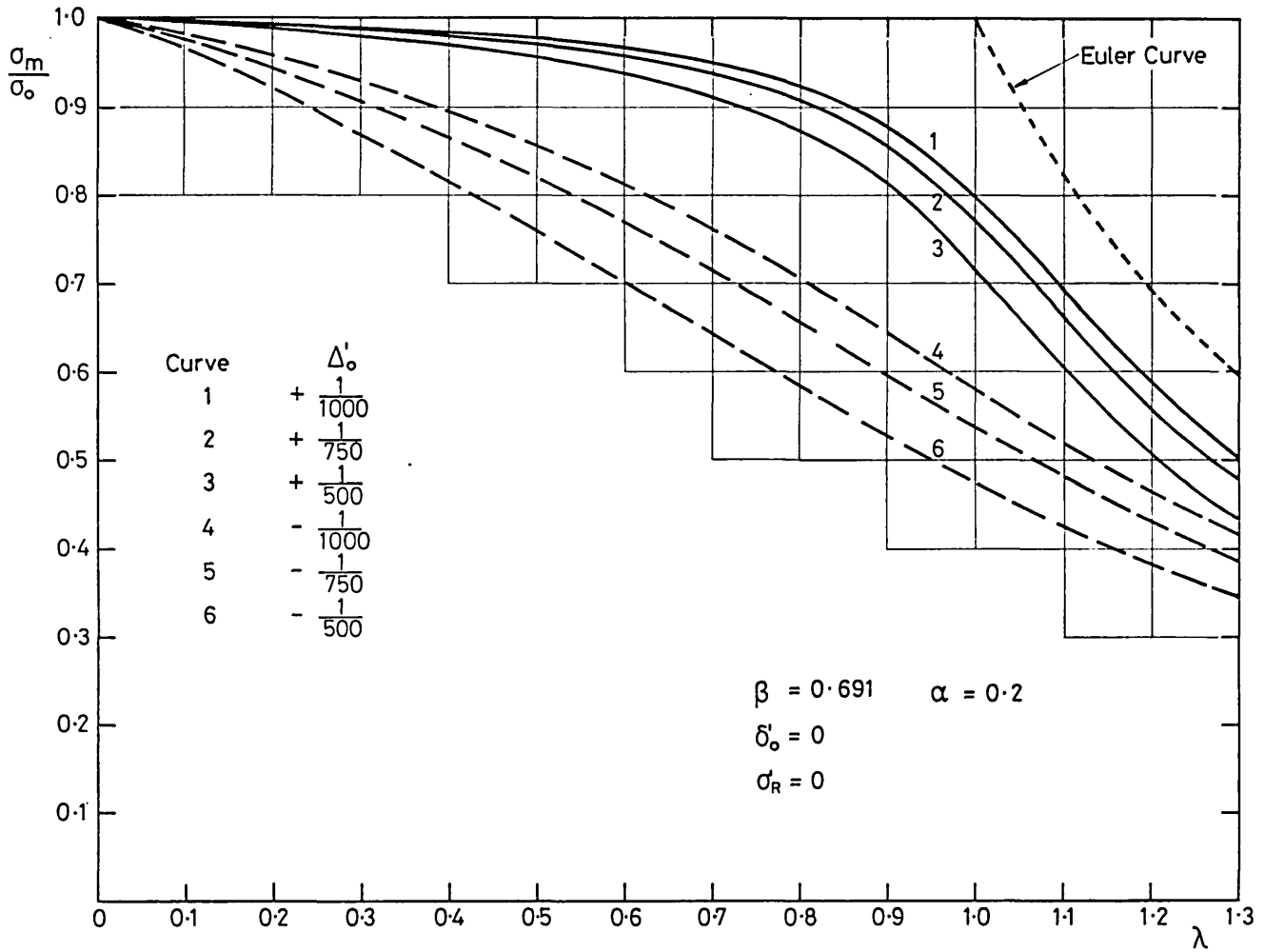

Fig. 5.12a Maximum Strength-Slenderness Curves for One-Span Columns

Effect of Varying Stiffener Initial Deflections

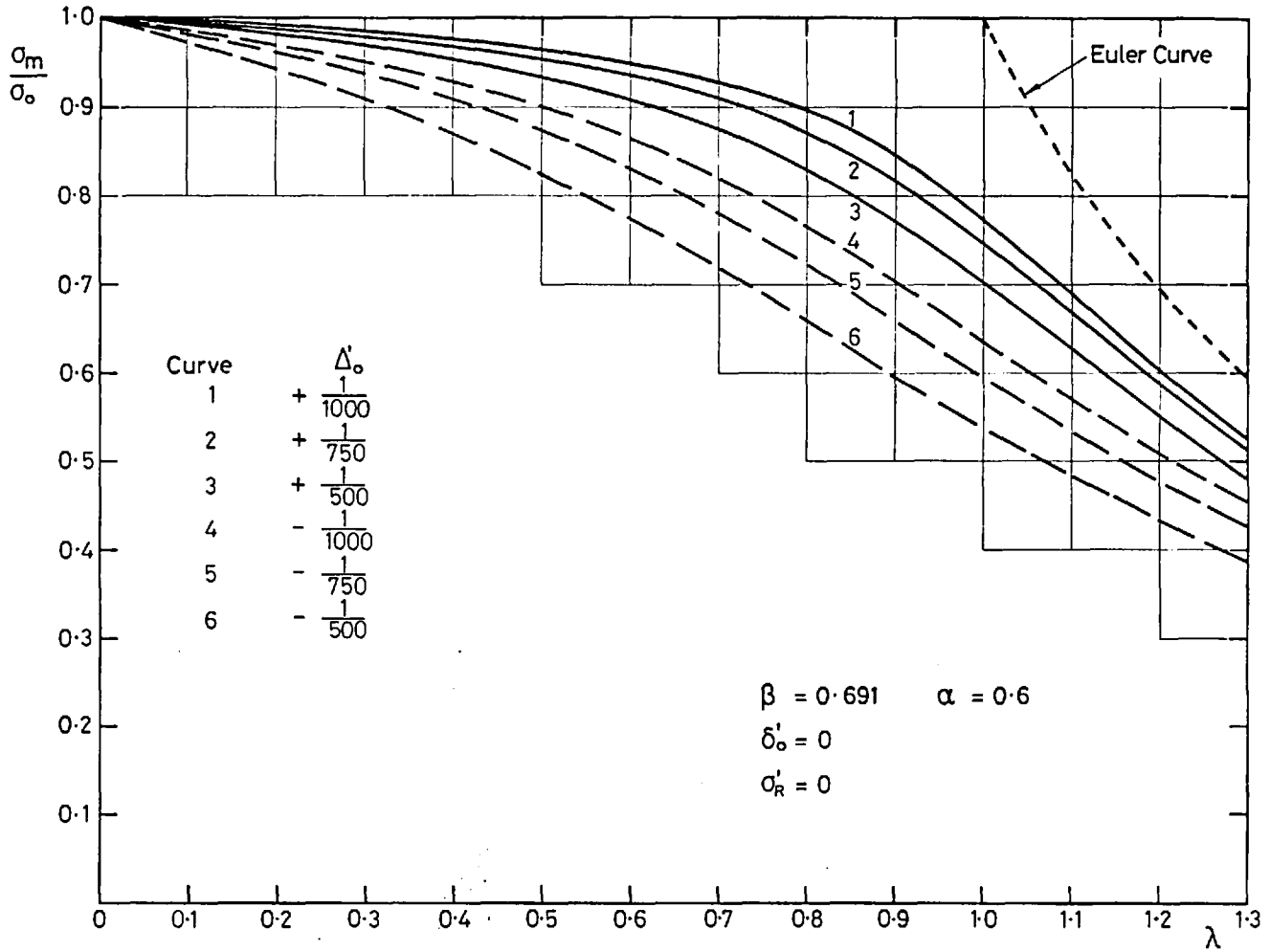

Fig. 5.12 b Maximum Strength-Slenderness Curves for One-Span Columns

Effect of Varying Stiffener Initial Deflections

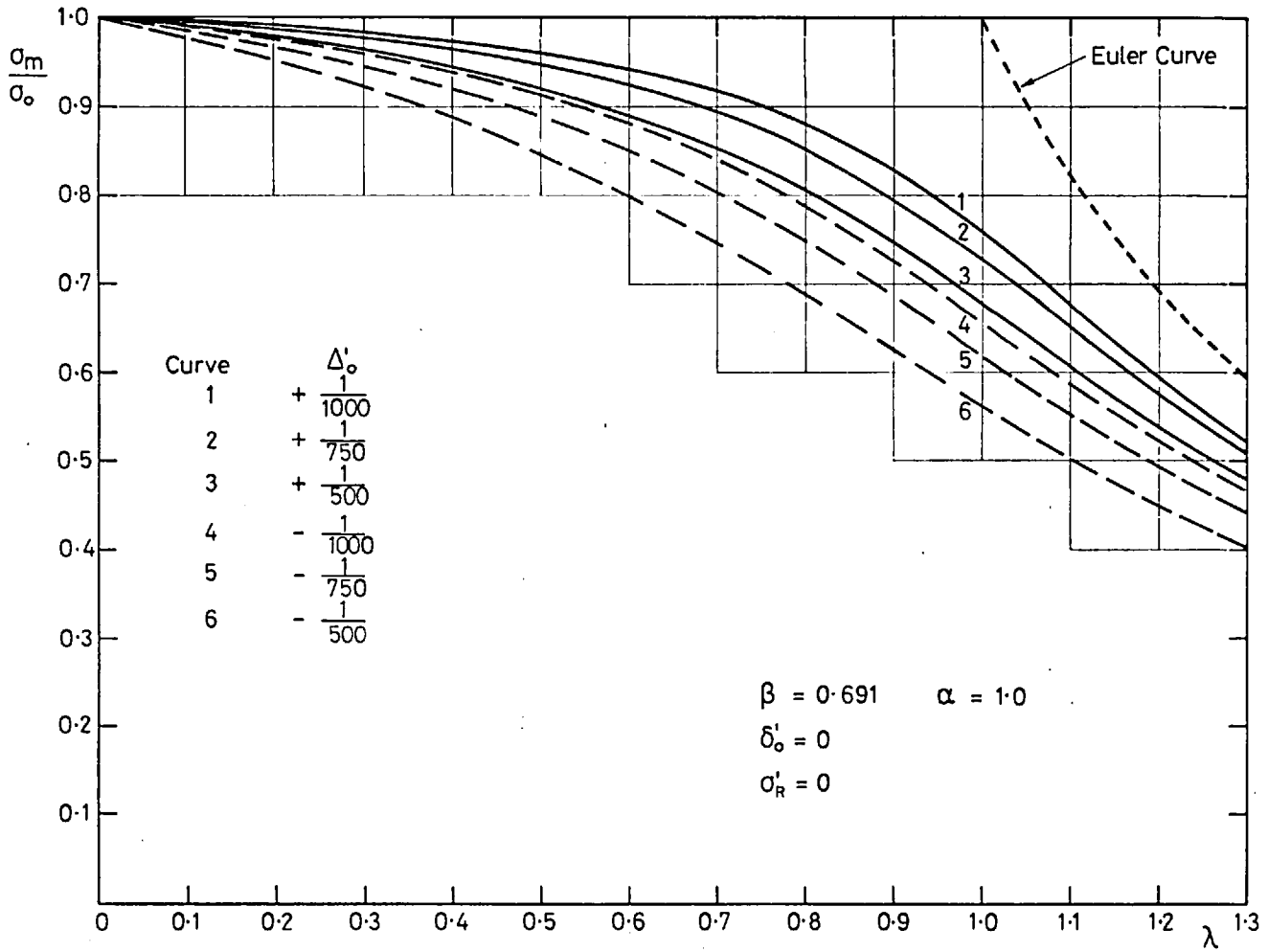

Fig. 5.12c Maximum Strength-Slenderness Curves for One-Span Columns

Effect of Varying Stiffener Initial Deflections

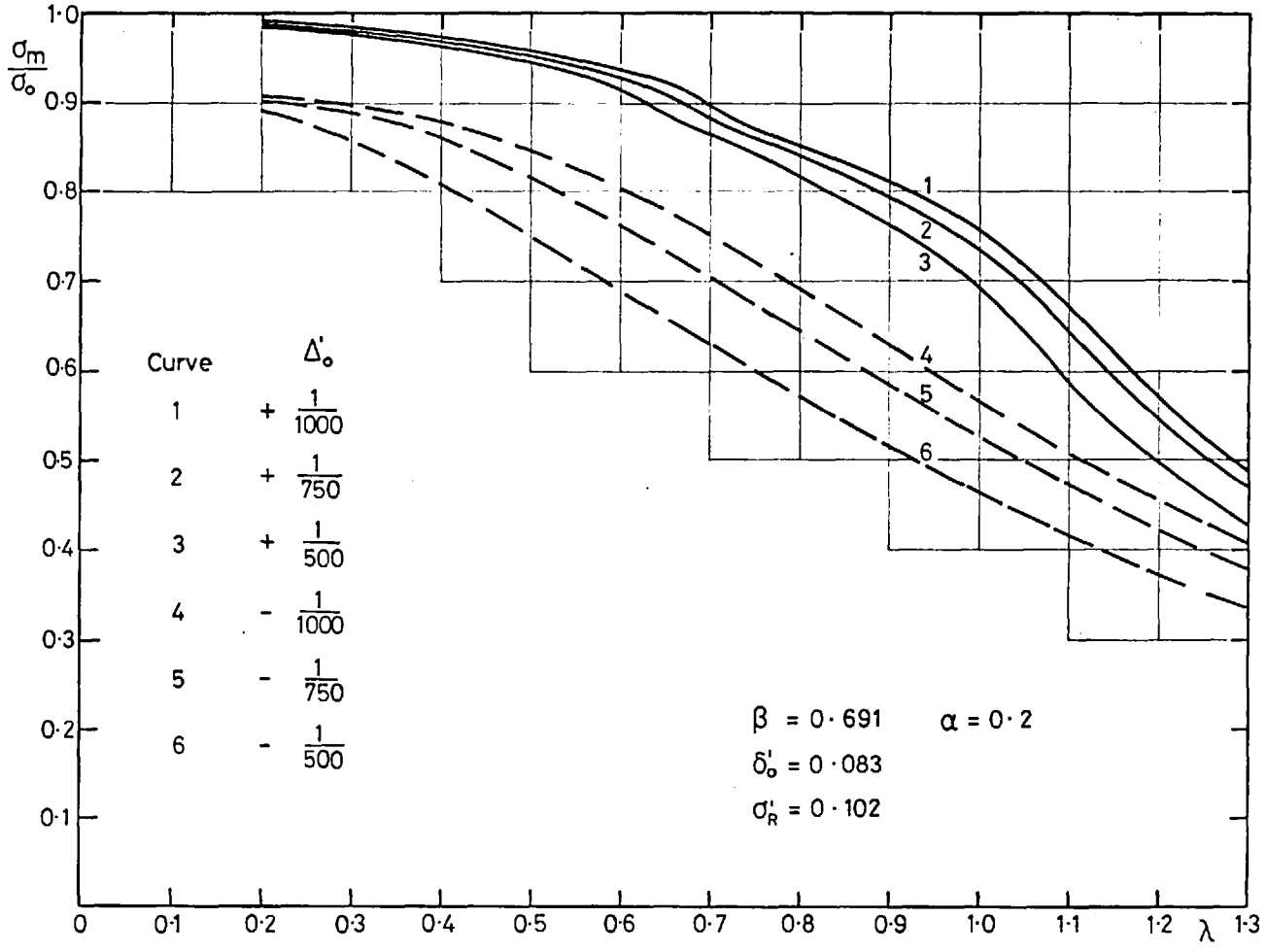

Fig. 5.13a Maximum Strength–Slenderness Curves for One-Span Columns

Effect of Varying Stiffener Initial Deflections

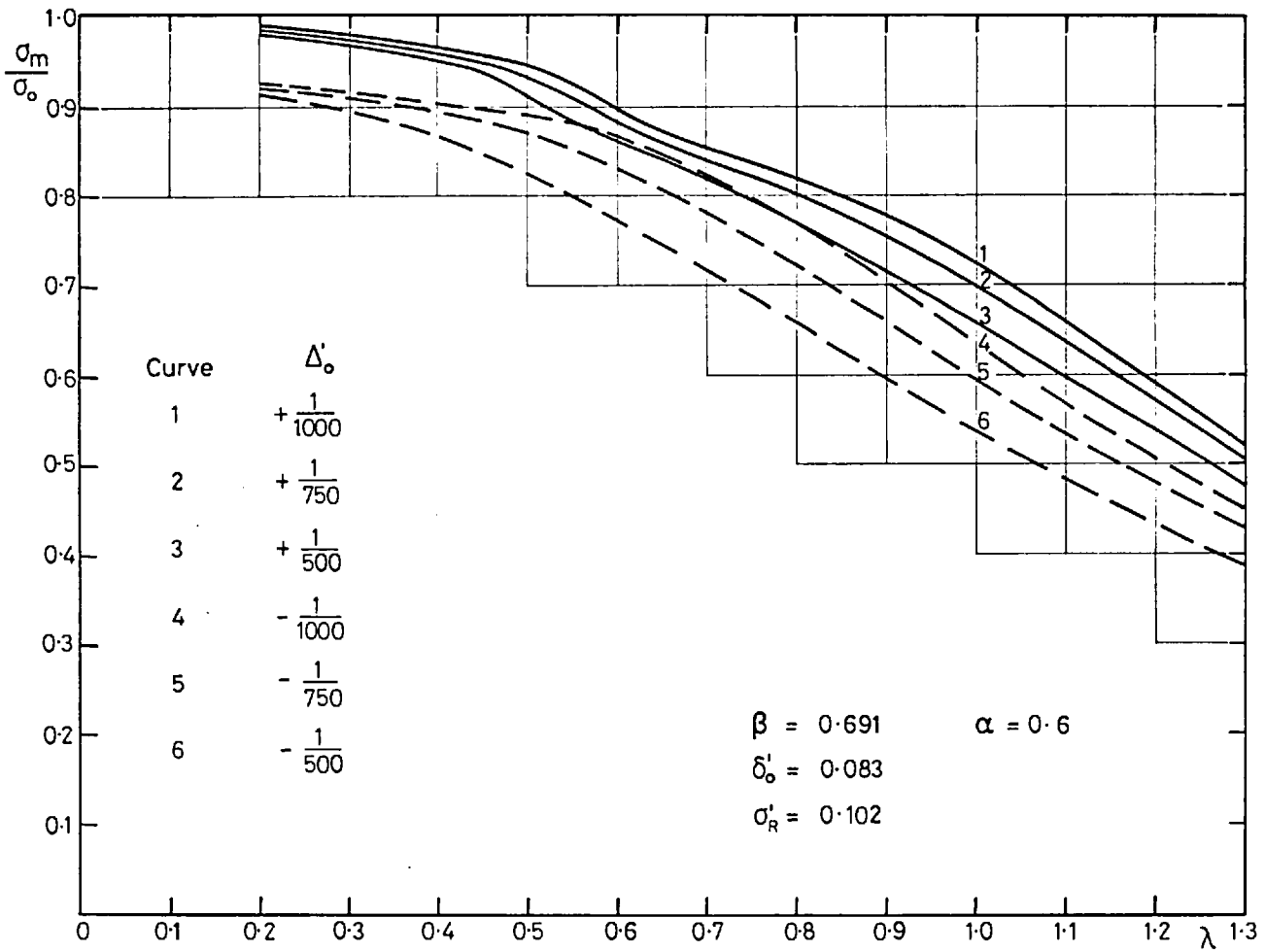

Fig. 5.13b Maximum Strength–Slenderness Curves for One-Span Columns

Effect of Varying Stiffener Initial Deflections

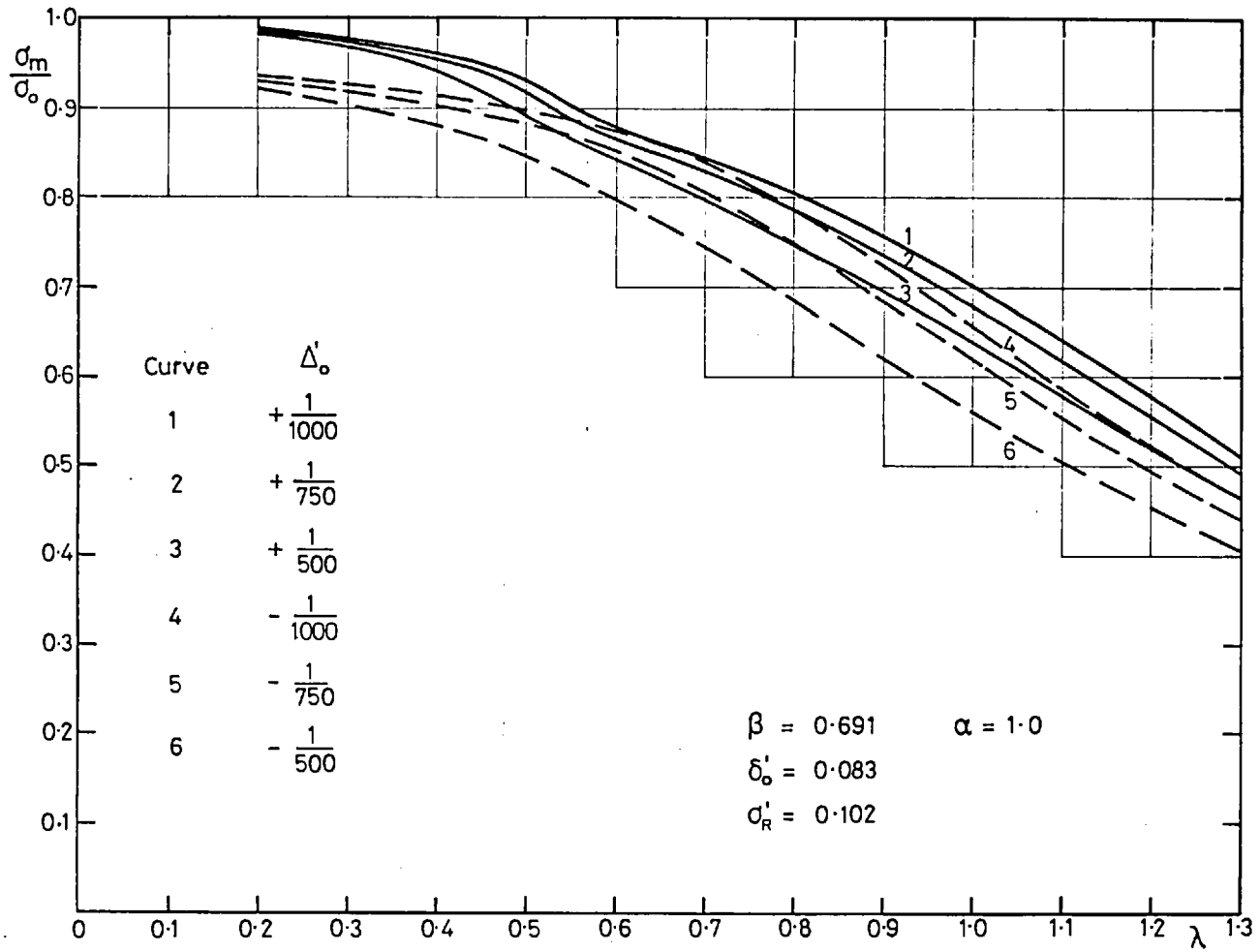

Fig. 5.13c Maximum Strength-Slenderness Curves for One-Span Columns

Effect of Varying Stiffener Initial Deflections

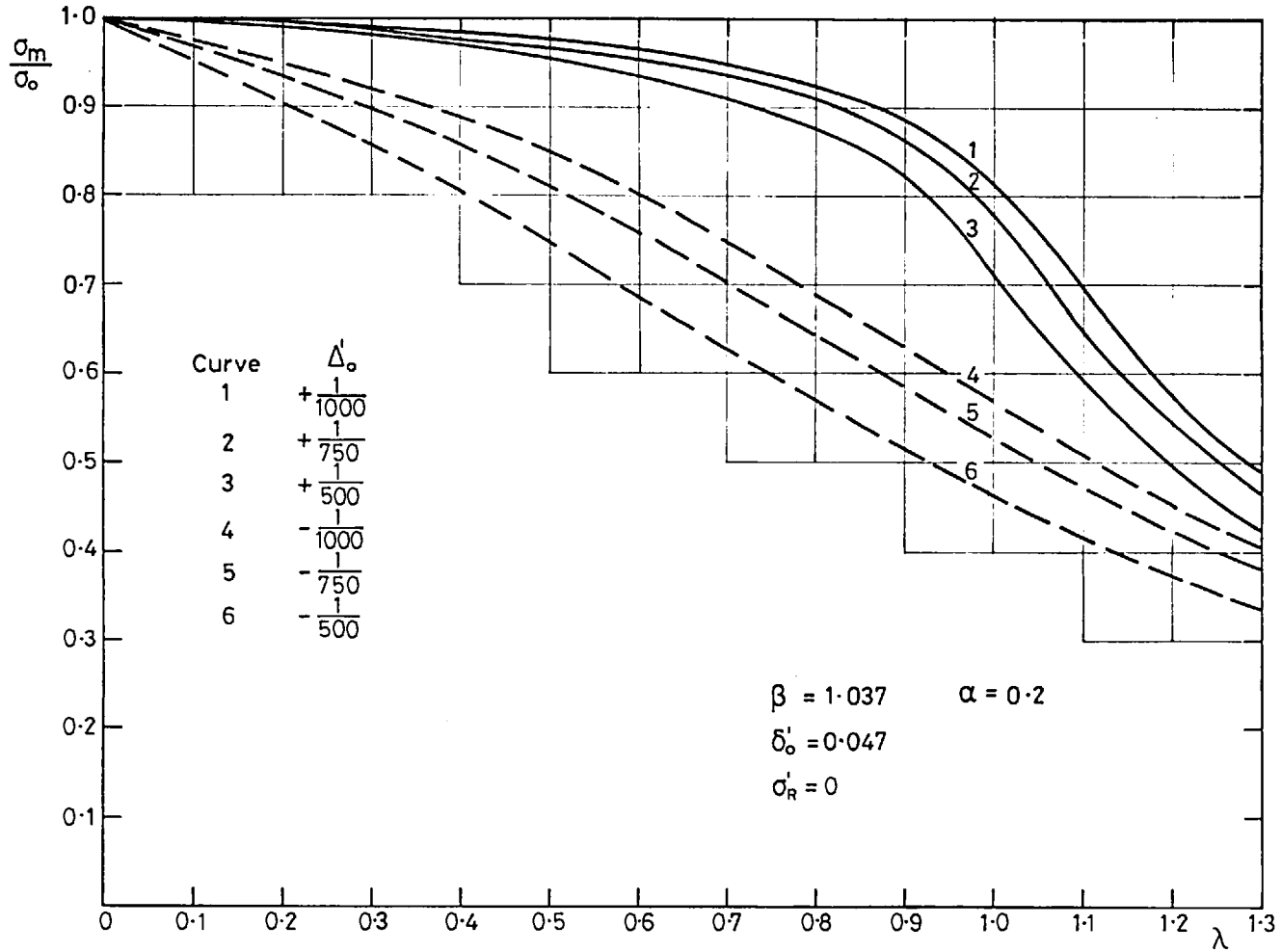

Fig. 5.14a Maximum Strength-Slenderness Curves for One-Span Columns

Effect of Varying Stiffener Initial Deflections

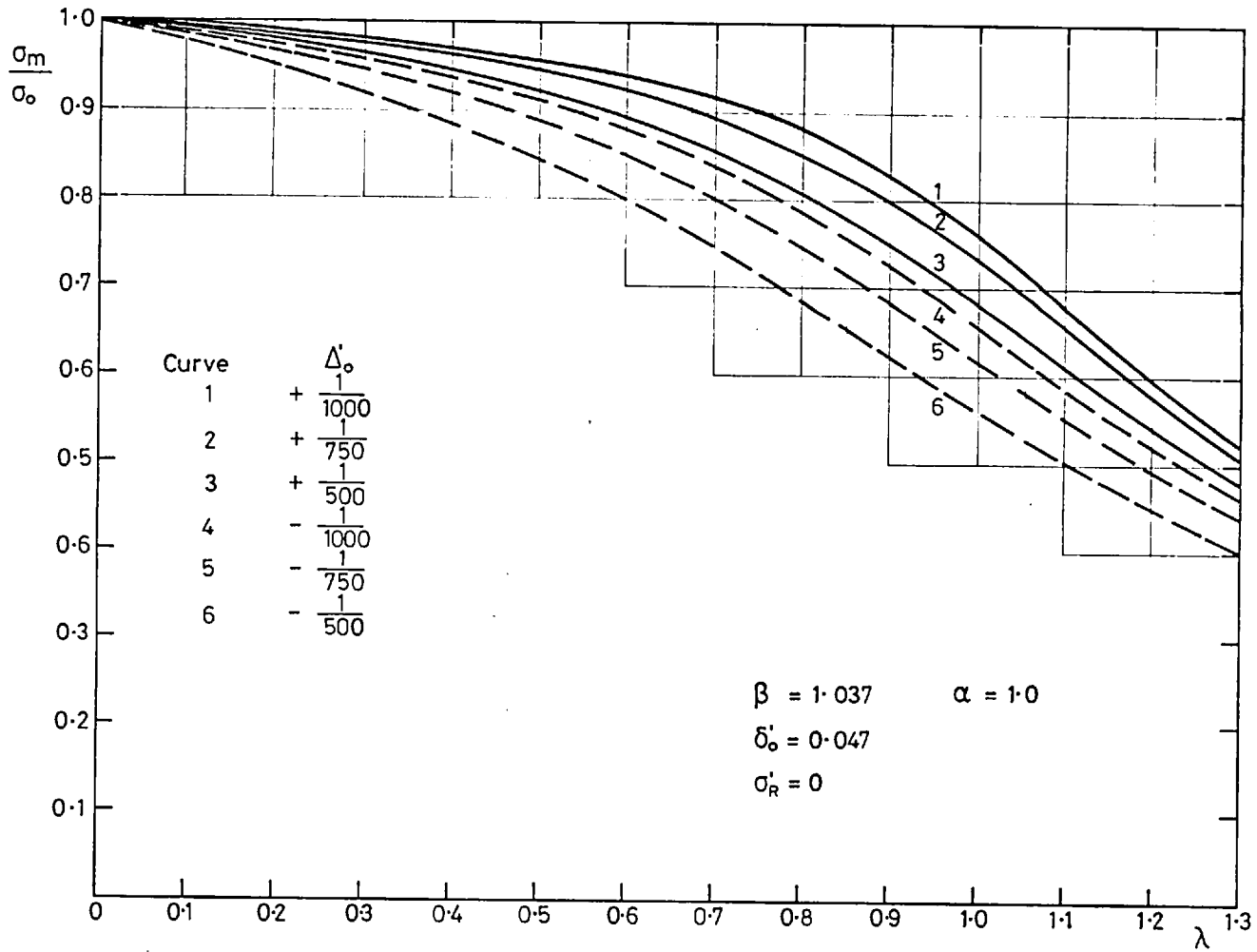

Fig. 5.14b Maximum Strength-Slenderness Curves for One-Span Columns

Effect of Varying Stiffener Initial Deflections

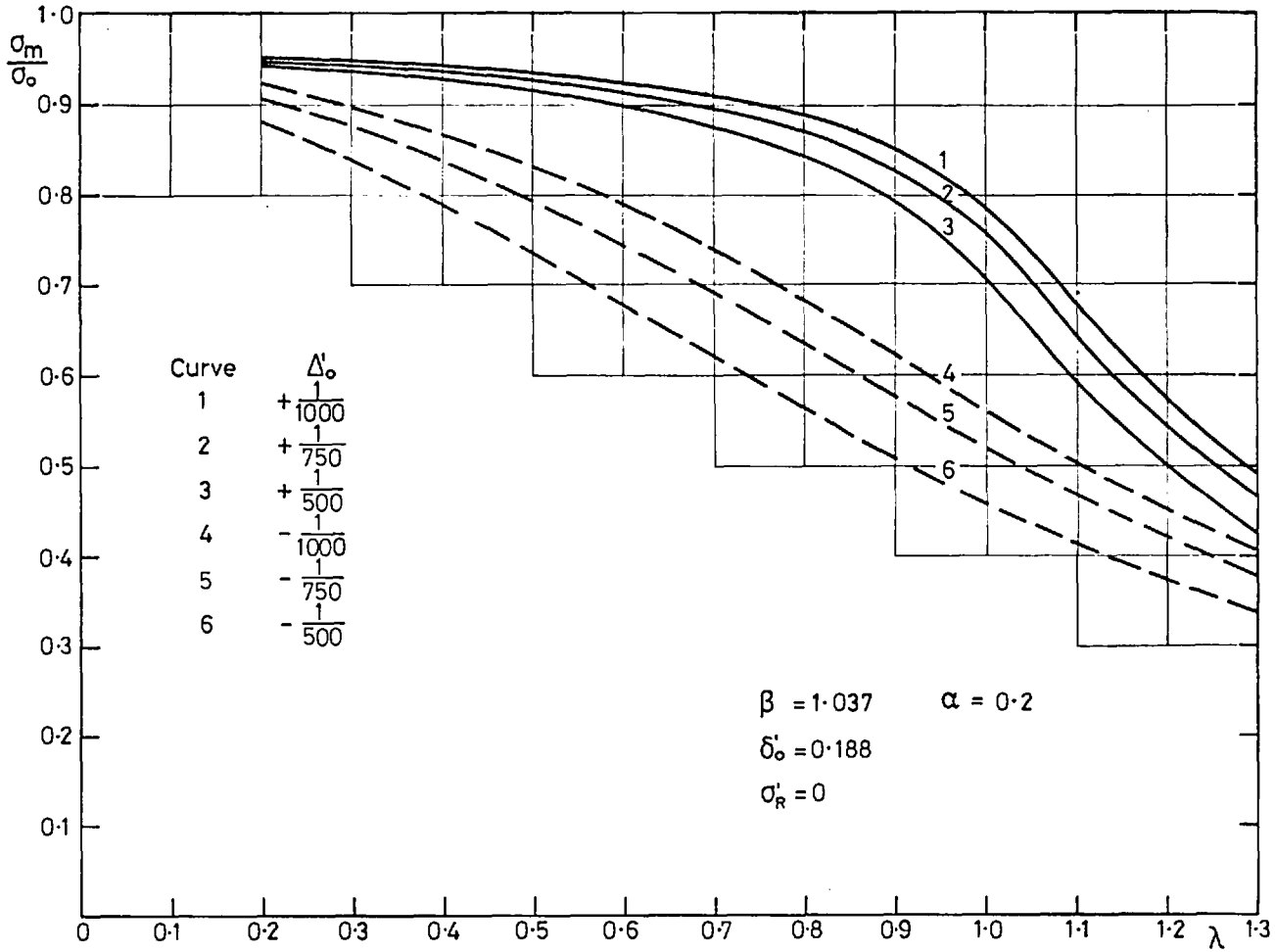

Fig. 5.15a Maximum Strength-Slenderness Curves for One-Span Columns

Effect of Varying Stiffener Initial Deflections

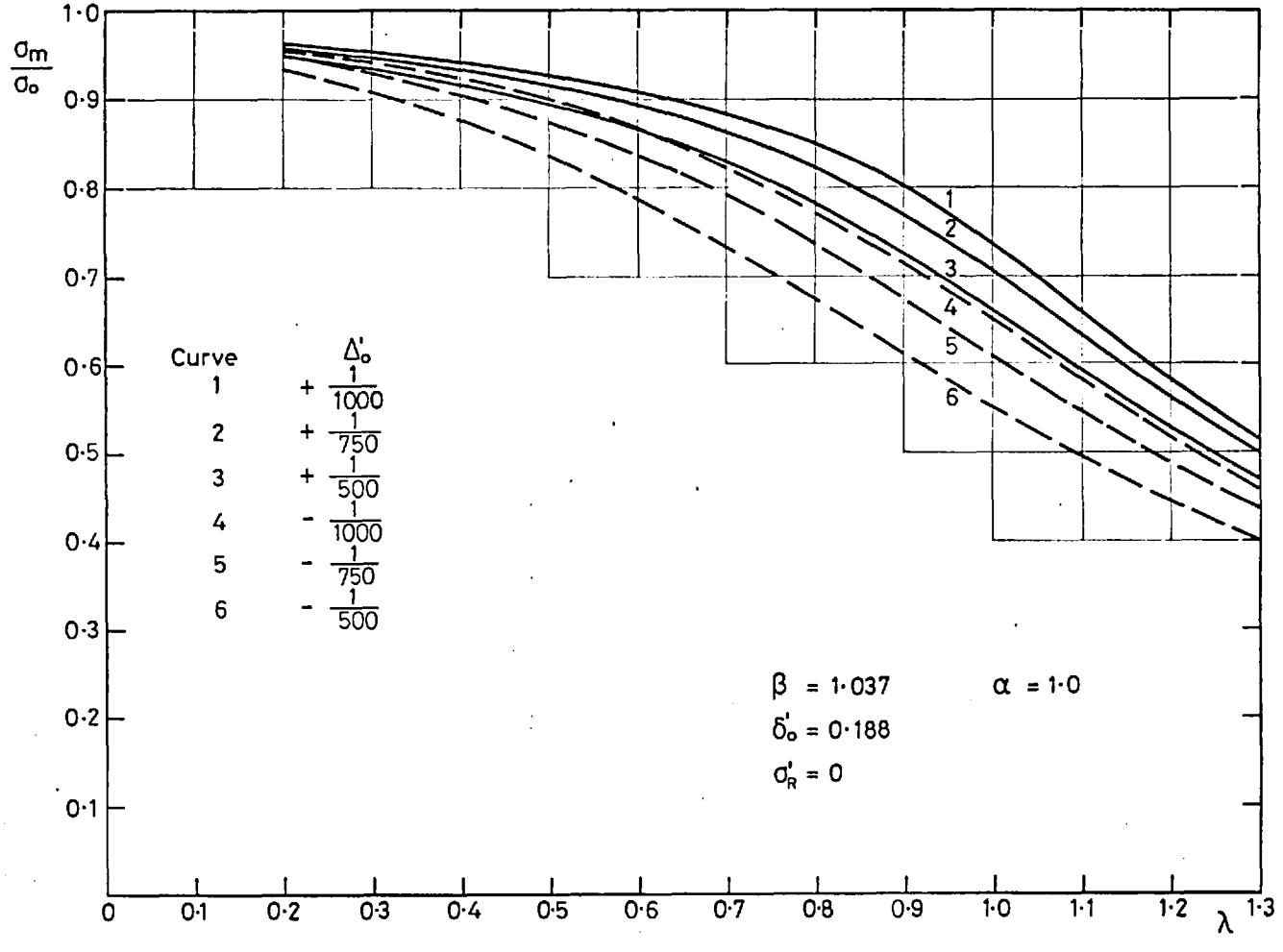

Fig.5.15b Maximum Strength-Slenderness Curves for One-Span Columns

Effect of Varying Stiffener Initial Deflections

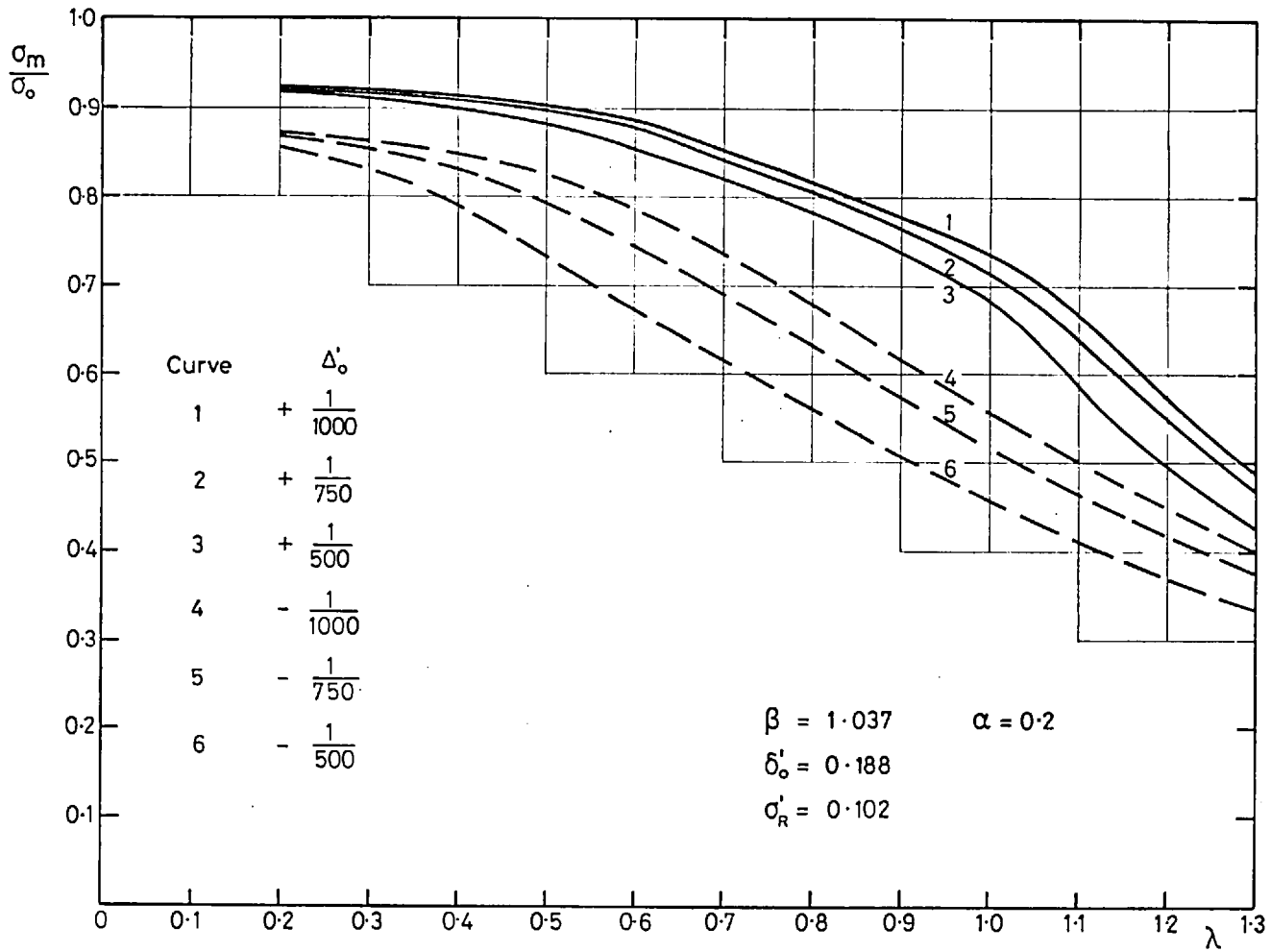

Fig. 5.16a Maximum Strength-Slenderness Curves for One-Span Columns

Effect of Varying Stiffener Initial Deflections

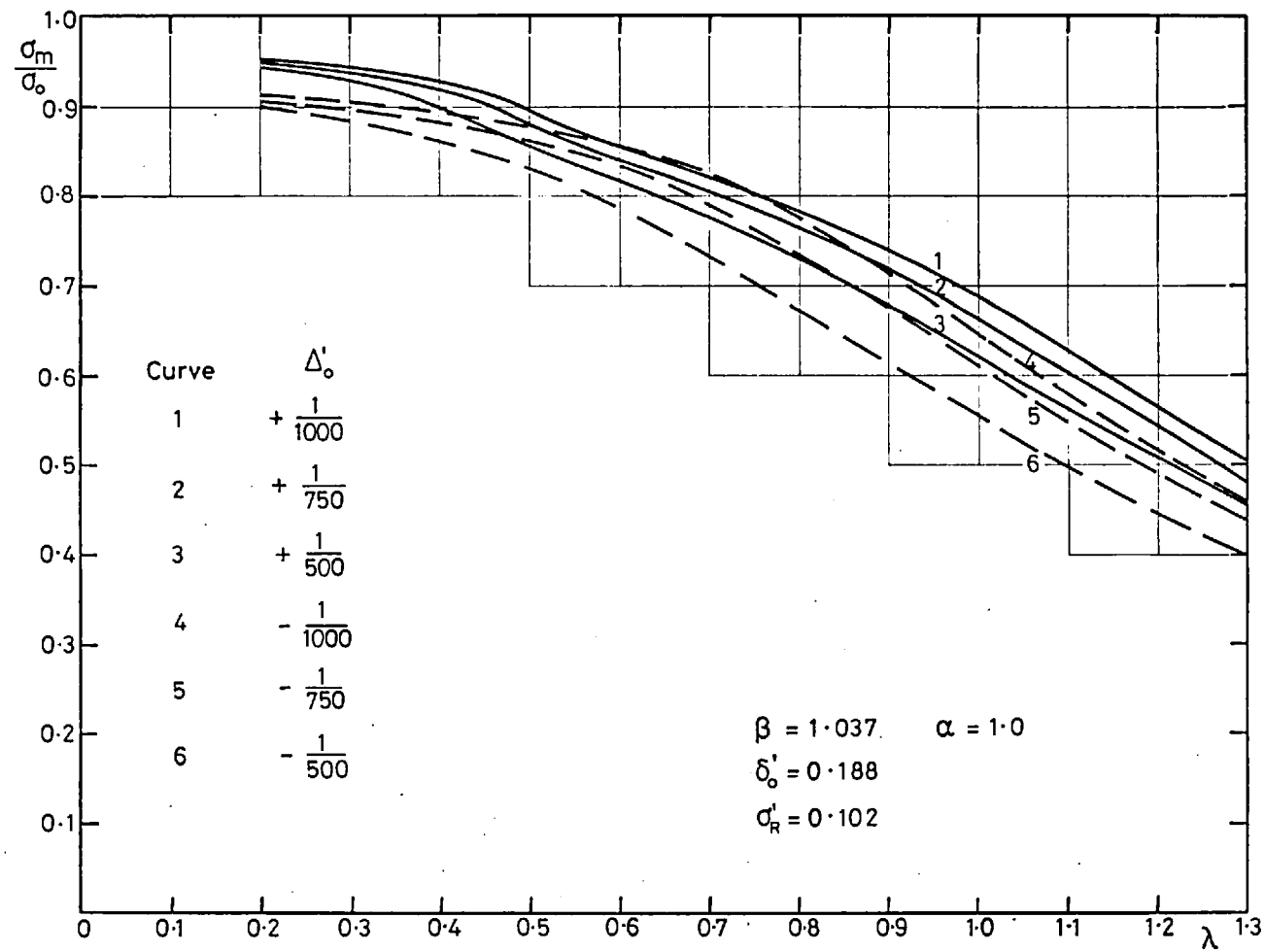

Fig. 5.16b Maximum Strength-Slenderness Curves for One-Span Columns

Effect of Varying Stiffener Initial Deflections

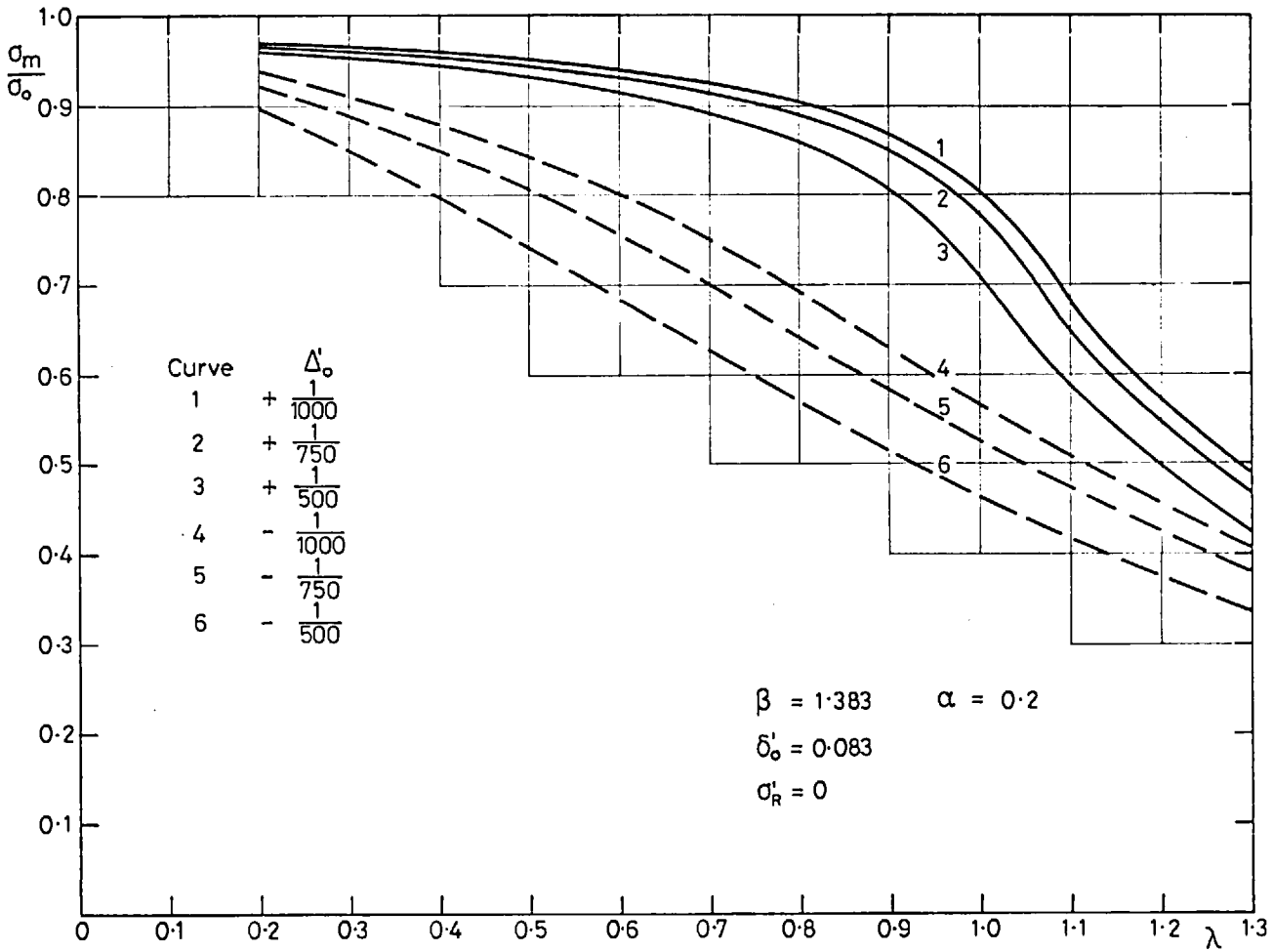

Fig. 5.17a Maximum Strength-Slenderness Curves for One-Span Columns

Effect of Varying Stiffener Initial Deflections

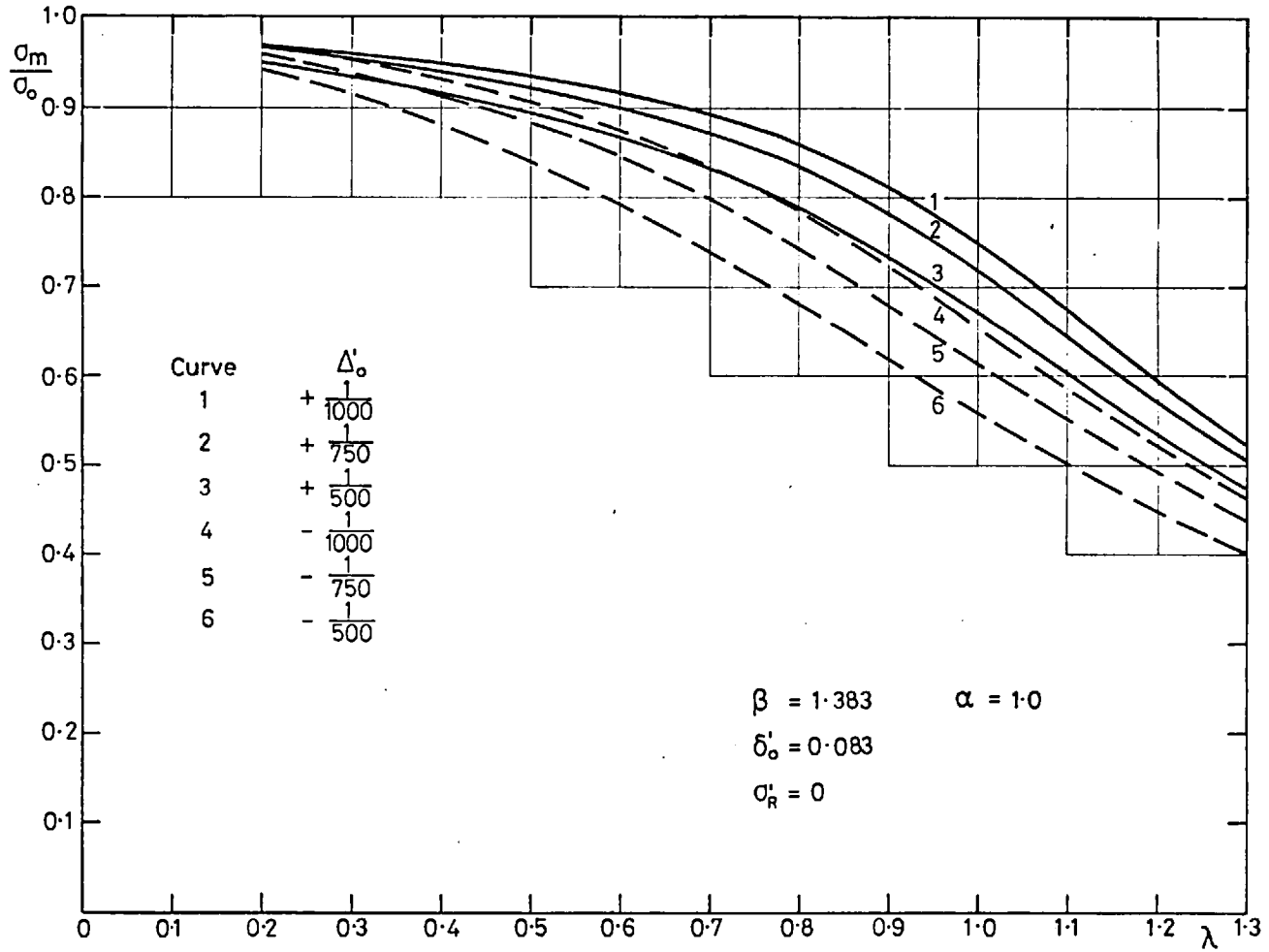

Fig. 5.17b Maximum Strength–Slenderness Curves for One-Span Columns

Effect of Varying Stiffener Initial Deflections

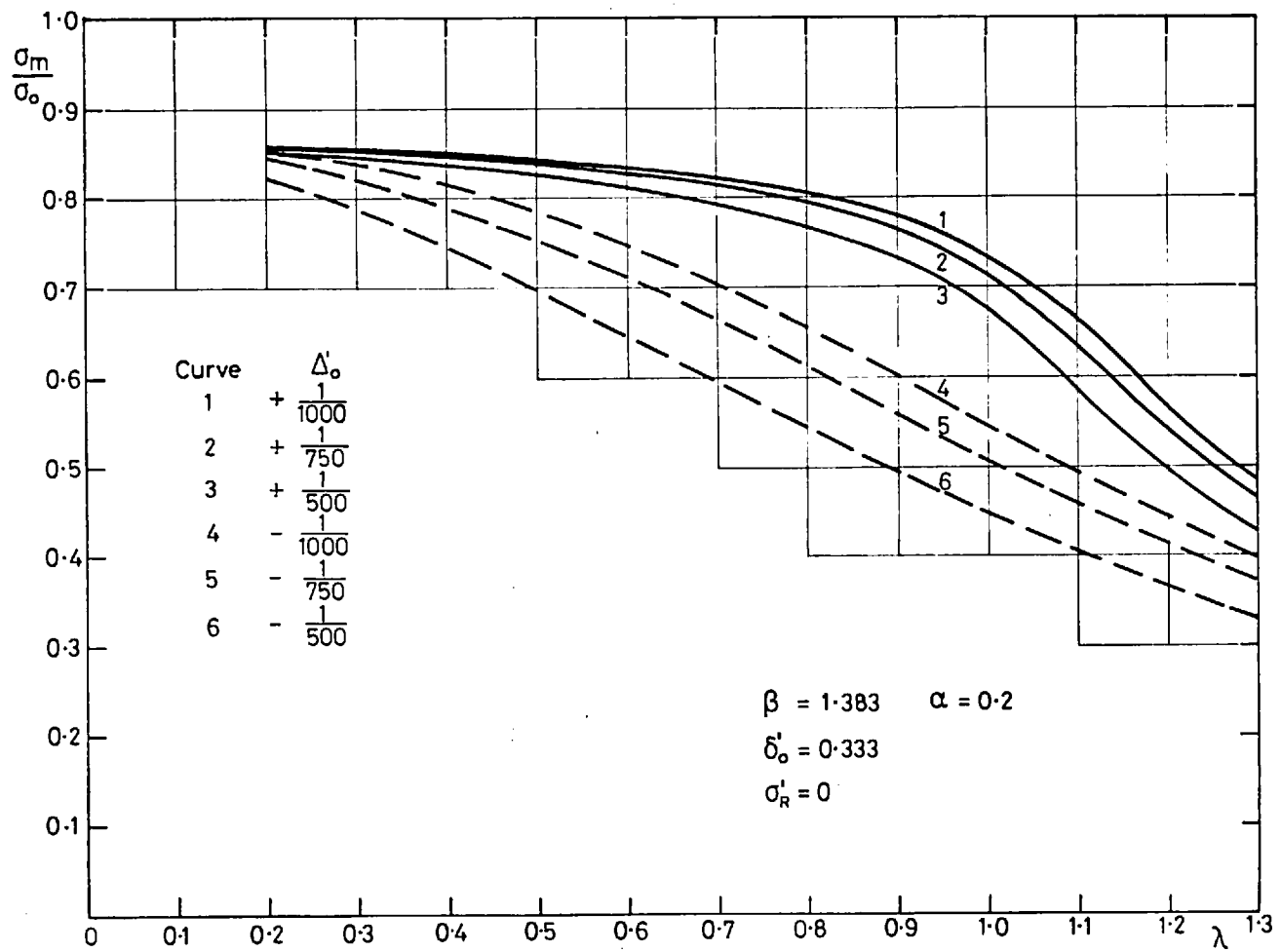

Fig. 5.18a Maximum Strength-Slenderness Curves for One-Span Columns

Effect of Varying Stiffener Initial Deflections

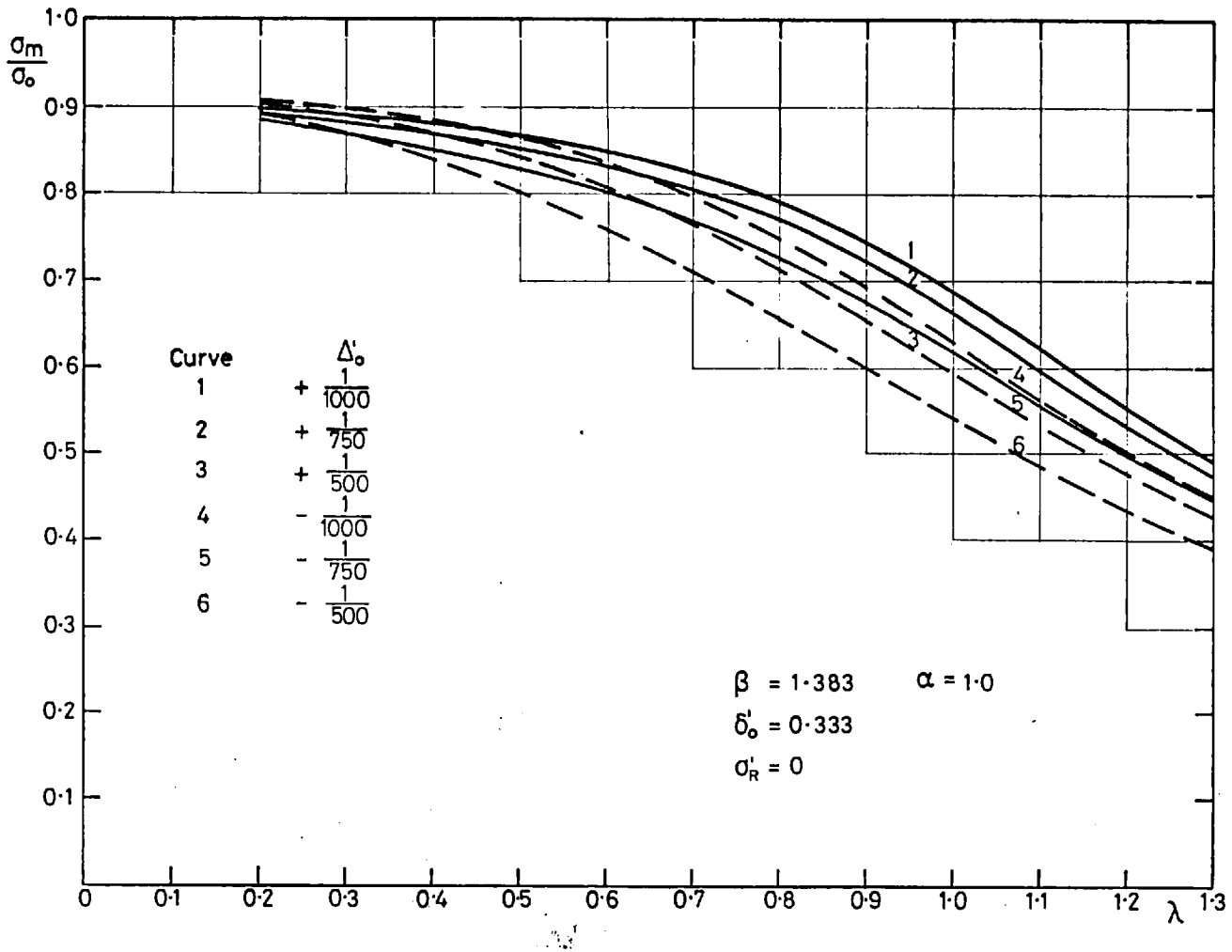

Fig. 5.18b Maximum Strength-Slenderness Curves for One-Span Columns

Effect of Varying Stiffener Initial Deflections

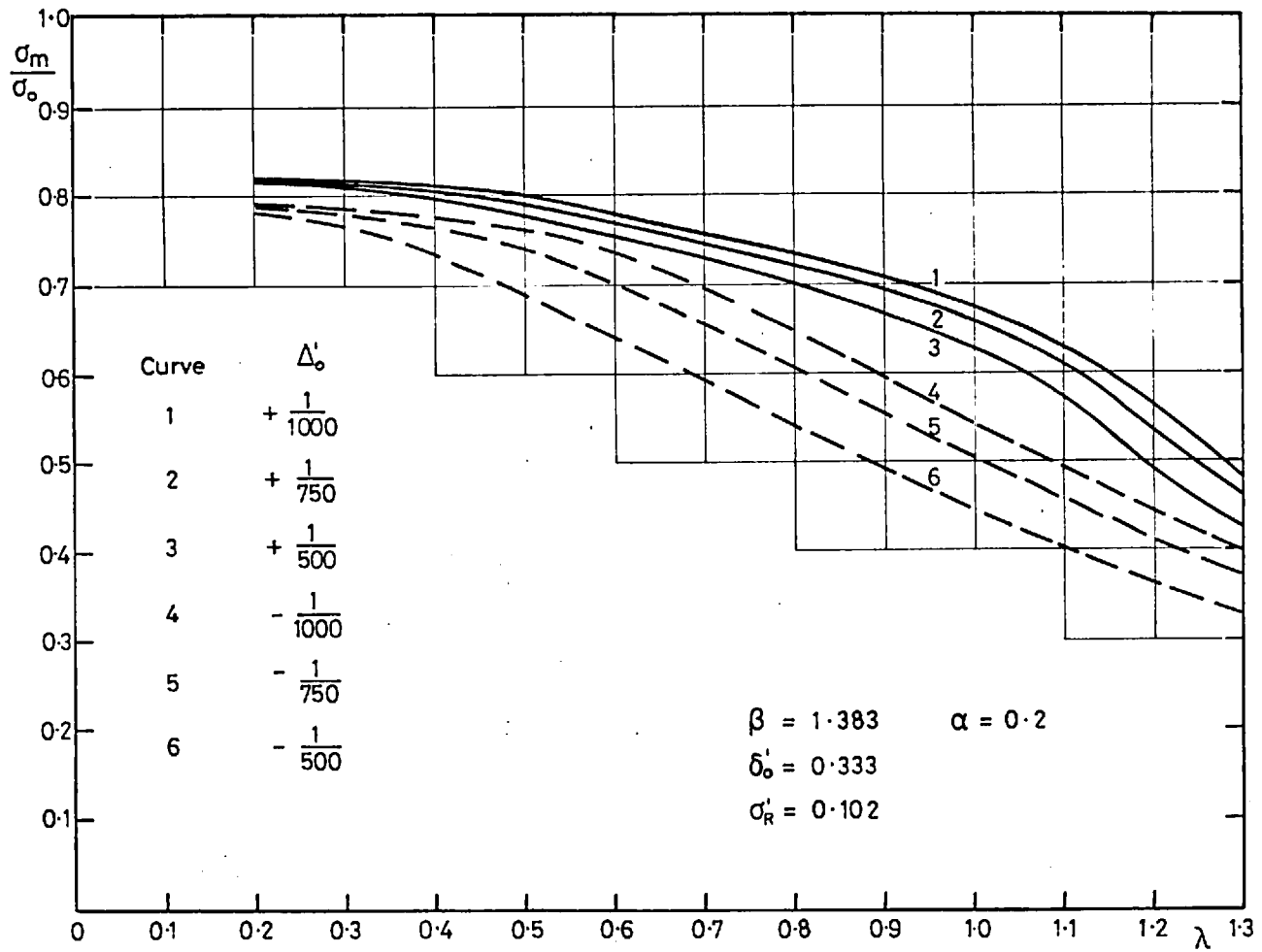

Fig. 5.19a Maximum Strength-Slenderness Curves for One-Span Columns

Effect of Varying Stiffener Initial Deflections

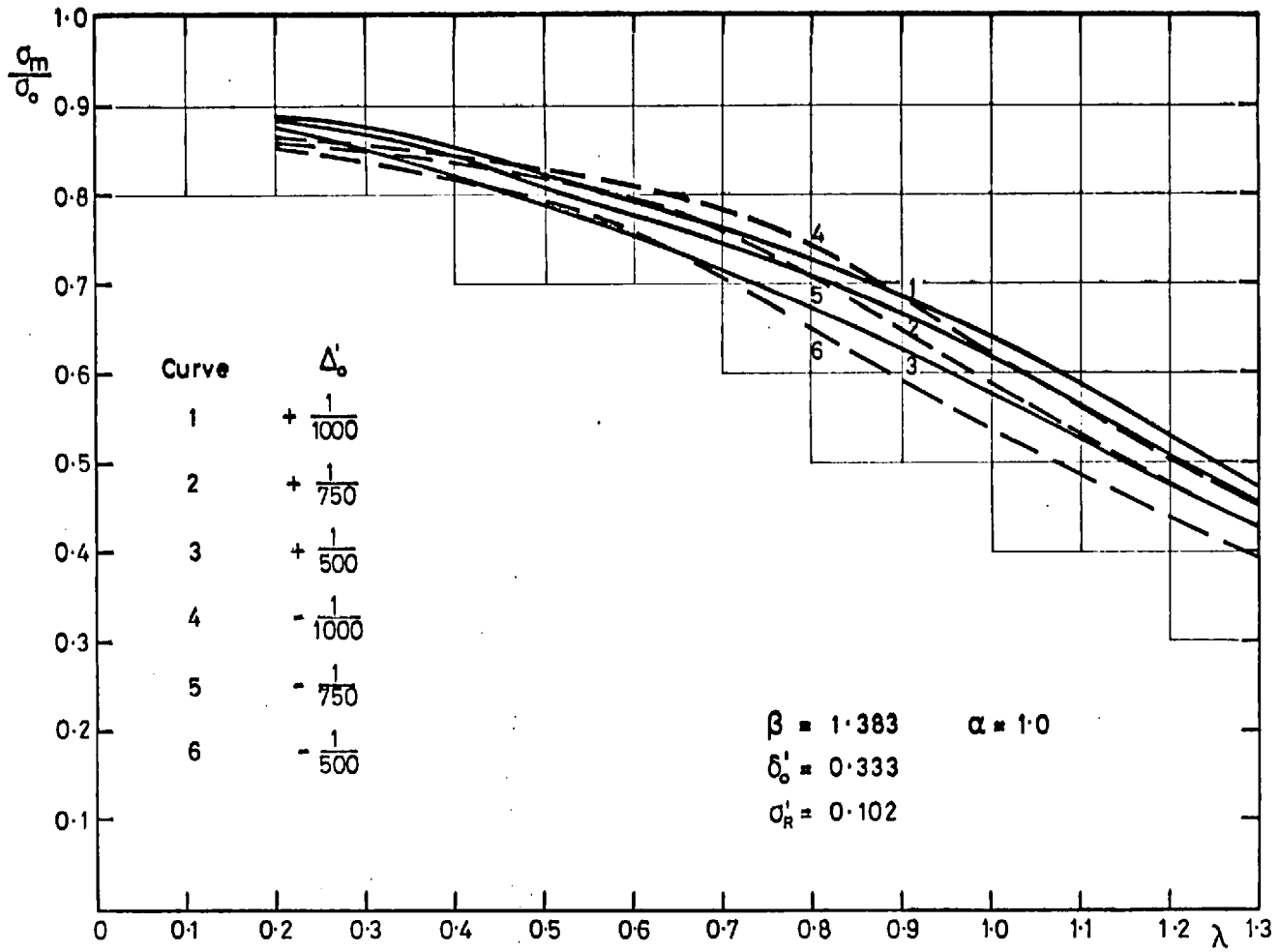

Fig.5.19b Maximum Strength-Slenderness Curves for One-Span Columns

Effect of Varying Stiffener Initial Deflections

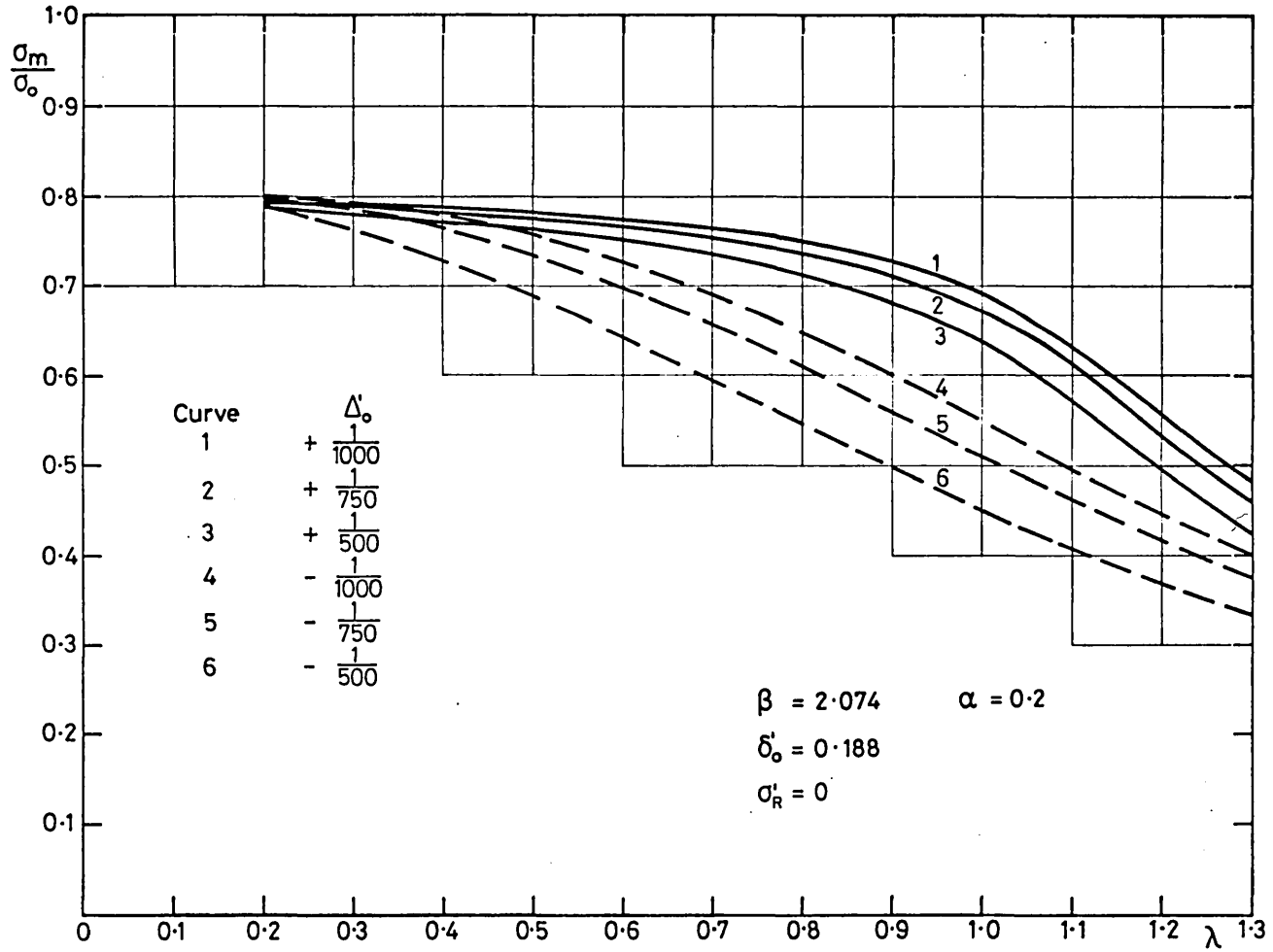

Fig. 5.20a Maximum Strength-Slenderness Curves for One-Span Columns

Effect of Varying Stiffener Initial Deflections

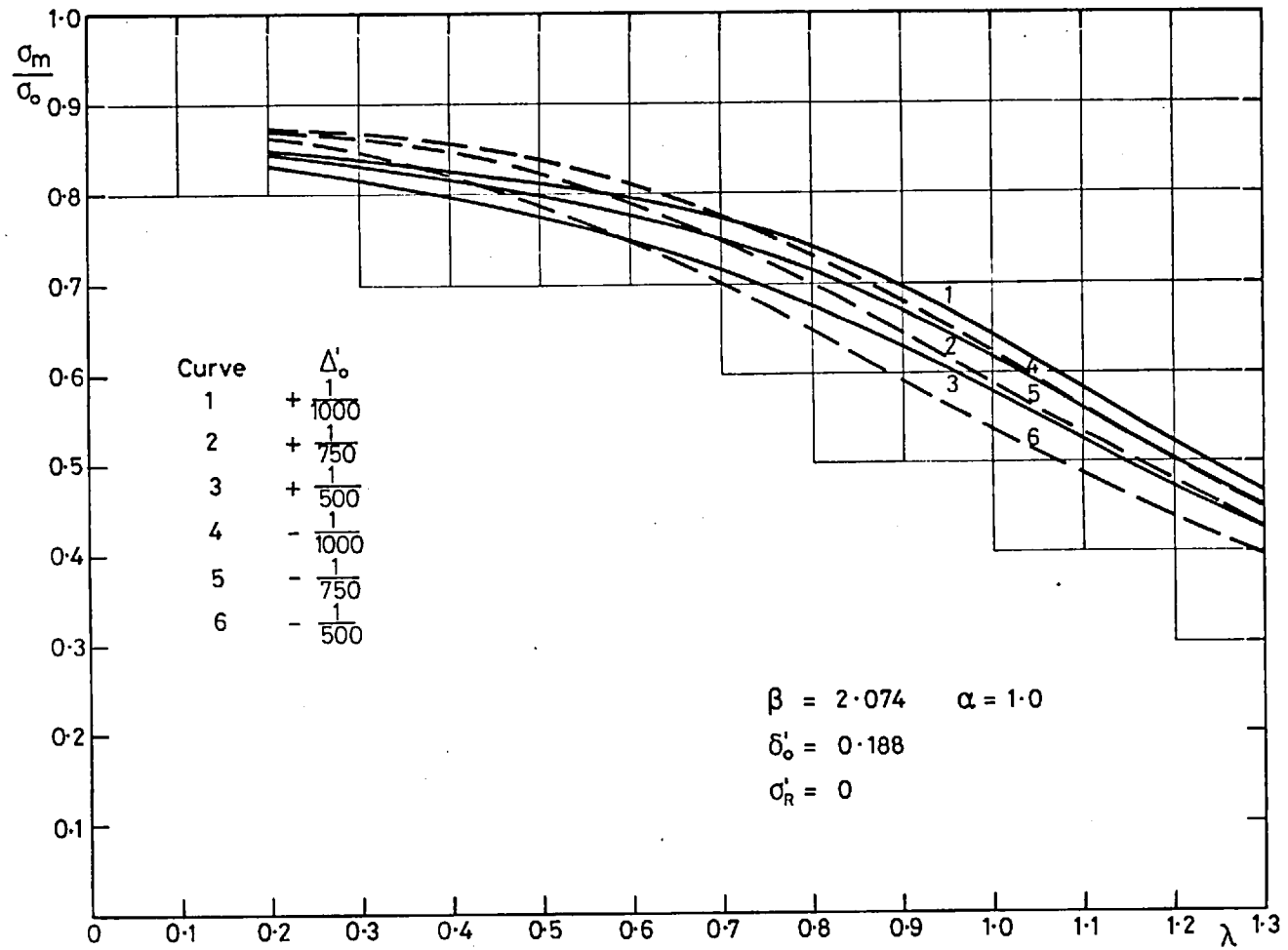

Fig. 5.20b Maximum Strength-Slenderness Curves for One-Span Columns

Effect of Varying Stiffener Initial Deflections

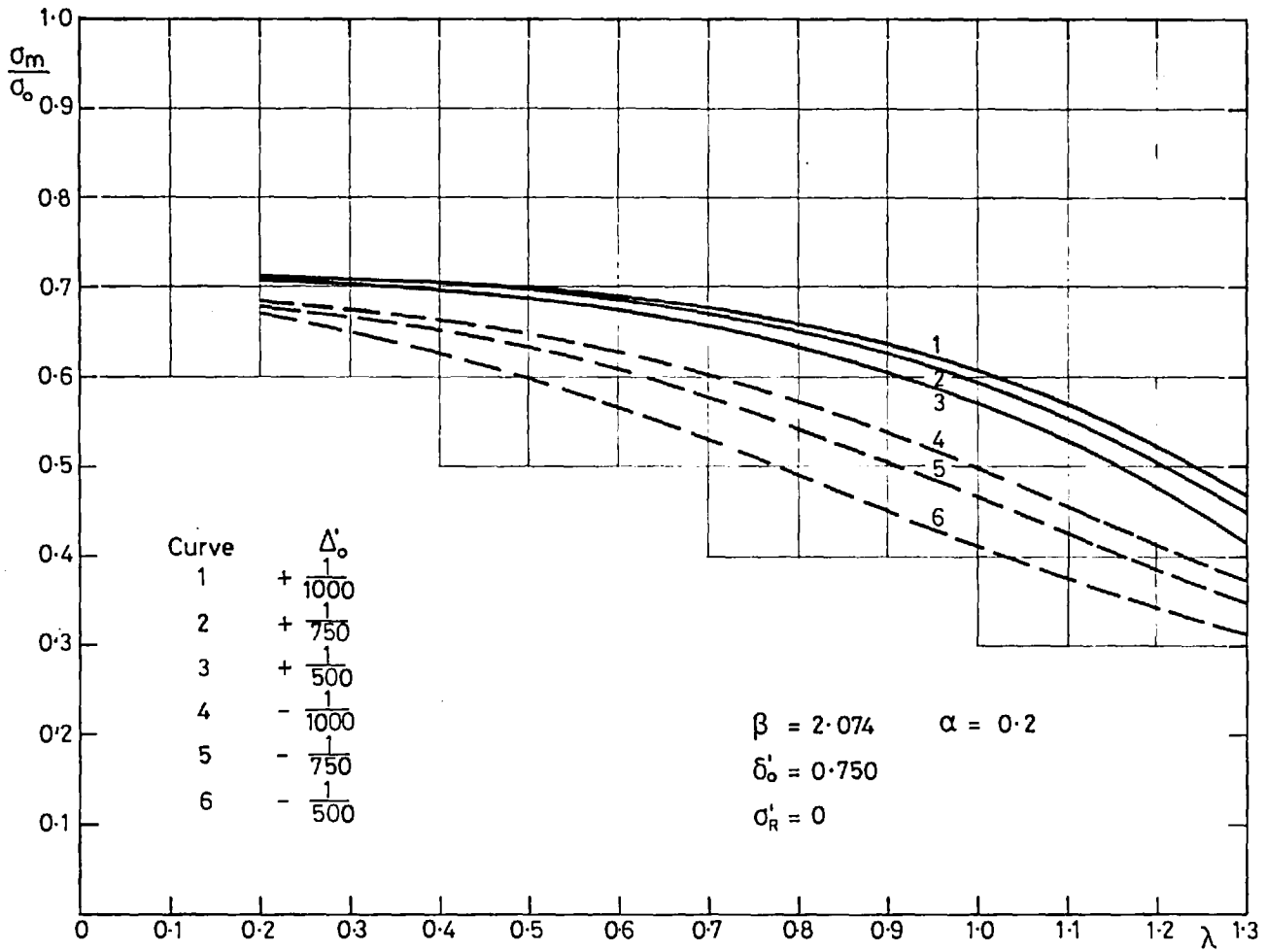

Fig. 5.21a Maximum Strength-Slenderness Curves for One-Span Columns

Effect of Varying Stiffener Initial Deflections

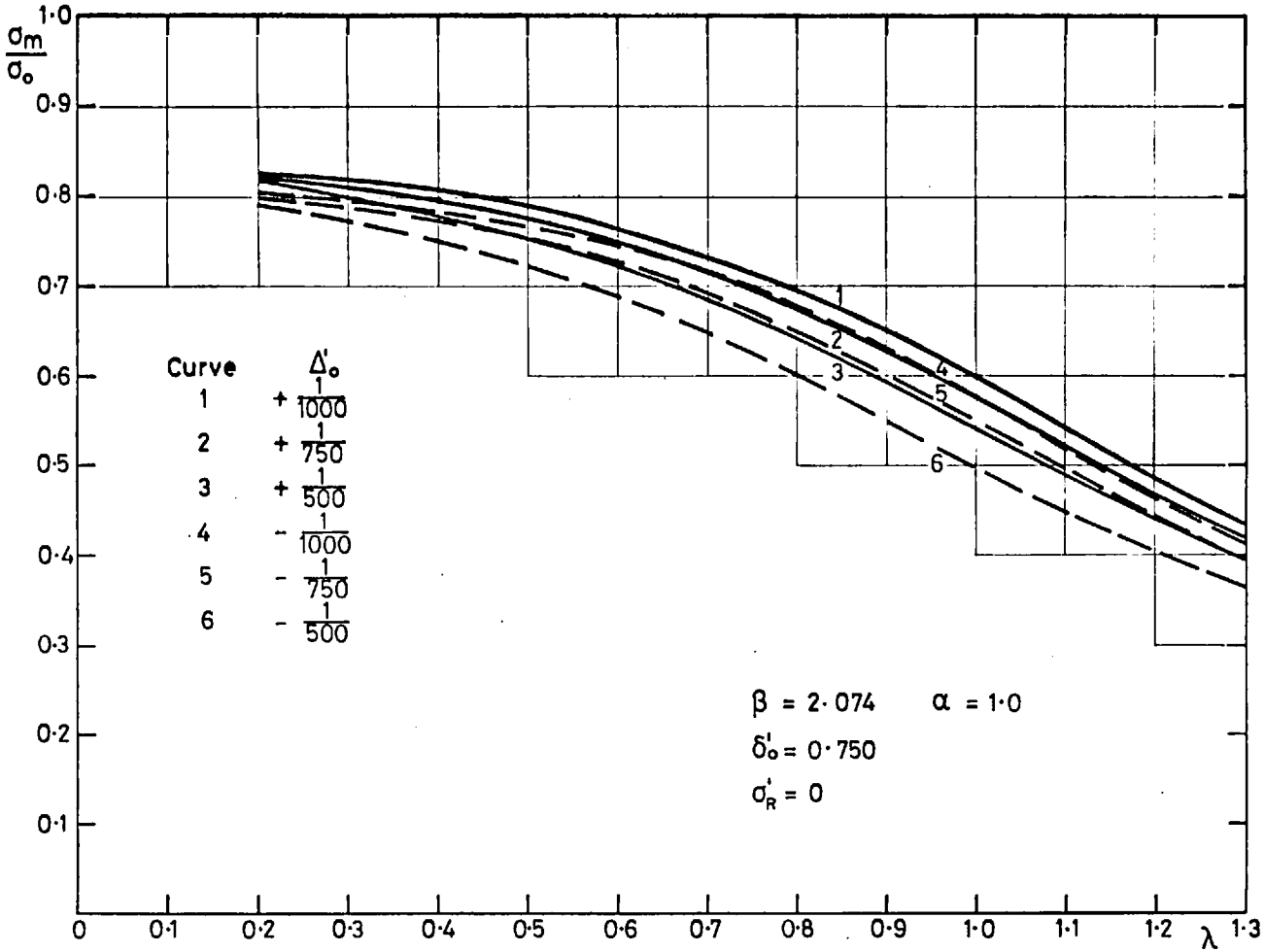

Fig. 5.21b Maximum Strength-Slenderness Curves for One-Span Columns

Effect of Varying Stiffener Initial Deflections

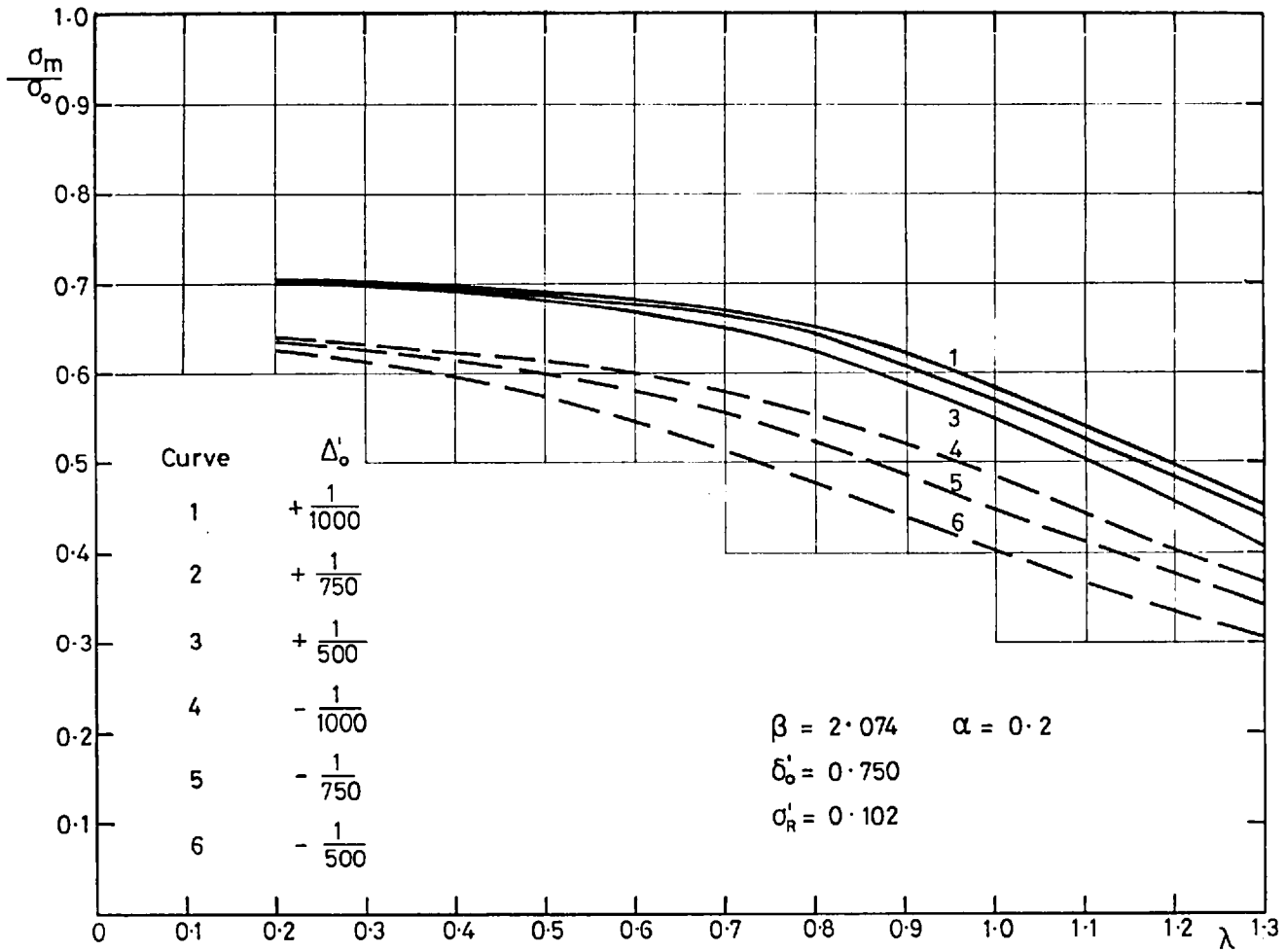

Fig. 5.22a Maximum Strength-Slenderness Curves for One-Span Columns

Effect of Varying Stiffener Initial Deflections

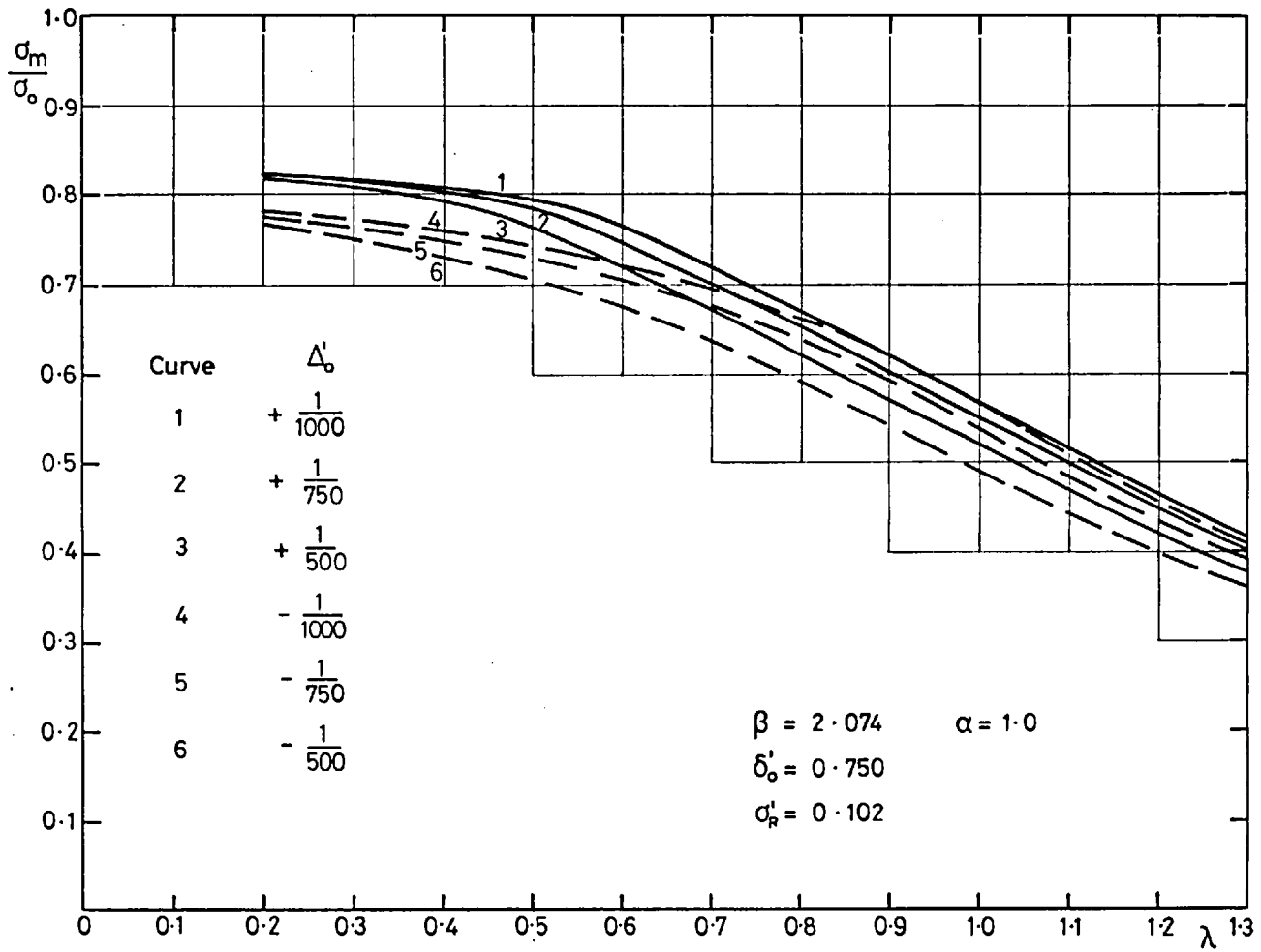

Fig. 5.22b Maximum Strength-Slenderness Curves for One-Span Columns

Effect of Varying Stiffener Initial Deflections

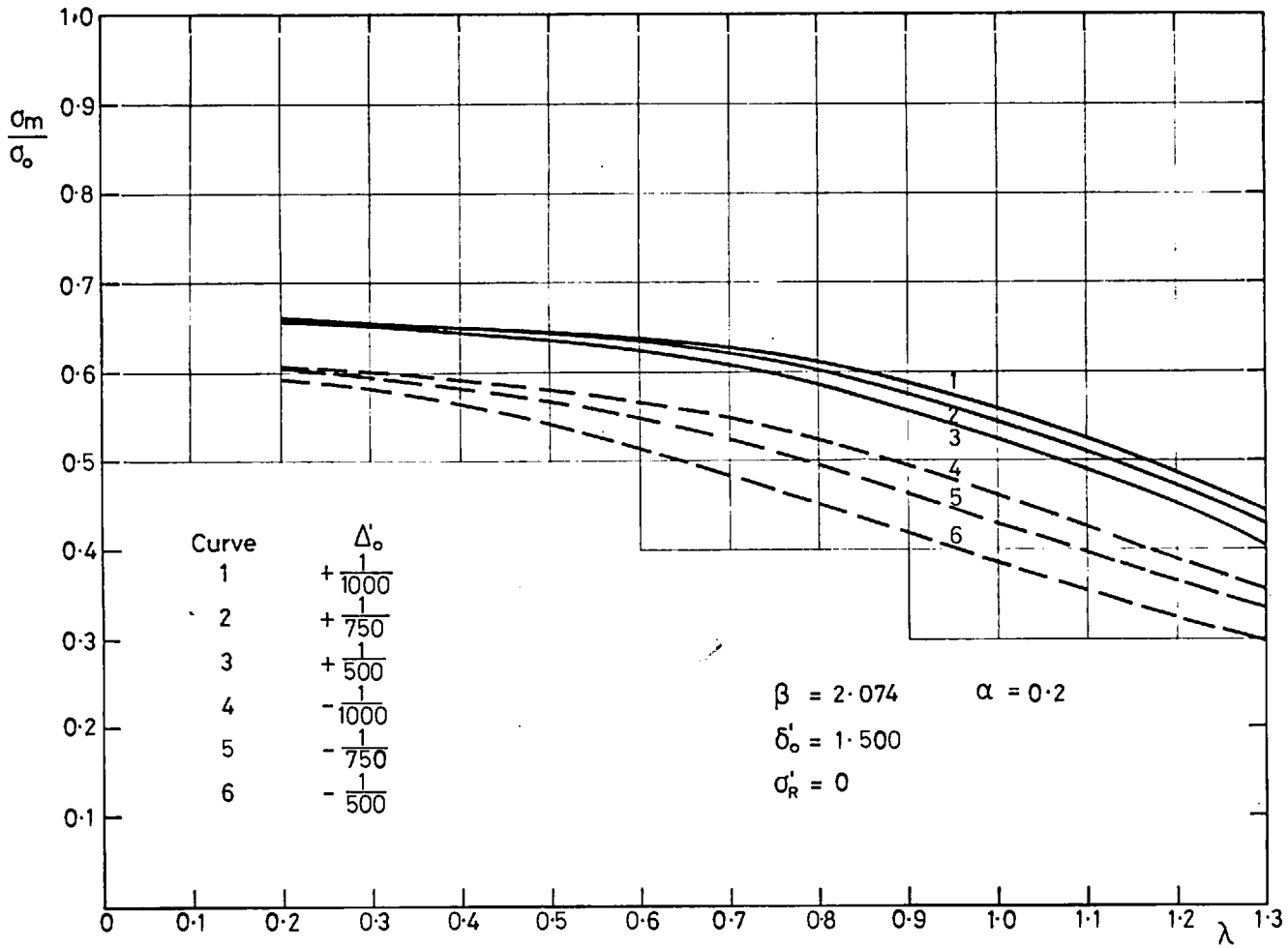

Fig. 5.23a Maximum Strength-Slenderness Curves for One-Span Columns

Effect of Varying Stiffener Initial Deflections

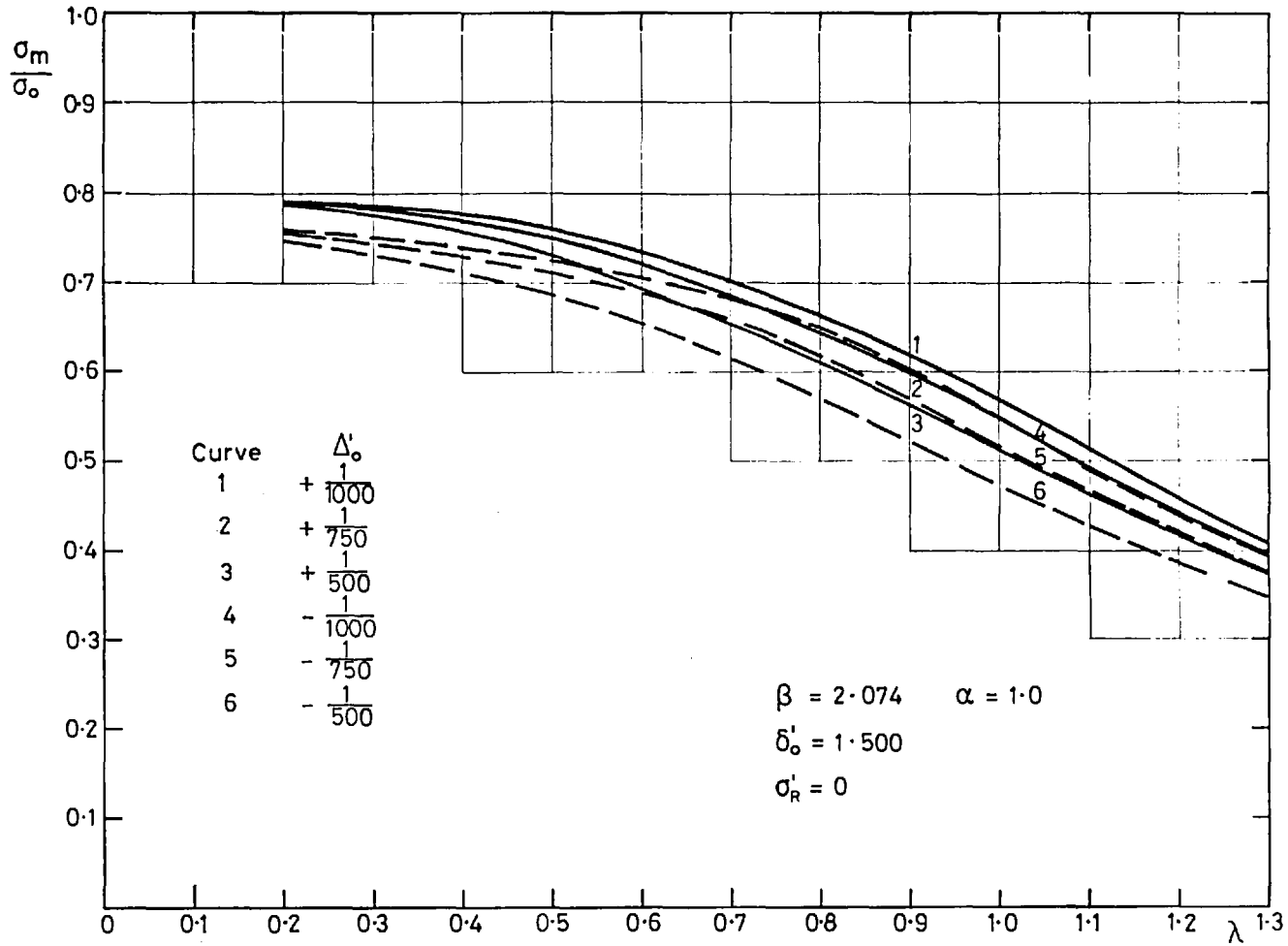

Fig. 5.23b Maximum Strength-Slenderness Curves for One-Span Columns

Effect of Varying Stiffener Initial Deflections

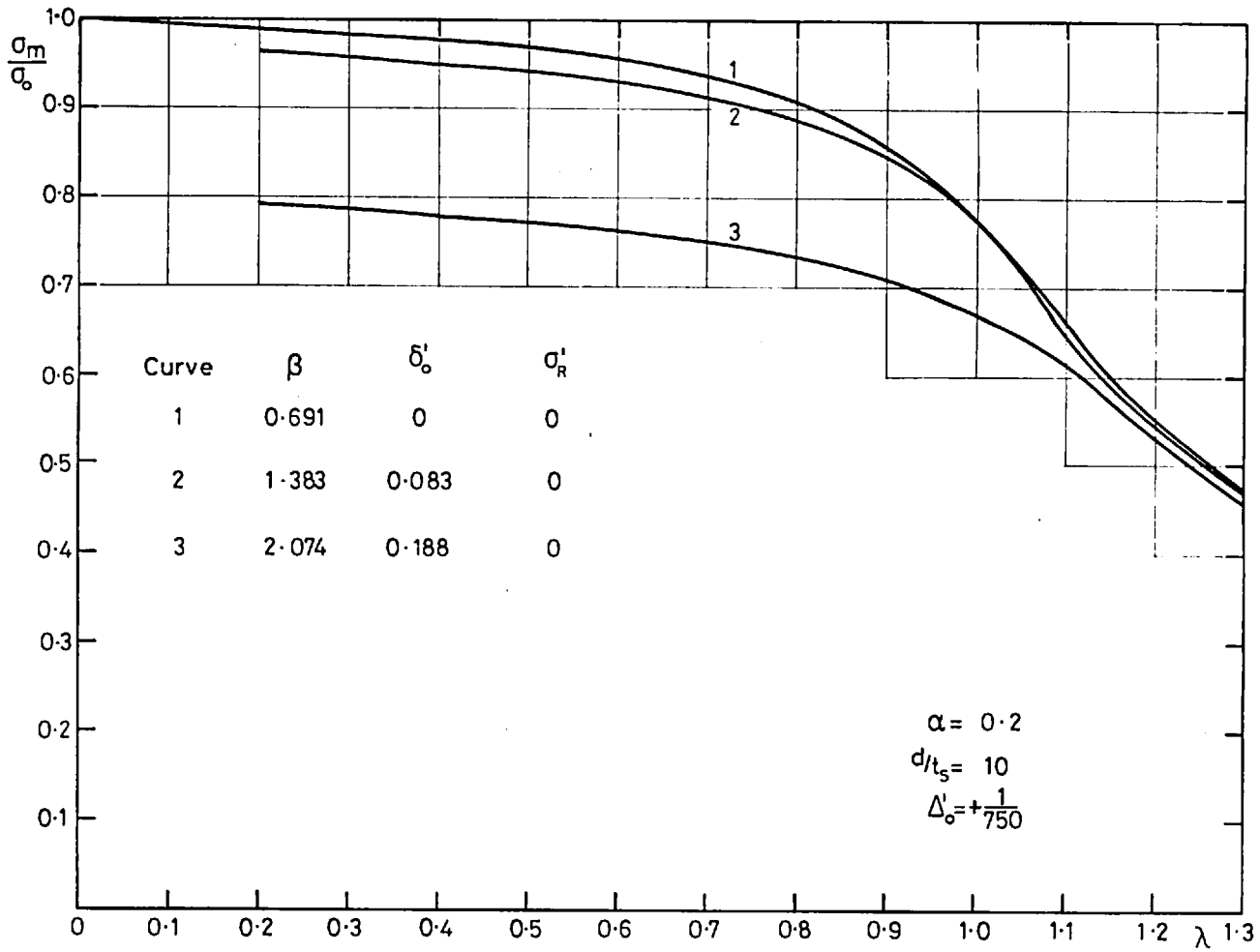

Fig. 5.24a Maximum Strength-Slenderness Curves for One-Span Columns

Effect of Varying Plate Slenderness

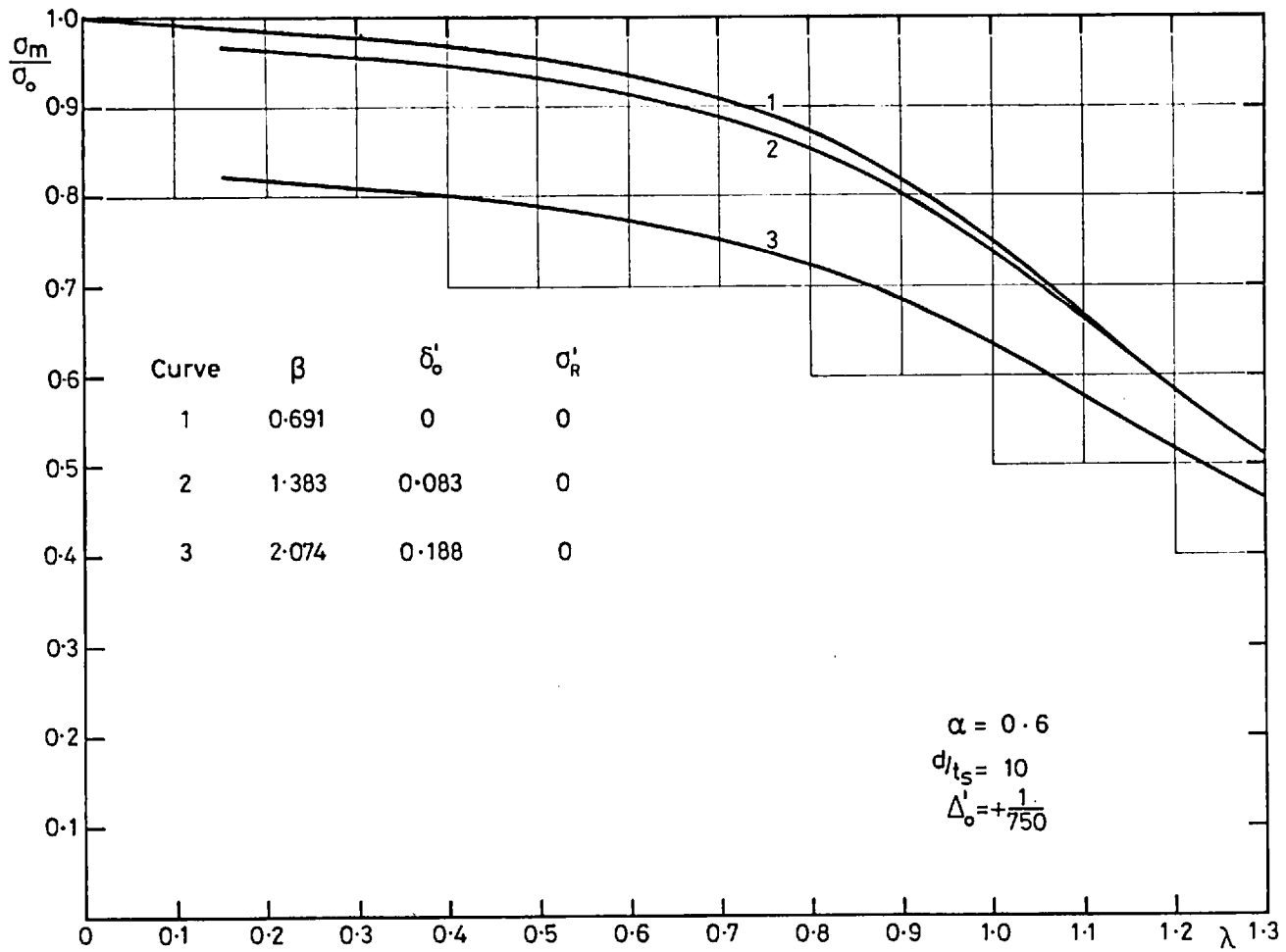

Fig.5.24b Maximum Strength-Slenderness Curves for One-Span Columns

Effect of Varying Plate Slenderness

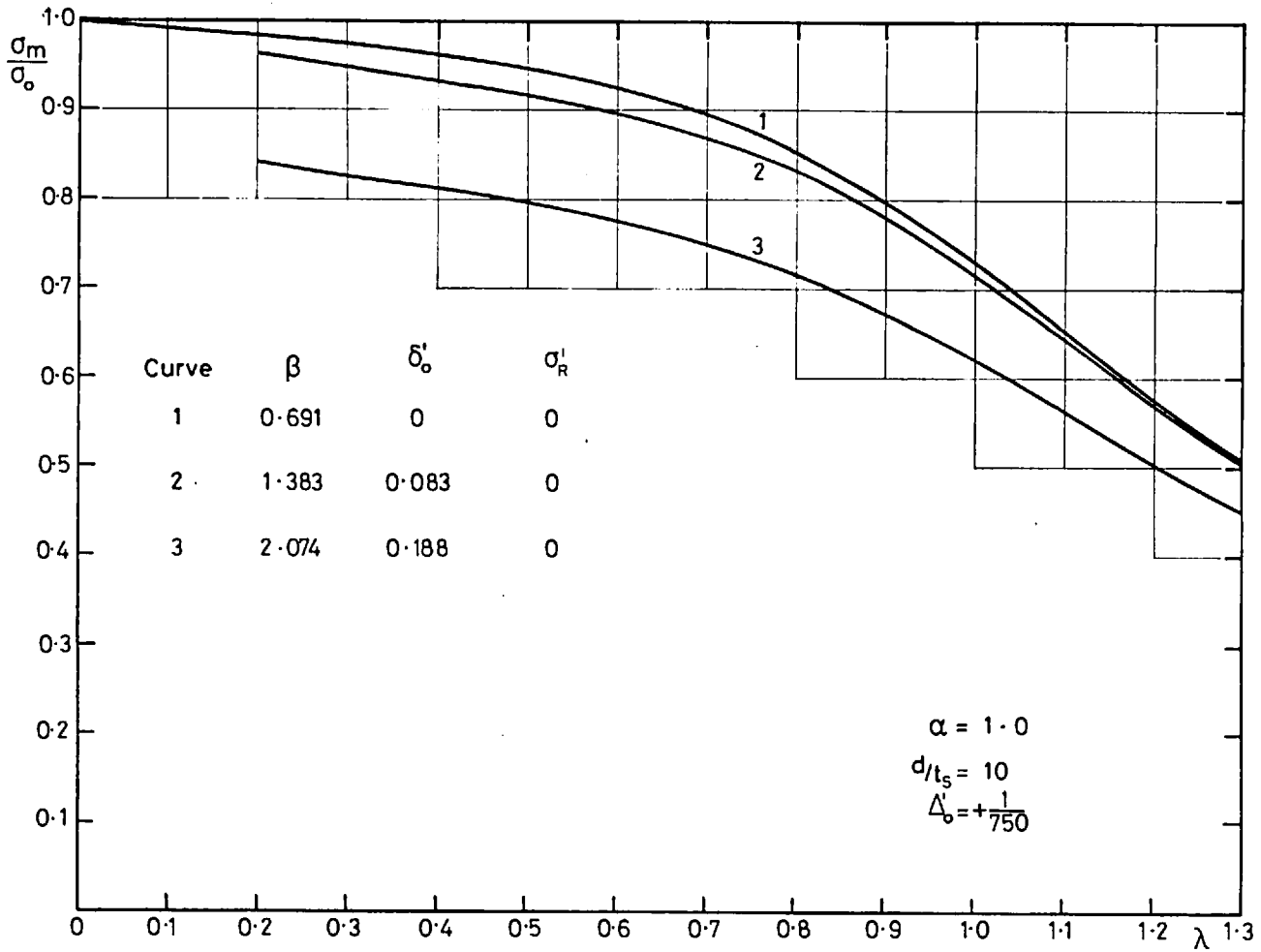

Fig.5.24c Maximum Strength-Slenderness Curves for One-Span Columns

Effect of Varying Plate Slenderness

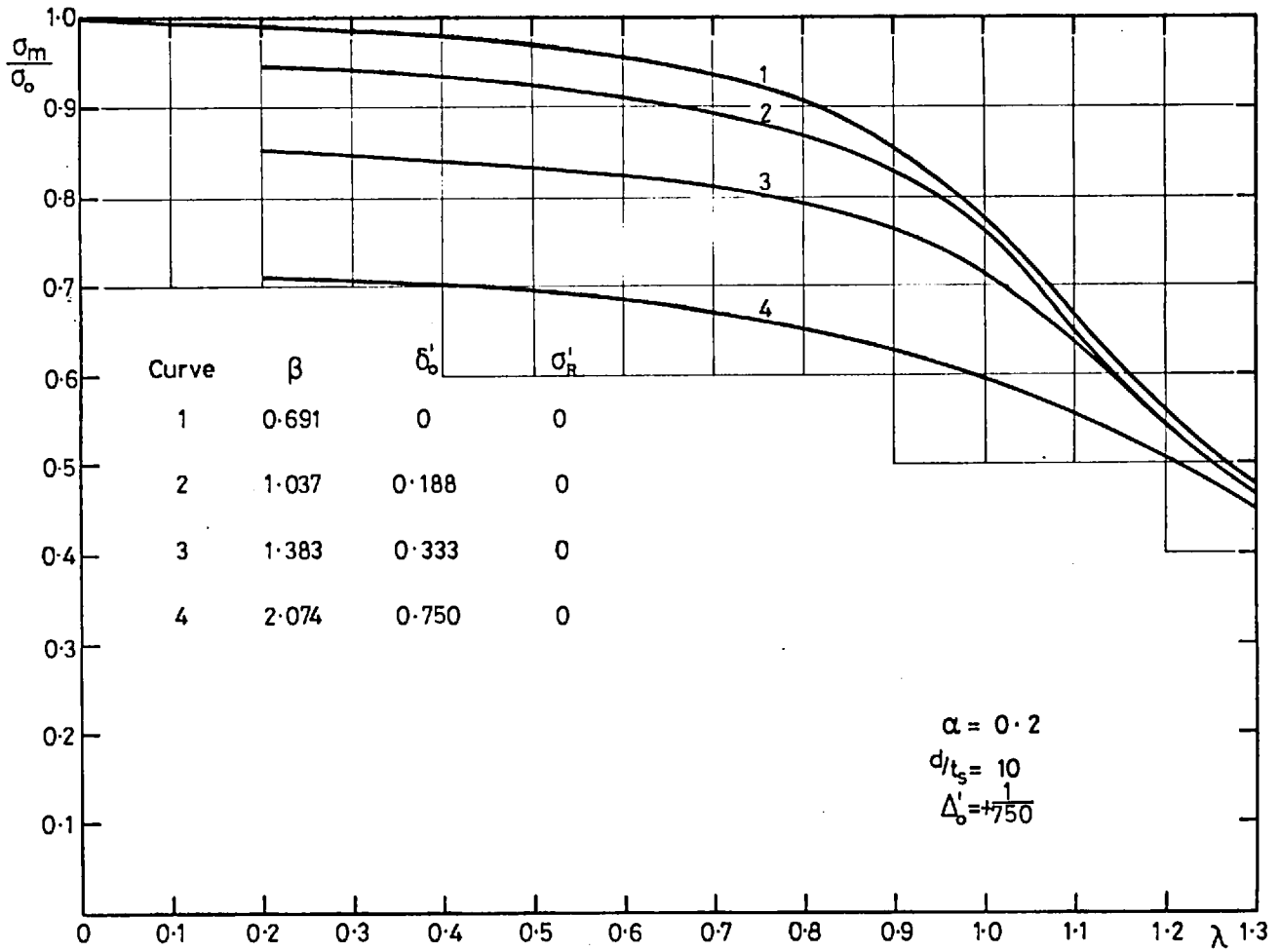

Fig. 5.25a Maximum Strength-Slenderness Curves for One-Span Columns

Effect of Varying Plate Slenderness

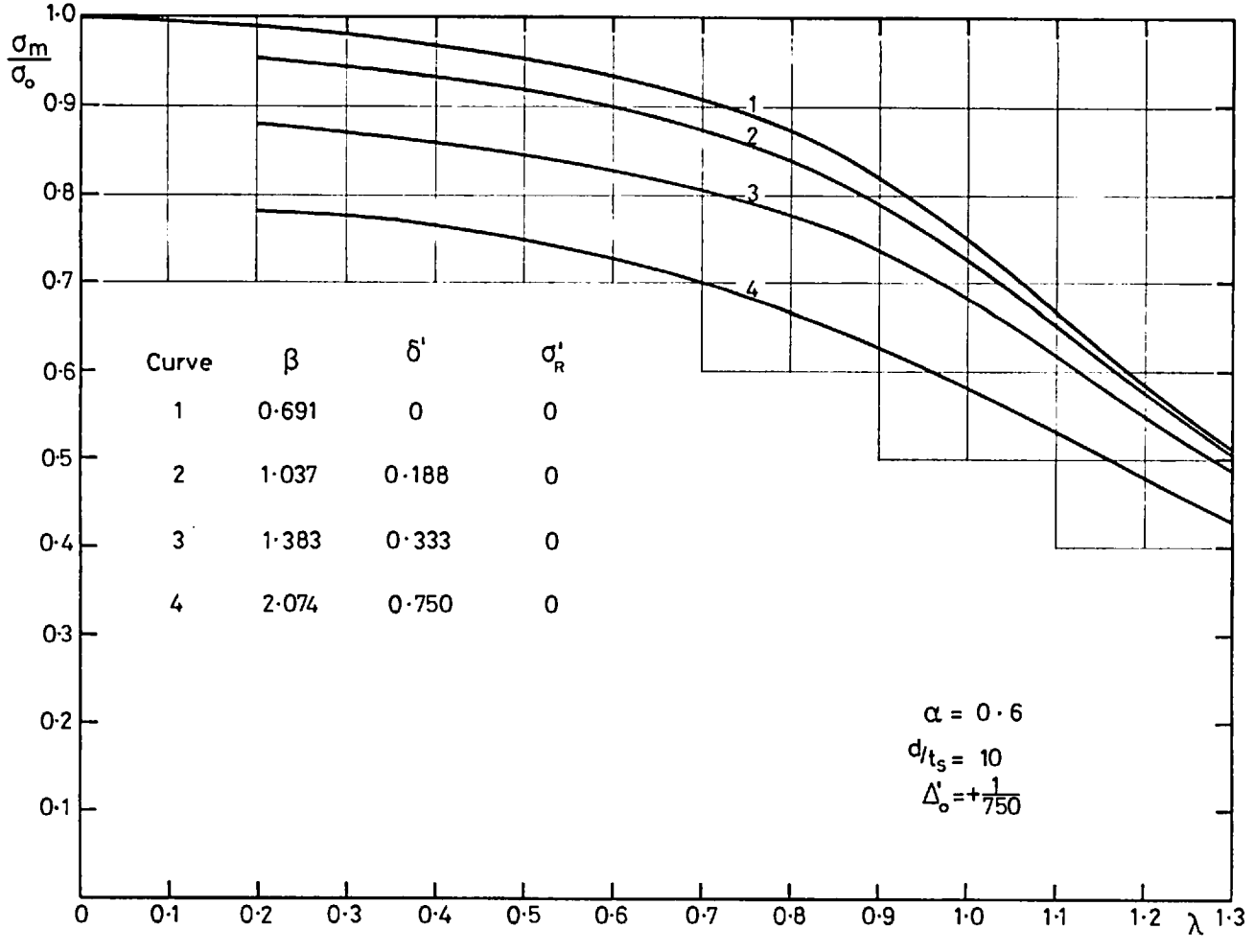

Fig. 5.25b Maximum Strength-Slenderness Curves for One-Span Columns

Effect of Varying Plate Slenderness

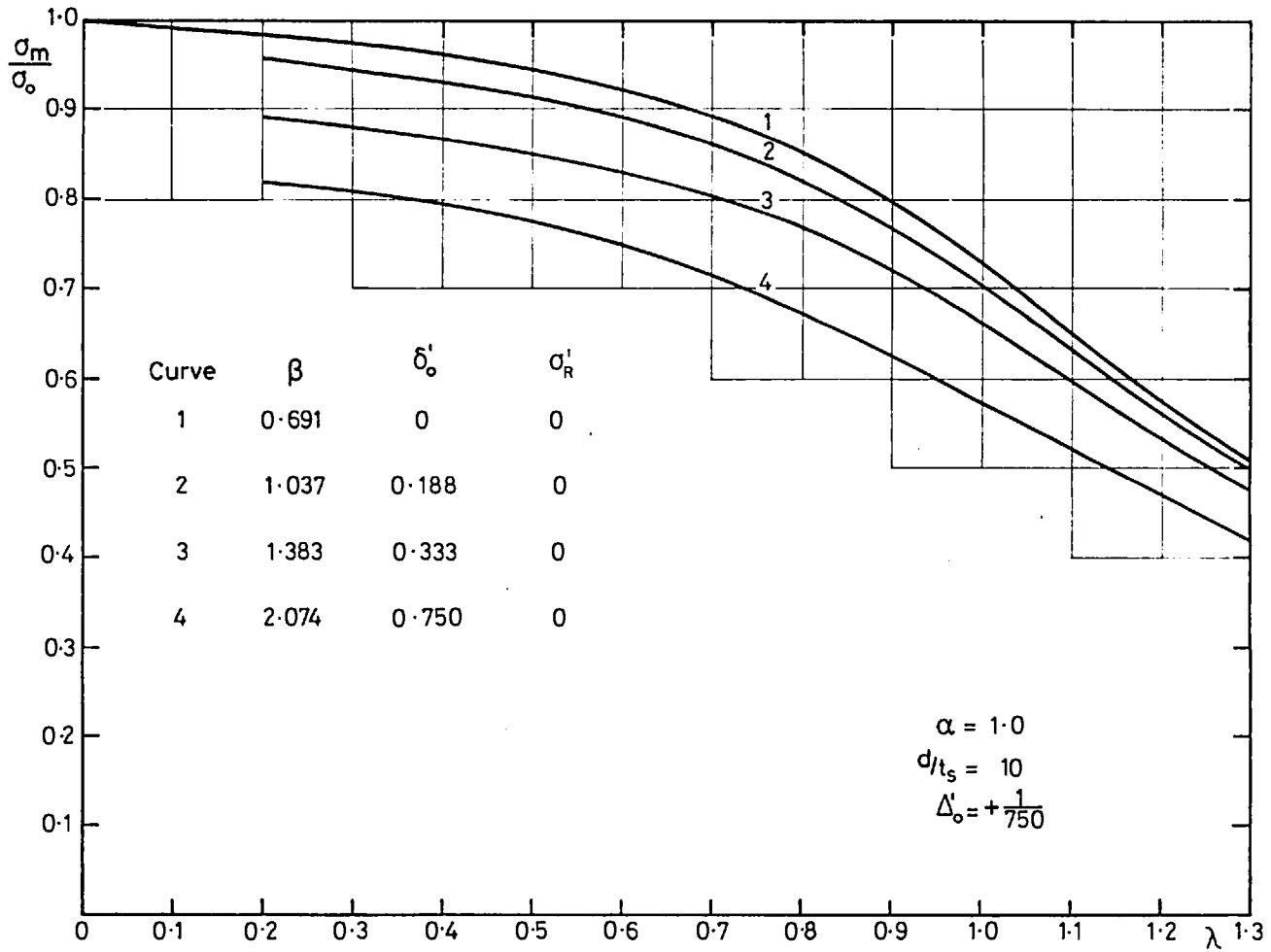

Fig.5.25c Maximum Strength-Slenderness Curves for One-Span Columns

Effect of Varying Plate Slenderness

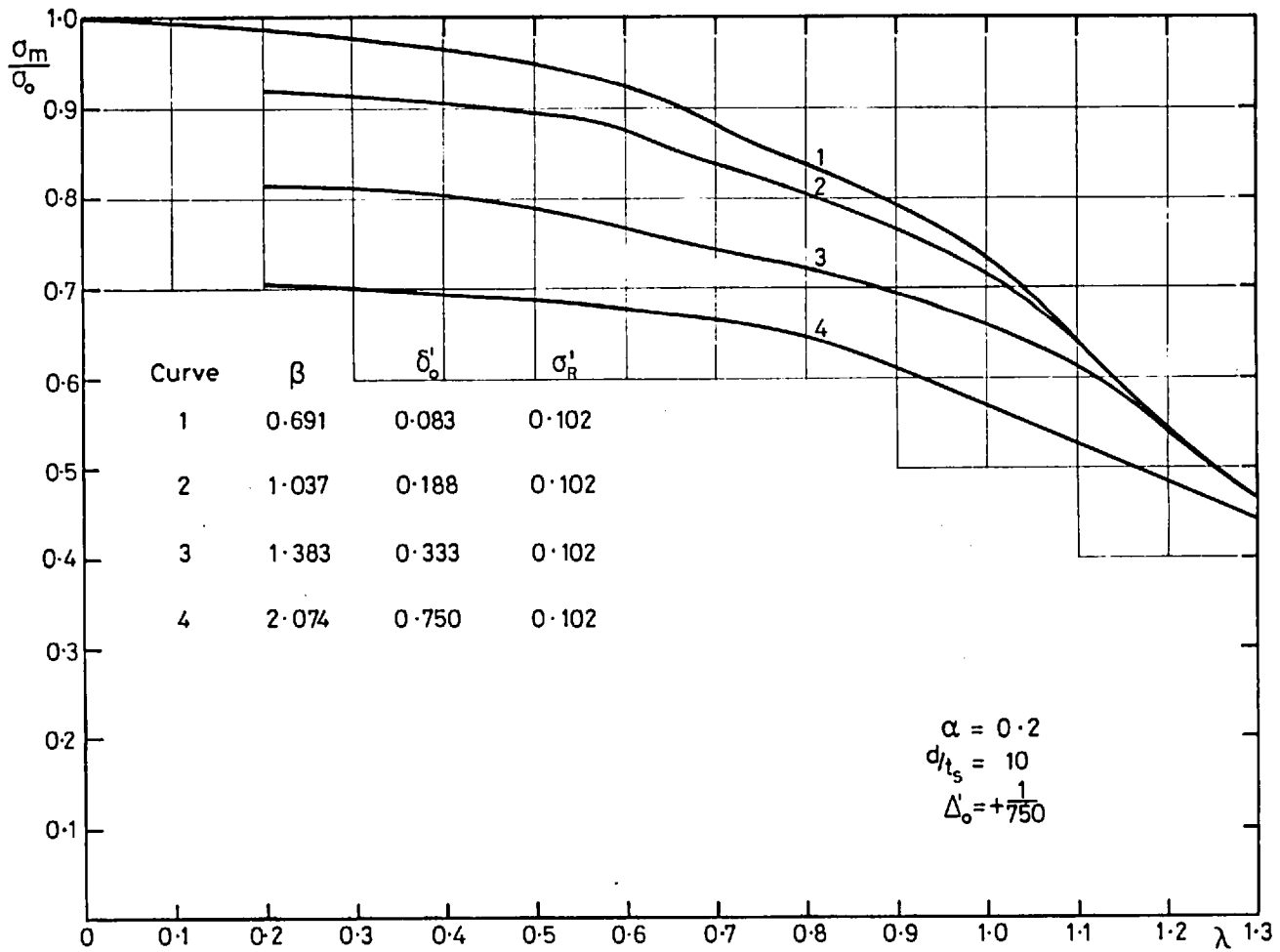

Fig. 5.26a Maximum Strength-Slenderness Curves for One-Span Columns

Effect of Varying Plate Slenderness

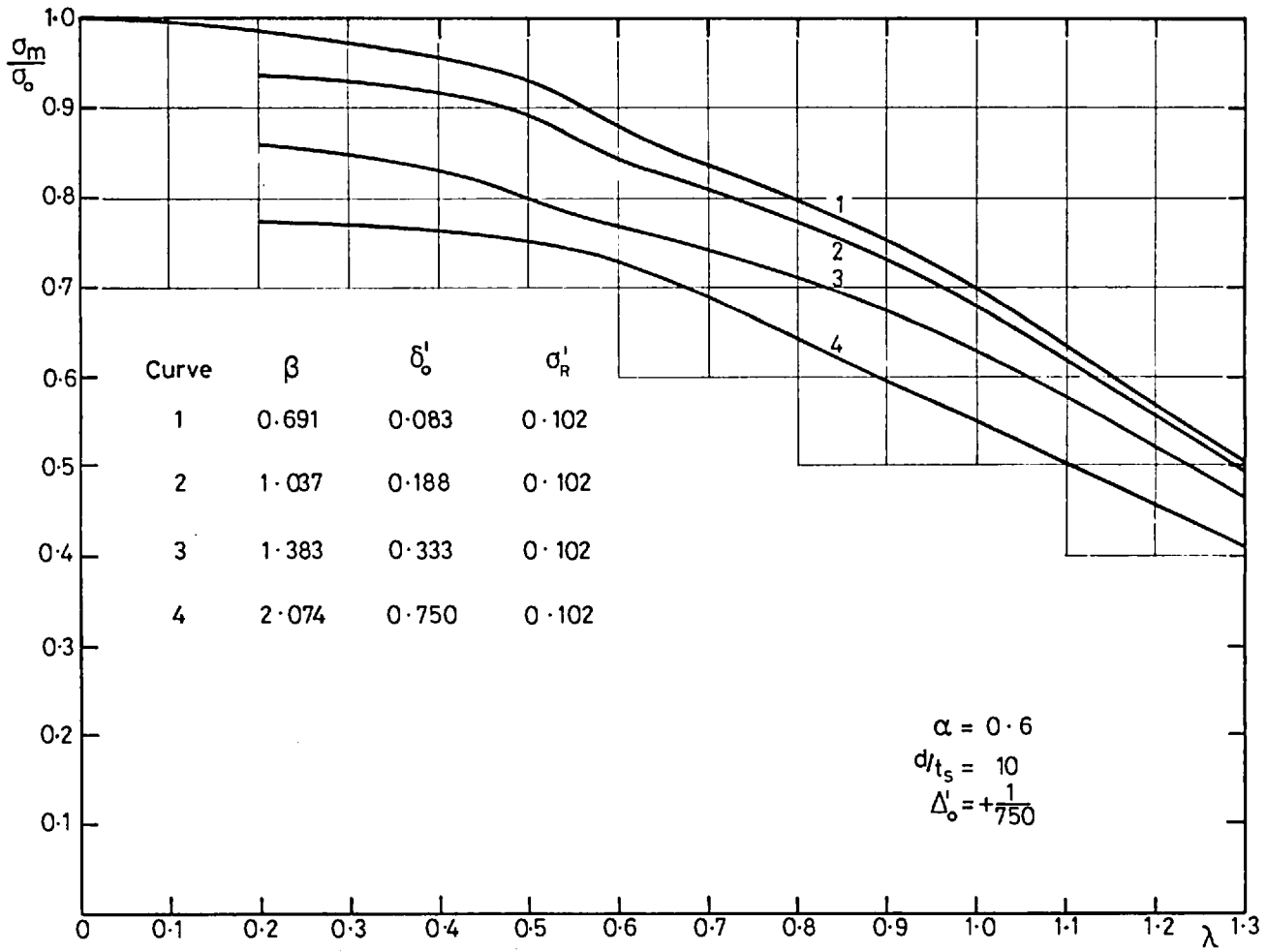

Fig. 5.26b Maximum Strength-Slenderness Curves for One-Span Columns

Effect of Varying Plate Slenderness

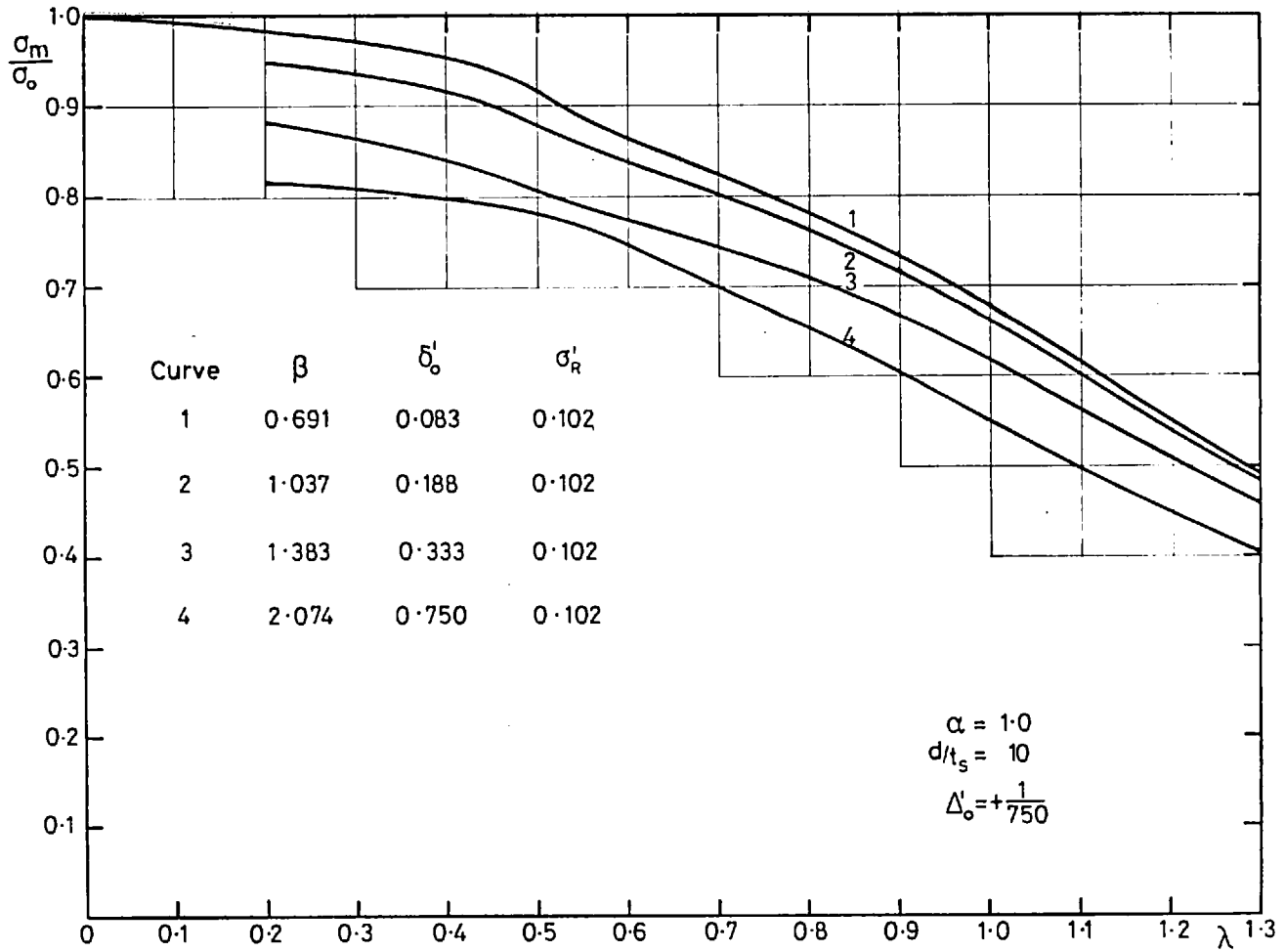

Fig. 5.26c Maximum Strength-Slenderness Curves for One-Span Columns

Effect of Varying Plate Slenderness

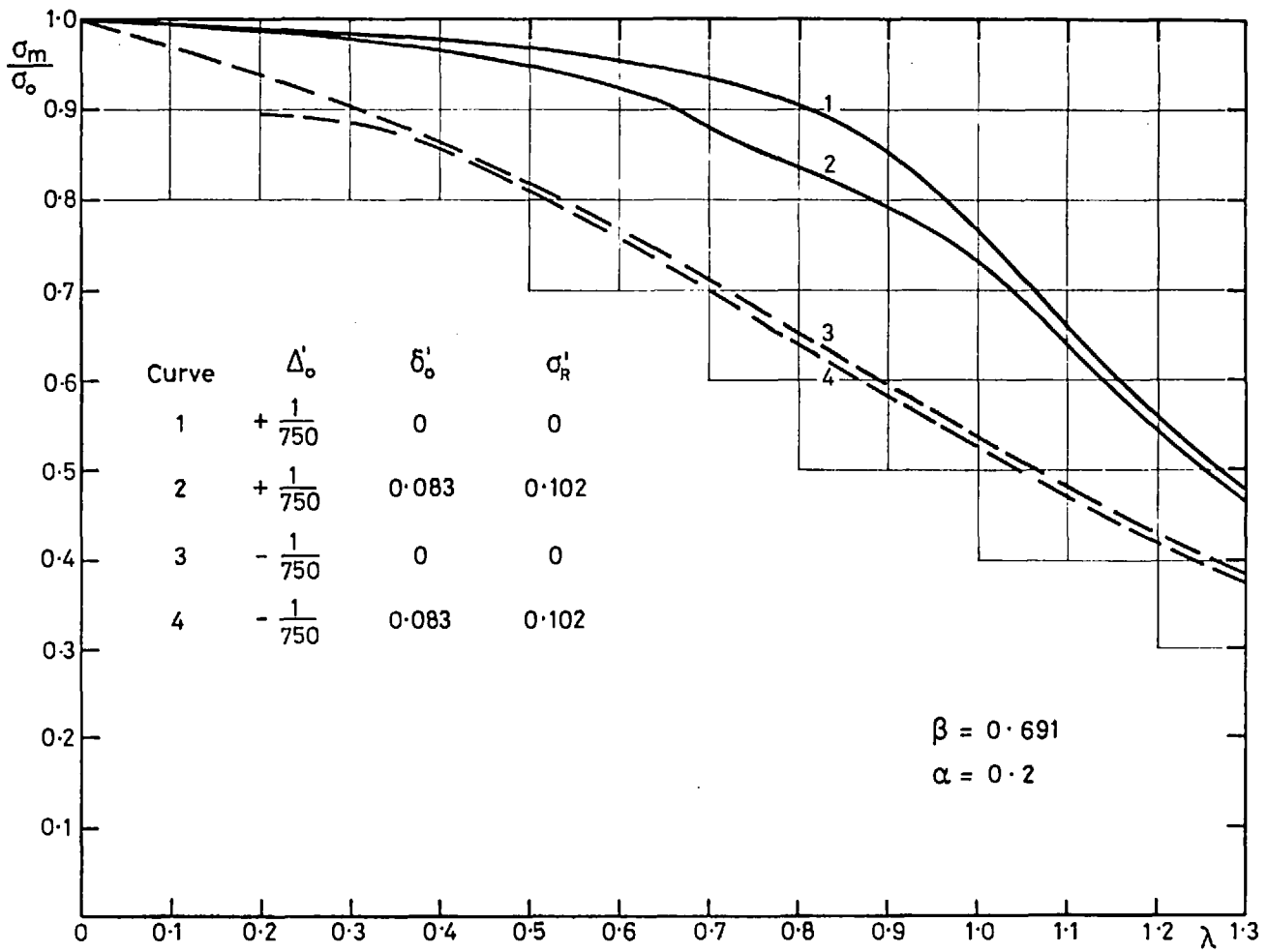

Fig.5.27a Maximum Strength-Slenderness Curves for One-Span Columns

Effect of Varying Plate Initial Imperfections

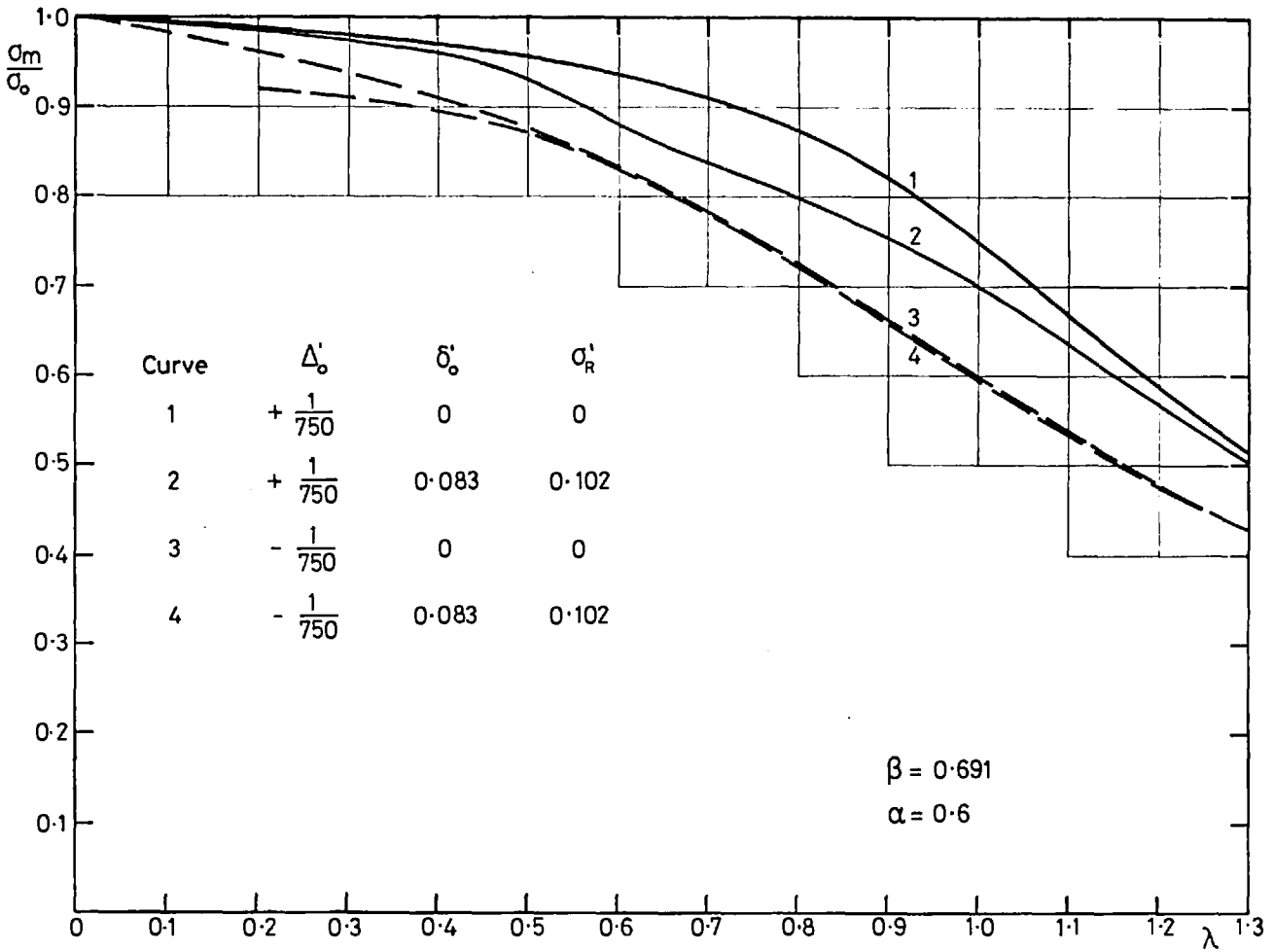

Fig. 5.27b Maximum Strength–Slenderness Curves for One-Span Columns

Effect of Varying Plate Initial Imperfections

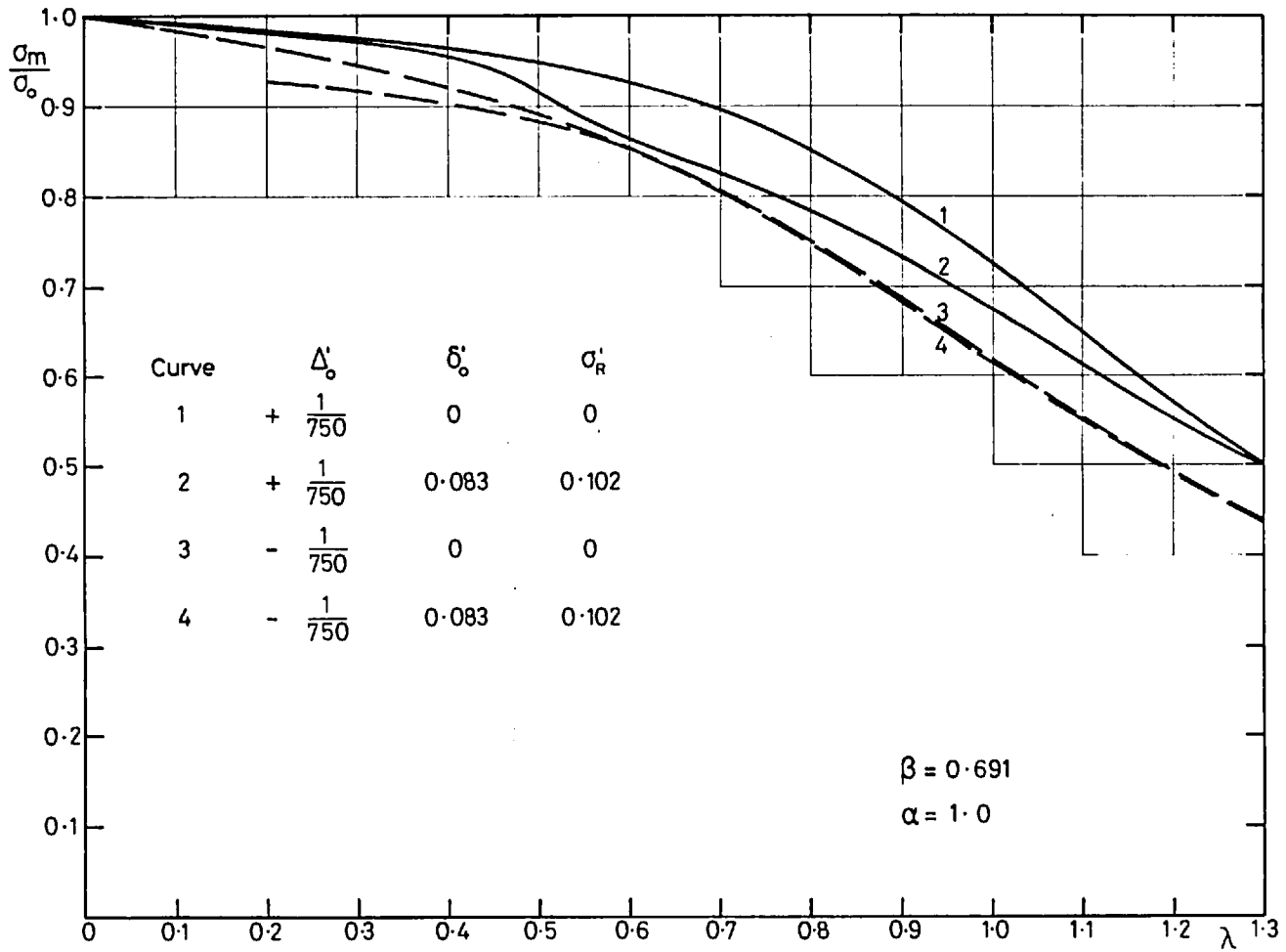

Fig. 5.27c Maximum Strength-Slenderness Curves for One-Span Columns

Effect of Varying Plate Initial Imperfections

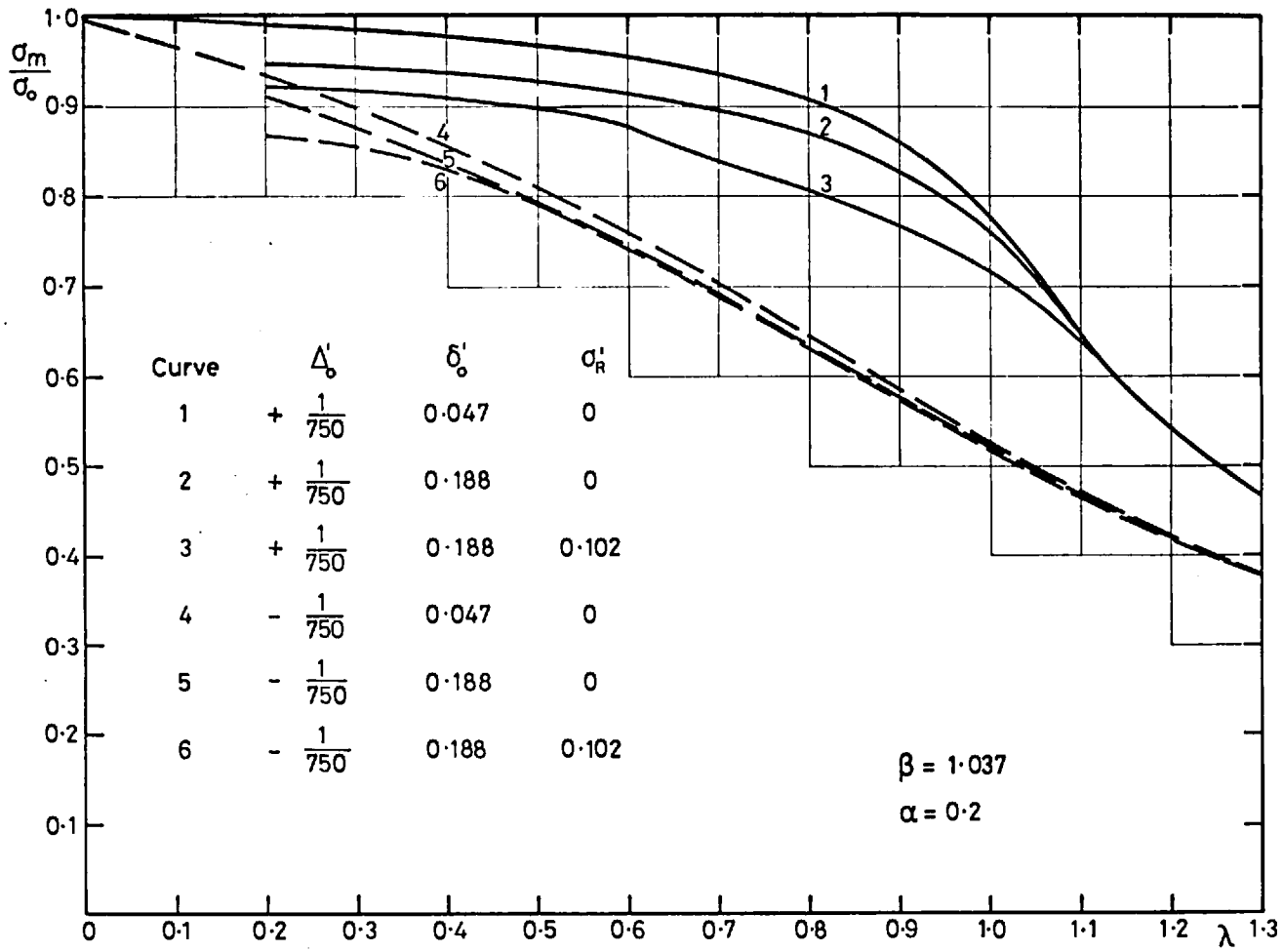

Fig. 5.28a Maximum Strength-Slenderness Curves for One-Span Columns

Effect of Varying Plate Initial Imperfections

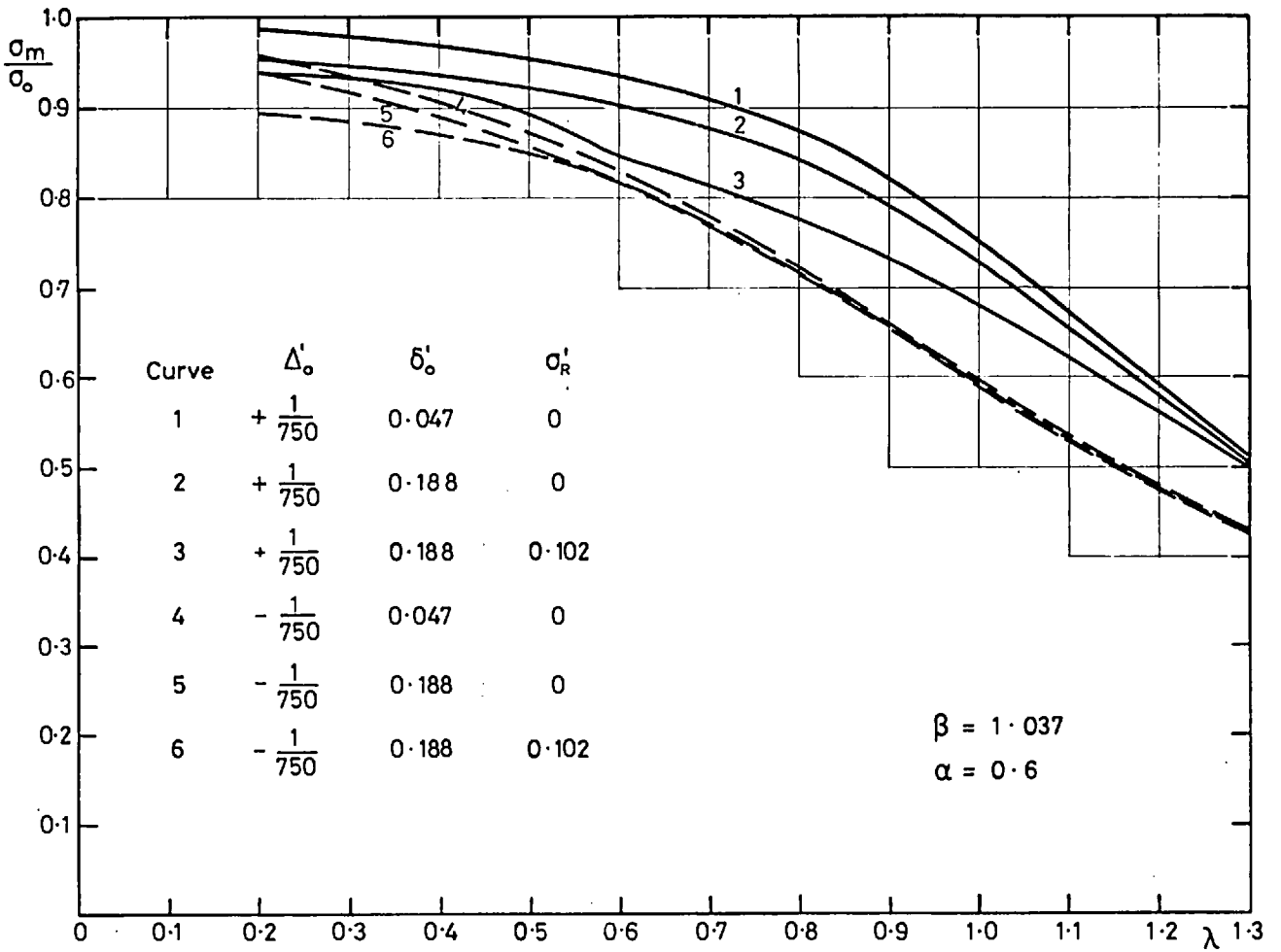

Fig.5.28b Maximum Strength-Slenderness Curves for One-Span Columns

Effect of Varying Plate Initial Imperfections

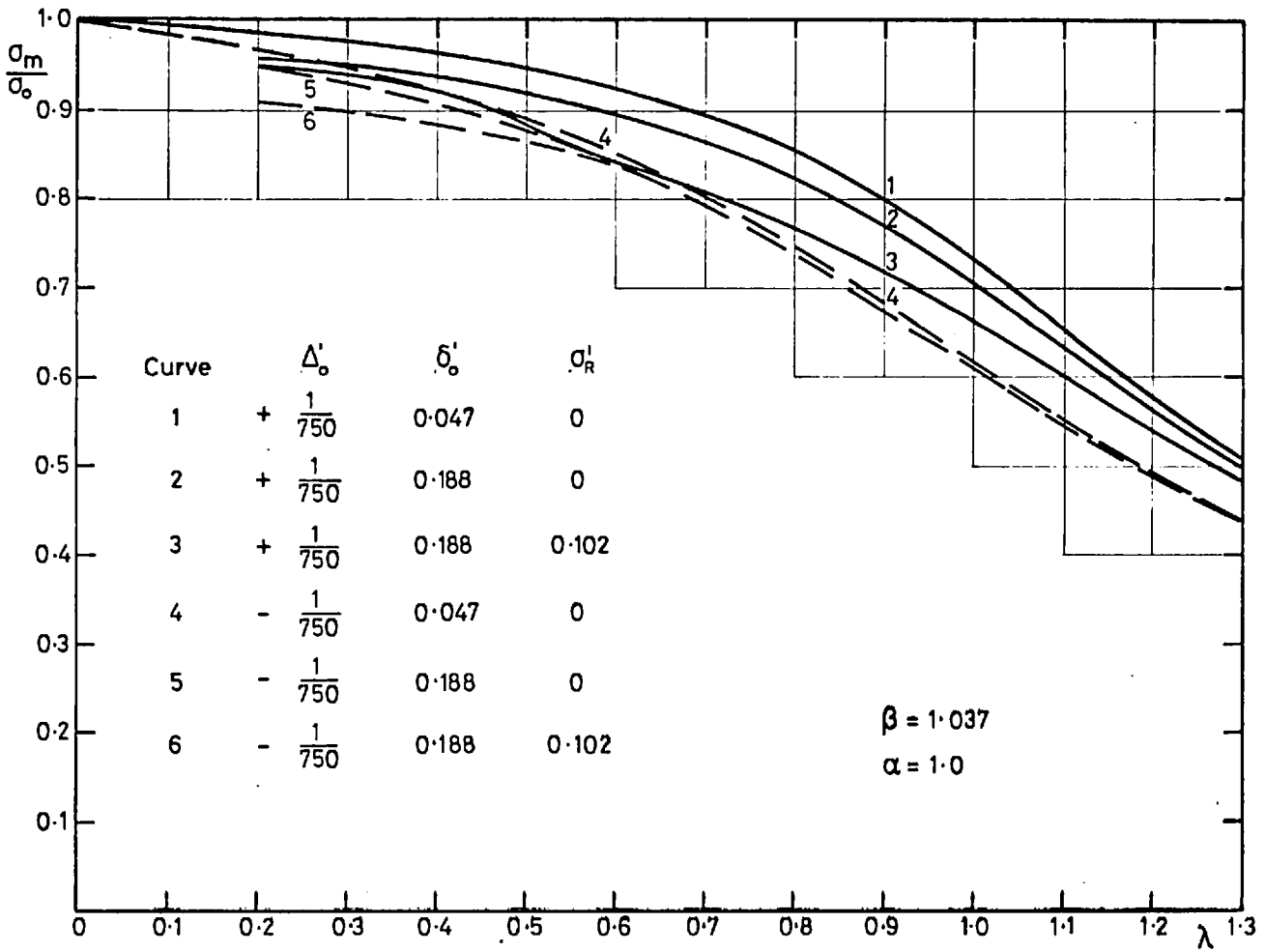

Fig. 5.28c Maximum Strength-Slenderness Curves for One-Span Columns

Effect of Varying Plate Initial Imperfections

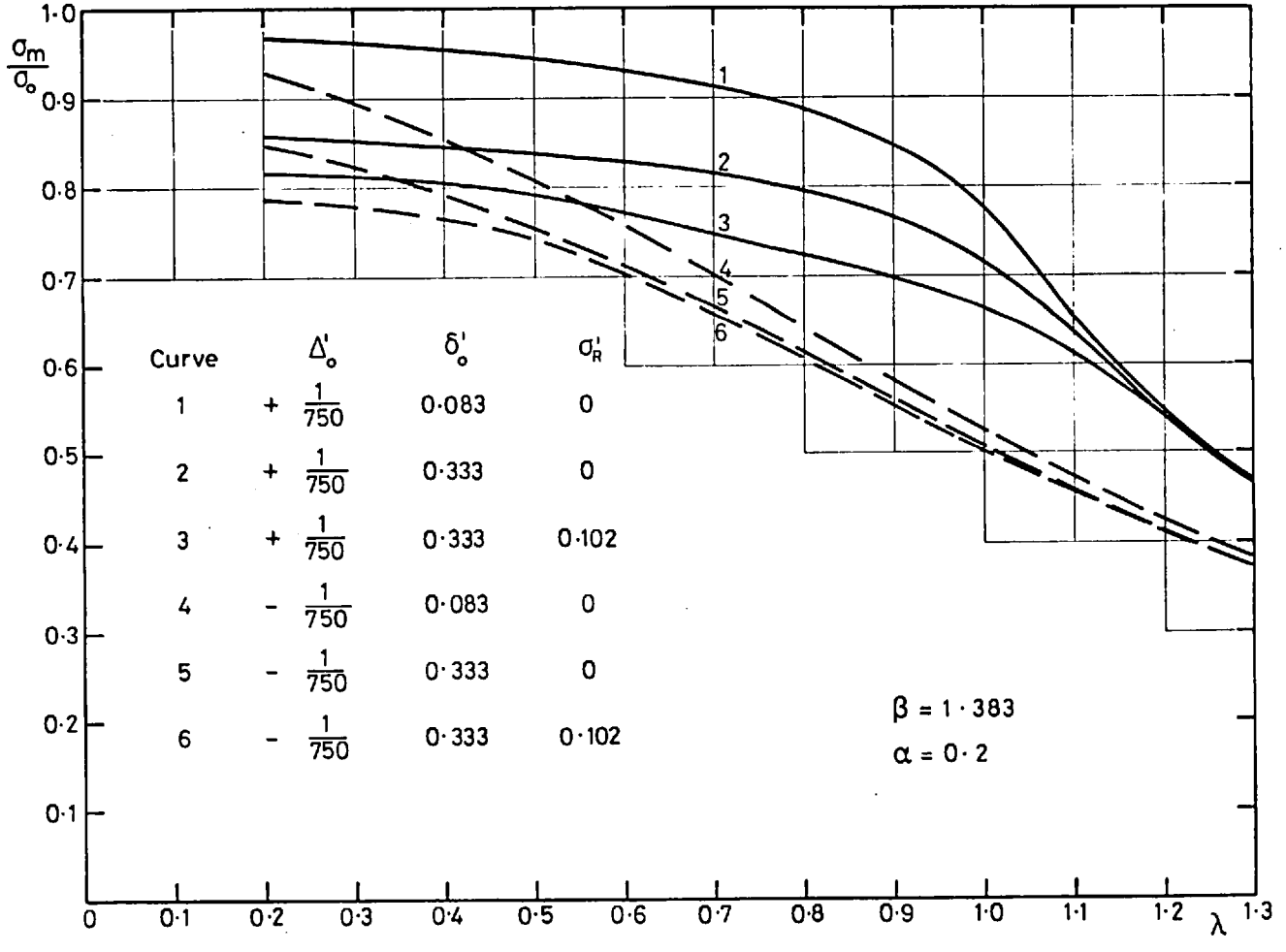

Fig. 5.29a Maximum Strength-Slenderness Curves for One-Span Columns

Effect of Varying Plate Initial Imperfections

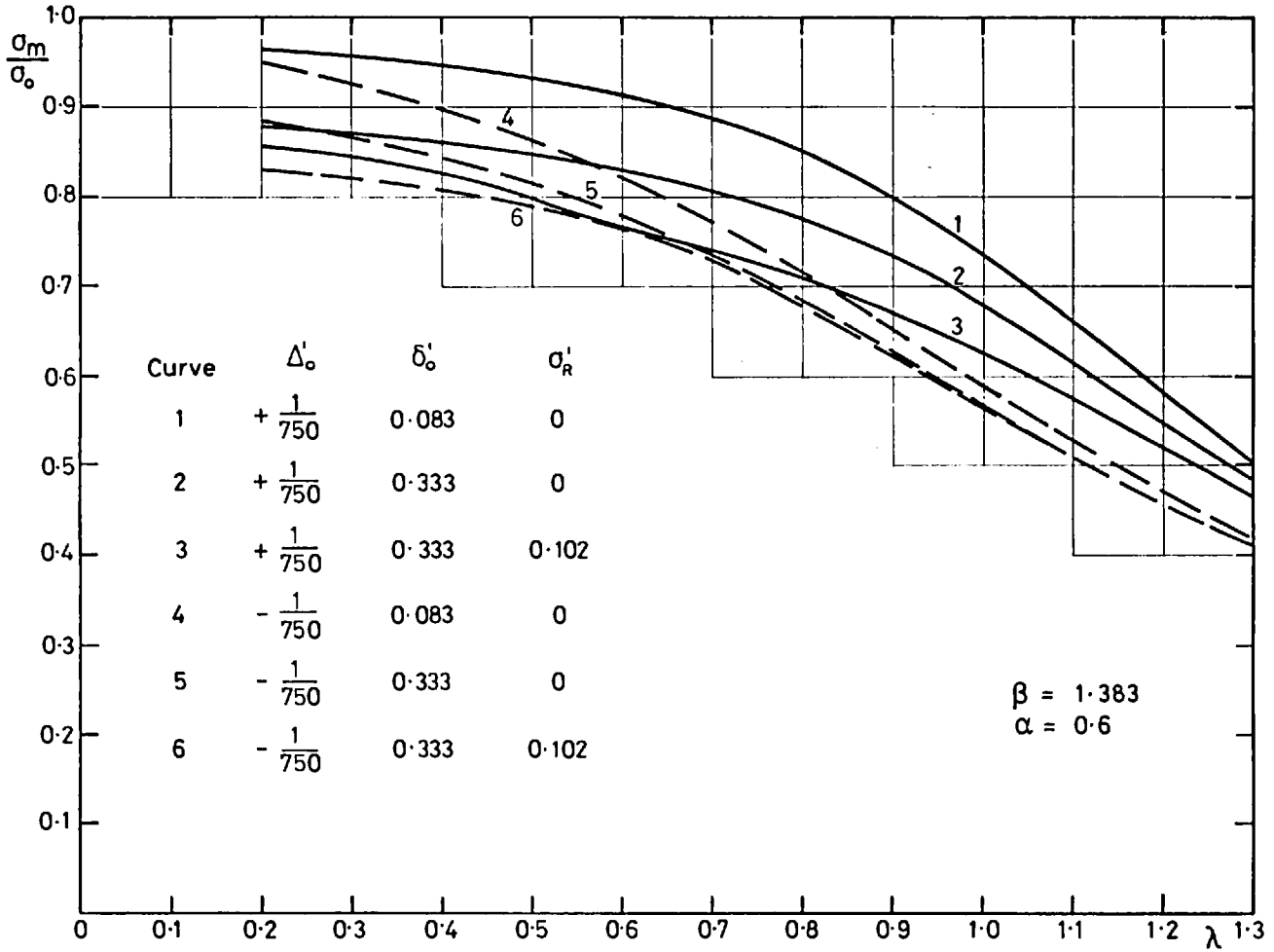

Fig. 5.29b Maximum Strength-Slenderness Curves for One-Span Columns

Effect of Varying Plate Initial Imperfections

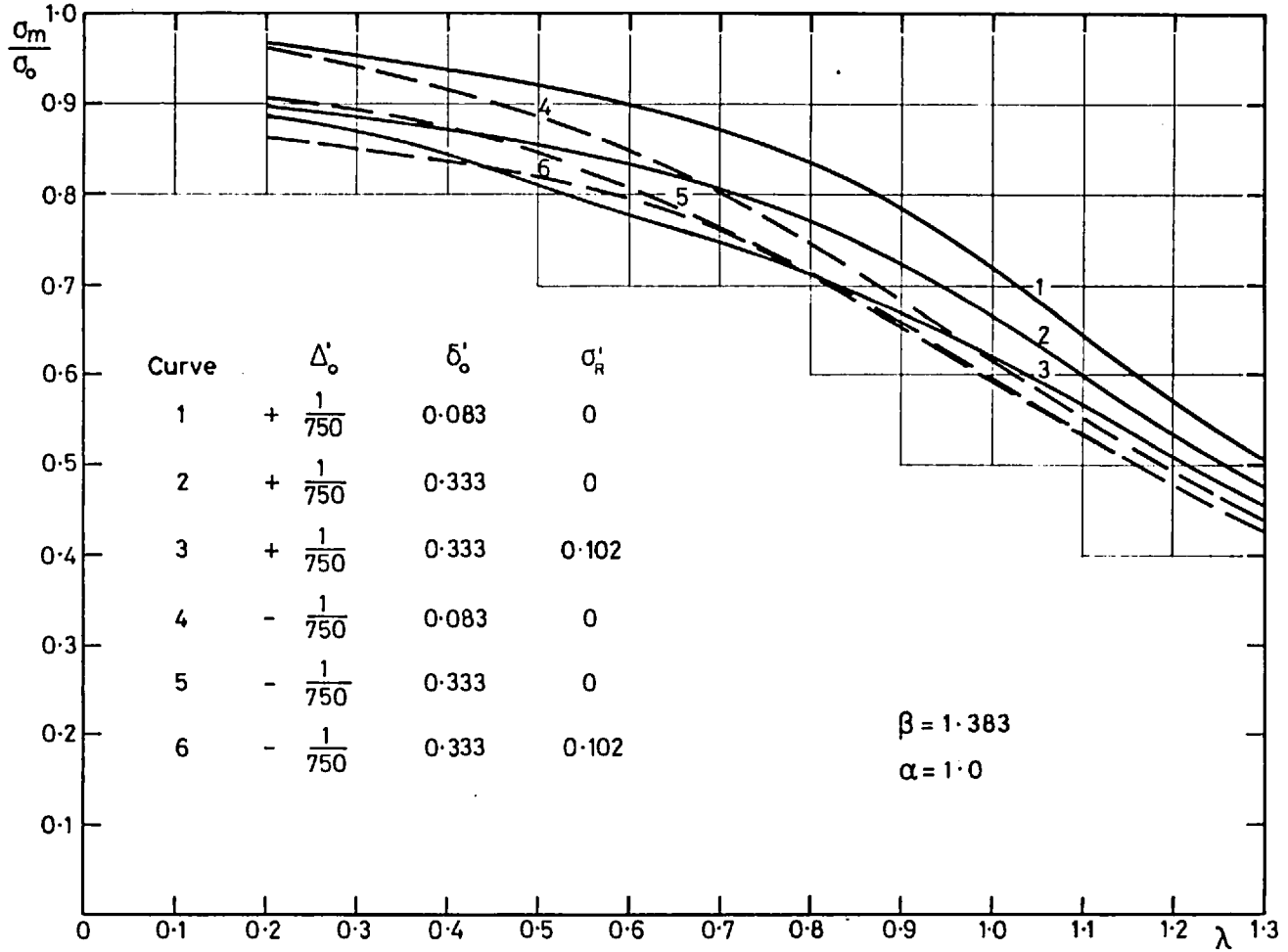

Fig. 5.29c Maximum Strength-Slenderness Curves for One-Span Columns

Effect of Varying Plate Initial Imperfections

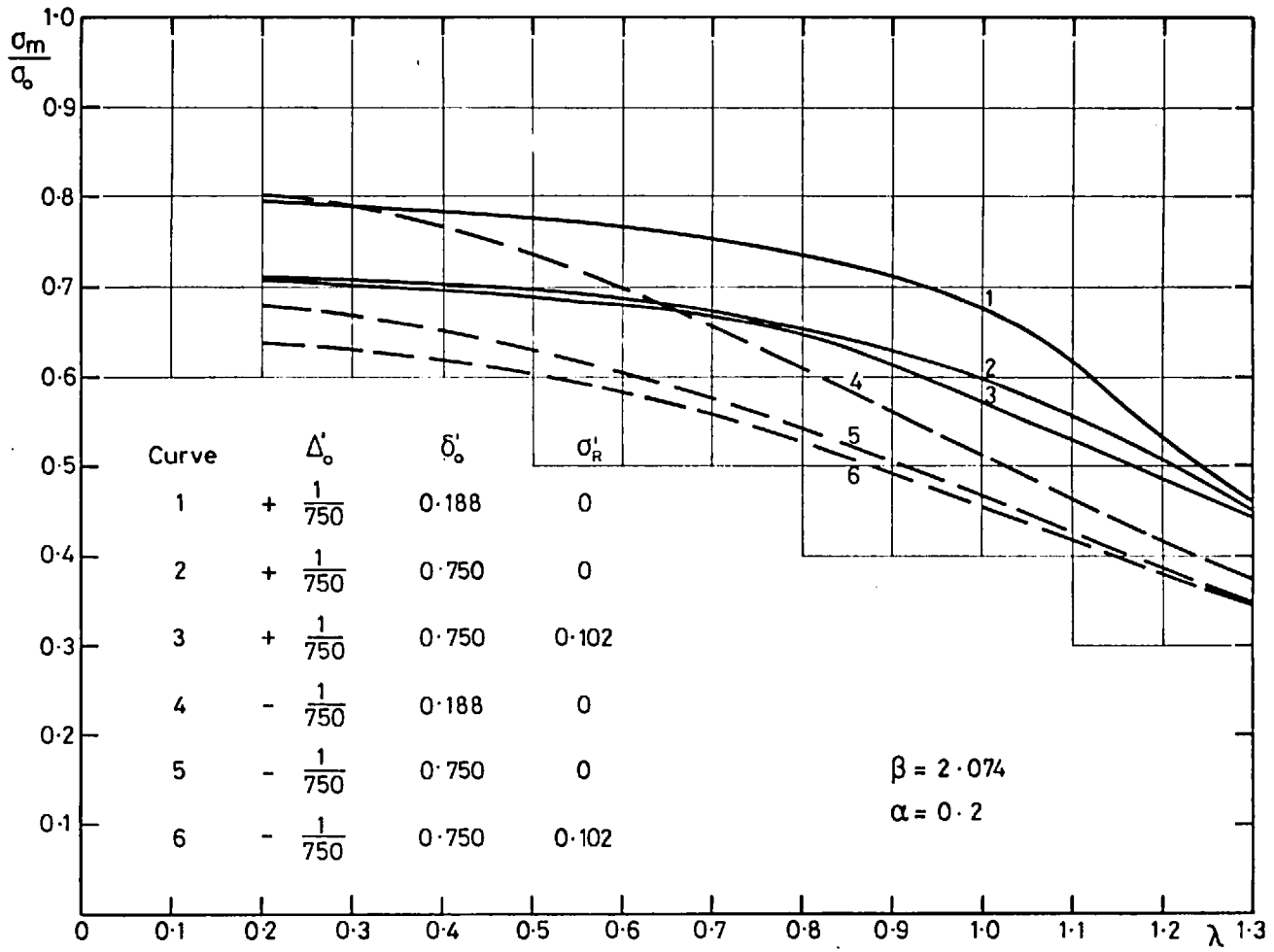

Fig. 5.30a Maximum Strength-Slenderness Curves for One-Span Columns

Effect of Varying Plate Initial Imperfections

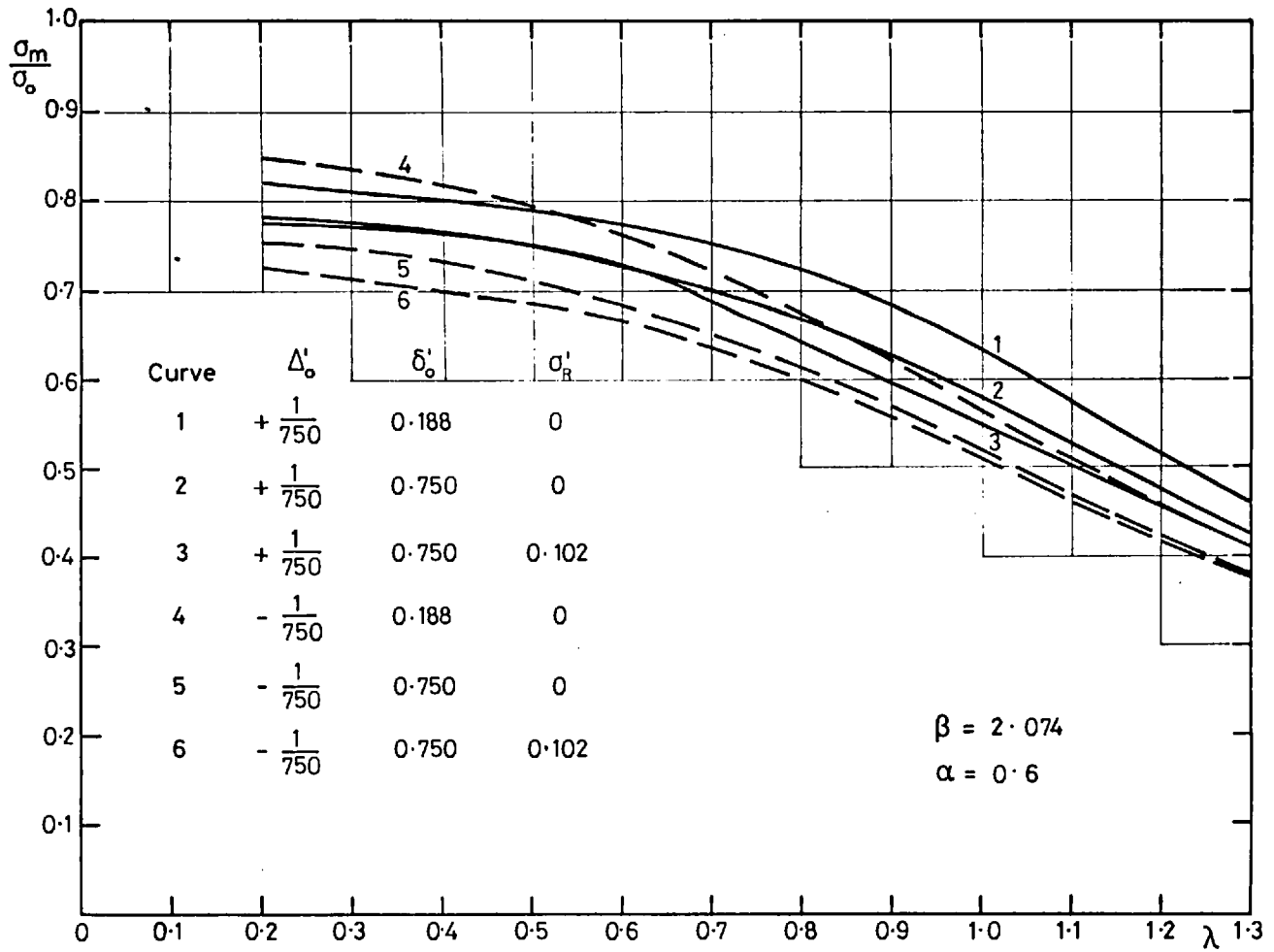

Fig. 5.30b Maximum Strength-Slenderness Curves for One-Span Columns

Effect of Varying Plate Initial Imperfections

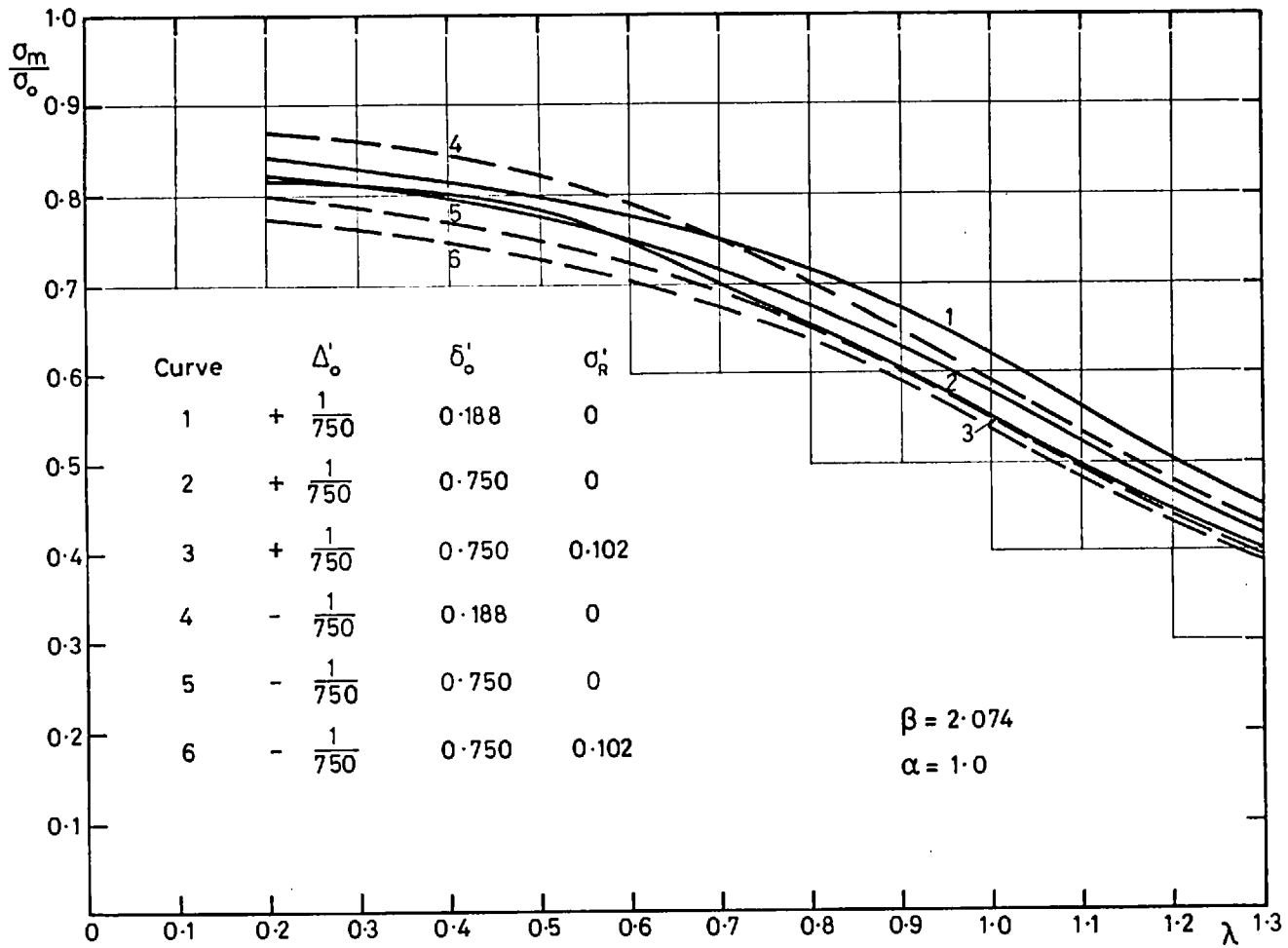

Fig.5.30c Maximum Strength-Slenderness Curves for One-Span Columns

Effect of Varying Plate Initial Imperfections

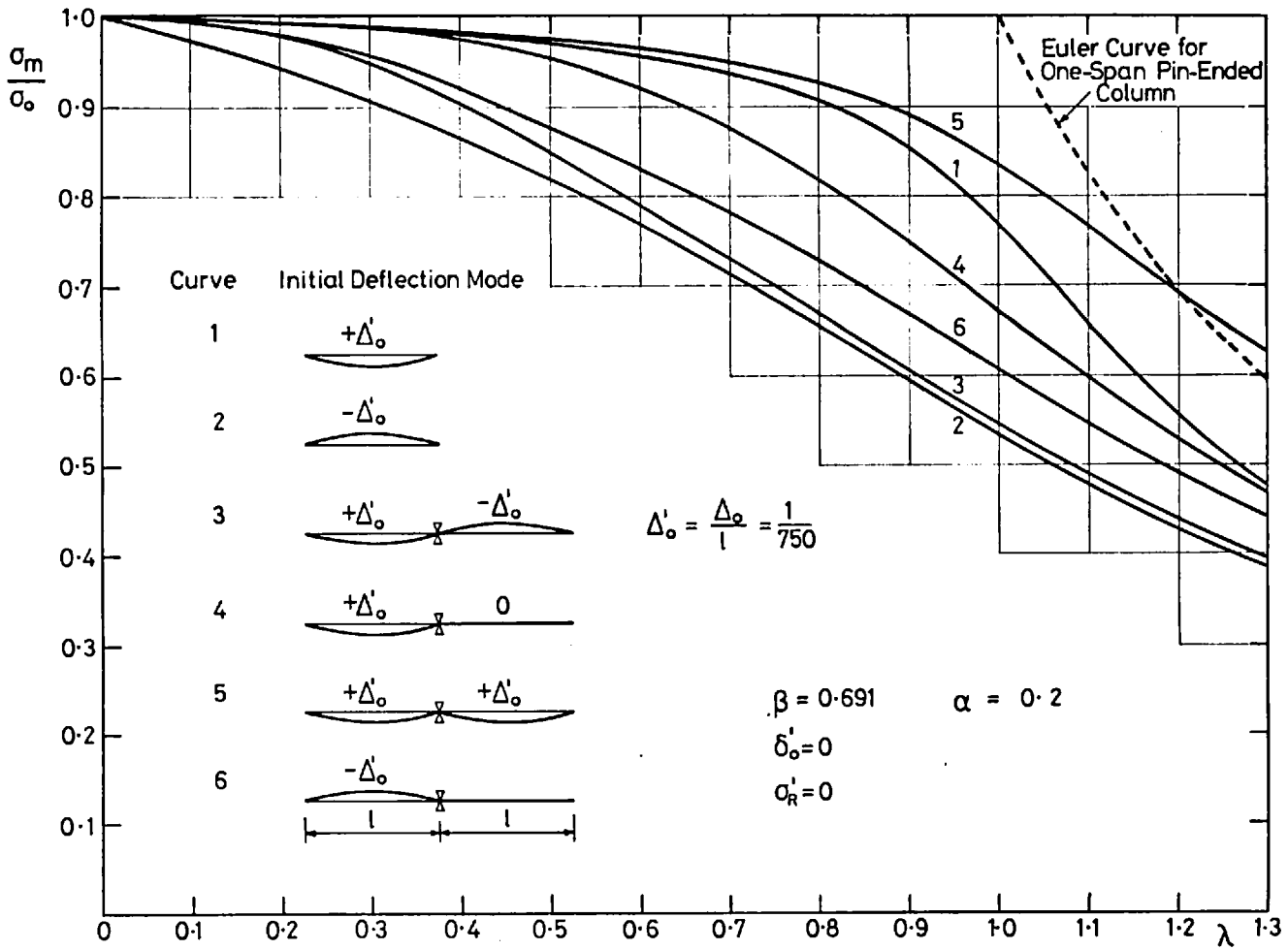

Fig. 5.31a Maximum Strength-Slenderness Curves for Two-Span Continuous Beam-Columns

Effect of Varying Stiffener Initial Deflection Modes

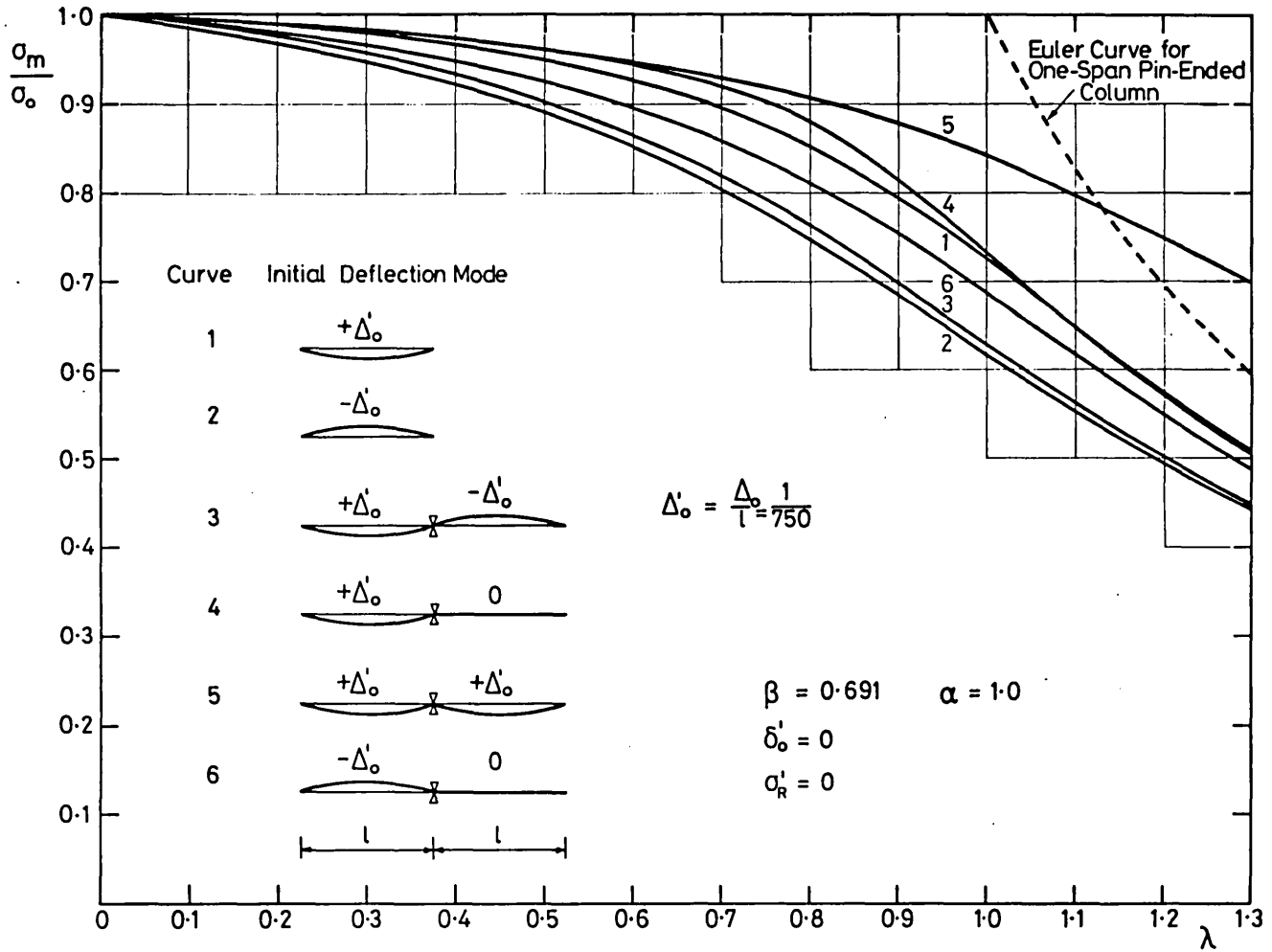

Fig. 5.31b Maximum Strength-Slenderness Curves for Two-Span Continuous Beam-Columns

Effect of Varying Stiffener Initial Deflection Modes

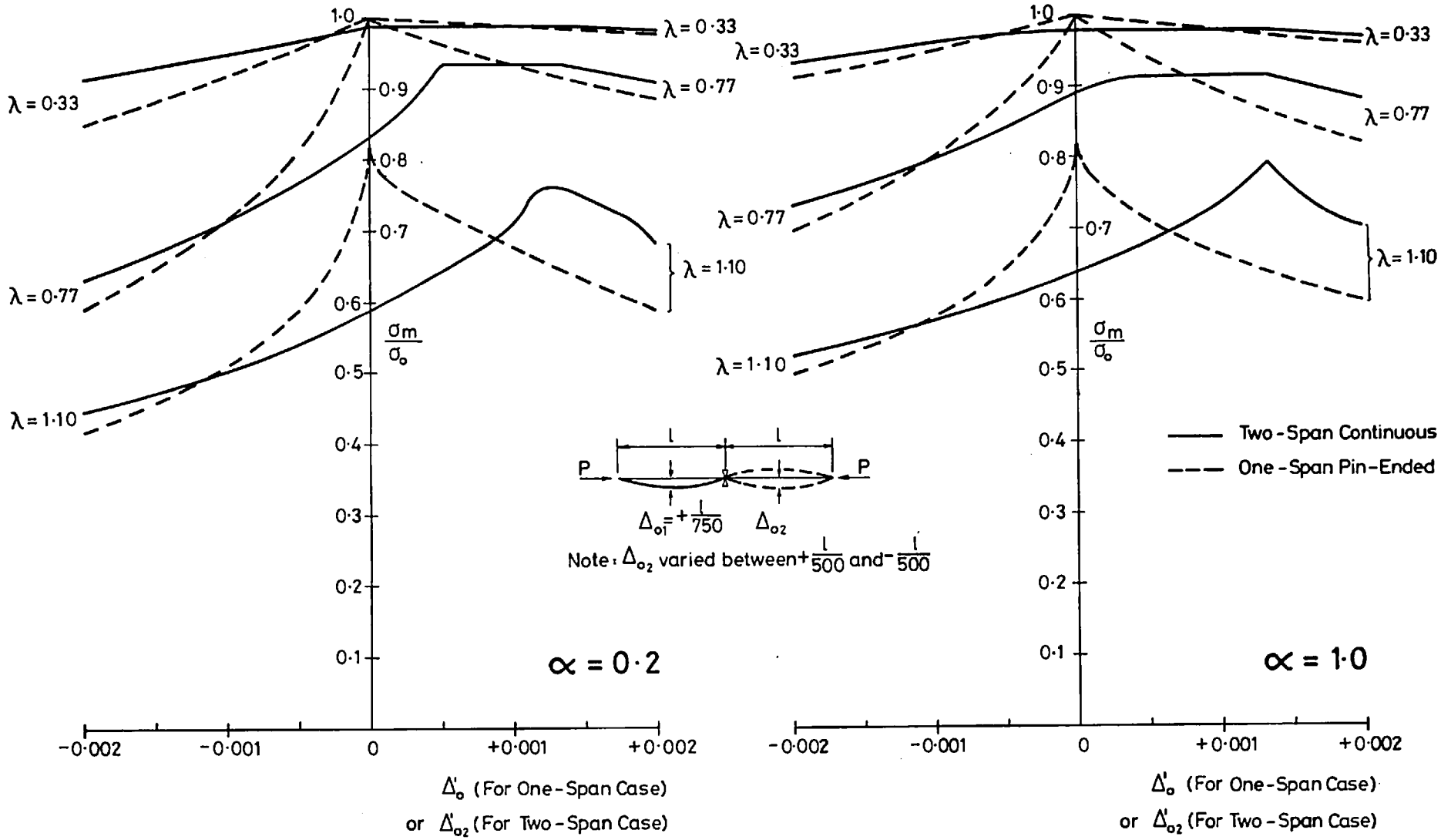

Fig. 5.32 Variation of Maximum Strength with Initial Deflection for One-Span Pin-Ended and Two-Span Continuous Beam-Columns.

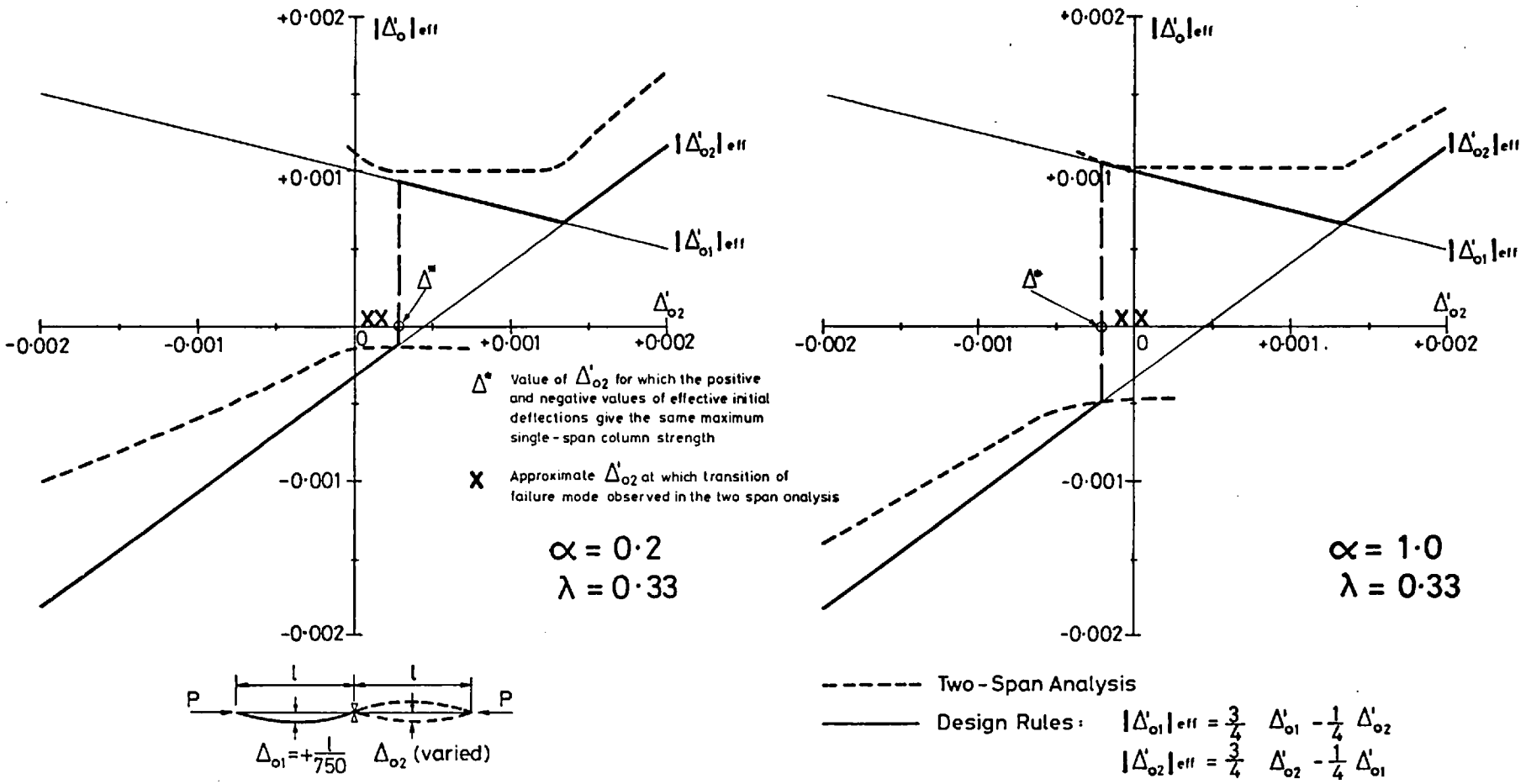

Fig.5.33a Effective Values of Stiffener Initial Deflections for Two-Span Continuous Beam-Columns.
Comparison Between Deflections Derived from the Analysis and Deflections Given by the Design Rules Formulae

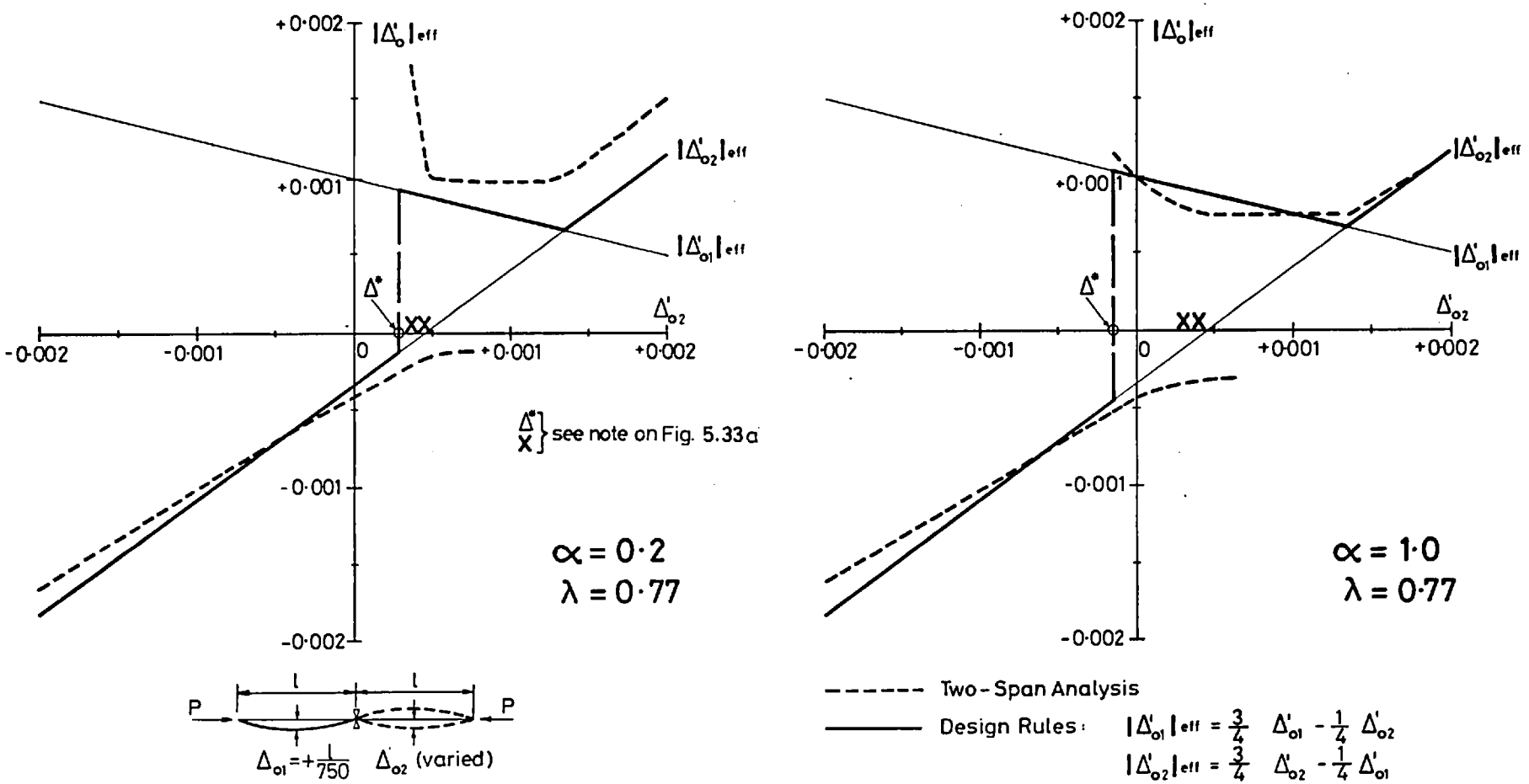

Fig. 5.33b Effective Values of Stiffener Initial Deflections for Two-Span Continuous Beam-Columns.
Comparison Between Deflections Derived from the Analysis and Deflections Given by the Design Rules Formulae

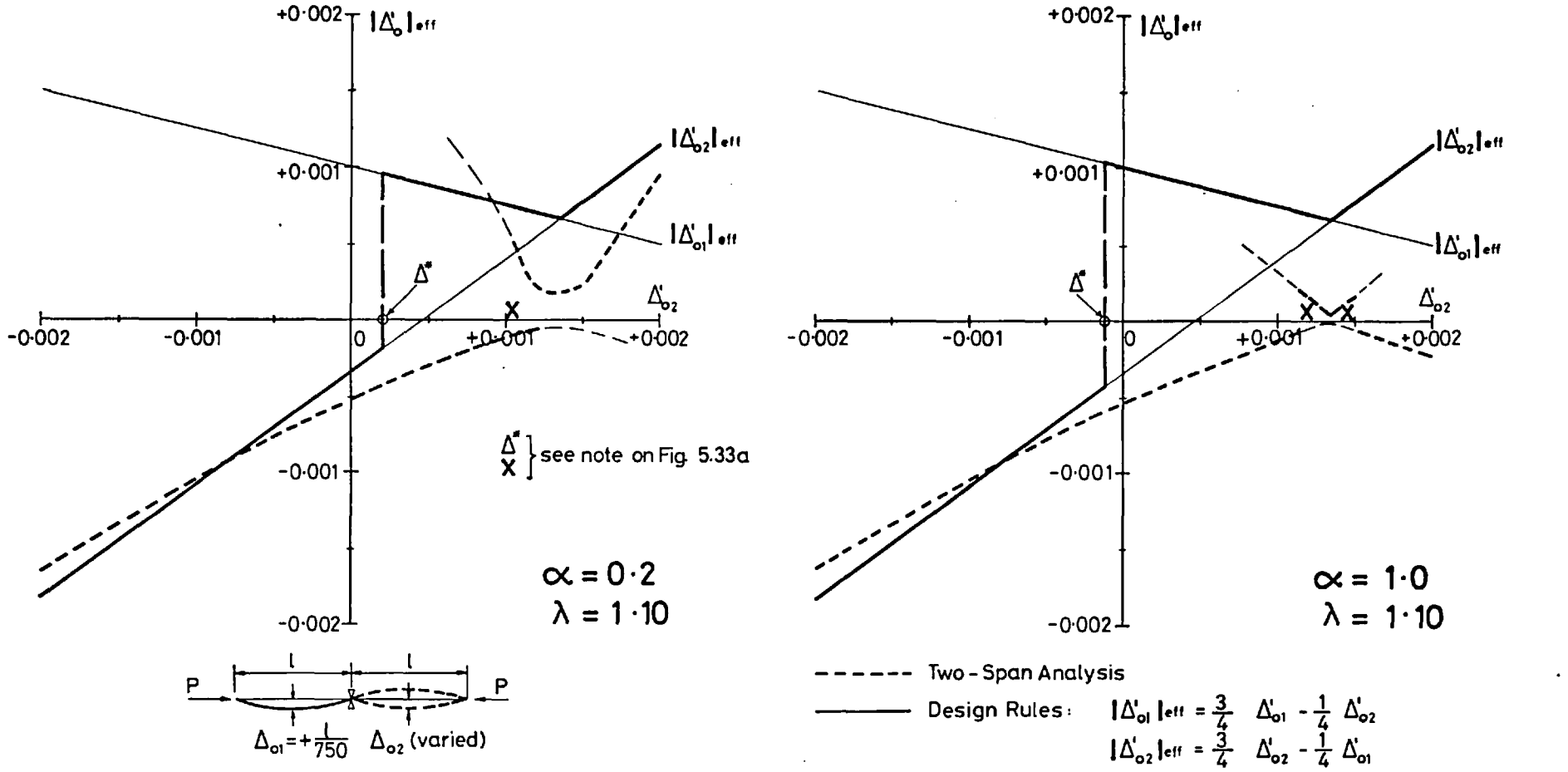

Fig. 5.33c Effective Values of Stiffener Initial Deflections for Two - Span Continuous Beam-Columns.
Comparison Between Deflections Derived from the Analysis and Deflections Given by the Design Rules Formulae

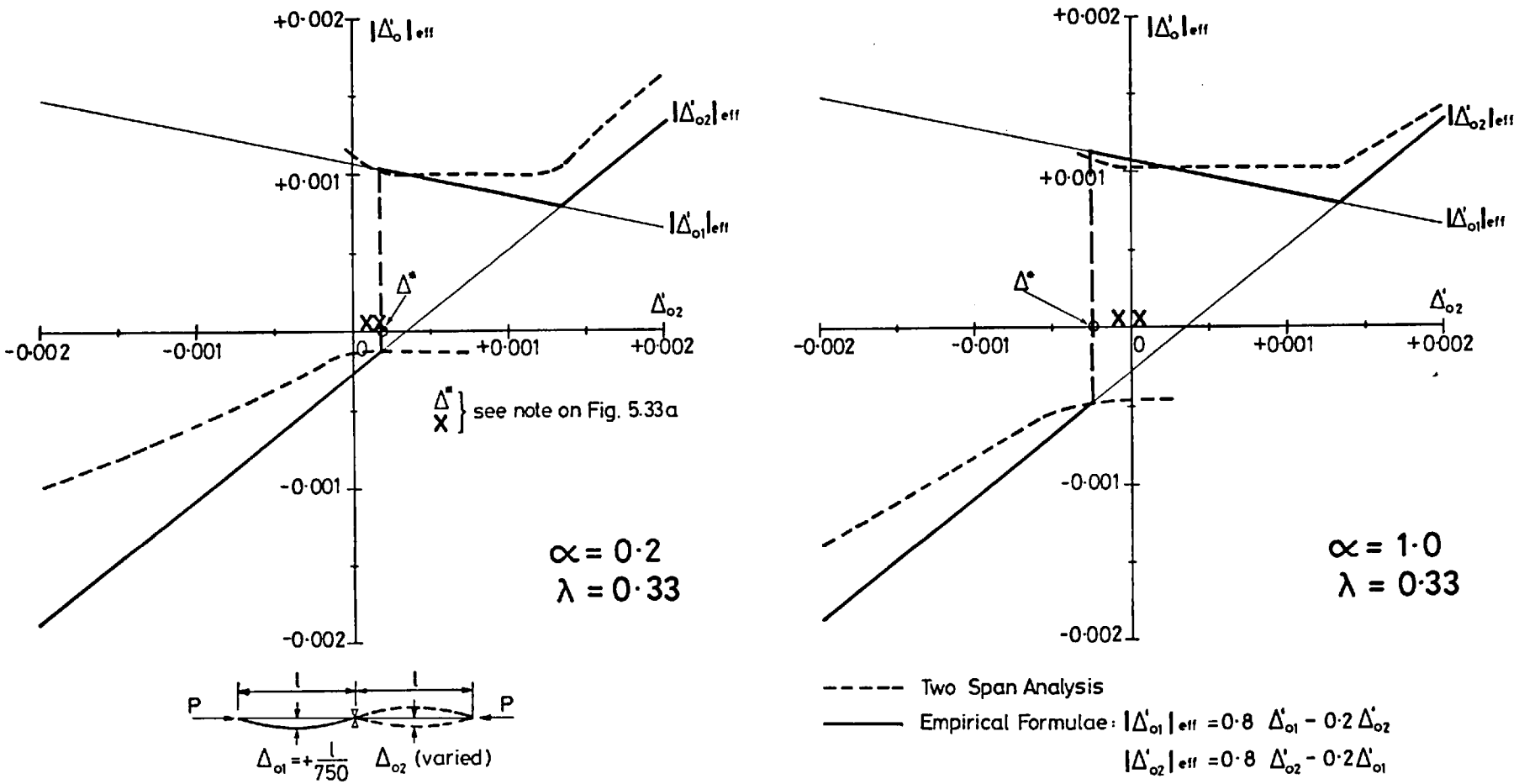

Fig. 5.34a Effective Values of Stiffener Initial Deflections for Two-Span Continuous Beam-Columns

Comparison Between Deflections Derived from the Analysis and Deflections Given by the Modified Design Rules Formulae

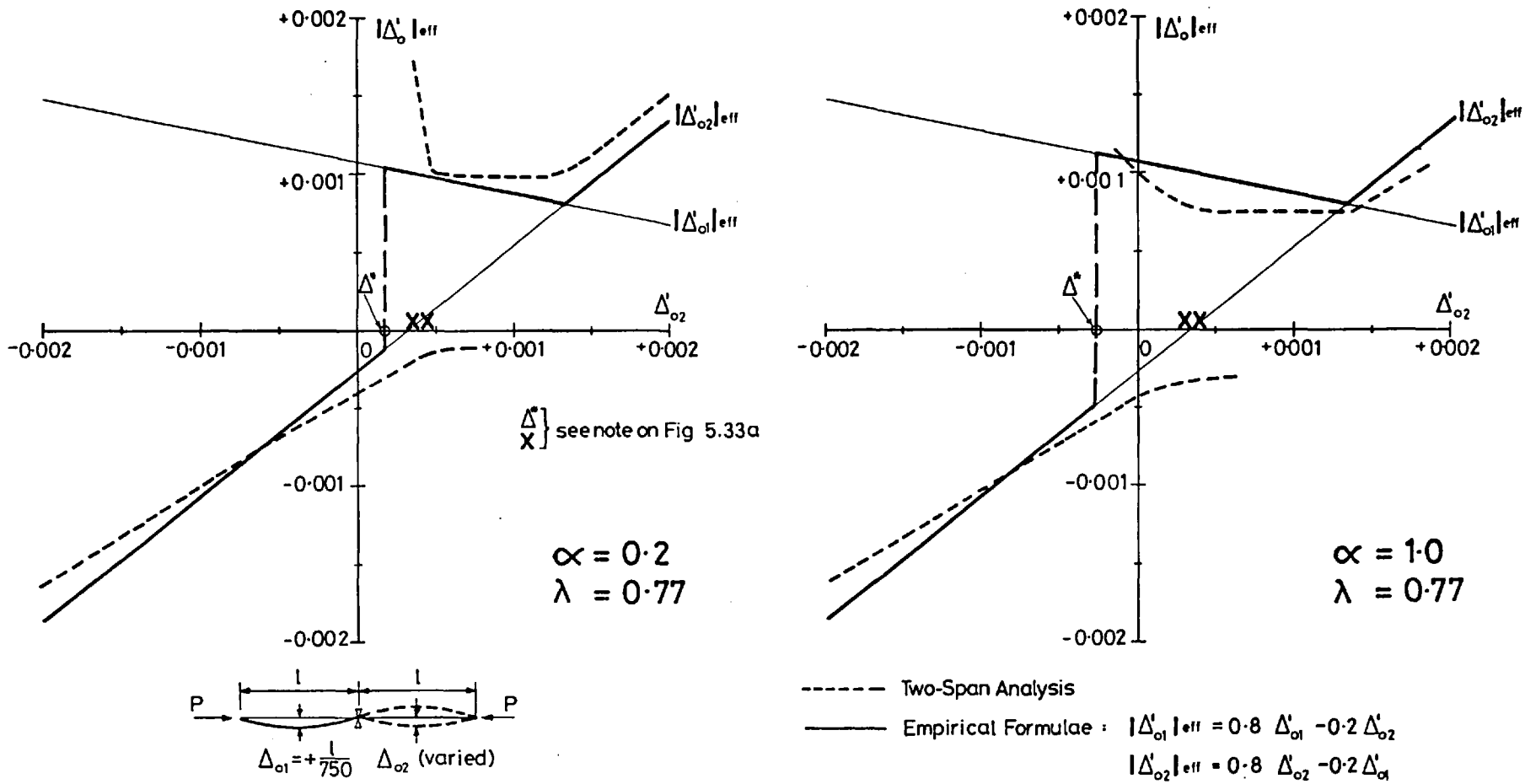

Fig. 5.34b Effective Values of Stiffener Initial Deflections for Two-Span Continuous Beam-Columns

Comparison Between Deflections Derived from the Analysis and Deflections Given by the Modified Design Rules Formulae

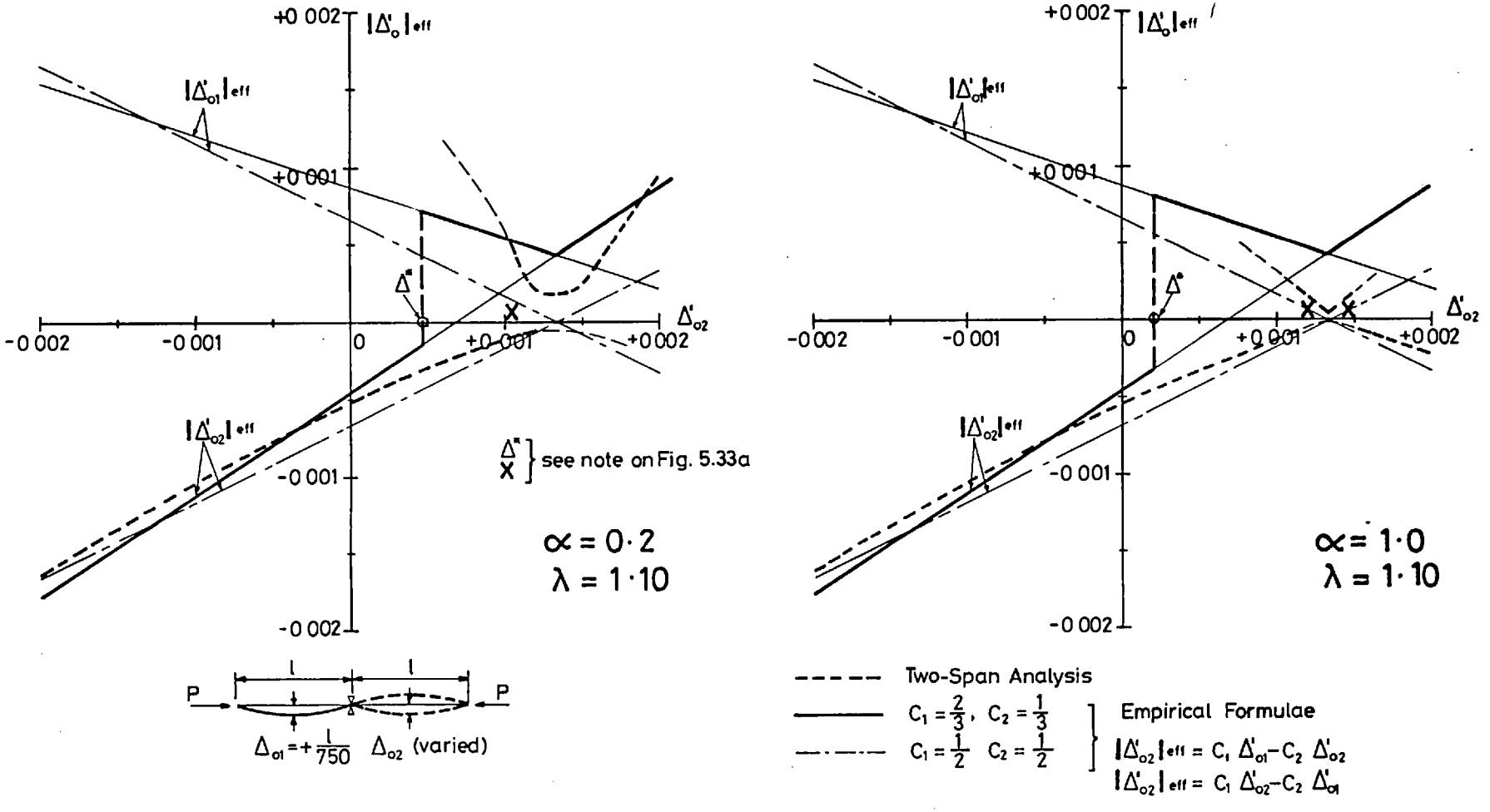

Fig. 5.34c Effective Values of Stiffener Initial Deflections for Two-Span Continuous Beam-Columns

Comparison Between Deflections Derived from the Analysis and Deflections Given by the Modified Design Rules Formulae

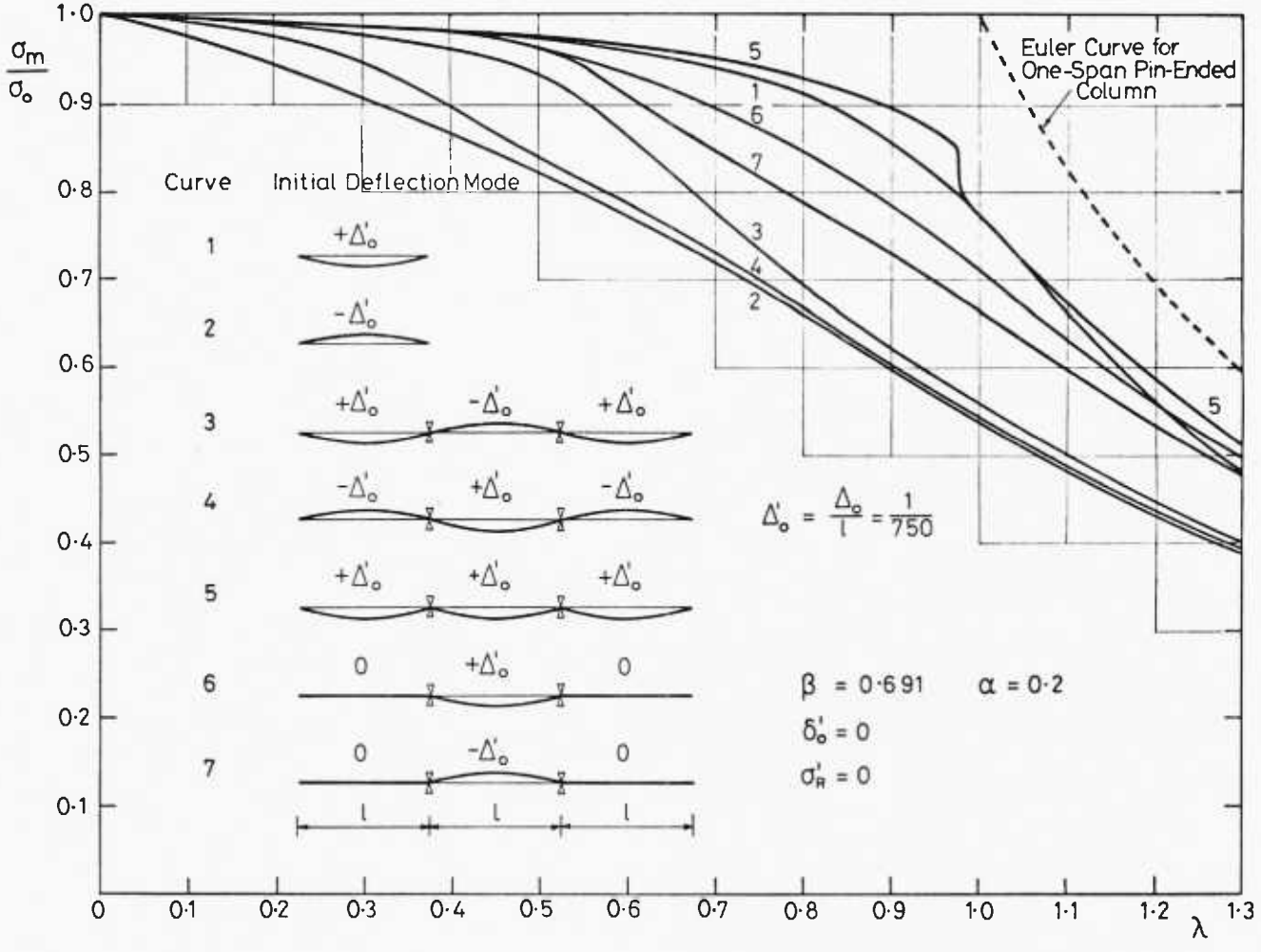

Fig. 5.35a Maximum Strength-Slenderness Curves for Three-Span Continuous Beam-Columns

Effect of Varying Stiffener Initial Deflection Modes

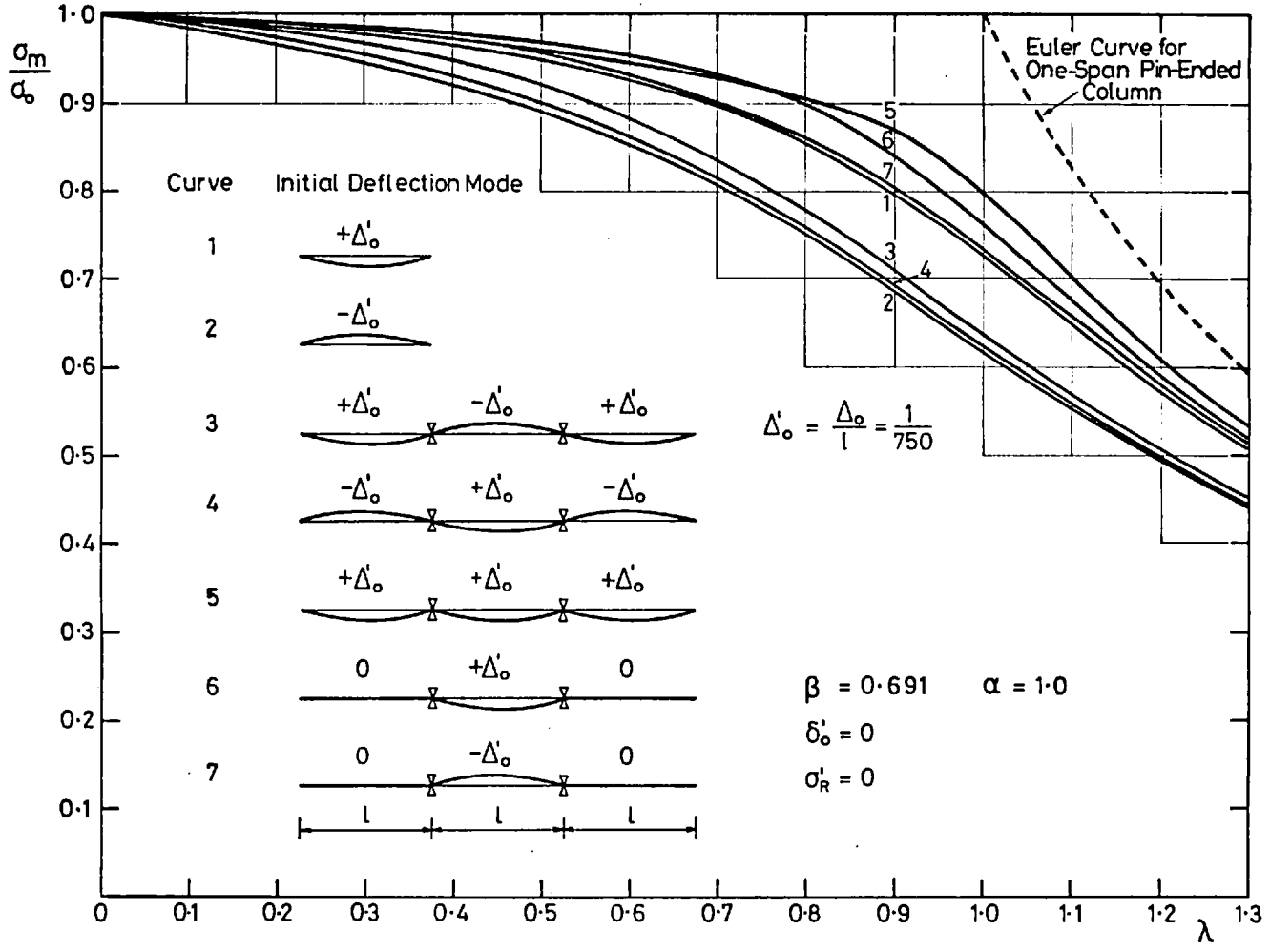

Fig. 5.35b Maximum Strength-Slenderness Curves for Three-Span Continuous Beam-Columns

Effect of Varying Stiffener Initial Deflection Modes

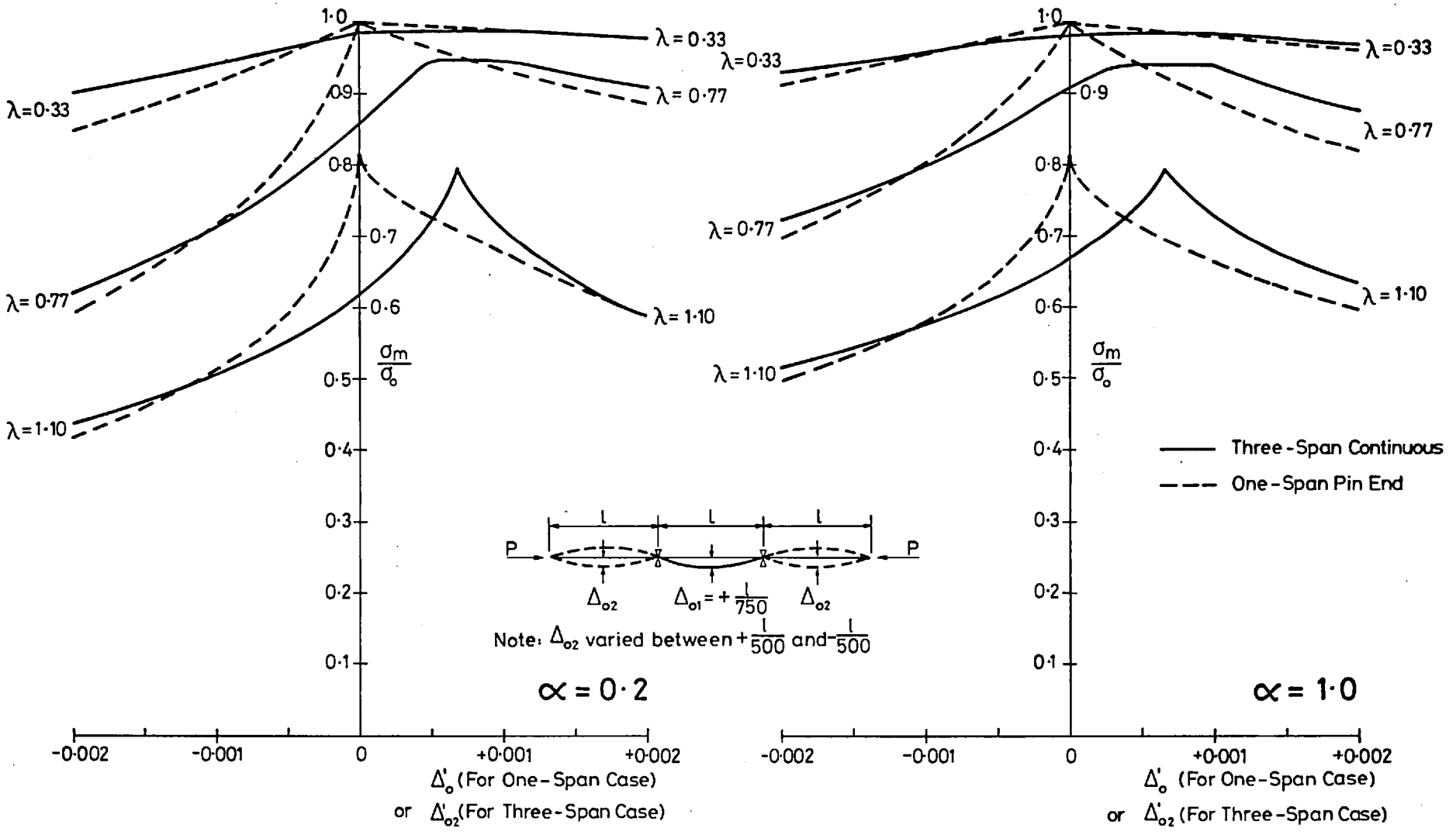

Fig. 5.36 Variation of Maximum Strength with Initial Deflection for One-Span Pin-Ended and Three-Span Continuous Beam-Columns

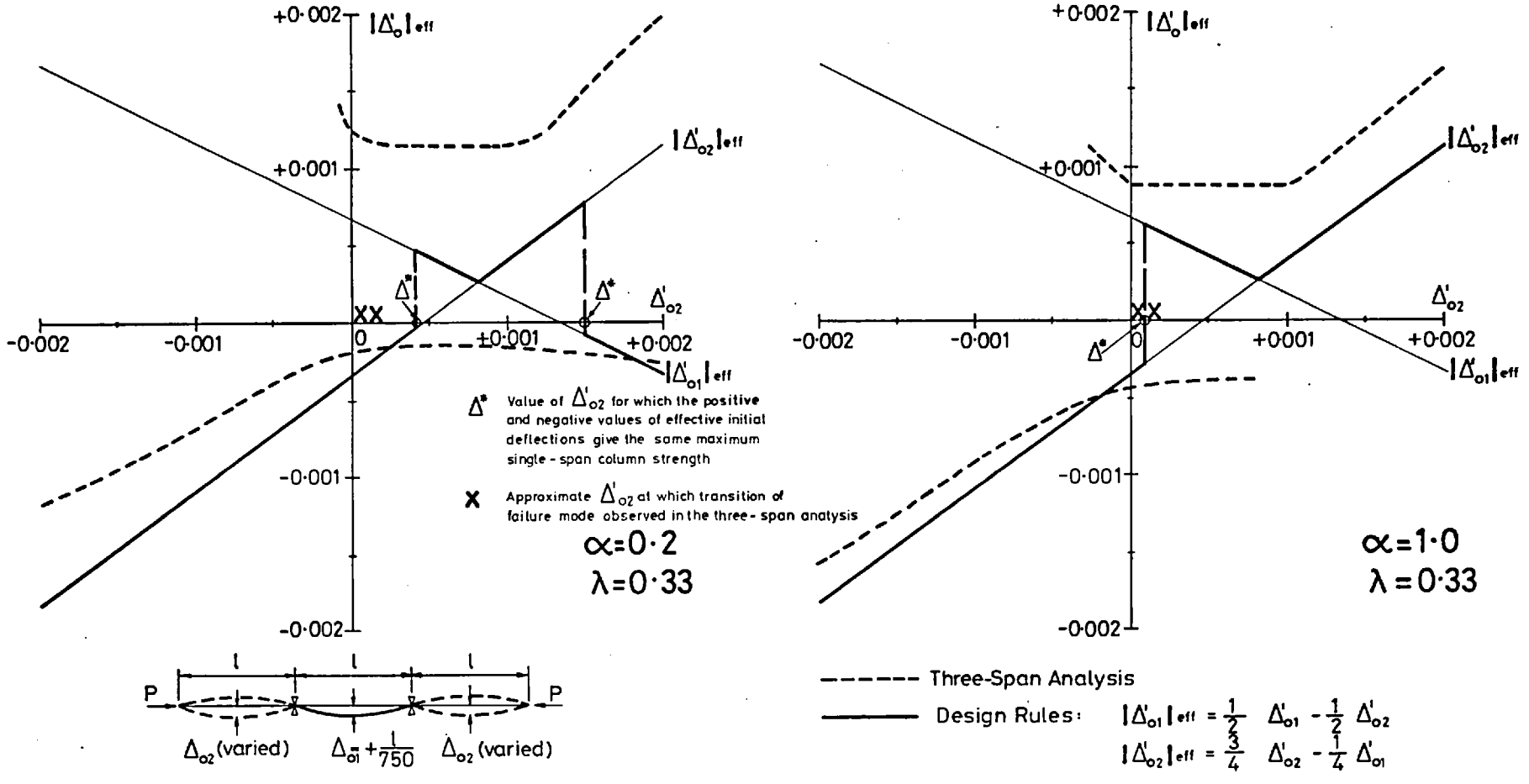

Fig. 5.37a Effective Values of Stiffener Initial Deflections for Three-Span Continuous Beam-Columns.
Comparison Between Deflections Derived from the Analysis and Deflections Given by the Design Rules Formulae

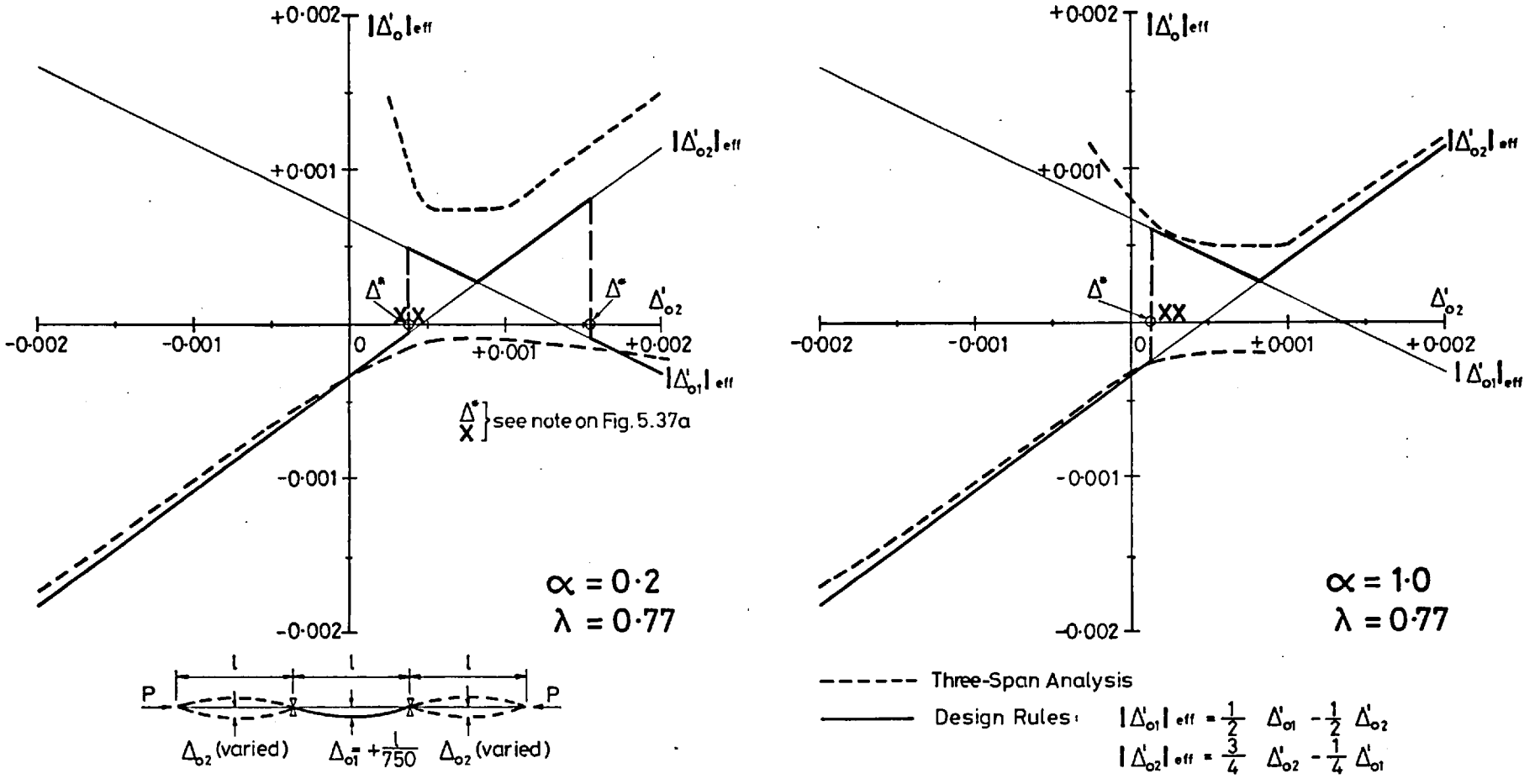

Fig. 5.37b Effective Values of Stiffener Initial Deflections for Three-Span Continuous Beam-Columns.
Comparison Between Deflections Derived from the Analysis and Deflections Given by the Design Rules Formulae

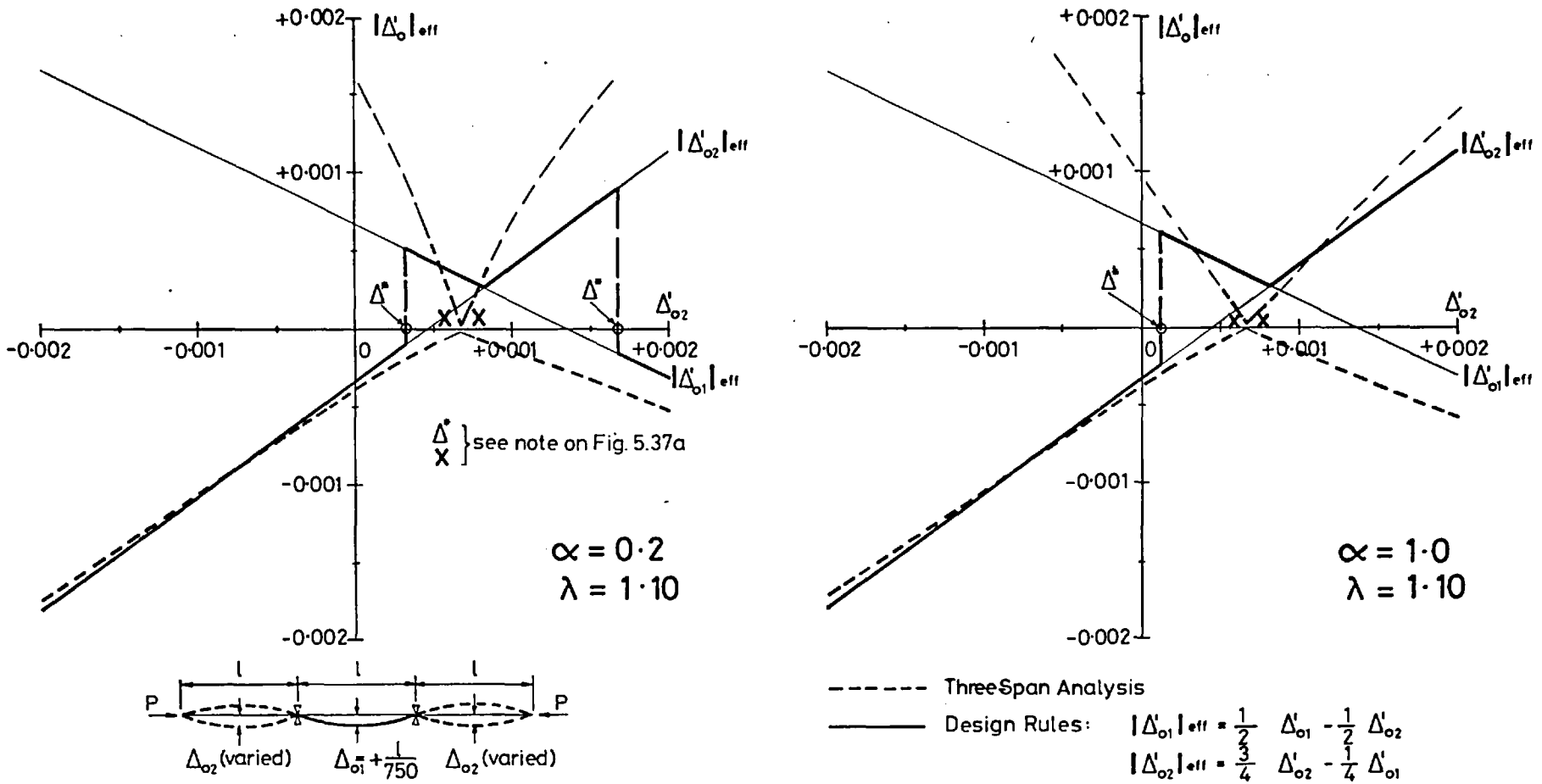

Fig. 5.37c Effective Values of Stiffener Initial Deflections for Three-Span Continuous Beam-Columns.
Comparison Between Deflections Derived from the Analysis and Deflections Given by the Design Rules Formulae

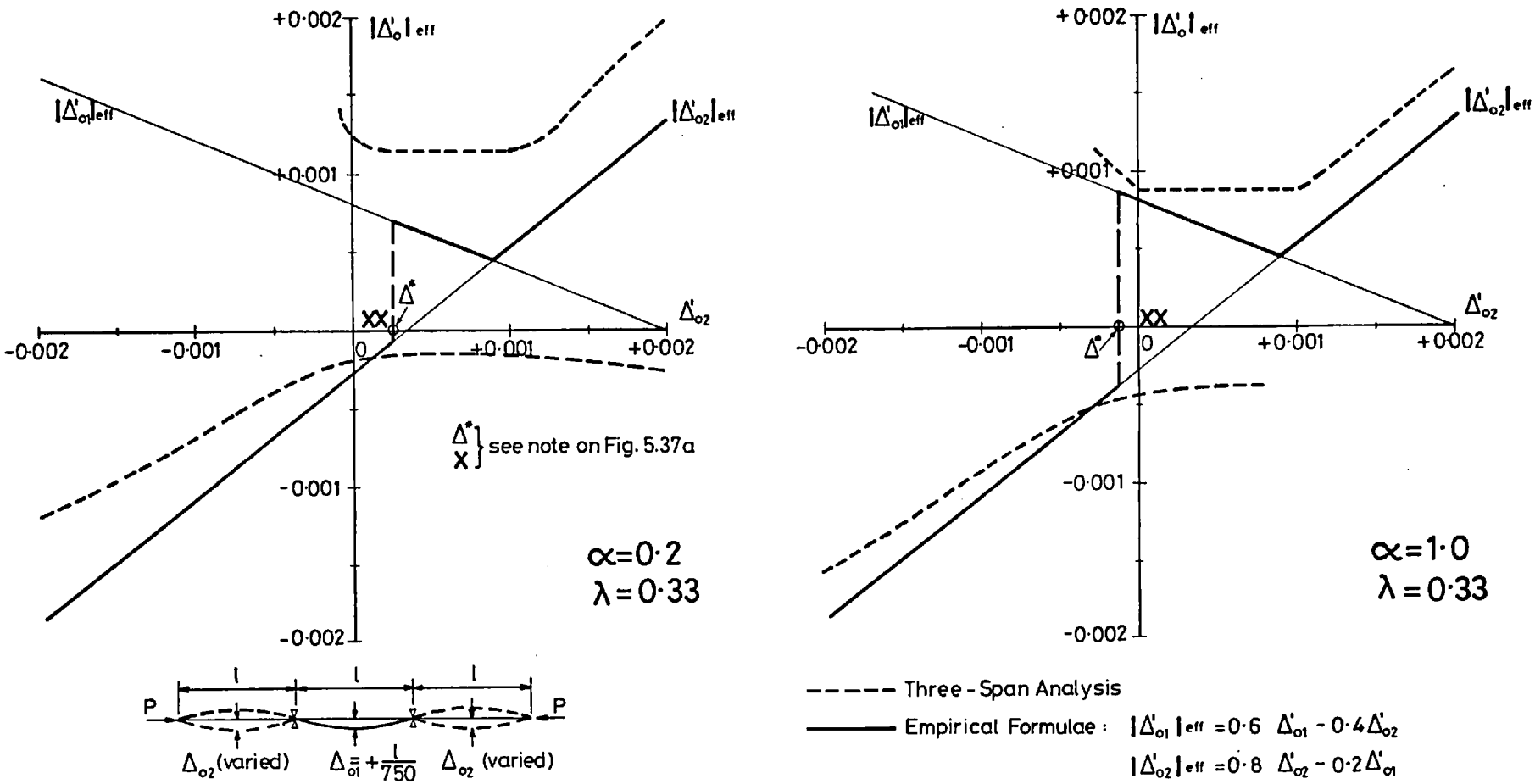

Fig. 5.38a Effective Values of Stiffener Initial Deflections for Three-Span Continuous Beam-Columns

Comparison Between Deflections Derived from the Analysis and Deflections Given by the Modified Design Rules Formulae

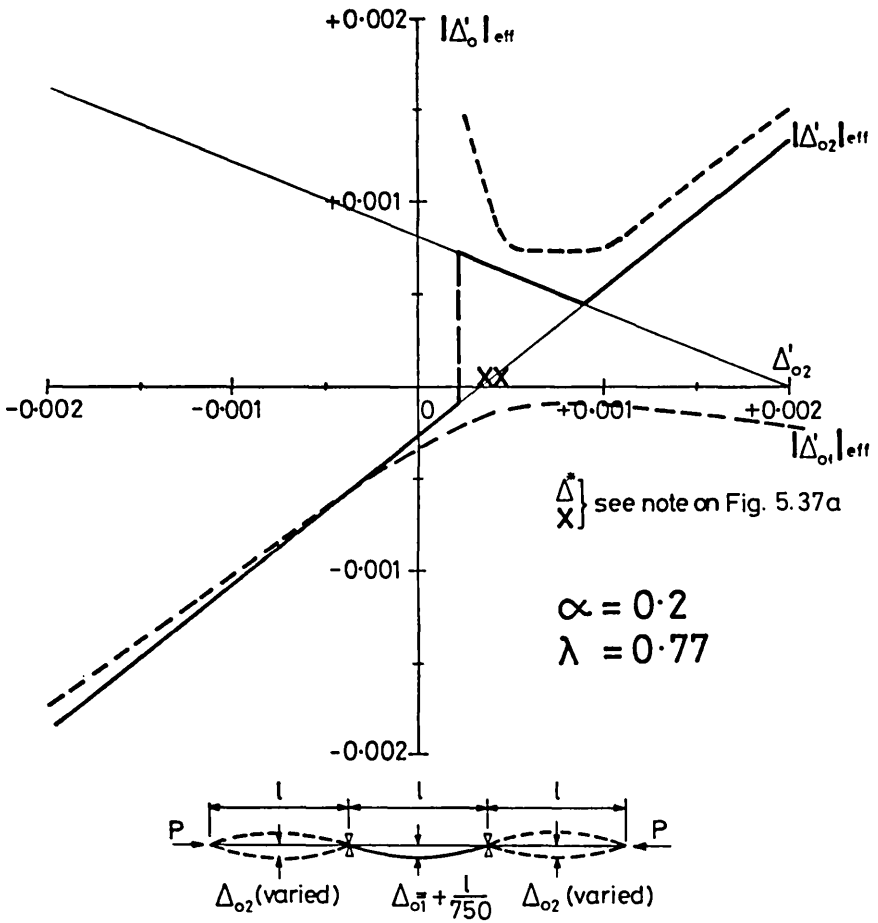

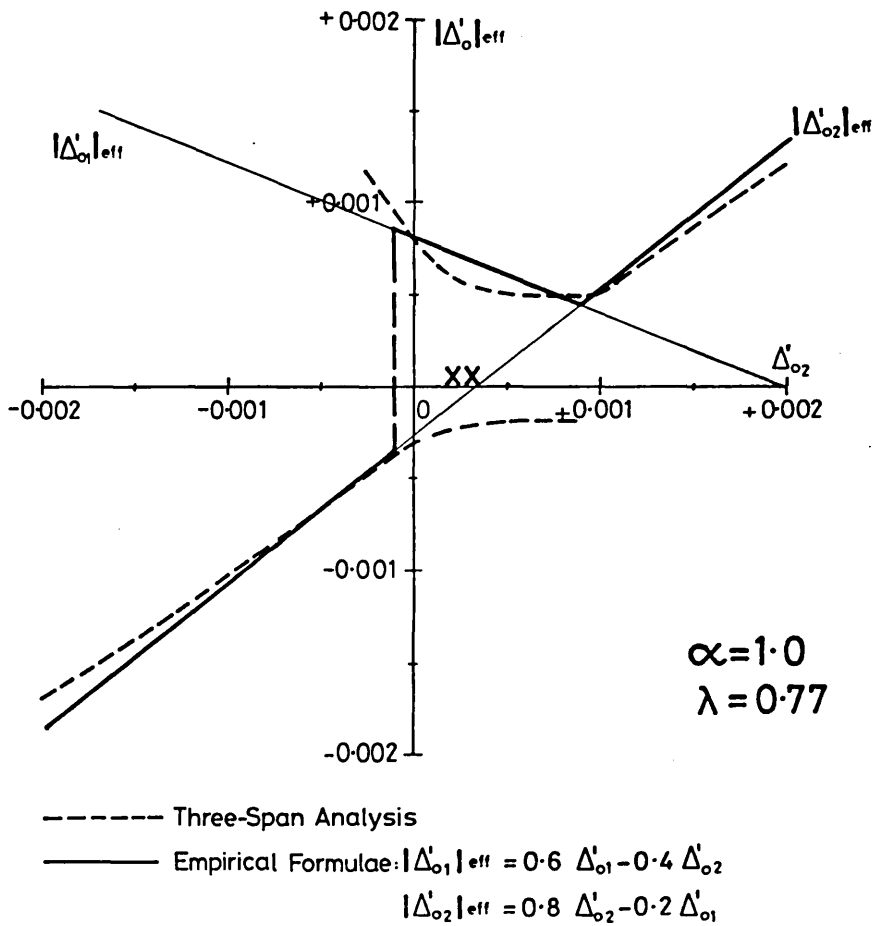

Fig. 5.38b Effective Values of Stiffener Initial Deflections for Three-Span Continuous Beam-Columns

Comparison Between Deflections Derived from the Analysis and Deflections Given by the Modified Design Rules Formulae

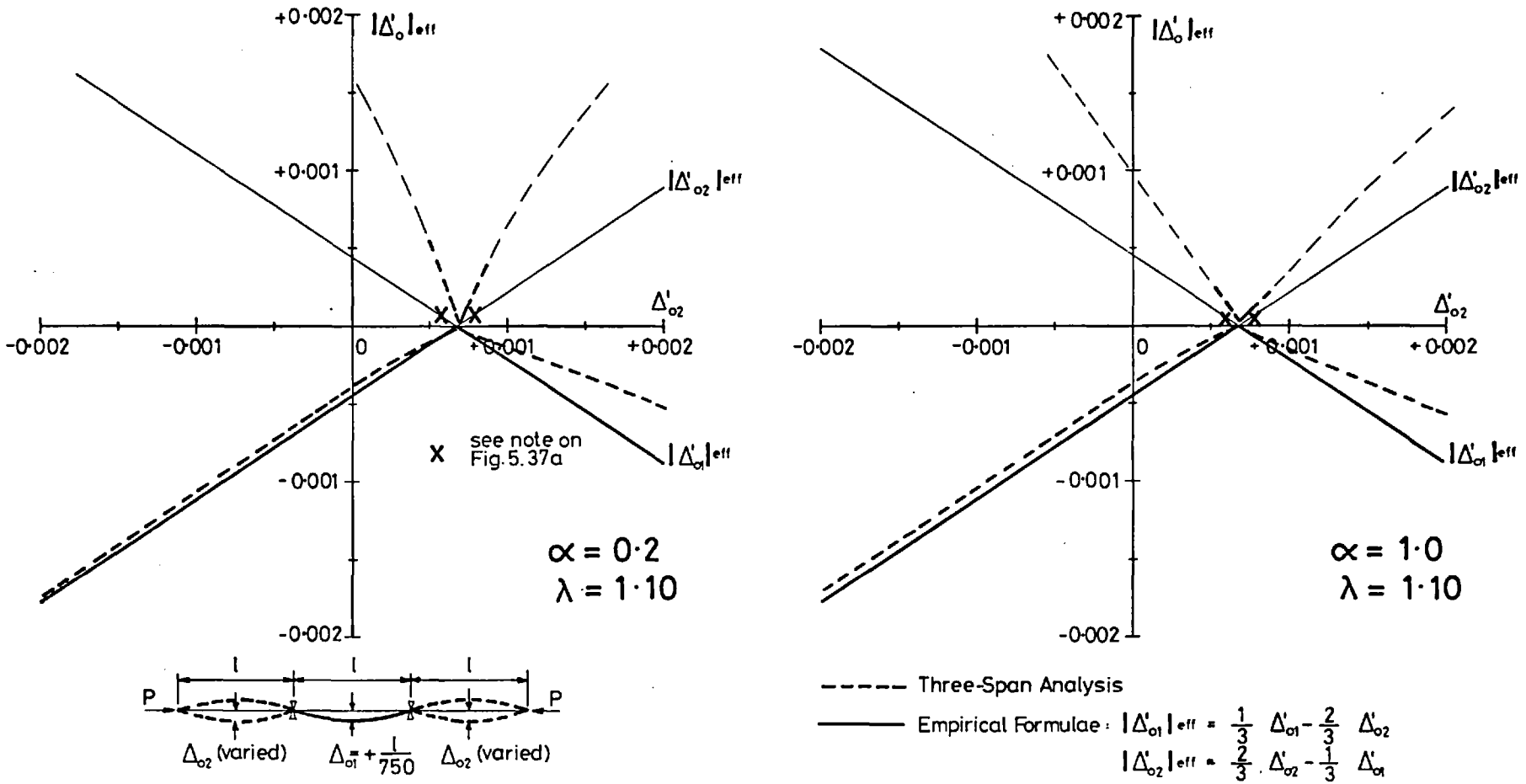

Fig. 5.38c Effective Values of Stiffener Initial Deflections for Three-Span Continuous Beam-Columns.
Comparison Between Deflections Derived from the Analysis and Deflections Given by the Modified Design Rules Formulae.

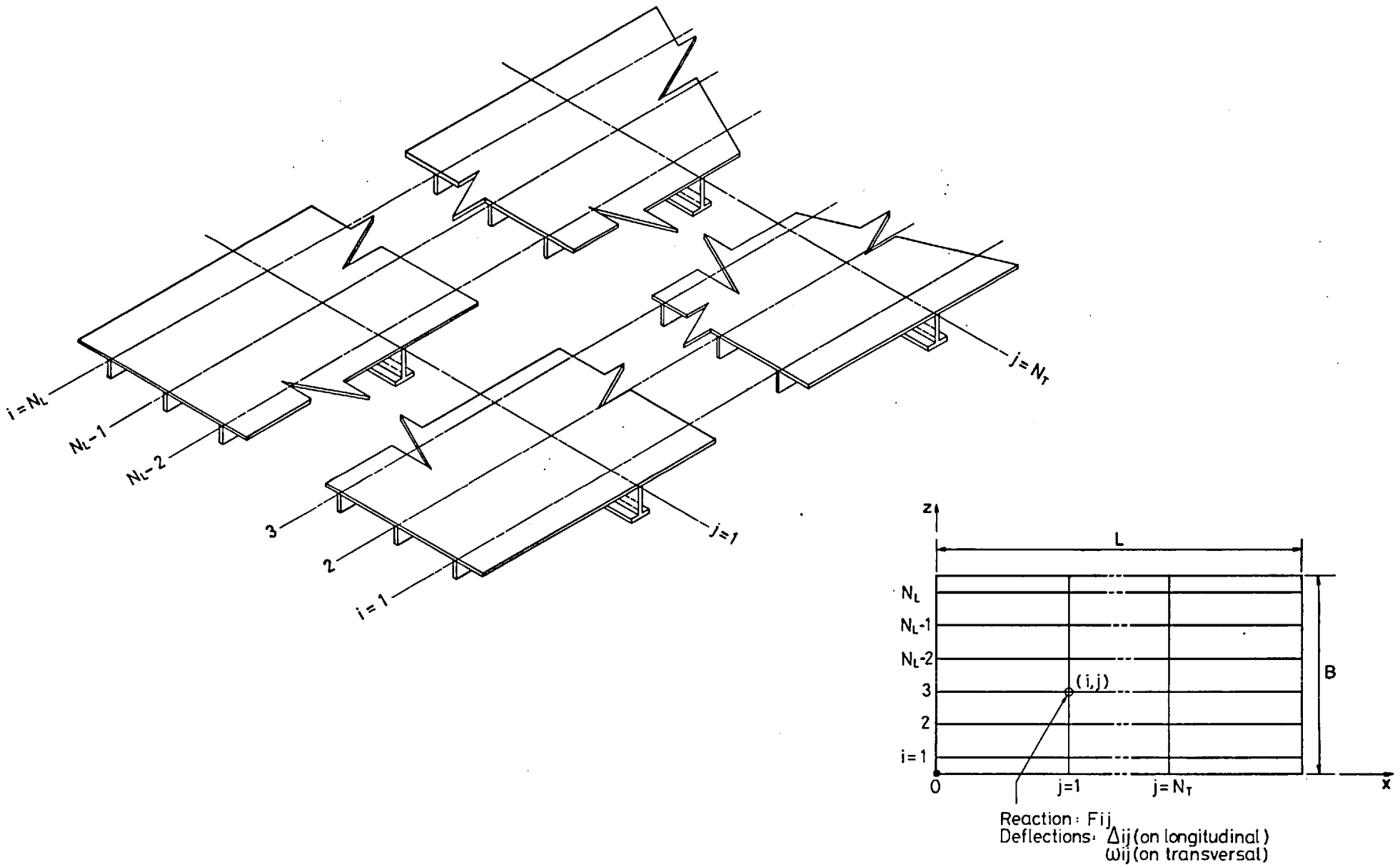

Fig A.1 Grillage of Beam-Columns

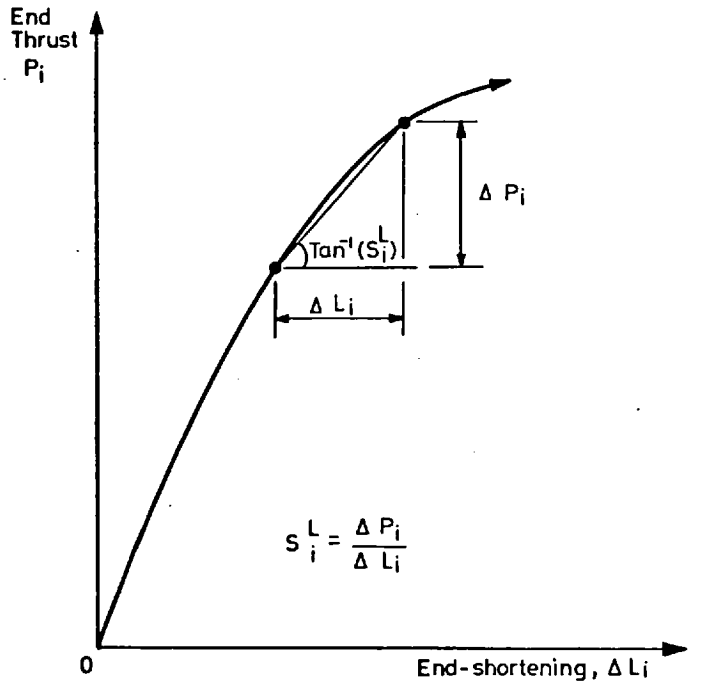

Fig.A.2 End Thrust versus End-Shortening Curve for ith Longitudinal

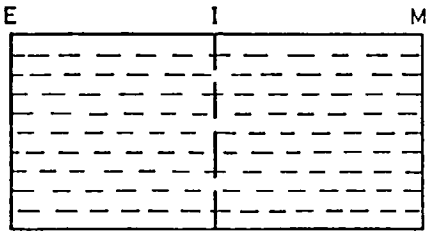

Bays E-I and I-M of
Compression Flange of Model 8

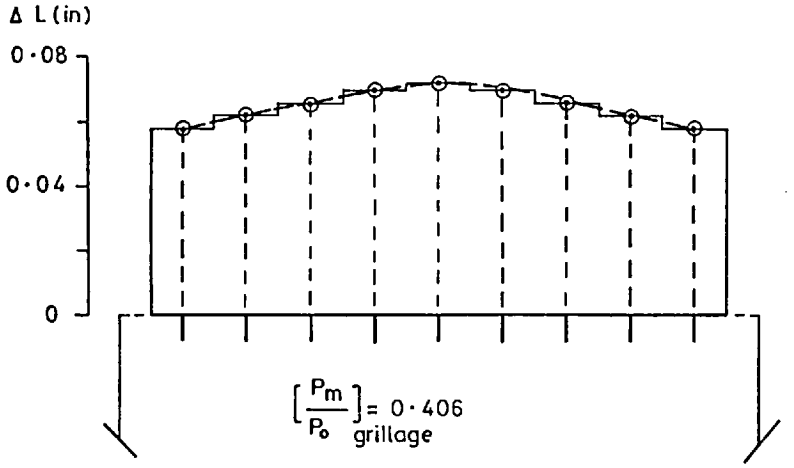

End-shortening of the Longitudinals
For Constant Axial Thrust Across
the Flange Width.

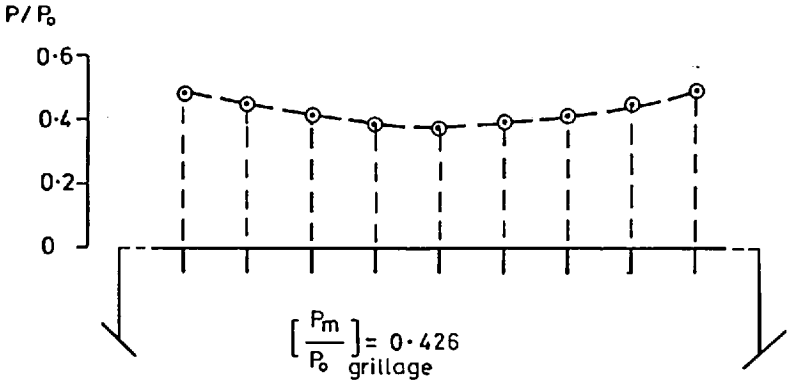

Distribution of Axial Thrust
For Constant End Displacement
Across the Flange Width

Fig. A.3 End-Shortening and Axial Thrust Distribution As Obtained From the Grillage Analysis

(Geometry and Stress-Strain Data as for Model 8)